

Understanding the mechanisms of host-tissue colonisation by *Fusarium graminearum*

Victoria Armer

Thesis submitted to the University of Exeter for the degree of Doctor of Philosophy in Biology

September 2024

This dissertation is available for Library use on the understanding that it is copyright material and that no quotation from the thesis/dissertation may be published without proper acknowledgement.

I certify that all material in this thesis which is not my own work has been identified and that any material that has previously been submitted and approved for the award of a degree by this or any other University has been acknowledged.

Acknowledgements

To my supervisors, Prof Kim Hammond-Kosack and Dr Mike Deeks: this PhD would not have been possible without your guidance and support. I am forever grateful for your inspiration, patience and trust. Your ardent enthusiasm for plant pathology is both infectious and stimulating and I will miss our weekly discussions, which have very much been a highlight, over the past four years.

I want to extend my gratitude also to the Fusarium group at Rothamsted Research who have been a constant source of encouragement and support. I would like to especially thank Erika Kroll, for being an incredible friend throughout this process as we progressed in tandem. In addition, to Dr Martin Darino, Dr Claire Kanja, Dr Rey Dharma and Dr Martin Urban – many of the experiments enclosed within this thesis would not have been possible without your expert knowledge and assistance, thank you. Also to Dr Navneet Kaur, Dr Wanxin Chen and Jade Smith, your company and discussions in weekly lab meetings I will always treasure. To the wider Wheat Pathogenomics Group, thank you for your support throughout this journey and contributions, which have shaped the direction of this project.

Thanks are also due to Kirstie Halsey, Dr Anjana Magaji-Umashankar and Hannah Walpole. I am very much indebted to you for your guidance, training and patience through my many, many questions in bioimaging. Thank you also to Max Fontaine for being a fantastic BSPP summer student and to Cian, Imogen, Pankhuri, Rovenia and Miles at Resurrect bio for hosting me for my 3 month internship.

Finally, this PhD would not have been possible without the support and encouragement of my friends and family. Mum, Dad, James and Robert, Arya, and my friends (you know who you are), thank you for being steadfast in your encouragement and presence. This thesis is dedicated to you.

Abstract

Fusarium graminearum is an ascomycete fungal pathogen that infects small grain cereals and leads to large reductions in yields due to reduced grain weights and contamination of developing grain with potent mycotoxins. Some of these are trichothecene mycotoxins, and are required for virulence when infecting wheat. Their potent toxicity to eukaryotic ribosomes dampens broad-spectrum protein translation and facilitates host-tissue colonisation by invasive hyphae. This thesis explores the intracellular role of deoxynivalenol (DON), one of the most prolific mycotoxins, and its role in wheat spikelet infection with respect to the crossing of wheat cell walls through plasmodesmatal pit fields.

Single gene deletion of an essential enzyme for the biosynthesis of trichothecene mycotoxins, $\Delta Tri5$, leads to restriction of infection to inoculated wheat spikelets by failing to prevent the deposition of callose, a β -1,3-glucan polymer, at plasmodesmata during biotic and abiotic stress to symplastically isolate cells. In the wild-type (WT) compatible interaction, invasive hyphae break through plasmodesmatal pit fields to facilitate host-tissue colonisation. This led to studies exploring PAMP-triggered immunity in the absence of DON in wheat floral tissues and the role of cell wall components as resistance or susceptibility factors to hyphal colonisation. On the other side of the interaction, studies contained within this thesis have identified a *Fusarium graminearum*-secreted Glycoside Hydrolase family 81 (GH81) enzyme that is predicted to hydrolyse callose deposited at plasmodesmatal pit fields during infection. Overall, this thesis both advances our understanding of the use of plasmodesmatal pit fields by *F. graminearum* during host-tissue colonisation in wheat spikes and opens new avenues for exploration.

Table of contents

Acknowledgements	2
Abstract.....	3
Table of contents.....	4
List of Figures and Tables	11
Chapter 1: Introduction	11
Chapter 2: General Materials and Methods	11
Chapter 3: The role of trichothecene mycotoxins in cell-to-cell invasion....	12
Chapter 4: Sequential inoculation of DON producing and DON non-producing <i>F. graminearum</i> isolates and the triggering of PTI-mediated defences	12
Chapter 5: Callose balancing at plasmodesmata.....	13
Chapter 6: The role of plant cell wall composition and fungal resistance...	14
Chapter 7: General Discussion	15
List of Appendices	16
List of Abbreviations	17
List of Units	21
Chapter 1: Introduction.....	23
1.1 Acknowledgments	23
1.2 Global food security.....	23
1.2.1 Wheat production.....	24
1.2.2 Globally important plant phytopathogens.....	27
1.2.3 Impact of fungal pathogens on food security	29
1.3 The plant immune system	30
1.3.1 PAMP-triggered immunity	33
1.3.2 Chitin reception by PRRs.....	34
1.3.3 Systemic Acquired Resistance (SAR).....	35
1.4 Plasmodesmata	36

1.4.1 PD structure and formation	36
1.4.2 Plasmodesmatal responses to pathogens	38
1.4.3 Fungal pathogens that use plasmodesmata	40
1.5 Fusarium Head Blight (FHB)	43
1.5.1 Causal agents of FHB.....	44
1.5.2 Genetic and population structure of <i>Fusarium graminearum</i>	45
1.5.3 Epidemiology of <i>F. graminearum</i>	49
1.5.4 Symptoms of FHB in small grain cereals	52
1.5.5 Mycotoxins.....	53
1.5.6 Virulence factors	57
1.5.7 Control strategies.....	58
1.6 PhD outline.....	60
1.6.1 Research questions	60
1.6.2 Hypotheses.....	60
1.6.3 Chapter overview	61
1.7 References.....	62
Chapter 2: General materials and methods.....	73
2.1 Acknowledgement of contributions.....	73
2.2 Media and chemicals	73
2.2.1 Plant growth media	73
2.2.2 Fungal growth media	73
2.2.3 Fungal strains	74
2.3 Molecular protocols	76
2.3.1 DNA extraction	76
2.3.3 cDNA synthesis.....	77
2.3.4 Polymerase Chain Reaction (PCR).....	77
2.3.5 Gel Electrophoresis.....	79
2.3.6 DNA quantification by qPCR	79

2.4 Bioassays.....	81
2.4.1 Fungal growth.....	81
2.4.2 Wheat growth.....	81
2.4.3 Arabidopsis growth.....	82
2.4.4 Wheat coleoptile inoculations	82
2.4.5 Wheat spike inoculations	83
2.4.6 Assessment of Disease Progression.....	83
2.4.7 Deoxynivalenol (DON) quantification	84
2.4.8 DNA quantification by quantitative real time PCR (qRT-PCR).....	84
2.5 Bioimaging	84
2.5.1 Photography	84
2.5.2 Sample fixation and resin embedding	85
2.5.3 Sectioning of resin samples for light microscopy	85
2.5.4 Immuno-labelling of callose deposits at plasmodesmata	85
2.6 Statistics.....	86
2.6.1 R scripts.....	86
2.7 References.....	86
Chapter 3: The role of trichothecene mycotoxins in cell-to-cell invasion	88
3.1 Acknowledgement of contributions.....	88
3.2 Introduction	88
3.3 Materials and Methods.....	94
3.3.1 Determination of DON concentration for exogenous application	94
3.3.2 Red Green Blue (RGB) colour classification for disease assessment of dissected spikelets.....	95
3.3.3 Light microscopy.....	95
3.3.4 Electron microscopy.....	95
3.3.5 Immuno-labelling of callose deposits at plasmodesmata for light microscopy.....	97

3.3.6 DON quantification.....	98
3.3.7 Expression of the <i>TRI5</i> gene during coleoptile infection	98
3.3.8 Phloroglucinol staining for presence of lignin	99
3.3.9 Formation of perithecia <i>in vitro</i>	99
3.3.10 Statistical analysis.....	99
3.4 Results	99
3.4.1 DON is toxic to plant tissue and is not required for the formation of perithecia <i>in vitro</i>	100
3.4.2 DON is not required for virulence on wheat coleoptiles and chemical complementation does not restore the WT disease phenotype on wheat spikes.....	101
3.4.3 The $\Delta Tri5$ mutant is inhibited in its ability to traverse plasmodesmata during host-tissue colonisation.....	106
3.4.4 TEM micrographs reveal pit fields in the plant cell wall at sites where secondary thickenings are absent	112
3.3.3 Immuno-labelling of callose during infection reveals reduced deposits in the WT infection and phloroglucinol staining indicates lignin-based defence response(s).....	114
3.5 Discussion	118
3.6 References	124
Chapter 4: Sequential inoculation of DON producing and DON non-producing <i>F. graminearum</i> isolates and the triggering of PTI-mediated defences	130
4.1 Acknowledgement of contributions.....	130
4.2 Introduction	130
4.3 Materials and Methods	131
4.3.1 Point inoculations.....	132
4.3.2 Spray inoculations.....	132
4.3.3 Co- and sequential inoculations.....	132
4.3.4 Disease assessment.....	133
4.3.5 Determination of $\Delta Tri5$ presence in wheat spike tissue.....	133

4.3.6 Callose deposition in rachis tissues	133
4.4 Results	134
4.4.1 Inoculation with DON-deficient $\Delta Tri5$ mutant prevents subsequent infection of WT <i>F. graminearum</i>	134
4.4.2 <i>In planta</i> growth of the <i>Fg</i> $\Delta Tri5$ mutant tracks behind PH-1.....	135
4.4.3 Application of the PTI-elicitor chitin prevents subsequent <i>F. graminearum</i> infections.....	138
4.4.4 Pre-inoculation treatments are not inducing resistance through tissue disturbance	140
4.4.5 Induced resistance is durable for 48 hours at a local scale.....	142
4.4.6 Induction of PTI defence mechanisms has local, but not systemic, durability	143
4.4.7 PTI elicitors trigger callose deposition in wheat rachis tissue	144
4.5 Discussion.....	151
4.6 References.....	159
Chapter 5: Callose balancing at plasmodesmata	164
5.1 Acknowledgement of contributions.....	164
5.2 Introduction	164
5.3 Methods	169
5.3.1 Identification of putative GH81 targets in <i>F. graminearum</i>	169
5.3.2 Structural prediction of putative GH81 target	169
5.3.3 Phylogenetic analysis of GH81 orthologues	170
5.3.2 Fragment amplification.....	170
5.3.3 Gibson Assembly	171
5.3.4 <i>E. coli</i> cloning.....	174
5.3.5 Preparation of bulk PCR fragments for fungal transformation.....	174
5.3.6 Fungal transformation	175
5.3.7 Transformant diagnostics.....	176
5.3.8 Generation of conidia for wheat inoculations	180

5.3.10 Phenotyping $\Delta GH81$ transformants <i>in vitro</i>	180
5.3.11 Plant inoculations	181
5.3.12 Disease assessment	181
5.3.12 DON quantification	181
5.4 Results	181
5.4.1 Identification of target GH81 gene	181
5.4.2 Structural prediction of FgGH81	183
5.4.2 GH81 target orthologues in <i>Fusarium</i> species complex	184
5.4.3. Fungal orthologues of FgGH81	187
5.4.5 PCR confirmation of GH81 transformants	189
5.4.6 <i>In vitro</i> phenotyping of $\Delta GH81$ growth	190
5.4.7 Wheat spike disease assessment of $\Delta GH81$	192
5.4.8 DON quantification	195
5.5 Discussion	195
5.5.1 Future experiments	199
5.6 References	200
Chapter 6: The role of plant cell wall composition and fungal resistance	203
6.1 Acknowledgement of contributions	203
6.2 Introduction	203
6.3 Materials and methods	209
6.3.1 Curation of cell wall mutants	209
6.3.2 SALK line T-DNA insertion model and genotyping	209
6.3.3 Arabidopsis thaliana detached leaf assay	211
6.3.4 Arabidopsis thaliana leaf disease assessment	211
6.3.5 Morphological assessment of wheat tissues throughout growth	212
6.3.6 Lignin staining and quantification in wheat tissue sections	212
6.3.7 RAMAN spectroscopy of rachis cell wall matrix	213
6.4 Results	215

6.4.1 Identification of wheat cell wall components postulated for susceptibility and/or resistance to <i>F. graminearum</i> infection	215
6.4.2 Identification of <i>Arabidopsis</i> orthologues and SALK lines	215
6.4.3 <i>Arabidopsis thaliana</i> detached leaf assay	217
6.4.5 Exploration of wheat stem and floral tissue morphology	219
6.4.7 BCARS-Raman spectroscopy for exploration of rachis cell wall matrix	230
6.5 Discussion.....	232
6.6 References.....	236
6.7 Appendix	241
6.7.1 Wheat cell wall orthologues for lignin targets.....	241
Chapter 7: General discussion	246
7.1 Summary of Key findings	246
7.2 Original hypotheses and research questions	247
7.3 Technological advancements	252
7.4 Challenges and future perspectives	255
7.5 Final conclusion and summary.....	256
7.6 References.....	257
Appendix 1	260
Appendix 2	261
Appendix 3	262

List of Figures and Tables

Chapter 1: Introduction

Fig. 1.2.1 The domestication of wheat from wild relatives

Fig. 1.2.2 Global wheat production

Table 1.2.1. Top 10 fungal pathogens in plant pathology

Table 1.2.2. Selected ascomycete fungal pathogens of wheat

Fig. 1.3.1. Adapted version of Jones and Dangl (2006) Zig-Zag model of proportional immune responses to pattern-triggered immunity (PTI) and effector triggered immunity (ETI)

Fig. 1.3.2. Simplified schematic of chitin-triggered immune signalling pathways

Fig. 1.4.1. PD ultrastructure

Table 1.4.1. Fungal pathogens reported to use plasmodesmata and/or pit fields during plant host infection

Fig. 1.4.2 Use of PD pit fields in wheat rachis tissue by *F. graminearum*

Fig. 1.5.1. Spore morphology and hyphal branching structure

Fig. 1.5.2 Phylogeny of the *Fusarium* genus with reference to genome size and host ranges

Fig. 1.5.3. Circos plot of the WT reference strain PH-1 of *F. graminearum*

Fig. 1.5.4. Typical lifecycle of *Fusarium graminearum* (teleomorph *Gibberella zeae*)

Fig. 1.5.5. Infection cushions (IC) and runner hyphae (RH) visible on the palea wheat spikelet tissue

Fig. 1.5.6 Biphasic infection pattern of *F. graminearum* in wheat spikes

Fig. 1.5.7. Symptoms of *F. graminearum* displaying the typical bleaching phenotype on several species of small grain cereals

Fig. 1.5.8. The type B epoxy-sesquiterpenoid trichothecene mycotoxin deoxynivalenol and *Fg* contamination of wheat grain

Fig. 1.5.9. Reports of mycotoxin production by *Fusarium* spp.

Chapter 2: General Materials and Methods

Table 2.2.1. Fungal growth media components

Table 2.3.1. Primers used throughout this study

Table 2.3.2. Buffer and media components

Chapter 3: The role of trichothecene mycotoxins in cell-to-cell invasion

Fig. 3.2.1. *TRI* gene expression is highest during the symptomless phase of infection.

Fig. 3.2.2. The trichothecene mycotoxin biosynthetic cluster.

Table 3.2.1. Function and mutant phenotypes of *TRI* genes in *Fusarium sporotrichioides*.

Fig. 3.2.3. Simplified model of the DON biosynthetic pathway.

Fig. 3.3.1. Example methodology for the quantification of immunofluorescence detection of callose in sectioned floral tissues.

Fig. 3.4.1. Demonstration of DON toxicity on plant material.

Figure 3.4.2. *F. graminearum* disease formation on wheat coleoptiles.

Figure 3.4.3. Analysis of whole wheat floral tissues following point inoculations.

Fig. 3.4.4 Fungal burden at 5- and 7-days post inoculation on spikelets

Figure 3.4.5. Quantitative spikelet analysis for disease symptom development

Figure 3.4.6. WT-infected wheat floral tissues at 5 and 7 dpi demonstrating aspects of typical infection

Figure 3.4.7. Comparison of $\Delta Tri5$ -infected and $\Delta Tri5$ + DON infected wheat floral tissues at 5dpi and 7dpi showing the similarities and differences between tissue types in various aspects of a typical infection

Fig. 3.4.8. Cell wall thickness of adaxial cell layer in resin samples.

Fig. 3.4.9. SEM micrographs of PH-1 and $\Delta Tri5$ - wheat floral interactions.

Fig. 3.4.10. Stained TEM micrographs of PH-1 infected lemma tissues at 5dpi demonstrating pit fields at breaks in the secondary cell wall.

Fig. 3.4.11. TEM micrographs with callose gold immunolabelled at pit fields in lemma tissues at 5dpi.

Fig. 3.4.12. Immunofluorescence detection of callose in rachis and lemma tissues.

Fig. 3.4.13. Immunofluorescence detection of callose in sectioned floral tissues.

Fig. 3.4.15. Phloroglucinol staining of fresh infected spikelets.

Chapter 4: Sequential inoculation of DON producing and DON non-producing *F. graminearum* isolates and the triggering of PTI-mediated defences

Fig. 4.4.1. Pre-treatment of spikelets with the DON-deficient *Fg* strain $\Delta Tri5$ prevents subsequent WT-infection

Fig. 4.4.2 $\Delta Tri5$ tracking behind WT *F. graminearum* in wheat spikes.

Fig. 4.4.3. Pre-treatment of spikelets with the PAMP elicitor chitin and mycotoxin DON prevents subsequent WT-infection

Fig. 4.4.4. Disease progression of water and chitin pre-treated wheat spikes with subsequent *Fg* inoculation 24 hrs later.

Fig. 4.4.5. Disease progression with elicitation of defences at 24hrs pre-inoculation and 48hrs pre-inoculation.

Fig. 4.4.6. Exemplar images of disease at 10dpi from spray co-inoculations

Fig. 4.4.7. Immunolabelling of callose at 24hrs post inoculation in wheat rachis tissue

Fig. 4.4.8. 3D render of immunolabelled callose deposits at 24hrs post inoculation with PH-1 in wheat rachis tissue

Fig. 4.4.9. Immunolabelling of callose at 48hrs post inoculation in wheat rachis tissue

Fig. 4.4.10. Immunolabelling of callose deposits in resin-embedded rachis sections taken at 24 and 48hrs post inoculation.

Fig. 4.4.11. Tissue specific responses of callose in lemma and rachis tissues at 5dpi.

Fig. 4.5.1. Schematic diagram of induced resistance in wheat spikes by chitin, DON and $\Delta Tri5$.

Table 4.5.1. Summary of sequential inoculation experimental challenges and future perspectives

Chapter 5: Callose balancing at plasmodesmata

Fig. 5.2.1 Structural differences between the glucose polymers callose and cellulose.

Fig. 5.2.2. Callose responses to plant microbe interactions.

Fig. 5.2.3. Schematic diagram of fungal cell wall composition

Table 5.3.1. Primers used for Gibson Assembly

Fig. 5.3.1 Schematic diagram of pGEM-T Easy vector used for split-marker fragment ligation

Fig. 5.3.2 Schematic diagram of Gibson Assembly.

Table 5.3.2. Primers used for sequencing and diagnostics of $\Delta FgGH81$

Table 5.3.3 Media preparations for fungal transformation.

Table 5.4.1. Expression of FgGH81 (FGRAMPH1_01G10749).

Fig. 5.4.2. Schematic diagram of rachis internode samples from point of infection used for RNASeq analysis

Fig. 5.4.3. AlphaFold 3 (DeepMind) structural predictions of FGRAMPH1_01G10749 (FgGH81).

Table 5.4.2 Sequence identity of orthologues in top 6 *Fusarium* species

Fig. 5.4.4 Phylogenetic tree of FgGH81 orthologues in *Fusarium* species.

Fig. 5.4.5. Alignment of top 6 *Fusarium* species orthologues.

Fig. 5.4.6. Phylogenetic tree across the fungal kingdom of FgGH81 orthologues.

Fig. 5.4.7. Transformant diagnostics by PCR.

Fig. 5.4.8. Spore morphology.

Fig. 5.4.9. Stress test plates of WT and $\Delta GH81$ transformants.

Fig. 5.4.10. Production of perithecia *in vitro*.

Fig. 5.4.11. Wheat spike disease assessment for $\Delta GH81$ *in planta* phenotype.

Chapter 6: The role of plant cell wall composition and fungal resistance

Fig. 6.2.1. Example diagram of the plant cell wall matrix.

Table 6.2.1 Plant cell wall (CW) components, relative enzyme classes for degradation and number of CWDEs present in *F. graminearum* (Fg) genome.

Fig. 6.2.2. Lignin biosynthesis pathway.

Fig. 6.3.1 Schematic representation of SALK line verification for T-DNA insertion.

Table 6.3.1. Primers used for genotyping *A. thaliana* SALK lines.

Fig. 6.3.2. Demonstration of image analysis for relative lignification in wheat tissues stained with potassium permanganate

Fig. 6.3.3. Schematic diagram of BCARS imaging system.

Table 6.4.1. *Arabidopsis thaliana* genotypes used in the initial detached leaf assay study.

Fig 6.4.1. Exemplary rosettes for *Arabidopsis thaliana* mutants at 4 weeks old.

Fig. 6.4.2. Example images of *Arabidopsis thaliana* detached leaf assay mutants.

Fig. 6.4.3. Apogee wheat growth.

Fig. 6.4.4. WT-Fg infection two weeks after anthesis infection window.

Fig. 6.4.5. Transverse sections of rachis internodes of wheat cv. 'Apogee' stained with TB showing morphology through growth at 6, 7 and 12 weeks.

Fig. 6.4.6. Longitudinal sections of rachis nodes stained with TB showing morphology through growth at 6, 7 and 12 weeks (left to right).

Fig. 6.4.7. Serial longitudinal sections of rachis nodes and internodes stained with Toluidine Blue at week 7 of growth.

Fig. 6.4.8. Selected sections from outer edge to centre of rachis, stained with Toluidine Blue.

Fig. 6.4.9. Longitudinal rachis sections stained with potassium permanganate for lignin visualisation.

Fig. 6.4.10. Percentage of high lignification in wheat tissues at different growth stages.

Fig. 6.4.11. Example images of potassium permanganate-stained 1 μ m thick sections.

Fig. 6.4.12. BCARS-Raman spectroscopy.

Fig. 6.4.13. Cellulose microfibrils in wheat rachis tissue.

Chapter 7: General Discussion

Fig. 7.1.1 Working model for cell wall traversing through plasmodesmatal pit fields in wheat rachis tissue by *Fusarium graminearum*.

Fig. 7.2.1 The DON hypothesis.

List of Appendices

Publications

- Appendix 1 Armer VJ, Kroll E, Darino M, Smith DP, Urban M, Hammond-Kosack KE, (2024). Navigating the *Fusarium* Species Complex: Host-Range Plasticity, Niche Diversification and Genome Variations. *Fungal Biology*. **In Press**. doi: 10.1016/j.funbio.2024.07.004.
- Appendix 2 Armer VJ, Urban M, Ashfield T, Deeks MJ, Hammond-Kosack KE. (2024). The trichothecene mycotoxin deoxynivalenol facilitates cell-to-cell invasion during wheat-tissue colonisation by *Fusarium graminearum*. *Molecular Plant Pathology*. **25**(6): e13485. doi: 10.1111/mpp.13485
- Appendix 3 Armer VJ, Deeks MJ, Hammond-Kosack KE. (2024). *Arabidopsis thaliana* detached leaf assay for the disease assessment of *Fusarium graminearum*. *Protocols.io*. doi: 10.17504/protocols.io.261gedmwov47/v1.

List of Abbreviations

ANOVA	Analysis of variance
Avr	Avirulence
BF	Brightfield
BLAST	Basic Local Alignment Tool
CalS	Callose synthase
CTAB	Cetyltrimethylammonium bromide
CRISPR	Clustered regularly interspaced short palindromic repeats
cv	Cultivar
CWDE	Cell wall degrading enzyme
dH ₂ O	Deionized water
DNA	Deoxyribonucleic acid
DON	Deoxynivalenol
EDTA	Ethylenediamine tetra-acetic acid
ELISA	Enzyme linked immunosorbent assay
EMBL	European molecular biology laboratory
EMS	Ethyl methanesulfonate
ER	Endoplasmic reticulum
ETI	Effector triggered immunity
FAO	Food and Agriculture Organisation
f. sp.	<i>formae speciales</i>
FHB	<i>Fusarium</i> Head Blight

FKM	Fragments per kilobase million
FP	Fluorescent protein
FRET	Förster resonance energy transfer
GFP	Green fluorescent protein
GH	Glycoside hydrolase
GM	Genetic modification
HR	Hypersensitive response
H ₂ O ₂	Hydrogen peroxide
HYG	Hygromycin cassette
KCl	Potassium Chloride
KO	Knock out
LN ₂	Liquid nitrogen
MAPK	Mitogen activated protein kinase
MS	Murashige and Skoog
NaCl	Sodium Chloride
NCBI	National Centre for Biotechnology Information
NEB	New England Biosciences
NIV	Nivalenol
PAMP	Pathogen associated molecular pattern
PBS	Phosphate Buffered Saline
PCR	Polymerase chain reaction
PD	Plasmodesmata

PDA	Potato dextrose agar
PDCB	Plasmodesmata callose-binding protein
PDLP	Plasmodesmata-located protein
PEG	Polyethylene glycol
PI	Propidium Iodide
PM	Plasma membrane
PRR	Pathogen recognition receptor
PTI	Pathogen triggered immunity
qPCR	Quantitative polymerase chain reaction
R	Resistance gene
RI	Rachis internode
RFP	Red fluorescent protein
RNA	Ribonucleic acid
ROS	Reactive oxygen species
RT	Room temperature
SA	Salicylic acid
SAR	Systemic acquired resistance
SC	Species complex
SEM	Scanning electron microscopy
SNA	Single nutrient Agar
TBE	Tris-Borate-EDTA
TE	Tris-EDTA

TEM	Transmission Electron Microscopy
TMD	Transmembrane domain
TMV	Tobacco mosaic virus
UK	United Kingdom
UN	United Nations
USA	United States of America
UV	Ultraviolet
VIGS	Virus-induced gene silencing
VOX	Virus mediated overexpression
WHO	World Health Organisation
WT	Wild type
YPD	Yeast peptone dextrose
ZEA	Zearalenone

List of Units

bp	Base pairs
cm	Centimetre
dpi	Days post inoculation
°C	Degrees Celsius
€	Euro
g	Gram
h	Hour
kb	Kilobase
kDa	Kilo Dalton
kg	Kilogram
T_m	Melting temperature
μg	Microgram
μl	Microlitre
μm	Micrometre
μM	Micromole
ml	Millilitre
mm	Millimetres
mM	Millimole
min	Minutes
M	Mole

nm	Nanometres
%	Percent
s	Seconds
Tpm	Transcripts per million
V	Volts

Chapter 1: Introduction

1.1 Acknowledgments

Aspects of this chapter contributed to a review article, entitled 'Navigating the *Fusarium* species complex: Host-Range Plasticity and Genome Variations', published in *Fungal Biology* (Armer et al., 2024a). For contribution to this publication I thank Erika Kroll, Martin Darino, Martin Urban, Dan Smith and Kim Hammond-Kosack.

1.2 Global food security

The challenge of achieving food security, defined in the 1996 World Food Summit as '*when all people, at all times, have physical and economic access to sufficient safe and nutritious food that meets their dietary needs and food preferences for an active and healthy life*', is still pertinent in the modern age (World Bank, 2024). This definition is further broken down into four dimensions which must all be fulfilled for food security to be achieved, and are briefly: Physical availability of food, economic and physical access, food utilisation, and the stability of the three dimensions.

Almost 30 years on, we are yet to achieve food security, and the challenges towards doing so are multifaceted. According to the World Food Programme's Global Report on Food Crises (GRFC) 2024, which analyses regions across the globe that are at high risk or, or currently undergoing food insecurity, 21.5 % (281.6 million people) of the global population face high levels of acute food insecurity. Drivers of this are cited to be conflict, cyclic weather extremes (El Niño-caused flooding and/or drought) and economic shocks. Yet the remainder of the world's large food producing regions are also grappling with crises. Deteriorating soil health (Bagnall et al., 2021), unpredictable weather patterns caused by climate change disrupting harvest predictability, increased demand for meat products requiring grain feed or soy-based feed (GRFC, 2024), and increasing costs of raw materials such as pesticides, fertilisers and fuel all applying pressure to food production systems (AHDB, 2024). Acute drivers of food insecurity in 2024 include repercussions from the COVID-19 pandemic, war in Ukraine, the middle

East and Africa, and environmental impacts on harvest yields (GRFC, 2024). In addition, there is a desperate need to balance food production and the negative impact it has on the environment, which ultimately supports sustainability of productive agriculture for future generations.

1.2.1 Wheat production

Wheat is a major staple crop in temperate regions across globe, accounting for 18% of global calories and 19% of protein (Erenstein et al., 2022) and in many regions is an important source of plant-based iron, B vitamins and dietary fibre (Shewry and Hey, 2015). Modern demand for wheat stems from its ability to produce many products associated with western diets, due to the gluten protein fraction, such as bread, pasta and other baked goods (Shewry and Hey, 2015). Now grown globally, the cereal crop originated from the south-eastern region of Turkey, in a region known as 'fertile crescent' (Peng, Sun and Nevo, 2011) and was domesticated over 10,000 years ago as part of the 'Neolithic Revolution' from hunter-gatherer to settled civilisations (Shewry, 2009). Modern hexaploid (AABBDD) wheat formed from the hybridisation of 3 progenitor cereal species: *Triticum uratu* (AA) and *Aegilops speltoides* (BB) hybridized to form *Triticum turgidum* (AABB) and *T. tauschii* (also known as *Ae. tauschii*) (DD) donated the third and final genome to hexaploid wheat via *T. spelta* (AABBDD), as demonstrated in Fig. 1.2.1 (Shewry, 2009). Hybridization events probably occurred several times, with favourable properties, such as free-threshing ability of grain created through mutations in the *brittle rachis* locus (Nalam et al., 2006), selected for by growers over millennia, with the polyploid nature of wheat generating genetic diversity on relatively fast scales (Dubcovsky and Dvorak, 2007).

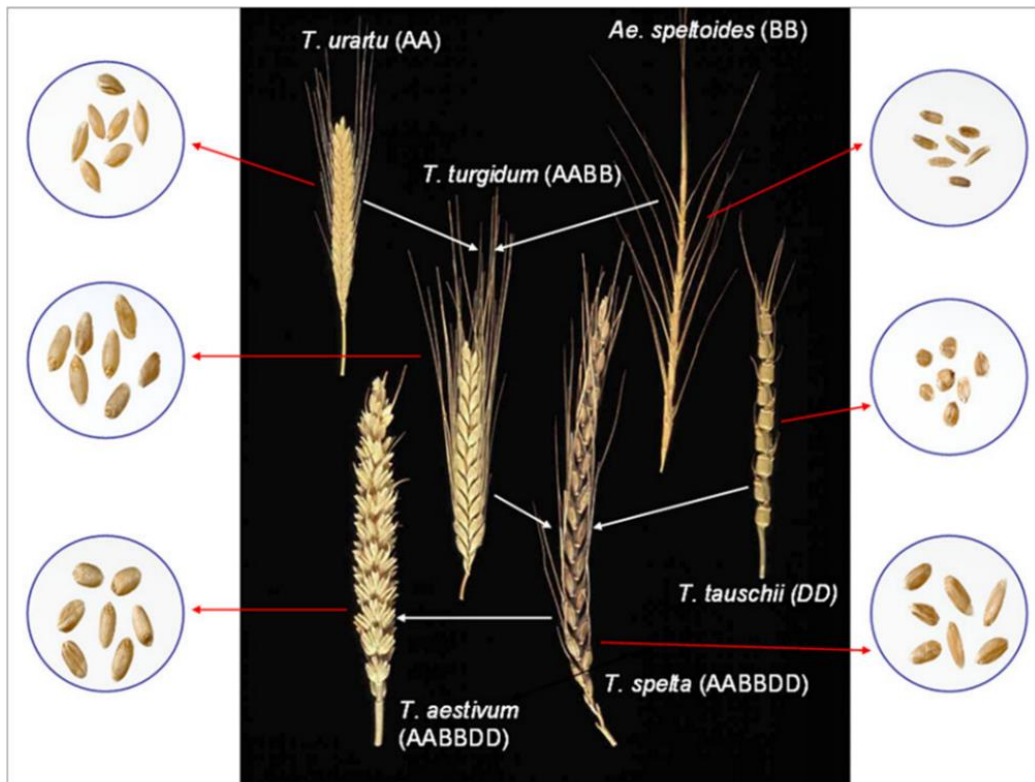


Fig. 1.2.1 The domestication of wheat from wild relatives. *Triticum urartu* (AA) hybridized with *Aegilops speltoides* (BB) to form *Triticum turgidum* (AABB). Further hybridisation with *T. tauschii* (DD) formed *T. spelta* (AABBDD) which was selectively bred to modern wheat *T. aestivum* (AABBDD). Taken from Shewry (2009).

In the 1950s and 60s, driven by efforts of American agronomist Norman Borlaug, wheat was selectively dwarfed, by identification of dwarfing genes *Rht1* and *Rht2*, increasing yields with simultaneous application of synthetic fertilisers and pesticides (Hedden, 2003). However, this also reduced genetic diversity among modern wheat varieties, limiting the ability to breed in useful genetic components that confer resistance to pests and pathogens and environmental perturbations. The recently published Watkins collection of wheat landraces collected in the 1920s and 30s (Cheng et al., 2024) has the potential to be a source of ‘novel’ resistance into modern wheat varieties to improve yields (Wingen et al., 2014). As demand for wheat grain increases with human population pressures and coinciding pathogen evolution, the drive for resistant, high yielding wheat that can be cultivated with minimal environmental impact remains.

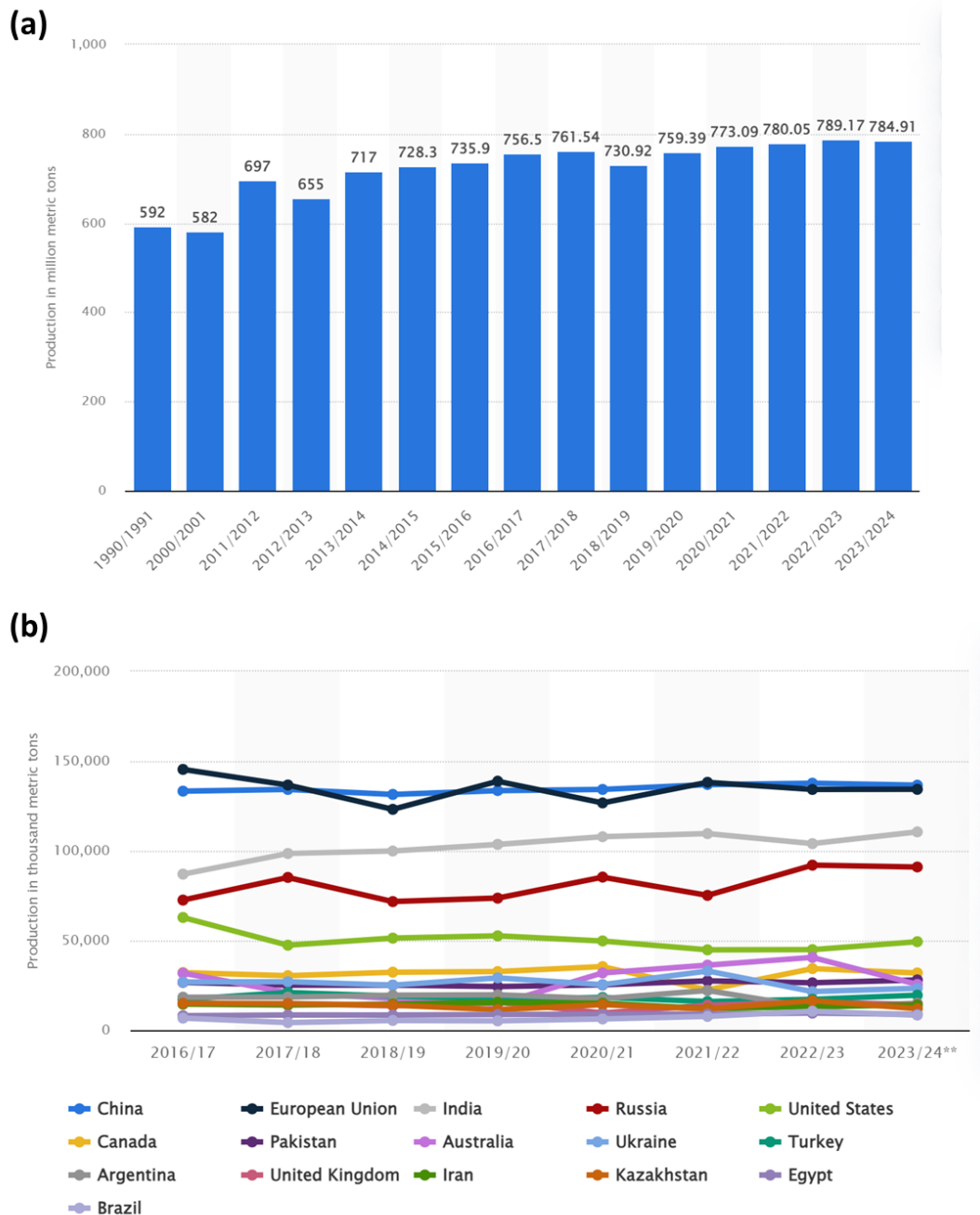


Fig. 1.2.2 Global wheat production. (a) Global wheat production from 1990/1991 to 2023/2024 (in million metric tons)* and (b) Leading wheat producers worldwide from 2016/2017 to 2023/2024 (in 1,000 metric tons). Taken from Statista (2024).

The United Nations (UN) predicts that the human population is expected to rise by 2 billion to 9.7 billion between 2020 and 2050 (UN, 2017). Wheat is an ideal candidate for meeting increased food requirement, with year-round growth in spring and winter varieties, and for its ability to be grown across temperate regions of the globe. However, global wheat production is currently stagnating around 780 million metric tonnes per year (Fig. 1.2.2(a); Statista, 2024) with top producers being China and the European Union, followed by India, Russia and

the United States (Fig. 1.2.2(b); Statista, 2024). Meeting this demand will require a doubling in global crop yields, and are currently not increasing at a rate fast enough to achieve this projected requirement (Ray et al., 2013).

However, one aspect that continues to impact yields, accounting for an average 20-40% loss of harvests, is the impact of pests and pathogens (Flood, 2010). These can include insects, bacterial, fungal and viral diseases, and affect all crops worldwide. Whilst regional challenges differ, it is imperative that the challenge of achieving food security is met by identifying control mechanisms, either genetic or chemical, to reduce crop losses.

1.2.2 Globally important plant phytopathogens

Pests and pathogens account for yield losses of between 20-40% across all crops. In wheat, the global average estimate is around 20% (Savary et al., 2019), of which a portion is attributed to fungal pathogens. In 2010, the scientific research field of plant pathology was surveyed for their analysis of the most important fungal pathogens affecting food security (Table 1.2.1, Dean et al., 2012).

Table 1.2.1. Top 10 fungal pathogens in plant pathology (adapted from Dean et al., 2012).

Pathogen	Disease	Crops affected
<i>Magnaporthe oryzae</i>	Rice and wheat blast	Rice and wheat
<i>Botrytis cinerea</i>	Grey mould	Typically soft fruits, more than 200 plant species
<i>Puccinia f. sp. tritici</i>	Wheat rust: stem (black) rust, stripe (yellow) rust and leaf (brown) rust	Wheat
<i>Fusarium graminearum</i>	Fusarium Head Blight (FHB)	Wheat and other small grain cereals
<i>Fusarium oxysporum</i>	Vascular wilts	Vast host ranges caused by f sp. strains.
<i>Blumeria graminis</i>	Powdery mildew	Vast host ranges, including wheat and barley
<i>Mycosphaerella graminicola</i> / <i>Zymoseptoria tritici</i>	Septoria tritici Blotch (STB)	Wheat
<i>Colletotrichum</i> spp.	Black/ leaf spot	Very wide host range / all crops

<i>Ustilago maydis</i>	Corn smut	Corn/ maize. Although not globally devastating is important for molecular plant pathology research.
<i>Melampsora lini</i>	Flax rust	Flax and linseed. Again, not globally devastating to food security but an important model for studying plant immunity.

Fungal pathogens are often highly adapted to their hosts and have honed infection mechanisms to be reliable and effective. While not an exhaustive list, this section aims to highlight various infection mechanisms of ascomycete fungal pathogens on the wheat host. Comparative analyses between the pathogens discussed can aid understanding of host and tissue specific immunity, and factors of infection that are maintained between them are essential for virulence in this major staple crop.

Fungal pathogens differ in their lifestyles and thus require different infection strategies. These are broadly classed as biotrophic, hemi-biotrophic and necrotrophic. Biotrophic fungal phytopathogens, such as *Blumeria graminis* and *Ustilago maydis*, require living plant tissue to colonise (Fei and Liu, 2022). Evading the plant immune system in these instances is essential. Sitting between the biotrophic and necrotrophic lifestyles, hemi-biotrophic pathogens are so-called for an initial symptomless, or latent, phase which causes minimal damage to host tissues and also must evade plant immunity (McCombe et al., 2022). This is followed by a 'switch' to necrotrophic growth that causes substantial damage and allows for release of nutrients to the colonising fungus. Examples of hemi-biotrophic pathogens include *F. graminearum* and *Magnaporthe oryzae*. On the other hand, necrotrophic pathogens such as *Botrytis cinerea*, have destructive colonisation strategies, attacking the host cells and often causing immediate cell death (apoptosis).

Fungal phytopathogens can also attack different host tissues. In wheat, *F. graminearum* typically infects the floral organs (spikelets) of cereals. However, the causative agents of wheat blast and Septoria tritici blotch (STB), *Magnaporthe oryzae* f. sp. *tritici* and *Zymoseptoria tritici* respectively, both infect leaves, with *F. graminearum* and *Z. tritici* estimated to cause some of the most extensive losses

to wheat crops globally of all phytopathogens surveyed by Savary et al. (2019). Underground, *Gaeumannomyces graminis* causes Take-All disease of roots (Table 1.2.2). Different plant host tissues pose different challenges to ascomycete fungal pathogens.

Table 1.2.2. Selected ascomycete fungal pathogens of wheat. Pathogens infect different wheat tissues and cause different symptoms on wheat.

Pathogen	Disease	Tissue
<i>Fusarium graminearum</i>	Fusarium Head Blight (FHB)	Spike/ floral
<i>Magnaporthe oryzae</i> f. sp. <i>tritici</i>	Wheat blast	Foliar
<i>Zymoseptoria tritici</i>	Septoria tritici blotch (STB)	Foliar
<i>Gaeumannomyces graminis</i>	Take-all disease	Roots

Fusarium spp., not just those that have host-range restriction to cereals, have global impacts on food security. All of the top staple and commodity crops are to some extent infected by *Fusarium* spp. such as cereals, tree fruits, coffee and members of the *Solanaceae* family such as tomatoes (Armer et al., 2024a). These include the devastating *F. odoratissimum* (known until recently as *F. oxysporum* f. sp. *cubense* pv. Tropical Race 4), the causal agent of Panama disease (Maryani et al., 2019), is devastating banana production worldwide, particularly the Cavendish variety which accounts for 99% of banana exports (Dita et al., 2018).

1.2.3 Impact of fungal pathogens on food security

At the time of writing (Summer 2024), global average temperatures are likely to surpass the 1.5°C warming limit set in the 2015 Paris Climate Agreement (Betts et al., 2023). With temperature-dependent risk of many fungal and oomycete phytopathogens increasing in high latitudes such as Europe (Chaloner, Gurr and Bebbler, 2021), this increase may increase crop losses to fungal pathogens. Most importantly, however, an increasingly globalised world is leading to the introduction of novel pathogens into crop populations with little genetic resistance. This likely occurred in *Magnaporthe oryzae* f. sp. *tritici* isolates

identified in Bangladesh which had high homology with isolates first identified in South America (Islam et al., 2016). The first reports of wheat blast (*Magnaporthe oryzae* f. sp. *tritici*) have also emerged in recent years from Zambia, Africa (Tembo et al., 2020).

In wheat, dense monocultures are highly conducive to the epidemic spread of pests and pathogens (Fones et al., 2020). In wheat, the foliar ascomycete fungal pathogen *Zymoseptoria tritici* is particularly damaging in the UK, costing €240 million annually to UK farmers (Fones and Gurr, 2015) and is attributed to 70% of EU fungicide use (Torriani et al., 2015).

One of the largest issues of *F. graminearum* infection is not just yield losses, but contamination of the grain with potent mycotoxins that are incredibly harmful to human and livestock health (Kanja et al., 2021; Johns et al., 2022; [1.5.5](#)). In global harvests, it is estimated that 60-80% are contaminated with mycotoxins to some extent, with *Fusarium* spp., *Aspergillus* spp. and the *Penicillium* spp. of highest concern (Eskola et al., 2019). Understanding how fungal pathogens cause disease in crops can aid our efforts to preventing physical yield losses and contamination of harvests with mycotoxins.

1.3 The plant immune system

The plant immune system can be broadly divided into two branches, or layers, according to way in which the response is triggered (reviewed: Dodds and Rathjen, 2010). Pattern triggered immunity (PTI) represents the first layer of the immune system, detecting generic components of biotic (pathogen) and abiotic (damage). The biotic elicitation of PTI involves the detection of Pathogen Associated Molecular Patterns (PAMPs) and the abiotic through Damage Associated Molecular Patterns (DAMPs) (Boller and Felix, 2009). PAMPs include cell wall and structural components of pathogens, such as the polysaccharide polymer chitin in the case of fungi and flagellin proteins in the case of bacteria. DAMPs are endogenous plant molecules, sometimes referred to as 'danger molecules' that are released in response to stress or physical cellular damage (Boller and Felix, 2009). Examples of DAMPs include proteins present in the cytosol, amino acids, fragments of cell wall oligosaccharides, peptides and nucleotides that are released from damaged cells through abiotic damage or

biotic attack (Hou et al., 2019). Like PAMPs, DAMPs trigger early processes of PTI such as the rapid generation and release of reactive oxygen species (ROS), activation of mitogen-activated protein kinases (MAPKs) and the upregulation of defence-related genes through the Pattern Recognition Receptor (PRR) system (Macho and Zipfel, 2014). Under non-stress conditions, these molecules do not trigger PTI, but changes in sub-cellular distribution or concentration in response to stress and/or damage are detected and initiate downstream signalling responses (Torres, Jones and Dangl, 2006; Camejo, Guzmán-Cedeño and Moreno, 2016). PAMPs and DAMPs are typically actioned by the immune system through PRRs, with all known plant PRRs localising to the plant cell surface plasma membrane, unlike mammalian PRRs which are also found on intracellular compartment membranes (Macho and Zipfel, 2014). However, a leucine-rich receptor present in the apoplast has recently been shown to respond to the ROS species H_2O_2 in *Arabidopsis* (Wu et al., 2020), indicating that ROS-mediated PTI may have other avenues for activation of immunity.

The second layer of the plant immune system is Effector Triggered Immunity (ETI). Effectors, small, secreted proteins produced by pathogens, are recognised by intracellular nucleotide-binding domain leucine-rich repeat receptors, known as NLRs, that trigger downstream signalling cascades in response to direct recognition of specific effectors. Effectors aim to facilitate infection, through processes such as masking pathogen presence, targeting physical *in planta* barriers, interfering with normal plant cell functioning and targeting components of plant immunity (Zhang et al., 2022). NLRs are located intracellularly and detect effectors, some of which recruit helper NLRs to activate downstream signalling processes (Chen et al., 2022). This response is typically stronger and more specific towards the invading pathogen than PTI responses (Jones and Dangl, 2006).

Jones and Dangl (2006) proposed the 'zig-zag' model, whereby the amplitude of the defence response increases between PTI to ETI layers of plant immunity (Fig. 1.3.1). The model describes how PAMPs are first detected by PRRs and initiate PTI, beyond the threshold for resistance. When effectors are secreted by the invading pathogen, these are detected by NLRs in the plant and subsequently activate ETI, beyond the threshold required for activation of the hypersensitive response (HR). The HR is a powerful defence response that often involves NLR-

mediated localised cell death restricted to the locality of the pathogen infection (Dallo et al., 2020).

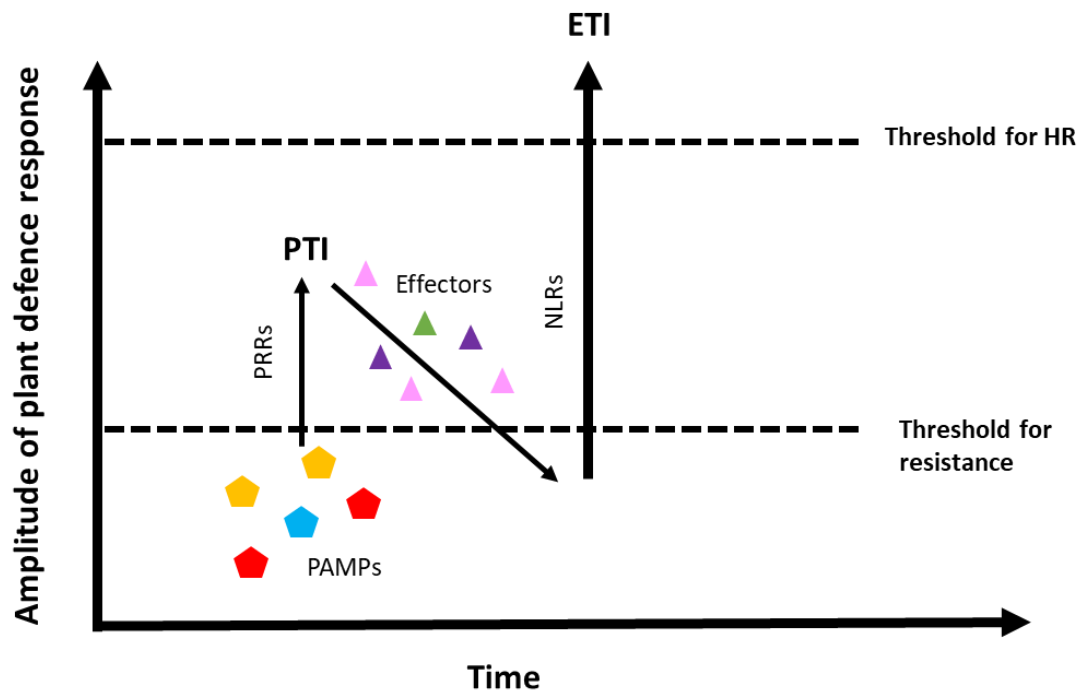


Fig. 1.3.1. Adapted version of Jones and Dangl (2006) Zig-Zag model of proportional immune responses to Pattern Triggered Immunity (PTI) and Effector Triggered Immunity (ETI). Detection of an invading pathogen is first triggered by the recognition of Pathogen associated molecular patterns (PAMPs) on plant cell membranes (pentagons), which triggers generic host defence responses of moderate amplitude and is known as pattern triggered immunity (PTI). Subsequently, effectors (triangles) secreted by the pathogen are recognised by NLRs within plant cells which trigger the second layer of the immune system, effector triggered immunity (ETI). This activates a stronger, specific response to the invading pathogen that surpasses the threshold for the hypersensitive response (HR). Pathogens overcome ETI recognition by gaining novel effectors either through mutation, horizontal gene transfer or sexual recombination that can evade the plant immune system until natural selection favours plants that contain NLRs alleles that are able to recognise the novel effectors and trigger ETI responses. (Figure adapted from the original in Jones and Dangl, 2006).

Plant immunity, by recognition of effectors, is broken when novel effectors are produced by the invading pathogen, either gained through mutation (to evade NLR recognition), horizontal gene transfer and sexual recombination. Pathogens which have multiple sexual recombination cycles within the cropping season often break genetic resistances faster. Therefore, most researchers consider that multiple sources of resistance need to be deployed to reduce the resistance gene selection pressure, otherwise a one single *NLR* gene may rapidly be 'broken'. For

example, populations of the wheat stem rust fungal pathogen *Puccinia graminis* f. sp. *tritici*, although requiring the alternate host common barberry to complete its lifecycle, have high genetic diversity when sampled in regions where the alternate host coincides in locality (Patpour et al., 2022). Populations with higher genetic diversity have greater opportunity to break genetic resistance in wheat hosts. This begins the 'arms race' between effector recognition by the host and selection for NLRs that are able to recognise different pathogen effectors.

Successful host immune responses must be tightly controlled with regards to timing, amplitude of the defence response and duration. Deviations from these optimal factors can have negative implications for plant growth, reproduction and subsequent elicitation of defence responses. Overstimulation of PAMP-triggered immunity can lead to autoimmunity, a phenomenon which causes detrimental disadvantages to the plant, exhibited through phenotypes such as stunted growth, uncontrolled cell death, reduced reproductive fitness and on leaves, chlorosis (yellow discolouration) and necrosis (cell death) (reviewed: Freh et al., 2022).

1.3.1 PAMP-triggered immunity

PAMPs are small molecular motifs that are present in microbes, but not hosts and are detected by PRRs. PAMPs can be formed from various types of molecules, for example, polysaccharides such as chitin, which is a component of fungal cell walls, proteins such as flagellin, present in bacteria, but can also be DNA and RNA species, surface glycoproteins and lipoproteins and other membrane components. The reception of PAMPs by PRRs leads to the activation of PTI (Boller and Felix, 2009). All currently identified PRRs in plants are receptor kinases, which often complex with receptor-like kinases (RLKs) that are able to relay signals, due to the lack of an intracellular domain in PRRs which present extracellularly (Jamieson, Shan and He, 2018). PRRs detect PAMPs and initiate a variety of signalling pathways as part of the PTI layer of the plant immune system. Upon triggering by PAMPs, such as flagellin (flg22) and elongation factor Tu (elf18 and 26), PRRs located in the cell surface membrane lead to the activation of BOTRYTIS-INDUCED KINASE 1 (BIK1), through direct phosphorylation of the C-terminus of the NADPH protein (Lee et al., 2020). This increases the affinity for binding with RBOH proteins, which becomes

phosphorylated by the activated BIK1 PRR and releases reactive oxygen species (Kadota, Shirasu and Zipfel, 2015).

Rapid ROS bursts are typical of PAMP-triggered immune responses and the different ROS molecules (i.e., hydrogen peroxide, H₂O₂ and superoxide O₂⁻) are major regulatory molecules in plants and stress signaling (Mittler et al., 2022). In plant-pathogen interactions, ROS bursts have a direct antimicrobial effect, but are also signalling molecules over both local and systemic scales, activating alternative antimicrobial defences (Waszczak, Carmody and Kangasjärvi, 2018). ROS bursts in plant-pathogen interactions rely on the action of respiratory burst oxidase homolog (RBOH) family proteins, which includes the NADPH proteins (Kadota, Shirasu and Zipfel, 2015). Pathogen interactions in *Arabidopsis thaliana* rely on the action of the RESPIRATORY BURST OXIDASE HOMOLOG PROTEIN D (RBOHD), a membrane-localised NADPH oxidase protein with six transmembrane helices (Lee et al., 2020), of which the promoter is highly receptive to PAMP mediated signalling (Morales et al., 2016).

1.3.2 Chitin reception by PRRs

Chitin perception is known to occur through separate and independent pathways. CHITIN ELICITOR RECEPTOR-LIKE KINASE 1 (CERK1) is a LysM receptor-like kinase that perceives chitin and is essential for chitin reception: in the model plant species *A. thaliana*, a loss of function of CERK1 leads to the lack of MAPK activation, no ROS burst and no upregulation of defence gene expression (Miya et al., 2007). Chitin is also perceived by plants through the LYSIN MOTIF DOMAIN-CONTAINING GLYCOSYLPHOSPHATIDYLINOSITOL-ANCHORED PROTEIN 2 (LYM2), a CEBiP, which was first identified in the model plant species *Arabidopsis thaliana* (Mita et al., 2007). Although LYM2, and other CEBiP homologues in other species, interact with CERK1 to coordinate chitin perception, the two receptors have been shown to be independently controlled and that chitin perception differs between species (Shina et al., 2012).

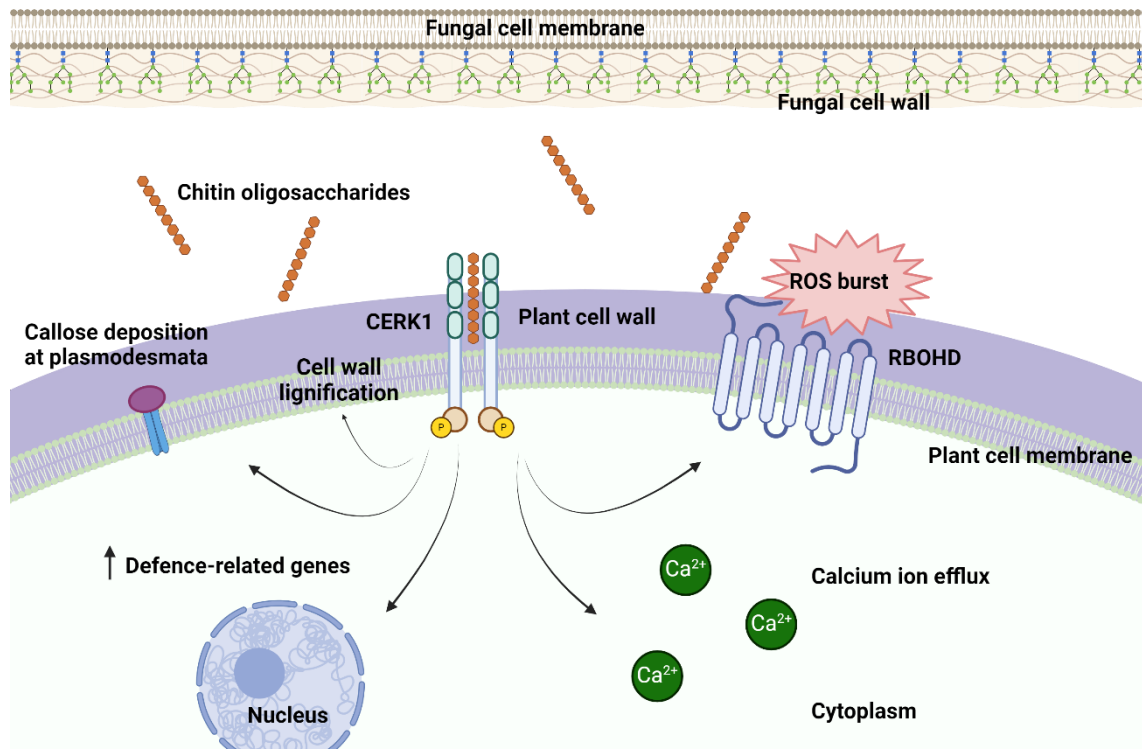


Fig. 1.3.2. Simplified schematic of chitin-triggered immune signalling pathways. Chitin fragments are shed/released by fungal cell walls and are recognised by PRRs on the plant cell membrane, including the LysM-receptor kinase CERK1. This triggers downstream signalling pathway, including MAPK activation, which leads to defence responses such as the generation of reactive oxygen species (ROS bursts), upregulation of defence-related genes, deposition of the β -1,3-glucan polymer callose at plasmodesmata/ pit fields, cell wall lignification and calcium ion efflux.

1.3.3 Systemic Acquired Resistance (SAR)

Induction of broad-spectrum immune responses across the systemic scale is known as Systemic Acquired Resistance (SAR) and forms part of the PTI layer of plant immunity (Fu and Dong, 2013). SAR can be induced by the reception of avirulent pathogens through the PTI layer of plant immunity.

Within the wider *Fusarium* species phylogeny SAR has been studied between virulent and avirulent strains of the *F. oxysporum* species complex (FOSC) on various plant hosts, which is largely conferred by the composition of lineage specific (LS) chromosomes (reviewed: Armer et al., 2024a). For example, for infection of tomato (*Solanum lycopersicum* L.) the *F. oxysporum* f. sp. *lycopersici* must have the presence of a specific LS (Ma et al., 2010). Further studies in this area have determined that the presence of Secreted In Xylem (SIX) effectors on

LS chromosomes, which are secreted during early root colonisation, determine the degree of virulence to host plants, but interestingly the deletion of SIX effectors from non-pathogenic *F. oxysporum* isolates diminished their ability to endophytically colonise plant roots (Redkar et al., 2022), indicating a further conserved role for these effectors beyond colonisation of vasculature.

Fungal endophytes of different species have been shown to confer resistance to closely related pathogenic species, such as the wheat root pathogen *Gaeumannomyces tritici*, causal agent of Take-all disease. A study by Chancellor et al. (2024) identified how local lignification in the host cell wall in response to interaction with the closely related *G. hyphodiodes* root endophyte and wheat roots can be a potential source of resistance against subsequent *G. tritici* infection. Further studies into biological control of pathogenic fungi through inoculation of hosts plants with avirulent pathogens could be an effective control measure, but analyses of yield penalties in this instance must be considered.

1.4 Plasmodesmata

Plasmodesmata (PD) are cytoplasmic communication channels that symplastically connect adjacent cells within plant tissues. Acting as molecular signaling highways, they are essential for the normal growth and development of plants, allowing for the movement of signaling molecules such as ions, sugars and small proteins between cells. They often colocalise together into what are known as pit fields. PD also play integral roles in the plant's response to biotic and abiotic stressors, with adjustable permeability by the deposition of a carbohydrate polymer, callose, which occludes the pore for the movement of signaling molecules, including those that are detrimental to plant health such as effectors, toxins and CWDEs (Tee and Faulkner, 2024).

1.4.1 PD structure and formation

Plasmodesmata are composed of an appressed endoplasmic reticulum (ER), known as a desmotubule, within a plasma membrane (PM) continuum stabilised by proteins connected to both the ER and PM (Sager and Lee, 2018). Spokes of endoplasmic reticulum connected to the surrounding cell wall stabilise the desmotubule structure (Fig. 1.5.1). Plasmodesmata (sing. Plasmodesma) can be

primary or secondary, based on their time of formation. Primary PD are formed during cell plate formation, in a process known as cytokinesis (Sager and Lee, 2018). As the cell plate forms, the plasma membrane remains intact between the two daughter cells, preventing complete isolation, and leading to the formation of PD. Distribution of primary PD within new cell walls are random (Faulkner et al., 2008). Secondary PD form often during cell expansion (Burch-Smith et al., 2011). Whilst the formation mechanisms of primary plasmodesmata have long been accepted to be at cytokinesis, the determinants of secondary plasmodesmata initiation and positioning have yet to be elucidated.

A group of plasmodesmata-associated proteins (PDLPs) have been identified that have both structural integrity roles throughout the lumen of the desmotubule portal, but many also have roles in conducting signaling events. Mutants of the PDLP family of proteins typically increase molecular flux/ PD permeability to signaling molecules (Thomas et al., 2008), indicating that they gate movement. Proteins associated with plasmodesmata have been identified through the generation of a proteome in the model plant species *Arabidopsis thaliana* (Fernandez-Calvino et al., 2011).

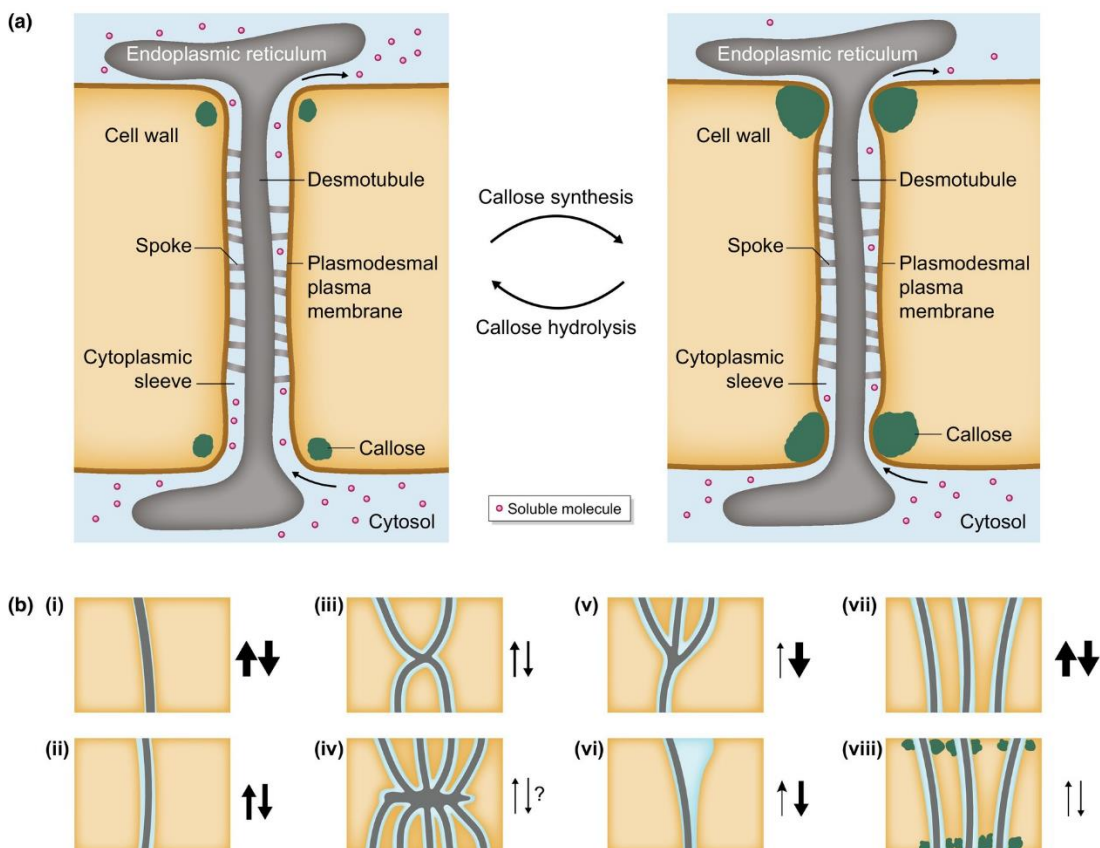


Fig. 1.4.1. PD ultrastructure. (a) PD are composed of an appressed endoplasmic reticulum (ER), also known as a desmotubule, which is held in place by ER spokes. The ER is surrounded by a cytoplasmic sleeve, through which signalling molecules can pass and is known as the lumen. PD permeability can be adjusted by the deposition of callose at the neck of PD (green) to prevent molecule movement between adjacent cells. (b) Structure of PD varies, with the size of the ER and branching determining directional flux of molecules. From Tee and Faulkner (2024).

PD also vary in their size and form (Fig. 1.4.1). Simple PD are characterised by a single opening and desmotubule strand and are common in younger tissues. In specialised tissues branched structures are more common, which can have several openings and branch as they span the cell wall, sometimes also with central cavities (Fig. 1.4.1 (b)). The shape and direction of branching within the cell wall span determines the flux potential and directionality (Nicolas *et al.*, 2017). In simple PD, the flux of molecules is larger than branched PD, possibly indicating that these are net-recipients of compounds from more mature tissues in the plant (Nicolas *et al.*, 2017). This supports early findings by Oparka (1999), who found that sink organs contain over 90% simple plasmodesmata, in contrast to just 20% in photosynthesising leaf cells. Conversely, this indicates that structurally more complicated forms of plasmodesmata in mature tissues is associated with increased control of molecule transport. Some plasmodesmata have been noted to have no evidence of the cytoplasmic sleeve, namely in the columella cells of *Arabidopsis thaliana* roots, which appear to be correlated with higher molecular traffic (Nicolas *et al.*, 2017). In size, PD are typically around 50nm in width but can be up to 5µm in sieve plate elements where the endoplasmic reticulum/desmotubule structure is no longer present and thus indicates no control of molecule transport (reviewed: Peters *et al.*, 2021).

In healthy tissues, plasmodesmata are important facets of cell signaling. In the phloem, products from photosynthesis move from the chloroplasts, primarily in the mesophyll layers of leaves, through PD and are transported to sink organs such as developing fruit, where PD again are implicated in the unloading of sugar from the column (Paniagua, 2021). Equally, during plant growth and development, hormones such as auxin, synthesised in the apical meristem, are transported across plants tissues in a passive, concentration-dependent manner through plasmodesmata (Band, 2021).

1.4.2 Plasmodesmatal responses to pathogens

PD have vital roles in protecting plant tissues from biotic and abiotic stress by transducing stress signaling molecules. In response to light stress induced ROS release, plasmodesmatal pore size has been shown to increase by the action of two PDLPs (PDLP1 and PDLP5), ultimately increasing molecular flux between cells (Fichman et al., 2021). Another PD-localised protein NOVEL CYS-RICH RECEPTOR KINASE (NCRK) is implicated in ROS-mediated plasmodesmal closure through callose deposition (Vu et al., 2023). The difference between the ROS signals that increase or decrease the molecular flux in these respective manners has not been fully explored.

In response to stress, plants can adjust the permeability to signaling molecules of PD by depositing a β -1,3-glucan polymer called callose at the 'neck' of plasmodesmata (Fig 1.4.1 (a)), thereby symplastically isolating a damaged cell from its healthy neighbours and limiting systemic damage (Sager, 2018). Through PD occlusion with callose, pathogen-excreted molecules such as effectors, toxins and enzymes are restricted to infected cells and thus limit damage. Callose deposition is post-transcriptionally controlled through the competitive action of callose synthases (CaLS) and β -1,3-glucanases which degrade callose to open PD channels (Tilsner et al., 2016).

Chitin reception, as previously discussed, is an essential part of Pattern Triggered Immunity (PTI). Research into plasmodesmatal-specific responses to chitin is still in its infancy, and whilst the broad-spectrum PTI response of callose accumulation at plasmodesmata is well established (Cheval and Faulkner, 2017), more recent research is elucidating potentially unique pathways of chitin perception to PD. Cheval et al. (2020) found that plasmodesmata possess their own chitin perception machinery that leads to stomatal closure, demonstrating 'microdomain specificity' and that the cytoplasmic communication channels can act independently. Interestingly, activation of LYM2 is also implicated in molecular flux through plasmodesmata, but this is independent of CERK1 (Faulkner et al., 2013), which indicates that LYM2 chitin perception may be involved in the deposition of callose at plasmodesmata. However, activation of RBOHD functions in both LYM2 and CERK1 mediated chitin perception, by different phosphorylation signatures (Cheval et al., 2020). How and why chitin-induced plasmodesmatal closure is independent is not yet known and still under speculation (Tee and Faulkner, 2024).

1.4.3 Fungal pathogens that use plasmodesmata

In recent years a number of plasmodesmata-targeting effectors and molecules have been identified as virulence factors for the successful infection of numerous fungi in plant-pathogen interactions and a number of other fungal species physically use PD pit fields as portals for advancing infection (Table 1.4.1).

Table 1.4.1. Fungal pathogens reported to use plasmodesmata and/or pit fields during plant host infection.

Species	Host species	PD use	Source
<i>Fusarium graminearum</i>	Wheat	Physical	Brown et al. (2010)
<i>Magnaporthe oryzae</i>	Rice	Physical	Kankanala, Czymmek and Valent (2007)
<i>Fusarium oxysporum</i>	Various	Effectors – SIX5/ Avr2 pair increase molecular flux through PD	Cao et al. (2018)
<i>Ustilago maydis</i>	Maize	Effectors – cmu1 passes through PD to repress Salicylic acid production to prime cells for infection	Djamei et al. (2011)
<i>Colletotrichum acutatum</i>	Pepper	Physical	Liao et al. (2011)
<i>Colletotrichum higginsianum</i>	Various, including brassicas	Physical and effectors	Ohtsu et al. (2024)

Several filamentous ascomycete fungal pathogens are reported to routinely use plasmodesmata pit fields as physical structures to squeeze through to advance their infection of the host plant tissue. These are the rice blast fungus *Magnaporthe oryzae* (Kankanala, Czymmek and Valent, 2007), *Colletotrichum* spp. (Liao et al., 2011; Ohtsu et al., 2024) and the Fusarium Head Blight (FH) causal agent *Fusarium graminearum* (Fig. 1.4.1; Brown et al., 2010). How fungi identify where plasmodesmata are is currently unknown, but the localisation of excreted effectors could act as crossing markers (Tee and Faulkner, 2024).

The physical constriction of fungal hyphae through pit fields in the host plant cell wall requires the co-ordination of several components. This transition is controlled by an apical body known as the Spitzenkörper (SPK) and is composed of a collection of vesicles and polarity-related proteins, cytoskeleton components such as actin, and ribosomes, assembled in such a way that controls polarised growth of filamentous fungal hyphae at the elongating tip (Steinberg, 2007). Tip elongation by fungal hyphae requires large membrane insertions and extension of the chitin cell wall which is curated by a steady stream of cell wall synthesising enzymes and component material deposited by vesicles at the growth site. The SPK acts as a marker for this deposition (Steinberg, 2007). During constriction, polarisation of the membrane needs to be maintained while growing under physical pressure. In the rice blast fungus *Magnaporthe oryzae* the structure used to facilitate cell-to-cell invasion has been named the transpressorium, picking up on prior reports half a century ago and is regulated by the Pmk1 MAP kinase pathway (Cruz-Mireles *et al.*, 2021). Single gene deletion knock out of the *F. graminearum* homologue *MAP1* leads to completely attenuated virulence *in planta* (Urban *et al.*, 2003) but a specific link to the ability to cross cell walls through pit fields has not yet been established.

Different fungal species manage cell wall integrity during hyphal tip elongation with varying success. Fukuda *et al.* (2021) investigated the ability of several fungal pathogens to maintain polarity post-constriction, studying also their respective growth rates. *F. oxysporum*, a prolific vascular pathogen of many plant species, never failed to retain cell wall integrity after constriction, but in the faster growing bread mould species *Neurospora crassa*, the hyphal tip depolarised after contraction, indicating a trade-off between plasticity and velocity of mycelial growth (Fukuda *et al.*, 2021). More recently, Cho *et al.* (2023) reported a link between fungal lifestyle and ability to constrict through plasmodesmatal-sized pit fields in a microfluidic (2 μm) and a nitrocellulose-based system (0.3 μm), finding that hemibiotrophs such as *F. graminearum* and *M. oryzae*, and saprotrophs such as *Aspergillus* spp. can pass through a grid of 0.3 μm , whereas necrotrophic pathogens such as *Botrytis cinerea* typically don't. However, the limits of hyphal constriction was shown to be limited to between 0.22 and 0.3 μm in *M. oryzae* (Cho *et al.*, 2023).

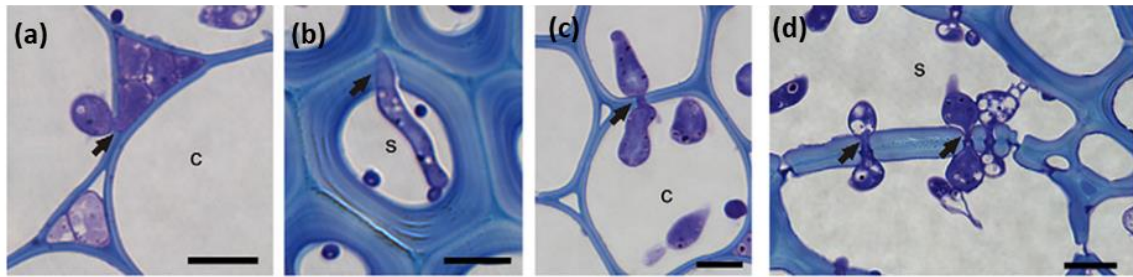


Fig. 1.4.2 Use of PD pit fields in wheat rachis tissue by *F. graminearum*. (a) Hyphal growth breaking into a cell from the apoplast, (b) Crossing as lignified cell wall, through a pit field, (c-d) Crossing cell walls through pit fields to accelerate host-tissue colonisation. Scale bar = 10µm. From Brown et al. (2010).

Research into how filamentous fungi navigate through constrained environments is still in its infancy but is accelerating due to the application of PDMS-based microfluidic platforms to fungal research. The collision with obstacles such as cell walls involves rearrangement of the Spitzenkörper and associated microtubules, often utilising the ‘shortest’ path and branching, whereby a subsequent SPK appears in the daughter cell and a second polarised hyphal tip is generated (Held et al., 2019). However, in natural environments, the navigation and directionality of fungal polar growth may rely on external cues such as chemical gradients from nutrient sources such as developing wheat grain or phloem vascular elements in the case of *F. graminearum*.

Fungal effectors are known to directly, or indirectly, suppress the deposition of callose triggered by PAMPs (Iswanto *et al.*, 2022). In the ascomycete fungal pathogen *F. graminearum*, an effector known as FGL1 (for FUSARIUM GRAMINEARUM LIPASE 1) is known to inhibit callose deposition, with no evidence of disruption to callose biosynthesis, in sieve elements in the phloem of wheat. This aspect of infection is integral for the movement of *F. graminearum* from the infected rachis to the remaining wheat spike.

Fusarium oxysporum, a vascular wilt pathogen of many plant hosts, secretes an effector known as Avr2 that interrupts major immunity-related pathways of salicylic acid (SA), Ethylene (ET) and Jasmonic acid (JA) in tomato (Di, Gomila and Takken, 2017). Arv2 (synonym SIX3) is known to interact with another effector called SIX5 (for SECRETED IN XYLEM 5), forming a heterodimer that localises to plasmodesmata in the model species *Nicotiana bethamiana* (Cao, 2018). SIX5 has been shown to increase the size exclusion limit of PD to between

53 and 80kDa and does not do so through alteration of callose homeostasis (Blekemolen et al., 2022). This modulates the plasmodesmata conductance (gating), through as yet unknown mechanisms, allowing larger molecules to traffic through that facilitate infection, such as effectors and toxins.

Several rust pathogens have also been identified as having interactions with plasmodesmata. In wheat, *Puccinia striiformis* f. sp. *tritici*, the causal agent of yellow rust, secretes an effector known as Pst_12806, which was demonstrated by Xu et al. (2019) to reduce callose deposition, as well as repress defence related genes, as part of a broad-spectrum dampening of PAMP-induced host defence responses. Further to this, effectors Pst4 and 5 from the same pathogen have been shown to dampen host responses, including callose accumulation, by inhibiting chloroplast protein rearrangement and importation during infection (Wang et al., 2021). In poplar trees, the rust pathogen *Melampsora larici-populina* secretes the effector Mlp37347 that interacts with GAD1 (for GLUTAMATE DECARBOXYLASE 1), an enzyme involved in the conversion of glutamate to GABA, a long-distance signaling molecule integral to stress responses, that accumulates at plasmodesmata to increase conductance and reduce callose deposition (Rahman et al., 2021).

Other fungal effectors that essentially dampen the PTI response, including ROS accumulation and callose deposition include Fs00367 from *Fusarium sacchari* (Huang et al., 2024) and CHORISMATE MUTASE 1 (Cmu1) from *Ustilago maydis* (Djamei et al. 2011), which is used for metabolic priming of adjacent cells for infection.

1.5 Fusarium Head Blight (FHB)

Fusarium Head Blight/ Scab (FHB) is a globally devastating fungal disease of small grain cereals, which includes wheat, oats and barley. It is caused by members of the *Fusarium* genus, which resides in the Ascomycota. Globally, FHB is present epidemically, with large outbreaks occurring annually in some regions, such as the USA, with climate change expected to increase the frequency and severity of occurrences (Vaughan et al., 2016). FHB leads to yield losses through direct reduction in grain weight and quantity, and through the contamination of grain with mycotoxins that are hazardous to human and livestock health (Kanja

et al., 2021; Johns et al., 2022). *F. graminearum* infection of grain also leads to the excretion of hydrophobin proteins, which cause the undesirable 'gushing' or 'foaming' in the distilling and fermenting industries (Sarlin et al., 2012).

Infection of cereals by causal agents of FHB occurs at anthesis (flowering) during wet weather. Spores germinate on the outer surfaces of the glumes and runner hyphae enter the wheat spike between the lemma and palea tissues, those that protect the developing grain, of wheat spikelets. Subsequently, a symptomless phase of infection is initiated which is characterised by apoplastic growth, prior to a switch where macroscopic disease symptoms become apparent (Brown et al. 2010). The destructive nature of *F. graminearum* has led to extensive research aiming to understand the infection biology of this filamentous ascomycete fungal pathogen, yet many fundamental aspects remain unknown and unexplored. The following sections detail known aspects of FHB epidemiology, infection and control.

1.5.1 Causal agents of FHB

A number of species within the *Fusarium sambucinum* species complex (FSAMSC) cause Fusarium Head Blight on small grain cereals. These include the ubiquitous *F. graminearum* (teleomorph *Gibberella zeae*), and *F. culmorum*, but *F. pseudograminearum*, *F. poae*, and *F. avenaceum* (colder regions) are also able to cause the disease with varying success in different geographic regions (Moonjely et al., 2023). One member of the FSAMSC, *F. venenatum* was until recently considered a saprotroph and unable to cause FHB, although on genome comparison was found to contain the Type A trichothecene gene cluster enabling the biosynthesis of trichothecene mycotoxins (King et al., 2018). It was recently reported that *F. venenatum* can in fact cause foot and root rot in wheat (*Triticum aestivum*) in Germany and may be an important pathogen in the region (Rigorth, Finckh and Šišić, 2021). First isolated from soil, it is this species that was selected for the production of the fungal-based meat alternative Quorn® (Trinci, 1992).

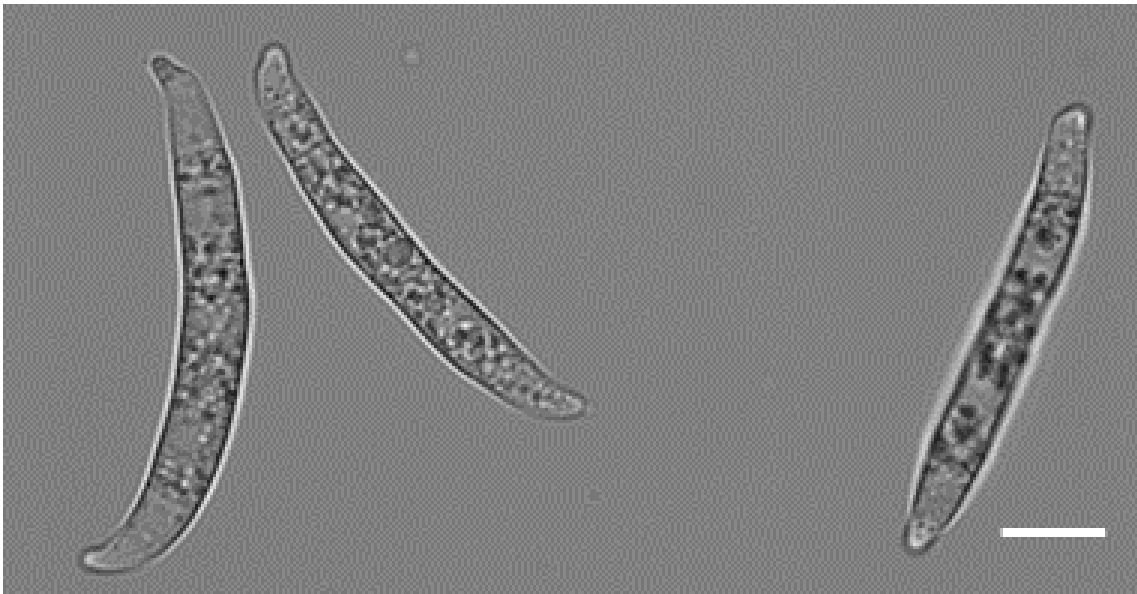


Fig. 1.5.1. Spore morphology. (a) *F. graminearum* spore morphology, which have 4-7 septa and typical 'banana' shape, scale bar = 10 μ m. Provided by Erika Kroll, Rothamsted Research, for Armer et al., 2024a.

1.5.2 Genetic and population structure of *Fusarium graminearum*

Due to its importance as a global fungal pathogen of wheat, *F. graminearum* was the third filamentous fungus to be sequenced, using Sanger sequencing, with the first genome release in 2003 by the BROAD institute (www.broad.mit.edu/annotation/genome/fusarium_group/MultiHome.html).

Subsequent genome sequences filled in some of the gaps (Cuomo et al., 2007), revealing very few repetitive sequences in this species but high levels of SNPs near telomeres. The isolate chosen for sequencing, PH-1, was isolated from Michigan, in the mid-West USA, and was selected for its ability to produce trichothecene mycotoxins and zearaleone, its economic importance in the region, ability to be cultured in the lab and sporulate *in vitro* and its high fertility (Trail and Common, 2000). This isolate is now considered the global reference strain. Now in its 5th iteration (King et al., 2015), the first fully assembled and well annotated reference genome is publicly available on ensembl (https://fungi.ensembl.org/Fusarium_graminearum/Info/Annotation/). Advances in sequencing technologies have allowed for continuous improvements to our knowledge of the species and the genetic drivers of its pathogenicity.

Most recently, it has been sequenced with the Oxford Nanopore technology MinION (Hao et al., 2021). The relative ease, affordability and portability of this

sequencing technology opens opportunity for sequencing field isolates, tracking populations and identifying genetic recombination hotspots and develops scope for extensive pangenome analyses. In addition, wider understanding of the *Fusarium* genus has been advanced by chromosome karyotyping using the germ tube burst method (Waalwijk et al., 2018). This can further lead to evolutionary insights into *F. graminearum* and closely related species.

Fusarium graminearum has 4 chromosomes, with no known lineage specific (LS) chromosomes (Armer et al., 2024a). Evolutionarily the youngest species in the *Fusaria*, the compaction of genomes was reported early in sequencing efforts of the genus (Cuomo et al., 2007; Ma et al., 2010; Lu et al., 2022). The *Fusarium sambucinum* species complex (FSAMSC), within which *F. graminearum* resides, remains the smallest of all the species complexes (Fig. 1.5.2). During sequencing efforts of the WT reference strain PH-1, ancient chromosome fusion events are postulated to have occurred, with probable regions identified (Cuomo et al., 2007; King et al., 2015), possibly indicating how genome compaction occurred.

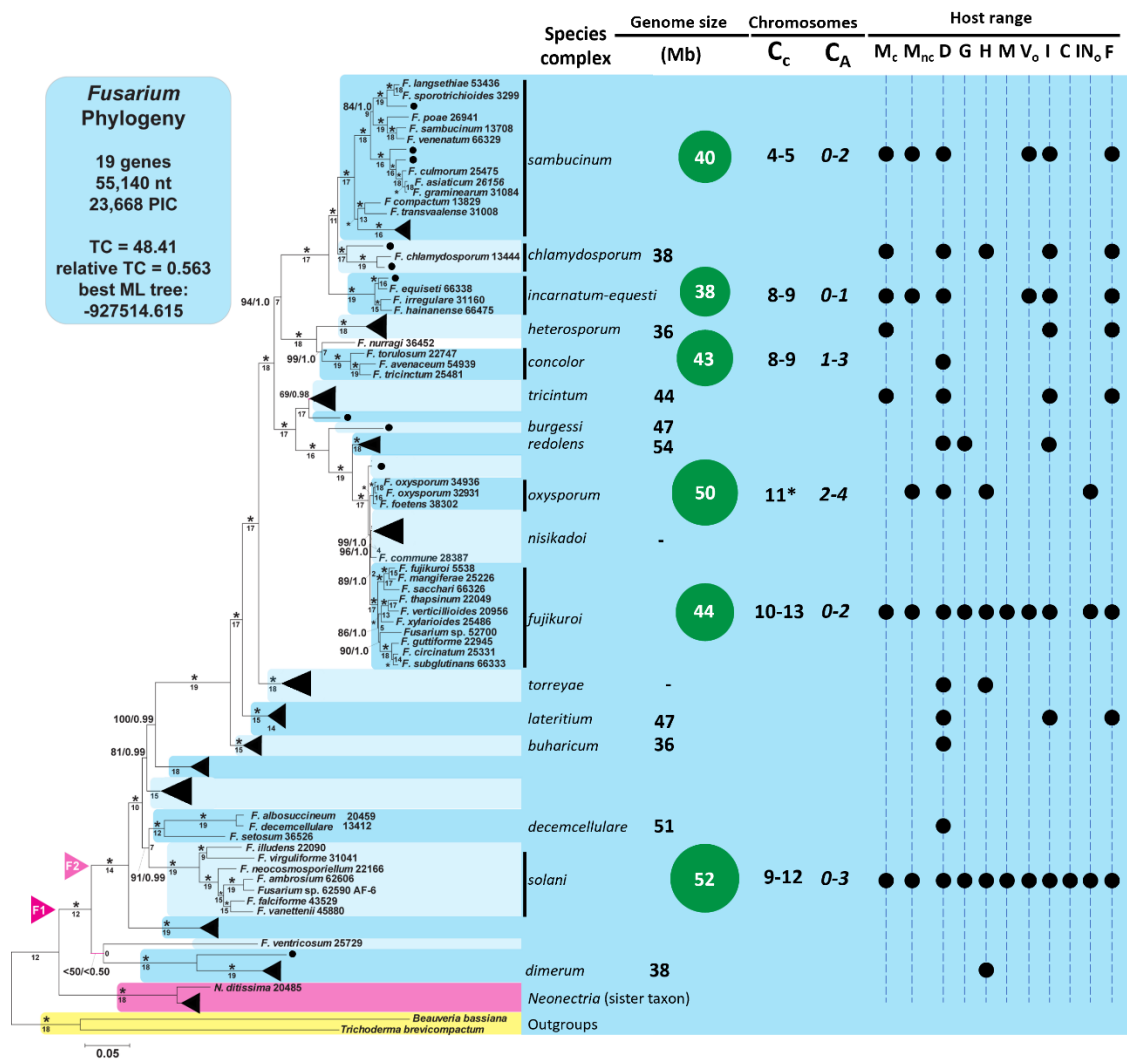


Fig. 1.5.2 Phylogeny of the *Fusarium* genus with reference to genome size and host ranges. Genomes that have complete, chromosome scale assemblies are highlighted with green circles and genome size is expressed as an average of publicly available ungapped genomes. The known number of Core (C_c) and Accessory (C_A) / Lineage Specific (LS) chromosomes are indicated, followed by the current known host ranges of each *Fusarium* species complex. Host range abbreviations are as follows: Monocot cereals (M_c), Other monocots (M_{nc}), Dicots (D), Gymnosperm (G), Human (H), Mammals (M), Other vertebrates (V_o), Insects (I), Crustacea (C), Other invertebrates (IN_o), and Fungi (F). A detailed list of sources for host ranges can be found in Appendix A.1 of Armer et al., 2024a. Figure is taken from Armer et al. (2024a) and is adapted from Geiser et al. (2021).

Most isolates of *F. graminearum* are homothallic, that being able to reproduce asexually, but can often outcross to other isolates in laboratory studies. How often this occurs in the field is currently unclear, but regional analyses in Germany determined a large quantity of sexual recombination that is not evenly distributed across chromosomes, indicating sexual recombination hotspots (Talas and McDonald, 2015). Similarly, a population analysis of *F. graminearum* isolates in

North America assembled the first pangenome, identified genetic differences across the population scale that may contribute to pathogen diversity. Kelly and Ward (2018) reported 13 distinct genomic regions with frequent sexual recombination, including divergence at the trichothecene biosynthetic cluster (see [chapter 3](#) for further reading). The identification of areas of the genome with high genetic diversity, versus those which are more conserved, has led to the postulation of the ‘two speed genome’, with regions of high recombination causing high genetic diversity leading to the rapid evolution of virulence genes essential for pathogenicity (Dong et al., 2015).

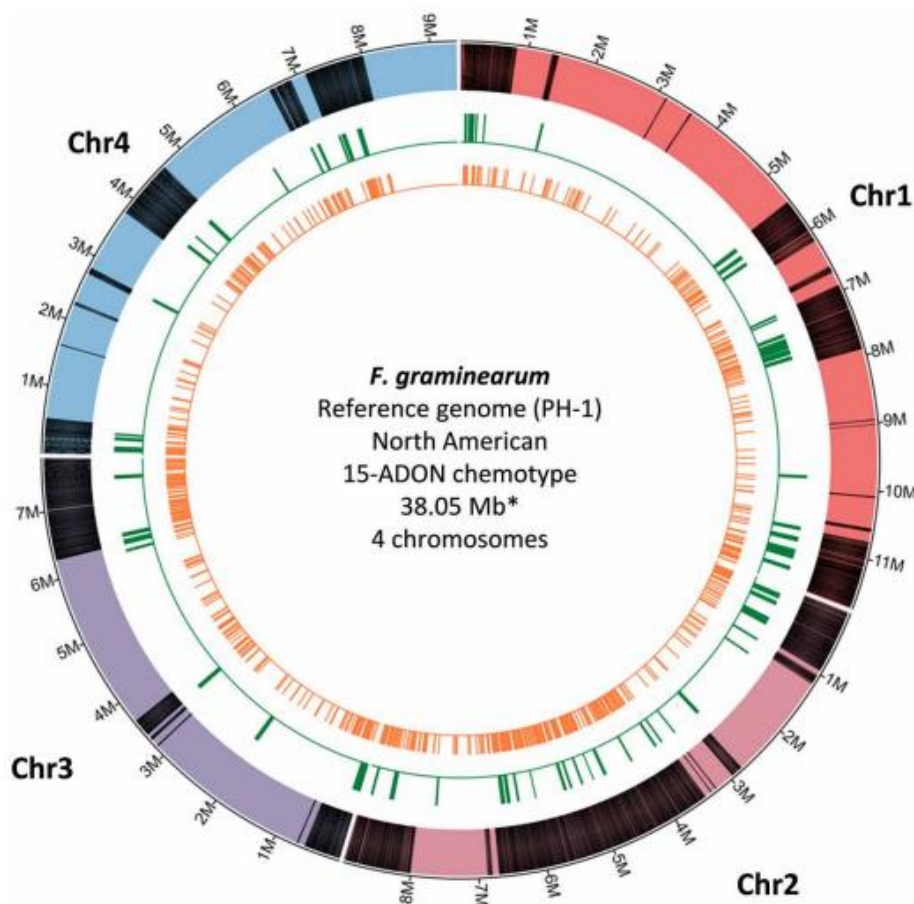


Fig. 1.5.3. Circos plot of the WT reference strain PH-1 of *F. graminearum*. Composed of 4 chromosomes, the genome is approximately 38Mb in size. Black lines highlight regions of high genetic diversity, green lines secondary metabolite clusters and orange lines genes predicted to encode secreted proteins. Chromosome 1 is highlighted in red, chromosome 2 in pink, chromosome 3 in purple and chromosome 4 in blue. Taken from Kanja et al., 2021.

Many of the *Fg* isolates in North America are of the 15-ADON chemotype, meaning that they exclusively synthesise the 15-ADON acetylated variant of the trichothecene mycotoxin deoxynivalenol (DON), a virulence factor in wheat

(Proctor et al., 1995). This is also the variant of the global reference strain PH-1 (NRRL 31084; Trail and Common, 2000). Despite dominance of 15-ADON producing isolates of *F. graminearum*, a population subdivision has emerged endemically with the 3-ADON variant in some regions of the USA (Kelly and Ward, 2018). The emergence of the 3-ADON chemotype may indicate an evolutionary advantage selected for by extensive growth of some wheat cultivars, as it has been shown that 3-ADON isolates can grow faster and deposit more mycotoxins within the developing grain on certain wheat isolates (Ward et al., 2008). These aspects of virulence may be driven by other, as yet unknown, genetic factors.

More extensive genomic surveillance, utilising technologies such as the MinION, will elucidate chemotype variation further in the future and enable us to better predict risk factors such as environmental conditions, which promote sexual reproduction and thus genetic diversity.

1.5.3 Epidemiology of *F. graminearum*

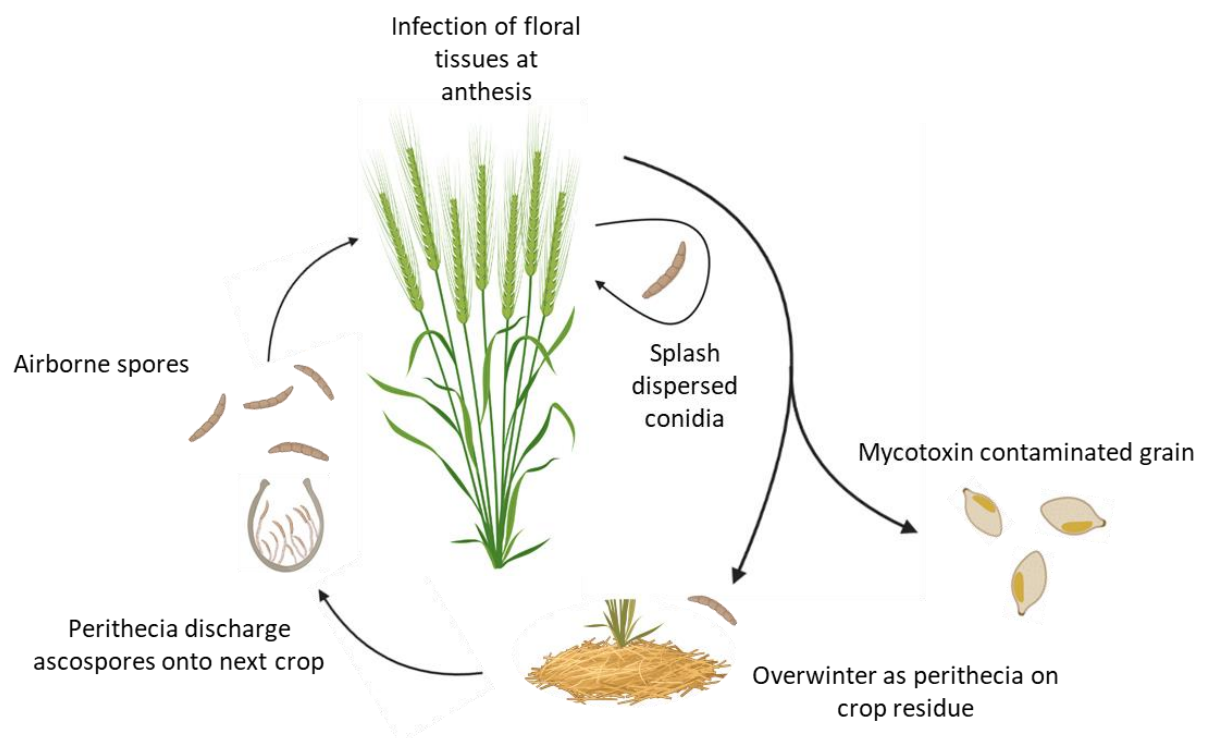


Fig. 1.5.4. Typical lifecycle of *Fusarium graminearum* (teleomorph *Gibberella zeae*). Infection is initiated by the dispersal and contact of *F. graminearum* spores onto a susceptible host, such as wheat (*Triticum aestivum*), at anthesis (flowering) and coinciding with conducive conditions of warm, wet weather to promote fungal infection. Germination of the spore on the

wheat spike is followed by elongation of the invasive hyphae into natural openings between the wheat spikelet tissues of the lemma and palea, that surround the developing wheat grain. Infection structures are evident as fungal biomass increases and intracellular hyphal growth occurs. As fungal burden increases, macroscopic symptoms appear on the wheat head, typically the premature bleaching and destruction of the developing wheat grain. Perithecia form from the chlorenchyma band of the rachis internode tissue and discharge spores onto subsequent wheat tillers within a cropping cycle. When live plants are removed at harvest, *F. graminearum* overwinters in resting structures called perithecia on crop residue, until suitable conditions and susceptible hosts reappear. Harvested grain is contaminated with mycotoxins which can proliferate in storage when *F. graminearum* is present. Figure created in Biorender.com.

F. graminearum has the ability to reproduce both sexually and asexually. The sexual stage begins with the discharge of ascospores from overwintering structures called perithecia (Fig. 1.5.4) onto a suitable, susceptible host. The perithecia are dark blue in colour when mature and forcibly discharge ascospores in favourable conditions through an opening known as an ostiole. Ascospores can travel over large distances through rain and wind dispersal. Similarly, sexual spores can be produced from an infected host plant by structures called perithecia from the chlorenchyma band of the rachis tissue (Guenther and Trail, 2005). Both sexual and asexual spores land on the outer surfaces of a susceptible host, such as wheat (*Triticum aestivum*), and germinate. The elongating germ tube tracks across the surface of the wheat head, forming runner hyphae (RH) which grow across the host surface and from infection cushions (IC), in which a high number of infection-related genes to facilitate infection are upregulated such as enzymes, effectors and secondary metabolites such as mycotoxins (Mentges et al., 2020; Fig. 1.5.5).

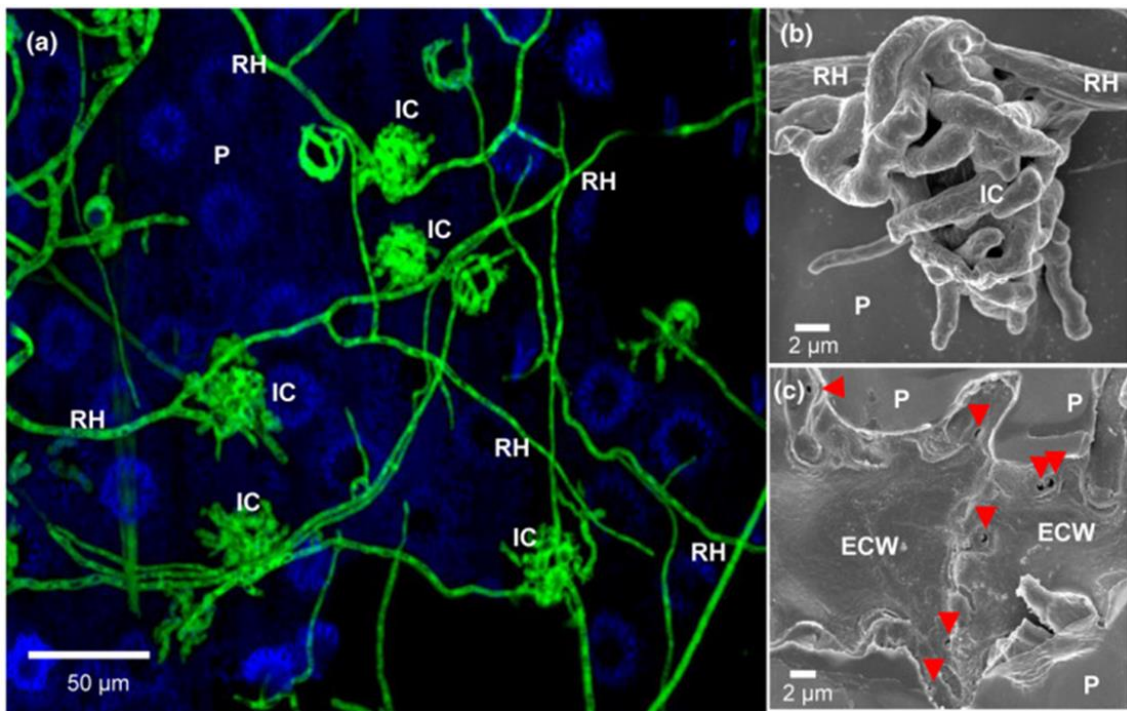


Fig. 1.5.5. Infection cushions (IC) and runner hyphae (RH) visible on the palea wheat spikelet tissue. (a) *F. graminearum* strain expressing the green fluorescent protein (GFP), imaged under confocal microscopy. RH = runner hyphae, IC = infection cushion, P= palea, scale bar = 50µm. (b) SEM micrograph of IC, scale bar = 2µm. (c) Palea tissue underneath a removed IC, showing evidence of penetration pegs indicated by red arrows, scale bar = 2µm. From Mentges et al. (2020).

Through microscopic analysis of *F. graminearum*, Brown et al. (2010) identified the biphasic colonisation pattern of infection, whereby hyphae were found to colonise the wheat spike ahead of the appearance of macroscopic symptoms (Fig. 1.5.6). Subsequent RNASeq transcriptional analysis found distinctive patterns of transcription accompanying the microscopic phenotype and became known as the symptomless and symptomatic phases of infection. Many effectors, small, secreted proteins involved in virulence, are differentially expressed depending on the phase of infection (Brown et al., 2017; Dilks et al., 2019).

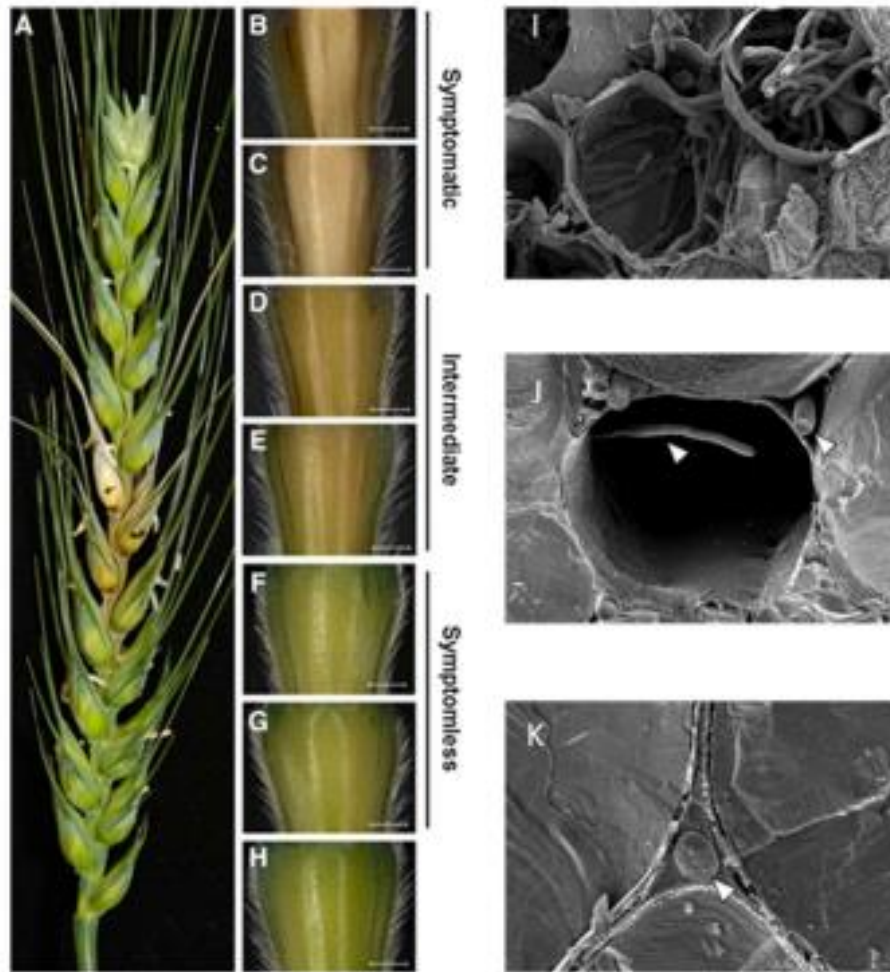


Fig. 1.5.6 Biphasic infection mechanism of *F. graminearum* in wheat spikes. (a) Typical disease symptoms on a wheat spike and (b) to (h) show dissected rachis internodes with decreasing infection severity further from point of inoculation. (i) Extensive hyphal colonisation is evident at later stages of infection, (j) pioneer hyphae are seen intracellularly in the intermediate macro-symptomatic phase and (k) restriction of hyphal growth to the apoplast is evident in the symptomless phase. (Taken from Kanja et al., 2022 (Thesis), adapted from Brown et al. (2017) and Brown et al. (2011).

1.5.4 Symptoms of FHB in small grain cereals

Symptoms of FHB appear after the symptomless phase and correlates with the switch from apoplastic to intracellular growth (Brown et al., 2010). Symptoms appear 3-5 days after initial infection and begin with the appearance of dark discoloration on the outer surfaces of the wheat spikelet, namely the glume, which are followed by the typical premature bleaching of the wheat head and shrivelling

of the developing wheat grain (Goswami and Kistler, 2004). Macroscopic symptoms on small grain cereals such as wheat, rye and oats are broadly similar (Fig. 1.5.7).



Fig. 1.5.7. Symptoms of *F. graminearum* displaying the typical bleaching phenotype on several species of small grain cereals. (a) wheat, (b) rye and (c) oats.

Grain contaminated with *F. graminearum* is shrivelled, reduced in size and weight, and sometimes with pink or bleached discolouration (Fig. 1.5.8(b)), and also indicate contamination with trichothecene mycotoxins such as deoxynivalenol (DON) (Fig. 1.5.8(a)).

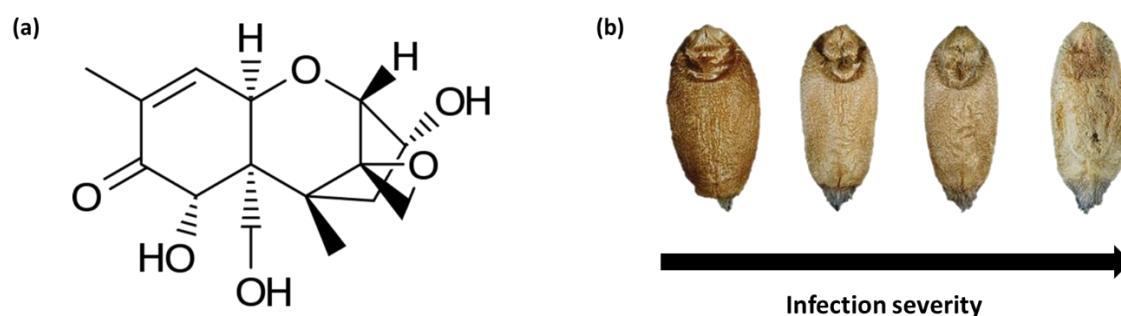


Fig. 1.5.8. The type B epoxy-sesquiterpenoid trichothecene mycotoxin deoxynivalenol (DON) and grain symptoms when contaminated with *F. graminearum*. (a) Chemical structure of DON and (b) increasing infection severity (left to right) of wheat grain infected with *F. graminearum*, indicating increasing DON levels.

1.5.5 Mycotoxins

One key aspect of *F. graminearum*'s destructive nature as a fungal pathogen is the contamination of developing grains with mycotoxins. While these can vary according to the causal species of FHB, and even between isolates of *F.*

graminearum, mycotoxins are still considered of high concern. Mycotoxins are secondary metabolites, meaning that they are not required for normal biological process relating to growth or reproduction, but are used to communicate and/or interfere with other organisms such as plant hosts (Khachatourians and Arora, 1999). Harvests of small grain cereals are routinely tested for the presence of DON (Fig. 1.5.7 (a)), the most prevalent mycotoxin, for their potential to harm human and livestock health, with strict thresholds for unprocessed grain worldwide (AHDB, 2023). Trichothecenes, among many other toxic characteristics, are carcinogenic and deoxynivalenol (DON) is nicknamed 'Vomitoxin' for its symptoms of nausea, sickness, feed refusal in livestock and birth defects (Hoofft and Bureau, 2021). Although typically not an issue, in years of particularly conducive environmental conditions around wheat anthesis, thresholds can be exceeded (Johns et al., 2022). However, if the water content of harvest grain mildly contaminated with *F. graminearum* is not carefully controlled, *F. graminearum* can proliferate in grain storage, continuing to synthesise trichothecene mycotoxins (Magan et al., 2010).

Sesquiterpenoid type B toxins of the trichothecene class include deoxynivalenol (DON), nivalenol (NIV), and T-2 toxin (McCormick et al., 2011). All trichothecene mycotoxins target the 16s subunit of eukaryotic ribosomes and hence inhibit broad spectrum protein synthesis (Brown et al., 2004). The biosynthetic gene cluster underpinning the biosynthesis of trichothecenes has been widely studied (McCormick et al., 2011) and presence of these toxins are essential for virulence in wheat (Proctor et al., 1995). By single gene deletion of the trichodiene synthase enzyme TRI5, the first committed step in biosynthesis, all trichothecene biosynthesis is inhibited. By utilising the $\Delta Tri5$ single gene deletion knock-out mutant, the role of trichothecene mycotoxins in host-tissue colonisation was explored in [chapter 3](#), and published (Armer et al., 2024b). While T-2 is the most toxic of the trichothecene mycotoxins it is rarely detected at clinically unsafe concentrations in grain (Janik et al., 2011).

Other mycotoxins produced by *Fusarium* spp., not of the trichothecene class, include fumonisins and zearalenone (ZEA). Fumonisin, are some of the most carcinogenic and cytotoxic mycotoxins (Gelderblom et al., 1988). ZEA is a mycoestrogen mycotoxin and synthesised through a polyketide pathway, but usually at low concentrations and contingent on the presence of other

trichothecene mycotoxins such as DON (Ekwomadu, Akinola and Mwanza, 2021). The types of mycotoxins produced by *Fusarium* spp. were recently reviewed by Qu et al. (2024). The *Fusarium sambucinum* species complex (FSAMSC) where *F. graminearum* resides, produce many of the known mycotoxins found in the *Fusarium* genus (Fig. 1.5.9), including trichothecenes, fumonisins and ZEA. Considered evolutionary the youngest, it is interesting that breadth of mycotoxin production has increased as genomes have decreased in size (Armer et al., 2024a), indicating essential roles for these in virulence and redundancy of other genetic factors required when mycotoxins are absent in other *Fusaria*.

Cereals are able to 'disarm' mycotoxins such as DON through the addition of sugars by the action of UDP-glycosyltransferases to generate DON-3-glucoside: transgenic wheat expressing a UDP-glycosyltransferase identified from barley demonstrated type II resistance (see [1.5.7](#)) and was found to conjugate DON to DON-3-glucoside (Li et al., 2015). This conversion prevents easy detection of DON and hence is known as a 'masked mycotoxin' (Berthiller et al., 2005). While not rendering it completely non-toxic, it enables trafficking of the water-soluble toxin.

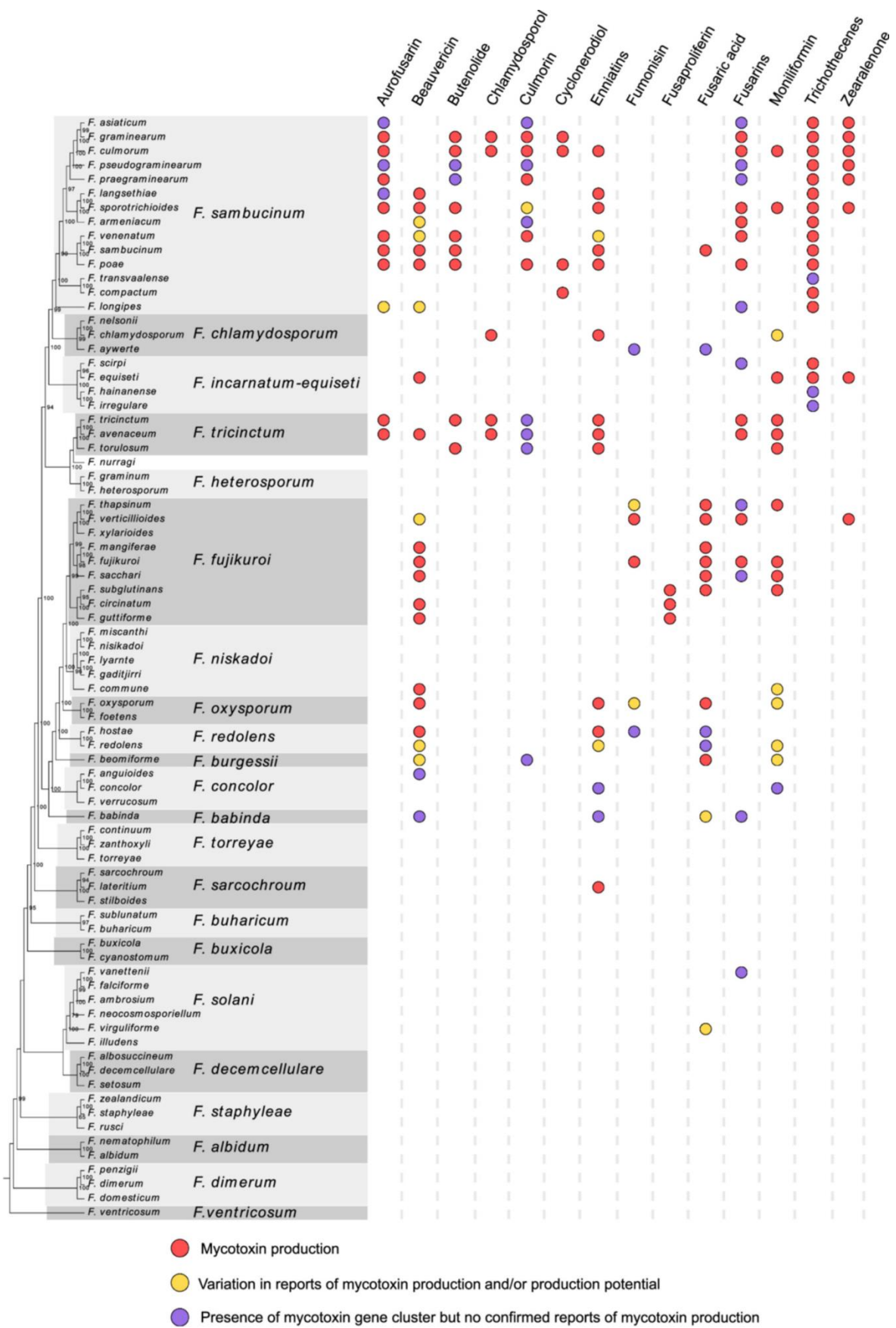


Fig. 1.5.9. Reports of mycotoxin production by *Fusarium* spp. The *F. sambucinum* species complex (FSAMSC), within which *F. graminearum* resides, produces many of the known mycotoxins in *Fusarium* spp. Taken from Qu et al., 2024.

1.5.6 Virulence factors

Alongside mycotoxins, *F. graminearum* also secretes a number of proteins, namely effectors and cell wall degrading enzymes (CWDEs) to aid infection of cereals. Effectors are small, secreted proteins that facilitate infection by manipulating or modulating plant immunity and so promote infection (Kamoun, 2006). In filamentous fungal pathogens, hundreds of effectors are predicted and most without known functions, domains or sequence homology to known proteins (Wilson and McDowell, 2022). However, the presence and/or absence of effectors greatly determines compatibility with the host (Sánchez-Vallet et al., 2018). Many effectors are differentially expressed depending on the phase of infection, for example, the symptomless or symptomatic, in *F. graminearum* infection (Brown et al., 2017). Many of the LS chromosomes in the *F. oxysporum* species complex contain effectors that are predicted to determine host specificity (Armer et al., 2024a). Efforts to characterise *F. graminearum* effectors, and those of other filamentous phytopathogens, are underway, with methods for discovery recently reviewed (Kanja and Hammond-Kosack, 2020), including gene knock out studies, protein localisations and transient protein expression in the *N. benthamiana*-*Agrobacterium* system.

Equally, CWDEs are secreted hydrolytic enzymes and have been shown to be integral to host-tissue colonisation by *F. graminearum*. The secretion of these may contribute to host-tissue colonisation by directly damaging the plant host through hydrolysis the cell wall, thereby making it easy for *F. graminearum* hyphae to break through cell walls. CWDEs include endo-polygalacturonases (PGs), which catalyse the degradation of pectin polymers, and xylanses, which hydrolyse xylan, a major component of hemicelluloses in plant cell walls. Knocking out essential genes for the synthesis of these enzymes alone does not seem to impair virulence, but double knock out of $\Delta pg1\Delta xyf$ led to significantly reduced virulence in wheat (Paccanaro et al., 2017). This indicates that *F. graminearum* may compensate for a lack of hydrolysis enzymes for particular aspects of plant cell walls with others, in order to dismantle the matrix, and so multiple targets need to be investigated if this is to be a durable strategy for controlling *F. graminearum* host-tissue colonisation. The role of CWDEs is further explored in [chapter 6](#).

1.5.7 Control strategies

Multiple factors contribute to the difficulty of *F. graminearum* control. First, the aforementioned biphasic lifestyle of *F. graminearum* enables fungal establishment within the host tissues prior to macroscopic disease symptoms becoming apparent. The ban on prophylactic treatment of crops in the EU and UK, to combat rising resistance and environmental concerns of the application of fungicides prevents farmers and agronomists predicting and preventing *F. graminearum* infection, even when conditions around anthesis are extremely conducive to *F. graminearum* establishment. Fungicides of the triazole class are currently the most effective and work by targeting the CYP51 enzyme that is required for the biosynthesis of the essential fungal membrane component ergosterol (Yin et al., 2009). However, some populations of *F. graminearum* have exhibited reduced sensitivity to triazoles due to allele duplication (Liu et al., 2011). Rising resistance to the triazole fungicides class is also proving difficult to work around, but by applying mixtures of fungicides from multiple classes with different targets, the genetic selection pressure on *F. graminearum* is reduced (McMullen et al., 2008).

Genetic resistance in wheat is an important component of FHB control. As previously discussed, the ubiquitous use of particular wheat cultivars may be driving population changes in *F. graminearum*, shifting from the previously dominant 15-ADON chemotype to the 3-ADON chemotype (Kelly and Ward, 2018), demonstrating selection pressure from genetic resistance.

Resistance of wheat cultivars to FHB infection is classified into 5 categories, whereby Type I is the most desirable (Mesterhazy, 1995):

- Type I – Resistance to fungal establishment and hyphal penetration
- Type II – Resistance to hyphal inter- and intracellular hyphal colonisation
- Type III – Resistance to grain colonisation
- Type IV – Resistance to hyphal spread throughout the wheat
- Type V – Ability to resist or degrade *Fg* toxins

Genes contributing to FHB resistance are quantitative, with over 500 QTLs having been reported within the literature and mapped to twenty-one of wheat's chromosomes; 7 alleles have been characterised (Ma et al., 2020). However,

large genetic diversity within *F. graminearum* has thus far failed to produce a single 'silver bullet' solution to FHB susceptibility. *F. graminearum* has so far proven not to conform to Flor's gene-for-gene model explaining plant host susceptibility and resistance to infection (Flor, 1971).

The most widely studied QTL, FHB1, located on the short arm of chromosome 3B, has been shown to confer type II resistance to *F. graminearum* (Cuthbert et al., 2006). The source of this resistance is still to be dissected, with three plausible sources within this QTL so far postulated within the literature. Firstly, TaHRC, a histidine rich calcium binding protein which may be nuclear localised (Su et al., 2019, Li et al., 2019), the WFhb1-1 gene, of probable anti-fungal but as yet unknown function, which has been shown to inhibit in vitro growth of *Fg* (Paudel et al., 2020), and a chimeric lectin containing pore forming toxin-like gene (Rawat et al., 2016). Interestingly, it has recently been reported that two loci, on chromosomes 5B and 6A, present in predominately in Chinese wheat cultivars with Fhb1, actually repress the resistance induced by FHB1, explaining the variable phenotypes previously reported (Li et al., 2023). Other known sources of type II resistance include the removal of transcription factor NFXL1, a susceptibility gene, which represses trichothecene mycotoxin-induced wheat defence responses (Brauer et al., 2020).

Finding and integrating novel sources of resistance into modern wheat cultivars is becoming easier with advancing sequencing technologies and genetic modification techniques. CRISPR/Cas9 gene editing in wheat has been successful, with Europe's first CRISPR field trial for low acrylamide wheat being conducted at Rothamsted Research (Raffan et al., 2023) and legislation surrounding field trials of wheat edited through this technique are now being allowed in the UK with the passing of a bill in parliament in March 2023 (Genetic Technology (Precision Breeding) Act 2023). In addition, so long as no foreign DNA is being inserted into the target genome, these crops will now be classified as Genetically Engineered (GE) and not GM. This technique is ideal for knocking out susceptibility factors, such as NFXL1. Sources of novel resistance to FHB are yet to be unlocked. However, the recent release of the Watkin's wheat collection of ancient wheat landraces (locally adapted wheat varieties), has the potential to expand genetic diversity of germplasm in wheat breeding pipelines and provide

novel traits, including disease resistance, currently missing from the relative low diversity currently present in modern wheat (Cheng et al., 2024).

With increasing concern among scientists and the wider public regarding the distribution of fungicides into the environment, genetic resistance remains the more sustainable solution for long term control of FHB. Developing resistant cultivars, either through GM or integrating ancient wheat genetic diversity as recently unlocked through the A. E. Watkin's wheat collection (Cheng et al., 2024) remains plausible and desirable.

1.6 PhD outline

1.6.1 Research questions

The overall aim of this thesis is to understand the physical interactions between invasive *F. graminearum* hyphae and wheat floral tissues during host tissue colonisation. The following research questions are addressed, in turn, in this thesis and aim to deliver a thorough exploration of *F. graminearum* infection mechanisms at the cellular, tissue and whole plant scale.

1. *What is the role of DON during infection of wheat floral tissues?*
2. *Does DON overcome PAMP-triggered immunity during *F. graminearum* infection?*
3. *Does *F. graminearum* directly degrade callose at plasmodesmata through the excretion of glycoside hydrolase enzymes?*
4. *What cell wall components pose an effective barrier to *F. graminearum*, forcing cell wall traversing through plasmodesmatal pores?*

1.6.2 Hypotheses

This thesis addresses key hypotheses surrounding the wheat- *F. graminearum* interaction:

1. *The mycotoxin Deoxynivalenol (DON) facilitates host-tissue colonisation in wheat rachis tissue.*

2. *Callose deposition is a defence response to F. graminearum infection in wheat spikes.*
3. *Developmental changes in wheat rachis morphology control the short infection window surrounding anthesis of F. graminearum in wheat spikes.*
4. *F. graminearum hyphae need to pass through PD pit fields due to lignin-rich cell wall composition in the wheat rachis.*

1.6.3 Chapter overview

Chapter 1 – Introduction to importance of wheat in food security, fungal phytopathogens, plant immunity, plasmodesmata and *Fusarium graminearum*.

Chapter 2 – The general materials and methods used within this thesis.

Chapter 3 – Addresses the first research question above and presents evidence for the role of DON during infection. By analysis of the single gene deletion mutant of the trichothecene synthase gene, $\Delta Tri5$, the role of DON is alluded to facilitate host-tissue colonisation by movement of invasive hyphae through plasmodesmatal pit fields. Work in this chapter also led to a further hypothesis that DON is excreted with spatial and temporal precision, as chemical complementation failed to reproduce the WT disease phenotype. Assays in the alternative tissue of the wheat coleoptile also revealed that TRI5 is a tissue-specific virulence factor, as no disease attenuation was observed.

Chapter 4 – Aimed to further understand the wheat defence response to *F. graminearum* in the absence of trichothecene mycotoxins. Surprisingly, inoculation with the avirulent $\Delta Tri5$ strain prevented subsequent WT infection establishment. Thereafter, this chapter explored PTI and ETI responses, identifying that $\Delta Tri5$ triggers PTI responses, and the ability to synthesise DON during infection appears to dampen PTI responses to facilitate WT infection. To follow on from the observations in chapter 3, the response of callose at plasmodesmata in the WT, $\Delta Tri5$ and PAMP-induced (chitin) interactions were explored.

Chapter 5 – Spurred on by the results of the prior chapters which indicated that PTI-triggered immunity is overcome by the presence of DON, and that this likely involves callose deposition at plasmodesmata, it was hypothesised that to facilitate infection *F. graminearum* secretes glycoside hydrolase enzymes to

break down callose at plasmodesmatal pit fields. After a bioinformatics search, it was found that *F. graminearum* carries a single copy of a GH81 enzyme that is predicted to break down β -1,3-glycosidic bonds present in the glucose polymer callose. To determine if this plays an essential role in infection, a knock-out mutant, denoted $\Delta FgGH81$ was generated and tested *in planta*, with independent transformants all having attenuated virulence *in planta*.

Chapter 6 – To elucidate why *F. graminearum* requires the use of pit fields during host-tissue colonisation of the wheat rachis, cell wall compositional elements were tested through application of the *Arabidopsis thaliana* SALK lines and a detached leaf assay set up. This chapter aimed to determine if particular cell wall elements conferred resistance and/or susceptibility to *F. graminearum* infection and translate to the native wheat- *F. graminearum* pathosystem. This led to the identification that lignin has an integral role in resistance to *F. graminearum* and may also be casual of the developmental resistance to *F. graminearum* infection post-anthesis.

Chapter 7 – General discussion that provides an overview of the results and studies presented within this thesis, with discussion of future directions for FHB control and remaining open research questions.

1.7 References

AHDB (2023). Risk assessment for *Fusarium* mycotoxins in wheat. Available online: <https://ahdb.org.uk/mycotoxins>. [Accessed 1st September 2023].

AHDB (2024). Inflation and cost of living put long-term resilience of farming under pressure in 2024. Available online: <https://ahdb.org.uk/news/agri-market-outlook-2024#:~:text=This%20has%20the%20potential%20to,fertiliser%20being%20a%20prime%20example>. . [Accessed 2nd August 2024].

Armer VJ, Kroll, E, Darino M, Smith D, Urban M, Hammond-Kosack KE. (2024a). Navigating the *Fusarium* species complex: Host-Range Plasticity and Genome Variations. *Fungal Biology*. **In press**. doi: 10.1016/j.funbio.2024.07.004.

Armer VJ, Urban M, Ashfield T, Deeks MJ, Hammond-Kosack KE. (2024b). The trichothecene mycotoxin deoxynivalenol facilitates cell-to-cell invasion during wheat-tissue colonisation by *Fusarium graminearum*. *Molecular Plant Pathology*. **25**(6): e13485. 10.1111/mpp.13485

Bagnall DK, Shanahan JF, Flanders A, Morgan CLS, Honeycutt CW. (2021). Soil health considerations for global food security. *Agronomy Journal*. **113**(6): 4581-4589.

Betts RA, Belcher SE, Hermanson L, Tank AK, Lowe JA, Jones CD, Morice CP, Rayner NA, Scaife AA, Scott PA. (2023). Approaching 1.5 °C: how will we know we've reached this crucial warming mark? *Nature*. **624**: 33-35. doi: 10.1038/d41586-023-03775-z.

Blekemolen MC, Cao L, Tintor N, de Groot T, Papp D, Faulkner C, Takken FLW. (2022). The primary function of Six5 of *Fusarium oxysporum* is to facilitate Avr2 activity by together manipulating the size exclusion limit of plasmodesmata. *Frontiers in plant science*, **13**: 910594. doi: 10.3389/fpls.2022.910594.

Blümke A, Falter C, Herrfurth C, Sode B, Bode R, Schafer W, Feussner I, Voigt CA (2014). Secreted fungal effector lipase releases free fatty acids to inhibit innate immunity-related callose formation during wheat head infection. *Plant Physiology*, **165**(1): 346-58. doi: 10.1104/pp.114.236737

Brauer EK, Balcerzak M, Rocheleau H, Leung W, Scherthner J, Subraniam R, Ouelett T. (2020). Genome Editing of a Deoxynivalenol-Induced Transcription Factor Confers Resistance to *Fusarium graminearum* in Wheat. *Molecular Plant-Microbe Interactions*, **33**(3): 553-560. doi: 10.1094/MPMI-11-19-0332-R.

Brown NA, Evans J, Mead A, Hammond-Kosack KE. (2017). A spatial temporal analysis of the *Fusarium graminearum* transcriptome during symptomless and symptomatic wheat infection. *Molecular Plant Pathology*. **18**(9): 1295-1312. doi: 10.1111/mpp.12564.

Brown NA, Urban M, Van De Meene AML, Hammond-Kosack KE. (2010). The infection biology of *Fusarium graminearum*: defining the pathways of spikelet to spikelet colonisation in wheat ears. *Fungal Biology*. **114**: 555-571. doi: 10.1016/j.funbio.2010.04.006.

Cao L, Blekemolen MC, Tintor N, Cornelissen BJC, Takken FLW. (2018). The *Fusarium oxysporum* Avr2-Six5 Effector Pair Alters Plasmodesmatal Exclusion Selectivity to Facilitate Cell-to-Cell Movement of Avr. *Molecular Plant*, **11**(5): 691–705. doi: 10.1016/j.molp.2018.02.011

Chaloner TM, Gurr SJ, Bebbler DP. (2021). Plant pathogen infection risk tracks global crop yields under climate change. *Nature Climate Change*. **11**: 710-715. doi: 10.1038/s41558-021-01104-8.

Cheng S. *et al.* (2024). Harnessing landrace diversity empowers wheat breeding. *Nature*. **Accelerated peer review**. doi.org/10.1038/s41586-024-07682-9.

Cheval C, Faulkner C. (2017). Plasmodesmal regulation during plant–pathogen interactions. *New Phytologist*. **217**(1): 62-67. doi: 10.1111/nph.14857.

Cheval C, Samwald S, Johnston MG, de Keijzer J, Breakspear A, Liu X, Bellandi A, Kadota Y, Zipfel C, Faulkner C. (2020). Chitin perception in plasmodesmata characterizes submembrane immune-signaling specificity in plants. **117**(17): 9621-9629. doi: 10.1073/pnas.1907799117

Cho E, SH Lee, Jeong M, De Mandal S, Park S, Nam SW, Byeun DG, Choi JK, Lee Y, Shin J, Jeon J. (2023). Genetic and transcriptomic analysis of hyphal constriction based on a novel assay method in the rice blast fungus. *bioRxiv*. doi: 10.1101/2023.06.14.545034.

Cruz-Mireles N, Eseola AB, Osés-Ruiz M, Ryder LS, Talbot NJ. (2021). From appressorium to transpressorium-Defining the morphogenetic basis of host cell invasion by the rice blast fungus. *PLoS Pathogens*, **17**(7): e1009779. doi: 10.1371/journal.ppat.1009779.

Cuomo CA *et al.* (2007). The *Fusarium graminearum* Genome Reveals a Link Between Localized Polymorphism and Pathogen Specialization. *Science*. **317**:1400-1402. doi: 10.1126/science.1143708.

Cuthbert PA, Somers DJ, Thomas J, Cloutier S, Brulé-Babel A. (2006). Fine mapping Fhb1, a major gene controlling *Fusarium* head blight resistance in bread wheat (*Triticum aestivum* L.). *Theoretical and Applied Genetics*. **112**(8): 1465-1472. doi: 10.1007/s00122-006-0249-7.

Dean R, Van Kan JAL, Pretorius ZA, Hammond-Kosack KE, Di Pietro A, Spanu PD, Rudd JJ, Dickman M, Kahmann R, Ellis J, Foster GD. (2012). The Top 10 fungal pathogens in molecular plant pathology. *Molecular Plant Pathology*, **13**: 414-430. doi: 10.1111/j.1364-3703.2011.00783.x

Di X, Gomila J, Takken FLW. (2017). Involvement of salicylic acid, ethylene and jasmonic acid signalling pathways in the susceptibility of tomato to *Fusarium oxysporum*. *Molecular Plant Pathology*, **18**(7): 1024-1035. doi: 10.1111/mpp.12559.

Dilks T, Halsey K, De Vos RP, Hammond-Kosack KE, Brown NA. (2019). Non-canonical fungal G-protein coupled receptors promote *Fusarium* head blight on wheat. *PLOS Pathogens*. **15**(4): e1007666. doi: 10.1371/journal.ppat.1007666

Dita M, Barquero M, Heck D, Mizubuti ESG, Staver CP. (2018). *Fusarium* Wilt of Banana: Current Knowledge on Epidemiology and Research Needs Toward Sustainable Disease Management. *Frontiers in Plant Science*. **9**: 1468. doi: 10.3389/fpls.2018.01468.

Djamei A, Schipper K, Rabe F, Ghosh A, Vincon V, Kahnt J, Osorio S, Tohge T, Fernie AR, Feussner I, Feussner K, Meinicke P, Stierhof Y, Schwarz H, Macek B, Mann M, Kahmann R. (2011). Metabolic priming by a secreted fungal effector. *Nature*. **478**: 395–398. doi: 10.1038/nature10454.

Dong S, Raffaele S, Kamoun S. (2015). The two-speed genomes of filamentous pathogens: waltz with plants. *Current Opinion in Genetics & Development*. **35**: 57-65. doi: 10.1016/j.gde.2015.09.001.

Dubcovsky J, Dvorak J. (2007). Genome plasticity a key factor in the success of polyploid wheat under domestication. *Science*. **316**(5833): 1862–1866. doi: 10.1126/science.1143986.

Ekwomadu TI, Akinola SA, Mwanza M. (2021). *Fusarium* Mycotoxins, Their Metabolites (Free, Emerging, and Masked), Food Safety Concerns, and Health Impacts. *International Journal of Environmental Research and Public Health*. **18**(22):11741. doi: 10.3390/ijerph182211741.

Erenstein O, Jaleta M, Mottaleb KA, Sonder K, Donovan J, Braun H. (2022). Global Trends in Wheat Production, Consumption and Trade. In: Reynolds, M.P., Braun, H.J. (eds) *Wheat Improvement*. Springer, Cham. doi: 10.1007/978-3-030-90673-3_4.

- Eskola M, Kos G, Elliott CT, Hajšlová J, Mayar S, Krska R. (2019). Worldwide contamination of food-crops with mycotoxins: validity of the widely cited 'FAO estimate' of 25%. *Critical Reviews in Food Science and Nutrition*, **60**(16): 2773–2789. doi: 10.1080/10408398.2019.1658570
- Faulkner C, Akman OE, Bell K, Jeffree C, Oparka K. (2008). Peeking into Pit Fields: A Multiple Twinning Model of Secondary Plasmodesmata Formation in Tobacco. *Plant Cell*, **20**(6): 1504-1518. doi: 10.1105/tpc.107.056903.
- Faulkner C, Petutschnig E, Benitez-Alfonso Y, Beck M, Robatzek S, Lipka V, Maule AJ. (2013). LYM2-dependent chitin perception limits molecular flux via plasmodesmata. *PNAS*, **110**(22): 9166-70. doi: 10.1073/pnas.1203458110.
- Fei W, Liu Y. (2022). Biotrophic Fungal Pathogens: a Critical Overview. *Applied Biochemistry and Biotechnology*. **195**: 1-16. doi: 10.1007/s12010-022-04087-0.
- Fernandez-Calvino L, Faulkner C, Walshaw J, Saalbach G, Bayer E, Benitez-Alfonso Y, Maule A. (2011) *Arabidopsis* Plasmodesmal Proteome. *PLOS ONE*. **6**(4): e18880. doi: 10.1371/journal.pone.0018880.
- Fichman Y, Myers Jr RJ, Grant AG, Mittler R. (2021). Plasmodesmata-localized proteins and ROS orchestrate light-induced rapid systemic signaling in *Arabidopsis*. *Science Signaling*. **14**(671): eabf0322. doi: 10.1126/scisignal.abf0322.
- Flood, J. (2010). The importance of plant health to food security. *Food Security*. **2**: 215–231 doi: 10.1007/s12571-010-0072-5.
- Flor HH. (1971). Current states of the gene-for-gene concept. *Annual Review of Phytopathology*. **9**: 275-296. doi: 10.1146/annurev.py.09.090171.001423.
- Fones H, Gurr S. (2015). The impact of *Septoria tritici* blotch disease on wheat: an EU perspective. *Fungal Genetics and Biology*. **79**: 3-7. doi: 10.1016/j.fgb.2015.04.004.
- Fones HN, Bebber DP, Chaloner TM, Kay WT, Steinberg G, Gurr SJ. (2020). Threats to global food security from emerging fungal and oomycete crop pathogens. *Nature Food*. **1**: 332–342 doi: 10.1038/s43016-020-0075-0.
- Fu ZQ, Dong X. (2013). Systemic Acquired Resistance: Turning Local Infection into Global Defense. *Annual Review of Plant Biology*. **64**: 839-63. doi: 10.1146/annurev-arplant-042811-105606.
- Fukuda S, Yamamoto R, Yanagisawa, N, Takaya N, Sato Y, Riquelme M, Takeshita N. (2021). Trade-off between Plasticity and Velocity in Mycelial Growth. *mBio*, **12**(2): e03196-20. doi: 10.1128/mbio.03196-20.
- Gelderblom WC, Jaskiewicz K, Marasas WF, Thiel PG, Horak RM, Vleggaar R, Kriek NP Fumonisin—Novel mycotoxins with cancer-promoting activity produced by *Fusarium moniliforme*. *Applied and Environmental Microbiology*. **54**:1806–1811. doi: 10.1128/aem.54.7.1806-1811.1988

Genetic Technology (Precision Breeding) Bill. 2023. (HC Bill 11, 2022-2023). [Online]. London: The Stationary Office. [Accessed 26th July 2024]. Available from: <https://commonslibrary.parliament.uk/research-briefings/cbp-9557/>

Goswami RS, Kistler HC. (2004). Heading for disaster: *Fusarium graminearum* on cereal crops. *Molecular Plant Pathology*. **5**(6): 515-524. doi: 10.1111/j.1364-3703.2004.00252.x.

Guenther JC, Trail F. (2005). The development and differentiation of *Gibberella zeae* (anamorph: *Fusarium graminearum*) during colonization of wheat. *Mycologia*. **97**(1), 229-237. doi: 10.1080/15572536.2006.11832856.

Hao Z, Li Y, Jiang Y, Xu J, Li J, Luo L. (2021). Genome Sequence Analysis of the Fungal Pathogen *Fusarium graminearum* Using Oxford Nanopore Technology. *Journal of Fungi (Basel)*. **7**(9): 699. doi: 10.3390/jof7090699.

Hedden P. (2003). The genes of the Green Revolution. *Trends in Genetics*. **19**(1): 5-9. doi: 10.1016/S0168-9525(02)00009-4.

Held M, Kaspar O, Edwards C, Nicolau DV. (2019). Intracellular mechanisms of fungal space searching in microenvironments. *PNAS*, **116**(27): 13543-13552. doi: 10.1073/pnas.1816423116.

Hooft JM, Bureau DP. (2021). Deoxynivalenol: Mechanisms of action and its effects on various terrestrial and aquatic species. *Food and Chemical Toxicology*. **157**: 112616. doi: 10.1016/j.fct.2021.112616.

Hou S, Liu Z, Shen H, Wu D. (2019). Damage-Associated Molecular Pattern-Triggered Immunity in Plants. *Frontiers in Plant Science*. **10**: 646. doi: 10.3389/fpls.2019.00646.

Islam MT, Croll D, Gladioux P, Soanes DM, Persoons A, Bhattacharjee P, Hossain MS, Gupta DR, Rahman MM, Mahboob MG, Cook N, Salam MU, Surovy MZ, Sancho VB, Maciel JL, Nhani Júnior A, Castroagudín VL, Reges JT, Ceresini PC, Ravel S, ... Kamoun S. (2016). Emergence of wheat blast in Bangladesh was caused by a South American lineage of *Magnaporthe oryzae*. *BMC biology*. **14**(1): 84. doi: 10.1186/s12915-016-0309-7.

Iswanto ABB, Vu MH, Pike S, Lee J, Kang H, Son GH, Kim JY, Kim SH. (2022). Pathogen effectors: What do they do at plasmodesmata? *Molecular Plant Pathology*, **23**(6): 795-804. doi: 10.1111/mpp.13142.

Janik E, Niemcewicz M, Podogrocki M, Ceremuga M, Stela M, Bijak M. (2021). T-2 toxin—The most toxic trichothecene mycotoxin: Metabolism, toxicity, and decontamination strategies. *Molecules*. **26**(22): 6868. doi: 10.3390/molecules26226868.

Johns LE, Bebbler DP, Gurr SJ, Brown NA. (2022). Emerging health threat and cost of *Fusarium* mycotoxins in European wheat. *Nature Food*. **3**: 1014–1019. doi: 10.1038/s43016-022-00655-z.

Kadota Y, Shirasu K, Zipfel C. (2015). Regulation of the NADPH Oxidase RBOHD During Plant Immunity. *Plant and Cell Physiology*. **56**(8): 1472–1480. doi: 10.1093/pcp/pcv063.

- Kamoun S. (2006). A catalogue of the effector secretome of plant pathogenic oomycetes. *Annual Review of Phytopathology*, **44**: 41–60. doi: 10.1146/annurev.phyto.44.070505.143436.
- Kanja C, Hammond-Kosack KE. (2020). Proteinaceous effector discovery and characterisation in filamentous plant pathogens. *Molecular Plant Pathogens*. **21**(10): 1353-1376. doi: 10.1111/mpp.12980.
- Kanja C, Machado Wood AK, Baggaley L, Walker C and Hammond-Kosack KE. (2021). Cereal-*Fusarium* interactions: Improved fundamental insights into *Fusarium* pathogenomics and cereal host resistance reveals new ways to achieve durable disease control. In: Achieving durable disease resistance in cereals, Ed R. Oliver, Burleigh Dodds Science Publishing, UK. doi: 10.1201/9781003180715.
- Kankanala P, Czymmek K, Valent B. (2007). Roles for rice membrane dynamics and plasmodesmata during biotrophic invasion by the blast fungus. *Plant Cell*, **19**(2): 706-24. doi: 10.1105/tpc.106.046300.
- Kelly AC, Ward TJ. (2018). Population genomics of *Fusarium graminearum* reveals signatures of divergent evolution within a major cereal pathogen. *PLoS One*. **13**(3):e0194616. doi: 10.1371/journal.pone.0194616.
- Khachatourians GG, Arora DK (1999). Biochemical and modern identification techniques: microfloras of fermented foods. In: *Encyclopaedia of Food Microbiology*. Robinson RK (eds). Elsevier, UK.
- King R, Urban M, Hammond-Kosack MCU, Hassani-Pak K, Hammond-Kosack KE. (2015). The completed genome sequence of the pathogenic ascomycete fungus *Fusarium graminearum*. *BMC Genomics*. **16**: 544. doi: 10.1186/s12864-015-1756-1.
- Li G, Yuan Y, Zhou J, Cheng R, Chen R, Luo X, Shi J, Wang H, Xu B, Duan Y, Zhong J, Wang X, Kong Z, Jia H, Ma Z. (2023). FHB resistance conferred by Fhb1 is under inhibitory regulation of two genetic loci in wheat (*Triticum aestivum* L.). *Theoretical and Applied Genetics*. **136**(6), 134. doi: 10.1007/s00122-023-04380-4.
- Li G, Zhou J, Jia H, Gao Z, Fan M, Luo Y, Zhao P, Xue S, Li N, Yuan Y, Ma S, Kong Z, Jia L, An X, Jiang G, Liu W, Cao W, Zhang R, Fan J, Xu X et al., Ma Z. (2019). Mutation of a histidine-rich calcium-binding-protein gene in wheat confers resistance to *Fusarium* head blight. *Nature Genetics*, **51**(7): 1106–1112. doi: 10.1038/s41588-019-0426-7.
- Li X, Shin S, Heinen S, Dill-Macky R, Berthiller F, Nersesian N, Clemente T, McCormick S, Muehlbauer GJ. (2015). Transgenic Wheat Expressing a Barley UDP-Glucosyltransferase Detoxifies Deoxynivalenol and Provides High Levels of Resistance to *Fusarium graminearum*. *Molecular Plant Microbe Interactions*. **28**(11): 1237–1246. doi: 10.1094/MPMI-03-15-0062-R.
- Liao CY, Chen MY, Chen YK, Kuo KC, Cung KR, Lee MH. (2011). Formation of highly branched hyphae by *Colletotrichum acutatum* within the fruit cuticles of *Capsicum* spp. *Plant Pathology*. **61**(2): 262-270. doi: 10.1111/j.1365-3059.2011.02523.x.

- Liu X, Yu F, Schnabel G, Wu J, Wang Z, Ma Z. (2011). Paralogous cyp51 genes in *Fusarium graminearum* mediate differential sensitivity to sterol demethylation inhibitors. *Fungal Genetics and Biology*, **48**(2): 113-123. doi: 10.1016/j.fgb.2010.10.004.
- Lu P, Chen D, Qi Z, Wang H, Chen Y, Wang Q, Jiang C, Xu JR and Liu H. (2022). Landscape and regulation of alternative splicing and alternative polyadenylation in a plant pathogenic fungus. *New Phytologist*. **235**(2): 674-689. doi: 10.1111/nph.18164.
- Ma L, van der Does HC, Borkovich KA, Coleman JJ, Daboussi M, Di Pietro A, Dufresne M, Freitag M. et al. (2010). Comparative genomics reveals mobile pathogenicity chromosomes in *Fusarium*. *Nature*. **464**: 367-73. doi: 10.1038/nature08850.
- Ma Z, Xie Q, Li G, Jia H, Zhou J, Kong Z, Li N, Yuan Y. (2020). Germplasms, genetics and genomics for better control of disastrous wheat *Fusarium* head blight. *Theoretical and Applied Genetics*, **133**: 1541-1568. doi: 10.1007/s00122-019-03525-8.
- Magan N, Aldred D, Mylona K, Lambert RJW. (2010). Limiting mycotoxins in stored wheat. *Food Additives & Contaminants*. **27**(5): 64-650. doi: 10.1080/19440040903514523.
- Maryani N, Lombard L, Poerba YS, Subandiyah S, Crous PW, Kema GHJ. (2019). Phylogeny and genetic diversity of the banana *Fusarium* wilt pathogen *Fusarium oxysporum* f. sp. *ubense* in the Indonesian centre of origin. *Studies in Mycology*. **92**: 155–194. doi: 10.1016/j.simyco.2018.06.003
- McCombe CL, Greenwood JR, Solomon PS, Williams SJ. (2022). Molecular plant immunity against biotrophic, hemibiotrophic, and necrotrophic fungi. *Essays in Biochemistry*. **66**(5): 581–593. doi: 10.1042/EBC20210073.
- McCormick SP, Stanley AM, Stover NA, Alexander NJ. (2011). Trichothecenes: from simple to complex mycotoxins. *Toxins*. **3**(7), 802-814. doi: 10.3390/toxins3070802.
- McMullen M, Halley S, Schatz B, Meyer S, Jordahl J, Ransom J. (2008). Integrated strategies for *Fusarium* head blight management in the United States. *Cereal Research Communications*. **36**: 563-568. doi: 10.1556/CRC.36.2008.Suppl.B.45.
- Mentges M, Glasenapp A, Boenisch M, Malz S, Henrissat B, Frandsen RJN, Güldener U, Münsterkötter M, Bormann J, Lebrun MH, Schäfer W, Martinez-Rocha AL. (2020). Infection cushions of *Fusarium graminearum* are fungal arsenals for wheat infection. *Molecular Plant Pathology*. **21**(8):1070-1087. doi: 10.1111/mpp.12960.
- Mesterházy A. (1995). Types and components of resistance to *Fusarium* head blight of wheat. *Plant Breeding*. **114**(5): 377-386. doi: 10.1111/j.1439-0523.1995.tb00816.x.
- Mittler R, Zandalinas SI, Fichman Y, Van Breusegem F. (2022). Reactive oxygen species signalling in plant stress responses. *Nature Reviews Molecular Cell Biology*. **23**: 663–679 doi: 10.1038/s41580-022-00499-2

- Moonjely S, Ebert M, Patan-Glassbrook D, Noel ZA, Roze L, Shay R, Watkins T, Trail F. (2023). Update on the state of research to manage *Fusarium* head blight. *Fungal Genetics and Biology*. **169**: 103829. doi: 10.1016/j.fgb.2023.103829.
- Nalam VJ, Vales MI, Watson CJ, Kianian SF, Riera-Lizarazu O. (2006). Map-based analysis of genes affecting the brittle rachis character in tetraploid wheat (*Triticum turgidum* L.). *Theoretical and Applied Genetics*. **112**(2): 373–381. doi: 10.1007/s00122-005-0140-y.
- Nicolas WJ, Grison MS, Trepout S, Gaston A, Fouche M, Cordelieres FP, Oparka K, Tilsner J, Brocard L, Bayer EM. (2017). Architecture and permeability of post-cytokinesis plasmodesmata lacking cytoplasmic sleeves. *Nature Plants*, **3**: 17082. doi: 10.1038/nplants.2017.82.
- Ohtsu M, Jennings J, Johnston M, Breakspear A, Liu X, Stark K, Morris RJ, de Keijzer J, Faulkner C. (2024). Assaying Effector Cell-to-Cell Mobility in Plant Tissues Identifies Hypermobility and Indirect Manipulation of Plasmodesmata. *Molecular Plant Pathology*. **37**(2): 84-92. doi: 10.1094/MPMI-05-23-0052-TA.
- Oparka KJR, Roberts AG, Boevink P, Santa Cruz S, Roberts I, Pradel KS, Imlau A, Kotlizky G, Sauer N, Epel B. (1999). Simple, but not branched, plasmodesmata allow the nonspecific trafficking of proteins in developing tobacco leaves. *Cell*, **97**(6): 743-754. doi: 10.1016/s0092-8674(00)80786-2.
- Paccanaro MC, Sella L, Castiglioni C, Giacomello F, Martínez-Rocha AL, D'Ovidio R, Schäfer W, Favaron F. (2017). Synergistic Effect of Different Plant Cell Wall–Degrading Enzymes Is Important for Virulence of *Fusarium graminearum*. *Molecular Plant Microbe Interactions*. **30**(11): 886-895. doi: 10.1094/MPMI-07-17-0179-R.
- Paniagua C, Sinanaj B, Benitez-Alfonso Y. (2021). Plasmodesmata and their role in the regulation of phloem unloading during fruit development. *Current Opinion in Plant Biology*, **64**: 102145. doi: 10.1016/j.pbi.2021.102145.
- Paudel B, Zhuang Y, Galla A, Dahal S, Qiu Y, Ma A, Raihan T, Yen Y. (2020). WFhb1-1 plays an important role in resistance against *Fusarium* head blight in wheat. *Scientific Reports*. **10**: 7794 doi: 10.1038/s41598-020-64777-9.
- Peng JH, Sun D, Nevo E. (2011). Domestication evolution, genetics and genomics in wheat. *Molecular Breeding*. **28**: 281-301. doi: 10.1007/s11032-011-9608-4.
- Peters WS, Jensen KH, Stone HA, Knoblauch M. (2021). Plasmodesmata and the problems with size: Interpreting the confusion. *Journal of Plant Physiology*, **257**: 153341. doi: 10.1016/j.jplph.2020.153341.
- Proctor RH, Hohn TM, McCormick SP. (1995). Reduced virulence of *Gibberella zeae* caused by disruption of a trichothecene toxin biosynthetic gene. *Molecular Plant Microbe Interactions*. **8**(4), 593-601. doi: 10.1094/mpmi-8-0593.
- Qu Z, Ren X, Du Z, Hou J, Li Y, Yao Y, An Y. (2024). *Fusarium* mycotoxins: The major food contaminants. *mLife*. **3**(2): 176-206. doi: 10.1002/mlf2.12112.

- Raffan S, Oddy J, Mead A, Barker G, Curtis T, Usher S, Burt C, Halford NG. (2023). Field assessment of genome-edited, low asparagine wheat: Europe's first CRISPR wheat field trial. *Plant Biotechnology Journal*. **21**(6):1097-1099. doi: 10.1111/pbi.14026.
- Rahman MS, Madina MH, Plourde MB, dos Santos KCG, Huang X, Zhang Y, Laliberté J-F, Germain H. (2021). The Fungal Effector Mlp37347 Alters Plasmodesmata Fluxes and Enhances Susceptibility to Pathogen. *Microorganisms*. **9**(6): 1232. doi: 10.3390/microorganisms9061232.
- Rawat N, Pumphrey MO, Liu S, Zhang X, Tiwari VK, Ando K, Trick HN, Bockus WW, Akhunov E, Anderson JA, Gill BS. (2016). Wheat Fhb1 encodes a chimeric lectin with agglutinin domains and a pore-forming toxin-like domain conferring resistance to *Fusarium* head blight. *Nature Genetics*, **48**(12): 1576–1580. doi: 10.1038/ng.3706.
- Ray DK, Mueller ND, West PC, Foley JA. (2013). Yield Trends Are Insufficient to Double Global Crop Production by 2050. *PLoS ONE*. **8**(6): e66428. doi: 10.1371/journal.pone.0066428.
- Rigorth KS, Finckh MR, Šišić A. (2021). First Report of *Fusarium venenatum* Causing Foot and Root Rot of Wheat (*Triticum aestivum*) in Germany. *Plant Disease*. **105**(6): 1855. doi: 10.1094/PDIS-10-20-2202-PDN.
- Rotkina L, Zanini A, Burch-Smith T, Wickramanayake J, Czymmek K. (2024). High-Resolution Volume Electron Microscopy of an Entire Epidermal Plant Cell Using Plasma-Focused Ion Beam Scanning Electron Microscopy. *Microscopy and Microanalysis*. **30**(1): 981-982. doi: 10.1093/mam/ozae044.483.
- Sager RE, Lee JY. (2018). Plasmodesmata at a glance. *Journal of Cell Science*, **131**(11): jcs209346. doi: 10.1242/jcs.209346.
- Sánchez-Vallet A, Fouché S, Fudal I, Hartmann FE, Soyer JL, Tellier A, Croll D. (2018). The genome biology of effector gene evolution in filamentous plant pathogens. *Annual review of phytopathology*, **56**, 21-40. doi: 10.1146/annurev-phyto-080516-035303.
- Sarlin T, Kivioja T, Kalkkinen N, Linder MB, Nakari-Setälä T. (2012). Identification and characterization of gushing-active hydrophobins from *Fusarium graminearum* and related species. *Journal of Basic Microbiology*. **52**(2): 184-194. doi: 10.1002/jobm.201100053.
- Savary S, Willocquet L, Pethybridge SJ, Esker P, McRoberts N, Nelson A. (2019). The global burden of pathogens and pests on major food crops. *Nature Ecology and Evolution*. **3**: 430–439 doi: 10.1038/s41559-018-0793-y.
- Shewry PR. (2009). Wheat. *Journal of Experimental Botany*. **60**(6): 1537-1553. doi: 10.1093/jxb/erp058.
- Shewry PR, Hey SJ. (2015). The contribution of wheat to human diet and health. *Food and Energy Security*. **4**(3):178-202. doi: 10.1002/fes3.64.
- Shinya T, Motoyama N, Ikeda A, Wada M, Kamiya K, Hayafune M, Kaku H, Shibuya N. (2012). Functional Characterization of CEBiP and CERK1 Homologs in Arabidopsis and Rice Reveals

- the Presence of Different Chitin Receptor Systems in Plants. *Plant and Cell Physiology*. **53**(10): 1696–1706. doi: 10.1093/pcp/pcs113.
- Steinberg G. (2007). Hyphal growth: a tale of motors, lipids, and the Spitzenkörper. *Eukaryotic Cell*. **6**(3): 351-360. doi: 10.1128/EC.00381-06.
- Su Z, Bernado A, Tian B, Chen H, Wang S, Ma H, Cai S, Lui D, Zhang D, Li T. (2019). A deletion mutation in TaHRC confers Fhb1 resistance to *Fusarium* head blight in wheat. *Nature Genetics*, **51**: 1099-1105. doi: 10.1038/s41588-019-0425-8.
- Talas F, McDonald BA. (2015). Genome-wide analysis of *Fusarium graminearum* field populations reveals hotspots of recombination. *BMC Genomics*. **16**: 996. doi: 10.1186/s12864-015-2166-0.
- Tee EE, Faulkner C. (2024). Plasmodesmata and intercellular molecular traffic control. *New Phytologist*. **243**(1): 32-47. doi: 10.1111/nph.19666.
- Tee EE, Faulkner C. (2024). Plasmodesmata and intercellular molecular traffic control. *New Phytologist*. **243**(1): 32-47. doi: 10.1111/nph.19666.
- Tembo B, Mulenga RM, Sichilima S, M'siska KK, Mwale M, Chikoti PC, Singh PK, He X, Pedley KF, Peterson GL, Singh RP, Braun HJ. (2020). Detection and characterization of fungus (*Magnaporthe oryzae* pathotype *Triticum*) causing wheat blast disease on rain-fed grown wheat (*Triticum aestivum* L.) in Zambia. *PLoS ONE*. **15**(9): e0238724. <https://doi.org/10.1371/journal.pone.0238724>.
- Thomas CL, Bayer EM, Ritzenthaler C, Fernandez-Calvino L, Maule AJ. (2008). Specific targeting of a plasmodesmal protein affecting cell-to-cell communication. *PLoS Biology*. **6**(1): e7. doi: 10.1371/journal.pbio.0060007.
- Tilsner J, Nicolas W, Rosado A, Bayer EM. (2016). Staying Tight: Plasmodesmal Membrane Contact Sites and the Control of Cell-to-Cell Connectivity in Plants. *Annual review of plant biology*, **67**: 337–364. doi: 10.1146/annurev-arplant-043015-111840.
- Torriani SFF, Melichar JPE, Mills C, Pain N, Sierotzki H, Courbot M. (2015). *Zymoseptoria tritici*: A major threat to wheat production, integrated approaches to control. *Fungal Genetics and Biology*. **79**: 8-12. doi: 10.1016/j.fgb.2015.04.010.
- Trail F, Common R. (2000) Perithecial development by *Gibberella zeae*: a light microscopy study. *Mycologia*, **92**: 130–138. doi: 10.1080/00275514.2000.12061137.
- Trinci APJ. (1992). Myco-protein: A twenty-year overnight success story. *Mycological Research*. **96**(1): 1–13. doi: 10.1016/S0953-7562(09)80989-1.
- United Nations, Department of Economic and Social Affairs, Population Division (2017). World Population Prospects 2017 – Data Booklet (ST/ESA/SER.A/401). [Available online, https://www.un.org/development/desa/pd/sites/www.un.org.development.desa.pd/files/files/documents/2020/Jan/un_2017_world_population_prospects-2017_revision_databooklet.pdf, accessed 31st July 2024].

- Urban M, Mott E, Farley T, Hammond-Kosack K. (2003). The *Fusarium graminearum* MAP1 gene is essential for pathogenicity and development of perithecia. *Molecular Plant Pathology*. **4**(5): 347-359. doi: 10.1046/j.1364-3703.2003.00183.x.
- Vaughan M, Backhouse D, Del Ponte EM. (2016). Climate change impacts on the ecology of *Fusarium graminearum* species complex and susceptibility of wheat to Fusarium head blight: a review. *World Mycotoxin Journal*. **9**(5): 685-700. doi: 10.3920/WMJ2016.2053
- Vu MH, Hyun TK, Bahk S, Jo Y, Kumar R, Thiruppathi D, Iswanto ABB, Chung WS, Shelake RM, Kim JY. (2023). ROS-mediated plasmodesmal regulation requires a network of an Arabidopsis receptor-like kinase, calmodulin-like proteins, and callose synthases. *Frontiers in Plant Science*. **13**: 1107224. doi: 10.3389/fpls.2022.1107224.
- Waalwijk C, Taga M, Zheng S, Proctor RH, Vaughan MM, O'Donnell K. (2018). Karyotype evolution in *Fusarium*. *IMA Fungus*. **9**(1): 13-26. doi: 10.5598/imafungus.2018.09.01.02.
- Wang X, Zhai T, Zhang X, Tang C, Zhuang R, Zhao H, Xu Q, Cheng Y, Wang J, Duplessis S, Kang Z, Wang X. (2021). Two stripe rust effectors impair wheat resistance by suppressing import of host Fe-S protein into chloroplasts. *Plant Physiology*, **187**(4): 2530-2543. doi: 10.1093/plphys/kiab434.
- Ward TJ, Clear RM, Rooney AP, O'Donnell K, Gaba D, Patrick S, Starkey DE, Gilbert J, Geiser DM, Nowicki TW. (2008). An adaptive evolutionary shift in *Fusarium* head blight pathogen populations is driving the rapid spread of more toxigenic *Fusarium graminearum* in North America. *Fungal Genetics and Biology*. **45**(4): 473-484. doi: 10.1016/j.fgb.2007.10.003.
- Wilson RA, McDowell JM. (2022). Recent advances in understanding of fungal and oomycete effectors. *Current Opinion in Plant Biology*. **68**: 102228. doi: 10.1016/j.pbi.2022.102228.
- Wingen LU, Orford S, Goram R, Leverington-Waite M, Bilham L, Patsiou TS, Ambrose M, Dicks J, Griffiths S. (2014). Establishing the A. E. Watkins landrace cultivar collection as a resource for systematic gene discovery in bread wheat. *Theoretical and applied genetics*. **127**(8): 1831–1842. doi: 10.1007/s00122-014-2344-5.
- World Bank (2024). <https://www.worldbank.org/en/topic/agriculture/brief/food-security-update/what-is-food-security>
- Wu F, Chi Y, Jiang Z. *et al.* (2020). Hydrogen peroxide sensor HPCA1 is an LRR receptor kinase in *Arabidopsis*. *Nature*. **578**: 577–581. doi: 10.1038/s41586-020-2032-3.
- Xu Q, Tang C, Wang X, Sun S, Zhao J, Kang Z, Wang, X. (2019). An effector protein of the wheat stripe rust fungus targets chloroplasts and suppresses chloroplast function. *Nature Communications*, **10**: 5571. doi: 10.1038/s41467-019-13487-6.
- Yin Y, Liu X, Li B, Ma Z. (2009). Characterization of Sterol Demethylation Inhibitor-Resistant Isolates of *Fusarium asiaticum* and *F. graminearum* Collected from Wheat in China. **99**(5): 472-631. doi: 10.1094/PHYTO-99-5-0487.

Chapter 2: General materials and methods

The materials and methods outlined in this chapter are used throughout this thesis. Any amendments to, or deviations from, these materials and methods will be detailed in the relevant chapters, as well as specific materials and methods not used in more than one chapter.

2.1 Acknowledgement of contributions

Unless otherwise referenced, I would like to thank all the members of Fusarium group within the larger Wheat Pathogenomics team at Rothamsted Research for their continued development of protocols for *Fusarium graminearum* growth, culturing *in vitro* and plant infection assays. In particular, I would like to thank Martin Urban for his long-standing contributions to the Fusarium Team, Martin Darino, Erika Kroll, Claire Kanja and Rey Dharma for molecular biology support and discussions. I would also like to thank Kirstie Halsey and Hannah Walpole from the bioimaging department for their advice and development of protocols for sample preparation and imaging. We also thank Harold Bockelman, the curator of the National Small Grains Collection, USDA-ARS, for providing seed for the space and time saving dwarf spring wheat variety 'Apogee' to Rothamsted Research.

2.2 Media and chemicals

2.2.1 Plant growth media

For the germination of *Arabidopsis thaliana* seed, $\frac{1}{2}$ Murashige and Skoog (MS) agar was prepared. For 1000ml, 1.1g MS basal salts were added to 1000ml dH₂O with stir bar and stirred until dissolved. The pH of the media was adjusted to pH 5.7 with 1M KOH and media aliquoted into Duran flasks for autoclaving with 1% (w/v) Agar Agar (VWR, UK) added to each.

2.2.2 Fungal growth media

Fungal cultures were grown either in liquid broth or on agar media per experimental requirements. Components of media used throughout this thesis are detailed in Table 2.2.1.

2.2.3 Fungal strains

The *Fusarium graminearum* strain PH-1 was used as the reference throughout this project. This strain is unanimously used throughout global *Fusarium* community as the reference strain and its chromosome-scale genome (version 5) is well annotated and available at <https://www.ebi.ac.uk/ena/browser/view/PRJEB5475> (King, Urban and Hammond-Kosack, 2017).

Table 2.2.1. Fungal growth media components. When converting a broth to agar, 1% w/v Agar No. 1 (Formedium, UK) is added prior to autoclaving.

Medium (broth/agar)	Components
Luria-Bertani (LB)	<i>Per litre:</i> 10 g Peptone, 5 g Yeast Extract, 5 g NaCl
Yeast Peptone Dextrose (YPD)	<i>Per litre:</i> 10 g Yeast Extract, 20 g Bacto peptone, 20 g Dextrose
Potato Dextrose (PD)	<i>Per litre:</i> 20 g dextrose, 4 g Potato infusion
Synthetic Nutrient Poor Agar (SNA)	0.1% KH ₂ PO ₄ , 0.1% KNO ₃ , 0.1%MgSO ₄ ·7H ₂ O, 0.05% KCl, 0.02% Glucose, 0.02% Saccharose, 2% Bacto Agar
Carrot agar	<i>For 400ml:</i> 200 g freshly purchased carrots diced into ~2cm ³ cubes, 200 ml dH ₂ O, 4 g Agar

2.3 Molecular protocols

2.3.1 DNA extraction

Genomic DNA was either extracted using the DNeasy DNA extraction kit as per the manufacturer's instructions (NEB, USA), or extracted using the CTAB DNA extraction protocol for *F. graminearum* cultures.

For DNA preparations from *F. graminearum*, conidia of desired strain were inoculated into 20ml PDB liquid culture in a 50ml falcon tube and incubated for 2 days at 28°C with agitation at 150rpm. Hyphae were then filtrated through 2 layers of miracloth under mild vacuum and the mycelial pad was then flash frozen in LN₂, ground to a fine powder in a sterile pestle and mortar in the presence of LN₂ and transferred to a 2ml microcentrifuge tube. To this, 750µl of CTAB lysis buffer (Table 2.3.2) amended with 5µl β-mercaptoethanol was added, and mixed by inversion to avoid shearing DNA. The microcentrifuge tube is then incubated in a water bath at 65°C for 30 mins, with inversion every 10 mins, and subsequently cooled down on ice. Subsequently, 500µl chloroform:isomyl (24:1) is added, gently mixed on a shaking platform for 15 mins and centrifuged for 5 mins in a tabletop centrifuge at 13.2k rpm. Upper aqueous DNA phase is removed and transferred into a fresh 2ml microcentrifuge tube and 1 volume 2-propanol (or 2 volumes ethanol) added. DNA is then precipitated by centrifugation at 13.2k rpm for 30 mins, supernatant is removed, and pellet is resuspended in 100µl TE buffer. Eluted DNA concentration is measure on a NanoDrop™ 2000 Spectrophotometer (ThermoFisher Scientific, MA, USA).

2.3.2 RNA extraction

Total RNA was extracted from biological samples of either fungal or plant origin using the Monarch® Total RNA Miniprep Kit (New England Biolabs, MA, USA) according to kit instructions. Briefly, LN₂ frozen tissue samples were ground to a fine powder in the presence of LN₂ and 800µl DNA/RNA protection solution, transferred to an RNase-free microcentrifuge tube and spun at 13.1k rpm (16,000g x g) in a centrifuge to pellet debris. Then, 800µl of RNA lysis buffer was added, the solution homogenised by vortexing, and transferred to a gDNA

removal column in two stages, spinning for 30s each time to bind the gDNA to the column. An equal volume of ethanol was added to the flow-through, mixed by pipetting and transferred to an RNA purification column, spun for 30s and flow-through discarded. A 500µl aliquot of an RNA wash buffer was added to wash each column, spun, and the optional DNase I treatment conducted (5 µl DNase I with 75 µl DNaseI reaction buffer) with 15 min incubation. Subsequently, 500µl RNA priming buffer was added, spun, and another 500µl RNA wash buffer before spinning again for 30 secs. A final 500µl RNA wash buffer was added to the column matrix and spun for 2 minutes to ensure sufficient drying and then RNA was eluted into 50µl dH₂O, recovering with a 30s spin into a fresh RNase-free microcentrifuge tube. Total RNA yield was measured on a NanoDrop™ 2000 Spectrophotometer (ThermoFisher Scientific, MA, USA).

2.3.3 cDNA synthesis

First strand cDNA was synthesised using RevertAid First Strand cDNA synthesis kit (Cat.K1621, Thermo Fisher Scientific, MA, USA) as per kit instructions and utilising random hexamer primers provided. Briefly, reverse transcription from RNA occurred at 42°C for 60 mins by RevertAid Reverse Transcriptase, in the presence of RiboLock RNase inhibitor and dNTPs in a reaction buffer, in a PCR machine (T100 Thermal Cycler, BioRad). Lid temperature was set to 105°C to prevent condensation of reaction.

2.3.4 Polymerase Chain Reaction (PCR)

Primers for PCR amplification were designed using geneious (version 10.2.3; www.geneious.com) from the *F. graminearum* genome version 5 (King, Urban and Hammond-Kosack, 20170). All primers used in this project were synthesised by Eurofins Genomics (UK) and obtained lyophilised and salt-free. Primers for Gibson assembly were designed and tested for specificity using the open-source tool NEBuilder (www.nebuilder.neb.com). Table 2.3.1 provides the list of primers used in this study.

Table 2.3.1. Primers used throughout this study.

Name	Forward Primer	Reverse Primer	Use
CDC48	GTCCTCCTGGCTGTGGTAAAAC	AGCAGCTCAGGTCCCTTGATAC	Housekeeping gene for wheat.
FgActin	ATGGTGTCACCTCACGTTGTCC	CAGTGGTGGAGAAGGTGTAACC	RNA expression by qPCR of cDNA; Housekeeping gene for <i>F. graminearum</i> .
TRI5	TCCGTAGCACTATGGACTTTTT	TAGGATGGGCTTCTGAGCCT	RNA expression by qPCR of cDNA.
HYG	TATGGTCTCAAGTCGCTGCAGGAATTCGA	TATGGTCTCAACTCTATTCCTTGC	Verification of hygromycin presence in single gene deletion knock outs.

2.3.5 Gel Electrophoresis

For the assessment of PCR products, gel electrophoresis was employed to separate fragments and determine size. For all gels, agarose (Formedium, UK) was dissolved at a concentration of 1% (w/v) in 1x TBE buffer (89mM Tris, 89mM boric acid, 2mM EDTA) and heated to boiling until dissolved. Once cooled to approximately 50°C, 3ul of ethidium bromide (5µg/ml) was added per 100ml agarose solution. Gels were cast with appropriate combs for the number of samples and once set transferred to a BioRad Mini-Sub Cell GT chamber filled with 1xTBE buffer. DNA samples were mixed with 6X loading dye (Promega, UK) by pipetting and loaded into gel wells. Samples were run at 75-100V for 30-60 mins depending on predicted band size, or until the loading dye had reached the end of the gel.

2.3.6 DNA quantification by qPCR

Sampled tissues of wheat infected with *F. graminearum* were disrupted by pestle and mortar in the presence of LN₂. Total gDNA was then extracted using the DNeasy Plant Mini Kit (Qiagen, Manchester, UK) according to kit instructions and concentrations analysed on a NanoDrop™ 2000 Spectrophotometer (ThermoFisher Scientific, MA, USA). For qPCR, each sample well contained 20ng gDNA. SYBR Green was used as the reporter, the passive reference was ROX, and the quencher was NFQ-MGB. The qPCR was conducted on a QuantStudio™ 6 Pro and results analysed on the complementary Design & Analysis Software v. 2.6.0 (ThermoFisher Scientific, MA, USA). A standard curve ranging from 0.01-100 ng gDNA was included in each qPCR run for respective housekeeping genes. No template controls (dH₂O) were also included in each qPCR run. For qPCR, a reaction volume of 20µl was used with 40 cycles of a 95°C hold followed by 1.6°C/S cooling to 60°C and completed with a melt curve. Three technical replicates of each biological replicate were completed for each experiment. Outliers or erroneous results were omitted through melt curve analysis. Primer efficiency was tested prior to qPCR testing on samples in order to optimise primer concentration.

Table 2.3.2. Buffer and media components

Buffer	Components
Extraction buffers	
DNA extraction buffer 'shorty'	0.2 M Tris-HCl (pH 9.0), 0.4 M LiCl, 25mM EDTA, 1% SDS
CTAB lysis buffer	<i>For 500ml:</i> CTAB 10g, TRISMA base 6.06g, EDTA 1.46g, NaCl 20.5g
TE buffer	10 mM Tris (pH 8.0), 1 mM EDTA
Sample preparation for bioimaging	
PBS buffer (10x stock)	1.37 M NaCl, 27 mM KCl, 100 mM Na ₂ HPO ₄ and 18 mM KH ₂ PO ₄
Sorensen's phosphate buffer (0.1 M)	NaH ₂ PO ₄ :Na ₂ HPO ₄ , adjusted to pH 7.2
Blocking buffer	3% (w/v) dried skimmed milk powder in 1x PBS

2.4 Bioassays

2.4.1 Fungal growth

All *Fusarium graminearum* strains used in this thesis are detailed in the relevant chapters, including the generation method if appropriate. For all experiments, the reference strain is PH-1 (NCBI: txid229533), for which an annotated genome (v. 5.0) is now available (King, Urban and Hammond-Kosack, 2017). Experiments were conducted under APHA plant licence number 101948/198285/6.

Conidia for glycerol stocks were prepared by culturing on Synthetic Nutrient Poor Agar (SNA) plates containing 0.1% KH_2PO_4 , 0.1% KNO_3 , 0.1% $\text{MgSO}_4 \cdot 7\text{H}_2\text{O}$, 0.05% KCl, 0.02% glucose, 0.02% sucrose and 2% agar (Table 2.2.1). Plates were left to grow for 8 days at RT with constant illumination under near-UV light (Philips TLD 36W/08). TB3 liquid medium (0.3% yeast extract, 0.3% Bacto Peptone and 20% sucrose) was added to plates to stimulate spore production and left for a further 2 days. Conidia were harvested and stored in 15% glycerol at -80°C in 2 ml cryotubes (Thermo Fisher Scientific, MA, USA).

Conidia for water inoculum were prepared by spreading conidia from glycerol stocks onto Potato Dextrose Agar (PDA, Sigma Aldrich, UK) plates and placed at RT for 2 days under constant illumination under near-UV light (Philips TLD 36W/08). Spores were harvested with sterile dH_2O and the concentration measured with the aid of a haemocytometer (Hausser Bright-line, USA). Typically, water inoculum was diluted to infection concentrations prior to storage. Water stocks were not kept for more than 4 months and were always stored at -80°C to ensure high spore viability.

2.4.2 Wheat growth

For all experiments, the dwarf spring wheat (*Triticum aestivum*) cultivar (cv.) 'Apogee' (Bugbee, 1999) was grown, sourced from the National Small Grains Collection, USDA-ARS, Aberdeen, Idaho, USA. This cultivar was selected for its fast growth, small and compact stature, and susceptibility to infection by the filamentous fungal pathogen *Fusarium graminearum*.

Apogee grain was sown in Rothamsted Prescription Mix (RPM) soil (Petersfield Growing Mediums, UK) in P15 pots (approx. volume 7cm³) and grown in controlled environment facilities at HSE category 2 (Fitotron®, Weiss Gallenkamp, UK), 16hr light: 8hr dark cycle at 22°C and 18°C respectively, 70% relative humidity and illumination at 2.2x10³ μmol m⁻³.

2.4.3 Arabidopsis growth

Arabidopsis thaliana (ecotype) Col-0 was used as the WT reference for all experiments. Seed were surface sterilised with 500μl of a fresh solution of 50:50 ratio of dH₂O and thin bleach (4.5% (v/v) sodium hypochlorite) in 2ml microcentrifuge tubes for 10 mins. Following this, a serial wash dilution was conducted, pipetting off 450μl sterilisation solution after seed had sunk (~1 min) and replacing with 1000μl dH₂O. Following this, the serial wash was repeated 4 times.

Seed was transplanted onto ½ Murashige-Skoog (MS) 1% agar ([section 2.2.1](#); Table 2.3.3) square petri plates (VWR, UK) using sterile toothpicks and stratified at 4°C in the dark for 2 days. Plates were then placed in a growth cabinet at 16 hour light: 8 hour dark, 22°C and 18°C respectively, 70% humidity and 140μmol m⁻² s⁻¹ light intensity. Plates were left to germinate for 7 days after which seedlings were transferred using surface sterilised (70% EtOH) tweezers to P15 pots filled compactly with Levington's F2+S soil and placed into a tray lined with capillary matting. Pots were always watered from below and for the first 14 days after transplantation a humidity lid was kept over the tray with vents closed to promote seedling establishment, after which *Arabidopsis thaliana* plants were left until fluorescence emergence.

2.4.4 Wheat coleoptile inoculations

Apogee grain was first stratified in dH₂O for 48 hrs at 5°C promote even germination. Grain was then placed onto wet cotton wool in a 24-well plate (CELLSTAR® 24 Well Cell Culture Multiwell Plate, Greiner Bio-One Ltd, UK) and left to germinate for 3 days. At 3 days, approximately 5 mm of the top of the coleoptile was cut with sterile scissors. Inoculations were conducted through the soaking of 1cm² filter paper with *F. graminearum* spores at 5x10⁵ spores/ml or

dH₂O as a negative control (Whatman® Qualitative Filter Papers, Grade 4, Sigma Aldrich) and then a cut 20µl pipette tip was placed on top of each cut coleoptile. Coleoptiles were subsequently left in the dark for 3 days to aid infection in a high humidity chamber (<90% RH), after which inoculation tips were subsequently removed, and coleoptiles were left to grow under normal growth conditions for a further 4 days (Darino et al., 2024). Disease phenotypes on the coleoptiles were assessed at 7 days post inoculation by imaging lesions on a Leica M205 FA Stereomicroscope (Leica Microsystems, UK). Each experimental replicate contained 5 biological samples for each treatment (3 mock-inoculated) and the experiment was repeated 3 times.

2.4.5 Wheat spike inoculations

At mid-anthesis, wheat plants were inoculated with 5×10^5 spores/ml water conidial suspension. As described in Lemmens et al. (2005) a 5µl droplet was placed between the palea and the lemma on each side of the 7th true (fertile) spikelet from the base. Inoculated plants were placed in a high (<90%) humidity for the first 72 hours of infection, with the first 24 hours in darkness. After 72 hours plants were returned to normal growth conditions ([2.4.2](#)).

2.4.6 Assessment of Disease Progression

As above, Apogee at mid-anthesis was inoculated and disease progression was assessed by counting spikelets showing visible symptoms every 2 days after inoculation until 14 dpi. As the 7th true (fertile) spikelet from the base was inoculated, 100% progression is deemed to be the 7 spikelets below the point of inoculation exhibiting complete symptoms. A score of 0.5 is assigned to spikelets whereby only the floral tissues of glume, lemma and palea are demonstrating disease symptoms, but not the rachis. In turn, a score of 1 is assigned where the rachis also exhibits macroscopic symptoms of *F. graminearum* infection.

Area Under Disease Progression Curve (AUDPC) (Van der Plank, 1963) values were calculated using the 'agricolae' package (version 1.4.0, de Mendiburu and Yaseen, 2020) in R (version 4.0.2). Statistical significance was determined by Kruskal-Wallis one-way analysis of variance through the R package 'ggplot2' (version 3.4.0, Wickham, 2016).

2.4.7 Deoxynivalenol (DON) quantification

Samples of either inoculated spikelets or whole wheat ear rachis internodes were flash frozen in LN₂ and ground to a fine powder using a mortar and pestle. For analysis, one gram of each sample was re-suspended in 5ml dH₂O and vortex until dissolved. The solution was then incubated in a water bath for 30 mins at 30°C and centrifuged for 15 mins at full speed (13.1krpm) at 30°C on a tabletop centrifuge. The supernatant was removed by pipette and the DON fraction taken forward for analysis.

The Beacon Analytical Systems Inc. Deoxynivalenol (DON) Plate Kit (Cat. 20-0016) was utilised for 15-ADON quantification by competitive enzyme-labelled immunoassay. Methodology for DON quantification followed the kit instructions provided. According to test instructions, a standard curve was utilised ranging from 0.1 to 5 ppm. The OD450 values were measured after a 5 min incubation at RT on a Thermo Varioskan Microplate reader (Thermo Fisher Scientific, UK). Three technical replicates of each biological replicate were conducted and the average taken as the final value after being reviewed for outliers.

2.4.8 DNA quantification by quantitative real time PCR (qRT-PCR)

Relative biomass of wheat and *F. graminearum* was determined by qPCR as outlined in [section 2.3.6](#). Housekeeping genes for wheat and *F. graminearum* were CDC48 (a cytosolic ATPase) and FgActin (a component of cell cytoskeleton) and were used at primers concentrations of at 400 nm and 200 nm respectively, as previously determined by qPCR reaction efficiency calculations (Table 2.4). Relative gDNA of wheat and *Fusarium* biomass was calculated from technical replicate average C_q values using the standard curve formulas for CDC48 and FgActin respectively. Fungal burden was calculated as the ratio of fungal genomic DNA (gDNA) to wheat gDNA.

2.5 Bioimaging

2.5.1 Photography

All images of plants and fungal plates were photographed under constant white light illumination against a black velvet background using an Olympus E-M10-Mark IV mirrorless digital camera (Olympus, Tokyo, Japan) and stored as TIFF image files for analysis.

2.5.2 Sample fixation and resin embedding

Samples were fixed in a 4% paraformaldehyde, 2.5% glutaraldehyde solution with 0.05M Sorensen's phosphate buffer ($\text{NaH}_2\text{PO}_4:\text{Na}_2\text{HPO}_4$, pH 7.0) and subsequently washed 3 x in 0.05M Sorensen's phosphate buffer for a minimum of 30 minutes per wash to remove fixative solution. Spikelets were dissected into constituent components of palea, lemma and rachis tissues for following preparations. Tissues underwent an ethanol dehydration (10-70%, 1 hour at each 10% interval; 70-100% had two dehydrations per 10% interval for minimum 1 hour each) and infiltrated with LR white resin (TAAB, UK) diluted with dry ethanol (100% EtOH) at increasing ratios (1:4, 2:3, 3:2, 4:1, 100%) for a minimum of 2 hours each. Samples were inserted into capsules (TAAB, UK) with fresh LR white resin and polymerised at 60°C for 16 hours in a TAAB nitrogen oven. Samples in polymerised resin were then stored at RT.

2.5.3 Sectioning of resin samples for light microscopy

Samples embedded within resins were shaped with razor blades and ultra-thin 1 μm sections cut on an ultramicrotome (Reichert-Jung, Ultracut) with freshly made glass knives from Superglass (TAAB, UK). Resin slices were placed onto glass polysine slides (Sigma Aldrich, UK) and left to dry on a hot plate at 70°C for standard light microscopy and 35°C for immuno-labelling.

Resin sections for light microscopy were stained with 0.1% (w/v) Toluidine Blue O and mounted with Permount mounting medium (Thermo Fisher Scientific, UK). Samples were imaged on a Zeiss Axioimager (AxioCam 512 color, Zeiss, Jena, Germany) light microscope with BF illumination.

2.5.4 Immuno-labelling of callose deposits at plasmodesmata

For immuno-labelling of callose deposits at plasmodesmata, the methods previously described by Amsbury and Benitez-Alfonso (2022) were used. Briefly, ultrathin 1 μ m LR White-embedded samples were blocked with 3% (w/v) dried milk powder in PBS (Table 2.3.2) and subsequently washed twice with PBS to remove residual blocking solution. Callose monoclonal antibody (β -1,3-glucan) (Cat. 400-2, Biosupplies, Australia) was diluted 1:80 in blocking solution and the resin sections incubated overnight at 4°C in a dark humidity box. Samples were then washed 4 times with PBS prior to incubation with the secondary antibody Alexafluor-488 goat anti-mouse (Invitrogen, Thermo Fisher Scientific) diluted 1:100 in blocking solution for 2 hrs at RT. Again, samples were washed 4 times in PBS and plant cell walls counterstained with 0.25% (w/v) calcofluor white (Sigma Aldrich, UK) in dH₂O for 10 mins, and washed 4 times in PBS again before imaging by confocal microscopy.

For visualisation of alexafluor-488-labelled callose deposits, excitation-emission spectra of 488 nm - 525 nm were used respectively, and for calcofluor counterstained wheat cell walls, excitation-emission of 405 nm - 475 nm were used. All images were captured on as Stellaris FALCON Confocal microscope (Leica Microsystems, Milton Keynes, UK) and processed using Las X office software (version, 1.4.4., Leica Microsystems, Milton Keynes, UK).

2.6 Statistics

2.6.1 R scripts

Unless otherwise stated, all statistics were conducted on custom R scripts for individual experiments (R studio version 2023.03.1+446). Packages and statistical methods are detailed with individual experiments. Graphs are plotted using the ggplot2 package (Wickham, 2016).

2.7 References

Amsbury S, Benitez-Alfonso Y. (2022). Immunofluorescence Detection of Callose in Plant Tissue Sections. *Methods in Molecular Biology*, 2457: 167-176. doi: 10.1007/978-1-0716-2132-5_10

- Armer VJ, Deeks MJ, Hammond-Kosack KE. (2024a). *Arabidopsis thaliana* detached leaf assay for the disease assessment of *Fusarium graminearum* infection. *Protocols.io*. doi: 10.17504/protocols.io.261gedmwov47/v1.
- Bugbee B, Koerner G, Albrechtsen R, Dewey W, Clawson S. (1999). 'USU-Apogee' Wheat - Registration. *Dwarf Crops*. Paper 11. https://digitalcommons.usu.edu/cpl_dwarfcrops/11. [Accessed 16/05/2024].
- Darino M, Urban M, Kaur N, Machado-Wood A, Grimwade-Mann M, Smith D, Beacham A, Hammond-Kosack K. (2024). Identification and functional characterisation of a locus for target site integration in *Fusarium graminearum*. *Fungal Biology and Biotechnology*. **11**: 2. doi: 10.1186/s40694-024-00171-8.
- de Mendiburu F and Yaseen M. (2023). agricolae: Statistical Procedures for Agricultural Research. R package version 1.3-7.
- King R, Urban M, Hammond-Kosack KE (2017). Annotation of *Fusarium graminearum* (PH-1) Version 5.0. *Genome Announcements*, 5: e01479-16. doi: 10.1128/genomeA.01479-16
- King R, Urban M, Lauder RP, Hawkins N, Evans M, Plummer A, Halsey K, Lovegrove A, Hammond-Kosack KE, Rudd JJ. (2017). A conserved fungal glycosyltransferase facilitates pathogenesis of plants by enabling hyphal growth on solid surfaces. *PLOS Pathogens*. 13(10): e1006672. doi: 10.1371/journal.ppat.1006672
- Lemmens M, Scholz U, Berthiller F, Dall'asta C, Koutnik A, Schuhmacher R, Adam G, Buerstmayr H, Mesterházy A, Krska R, Ruckebauer P. (2005). The ability to detoxify the mycotoxin deoxynivalenol colocalizes with a major quantitative trait locus for *Fusarium* head blight resistance in wheat. *Molecular Plant Microbe Interactions*, 18: 1318-24. doi: 10.1094/MPMI-18-1318.
- Van Der Plank JE. (1963). *Plant diseases: epidemics and control*. Academic Press, New York.
- Wickham H. (2016). *ggplot2: Elegant Graphics for Data Analysis*. Springer-Verlag, New York.

Chapter 3: The role of trichothecene mycotoxins in cell-to-cell invasion

3.1 Acknowledgement of contributions

I would like to thank Martin Urban (Rothamsted Research) for the original generation of the $\Delta Tri5$ mutant, which was published in Cuzick, Urban and Hammond-Kosack (2008). We also thank Tom Ashfield at CHAP (Harpenden) for training and access to the Lemnagrid image analysis software. Many thanks also go to Anjana Magaji-Umashankar for help with TEM imaging. The majority of this work contributed to a publication entitled 'The trichothecene mycotoxin deoxynivalenol facilitates cell-to-cell invasion during wheat-tissue colonisation by *Fusarium graminearum*', published in the journal Molecular Plant Pathology (Armer et al., 2024). A copy of this is included in Appendix 2.

3.2 Introduction

Fusarium graminearum secretes mycotoxins during host-tissue colonisation of small grain cereals, which, as previously discussed, is one of the major causes of economic losses by the pathogen (McMullen et al., 1997) due to their rendering of the grain unsuitable for human or livestock consumption (McMullen et al., 2012). The sesquiterpenoid type B toxins of the trichothecene class are particularly potent and include deoxynivalenol (DON), nivalenol (NIV), zearalenone (ZEA), and T-2 toxin (reviewed McCormick et al., 2011), all of which target ribosomes and inhibit protein synthesis (Brown et al., 2004). The experiments outlined in this chapter set out to understand the role of trichothecene mycotoxins during host-tissue colonisation of wheat floral tissues by re-evaluating the $\Delta Tri5$ single gene deletion knock out, which renders *F. graminearum* unable to synthesise trichothecene mycotoxins including DON (Proctor et al., 1995).

F. graminearum has been noted to have a 'biphasic' lifestyle, whereby the advancing infection front is split between macroscopically symptomatic and symptomless phases (Fig. 3.2.1(a); Brown et al., 2011). The symptomless phase is hallmarked by apoplastic growth, and then switches to the symptomatic phase

characterised by extensive intracellular growth. What initiates this switch is not yet known and is a subject of great interest.

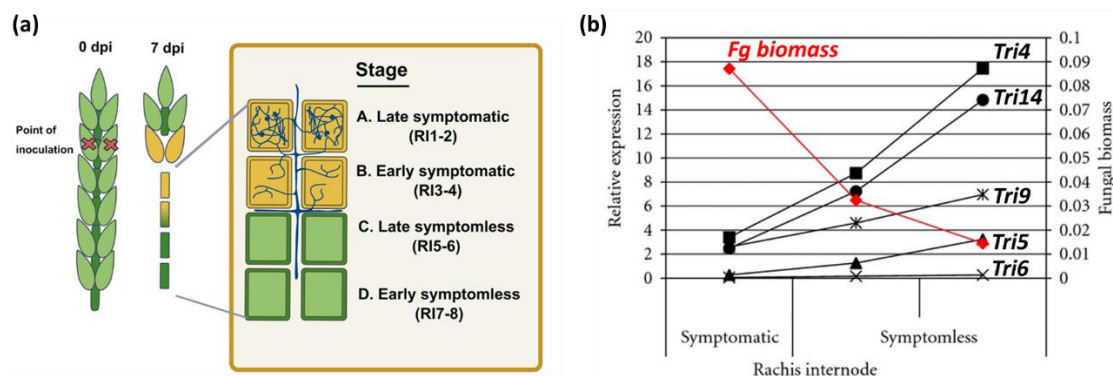


Fig. 3.2.1. *TRI* gene expression is highest during the symptomless phase of infection. (a) The symptomless and symptomatic phases of *Fg* infection (adapted from Kroll et al., 2024) and (b) Relative expression of selected *TRI* cluster genes during different phases of infection and relative *F. graminearum* biomass (adapted from Brown et al., 2011).

During later stages of infection, *F. graminearum* secretes CWDEs in abundance (Brown, Antoniw, and Hammond-Kosack, 2012) to facilitate infection by deconstructing wheat cell walls. At the rachis internode, the structural tissue at the base of the wheat spikelet and the continuum of which forms the basis of the wheat spike, invasive hyphae have been reported to enter vascular elements (Wanjiru et al., 2002). From here they grow through the wheat spike within the vasculature as well as in the cortical tissue surrounding the vascular bundles (Brown et al., 2010). Furthermore, within the chlorenchyma band of the rachis where photosynthesis occurs, *F. graminearum* produces perithecia, sexual reproductive structures, completing its lifecycle (Guenther and Trail, 2005). These aspects are of interest to this study due to the previously reported restriction of the $\Delta Tri5$ strain to inoculated spikelets, as we hypothesised that the absence of DON may impact the ability to digest wheat cell walls and enter the vascular elements.

In the initial symptomless phase of infection, the trichothecene biosynthetic gene cluster (BGC) that synthesise trichothecene mycotoxins such as DON are most upregulated (Fig. 3.2.1(b); Brown et al., 2011), indicating a role for these during fungal establishment in host tissues. Within this cluster, 15 genes are clustered across 3 chromosomal regions (Fig. 3.2.2), but just four (*TRI4*, *TRI6*, *TRI5* and *TRI10*) are required to build the toxic trichothecene skeleton isotrichodermol (Kimura et al., 2007; McCormick et al., 2013).

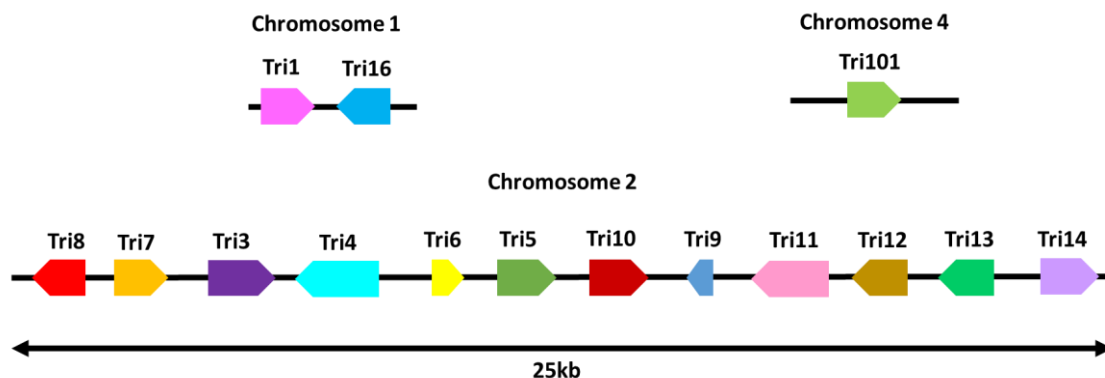


Fig. 3.2.2. The trichothecene mycotoxin biosynthetic cluster. Composed of three parts, residing on chromosome 1, 4 and 2. Genes are schematic only and not to scale. (Adapted from Kimura et al., 2003).

The largest of these clusters, consisting of 12 genes, spans a 25kb region of chromosome 2 (Fig. 3.2.2). *TRI101* is located on chromosome 4 and is responsible for the conversion of isotrichodermol to isotrichodermin, which serves to act as a self-preservation mechanism for trichothecene-producing species by reducing the toxicity of the toxins by the acetylation of the hydroxyl group at C-3 in isotrichodermol (Kimura et al., 1998). *TRI1* AND *TRI16* reside as a pair on chromosome 1 and are a C-8 hydroxylase and acyltransferase respectively (Fig. 3.2.2; Table 3.2.1; Wang et al., 2023), both essential for DON biosynthesis.

Table 3.2.1. Function and mutant phenotypes of *TRI* genes in *Fusarium sporotrichioides*. Adapted from Wang et al. (2023).

Tri Gene	Function	Mutant Phenotype
<i>Tri8</i>	C-3 deacetylase	3-acetyl T-2
<i>Tri7</i>	C-4 acetyltransferase	HT-2
<i>Tri3</i>	C-15 acetyltransferase	15-decalonectrin, 3,15-didecalonectrin
<i>Tri4</i>	multifunctional oxygenase	trichodiene
<i>Tri6</i>	zinc finger transcription factor	low levels of trichodiene
<i>Tri5</i>	trichodiene synthase	no trichothecenes
<i>Tri10</i>	regulatory gene	no trichothecenes
<i>Tri9</i>	unknown	not determined
<i>Tri11</i>	C-15 hydroxylase	isotrichodermin
<i>Tri12</i>	trichothecene efflux pump	no trichothecenes
<i>Tri13</i>	C-4 hydroxylase	8-hydroxycalonectrin, 4-deoxy T-2, 8-hydroxy-3-deacetylcalonectrin

<i>Tri14</i>	virulence factor	T-2
<i>Tri1</i>	C-8 hydroxylase	DAS
<i>Tri16</i>	C-8 acyltransferase	NEO, DAS
<i>Tri101</i>	C-3 acetyltransferase	isotrichodermol

Three genes residing in the *TRI* BGC are not essential for trichothecene biosynthesis: *TRI8*, *TRI3* and *TRI13* (Kimura et al., 2003). *TRI6* and *TRI10* are transcription factors, with a zinc finger binding motif (Hohn et al., 1999) and no known DNA-binding motif (Tag et al., 2001), respectively, but collectively are essential for trichothecene biosynthesis. The *TRI5* gene encodes the enzyme trichothecene synthase (Table 3.2.1; Hohn et al., 1993) which converts farnesyl diphosphate to trichodiene, marking the first committed step in trichothecene mycotoxin biosynthesis (Fig. 3.2.3.).

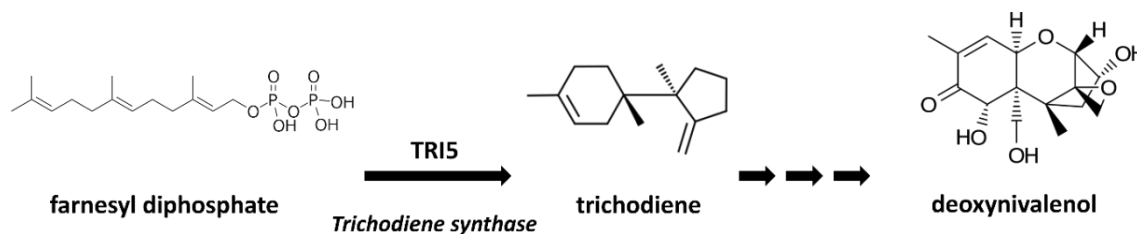


Fig. 3.2.3. Simplified model of the DON biosynthetic pathway. *TRI5* encodes the enzyme trichodiene synthase which catalyses the conversion of farnesyl diphosphate to trichodiene.

DON is a well-reported virulence factor in wheat floral tissues (Proctor et al., 1995; Jansen et al., 2005, Cuzick, Urban and Hammond-Kosack, 2008). It is synthesised and then secreted by *F. graminearum* hyphae during infection and is a potent ribosomal-binding translational inhibitor. Deletion of *TRI5* eliminates the ability of *F. graminearum* to synthesise DON (Proctor et al., 1995), and infection of wheat floral tissues by the single gene deletion mutant ($\Delta Tri5$) is restricted to the inoculated spikelet, and results in the production of eye-shaped lesions on the outer glume (Jansen et al., 2005; Cuzick, Urban and Hammond-Kosack, 2008). This broad-spectrum dampening of induced protein dependent defence responses by WT *F. graminearum* has thus far prevented the elucidation of specific components of host immunity that restrict *F. graminearum* in the DON-deficient interaction. The low molecular weight of trichothecenes and their water-solubility allow them to rapidly enter cells and target eukaryotic ribosomes. This causes what is known as the 'ribotoxic stress response' that can activate, among

other processes, mitogen-activated protein kinases (MAPKs) and apoptosis (reviewed Pestka, 2008). Expression of *TRI5* in wild-type *F. graminearum* is correlated with DON accumulation *in planta* (Hallen-Adams et al., 2011). In non-host pathosystems, such as the model plant species *Arabidopsis thaliana*, infection of floral tissues with the single gene deletion mutant $\Delta Tri5$ causes a wild-type disease phenotype, indicating that DON is not a virulence factor in this interaction (Cuzick, Urban and Hammond-Kosack, 2008). Current evidence indicates that the *TRI4* gene, which encodes a multi-functional cytochrome P450 monooxygenase and resides within the main trichothecene mycotoxin biosynthetic cluster (Tokai et al., 2007), is expressed during the *F. graminearum*--wheat coleoptile interaction (Qui et al., 2019), but the role of *TRI4* or *TRI5* as a virulence factors in coleoptiles has not yet been reported. The TRI4 protein is required for four consecutive oxygenation steps in trichothecene mycotoxin biosynthesis (McCormick, Alexander and Proctor, 2006; Tokai et al., 2007), thus indicating a role for trichothecene mycotoxins during coleoptile infection.

Through the use of fluorescent marker reporter strains, the *TRI5* gene has been shown to be induced during infection structure formation on wheat palea (Boenisch and Schäfer, 2011). However, the absence of *TRI5* in a *F. graminearum* $\Delta Tri5$ -GFP strain did not impact the ability of *F. graminearum* to form infection cushions during initial time points of infection (Boenisch and Schäfer, 2011). The DON mycotoxin naturally occurs as two chemotypes, 15-ADON and 3-ADON, and individual *F. graminearum* strains secrete either toxin type. The wild-type (WT) strain used in this study, PH-1, exclusively synthesises 15-ADON. Host-plant resistance to DON is a characteristic of type II FHB resistance, whereby fungal advancement does not proceed beyond the rachis node (reviewed Mesterházy, 1995). In the $\Delta Tri5$ -wheat interaction, *F. graminearum* fails to traverse beyond the rachis node, indicating that DON is required for this aspect of infection.

Intracellular growth by *F. graminearum* has been previously reported to traverse wheat cell walls through pits, or pit fields, where multiple plasmodesmata (PD) are present (Guenther and Trail, 2005; Jansen et al., 2005; Brown et al., 2010). PD are cytoplasmic communication channels that symplastically bridge the cell walls by an appressed endoplasmic reticulum (ER), known as a desmotubule, within a plasma membrane (PM) continuum stabilised by proteins connected to both the

ER and PM (Sager and Lee, 2018). PD are instrumental to cellular signalling, allowing for the transport of sugars, ions and small proteins, to name a few. However, plants can adjust the permeability of PD by the deposition of callose, mediated by the action of callose synthases and β -1,3-glucanases (Lee and Lu, 2011) at PD junctions. This callose plugging leads to the symplastic isolation of cells that are damaged or under pathogen attack thereby restricting the movement of secreted pathogen effector proteins, toxins and other metabolites. PD have a major role in host plant defence against viruses, bacteria and fungi (Lee and Lu, 2011). *F. graminearum* exploits the plasmodesmatal transit highways by excreting β -1,3-glucanases: enzymes that catalyse the breakdown of the 1,3-O-glycosidic bond between glucose molecules in callose. RNA-seq analysis of *F. graminearum* infection of wheat spikes found that several *Fusarium* β -1,3-glucanases are upregulated in the host plant from as early as 6 hours post-infection and peaking between 36-48 hours after inoculation (Pritsch et al., 2007).

Whilst the macro-biology and some aspects of the cellular biology of the single-gene deletion mutant $\Delta Tri5$ have been previously studied, the mode of restriction of $\Delta Tri5$ remains to be elucidated. Postulations have been made around the role of DON during host-tissue colonisation, specifically relating to the targeting of ribosomes and the subsequent, broad-spectrum, protein translation inhibition (Pestka, 2010). However, what host defence mechanisms are targeted and/or specifically affected by DON have not been explored *in planta*. This study aims to re-evaluate the infection biology of the $\Delta Tri5$ strain, and hence the role(s) of DON, during host-tissue colonisation through a combination of molecular and microscopy techniques. Through qualitative and quantitative image analysis of wheat floral tissues during WT and $\Delta Tri5$ infection, it is reported that the $\Delta Tri5$ single gene deletion mutant has an impaired ability to traverse PD. We also find no evidence to support the hypothesis that a general increase in plant cell wall thickening occurs in the absence of DON production, whereby the upregulation of cell wall defences occurs during pathogen attack (reviewed Ishida and Noutoshi, 2022). From the data gathered, we infer that the secretion of DON during host-tissue colonisation is highly specific both spatially and temporally. This is indicated by the lack of increase in virulence in the $\Delta Tri5$ mutant when supplied with DON at the point of inoculation in our study. In light of these

discoveries, we pose new questions surrounding *F. graminearum* infection biology, cell wall colonisation and wheat host defence mechanisms.

3.3 Materials and Methods

The methods outlined here are in addition to those detailed in the [general materials and methods chapter](#).

3.3.1 Determination of DON concentration for exogenous application

To determine the suitable concentration of DON for inoculum supplementation, a pilot experiment was conducted to demonstrate a lack of toxicity to *F. graminearum* at various concentrations ranging from 0.5 - 10 times concentrations used *in planta*. For this, 1.5ml microcentrifuge tubes containing 1ml YPD (Formedium Ltd, UK) were inoculated to a concentration of 5×10^4 spores/ml and incubated at 28°C for 24 hours with rotation at 180 rpm. Hyphal growth was measured at 6, 12, 18 and 24 hours after inoculation by light microscopy and analysed on Fiji image processing software (v. 2.3.0) (Schindelin et al., 2012). Concentrations up to 350ppm were non-detrimental to fungal proliferation in media.

Due to the inability to easily detect deoxynivalenol (DON; chemotype 15-ADON) in plant tissues once glycosylation has occurred, and the lack of macroscopic necrosis observed in wheat spikelets post-inoculation with water containing 35 ppm DON, we set out to confirm the potent toxicity of the DON chemistry (sourced from Sigma-Aldrich, USA) on plant tissues. We utilised an assay described by Shin et al. (2012) and DON concentrations of 0mg/l, 10mg/l (10ppm, 33 μ M) and 20mg/l (20ppm, 67 μ M) to produce comparable phenotypes on *Arabidopsis thaliana* (ecotype Col-0; NASC, UK) during germination and early growth. Briefly, Col-0 seeds were surface sterilised and germinated on the surface of ½ MS 1% (w/v) agar plates (as described in Armer et al., 2024), with each plate supplemented with a different DON concentration or no DON.

The concentration of 35ppm (118 μ M) was determined as a result of these experiments, demonstrating toxicity *in planta* but not to *F. graminearum* growth *in vitro*.

3.3.2 Red Green Blue (RGB) colour classification for disease assessment of dissected spikelets

To quantify disease progression on wheat spikelets at 5 and 7dpi, colour (RGB) spikelets were imaged (iPhone 6s, Apple Inc, US) on both sides with consistent illumination. Diseased area was quantified using a curated programme on the LemnaTec Lemnagrid software (CHAP, York, UK). Diseased area was classified by pixel colour segmentation after application of filters to threshold from the background, identify misclassified pixels and fill in gaps. Area attributed to anthers were omitted from further analysis. The relative area attributed to each classification was then calculated in a custom R script and all samples were normalised to the mean value of 'diseased' of the mock treatment due to inherent background parsing error.

3.3.3 Light microscopy

Inoculated spikelets were dissected from the wheat spikes for internal observations of infected floral tissues and fixed in LR-white resin as outlined in [chapter 2](#). Ultra-thin 1µm resin sections were cut from resin blocks using a microtome (Reichert-Jung, Ultracut), placed onto Polysine microscope slides (Agar Scientific, UK) and stained with 0.1% (w/v) Toluidine Blue O in 0.1M Sorensen's phosphate buffer (NaH_2PO_4 : $\text{Na}_2\text{HPO}_4 \cdot 7\text{H}_2\text{O}$, pH 7.2). Every 10th section was collected for a total of 10 sections per embedded block to fully explore floral tissues and mounted with Permount (Fisher Scientific, UK) prior to imaging on a Zeiss Axioimager 512 (Zeiss, Oberkochen, Germany) at x20 magnification under BF illumination. The experiment was repeated 3 times, with a total of 5 biological replicates for each treatment, with 2 mock samples per batch. In total, 111 resin blocks were explored across a 100µm sampling area in the centre of the sample, with sections cut every 10µm.

3.3.4 Electron microscopy

For SEM exploration of floral tissues, spikelets at 5dpi were excised and coated in 50:50 OCT compound (Sakura FineTek) with colloidal graphite (TAAB). SEM analysis was conducted on lemma rachis tissue infected with the WT reference strain PH-1 and lemma tissue with the ΔTri5 strain at 5dpi. Sample preparation

occurred in a Quorum Cryo low-pressure system before imaging on a JEOL LV6360 SEM at 5kV with software version 6.04 (Jeol, UK).

For TEM of lemma tissues at 5dpi inoculated with PH-1 (WT), Δ Tri5 or water (mock), samples were excised from plants grown and inoculated with *F. graminearum* as outlined in sections [2.4.2](#) and [2.4.4](#). To preserve the fine structures, such as the desmotubule, high pressure freezing was employed. Lemma tissues were dissected using a sterile razor blade placed into 0.1M sucrose solution and high pressure frozen using a Leica EM ice (Leica microsystems) for sample preservation. Samples were stored in LN₂ prior to freeze substitution in a Leica AFS (Leica microsystems) with anhydrous acetone. AFS freeze substitution protocol was as follows: -85°C 26 hrs hold before rising 2°C per hour to -60°C over a 12.5 hour period and held for 8 hrs, followed by another rise of 2°C per hour to -30°C over 15 hrs and held at -30°C for a further 24 hrs, before being transferred to a -20°C freezer for 2 days. Samples then underwent Spurr resin (Sigma Aldrich, UK) infiltration at 25% intervals to 100% overnight prior to embedding in capsules and polymerised at 60°C overnight.

For TEM imaging, 100nm sections of desired tissues were sectioned on a ultramicrotome (Leica UC7, Germany) and placed onto gold grids coated with formvar. For standard viewing, sections were stained with UranylLess EM stain (Electron Microscopy Services, UK) for 1 min and subsequently 3% lead citrate for 2 min at RT.

For immunogold of callose at plasmodesmata in TEM, the protocol from Deeks et al. (2012) was used. Briefly, the sections were incubated for 30 mins with a blocking solution of 0.1M Sørensen's Phosphate buffer (as described in section [2.5.2](#)) amended with 0.1% (v/v) Tween 20 and 1% (w/v) Bovine Serum albumin (BSA). Sections were then incubated in the blocking solution amended with 1:200 β -1,3-glucan antibody (Biosupplies, Australia) for 60 mins at 37°C, washed three times for 5 mins each with a wash buffer composed of 0.1M Sørensen's Phosphate buffer and 0.1% (v/v) Tween 20. Sections were then incubated for 30 mins at 37°C with goat anti-mouse 10nm colloidal gold (Sigma Aldrich, UK) diluted 1:20 in blocking buffer. Grids were then rinsed 3 times in wash buffer for 5 mins per wash and dried for storage at RT until imaging. Samples were washed by placing inverted grids onto drops of incubating solution on parafilm in a watch glass lined with damp tissue to prevent grids drying during incubation periods.

Imaging occurred on a Jeol 200plus Transmission Electron Microscope (Jeol, UK) at 200kV.

3.3.5 Immuno-labelling of callose deposits at plasmodesmata for light microscopy

Callose immuno-labelling of resin-embedded sectioned material was conducted according to Amsbury and Benitez-Alfonso (2022). Briefly, callose was localised by anti- β -1,3-glucan antibodies (Cat. 400-2, Biosupplies, Australia) and secondarily conjugated with rabbit anti-mouse Alexa Fluor™ 488 (Cat. A27023, Thermo Fisher Scientific, UK). Wheat cell walls were counterstained with calcofluor white. Sections were imaged by confocal microscopy on a Leica SP8 confocal microscope, with excitation-emission spectra for AlexFluor-488 at 488nm, 510nm-530nm and 405nm, 450nm-475nm for calcofluor white. Image analysis for the quantification of callose deposits per cell was conducted in Fiji (ImageJ) using maximum projections of Z stacks and channels converted to binary masks. The number of cells in the sample area was calculated using the cell counter tool and callose deposits were counted by the number of discrete Alexa 488-fluorescences between the size of 2 to 12 pixel units to eliminate cross-reactivity with β -1,3-glucans in the fungal cell walls. The number of callose deposits were averaged across the number of complete cells (all cell walls visible) in the sample area. Callose deposits were quantified in the lemma and rachis tissues only, with 3 biological replicates for each treatment (PH-1, $\Delta Tri5$, DON, Mock). Image analysis methodology is demonstrated in Fig. 3.3.1.

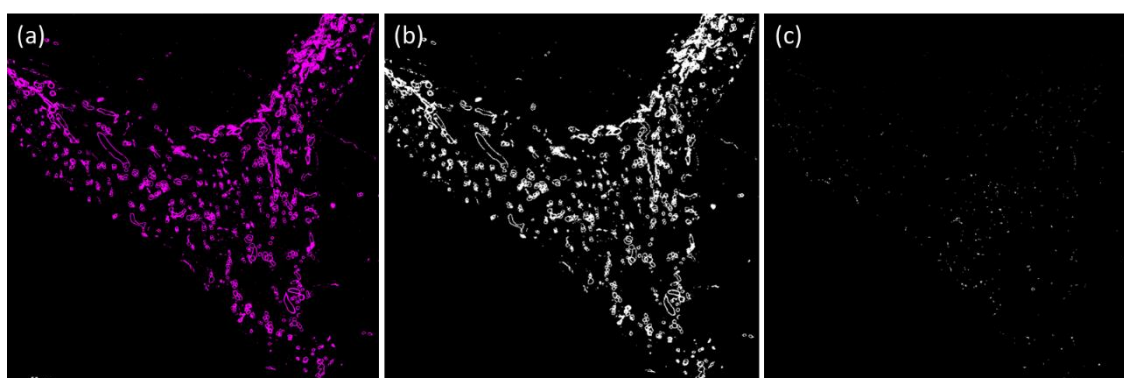


Fig. 3.3.1. Example methodology for the quantification of immunofluorescence detection of callose in sectioned floral tissues. Wheat palea tissue infected with the wildtype PH-1 strain of *F. graminearum* at 5dpi and immuno-labelled for callose, with the secondary antibody

conjugated to the fluorophore Alexa Fluor-488. (a) the RGB channel for the emission spectra 510nm- 530nm to detect callose (magenta). β -1,3-glucans in the fungal cell wall have cross-reactivity with the anti-callose antibody. (b) RGB images are converted into binary masks for measurement of particles. (c) Using the 'Analyse Particles' tool in Fiji, particles are counted between 2-19 pixel units in size. This reduces counts due to noise (1 pixel in size) but eliminates pixels attributed to β -1,3-glucans in the fungal cell wall.

3.3.6 DON quantification

To determine if the presence of DON in the WT strain inoculum stimulated further DON production, if administered DON could be detected in wheat spike tissues at the end of disease progression (14dpi), and the absence of DON in the $\Delta Tri5$ mutant interaction a competitive enzyme-labelled immunoassay for 15-ADON was employed. Whole wheat spikes were utilised for this quantification in the case the DON was trafficked or secreted beyond the inoculated spikelet due to its high water solubility. Whole wheat spikes after 14 days of disease progression were ground to a fine powder in the presence of liquid nitrogen and 1g of each sample was resuspended in 5ml dH₂O, vortexed until dissolved, incubated in a 30°C water bath for 30 mins and centrifuged for 15 minutes at full speed (13.1g). The supernatant was removed and analysed using the Beacon Analytical Systems Inc Deoxynivalenol (DON) Plate Kit (Cat. 20-0016) according to kit instructions. The OD₄₅₀ values were measured on a Thermo Varioskan microplate reader (Thermo Scientific, USA). Three technical replicates of each biological replicate (a single wheat spike) were conducted, and the experiment was repeated three times.

3.3.7 Expression of the *TRI5* gene during coleoptile infection

The trichodiene synthase gene *TRI5* was used as a proxy for the relative expression of the trichothecene biosynthesis pathway during coleoptile infection. Total RNA was extracted from whole coleoptiles at 3, 5 and 7dpi using a total RNA extraction kit (NEB, UK) and following the kit instructions. First strand cDNA was synthesised using RevertAid First Strand cDNA synthesis kit (Thermo Fisher Scientific, UK) as per kit instructions and utilising random hexamer primers provided. *TRI5* expression was then assessed by qPCR with melt curve using the primers outlined in Table 2.3.1, with SYBR as the reporter, passive reference as ROX and NFQ-MGB as the quencher. The qPCR with melt curve was conducted

in technical and biological triplicate on a QuantStudio™ 6 Pro and results analysed on the complementary Design & Analysis Software v. 2.6.0 (ThermoFisher Scientific, MA, USA). The experiment was conducted 3 times. Quantification of *TRI5* expression was normalised against the housekeeping gene FgActin (Table 2.3.1) for each sample, also included within the qPCR run in triplicate. At least one primer in a primer pair for qPCR targets was designed to span an exon-exon junction to avoid annealing to residual DNA.

3.3.8 Phloroglucinol staining for presence of lignin

A 3% Phloroglucinol (Sigma Aldrich, UK) - HCl solution (Weisner stain) was prepared fresh in accordance with methods by Mitra and Loqué (2014). Inoculated wheat spikelets were sampled at 5dpi and cleared in 100% EtOH for 4 days before going through a rehydration series (75%, 50%, 25% and 0% EtOH) at 1 hour per stage. Cleared spikelets were bathed in Weisner stain for 1 hour, or until staining of the tissues becomes evidently saturated. Spikelets were then imaged (OM-D E-M10, Olympus, Japan) under constant illumination and, subsequently, dissected tissues were imaged individually.

3.3.9 Formation of perithecia *in vitro*

Carrot agar was prepared using the method outlined by Cavinder et al. (2012) and supplemented with DON at 35ppm (w/v) to test for the ability of the WT strain, and the DON trichothecene-deficient deletion mutant, $\Delta Tri5$, to develop perithecia *in vitro*, for lifecycle completion viability. Ability of perithecia to discharge ascospores in the presence of DON was assessed using the same method as described in Cavinder et al. (2012).

3.3.10 Statistical analysis

Scripts were written in R (version 4.0.2) for each experimental analysis. Unless otherwise stated, ANOVA followed by Tukey post-hoc test was conducted for parametric datasets and Kruskal-Wallis for non-parametric datasets. The significance threshold was set to $P < 0.05$ in all cases.

3.4 Results

The role(s) of DON during *F. graminearum* infection of different wheat tissues was addressed through a multifaceted approach. We applied a combination of detailed cell and molecular biology and morphological analyses of floral and coleoptile infections to analyse the effect of DON on hyphae traversing cell walls at PD and the occurrence of the defence response, callose deposition, at PD during infections cause by either the wildtype (WT) strain or the single gene deletion mutant $\Delta Tri5$ *F. graminearum* strain.

3.4.1 DON is toxic to plant tissue and is not required for the formation of perithecia *in vitro*

The addition of DON to $\frac{1}{2}$ MS agar for *Arabidopsis thaliana* wild-type Col-0 demonstrated toxicity through reduced growth and delayed germination (Fig. 3.4.1). Notably, at 10mg/l root growth was completely attenuated (Fig. 3.4.1 (a)) and germination delay was concentration dependent (Fig. 3.4.1 (b)). This confirmed that the concentration of DON used for the chemical complementation in wheat floral spikes is biologically active.

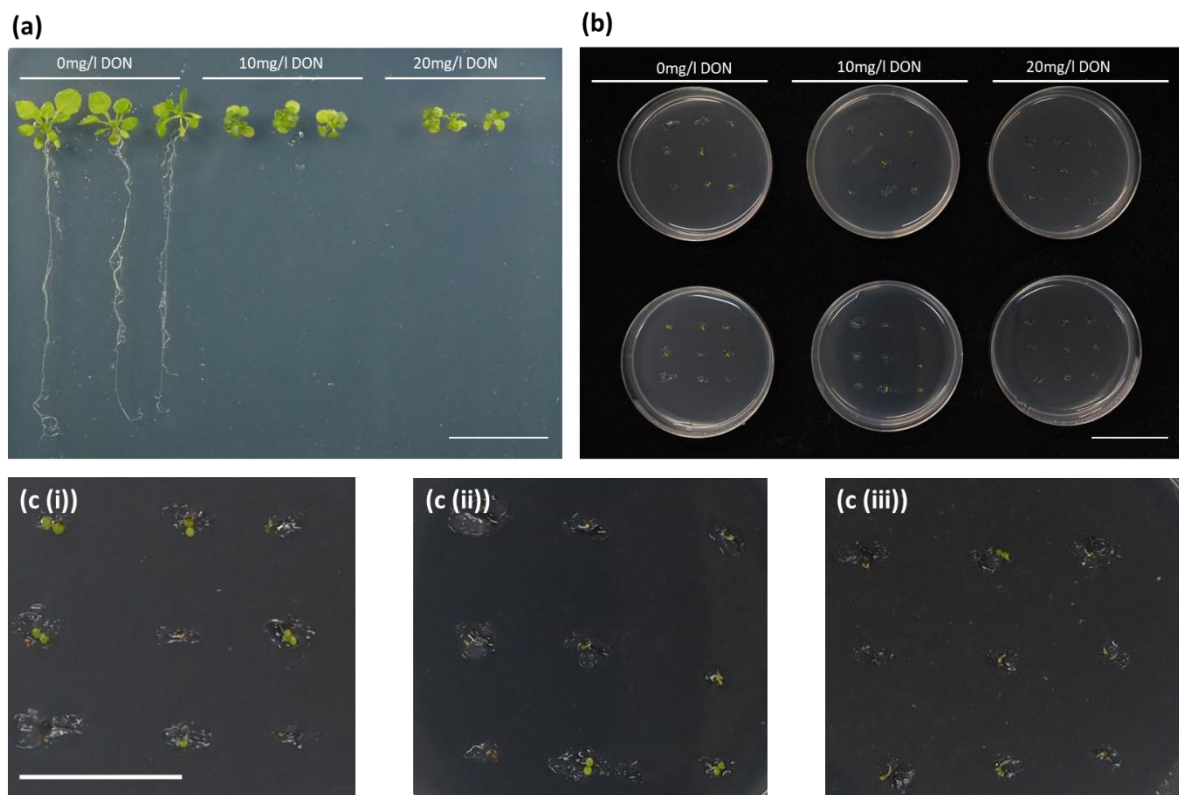


Fig. 3.4.1. Demonstration of DON toxicity on plant material. (a) Growth of *Arabidopsis thaliana* at 3 weeks on $\frac{1}{2}$ MS agar supplemented with 0mg/l DON, 10mg/l DON and 20mg/l DON. (b) Delayed germination on plates of *A. thaliana* on $\frac{1}{2}$ MS agar supplemented with DON, scale bar =

20mm. (c) Close up view of germination with 0mg/ml DON (i), 10mg/ml DON (ii) and 20mg/ml DON (iii). Scale bar = 10mm.

To determine if the production of DON is required for the production of perithecia, the DON-deficient $\Delta Tri5$ mutant was *in vitro* perithecia induction assay. It was found that $\Delta Tri5$ was able to produce abundant perithecia that were macroscopically indistinguishable in size to those produced by WT PH-1. Furthermore, to test the viability of formed perithecia, successful ascospore discharge from perithecia was observed by light microscopy for both the WT and $\Delta Tri5$ *F. graminearum* strains.

3.4.2 DON is not required for virulence on wheat coleoptiles and chemical complementation does not restore the WT disease phenotype on wheat spikes

To determine whether DON is or is not required for virulence on wheat coleoptiles under our conditions the fully susceptible cv. Apogee was tested. Inoculation of wheat coleoptiles revealed no differences in lesion length between the WT PH-1 strain and single gene deletion mutant $\Delta Tri5$ (Fig. 3.4.2 (a) and 1(b)). However, RT-qPCR analysis showed that the WT strain expressed TRI5 during coleoptile infection at 3, 5 and 7 days post inoculation (dpi), but remains at very low levels (x0.8 FgActin) and stationary throughout the infection progression (Fig. 3.4.2 (c)), indicating that TRI5 mRNA levels are not temporally altered for this interaction during the early to mid-time points explored. This finding supports a previous study by Qui et al. (2019), who reported accumulation of transcripts of the *TRI4* gene, also required for trichothecene mycotoxin biosynthesis.

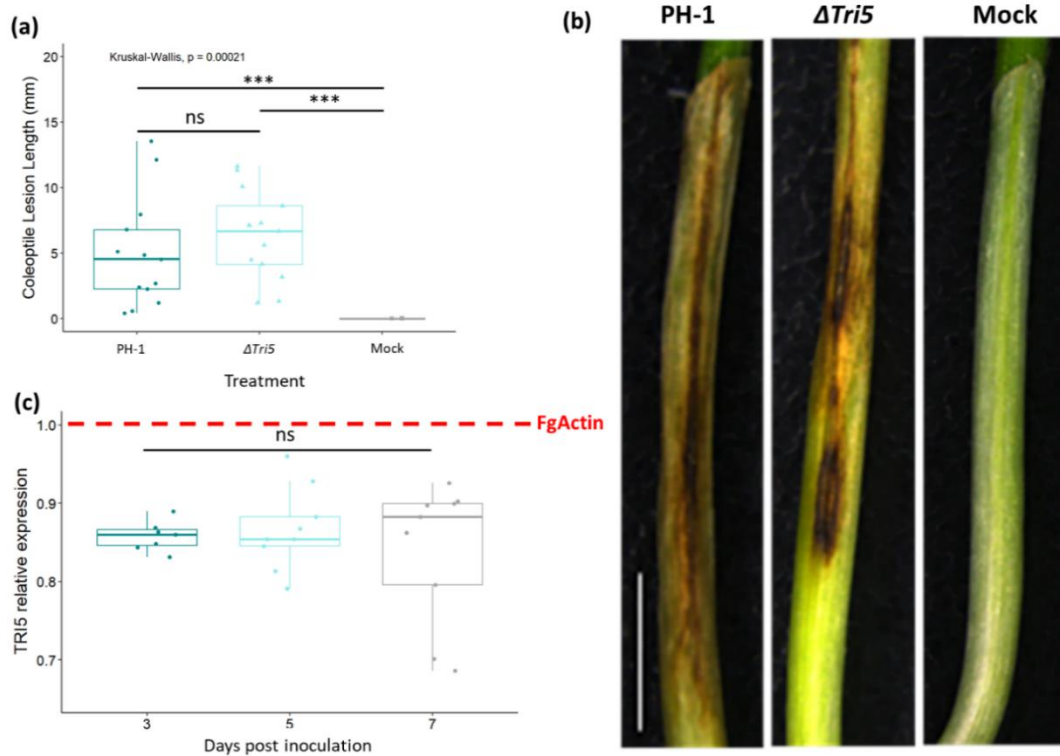


Figure 3.4.2. *F. graminearum* disease formation on wheat coleoptiles. (a) Length lesion at 7dpi for PH-1, the $\Delta Tri5$ mutant and mock inoculations, Kruskal-Wallis $p < 0.005$ (***). (b) Examples of disease lesion phenotypes at 7dpi for PH-1, $\Delta Tri5$ and mock inoculations from rep 2, scale bar = 20mm and (c) Relative expression of *TRI5* measured using RT-qPCR at 3, 5 and 7dpi in wheat coleoptiles, normalised against *FgActin* expression. ANOVA $F(2,22) = 0.421$, $p = 0.662$ (ns).

Next, we asked whether the same host and pathogen genotypes showed different DON dependencies during floral tissue interactions. Disease progression of WT, $\Delta Tri5$ and DON-complemented strains were analysed by tracking visible disease symptom development on the outer glume and rachis of inoculated wheat spikes. The single $\Delta Tri5$ mutant was restricted to the inoculated spikelet in all instances. Whereas chemical complementation of the $\Delta Tri5$ mutant with DON (35ppm) applied along with the conidia inoculum failed to restore the macroscopic WT spikelet phenotype occurring on the inoculated spikelet or spikelet-to-spikelet symptom development. This DON concentration was not detrimental to either spore germination or early spore germling growth in pilot studies. Interestingly, co-inoculation of WT *F. graminearum* with DON (35ppm) at the same concentration did not result in any observable advancement of disease symptoms (Fig. 3.4.3 (a)). Application of DON (35ppm) alone did not induce any

macroscopic disease symptoms and visually equated to the water only (dH₂O) mock-inoculated samples (Fig. 3.4.3 (d), 3.4.3(a)). The area under the disease progression curve (AUDPC) analysis revealed that the PH-1 and PH-1 + DON supplementation floral infections had significantly greater disease progression than the $\Delta Tri5$, $\Delta Tri5$ + DON, DON only, and mock-inoculated treatments (Kruskal-Wallis, $p=2.8e^{-10}$; Fig. 3.4.3 (b)). To quantify the levels of DON present in all treatments at the end of disease progression (day 14), a DON-ELISA test was carried out to determine the final 15-ADON concentrations. PH-1 and PH-1 + DON samples had an average DON concentration of over 30 ppm, whilst all other treatments had no detectable (<0.5ppm) DON (Fig. 3.4.3 (c)). This indicates that the addition of DON to WT inoculum did not stimulate further DON production and confirms that the $\Delta Tri5$ mutant is impaired in DON biosynthesis. Of note, the lack of detection of DON in the $\Delta Tri5$ + DON and DON alone samples is likely due to the detoxification of DON by wheat plants to DON-3-glucoside, the latter is undetectable by the competitive enzyme-labelled immunoassay kit used in this study. The conjugation of DON to DON-3-glucoside, catalysed by a UDP-glucosyltransferase, *in planta* is difficult to detect through its increased molecule polarity and is thus known as a 'masked mycotoxin' (Berthiller et al., 2005). A visual representation of disease progression occurring in each treatment is shown in Fig. 3.4.3 (d).

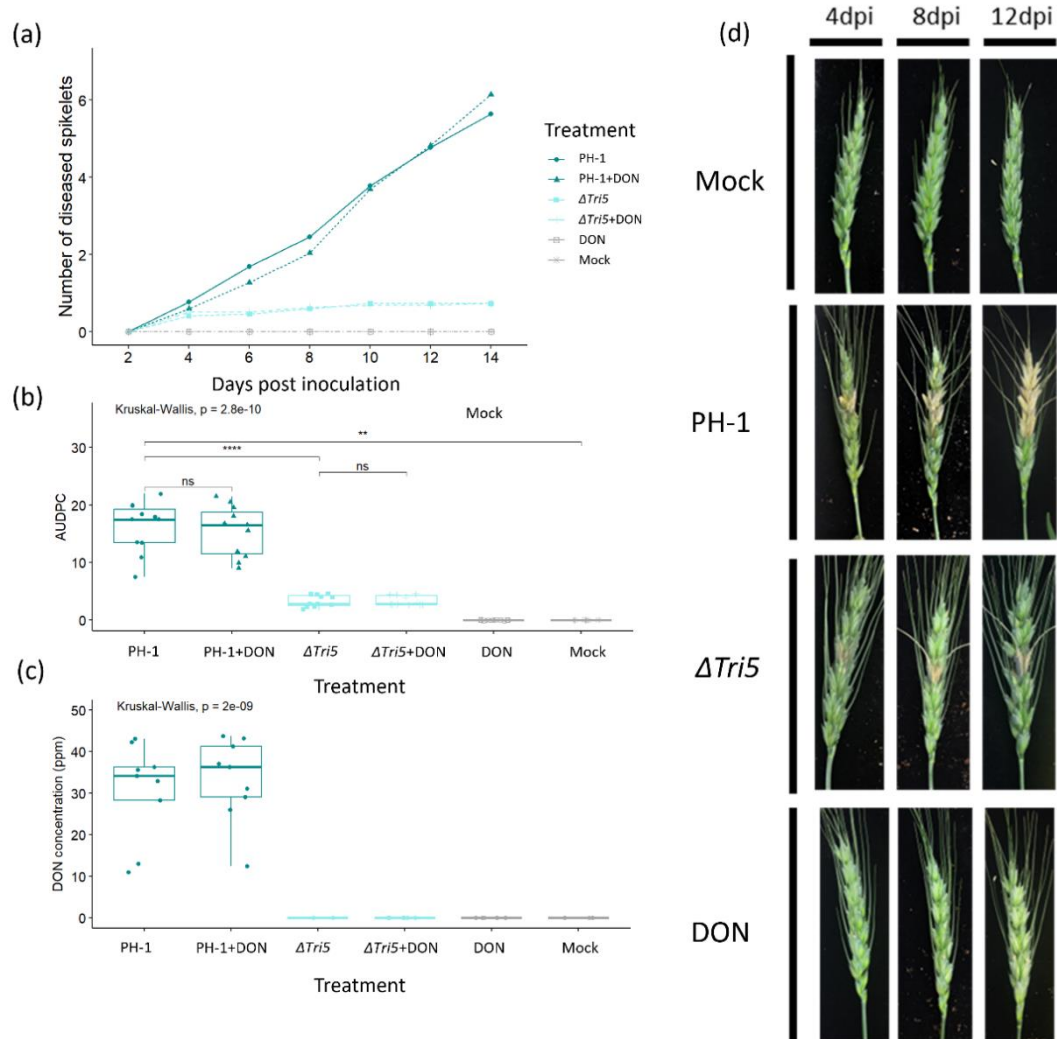


Figure 3.4.3. Analysis of whole wheat floral tissues following point inoculations. (a) Tracked visible disease progression at 2-day intervals to 14 dpi from below the inoculated spikelet. (b) Area Under Disease Progression Curve (AUDPC) for disease progression in panel (a), Kruskal-Wallis $p < 0.005$ (***). (c) DON concentrations of wheat spikes at 14 dpi, Kruskal-Wallis $p < 0.005$ (***). (d) Representative disease progression images at selected timepoints of 4, 8 and 12 days.

Fungal burden is the ratio of fungal to plant host genomic DNA and acts as a proxy for the internal severity of disease. In point-inoculated spikelets at 5 and 7 days post inoculation, fungal burden was calculated (Fig. 3.4.4). At 5dpi it was found that the WT interaction had the highest fungal burden at a ratio of 2.5:1, but this was not statistically significant from the treatments of $\Delta Tri5$ and the DON-supplemented WT and $\Delta Tri5$ samples, overall test statistic ANOVA $F(9,20) = 3.447$, $p < 0.05$ (*). However, it is speculated that as disease progresses and wheat tissue undergoes necrosis, cells become devoid of their contents and thus lose genomic material. Similarly, as the advancing hyphal front of infection moves

beyond the primary infection tissues, autophagy is known to occur, which leads to the formation of ‘ghost’ hyphae (Brown et al., 2011). These facet of infection could explain why fungal burden does not increase from 5 to 7 days in any of the treatments.

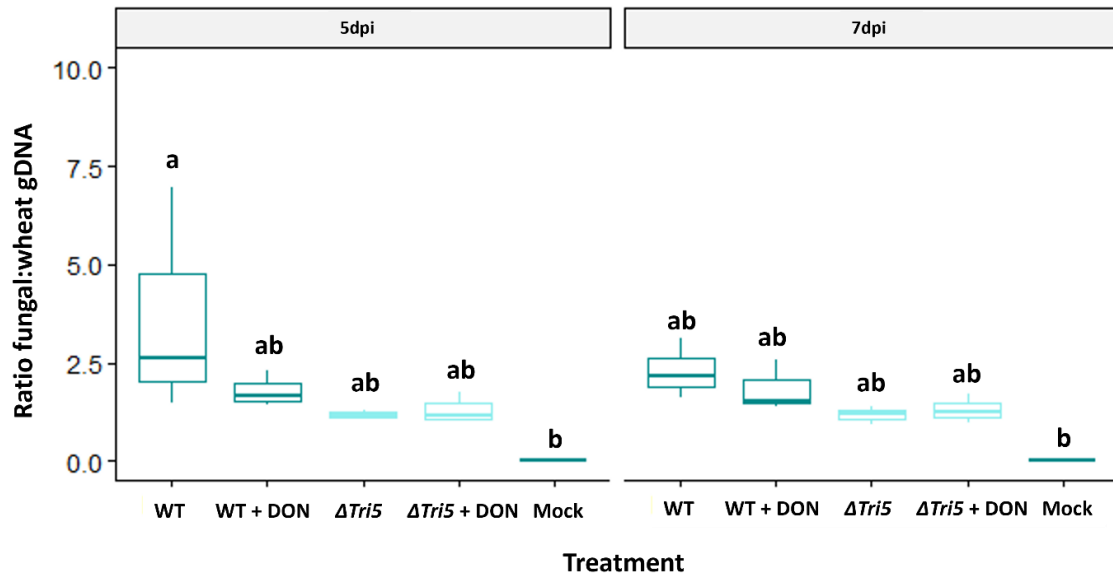


Fig. 3.4.4 Fungal burden at 5- and 7-days post inoculation on spikelets. 5dpi shown on the left and 7dpi shown on the right. ANOVA $F(9,20) = 3.447$, $p < 0.05$ (*).

Cuzick, Urban and Hammond-Kosack (2008) had previously shown that a qualitative difference in the appearance of macroscopic disease symptoms on the glumes between the WT and the $\Delta Tri5$ mutant. In this study, we have extended this observation and explored the macroscopic as well as the microscopic disease symptoms. Macroscopically, we were able to confirm the $\Delta Tri5$ -inoculated spikelets exhibited ‘eye-shaped’ lesions on the outer surface of the glume by 7dpi (Fig. 3.4.5 (a)). These differed from the characteristic fawn brown ‘bleaching’ of the spikelet tissues observed in the WT interaction at 7dpi (Fig. 3.4.5 (a)). Chemical complementation of $\Delta Tri5$ did not restore the WT phenotype nor visibly increase the severity of the WT disease phenotype. To quantify the diseased area, inoculated spikelets were imaged at 5 and 7dpi and analysed using the Lemnagrid software for diseased area. The PH-1 and PH-1 + DON spikelets had a greater area exhibiting disease symptoms than both the $\Delta Tri5$ and $\Delta Tri5 + DON$ treatments (Fig. 3.4.5 (b)). Computational restrictions in spikelet parsing from background led to minor, insignificant disease symptoms for DON and mock samples.

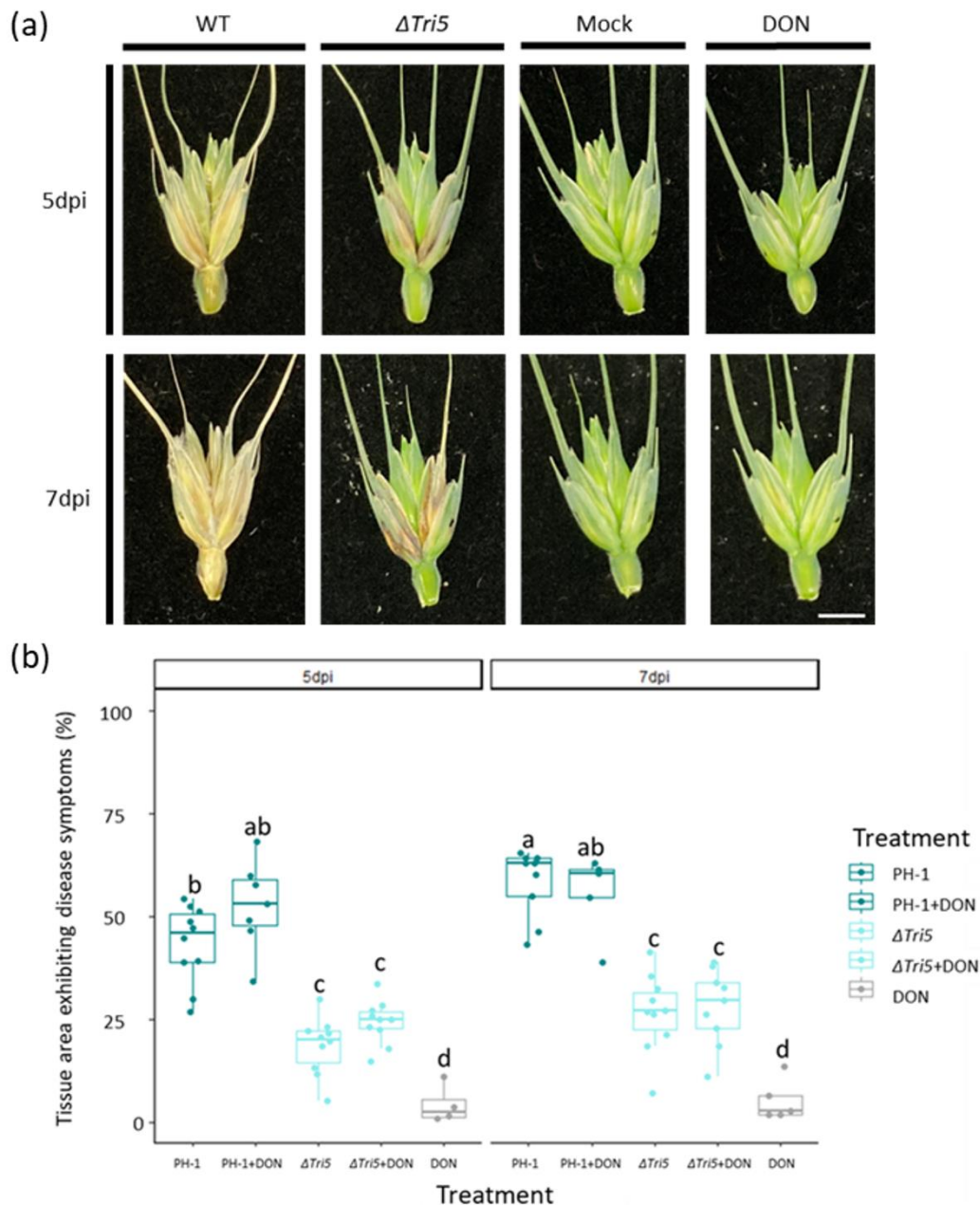


Figure 3.4.5. Quantitative spikelet analysis for disease symptom development. (a) Examples of dissected spikelets at 5 and 7dpi, scale bar = 10mm. (b) External tissue areas exhibiting disease symptoms at 5 and 7dpi as determined by Lemnagrid computational software. ANOVA, $P < 0.005$ (***) , Tukey post-hoc denotes group significance.

3.4.3 The $\Delta Tri5$ mutant is inhibited in its ability to traverse plasmodesmata during host-tissue colonisation

Resin-embedded samples of the lemma, palea and rachis spikelet components revealed changes in cellular morphology at different points of WT infection (Fig.

3.4.6). In all samples, extensive hyphal colonisation of the abaxial layer of the lemma and palea tissues are observed (Fig. 3.4.6 and Fig. 3.4.7).

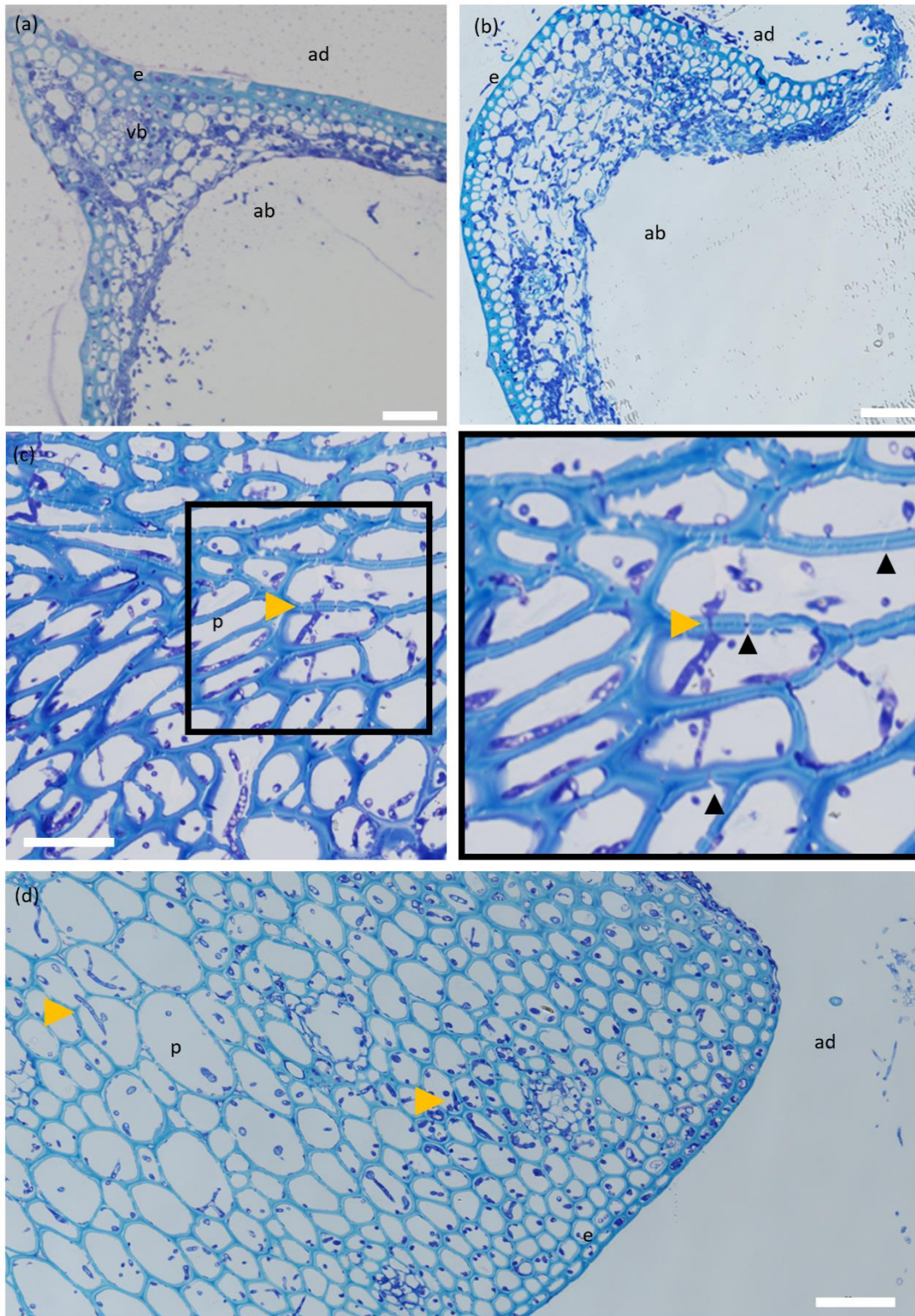


Figure 3.4.6. WT-infected wheat floral tissues at 5 and 7 dpi demonstrating aspects of typical infection. (a) Lemma at 5dpi infected with WT *F. graminearum* showing widespread hyphal colonisation throughout the tissue accompanied by hyphal proliferation protruding from

the abaxial layer. (b) A 7dpi WT-infected lemma showing further tissue degradation by cell wall degrading enzymes and considerable hyphal proliferation. (c) Rachis at 5dpi infected with WT *F. graminearum* showing a number of plasmodesmatal crossings by invasive hyphae, indicated by yellow arrowheads, and extensive cell wall degradation of the mesophyll layer by *F. graminearum*-secreted cell wall degrading enzymes. Plasmodesmata can be identified as gaps in the parenchyma layer cell walls, a number of which are indicated by black arrowheads. (d) A 7dpi WT-infected rachis demonstrating durability of parenchyma tissue against cell wall degrading enzymes at later infection timepoints. ab = abaxial layer, ad = adaxial layer, e = epidermal layer, mes = mesophyll, p = parenchyma tissue, vb = vascular bundle. Yellow arrowheads indicate plasmodesmatal crossings by invasive *F. graminearum* hyphae. Scale bar = 50µm.

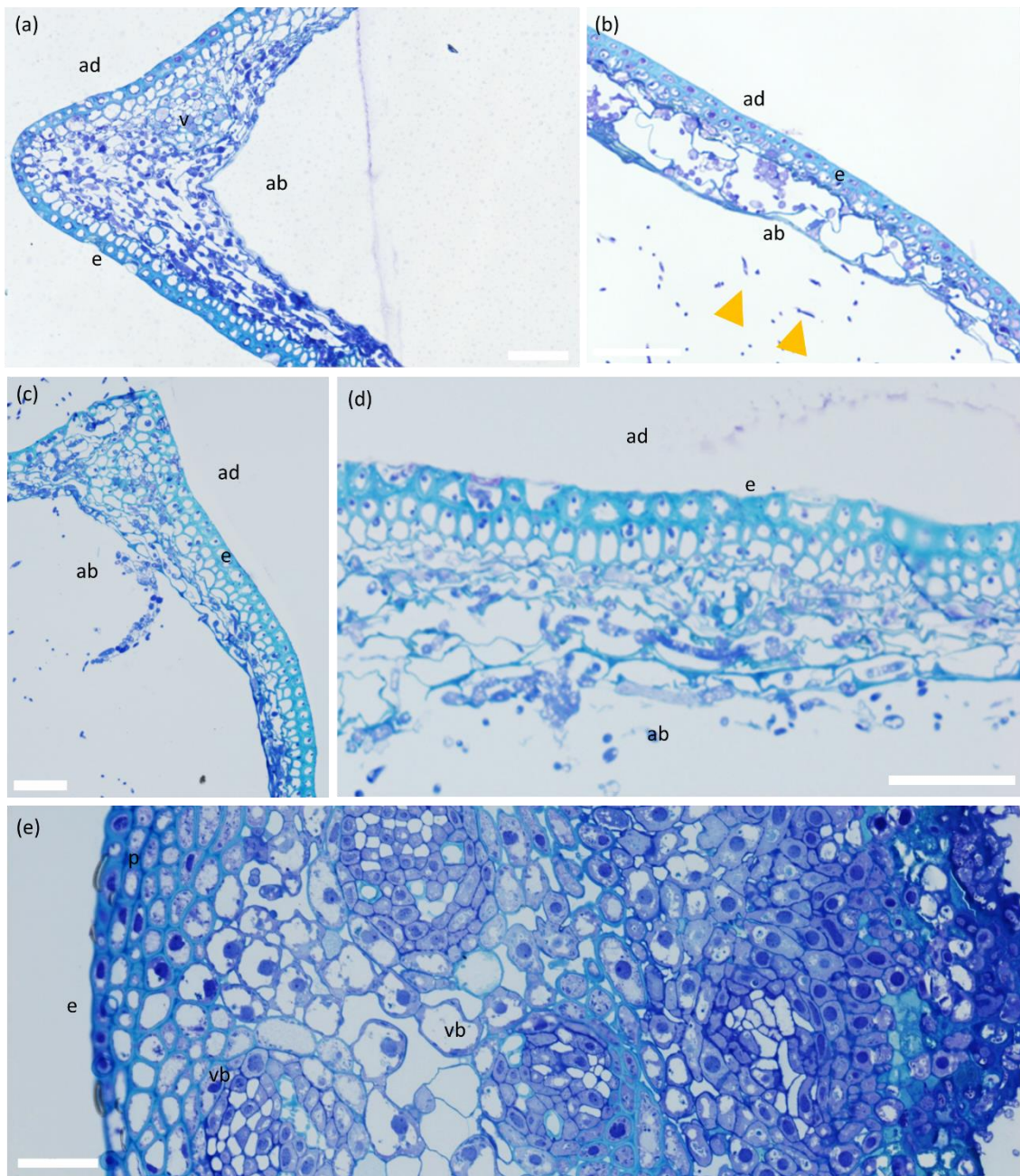


Figure 3.4.7. Comparison of $\Delta Tri5$ -infected and $\Delta Tri5 + DON$ infected wheat floral tissues at 5dpi and 7dpi showing the similarities and differences between tissue types in various

aspects of a typical infection. (a) Lemma at 7dpi infected with $\Delta Tri5$ *F. graminearum* with extensive proliferation of invasive hyphae throughout the abaxial layer, but rarely any penetration into the adaxial layer. (b). Palea at 5dpi infected with $\Delta Tri5$ and supplemented with 35ppm DON showing cell wall degradation in the abaxial layer and evidence of external fungal hyphae. Yellow arrows indicate hyphae external to the plant tissue. (c) Palea at 7dpi infected with $\Delta Tri5$, with similar symptoms to the lemma at the earlier 5dpi time point. (d) Lemma infected with $\Delta Tri5$ and supplemented with 35ppm DON at 7dpi showing cell wall degradation of the abaxial layer. (e) A rachis section at 5dpi infected with $\Delta Tri5$ and supplemented with 35ppm DON. No evidence of hyphae or cell wall degradation throughout the sample. ab = abaxial layer, ad = adaxial layer, e = epidermal layer, mes = mesophyll layer, p = parenchyma tissue, vb = vascular bundle. No plasmodesmatal crossings by invasive *F. graminearum* hyphae are evident. Scale bar = 50 μ m.

In the palea and lemma parenchyma tissue layer, the $\Delta Tri5$ and $\Delta Tri5$ + DON infected samples exhibited extensive cell wall degradation and colonisation by invasive hyphae (Fig. 3.4.7), similarly to the WT infection (Fig. 3.4.6). However, in the adaxial (outward facing) layer of the palea and lemma tissues, the hyphae in the $\Delta Tri5$ and $\Delta Tri5$ + DON samples rarely penetrated into the thicker-walled cells (Fig. 3.4.7 (a)-(d)). Mirroring the macroscopic lack of symptoms in the rachis, the $\Delta Tri5$ rachis samples never contained invasive hyphae at either 5 or 7 dpi (Fig. 3.4.7(e)). In the PH-1 and PH-1 + DON infected samples, invasive hyphae proliferated throughout the entirety of the lemma, palea and rachis tissues, causing extensive cell wall degradation (Fig. 3.4.6). To penetrate the adaxial layer, the PH-1 hyphae utilised cell wall pits resembling PD pit fields (Fig. 3.4.6 (c)). In these instances, the hyphae constricted considerably to traverse the cell wall. Traversing of the cell wall through PD pit fields was not observed in $\Delta Tri5$ and $\Delta Tri5$ + DON samples at either time point (Fig. 3.4.7). In general, where hyphae had invaded cells, the cell contents, notably nuclei, chloroplasts and evidence of cytoplasm, were not observed, indicating cell death. In the palea and lemma tissues of the PH-1 infected samples at 7dpi, putative evidence of 'ghost' hyphae was identified, which are characterised by a lack of cellular contents (Brown et al., 2011) in older infection structures as the infection front advances into the host plant.

To aid elucidation of the role of DON during infection of wheat floral tissues, cell wall thickness from resin-embedded wheat samples was measured along the adaxial layer of lemma and palea tissues, and in the visibly reinforced regions of rachis tissue, for all treatments. In the adaxial layer of the lemma, palea and rachis tissues, cell wall thickness was found not to differ between treatments,

particularly between those with and without the presence of DON (Fig. 3.4.8). This unanticipated result indicates that cell wall reinforcements are not evident at this level of resolution, and are not impacted by the presence of DON. However, it is worth noting that extensive cell wall degradation was present in the abaxial layer of palea and lemma tissues. This microscopic phenotype was not quantified but is most likely caused by the release of CWDEs from *F. graminearum* hyphae.

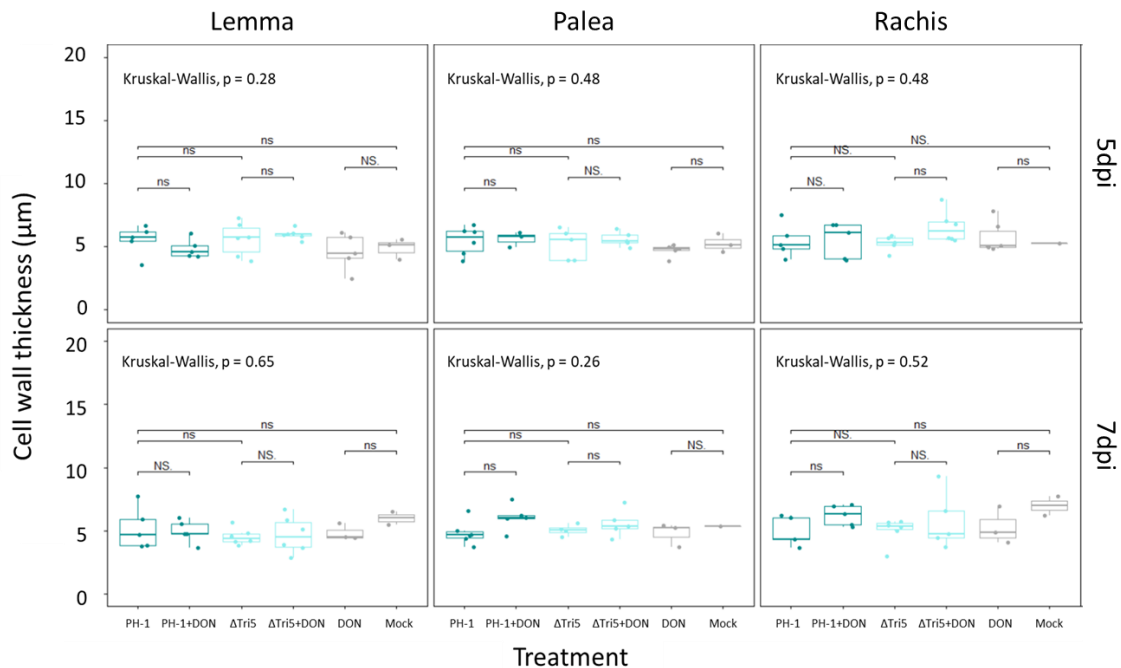


Fig. 3.4.8. Cell wall thickness of adaxial cell layer in resin samples. Wheat spikelet tissues of palea, lemma and rachis at 5 and 7dpi time points were analysed, with an average of 10 measurements from a representative resin image of each biological replicate analysed. No significance was determined by Kruskal-Wallis.

In order to gain a thorough understanding of infection, a scanning electron microscopy analysis was used. SEM micrographs of rachis tissues post spikelet inoculation with WT PH-1 at 5dpi revealed several notable interactions, including intracellular growth through cells still containing cytoplasm, apoplastic growth between cells, hyphal constriction and cell wall traversing and gaps in rachis cell walls (Fig. 3.4.9 (a), (b) and (d)). Micrographs of $\Delta Tri5$ -infected lemma tissue at 5dpi confirmed the resin analysis, whereby extensive cell wall degradation was observed in the parenchyma tissue layer (Fig. 3.4.9 (c)). Mock inoculated rachis tissues revealed gaps in the secondary cell wall, indicated with a yellow arrow, that are hypothesized to be the site of PD pit fields (Fig. 3.4.9 (e)). In the centre

of the rachis, aerenchyma are observed adjacent to parenchyma tissue layers (Fig. 3.4.9 (f)).

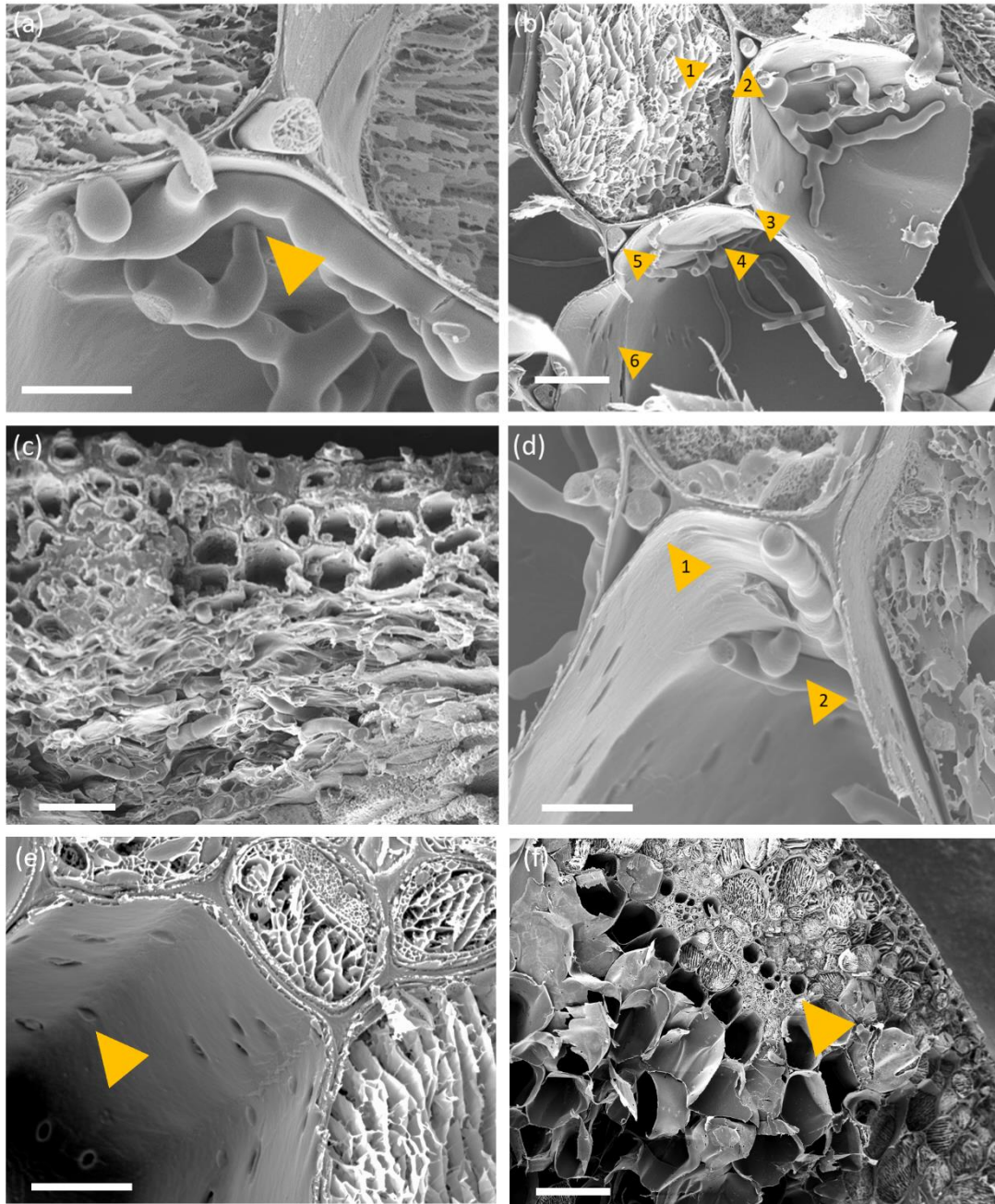


Fig. 3.4.9. SEM micrographs of PH-1 and $\Delta Tri5$ -wheat floral interactions. (a) A hypha of the wild-type PH-1 strain appears to cross through the cell wall at 5dpi in rachis tissue. Scale bar = 10 μ m. (b) Wild-type PH-1 infecting rachis tissue at 5dpi, the numbered yellow arrowheads indicate points of interest. 1. Intracellular growth in a cell where cytoplasm is still present; 2., 3., and 5. Apoplastic growth between cells, 4. Potential crossing of the cell wall by a hypha through a plasmodesma, and 6. 'Holes' in the cell wall that are potential sites of PD. Scale bar = 20 μ m. (c) $\Delta Tri5$ -infected lemma tissue at 5dpi demonstrating extensive hyphal colonisation and cell-wall degradation of the parenchyma tissue layer (bottom), but minimal infection in the thicker-walled adaxial layer (top), scale bar = 20 μ m. (d) Wild-type PH-1 infection of the rachis at 5dpi, 1. Growth

of two hyphae through the same apoplastic space in parallel to hyphae growing intracellularly in neighbouring cells to the left and right. 2. Hypha appear to constrict to traverse the cell wall. (e) Mock-inoculated rachis tissue, yellow arrow indicates pores in cell wall. (f) Mock inoculated rachis tissue showing lack of cellular contents in the central regions of the tissue. Yellow arrow indicates vascular bundle. (a)-(e) Scale bar = 10 μ m, (f) scale bar = 100 μ m.

3.4.4 TEM micrographs reveal pit fields in the plant cell wall at sites where secondary thickenings are absent

To better explore the gaps in the secondary cell wall observed in the SEM micrographs, TEM was employed to answer the hypotheses: '*Are the gaps locations of single plasmodesma or collections of plasmodesmata in pit fields?*' and '*Are the plasmodesmatal pores 'alive' (i.e. with an intact desmotubule) or 'dead' portals when used by *F. graminearum*?*'.

Firstly, lemma tissue samples inoculated with WT *F. graminearum* were explored through stained 100nm sections to explore whether the observed breaks in the secondary cell wall housed singular plasmodesma or multiple plasmodesmata in pit fields. Micrographs revealed that the approximately 1 μ m long breaks in the secondary cell wall contain multiple (3-6) plasmodesmata in the observed planes (Fig. 3.4.10), constituting pit fields. Secondly, the β -1,3-glucan polymer callose was localised to pit fields by conjugating anti-callose with 50nm colloidal gold nanoparticles (Fig. 3.4.11). In WT-infected lemma tissues at 5dpi, callose localised to one side of the cell wall (Fig. 3.4.11 (a)), while in the Δ *Tri5* DON-deficient mutant, a greater distribution of callose across the whole plasmodesmatal pit field was observed (Fig. 3.4.11 (b)). In the mock-inoculated lemma tissues at 5dpi, only callose localised to one side of the cell wall was evident (Fig. 3.4.11 (c)). Thus, WT-infected and mock-inoculated samples showed similar callose distributions, which differed from the *Tri5*-infected samples, indicating a role for DON in this component of wheat defence. For TEM analysis, one biological replicate per treatment was imaged, with 10-20 sections from each taken forward for imaging, resin quality depending.

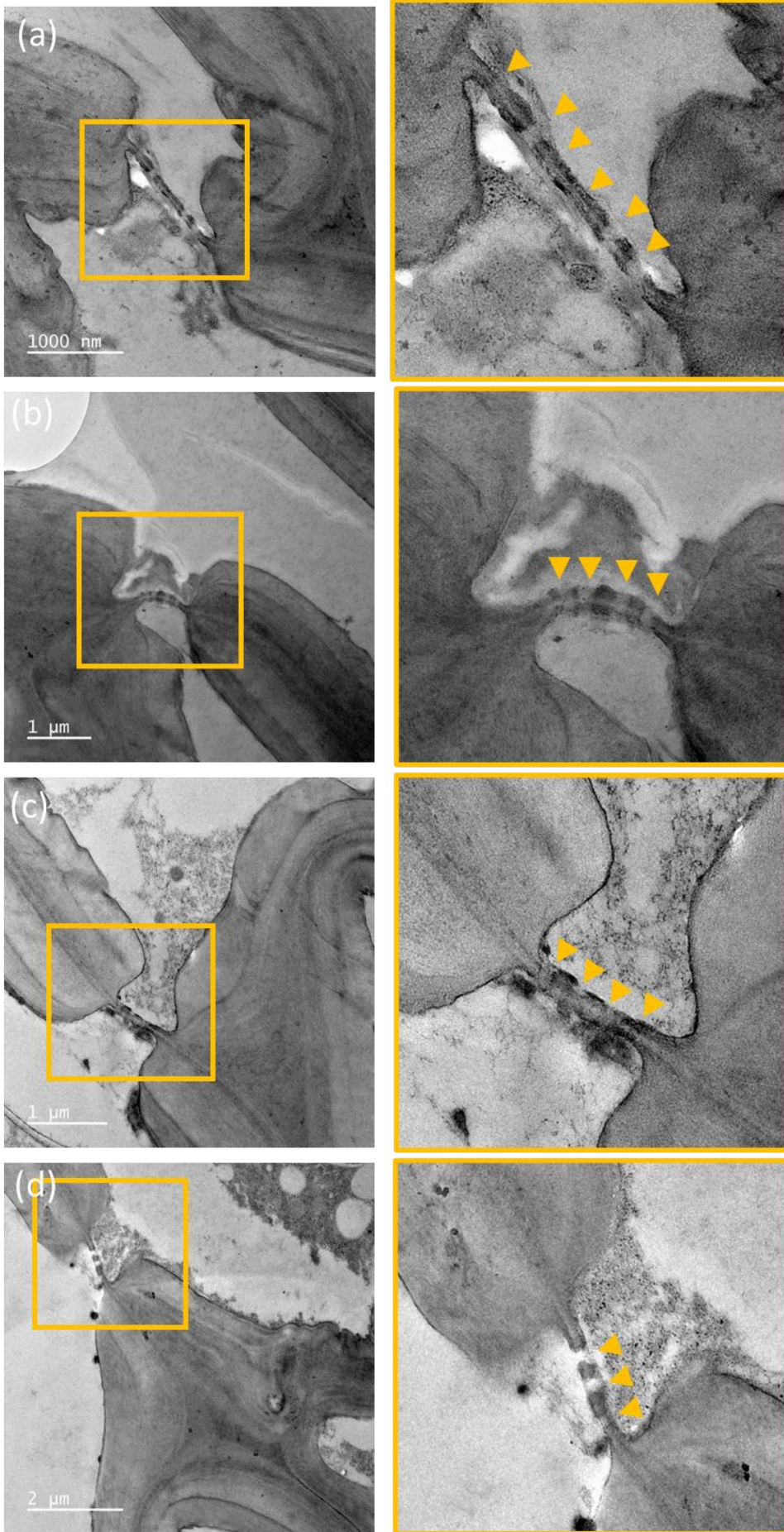


Fig. 3.4.10. Stained TEM micrographs of PH-1 infected lemma tissues at 5dpi demonstrating pit fields at breaks in the secondary cell wall. (a) Break in secondary cell wall exposes primary cell wall with middle lamella, punctuated with 6 visible plasmodesmatal pores. In all micrographs, the desmotubule structure of plasmodesmata is not visible. All samples were verified for presence of *F. graminearum* hyphae. 100nm sections stained with Uranylless and 3% Lead Citrate. Scale bars on individual panels.

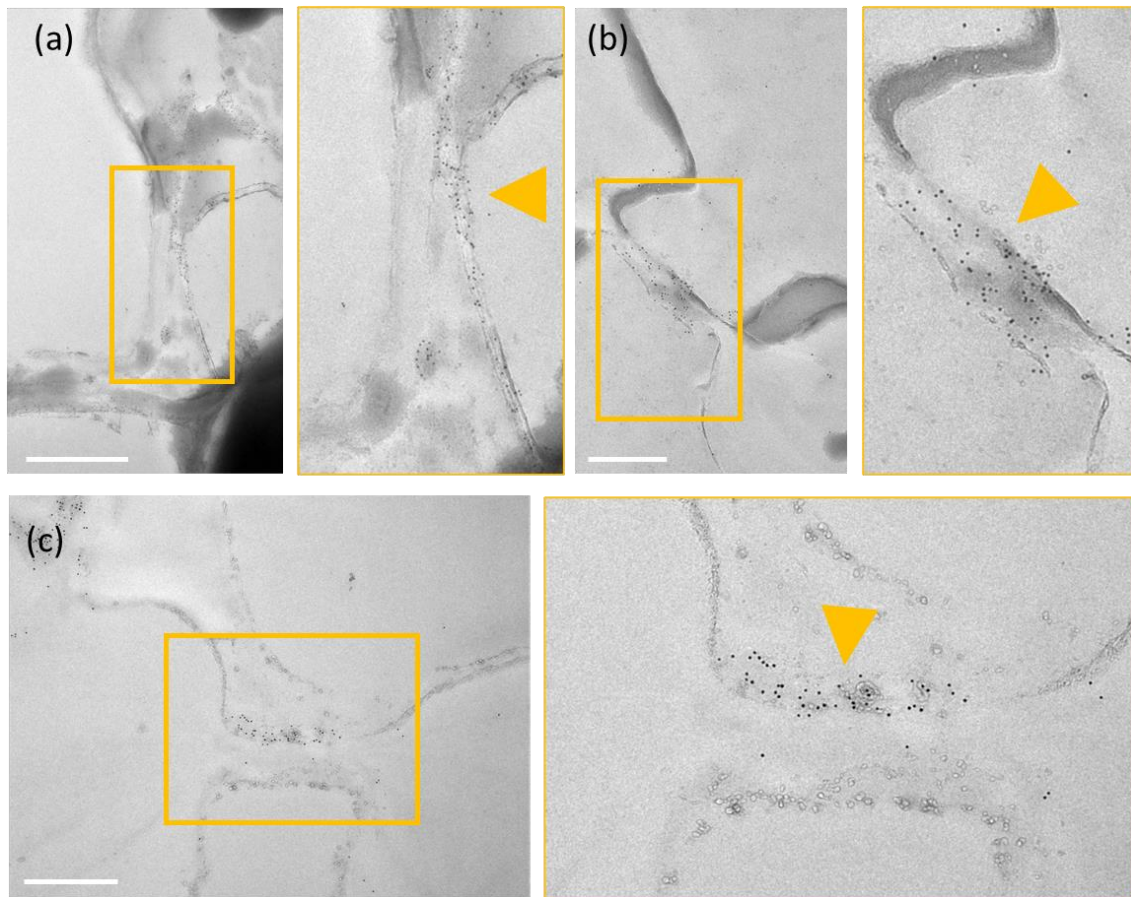


Fig. 3.4.11. TEM micrographs with callose gold immunolabelled at pit fields in lemma tissues at 5dpi. (a) WT (PH-1) -infected lemma at 5dpi showing callose localisation across one side of a secondary cell wall break, indicated with a yellow arrow, scale bar = 1µm. (b) $\Delta Tri5$ -infected lemma tissue at 5pi showing gold nanoparticles at a secondary cell wall break, spanning the entire junction and indicated by the yellow arrow, scale bar = 500nm. (c) Mock-inoculated lemma tissue at 5dpi showing gold-labelled callose on one side of the plasmodesmatal junction as indicated by the yellow arrow, scale bar = 500nm.

3.3.3 Immuno-labelling of callose during infection reveals reduced deposits in the WT infection and phloroglucinol staining indicates lignin-based defence response(s)

Resin sections of PH-1, $\Delta Tri5$ and mock-inoculated wheat floral tissues were analysed for the presence of callose at junctions in the cell wall (Fig. 3.4.12).

Immuno-labelling for the presence of callose confirmed the breaks in the secondary cell wall observed in resin sections was consistent with sites of plasmodesmatal pit fields. Imaging revealed that in both WT (PH-1) and DON-deficient ($\Delta Tri5$) *F. graminearum*-inoculated spikes there was an increased frequency of instances where callose was deposited at plasmodesmatal junctions compared to mock-inoculated controls (Fig. 3.4.12). However, the DON-only inoculated samples exhibited a marked increase in callose in both lemma and rachis tissues, indicating that callose deposition had been induced in a manner consistent with a basal immune response to symplastically isolate cells after the detection of the DON toxin, acting as a DAMP. Further examples are shown in Fig. 3.4.13.

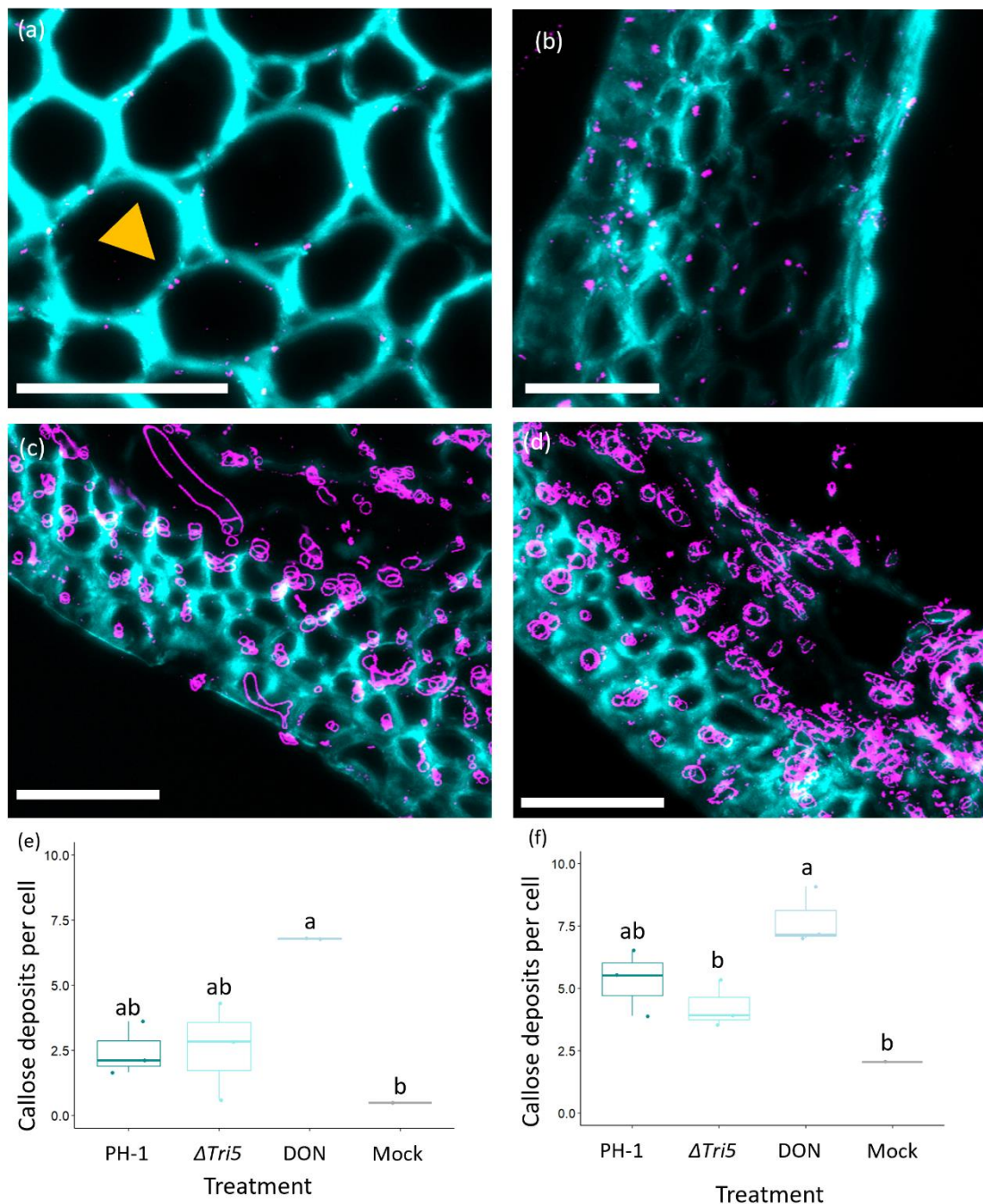


Fig. 3.4.12. Immunofluorescence detection of callose in rachis and lemma tissues. Magnified region of interest of the *Fg*-wheat interaction demonstrating callose deposits at plasmodesmata. (a) Control rachis, (b) rachis below DON-inoculated spikelet, (c) PH-1 infected lemma at 5dpi, (d) $\Delta Tri5$ -infected lemma at 5dpi. Sections were imaged by confocal microscopy with excitation-emission spectra for AlexFluor-488 488nm, 510nm-530nm and 405nm, 450nm-475nm for Calcofluor. Callose deposits are labelled in magenta with wheat cell walls in cyan. Scale bars = 50 μ m. In panels (c) and (d) the *Fusarium* hyphae also react positively to the antibody due to β -1,3-glucans in the fungal cell wall and are labelled in magenta. (e) Quantification of the number of immuno-labelled callose deposits, averaged across number of cells in the sample area, in lemma tissues at 5dpi, ANOVA = $p < 0.05$ (*), and (f) Rachis tissues at 5dpi, ANOVA = $p < 0.05$

(*). Letters indicate significance differences between groups from Tukey Post-hoc analysis following one-way ANOVA.

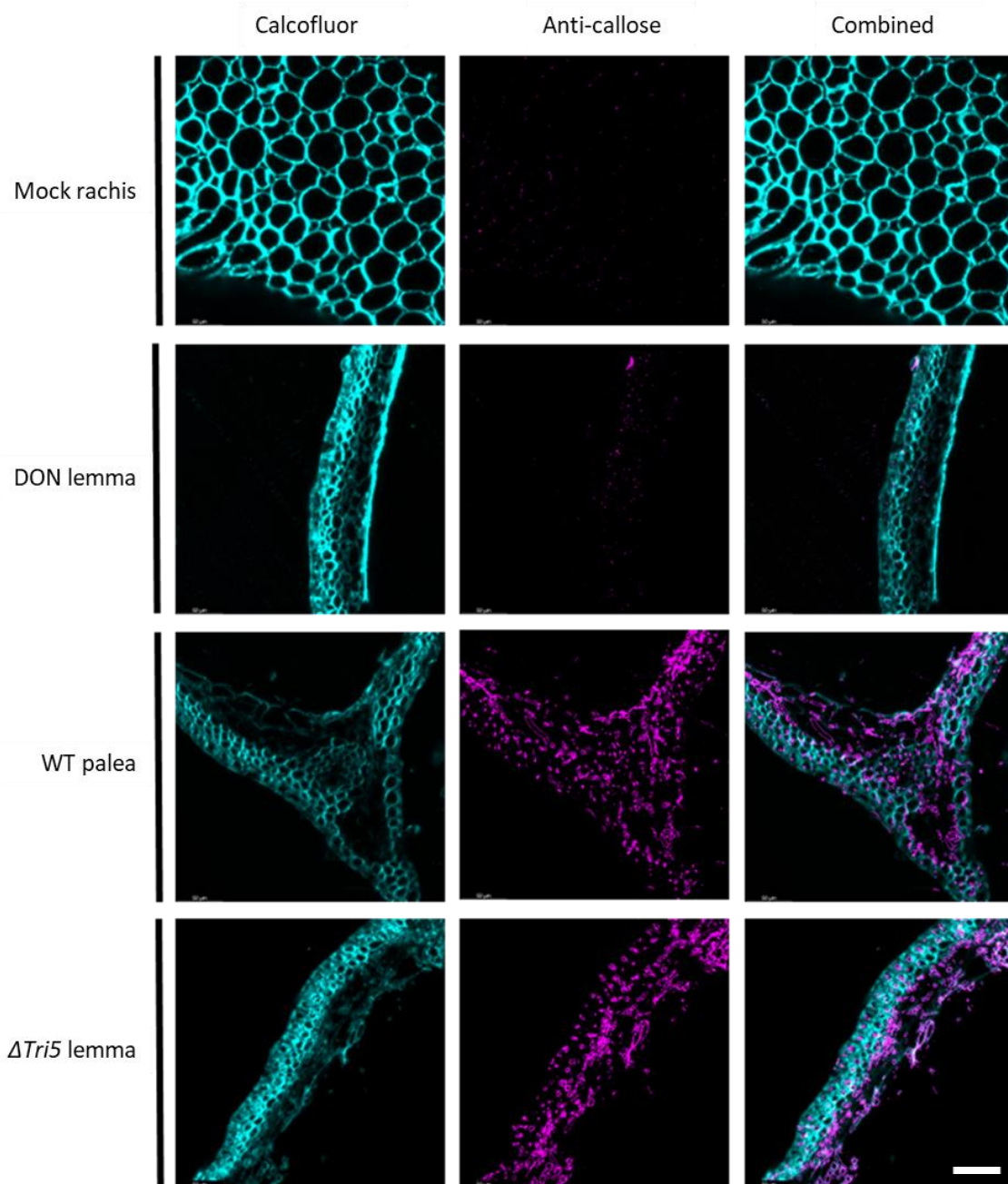


Fig. 3.4.13. Immunofluorescence detection of callose in sectioned floral tissues. Wheat floral tissues from palea, lemma and rachis embedded in LR white resin and sectioned to 1 μ m then immuno-labelled with anti-callose antibodies and secondarily conjugated with AlexaFluor-488 (magenta). Wheat cell walls are counterstained with calcofluor white (cyan). Selected images of Control, PH-1 (WT), DON, and $\Delta Tri5$ -infected wheat floral tissues at 5dpi demonstrating typical observations of each interaction. Scale bar = 50 μ m.

Spikelets of wheat inoculated with WT, PH-1 and $\Delta Tri5$ were sampled at 5dpi for analysis of a lignin response to *F. graminearum* infection. This investigation was prompted by the presence of localised 'eye-shaped' lesions in the $\Delta Tri5$ -infected

samples. Darker staining by the phloroglucinol indicates a higher lignin content, which was found to be most notable in the $\Delta Tri5$ -infected lemma tissue (Fig. 3.4.14). This was surprising, as the lesions were present on the glume. Whilst this was not quantified, the WT PH-1 and mock-inoculated controls were visually comparable, indicating that WT *F. graminearum* may have a role in dampening pathogen-induced lignin upregulations through the action of DON. This proposes the hypotheses that in the absence of trichothecene mycotoxins, wheat is able to upregulate lignin defence pathways.

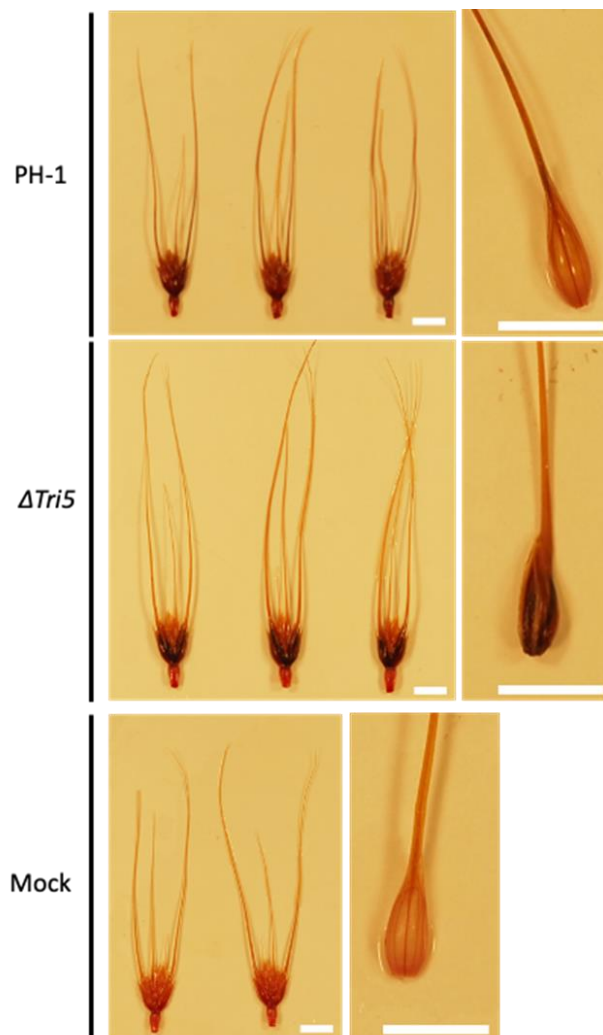


Fig. 3.4.14. Phloroglucinol staining of fresh infected spikelets. Darker staining of the tissues indicates a greater quantity of lignin. (a) PH-1 - infected spikelet, (b) $\Delta Tri5$ -infected spikelet, (c) Mock-inoculated spikelet. Spikelet component tissues: Lemma demonstrated an increase in phloroglucinol staining component, shown to the left of each treatment, indicating an increase in lignin content. N.B. Point inoculations occur between the lemma and palea tissues. All spikelets were collected at 5dpi and are of the wheat cv. Apogee. Scale bar = 10mm.

3.5 Discussion

This chapter has re-examined and extended knowledge on the restricted host tissue colonisation phenotype previously reported in wheat spikes for the non-DON-producing $\Delta Tri5$ single gene deletion mutant of *F. graminearum*. This study was catalysed by the lack of published cellular information available on how DON, produced and secreted by the advancing *F. graminearum* hyphae, actually facilitates the extraordinary effective and speedy disease progression consistently observed in the spikes of susceptible wheat cultivars. DON has long been classified as a key virulence factor in the *F. graminearum*-wheat interaction (Hohn et al., 1993; Jansen et al., 2005) and facilitates the host-tissue colonisation of the rachis and thus is essential for successful internal spikelet-to-spikelet growth of hyphae through the entire floral spike. However, prior to this study, the morphological and cellular responses underlying this macroscopically well documented phenomenon had not been explored. Our two primary aims were (a) to identify the morphological differences in the hyphal infection routes between the WT and $\Delta Tri5$ strains during wheat floral infections compared to coleoptile infections, and (b) to focus on the multifaceted role(s) of the cell wall and its constituent components as well as the pit fields during hyphal colonisation due to their potential to delay, minimise or cease fungal progression through the numerous internal complexities that the wheat spike architecture presents to the *Fusarium* hyphae.

As described above, our experimentation confirmed that the $\Delta Tri5$ mutant could sufficiently colonise the lemma and palea tissues but not the rachis (Jansen et al., 2005; Cuzick et al., 2007). Similarly, our results concurred with those of Jansen et al. (2005) that the DON-deficient *F. graminearum* strain could not grow beyond the rachis node due to the presence of inherently thicker cell walls in this tissue. Chemical complementation with DON did not restore the WT macroscopic phenotype, nor did it increase fungal burden, a proxy for internal disease. However, it could be the case that assessment of this at 5dpi was too late given previously reported increase in autophagy (Brown et al., 2011) and extensive cell death by the wheat host.

Our quantitative comparative analysis of the WT and DON-deficient interactions revealed no differences between cell wall thickness at two timepoints, or with the control mock inoculated tissues, indicating that cell walls do not increase in thickness *per se* as part of a locally occurring defence response. Upon further

microscopic analysis in the current study, we observed that the DON-deficient $\Delta Tri5$ mutant could not enter wheat cells with inherently thicker cell walls because the hyphae could not pass through pit fields containing plasmodesmata. This phenomenon was frequently observed in both the cortical and sclerenchyma cell layers. As a result, the $\Delta Tri5$ hyphae accumulated within and between the neighbouring thinner-walled parenchyma cells. In the absence of DON, potentially other so far uncharacterised secreted proteinaceous effectors fail to correctly manipulate these potential gateways into the neighbouring wheat cells. The analysis of resin sections revealed that cell walls within the adaxial layer of lemma and palea tissues were not thicker in infected samples. Although this rules out additional cell wall reinforcements, these findings do not eliminate cell wall compositional changes. Our results from phloroglucinol staining indicate that lignin content increases in the lemma tissue, which strengthens the tissue and hence emphasises the role of plasmodesmata as cell wall portals in host-tissue colonisation. We hypothesise that DON, through its intracellular target of the ribosomes, inhibits local protein-translation based defence responses. Whereas symplastic isolation of neighbouring cells by the deposition of callose at plasmodesmata is a largely post-translationally regulated process induced within the generic plant defence response (Wu et al., 2018).

The SEM inquiry of the infected tissues indicates that plasmodesmata, when used by the advancing hyphal front, are potentially 'dead portals', which lack the desmotubule symplastic bridge between neighbouring cells. This was followed up by TEM analysis of lemma tissues at 5dpi following inoculation with WT *F. graminearum*, the $\Delta Tri5$ mutant and mock inoculation. Whether callose deposits are eliminated prior to or coincident with hyphal constriction and traversing of the cell wall are still to be elucidated through further microscopic analysis. The analysis conducted failed to identify desmotubule connections in the tissue explored. However, immunolabelling of callose deposits in TEM micrographs indicate that the presence of DON in the WT strain may affect callose deposition. Where DON is present, callose deposition was observed to be similar to the WT with deposition on one side of the cell wall only, whilst in the $\Delta Tri5$ mutant, callose deposition spanned the entire pit field across both sides of the cell wall. As explored further in the following chapter ([chapter 4](#)), callose deposition at plasmodesmata may be implicated in localised, induced resistance to *F.*

graminearum infection and is stimulated by PAMP elicitors. Whilst further replicates are required to confirm these observations, these initial results support the hypothesis that DON interacts with deposition of callose at plasmodesmata.

Collectively, the data presented in this chapter suggest that the broad-spectrum consequences of DON targeting could prevent the synthesis and action of key defence enzymes at plasmodesmata. This could be further explored by a combined comparative proteomics, phosphoproteomics and RNAseq analysis of the WT and $\Delta Tri5$ -infections to elucidate the wheat defence responses occurring at the advancing *Fusarium* hyphal front that are reduced and/or eliminated by the presence of DON.

The deposition of callose at the plasmodesmatal junction by callose synthases has been demonstrated to be induced by various biotic stress-inducing pathogens (Wu et al., 2018). The role of callose differs with cellular location: callose polymers are a structural component of papillae in various cereal species that form below appressoria produced by fungal pathogens such as the powdery mildew *Blumeria graminis* f. sp. *hordeij*, whereby elevated callose deposition in highly localised papillae in epidermal cells result in resistance to fungal infection (Ellinger et al., 2013). In vascular tissue, callose can be deposited to restrict vascular advancements by wilt pathogens, including by *Fusarium* and *Verticillium* species (reviewed: Kashyap et al., 2021). To investigate the potential of DON impacting upon plasmodesmatal occlusion following our discovery of the impeded traversal of plasmodesmata by the $\Delta Tri5$ strain, we immuno-labelled callose in resin-embedded sections of wheat floral tissues. We found that DON strongly induced callose depositions, and callose deposition was also moderately increased in WT and $\Delta Tri5$ infected lemma and palea tissues. This indicates that callose deposition is increased as a defence response when DON or *Fusarium* hyphae are present. However, in the WT infection, we observed a frequency of callose depositions similar to the non-DON producing $\Delta Tri5$ strain indicating an interruption or targeted degradation of callose occlusions by *F. graminearum* invasive hyphae. The secretion of glycoside hydrolase (GH) proteins that break down β -1,3-glucans such as callose have not been explored with respect to the *F. graminearum*-wheat interaction, although the GH12 family proteins that break down xyloglucan in plant cell walls appear to be implicated in virulence (Wang et al., 2022). The GH81 family of proteins is predicted to catalyse the breakdown of

β -1-3-glycosidic bonds present between glucose monomers in the polysaccharide. The potential for a role for GH81 proteins excreted by *F. graminearum* to facilitate host-tissue colonisation in wheat is explored further in [Chapter 5](#). In the $\Delta Tri5$ infections, in the absence of DON other hyphal components and /or secreted molecules may be responsible for the modest callose deposition at the plasmodesmatal junction.

Intracellular colonisation through the rachis node and beyond in the rachis internode possibly requires DON and is therefore required for the second intracellular phase of the biphasic lifestyle described for *F. graminearum*, where extracellular apoplastic growth characterises the initial 'stealth' phase of infection (Brown et al., 2010). If this is the case, then lacking the ability to traverse plasmodesmata would restrict direct acquisition of nutrients from host cells by the fungal hyphae. The *TRI* biosynthetic gene cluster required for DON biosynthesis is transcriptionally activated early during wheat spike infection, peaking between 72 and 120 hrs post-inoculation (Evans, 2000; Cheng, Kistler and Ma, 2019), when infection is largely restricted to the palea, lemma and glume tissues. Trichothecene biosynthesis is regulated by two transcription factors, TRI6 and TRI10, within the biosynthetic pathway. Of note, DON is not required for full virulence of the developing wheat kernel seed coat (Jansen et al., 2005), in addition to our finding in coleoptiles, Ilgen et al. (2009) identified that trichothecene biosynthesis pathway induction was potentially tissue specific and somewhat restricted to the developing grain kernel and rachis node, and suggested that 'kernel tissue perception' by the *Fusarium* hyphae induce the biosynthesis of trichothecene mycotoxins. This suggestion concurs with Zhang et al. (2012) who report that the trichothecene biosynthesis genes were not induced during *F. graminearum* infection of wheat coleoptiles, whereas Qui et al. (2019) reported the expression of *TRI4* in wheat coleoptiles. We found *TRI5* expression to be detectable at low levels in the wheat coleoptiles, remaining around 0.8 x the expression levels of FgActin, but is not likely to be significantly upregulated.

Gardiner et al. (2009b) presented evidence that, in addition to their previous reports that exogenous application of amines, such as agmatine, *in vitro* induces *TRI5* expression (Gardiner et al., 2009a), low pH further accelerates expression of the *TRI* gene cluster. Other inducers of the DON biosynthetic pathway genes include carbon, nitrogen and light (Gardiner et al., 2009b). These factors could

explain the low and stationary levels of *TRI5* gene expression throughout infection of wheat coleoptiles, which have been noted to be particularly acidic plant tissue due to the optimum activity of expansion proteins around pH 4 (Gao et al., 2008). Other fungal pathogens that are reported to utilise plasmodesmata during infection of cereals include *Magnaporthe oryzae* and *M. oryzae* pathotype *tritricum* which respectively cause rice blast and wheat blast diseases on the floral panicles and floral spikes (Sakulukoo et al., 2018; Fernandez and Orth, 2018). Although *M. oryzae* does not synthesise trichothecene mycotoxins, the invading hyphae secrete another potent general protein translation inhibitor, namely tenuazonic acid (Wilson and Talbot, 2009). The effect of this mycotoxin on plasmodesmatal traversing and virulence in *Magnaporthe spp.* has not yet been reported.

F. graminearum progression into the rachis and through sequential rachis nodes and internodes allows for the successful completion of the disease infection cycle in wheat crops. Typically, perithecia form from the chlorenchyma band of the rachis following prolific hyphal colonisation of this highly specialised photosynthetic tissue layer within the wheat spike (Guenther and Trail, 2005). Hence, interruption of WT disease progression prior to this crucial point in the primarily monocyclic infection cycle is of great interest for reducing full virulence of FHB and in particular in reducing the abundance of air dispersed ascospores. Interestingly, infection of barley spikelets with WT *F. graminearum* is solely restricted to the inoculated spikelet, similarly to $\Delta Tri5$ infection of wheat (Jansen et al., 2005). How this occurs has not yet been explored, but we hypothesise that a lack of traversing of plasmodesmata by hyphae may have a role to play in barley rachis node tissue.

Overall, the results of this chapter indicate that plasmodesmata are the key to successful host-tissue colonisation by *F. graminearum* and that DON, directly or indirectly, facilitates this interaction. It is anticipated that the results of this study are considered in future working disease models of the *F. graminearum* - wheat interaction and suggest these incorporate a greater emphasis on tissue and cell wall architecture and composition when considering host susceptibility to fungal pathogens. To this end, a new working model is proposed (Fig. 3.5.1), that summarises our findings around the presence of DON during wheat infection and the impact on callose deposition at plasmodesmata.

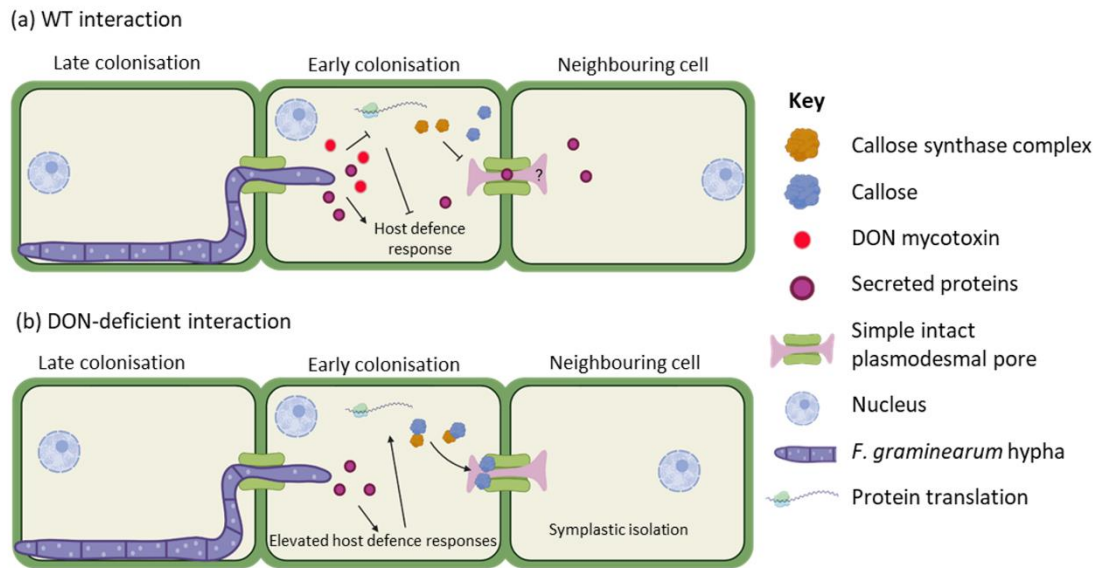


Fig. 3.5.1. Proposed working model for the role of DON in the *F. graminearum* – wheat interaction. (a) In the wild-type (WT) interaction, DON interferes with the wheat host defence response by inhibiting protein translation and reducing the ability of the host to deposit callose at plasmodesmata to restrict further hyphal infection. It is currently unknown how long the desmotubule remains functional, or in place. (b) In the absence of DON, *F. graminearum*-secreted proteins are detected by the host and trigger host defence responses, including the symplastic isolation of neighbouring cells by the deposition of callose at plasmodesmata.

3.6 References

Amsbury S, Benitez-Alfonso Y. (2022). Chapter 10: Immunofluorescence detection of callose in plant tissue sections. In: Benitez-Alfonso, Y. and Heinlein, M. (eds.): *Plasmodesmata: Methods and Protocols*, Methods in Molecular Biology, vol. 2457. doi: 10.1007/978-1-0716-2132-5_10.

Armer VJ, Deeks MJ, Hammond-Kosack KE. (2024). *Arabidopsis thaliana* detached leaf assay for the disease assessment of *Fusarium graminearum*. *Protocols.io*. doi: 10.17504/protocols.io.261gedmwov47/v1.

Armer VJ, Urban M, Ashfield T, Deeks MJ, Hammond-Kosack KE. (2024a). The trichothecene mycotoxin deoxynivalenol facilitates cell-to-cell invasion during wheat-tissue colonisation by *Fusarium graminearum*. *Molecular Plant Pathology*. **25**(6): e13485. 10.1111/mpp.13485.

Berthiller F, Dall'Asta C, Schuhmacher R, Lemmens M, Adam G, Krska R. (2005). Masked mycotoxins: determination of a deoxynivalenol glucoside in artificially and naturally contaminated wheat by liquid chromatography–tandem mass spectrometry. *Journal of Agricultural and Food Chemistry*. **53**(9), 3421-3425. doi: 10.1021/jf047798g.

- Boenisch MJ, Schafer W. (2011). *Fusarium graminearum* forms mycotoxin producing infection structures on wheat. *BMC Plant Biology*. **11**: 110. doi: 10.1186/1471-2229-11-110.
- Brown DW, Dyer RB, McCormick SP, Kendra DF, Plattner RD. (2004). Functional demarcation of the *Fusarium* core trichothecene gene cluster. *Fungal Genetics and Biology*. **41**(4), 454-462. doi: 10.1016/j.fgb.2003.12.002.
- Brown NA, Antoniw J, Hammon-Kosack KE. (2012). The Predicted Secretome of the Plant Pathogenic Fungus *Fusarium graminearum*: A Refined Comparative Analysis. *PLoS ONE*, **7**(4), e33731. doi:10.1371/journal.pone.0033731.
- Brown NA, Bass C, Baldwin TK, Chen H, Massot F, Carion PW, Urban M, van de Meene AM, Hammond-Kosack KE. (2011). Characterisation of the *Fusarium*-wheat floral interaction. *Journal of Pathogens*. Article ID 626345. doi: 10.4061/2011/626345.scholar.
- Brown NA, Urban M, van de Meene AML, Hammond-Kosack KE. (2010). The infection biology of *Fusarium graminearum* defining the pathways of spikelet to spikelet colonisation in wheat ears. *Fungal Biology*. **114**(7): 555-571. doi: 10.1016/j.funbio.2010.04.006.
- Cavinder B, Sikhakolli U, Fellows KM, Trail F. (2012). Sexual development and ascospore discharge in *Fusarium graminearum*. *Journal Visualized Experiments*. **61**: 3895. doi: 10.3791/3895.
- Chen Y, Kistler HC, Ma Z. (2019). *Fusarium graminearum* trichothecene mycotoxins: biosynthesis, regulation, and management. *Annual Review Phytopathology*. **57**: 15-39. doi: 10.1146/annurev-phyto-082718-100318.
- Cuzick A, Urban M, Hammond-Kosack K. (2008). *Fusarium graminearum* gene deletion mutants *map1* and *tri5* reveal similarities and differences in the pathogenicity requirements to cause disease on Arabidopsis and wheat floral tissue. *New Phytologist*. **177**(4), 990-1000. doi: 10.1111/j.1469-8137.2007.02333.x
- Darino M, Urban M, Kaur N, Machado-Wood A, Grimwade-Mann M, Smith D, Beacham A, Hammond-Kosack K. (2024). Identification and functional characterisation of a locus for target site integration in *Fusarium graminearum*. *Fungal Biology and Biotechnology*. **11**: 2. doi: 10.1186/s40694-024-00171-8.
- Deeks MJ, Calcutt JR, Ingle EKS, Hawkins TJ, Chapman S, Richardson AC, Mentlak DA, Dixon MR, Cartwright F, Smertenko AP, Oparka K, Hussey PJ. (2012). A Superfamily of Actin-Binding Proteins at the Actin-Membrane Nexus of Higher Plants. *Current Biology*. **22**(17): P1595-1600. doi: 10.1016/j.cub.2012.06.041.
- Dilks T, Halsey K, De Vos RP, Hammond-Kosack KE, Brown NA. (2019). Non-canonical fungal G-protein coupled receptors promote *Fusarium* head blight on wheat. *PLoS Pathogens*. **15**(4): e1007666. doi: 10.1371/journal.ppat.1007666.

- Ellinger D, Naumann M, Falter C, Zwikowics C, Jamrow T, Manisseri C, Somerville SC, Voigt CA. (2013). Elevated early callose deposition results in complete penetration resistance to powdery mildew in *Arabidopsis*. *Plant Physiology*. **161**(3): 1433-1444. doi: 10.1104/pp.112.211011
- Evans CK, Xie W, Dill-Macky R, Mirocha CJ. (2000). Biosynthesis of deoxynivalenol in spikelets of barley inoculated with macroconidia of *Fusarium graminearum*. *Plant Disease*. **84**(6): 654-660. doi: 10.1094/PDIS.2000.84.6.654.
- Fan J, Urban M, Parker JE, Brewer HC, Kelly SL, Hammond-Kosack KE, Fraaije BA, Liu X, Cools HJ. (2013). Characterization of the sterol 14 α -demethylases of *Fusarium graminearum* identifies a novel genus-specific CYP51 function. *New Phytologist*. **198**(3): 821–835. doi: 10.1111/nph.12193.
- Fernandez J, Orth K. (2018). Rise of a cereal killer: The biology of *Magnaporthe oryzae* biotrophic growth. *Trends in Microbiology*. **26**(7), 582-597. doi: 10.1016/j.tim.2017.12.007.
- Gao Q, Zhao M, Li F, Gau Q, Xing S, Wang W. (2008). Expansins and coleoptile elongation in wheat. *Protoplasma*. **233**: 73-81. doi: 10.1007/s00709-008-0303-1.
- Gardiner DM, Kazan K, Manners JM. (2009). Nutrient profiling reveals potent inducers of trichothecene biosynthesis in *Fusarium graminearum*. *Fungal Genetics and Biology*. **46**: 604–613. doi: 10.1016/j.fgb.2009.04.004.
- Gardiner DM, Osbourne S, Kazan K, Manners JM. (2009). Low pH regulates the productions of deoxynivalenol by *Fusarium graminearum*. *Microbiology*. **155**(9): 3149-3156. doi: 10.1099/mic.0.029546-0.
- Guenther JC, Trail F. (2005). The development and differentiation of *Gibberella zeae* (anamorph: *Fusarium graminearum*) during colonization of wheat. *Mycologia*. **97**(1): 229-237. doi: 10.1080/15572536.2006.11832856.
- Hallen-Adams HE, Wenner N, Kuldau GA, Trail F. (2011). Deoxynivalenol biosynthesis-related gene expression during wheat kernel colonization by *Fusarium graminearum*. *Phytopathology*. **101**(9): 1091-1096. doi: 10.1094/PHYTO-01-11-0023.
- Hohn TM, McCormick SP, Desjardins AE. (1993). Evidence for a gene cluster involving trichothecene-pathway biosynthetic genes in *Fusarium sporotrichioides*. *Current Genetics*. **24**: 291-295. doi: 10.1007/bf00336778.
- Ilgen P, Hadelar B, Maier FJ, Schäfer W. (2009). Developing Kernel and Rachis Node Induce the Trichothecene Pathway of *Fusarium graminearum* During Wheat Head Infection. *Molecular Plant Microbe Interactions*, **22**(8): 899-908. doi: 10.1094/MPMI-22-8-0899.
- Jansen C, von Wettstein D, Schäfer W, Kogel K-H, Felk A, Maier FJ. (2005). Infection patterns in barley and wheat spikes inoculated with wild-type and trichodiene synthase gene disrupted *Fusarium graminearum*. *PNAS*. **102**(46): 16892- 16897. doi: 10.1073/pnas.0508467102.

- Kashyap A, Planas-Marquès M, Capellades M, Valls M, Coll NS. (2021). Blocking intruders: inducible physico-chemical barriers against plant vascular wilt pathogens. *Journal of Experimental Botany*. **72**(2): 184-198. doi: 10.1093/jxb/eraa444.
- Kimura M, Kaneko I, Komiyama M, Takatsuki A, Koshino H, Yoneyama K, Yamaguchi I. (1998). Trichothecene 3-O-acetyltransferase protects both the producing organism and transformed yeast from related mycotoxins. *Journal of Biological Chemistry*. **273**: 1654–1661. doi: 10.1074/jbc.273.3.1654.
- Kimura M, Tokai T, O'Donnell K, Ward TJ, Fujimura M, Hamamoto H, Shibata T, Yamaguchi I. (2003). The trichothecene biosynthesis gene cluster of *Fusarium graminearum* F15 contains a limited number of essential pathway genes and expressed non-essential genes. **539**(1-3): 105-110. doi: 10.1016/S0014-5793(03)00208-4.
- Kroll EK, Bayon C, Rudd J, Armer V, Magaji- Umashankar A, Ames R, Urban M, Brown NA, Hammond-Kosack KE. (2024). A conserved fungal Knr4/Smi1 protein is vital for maintaining cell wall integrity and host plant pathogenesis. *bioRxiv*, 2024.05.31.596832; doi: 10.1101/2024.05.31.596832.
- Lee J, Lu H. (2011). Plasmodesmata: the battleground against intruders. *Trends in Plant Science*. **16**(4): 201-210. doi: 10.1016/j.tplants.2011.01.004.
- Lemmens M, Scholz U, Berthiller F, Dall'Asta C, Koutnik A, Schuhmacher R, Adam G, Buerstmayr H, Mesterházy A, Krska R, Ruckebauer P. (2005). The ability to detoxify the mycotoxin deoxynivalenol colocalizes with a major quantitative trait locus for Fusarium Head Blight resistance in wheat. *Molecular Plant Microbe Interactions*. **18**(12): 1318-1324. doi: 10.1094/MPMI-18-131.
- McCormick SP, Alexander NJ, Proctor RH. (2006). *Fusarium Tri4* encodes a multifunctional oxygenase required for trichothecene biosynthesis. *Canadian Journal of Microbiology*. **52**: 636–642. doi: 10.1139/w06-011.
- McCormick SP, Stanley AM, Stover NA, Alexander NJ. (2011). Trichothecenes: from simple to complex mycotoxins. *Toxins*. **3**(7): 802-814. doi: 10.3390/toxins3070802.
- McMullen M, Bergstrom G, De Wolf E, Dill-Macky R, Hershman D, Shaner G, Van Sanford D. (2012). A unified effort to fight an enemy of wheat and barley: Fusarium head blight. *Plant Disease*. **96**(12): 1712-1728. doi: 10.1094/PDIS-03-12-0291.
- McMullen M, Jones R, Gallenberg D. (1997). Scab of wheat and barley: a re-emerging disease of devastating impact. *Plant Disease*. **81**(12): 1340 – 1348. doi: 10.1094/PDIS.1997.81.12.1340.
- Mendiburu F, Yaseen M. (2020). *Agricolae: statistical procedures for agricultural research*. R package version 1.4.0.
- Mesterházy A. (1995). Types and components of resistance to *Fusarium* head blight of wheat. *Plant Breeding*. **114**: 377-386. doi: 10.1111/j.1439-0523.1995.tb00816.x

- Mitra PP, Loque D. (2014). Histochemical staining of *Arabidopsis thaliana* secondary cell wall elements. *Journal of Visualized Experiments*. **87**: 51381. doi: 10.3791/51381.
- Parry DW, Jenkinson P, McLeod L. (1995). *Fusarium* ear blight (scab) in small grain cereals—A review. *Plant Pathology*. **44**: 207–238. doi: doi.org/10.1111/j.1365-3059.1995.tb02773.x.
- Pestka JJ. (2008). Mechanisms of Deoxynivalenol-Induced Gene Expression and Apoptosis. *Food Additives and Contamination Part A: Chemistry, Analysis, Control, Exposure and Risk Assessment*. **25**(9): 1128–1140. doi: 10.1080/02652030802056626.
- Pestka JJ. (2010). Deoxynivalenol: mechanisms of action, human exposure, and toxicological relevance. *Archives of Toxicology*. **84**: 663-679. doi: 10.1007/s00204-010-0579-8.
- Pritsch C, Muehlbauer GJ, Bushnell WR, Somers DA, Vance CP. (2000). Fungal development and induction of defense response genes during early infection of wheat spikes by *Fusarium graminearum*. *Molecular Plant Microbe Interactions*. **13**(2): 159-169. doi: 10.1094/MPMI.2000.13.2.159.
- Proctor RH, Hohn TM, McCormick SP. (1995). Reduced virulence of *Gibberella zeae* caused by disruption of a trichothecene toxin biosynthetic gene. *Molecular Plant Microbe Interactions*. **8**(4), 593-601. doi: 10.1094/mpmi-8-0593.
- Qui H, Zhao X, Fang W, Wu H, Abubakar YS, Lu G, Wang Z, Zheng W. (2019). Spatiotemporal nature of *Fusarium graminearum*-wheat coleoptile interactions. *Phytopathology Research*. **1**, article 26. doi: 10.1186/s42483-019-0033-7.
- Sager RE, Lee J. (2018). Plasmodesmata at a glance. *Journal of Cell Science*. **131**(11), jcs209346. doi: 10.1242/jcs.209346.
- Sakulkoo W, Osés-Ruiz M, Garcia EO, Soanes DM, Littlejohn GR, Hacker C, Correia A, Valent B, Talbot NJ. (2018). A single fungal MAP kinase controls plant cell-to-cell invasion by the rice blast fungus. *Science*. **359**(6382): 1399-1403. doi: 10.1126/science.aaq0892.
- Shin S, Torres-Acosta JA, Heinen SJ, McCormick S, Lemmens M, Paris MPK, Berthiller F, Adam G, Muehlbauer GJ. (2012). Transgenic *Arabidopsis thaliana* expressing a barley UDP-glucosyltransferase exhibit resistance to the mycotoxin deoxynivalenol. *Journal of Experimental Biology*. **63**(13): 4731-4740. doi: 10.1093/jxb/ers141.
- Tag AG, Garifullina GF, Peplow AW, Ake C, Phillips TD, Hohn TM, Beremand MN. (2001). A novel regulatory gene, *Tri10*, controls trichothecene toxin production and gene expression. *Applied and Environmental Microbiology*. **67**: 5294–5302. doi: 10.1128/AEM.67.11.5294-5302.2001.
- Tokai T, Koshino H, Takahashi-Ando N, Sato M, Fujimura M, Kimura M. (2007). *Fusarium Tri4* encodes a key multifunctional cytochrome P450 monooxygenase for four consecutive oxygenation steps in trichothecene biosynthesis. *Biochemical and Biophysical Research Communications*. **353**(2): 412-417. doi: 10.1016/j.bbrc.2006.12.033.
- Van Der Plank JE. (1963). Plant diseases: epidemics and control. Academic Press, New York.

- Vaughan M, Backhouse D, Ponte EMD. (2016). Climate change impacts on the ecology of *Fusarium graminearum* species complex and susceptibility of wheat to Fusarium head blight: a review. *World Mycotoxin Journal*, **9**(5): 685–700. doi: 10.3920/WMJ2016.2053
- Wang J, Zhang M, Yang J, Yang X, Zhang J, Zhao Z. (2023). Type A Trichothecene Metabolic Profile Differentiation, Mechanisms, Biosynthetic Pathways, and Evolution in *Fusarium* Species-A Mini Review. *Toxins (Basel)*. **15**(7): 446. doi: 10.3390/toxins15070446.
- Wang Z, Yang B, Zheng W, Wang L, Cai X, Yang J, Song R, Yang S, Wang Y, Xiao J, Liu H, Wang Y, Wang X, Wang Y. (2022). Recognition of glycoside hydrolase 12 proteins by the immune receptor RXEG1 confers *Fusarium* head blight resistance in wheat. *Plant Biotechnology Journal*. **21**(4): 769-781. doi: 10.1111/pbi.13995.
- Wanjiru WM, Zhensheng K, Buchenauer H. (2002). Importance of cell wall degrading enzymes produced by *Fusarium graminearum* during infection of wheat heads. *European Journal of Plant Pathology*. **108**: 803-810. doi: 10.1023/A:1020847216155.
- Wickham H. (2016). *ggplot2: Elegant Graphics for Data Analysis*. Springer-Verlag, New York.
- Wilson RA, Talbot NJ. (2009). Under pressure: investigating the biology of plant infection by *Magnaporthe oryzae*. *Nature Reviews Microbiology*, **7**: 185-195. doi: 10.1038/nrmicro2032.
- Wu S, Kumar R, Iswanto ABB, Kim J. (2018). Callose balancing at plasmodesmata. *Journal of Experimental Botany*. **69**(22), 5325-5339. doi: 10.1093/jxb/ery317.
- Zhang X-W, Jia L-J, Zhang Y, Li X, Zhang D, Tang W-H. (2012). In planta stage-specific fungal gene profiling elucidates the molecular strategies of *Fusarium graminearum* growing inside wheat coleoptiles. *Plant Cell*. **24**(12). 5159-5176. doi: 10.1105/tpc.112.105957.

Chapter 4: Sequential inoculation of DON producing and DON non-producing *F. graminearum* isolates and the triggering of PTI-mediated defences

4.1 Acknowledgement of contributions

I would like to thank Martin Urban (Rothamsted Research) for the original generation of the $\Delta Tri5$ mutant, which was published in Cuzick, Urban and Hammond-Kosack (2008).

4.2 Introduction

The results described in [Chapter 3](#) encouraged us to consider the types of immune responses triggered by the single gene deletion mutant $\Delta Tri5$ that are normally inhibited in the WT-interaction when the trichothecene mycotoxin DON is present (see also Armer et al., 2024 (a)). It is hypothesised that in the absence of the trichothecene mycotoxin deoxynivalenol (DON), infection of wheat spikes by *Fusarium graminearum* is effectively prevented by induced wheat immune responses.

Plant immune responses occur through two layers, which are triggered by pathogen associated molecular patterns (PAMPs) and small pathogen-secreted proteins known as effectors. These underpin Pathogen Triggered Immunity (PTI) and Effector Triggered Immunity (ETI) specific responses, respectively, as described previously in [section 1.3](#). The experiments outlined in this chapter aimed to test the hypothesis that recognition of *F. graminearum* in the absence of DON, as occurs in the wheat spike $-\Delta Tri5$ mutant interaction, would initiate immune signalling and prevent subsequent WT infection. This was tested through a series of co-inoculation experiments with the virulent (WT) and avirulent ($\Delta Tri5$) *F. graminearum* strains. Subsequently, it is tested whether the specific defence pathways that are dampened by the presence of DON are triggered by PTI or ETI responses through application of the PAMP chitin prior to WT inoculation.

The co-inoculation of virulent and virulent strains of pathogens have been explored previously for effective control of plant pathogens. In *Fusarium*

oxysporum, a vascular wilt pathogen closely related to *F. graminearum* and causal agent of Panama Disease of banana (*Musa acuminata*), the highly destructive strain Tropical Race 4 (TR4) can be effectively controlled by pre-inoculating with an avirulent *F. oxysporum* strain known as Race 1 (García-Bastidas et al., 2022). The systemic defence response pathways of ethylene and jasmonate signaling were induced with Race 1 and significantly reduced disease progression of TR4. Similarly, various f. sp. of *F. oxysporum*, which cause vascular wilts of a wide variety of crops have been found to be reduced in virulence when also in the presence of a fungal endophyte (de Lamo and Takken, 2020), indicating that the presence of non-virulent pathogens can induce durable disease resistance and inoculation of avirulent strains may be an effective method of biocontrol of more destructive fungal pathogens. However, whether this occurs through the PTI or ETI branches of plant immunity was not deciphered.

In the case of mounting responses to fungal endophytes, there is a trade-off between resource allocation towards immunity and yield with plant resources usually directed towards normal growth and development, instead being diverted towards (Brown, 2002). However, identifying and deploying specific immune responses that confer resistance to destructive fungal pathogens with the potential to inflict high yield losses is of benefit, and may be an ideal focus for biocontrol. The specific infection window of *F. graminearum* timed to cereal spike anthesis poses a unique opportunity for induction of transient immunity through either a PTI or ETI pathway. This is particularly interesting when focusing on the induced callose deposition at plasmodesmatal pit fields which can prevent hyphal traversing cell walls rachis tissue, which has previously been shown to be an essential component of infection ([Chapter 3](#); Armer et al., 2024a).

The results of this chapter bring new questions to light surrounding the perception of fungal pathogens in the wheat spikelet, and the induction and subsequent durability of wheat defence responses. It also postulates the potential for biocontrol of *F. graminearum* with elicitors of the PTI branch of plant immunity and/or colonisation with fungal endophytes / avirulent strains of *F. graminearum*.

4.3 Materials and Methods

The methods outlined here are in addition to those detailed in the [general materials and methods chapter](#).

4.3.1 Point inoculations

The susceptible dwarf spring wheat cultivar 'Apogee' was used for all experiments and grown as per the conditions outlined in section [2.4.2](#). Fungal inoculum was prepared as outlined in [2.4.1](#) and a concentration of 5×10^5 spores/ml used for the WT reference strain PH-1 and the DON-deficient single gene deletion mutant $\Delta Tri5$. DON was applied at a concentration of 35ppm, as determined previously in [3.3.1](#). For the chitin application for elicitation of PAMP-triggered immunity, 100 μ g/ml shrimp chitin (Sigma Aldrich) concentration was used, as previously described (Hao et al., 2022).

Inoculations of wheat plants occurred at mid-anthesis in the 7th true (fertile) spikelet from the base of the wheat spike, as previously described [2.4.4](#).

4.3.2 Spray inoculations

To determine if PAMP-triggered immunity is local or systemic, a spray inoculation disease assessment was conducted. Chitin and the DON-deficient *F. graminearum* strain $\Delta Tri5$ were used as immune response elicitors, with water (dH₂O) as the mock treatment control, as concentrations previously described in [4.3.1](#). To ensure fungal infection, the non-ionic surfactant Tween 20 (Polysorbate 20; Sigma Aldrich) at a concentration of 0.02% (v/v) was added to all treatments for spray inoculations.

4.3.3 Co- and sequential inoculations

The PAMP elicitor chitin and the DON-deficient *Fg* strain $\Delta Tri5$ were used as pre-treatments for the subsequent assessment of immune system activation and inoculated by point or spray inoculation at early anthesis. For point inoculations only, the mycotoxin DON was included as an immune system elicitor. Water (dH₂O) and the *F. graminearum* WT strain PH-1 were also included as controls. After inoculation, plants were kept in high humidity boxes (RH < 90%) until the subsequent treatment. Either 24 hours or 48 hours after the initial treatment, WT *F. graminearum* was inoculated onto the wheat spike following the same

inoculation method (i.e., point or spray inoculation). As controls, dH₂O, chitin, $\Delta Tri5$, and PH-1 treatments were also included.

4.3.4 Disease assessment

To quantify disease levels after point inoculations, the number of spikelets exhibiting macroscopic disease symptoms were counted at day 3, 7, 10 and 14 of disease progression and the Area Under Disease Progression Curve (AUDPC) was calculated, both as outlined in section [2.4.5](#).

4.3.5 Determination of $\Delta Tri5$ presence in wheat spike tissue

To determine if the WT strain PH-1 facilitated subsequent tracking through the rachis by the DON-deficient strain $\Delta Tri5$, infected rachis tissue from the inoculated spikelet, i.e. 7th spikelet (1st true spikelet from base of wheat spike) was excised at the end of disease progression (14dpi). Other floral tissues were removed with a sterile razor blade and rachises placed onto SNA plates supplemented with the antibiotic selection marker for the $\Delta Tri5$ strain, namely hygromycin at 75mg/ml. Plates were left at RT under near UV light, as detailed in section [2.4.1](#). Fungal growth onto plates was then sampled for gDNA, and a PCR done using the hygromycin primers to determine if $\Delta Tri5$ was present or absent. DNA extraction occurred using the phenol/ chloroform method as detailed in [2.3.1](#) and PCR followed the protocol as detailed in section [2.3.4](#).

4.3.6 Callose deposition in rachis tissues

To determine if callose deposition at plasmodesmata/ pit fields was responsible for the local acquisition of resistance in spikelets, LR-white resin-embedded samples of rachis tissues were prepared, sectioned and immuno-localisation of callose was done as outlined in sections [2.4.2](#), [2.4.3](#) and [2.4.5](#), respectively. Rachis samples were prepared after 24 and 48 hrs post-inoculation with different prospective callose inducers, *F. graminearum* PH-1 (WT) or the $\Delta Tri5$ mutant at 5×10^5 spores/ml, the mycotoxin DON (35ppm) or chitin (100 μ g/ml). Two controls were included in this study, with water droplets (dH₂O) and no treatment at all into spikelets to control for tissue disturbance during inoculation. Inoculations occurred in the 7th true spikelet, as outlined in section [2.4.4](#).

Image analysis was done in ImageJ, using the thresholding parameters as outlined in section [3.3.5](#) and was applied to all treatments. The number of callose deposits, total area of callose deposits and number of callose deposits per cell were calculated.

4.4 Results

4.4.1 Inoculation with DON-deficient $\Delta Tri5$ mutant prevents subsequent infection of WT *F. graminearum*

To explore whether wheat defence responses were upregulated in the absence of the mycotoxin DON, the DON-deficient *F. graminearum* strain $\Delta Tri5$ was point-inoculated into wheat spikelets. Subsequently, the WT strain PH-1 was inoculated into the same spikelet 24 hrs and 48 hrs later. These experiments revealed that the inoculation of $\Delta Tri5$ prevented subsequent WT infection at both timepoints, indicating that defence responses that are upregulated in the presence of $\Delta Tri5$ are sustained for at least 48 hrs (Fig 4.4.1. (a)). Analysis of disease progression through area under disease progression curve (AUDPC) found that when PH-1 was inoculated first and $\Delta Tri5$ co-inoculated 24hrs later into wheat spikelets the AUDPC was comparable to the PH-1 control (Fig. 4.4.1 (b)). Although close examination of the dataset revealed that these mixed infections tracked ahead of the PH-1 alone during the mid-disease progression phase (Fig. 4.4.1. (a)). Symptoms on the $\Delta Tri5$ and WT sequentially inoculated wheat spikes were comparable to the $\Delta Tri5$ infected alone, with eye-shaped lesions on the outer glume and no symptoms in the rachis (Fig. 4.4.1. (c)), as also exemplified and discussed in section [3.4.3](#).

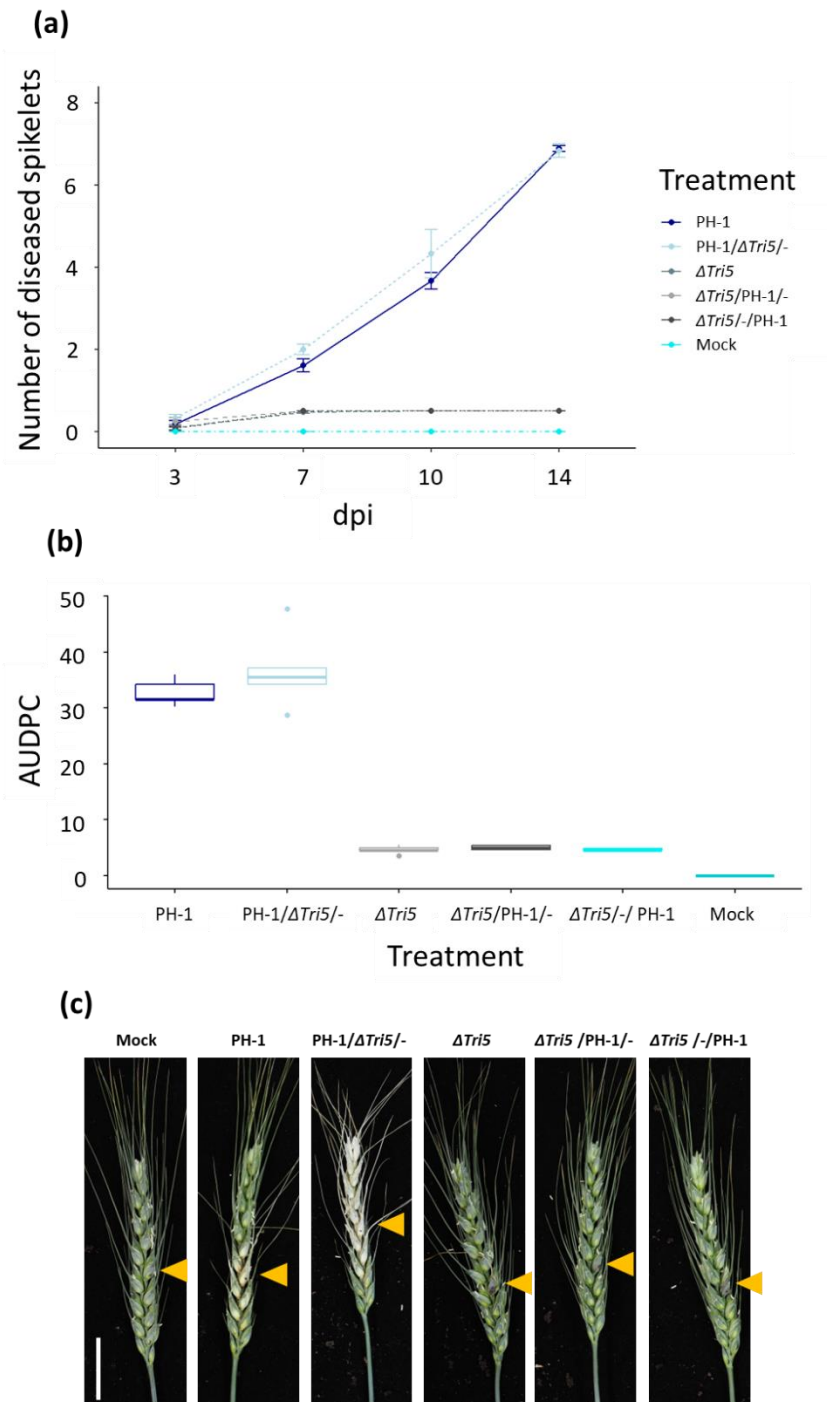


Fig. 4.4.1. Pre-treatment of spikelets with the DON-deficient *Fg* strain $\Delta Tri5$ prevents subsequent WT-infection. (a) Disease progression of WT (PH-1), WT with subsequent $\Delta Tri5$ infection 24hrs later (PH-1/ $\Delta Tri5$ /-), $\Delta Tri5$ with PH-1 at 24 hrs later ($\Delta Tri5$ /PH-1/-), $\Delta Tri5$ with PH-1 at 48 hrs later ($\Delta Tri5$ /-/PH-1) and mock (dH₂O) control treatment. (b) Area Under Disease Progression Curve (AUDPC) of disease progression curve. Kruskal-Wallis $\chi^2 = 35.669$, $df = 5$, p -value = $1.106e-06$. (c) Example images of co-inoculated wheat spikes at 10dpi. Yellow arrow indicates inoculated spikelet (7th), scale bar = 20mm. Experiment was repeated 3 times with 3 biological replicates per experimental replicate.

4.4.2 *In planta* growth of the *Fg* $\Delta Tri5$ mutant tracks behind PH-1

Sequential inoculation of wheat spikelets with the WT *F. graminearum* strain PH-1 and then $\Delta Tri5$ 24 hours later increased disease severity during the mid-disease progression phase (Fig. 4.4.1 (a)). To investigate whether the DON-deficient mutant $\Delta Tri5$ was able to track behind the DON-excreting WT strain into the rachis, rachis sections from below the inoculated wheat spikelet, i.e. rachis internodes 6 and 7 were dissected at 14dpi and placed onto SNA plates supplemented with the selection marker Hygromycin. In all three replicates hyphal growth into the agar was observed by day 3 (Fig. 4.4.2 (a)). Dissected rachis internodes 7 (the inoculated spikelet) and 6 (the rachis internode directly below) showed outgrowth on SNA amended with 20 μ g/ml hygromycin (Fig. 4.4.2 (b)) in three biological replicates. In a further serial dissection of whole wheat spike rachis internodes shows a visible distance-dependent outgrowth into the hygromycin-amended SNA, with the greatest outgrowth in RI-7, RI-6 and RI-5, closest to the point of inoculation. Interestingly, outgrowth is also observed in the peduncle despite no outgrowth in neighbouring rachis internodes, which may indicate use of vascular elements by $\Delta Tri5$. WT *F. graminearum* is unable to grow on SNA with 20 μ g/ml hygromycin.

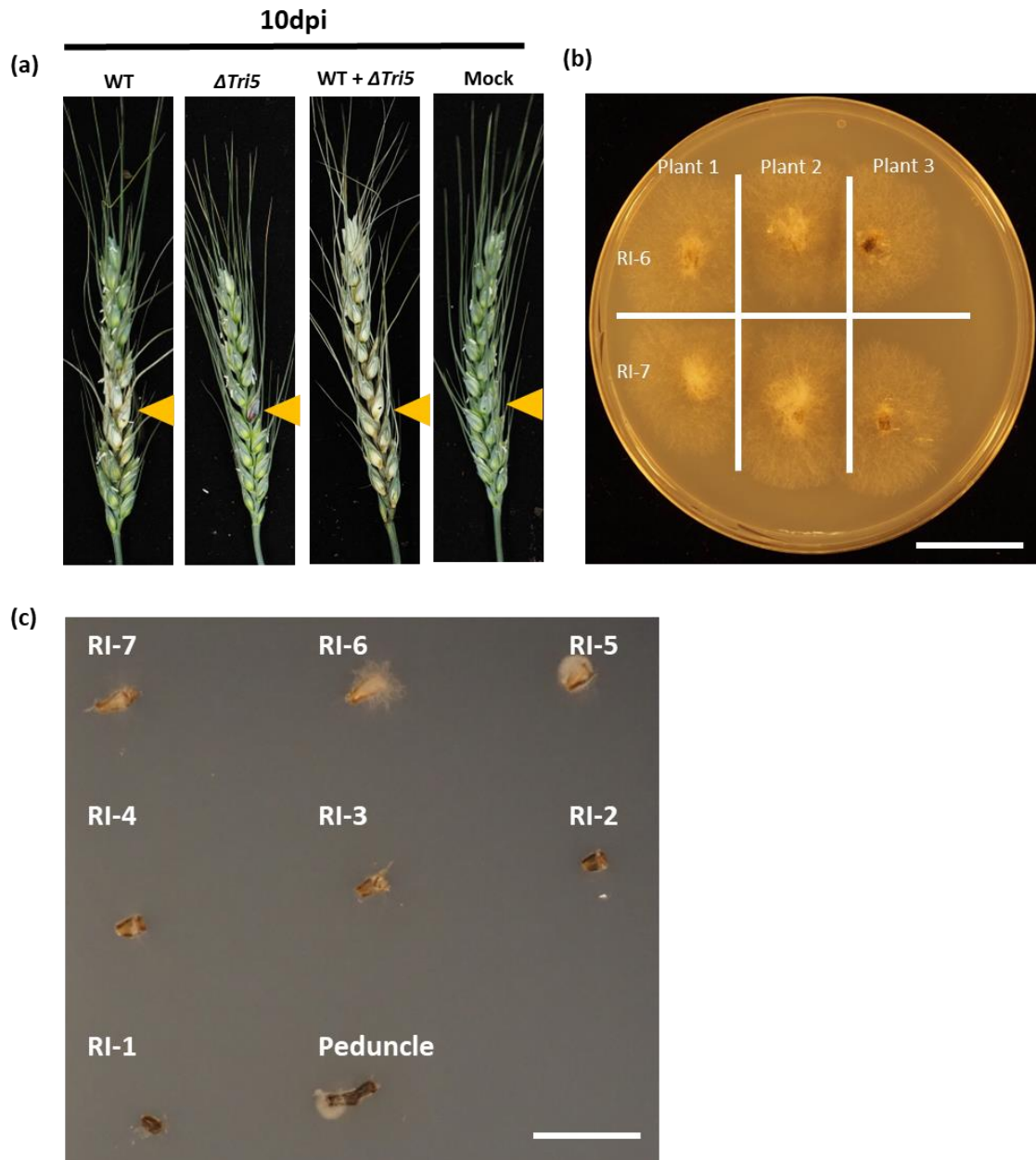


Fig. 4.4.2 $\Delta Tri5$ tracking behind WT *F. graminearum* in wheat spikes. (a) Appearance of wheat spikes after applying the four different treatments. The spikes inoculated with WT strain PH-1 and subsequently $\Delta Tri5$ have advanced disease progression compared to WT alone. Yellow arrows indicate inoculated spikelets. Images of exemplar wheat spikes were images at 10dpi. (b) Rachis internodes of PH-1 (WT) point-inoculated samples (RI-7) subsequently inoculated with $\Delta Tri5$ and adjacent rachis internode (RI-6) from wheat spikes at 10dpi, showing outgrowth into SNA amended with 20 μ g/ml hygromycin, scale bar = 20mm. (c) Serial dissection of whole wheat spike rachis internodes from infected wheat spike with WT infection and $\Delta Tri5$ infection 24 hours later at 10dpi, from point of infection (RI-7) to base of wheat spike (peduncle). Outgrowth into SNA amended with 20 μ g/ml hygromycin indicates presence of $\Delta Tri5$, scale bar = 20mm. Experiment was conducted once with 3 biological replicates.

4.4.3 Application of the PTI-elicitor chitin prevents subsequent *F. graminearum* infections

Following the results in section 4.4.1, we hypothesised that the induced resistance observed in both pre-inoculations at 24 and 48hrs by $\Delta Tri5$ was PAMP triggered. To test this, pre-inoculations of wheat spikes with the PAMP-elicitor chitin prior to *F. graminearum* inoculation were conducted. We also included the mycotoxin DON as a potential PAMP. These experiments revealed that application of chitin at 100 μ g/ml by point inoculation prevented symptoms of both WT (PH-1) infection and those characteristic of the DON-deficient strain $\Delta Tri5$ (Fig. 4.4.3). This was observed when the chitin pre-treatment was done at either 24 or 48hrs prior to WT inoculation, with disease symptoms only breaking through when spikelets were pre-treated with the mycotoxin DON (Fig. 4.4.3. (a) and (c)). However, some samples exhibited limited disease symptoms when pre-treated with chitin, as shown in Fig. 4.5 (c)), but did not break into the rachis tissue during the 14 day disease progression timeframe used in this study. AUDPC analysis demonstrated a significance, Kruskal-Wallis $\chi^2 = 21.602$, $df = 6$, p -value < 0.005 (**), between PAMP (DON and chitin) pre-treated samples with WT inoculation and the WT alone control (Fig. 4.4.3 (b)). In the DON pre-treatment at 24 hours, disease symptoms were evident in the inoculated spikelet, but this was not observed when WT *F. graminearum* was inoculated 48 hours later. This result needs to be verified through further experimental replicates but may indicate differing reception mechanisms between DON and chitin.

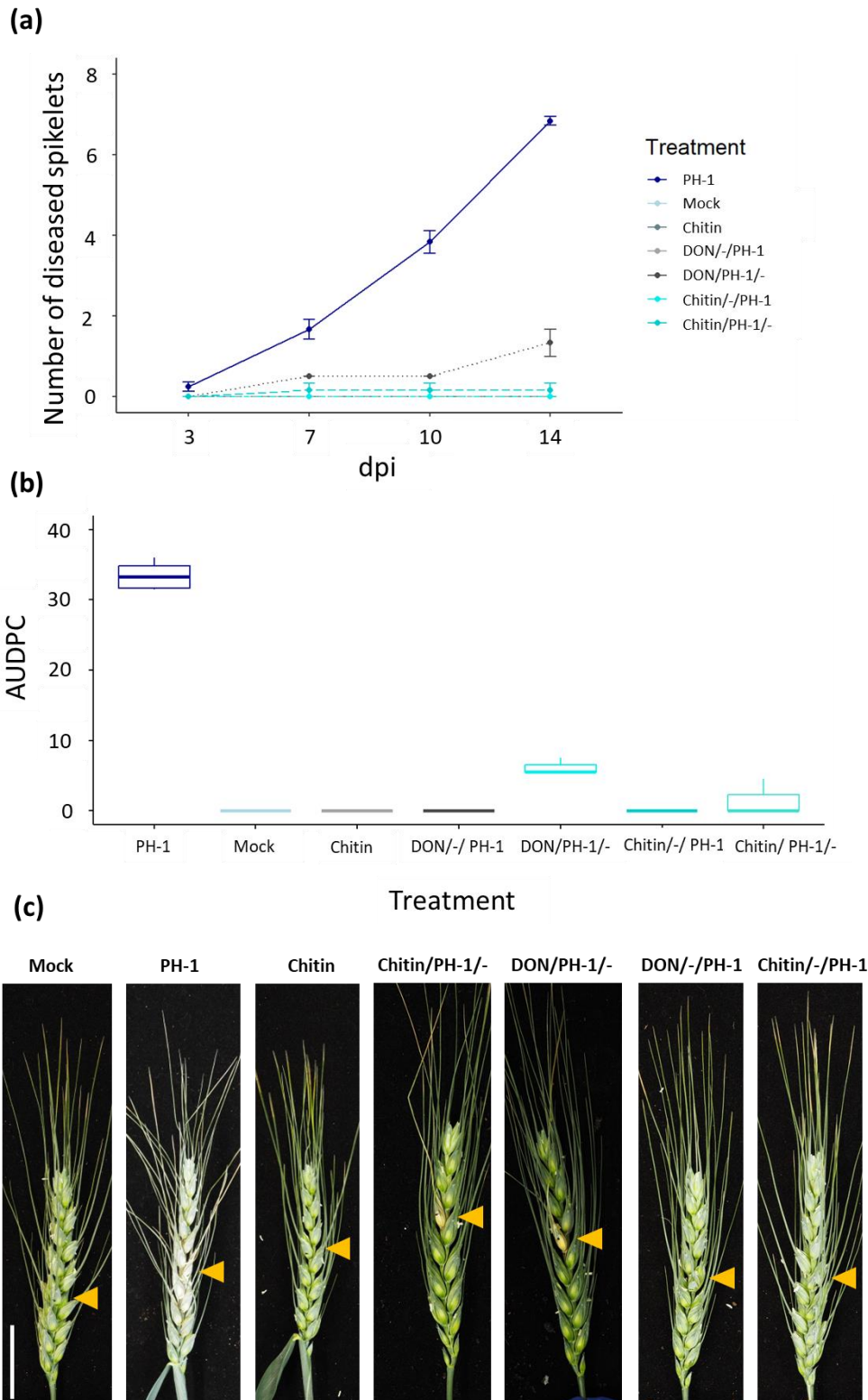


Fig. 4.4.3. Pre-treatment of spikelets with the PAMP elicitor chitin and mycotoxin DON prevents subsequent WT-infection. (a) Disease progression of WT (PH-1), chitin treatment with subsequent PH-1 inoculation at 24hrs later (Chitin/PH-1/-) or 48hrs later (Chitin/-/PH-1), DON treatment with PH-1 24 hrs later (DON/PH-1/-) and 48 hrs later (DON/-/PH-1) and mock (dH₂O) control treatment. (b) Area Under Disease Progression Curve (AUDPC) of disease progression curve. Kruskal-Wallis $\chi^2 = 21.602$, df = 6, p-value = 0.001429. (c) Example images of co-

inoculated wheat spikes at 10dpi. Yellow arrow indicates inoculated spikelet (7th), scale bar = 20mm. Experiment was conducted in triplicate with 3 biological replicates.

4.4.4 Pre-inoculation treatments are not inducing resistance through tissue disturbance

To rule out the potential of physical or physiological spikelet tissue disturbance through point-inoculation between the lemma and palea tissues causing the induced resistance observed by chitin, $\Delta Tri5$ or DON, a control experiment was devised. Sterile water (dH₂O) was inoculated into spikelets 24 and 48 hrs prior to subsequent inoculation with WT (PH-1) and $\Delta Tri5$ *F. graminearum* strains. These experiments showed that tissue disturbances did not induce any measurable resistances compared to control *F. graminearum* treatments alone (Fig. 4.4.4 (a) and (b)), Kruskal-Wallis $\chi^2 = 7.8873$, df = 3, p-value = 0.0484, confirming that induced resistance by $\Delta Tri5$ and chitin were due to PAMP-triggered immunity. Example disease symptoms are shown in Fig. 4.4.4 (c) at 7dpi, with typical symptoms of PH-1 (WT) and $\Delta Tri5$ shown despite prior tissue disturbance.

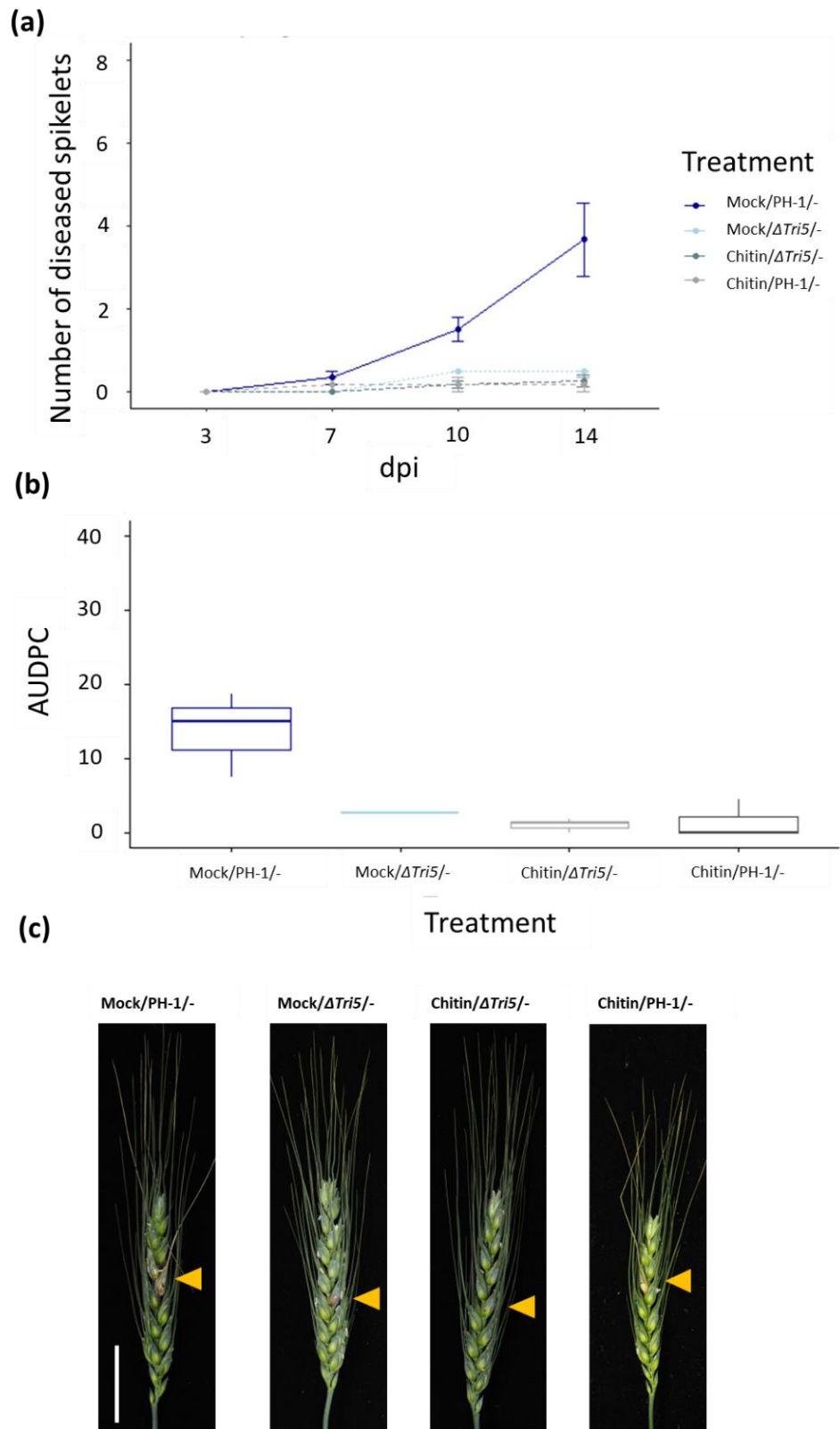
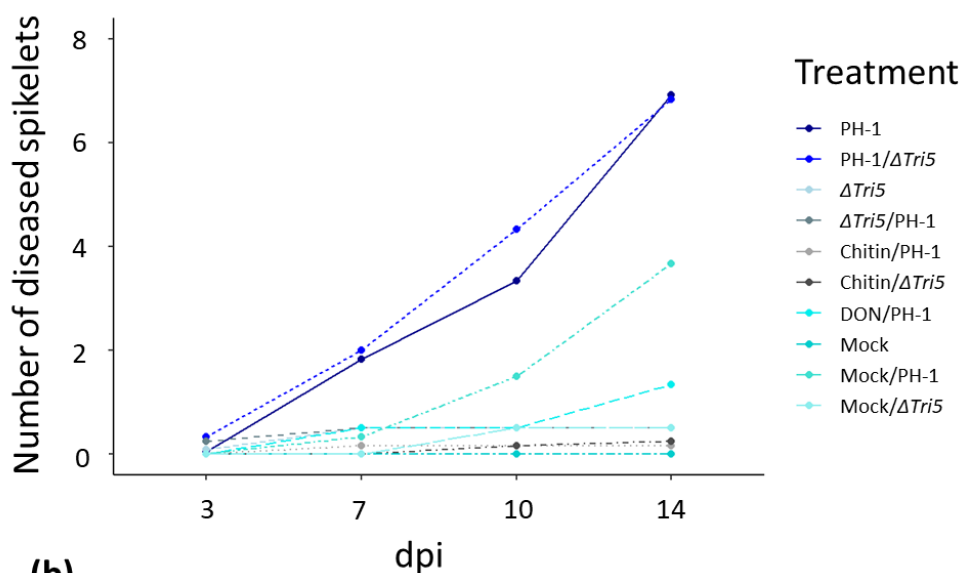


Fig. 4.4.4. Disease progression of water and chitin pre-treated wheat spikes with subsequent *Fg* inoculation 24 hrs later. (a) Disease progression of mock and chitin pre-inoculated spikes at 3, 7, 10 and 14dpi, with subsequent WT (PH-1) or Δ Tri5 inoculation 24 hrs later. (b) AUDPC, Kruskal-Wallis $\chi^2 = 7.8873$, $df = 3$, p -value = 0.0484. (c) Example images of co-inoculated wheat spikes at 7dpi. Yellow arrow indicates inoculated spikelet (7th), scale bar = 20mm, $n=3$ for all treatments.

4.4.5 Induced resistance is durable for 48 hours at a local scale

Sequential inoculation experiments were done with elicitation of defences at either 24 or 48 hours prior to inoculation with the WT *F. graminearum* strain PH-1. Other timepoints were not tested in this experiment. Similar disease levels were observed across 24hr pre-treatment with the elicitors chitin, DON, and the DON-deficient strain $\Delta Tri5$ (Fig. 4.4.5. (a)) and those at 48hrs (Fig. 4.4.5 (b)). Whilst further timepoints were not tested, these experiments indicate that induced resistance is sustained for at least 48hrs.

(a)



(b)

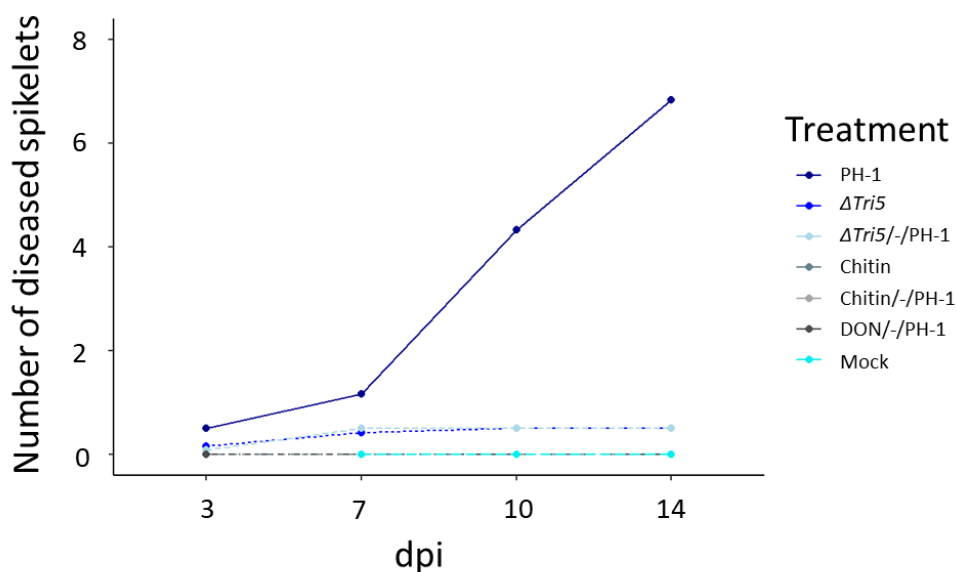


Fig. 4.4.5. Disease progression with elicitation of defences at 24hrs pre-inoculation and 48hrs pre-inoculation. (a) Pre-inoculation with PH-1 (dark blue), $\Delta Tri5$ (mid-blue), Chitin (grey), DON (cyan) and Mock (turquoise), 24hrs before PH-1 or $\Delta Tri5$ 24hrs later (day 0). (b) Pre-inoculation with PH-1 (dark blue), $\Delta Tri5$ (mid-blue), Chitin (light grey), DON (dark grey) and Mock (turquoise) followed by the WT strain PH-1 48hrs later. Line graph displays the mean of 12 biological replicates across 3 experimental replicates.

4.4.6 Induction of PTI defence mechanisms has local, but not systemic, durability

To test whether the PAMP-elicitor chitin and the DON-deficient strain $\Delta Tri5$ could induce resistance across the systemic scale, spray sequential inoculation experiments were conducted. Water (dH₂O; control), chitin and $\Delta Tri5$ pre-treatments, when sprayed, all failed to prevent subsequent *F. graminearum* infection of both WT (PH-1) and $\Delta Tri5$ strains, which both exhibited typical disease symptoms (Fig. 4.4.6 (a)). This result was also evident when there was a 48hr interval between the pre-treatment and subsequent inoculation (Fig. 4.4.6 (b)).

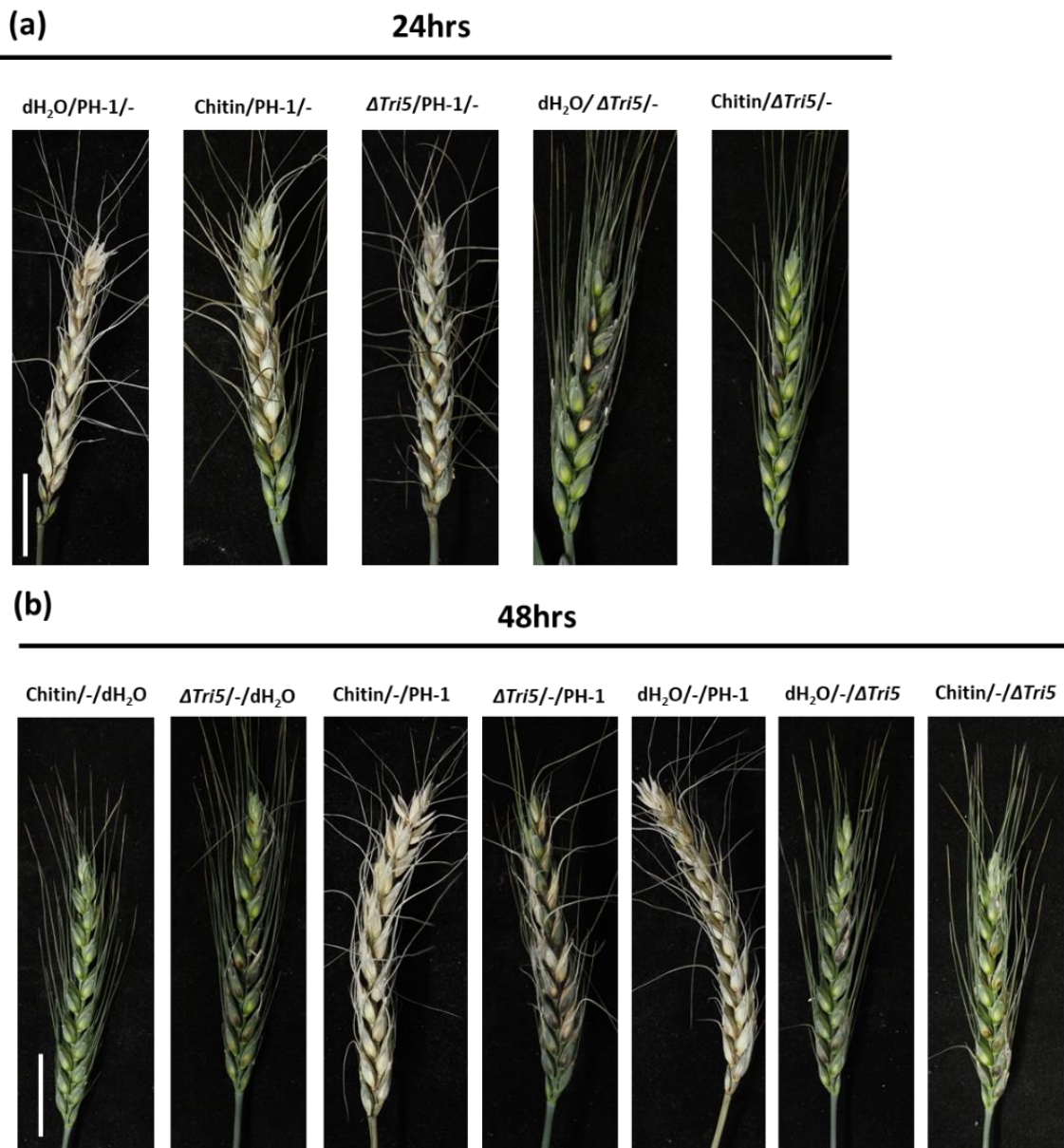


Fig. 4.4.6. Exemplar images of disease at 10dpi from spray co-inoculations. (a) Pre-treatments of water (dH₂O), chitin or $\Delta Tri5$ were used and subsequently the *Fg* strains PH-1 and $\Delta Tri5$ were spray inoculated 24 hrs later into wheat spikes. (b) Pre-treatments of water (dH₂O), chitin or $\Delta Tri5$ were applied 48hrs prior to inoculation with the *Fg* strains PH-1 and $\Delta Tri5$. Scale bar = 20mm. Experiment was repeated 3 times, n= 9 overall.

4.4.7 PTI elicitors trigger callose deposition in wheat rachis tissue

To determine if the induced resistance by known PTI elicitor chitin and the DON-deficient mutant $\Delta Tri5$ involved callose accumulation at plasmodesmata, immunolocalization of callose was conducted in fixed and sectioned rachis tissues at 24- and 48-hours post treatment. The selected time points aligned with

the induction of resistance in the sequential inoculation experiments (sections [4.4.1](#) – [4.4.6](#)).

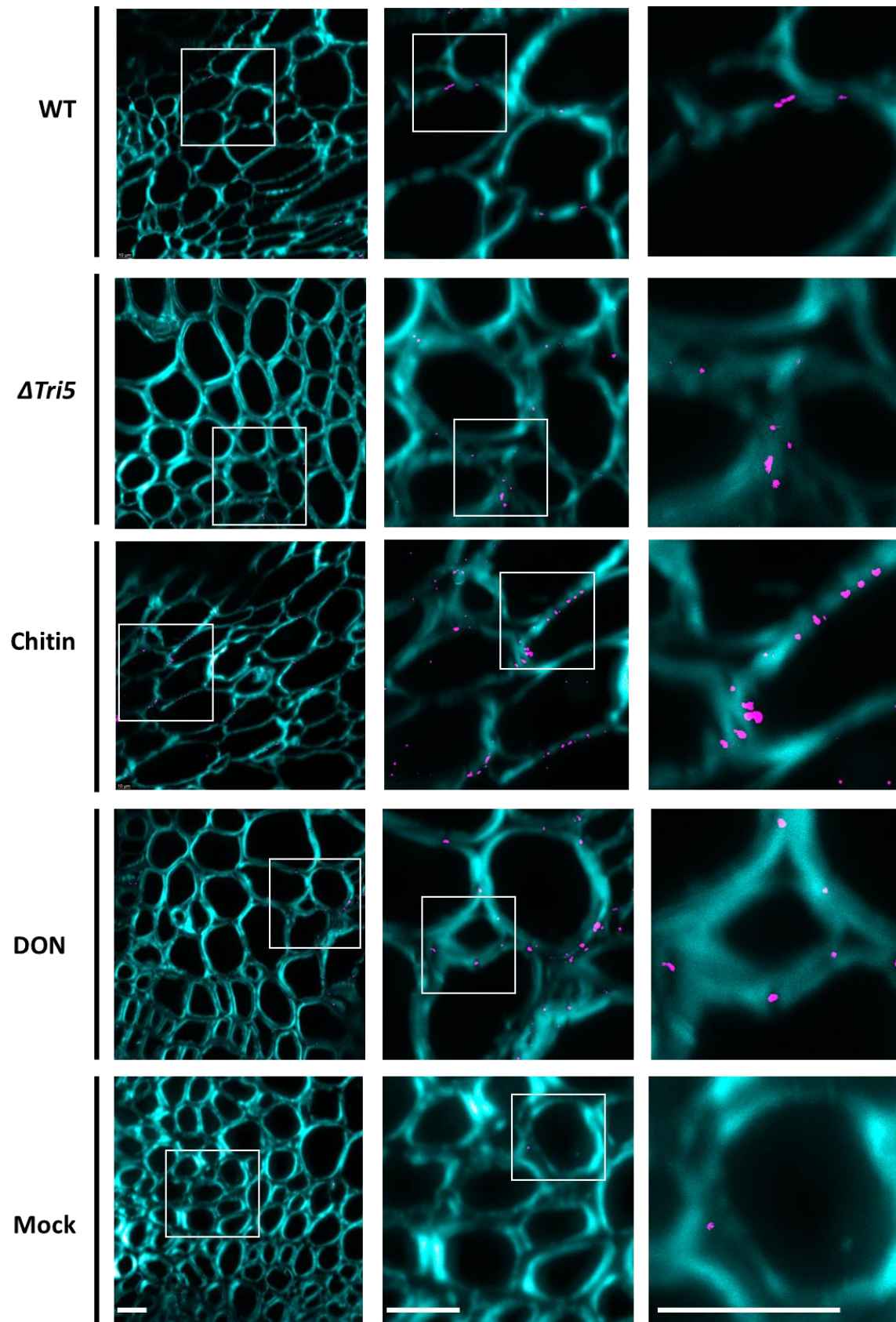


Fig. 4.4.7. Immunolabelling of callose at 24hrs post inoculation in wheat rachis tissue. The deposition of callose was observed after the inoculation with *F. graminearum* WT strain PH-1, the DON-deficient $\Delta Tri5$ mutant, chitin, DON and water (dH₂O; mock control). White boxes indicate area selected for magnification in subsequent box. Wheat cell walls were stained with calcofluor white and visible in cyan, and callose is visible through the conjugation of β -1,3-glucan antibodies and alexfluor-488-tagged antibodies, visible in magenta. Discrete deposits of callose (magenta) are visible in breaks in the secondary cell wall staining by calcofluor, indicating sites of pit fields. Scale bar = 100 μ m.

Localisations of callose in the parenchyma tissue layer of rachis internode samples were evident in all samples (Fig. 4.4.7). Callose deposits correlated with breaks in the secondary cell wall counterstain, indicating sites of pit fields as previously demonstrated in chapter 3, section [3.4.5](#) through TEM micrographs. Callose depositions spanned the breaks in the secondary cell wall, as observed in Fig. 4.4.8.

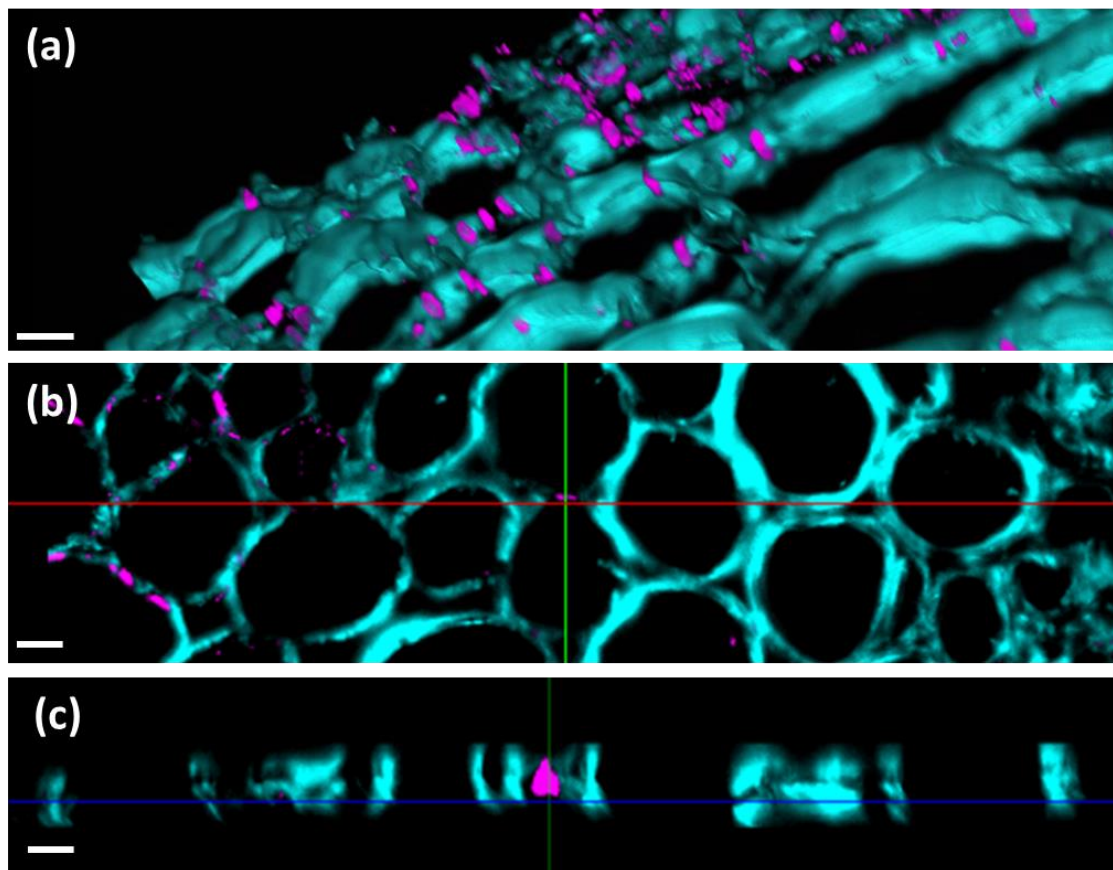


Fig. 4.4.8. 3D render of immunolabelled callose deposits at 24hrs post inoculation with PH-1 in wheat rachis tissue. Wheat cell walls are counterstained with calcofluor white and imaged with the excitation-emission spectra 405-475nm. Callose is immunolabelled with the β -1,3-glucan antibody and secondarily conjugated to the fluorophore alexfluor-488, imaged with excitation-emission spectra 488-525nm. Callose deposits are seen to span cell walls in breaks in the secondary cell wall staining and indicate sites of plasmodesmatal pit fields. (a) 45° angle of wheat

rachis section, (b) site selection of (c) showing callose deposit spanning wheat cell wall. Scale bar = 100µm. 3D render generated in ZEN Blue software (Zeiss Microsystems, Germany).

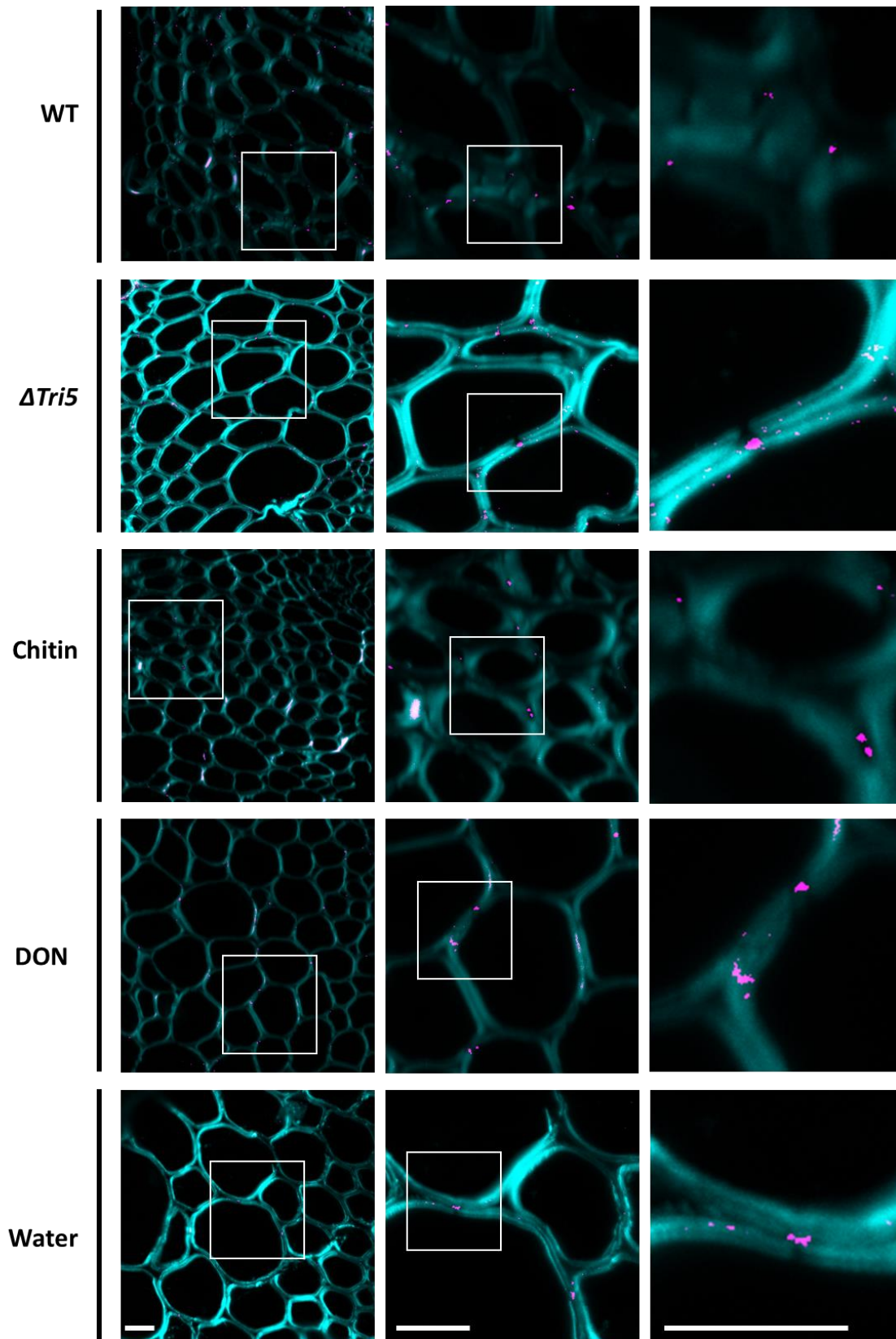


Fig. 4.4.9. Immunolabelling of callose at 48hrs post inoculation in wheat rachis tissue. The deposition of callose was observed after the inoculation with *F. graminearum* WT strain PH-1, the DON-deficient $\Delta Tri5$ mutant, chitin, DON and water (mock control). White boxes indicate area

selected for magnification in subsequent box. Wheat cell walls are stained with calcofluor white and visible in cyan, and callose is visible through the conjugation of β -1,3-glucan antibodies and alexfluor-488-tagged antibodies, visible in magenta. Discrete deposits of callose (magenta) are visible in breaks in the secondary cell wall staining by calcofluor, indicating sites of pit fields. Scale bar = 100 μ m.

Similar to the 24hr treatment, callose deposits were observed in all treatments (Fig. 4.4.9). To determine whether the defence elicitors chitin, DON and the DON-deficient *Fg* strain $\Delta Tri5$ elevated the frequency of callose deposits in rachis internodes, the immunolocalised resin sections were quantified. Due to lack of standardised protocols, three methodologies were employed to fully explore the callose deposition immune response. These analysed the number of discrete callose deposits averaged across the number of cells in the image (Fig. 4.4.10 (a); $F(11,21)= 0.807$, $p= 0.63$), the total area of callose immunolocalised in the image area (Fig. 4.4.10 (b); $F(11,21)= 1.177$, $p= 0.359$) and the total area averaged across the number of cells in the image sample (Fig. 4.4.10 (c); $(11,21)= 0.786$, $p= 0.651$). Whilst not statistically significant, trends are observed in the data, with a tendency for larger data point distribution in the DON and *Fg*-inoculated rachis samples at both 24 and 48hr timepoints, and in the chitin treatment at 48hr, but not in control, dH₂O and mock (no treatment, NT), samples.

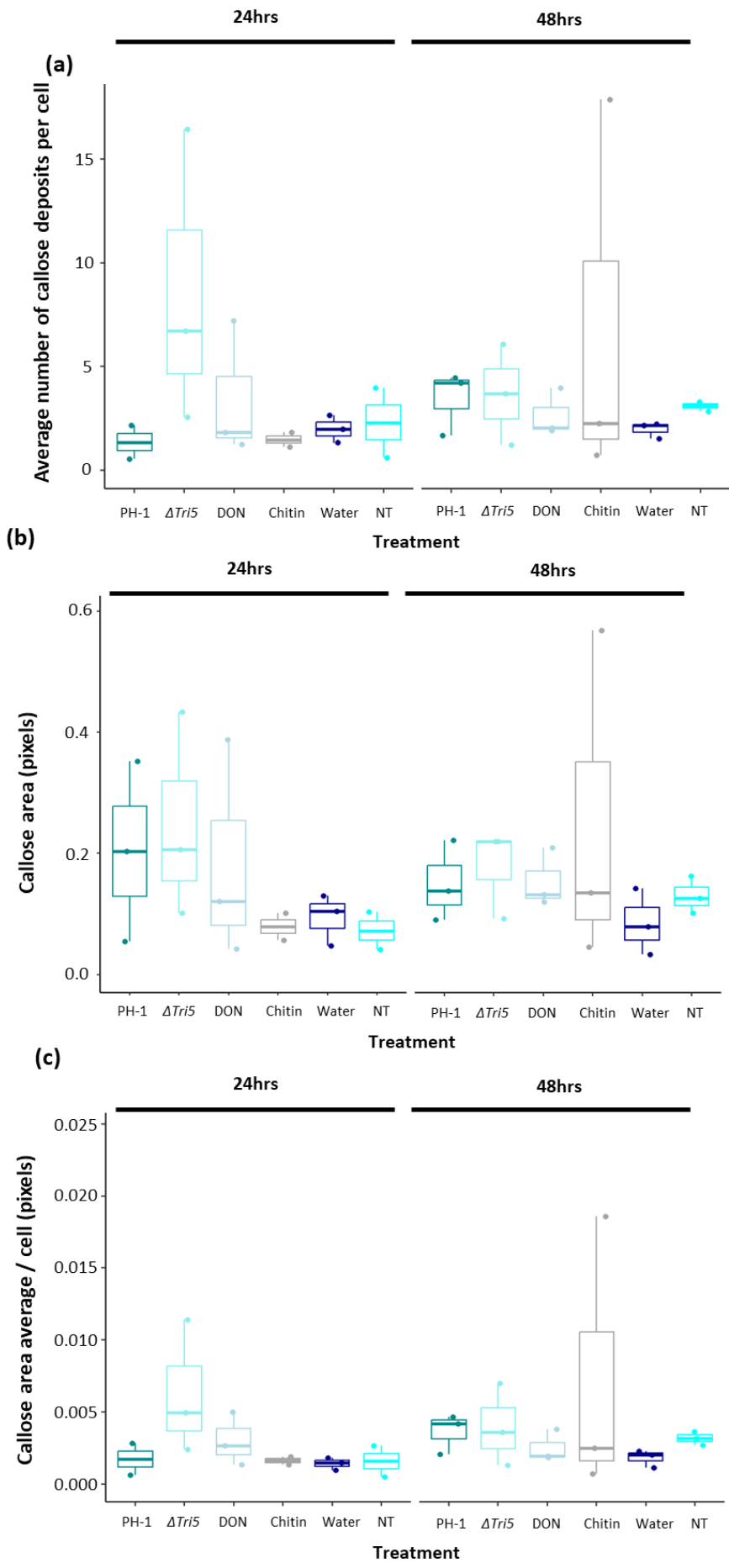


Fig. 4.4.10. Immunolabelling of callose deposits in resin-embedded rachis sections taken at 24 and 48hrs post inoculation. (a) Average number of discrete callose deposits averaged across the cell number at 24 hours (left) and 48 hours (right) post-inoculation, $F(11,21)= 0.807$, $p= 0.63$, (b) Average callose area determined through immunolocalization in pixel (arbitrary) units, $F(11,21)= 1.177$, $p= 0.359$, (c) Averaged callose area across cell number in image sample, $F(11,21)= 0.786$, $p= 0.651$. The experiment was conducted once with 3 biological replicated (i.e. three spikes from three different plants). Values were determined through averaging three technical replicates (sections taken x um apart) taken from each biological replicate.

Tissue-specific responses were also explored using the lemma and rachis tissues during early fungal establishment in host tissue at 5dpi. This aimed to determine whether proximity to the inoculation site (between the lemma and palea tissues) affected the strength of the callose deposition response across a biologically relevant timeframe to infection. Using the treatments of WT (PH-1), the DON-deficient strain $\Delta Tri5$, the mycotoxin DON and mock (dH₂O) treatments, this experiment aimed to dissect whether callose deposition varied between the WT and $\Delta Tri5$ samples, with and without the presence of DON. Hence, whether callose deposition may be affected by the excretion of DON by WT *Fg* when it is excreted with spatial and temporal precision, as opposed to generic application.

The absolute number of discrete callose deposits between the lemma and rachis tissues showed similar trends, with rachis tissue tending towards higher frequencies, despite a lack of significance (Fig. 4.4.11 (a)); ANOVA across lemma and rachis tissue samples $F(7,11) = 1.21$, $p = 0.41$. When averaged across the number of cells in the sample area, similar trends were also seen (Fig. 4.4.11 (b)).

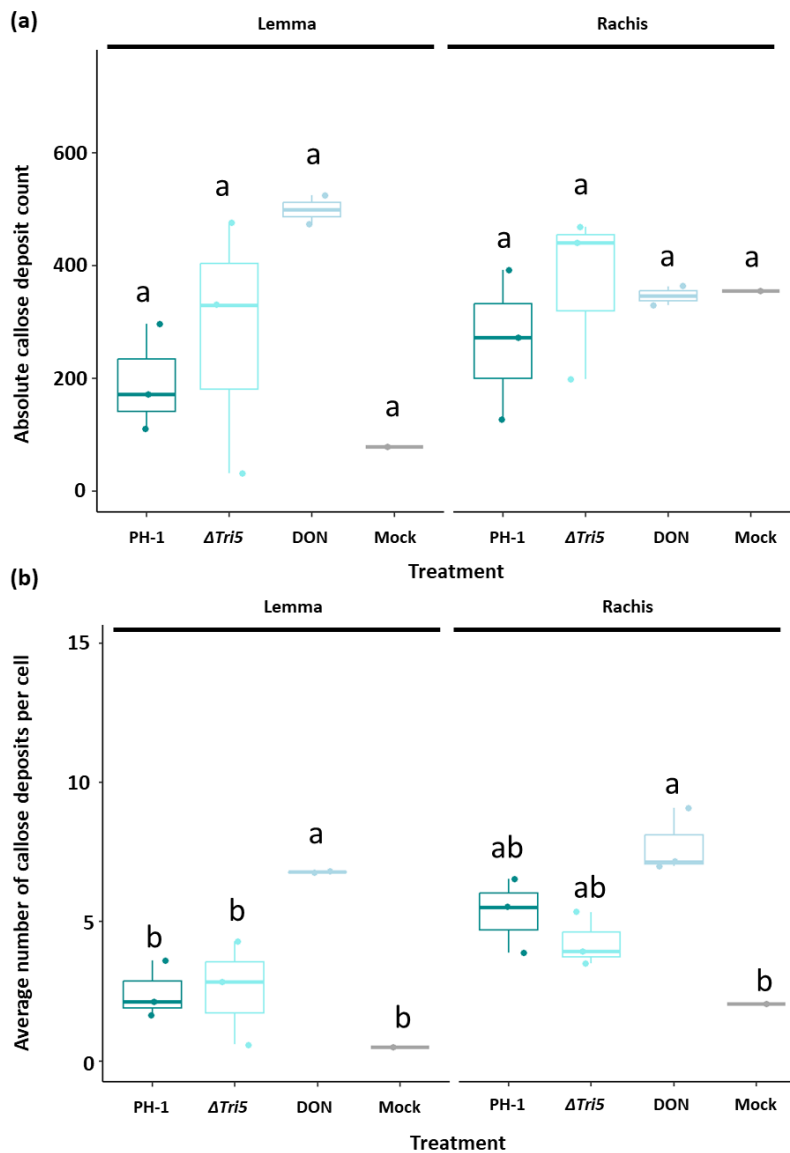


Fig. 4.4.11. Tissue specific responses of callose in lemma and rachis tissues at 5dpi. (a) Absolute counts of callose deposits in imaged resin samples through immunolabelling in lemma (left) and rachis (right) tissues. ANOVA across samples $F(7,11) = 1.21$, $p = 0.41$. Letters denote Tukey post-hoc test statistics. (b) Number of callose deposits averaged across total number of cells in imaged sample in lemma (left) and rachis (right) tissues. ANOVA $F(7,11) = 8.248$, $p < 0.005(**)$. Letters denote significant differences between groups through Tukey post-hoc analysis. The experiment was conducted once, with three biological replicates per treatment. Values are an average of three technical replicates per biological replicate, and one mock replicate was included.

4.5 Discussion

This chapter aimed to elucidate, in the absence of the mycotoxin DON, whether wheat can surmount an effective defence response to prevent subsequent WT infection. This was stimulated by the findings presented in [chapter 3](#), where the

role of virulence factor DON was re-examined. The DON-deficient strain $\Delta Tri5$ was found to be unable to traverse cell walls through pit fields in lignified tissue layers in the lemma, palea and rachis tissue components of the wheat spikelet. With this discovery, we hypothesised that effective callose deposition at plasmodesmata may be prevented by the excretion of DON by the WT *F. graminearum* strain (PH-1). As discussed in chapter 3, DON is known to dampen defence responses by targeting the 16s subunit of eukaryotic ribosomes, effectively inhibiting broad-spectrum host protein translation. When *F. graminearum* lacks the ability to synthesise DON through deletion of the *TRI5* gene, which encodes the essential enzyme trichodiene synthase and represents the first committed step in trichothecene biosynthesis, host tissue colonisation is restricted to the glume, lemma and palea tissue of wheat spikelets. Thus, we deduced as previously reported (Armer et al., 2024a) that DON is required for colonisation beyond the rachis node, into the rachis internode and into subsequent spikelets of wheat. In this chapter, these observations are extended and it was hypothesised that DON interferes with the mechanisms that lead to callose deposition in wheat rachis tissues and thus facilitates cell wall traversing through plasmodesmatal pit fields. In natural infections in the field, access to the rachis is required for sexual reproduction of *F. graminearum* with ascospores forming within perithecia that develop within the chlorenchyma bands in the rachis internode (Guenther and Trail, 2005). Therefore hyphal traversing beyond the rachis node is essential for the early and successful completion of the full lifecycle and further proliferation of disease to other hosts within a cropping cycle.

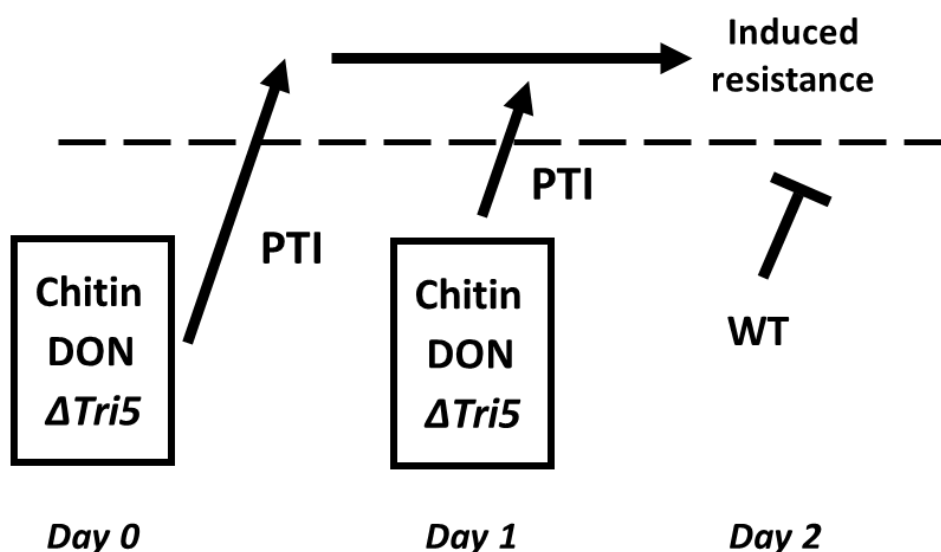


Fig. 4.5.1. Schematic diagram of induced resistance in wheat spikes by chitin, DON and $\Delta Tri5$. Whether pre-inoculation occurs 24hrs (day 1) or 48hrs (day 0) prior to WT infection, PTI-induced resistance is durable and sustained in wheat spikelets at a local scale.

Callose is deposited at plasmodesmatal pit fields during stress, caused by either biotic or abiotic factors (Wang, Andargie and Fang, 2022). The perception of PAMPs by PRRs triggers PTI, which activates downstream signalling pathways, one of which is the deposition of callose at plasmodesmata. During the inception of the experiments include within this chapter we hypothesised that DON interferes with this response, allowing the passage of invasive hyphae through pit fields in lignified tissue. It is widely known that the PAMP chitin, a constituent component of fungal cell walls, is perceived by the BIK1 receptor and subsequently triggers PTI in *Arabidopsis thaliana* (Huang and Joosten, 2024). Other filamentous ascomycete fungal pathogens of wheat, such as the foliar invading species *Zymoseptoria tritici*, secrete lysin domain (LysM) motif-containing proteins that 'mask' the presence of the fungus from the host plant by binding to chitin oligosaccharides and so interfering with the reception pathway. This prevents pathogen perception by the host plant during a long, latent, symptomless phase before switching to widespread necrotrophic damage (Marshall et al., 2011). *Fusarium graminearum* does not possess similar genes in its genome (Brown et al., 2012), and so we hypothesised that DON is excreted to dampen chitin reception after various PAMPs have been perceived and PTI has been triggered.

The results in this chapter confirmed the hypothesis that when *F. graminearum* infects wheat without the ability to synthesise the mycotoxin DON, defence responses are triggered that prevent subsequent infection by the WT strain PH-1. Interestingly, PH-1 was not able to overcome these induced defences across the entire infection period (14 days) and the defences triggered by $\Delta Tri5$ were swift, within 24hrs, and were sustained to at least 48hrs. However, as this coincided with the proliferation of the $\Delta Tri5$ mutant throughout the lemma and palea tissues of the wheat spikelet, it is unsurprising that defences were sustained, but this was similarly supported with chitin application in the wheat spikelet. The inability of the WT strain to break through $\Delta Tri5$ -induced defences at both 24 and 48 hours after initial infection, prompted further investigation into whether this was broadly triggered by the PTI or ETI layers of plant immunity or

indeed might constitute a mixture of PTI and ETI responses. Despite the presence of DON in the secondary inoculation with WT *F. graminearum*, these induced defence responses were durable and not broken.

Once established that pre-treatment of wheat spikelets with the DON-deficient strain $\Delta Tri5$ prevented subsequent WT infection, we proposed that the induction of defence responses occurred through the PTI layer, and not the ETI layer of plant immunity. To test this hypothesis the PAMP chitin was applied to wheat spikelets in a disease assessment assay, alongside the *F. graminearum* strain $\Delta Tri5$ and also the mycotoxin DON. Although the exogenous application of DON failed to chemically complement the $\Delta Tri5$ mutant in chapter 3, it was included in this assay as a potential PAMP elicitor due to its detection and detoxification by wheat, as discussed in section [3.4.2](#). When pre-treated with either chitin, the WT strain PH-1 failed to establish and no symptoms developed, whereas pre-treatment with the $\Delta Tri5$ strain lead to just the $\Delta Tri5$ dependent eye-shaped lesion development on the glumes. This indicates that $\Delta Tri5$ induced immunity through a PTI pathway, as a similar phenotype was observed. Interestingly, the mycotoxin DON also induced resistance, indicating a role for toxin perception in PTI. This induction is likely to occur through the reception of DAMPs, such as reactive oxygen species (ROS) released by the wheat host in response to ribosomal toxicity, as discussed in section [3.5](#). This result is supported by previous reports in the literature by Blümke et al. (2015), who demonstrated that application of DON to the cereal model species *Brachypodium distachyon* reduced susceptibility to subsequent infection with WT *F. graminearum*. DON has been shown to be perceived by wheat and acts as a trigger for PTI through the action of *Triticum aestivum* *Fusarium* Resistance Orphan Gene (TaFROG) of which expression is toxin dependent (Perochon et al., 2015). Another *F. graminearum* toxin, albeit not a trichothecene, is Fumonisin B1 has also been shown to act as a DAMP with ROS release, callose deposition and expression of Pathogenesis Related (PR) proteins (Wolpert et al., 2002).

The strength and duration of the DON defence response may be less than that induced by chitin, as the resistance is broken through by the WT strain PH-1 towards the end of the disease progression. Potentially, in this pathosystem, PAMP-induced PTI responses are stronger than DAMP-induced PTI responses in the wheat spike. Alternatively, the detoxification of DON by the addition of a

sugar molecule (glucoside) (Li et al., 2015) that allows for trafficking throughout the wheat spike may remove the PTI-triggering DON signal away from the inoculated spikelet to an extent to which it fails to reach the required thresholds in the different cell types within the wheat rachis tissues after several days.

Another interesting observation from this series of assays, that needs to be confirmed through further repeats, is that $\Delta Tri5$ tracked behind PH-1 *in planta*. This indicates that PH-1, either through direct WT hyphal actions or facilitated by DON excretion, the isogenic WT PH-1 strain manages to remove or suppress physical barriers and /or other activated defence responses in other cellular compartments to further $\Delta Tri5$ hyphal colonisation. This was confirmed by taking a series of rachis internodes from the PH-1 and $\Delta Tri5$ -co-inoculated wheat spikelets, excising them and placing on hygromycin selection plates. The $\Delta Tri5$ single gene deletion mutant was generated through a hygromycin split marker approach (Cuzick et al., 2008) and the presence of the hygromycin gene was further confirmed through PCR. Whether PH-1 facilitated the *in planta* growth of $\Delta Tri5$ by preventing or removing callose deposits due to DON excretion was not detected directly but was explored through immunolocalisation of callose deposits in lemma and rachis tissues at 5dpi post inoculation. In the PH-1 and $\Delta Tri5$ -infected lemma and palea tissues, measurements of callose deposition were increased compared to mock controls, but DON itself also increased callose deposition. It is hypothesised that DON, in this instance, is perceived by the plant and acts as a trigger for PTI. By targeting ribosomes and causing ribotoxicity, DON may act as a DAMP and trigger callose deposition at PD. It is worth noting that, in the samples imaged the variability of callose deposition between biological samples of chitin and DON was much smaller than the *F. graminearum* infected samples. While different PAMPs may lead to different responses *in planta*, the action of fungal enzymes that directly degrade callose may also be at play. This notion is explored further in [chapter 5](#). However, the limitations of this assay with respect to cost and time for sample preparation limited experimental replicates and only provide an indication of callose responses to *F. graminearum*, with and without the ability to synthesis DON, and just DON alone. These initial results should be followed up in further detailed studies using new technological advancements such as automatic histology system microtomes, thereby reducing the overall sample preparation burden.

To determine if the resistance induced by the PAMP chitin and the DON-deficient *F. graminearum* strain $\Delta Tri5$ occurred at a systemic scale, spray inoculations were conducted. However, disease establishment was found to vary considerably between wheat spikes. Although amended with the surfactant Tween 20 to enable wheat surface adhesion of the spore solution, the PTI pathways were not triggered beyond the required threshold when $\Delta Tri5$ or chitin was applied to the outer surface of the wheat spike. Instead, rather disappointingly typical FHB symptoms for both WT and $\Delta Tri5$ were observed at both 24 and 48hr timepoints. This may be explained by several factors, but the most pertinent is that different tissues had been directly exposed to chitin or the $\Delta Tri5$ strain. In spray inoculations, most of the inoculum is deposited on the outer glume surfaces, which is lignified and has a wax-coated cuticle that serves a protective role. Whereas in the droplet point inoculation experiments, inoculum is placed directly between the lemma and palea tissue, which sit underneath the glume, and do not pose such a significant barrier to *F. graminearum* infection. Under field conditions, the *Fusarium* spores would predominantly be deposited onto the glume and awn surfaces, and only a subfraction would directly alight on the lemma and palea tissues once florets open timed with anthesis lemma in order to infect the developing grain (Brown et al., 2010). Chitin has been reported to have tissue specific reception in wheat spikes, with the rachis node initiating the greatest ROS burst in response to chitin application (Hao, Tiley and McCormick, 2022). Tissue specific reception is the relative response to PAMPs, such as chitin, with differing gene expression and ROS release, that may play roles in susceptibility and/or resistance to plant pathogens. However, chitin reception on the outer glume has not yet been reported in the literature but given the results of this experiment is not likely to be detected to the threshold level required for PTI. Collectively, these results indicate that induction of PTI occurs over local, not systemic, tissue scales and so applicability in the field may be limited.

Plants highly resistant to biotic stresses, such as those imposed by fungal pathogens, typically yield higher than susceptible counterparts in high disease pressure situations, but under lower disease pressures may be lower yielding. This is in part due to plant immunity signalling pathways and plant growth promoting pathways being intrinsically intertwined. In doing so, when not attacked by a pathogen the plant ensures available resources are directed towards

promoting plant growth (Brown, 2002). As such, trade-offs occur when fitness is tested by environmental conditions. For example, in ETI, NLR immune receptors and their associated wall associated kinases (WAKs) balance immunity and yield, often through close genomic and genetic linkage between *R* genes and genes associated with yield reductions (Ning, Liu and Wang, 2017). In wheat, the *R* gene conferring resistance to stem rust, *Sr26*, has an average yield penalty of 9% (Brown, 2002). However, under high disease incidence, resistance to the pathogen would yield higher than faster growing, susceptible cultivars when balancing yield loss conferred by *F. graminearum* infection, directly through grain mass reduction and indirectly through contamination of grain with trichothecene mycotoxins (McMullen et al., 1997). Whilst not explored in the series of experiments here, it would be interesting to determine what, if any, yield penalty would occur after chitin application into the wheat spike. However, at the moment the field applicability such an approach would be limited due to the lack of systemic resistance induced by exogenous application to the whole wheat spike, as evidenced by the spray inoculation experiments presented in this chapter.

Callose deposition as a component of PTI defence in response to chitin, $\Delta Tri5$, DON and the WT strain was explored at the same timepoints as induced resistance was observed in the sequential inoculation studies. These experiments aimed to determine whether callose deposition was upregulated in the rachis tissue, where cell walls are highly lignified, and thus CWDEs have a limited ability to degrade cell walls, forcing hyphae to constrict and pass through plasmodesmatal pit fields. At both 24 and 48hrs post inoculation, all treatments increased callose deposition in the rachis when compared to the control, across all measurement metrics. While not statistically significant, trends observed in this dataset were that callose deposition between biological and technical replicates was variable, but this type of data distribution pattern was not observed in mock treatments. This may in part be due to the limited number of samples that were included in this study due to time and financial constraints, but recent advances have eluded that plasmodesmatal responses to fungal pathogens may be heterogenic, whereby plasmodesmata within close proximity respond differently in their callose deposition (Cheval et al., 2020). In the presence of chitin, molecular fluxes through plasmodesmata have been shown to be reduced, but this occurs through chitin reception by LYM2, not the chitin recognition receptor

CERK1 (Faulkner et al., 2013). While molecular flux was reduced after chitin application in wheat spikelets was not explored in this study. In lemma tissues, similar callose deposition patterns were observed at 5dpi, with WT, $\Delta Tri5$ and DON all inducing callose deposits, with no observed difference between the WT strain PH-1 and the DON-deficient strain $\Delta Tri5$, despite a trend towards a lower level of callose deposits in the WT-infected tissues. Similar numbers of callose deposits were observed in the rachis tissues at 24 and 48 hrs post-inoculation and the rachis tissue at 5dpi, indicating that callose deposition occurs early during host-tissue colonisation by *F. graminearum*, and is sustained throughout infection. This may indicate an important role for an early and sustained response to PAMPs such as chitin to symplastically isolate damage cells from the remaining healthy tissue through the action of callose deposition. Whether *F. graminearum* can effectively degrade callose at plasmodesmata through the action of glycoside hydrolase enzymes is explored in further detail in [chapter 5](#).

A summary of the inoculation experiments presented in this chapter are displayed in Table 4.5.1.

Table 4.5.1. Summary of sequential inoculation experimental challenges and future prospectives. Specific components discussed in this chapter that may be improved through future experimentation and application of alternative technologies.

Component	Challenge / Limitation	Future Perspectives
Point sequential inoculation	Artificially high induction of defence responses, triggering PTI.	Lower limit of threshold could be determined to replicate more natural infection pressures in controlled experiments.
Spray sequential inoculation	Disease symptoms not reproducible.	Low concentration 'dip' of wheat spikes could help to standardised amount of PAMP and/or inoculum deposited onto each biological sample.

Immunolocalisation of callose	High financial and time cost for sample preparation, immunolocalisation and imaging.	Use of automatic microtome could improve time to prepare samples for microscopy and thereby provide more samples for downstream analysis.
--------------------------------------	--	---

In summary, the evidence presented in this chapter indicates that PTI, by induction through the PAMP chitin or the DON-deficient reduced virulence $\Delta Tri5$ *F. graminearum* strain is sufficient to upregulate defence responses and prevent subsequent WT infection. This induced resistance was durable and not overcome, despite the presence of DON in the WT infection. DON itself may be considered a DAMP/ PAMP, as it also induced resistance, albeit broken by WT *F. graminearum* towards the end of the disease progression. This may be due to the host tissue ‘de-toxification’ of the trichothecene mycotoxins by the action of UDP-glycosyltransferases in wheat, which adds a glycosyl molecule to the toxin, allowing DON-Glu to be transported away from the site of inoculation and thus no longer stimulates the PTI layer of plant immunity. The observed induced resistance in wheat spikelets after induction of PTI may involve the deposition of callose at plasmodesmatal pit fields in the lemma and palea tissues of wheat spikelets, but further experiments, notably with more experimental replicates, are required to better assess this component of wheat floral defence. Future studies should look at whether this induced resistance wanes after a period of time beyond 48 hours post pre-treatment and if this durable resistance is dose-dependent on the PTI elicitor.

4.6 References

Armer VJ, Kroll E, Darino M, Smith DP, Urban M, Hammond-Kosack KE, (2024b). Navigating the *Fusarium* Species Complex: Host-Range Plasticity, Niche Diversification and Genome Variations. *Fungal Biology*. **In Press**. doi: 10.1016/j.funbio.2024.07.004.

Armer VJ, Urban M, Ashfield T, Deeks MJ, Hammond-Kosack KE, (2024a). The trichothecene mycotoxin deoxynivalenol facilitates cell-to-cell invasion during wheat-tissue colonisation by *Fusarium graminearum*. *Molecular Plant Pathology*. **25**(6): e13485. doi: 10.1111/mpp.13485.

- Berthiller F, Dall'Asta C, Schuhmacher R, Lemmens M, Adam G, Krska R. (2005). Masked mycotoxins: determination of a deoxynivalenol glucoside in artificially and naturally contaminated wheat by liquid chromatography–tandem mass spectrometry. *Journal of Agricultural and Food Chemistry*. **53**(9), 3421-3425. doi: 10.1021/jf047798g
- Bharath P, Gahir S, Raghavendra AS. (2021). Abscisic Acid-Induced Stomatal Closure: An Important Component of Plant Defense Against Abiotic and Biotic Stress. *Frontiers in Plant Science*. **12**: 615114. doi: 10.3389/fpls.2021.615114.
- Blümke A, Sode B, Ellinger D, Voigt CA. (2015). Reduced susceptibility to *Fusarium* head blight in *Brachypodium distachyon* through priming with the *Fusarium* mycotoxin deoxynivalenol. *Molecular Plant Pathology*. **16**(5): 472-483. doi: 10.1111/mpp.12203.
- Boller T, Felix G. (2009). A Renaissance of Elicitors: Perception of Microbe-Associated Molecular Patterns and Danger Signals by Pattern-Recognition Receptors. *Annual Review of Plant Biology*. **60**: 379-406. doi: 10.1146/annurev.arplant.57.032905.105346.
- Brown JKM. (2002). Yield penalties of disease resistance in crops. *Current Opinion in Plant Biology*. **5**: 339-344. doi: 10.1016/S1369-5266(02)00270-4.
- Brown NA, Urban M, van de Meene AML, Hammond-Kosack KE. (2010). The infection biology of *Fusarium graminearum* defining the pathways of spikelet to spikelet colonisation in wheat ears. *Fungal Biology*. **114**(7): 555-571. doi: 10.1016/j.funbio.2010.04.006.
- Brown NA, Antoniw J, Hammon-Kosack KE. (2012). The Predicted Secretome of the Plant Pathogenic Fungus *Fusarium graminearum*: A Refined Comparative Analysis. *PLoS ONE*, **7**(4), e33731. doi:10.1371/journal.pone.0033731.
- Camejo D, Guzmán-Cedeño Á, Moreno A. (2016). Reactive oxygen species, essential molecules, during plant–pathogen interactions. *Plant Physiology and Biochemistry*. **103**: 10-23. doi: 10.1016/j.plaphy.2016.02.035.
- Chancellor T, Smith DP, Chen W, Clack SJ, Venter E, Halsey K, Carrera E, McMillan V, Canning G, Armer VJ, Hammond-Kosack KE, Palma-Guerrero J. (2024). A fungal endophyte induces local cell-wall mediated resistance in wheat roots against take-all disease. *In Press*. doi: 10.3389/fpls.2024.1444271.
- Cheval C, Samwald S, Johnston MG, de Keijzer J, Breakspear A, Liu X, Bellandi A, Kadota Y, Zipfel C, Faulkner C. (2020). Chitin perception in plasmodesmata characterizes submembrane immune-signaling specificity in plants. *Proceedings of the National Academy of Sciences*. **117**(17): 9621-9629. doi: 10.1073/pnas.1907799117.
- Chouhan D, Mandal P. (2021). Applications of chitosan and chitosan based metallic nanoparticles in agrosociences – a review. *International Journal of Biological Macromolecules*. **166**: 1554-1569. doi: 10.1016/j.ijbiomac.2020.11.035.

- Dalio RJD, Paschoal D, Arena GD, Magalhães, Oliveira TS, Merfa MV, Maximo HJ, Machado MA. (2020). Hypersensitive response: From NLR pathogen recognition to cell death response. *Annals of Applied Biology*. **178**(2): 268-280. doi: 10.1111/aab.12657.
- de Lamo, FJ, Takken, FLW. (2020). Biocontrol by *Fusarium oxysporum* Using Endophyte-Mediated Resistance. *Frontiers in Plant Science*. **11**(37). doi: 10.3389/fpls.2020.00037.
- Dodds PN, Rathjen JP. (2010). Plant immunity: towards an integrated view of plant-pathogen interactions. *Nature Reviews Genetics*. **11**: 539-548. doi: 10.1038/nrg2812.
- Faulkner C, Petutschnig E, Benitez-Alfonso Y, Beck M, Robatzek S, Lipka V, Maule AJ. (2013). LYM2-dependent chitin perception limits molecular flux via plasmodesmata. *Proceedings of the National Academy of Sciences*. **110**(22): 9166-9170. doi: 10.1073/pnas.1203458110.
- Freh M, Gao J, Petersen M, Panstruga R. (2022). Plant autoimmunity – fresh insights into an old phenomenon. *Plant Physiology*. **188**(3): 1419-1434. doi: 10.1093/plphys/kiab590.
- García-Bastidas, FA, Arango-Isaza, R, Rodriguex-Cabal, HA, Seidl, MF, Cappadona, G, Segura, R, Salacinas, M, Kema, GHJ. (2022). Induced resistance to *Fusarium* wilt of banana caused by Tropical Race 4 in Cavendish cv Grand Naine bananas after challenging with avirulent *Fusarium* spp. *PLOS ONE*, 17(9): e0273335. doi: 10.1371/journal.pone.0273335.
- Guenther, J. C. and Trail, F. (2005). The development and differentiation of *Gibberella zeae* (anamorph: *Fusarium graminearum*) during colonization of wheat. *Mycologia*. 97(1), 229-237. doi: 10.1080/15572536.2006.11832856.
- Hao G, Tiley H, McCormick S. (2022). Chitin Triggers Tissue-Specific Immunity in Wheat Associated With *Fusarium* Head Blight. *Frontiers in Plant Science*. **13**: 832502. doi: 10.3389/fpls.2022.832502.
- Huang WRH, Joosten MHAJ. (2024). Immune signaling: receptor-like proteins make the difference. *Trends in Plant Science*. **In press**. doi: 10.1016/j.tplants.2024.03.012.
- Jamieson PA, Shan L, He P. (2018). Plant cell surface molecular cypher: Receptor-like proteins and their roles in immunity and development. *Plant Science*. **274**: 242-251. doi: 10.1016/j.plantsci.2018.05.030.
- Jones DG, Dangl JL (2006). The plant immune system. *Nature*. **444**: 323-329. doi: 10.1038/nature05286.
- Lee D, Lal NK, Lin ZD, Ma S, Liu J, Casto B, Toruño T, Dinesh-Kumar SP, Coaker G. (2020). Regulation of reactive oxygen species during plant immunity through phosphorylation and ubiquitination of RBOHD. *Nature Communications*. **11**: 1838. doi: 10.1038/s41467-020-15601-5.
- Li X, Shin S, Heinen S, Dill-Macky R, Berthiller F, Nersesian N, Clemente T, McCormick S, Muehlbauer GJ. (2015). Transgenic Wheat Expressing a Barley UDP-Glucosyltransferase Detoxifies Deoxynivalenol and Provides High Levels of Resistance to *Fusarium graminearum*. *Molecular Plant Microbe Interactions*. **28**(11): 1237–1246. doi: 10.1094/MPMI-03-15-0062-R.

- Ma, LJ, van der Does, HC, Borkovich, KA. *et al.* (2010). Comparative genomics reveals mobile pathogenicity chromosomes in *Fusarium*. *Nature* **464**: 367–373. doi: 10.1038/nature08850.
- Macho AP, Zipfel C. (2014). Plant PRRs and the Activation of Innate Immune System. *Molecular Cell*. **54**(2): 263-272. doi: 10.1016/j.molcel.2014.03.028.
- Marshall R, Kombrink A, Motteram J, Loza-Reyes E, Lucas J, Hammond-Kosack KE, Thomma BPHJ, Rudd JJ. (2011). Analysis of Two *in Planta* Expressed LysM Effector Homologs from the Fungus *Mycosphaerella graminicola* Reveals Novel Functional Properties and Varying Contributions to Virulence on Wheat. *Plant Physiology*. **156**(2): 756-769. doi: 10.1104/pp.111.176347.
- McMullen M, Jones R, Gallenberg D. (1997). Scab of wheat and barley: a re-emerging disease of devastating impact. *Plant Disease*. 81(12), 1340 – 1348. doi: 10.1094/PDIS.1997.81.12.1340.
- Miya A, Albert P, Shinya T, Desaki Y, Ichimura K, Shirasu K, Narusaka Y, Kawakami N, Kaku H, Shibuya N. (2007). CERK1, a LysM receptor kinase, is essential for chitin elicitor signaling in *Arabidopsis*. *PNAS*. **104**(49): 19613-19618. doi: 10.1073/pnas.0705147104.
- Morales J, Kadota Y, Zipfel C, Molina A, Torres M-A. (2016). The *Arabidopsis* NADPH oxidases *RbohD* and *RbohF* display differential expression patterns and contributions during plant immunity. *Journal of Experimental Botany*. **67**(6):1663–76. doi: 10.1093/jxb/erv558.
- Ning Y, Liu W, Wang GL. (2017). Balancing immunity and yield in crop plants. *Trends in Plant Science*. **22**(12): 1069-1079. doi: 10.1016/j.tplants.2017.09.0101.
- Patpour M, et al. (2022). Wheat Stem Rust back in Europe: Diversity, prevalence and impact on host resistance. *Frontiers in Plant Science*. **13**: 882440. doi: 10.3389/fpls.2022.882440.
- Perochon A, Jianguang J, Kahla A, Arunachalam C, Scofield SR, Bowden S, Wallington E, Doohan FM. (2015). TaFROG Encodes a Pooideae Orphan Protein That Interacts with SnRK1 and Enhances Resistance to the Mycotoxigenic Fungus *Fusarium graminearum*. *Plant Physiology*. 169(4): 2895–2906. doi: 10.1104/pp.15.01056.
- Redkar A, Sabale M, Schudoma C, Zechmann B, Gupta YK, López-Berges MS, Venturini G, Gimenez-Ibanez S, Turrà D, Solano R, Di Pietro A. (2022). Conserved secreted effectors contribute to endophytic growth and multihost plant compatibility in a vascular wilt fungus. *The Plant Cell*. **34**(9): 3214-3222. doi: 10.1093/plcell/koac174.
- Tee EE, Faulkner C. (2024). Plasmodesmata and intercellular molecular traffic control. *New Phytologist*. **243**(1): 32-47. doi: 10.1111/nph.19666.
- Torres MA, Jones JDG, Dangl JL. (2006). Reactive oxygen species signaling in response to pathogens. *Plant Physiology*. **141**(2): 373-378. doi: 10.1104/pp.106.079467.
- Wang B, Andargie M, Fang R. (2022). The function and biosynthesis of callose in high plants. *Heliyon*. **8**(4):e09248. doi: 10.1016/j.heliyon.2022.e09248.

Waszczak C, Carmody M, Kangasjärvi J. (2018). Reactive Oxygen Species in Plant Signaling. *Annual Review of Plant Biology*. **69**: 209-236.

Wolpert TJ, Dunkle LD, Ciufetti LM. (2002). Host-selective toxins and avirulence determinants: what's in a name? *Annual Review of Phytopathology*. **40**: 251-285. doi: 10.1146/annurev.phyto.40.011402.114210.

Zhang S, Li C, Si J, Han Z, Chen D. (2022). Action Mechanisms of Effectors in Plant-Pathogen Interaction. *International Journal of Molecular Sciences*. **23**(12): 6758. doi: 10.3390/ijms23126758.

Chapter 5: Callose balancing at plasmodesmata

5.1 Acknowledgement of contributions

I would like to extend thanks to Erika Kroll (Rothamsted Research) for providing RNASeq data processing from Dilks et al. (2019), which contributed to the selection of the GH81 target gene in *F. graminearum* for exploration in this chapter.

5.2 Introduction

Plant cell walls offer a physical barrier to pathogen colonisation (Underwood, 2012) and as such filamentous pathogens that find alternative routes to degrading the host cell wall matrix have an advantage. Previous experimentation in [chapter 3](#) demonstrated that movement between adjacent cells occurs through plasmodesmatal pit fields and requires the action of the trichothecene mycotoxin DON to dampen PTI-induced host defence responses. Wheat defences activated in response to the DON-deficient *F. graminearum* strain $\Delta Tri5$ were shown to be sufficient to prevent subsequent WT infection in [chapter 4](#). Due to the essential nature of hyphal constriction through pit fields in thick, lignified tissues such as the wheat rachis, it was hypothesised that *F. graminearum* should excrete an enzyme(s) to directly degrade the callose deposition at PD in wheat spikes. This chapter explores the action of a secreted glycoside hydrolase enzyme that is predicted to catalyse the hydrolysis of β -1,3-glycosidic bonds in the glucose polymer callose at pit fields during infection.

Glycoside hydrolases (GH) are a large group of enzymes that catalyse the hydrolysis of glycosidic bonds between two or more carbohydrate monomers, or with a non-carbohydrate moiety. This enzyme class is well classified by the CAZY database (cazy.org) (Drula et al., 2022). Plant-infecting fungal pathogens secrete many types of GH enzymes during host-tissue colonisation for the degradation of plant cell walls, which are primarily composed of the polysaccharides cellulose (β -1,4-D-glucose), hemicelluloses (heteropolymers e.g., xylans, xyloglucans, arabinoxylans, mannans and glucomannans) and pectin. While cellulose is the main carbohydrate polymer in plant cell walls, its microfibrils that provide

structural support are strengthened by the cross-linking glycans and pectic polysaccharides (Delmer et al., 2024). Cell wall composition, and alterations in response to *F. graminearum* host-tissue colonisation, are further explored and discussed in [chapter 6](#). Many of the cell wall degrading enzymes (CWDEs) identified in fungal pathogens of plants aid virulence by directly reducing the strength and structure of the host cell wall and also release carbohydrate nutrition to aid further fungal proliferation (Rafiei, Véléz and Tzelepis, 2021).

Callose, similarly to cellulose, is a glucan polymer of β -glucose subunits. However, the two differ in their carbon linkages, with callose forming glycosidic bonds between carbons 1-3 and cellulose between carbons 1-4 (Fig. 5.2.1). This linkage leads to the structural differences between the two, with cellulose forming long rigid polymers that contribute to plant cell wall strength and whilst callose forms globular, coat-like structures when deposited at plasmodesmatal pores/ pit fields (Wang, Andargie and Fang, 2022).

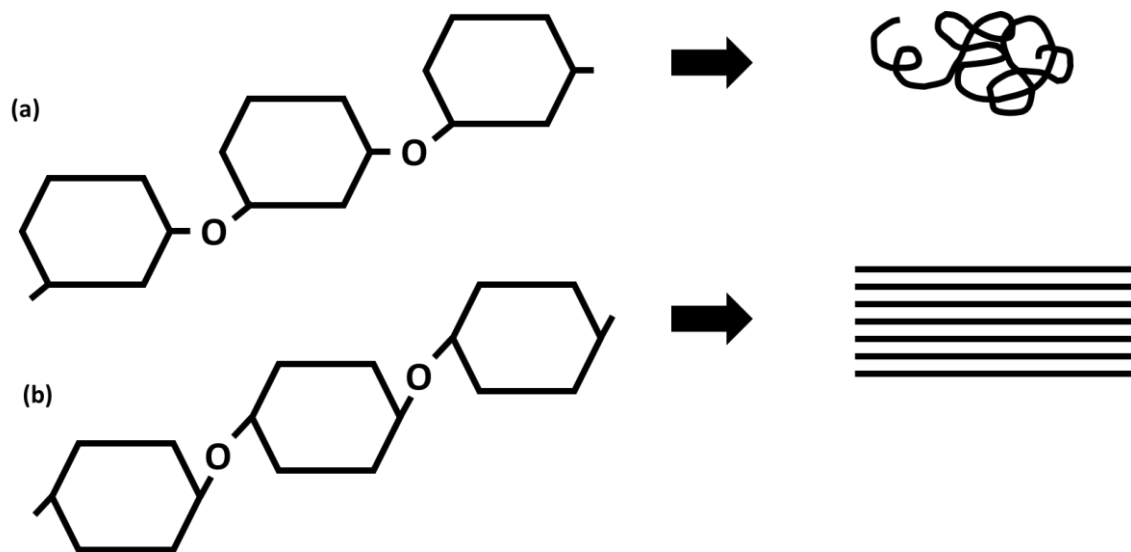


Fig. 5.2.1 Structural differences between the glucose polymers callose and cellulose. The different carbons linked through glycosidic bonds alter the overall structure of the glucose polymers, resulting in (a) unstructured (callose) with β -1,3-glycosidic bonds or (b) structured (cellulose) polysaccharides, with β -1,4-glycosidic bonds.

Despite being much lower in abundance relative to its closely related polymer cellulose, callose has integral roles in defence mechanisms to biotic and abiotic stress. Although present in small quantities within the plant cell wall itself, it's deliberate deposition at plasmodesmatal pores symplastically isolates neighbouring healthy cells, limiting cellular and widespread tissue damage by stress inducers.

Callose is synthesised in the plasma membrane at glucan-synthase complexes by Callose Synthases (CaS), also known as Glucan Synthase-Like (GSL), proteins embedded within the plasma membrane with multiple transmembrane domains (German, Yeshvekar and Benitez-Alfonso, 2022). CaS enzymes are glycosyl transferases that catalyse the polymerisation of UDP-glucose subunits into polymers with β -1,3-glycosidic bonds at membrane complexes that also include a GTP hydrolase, annexin and a sucrose synthase (Schneider et al., 2016). Both callose and cellulose share the same monomer substrate of UDP-glucose. The degradation of callose is mediated by the action of β -1,3-glucanases (BGs), including those of the GH81 family. Around plasmodesmata, specific BGs co-localise with plasmodesmata-callose binding proteins (Fig. 5.2.2; German, Yeshvekar and Benitez-Alfonso, 2022). Both the action of CaS and BGs are mediated by signaling pathways as part of the PTI response, including calcium (Holdaway-Clarke et al., 2000), but are likely to be triggered by other molecules yet to be determined, as well as some phytohormones. For example, in *Arabidopsis*, AUXIN RESPONSE FACTOR 7 (ARF7) increases expression of the CaS GLS8 which positively regulated callose synthesis at PD (Han et al., 2014).

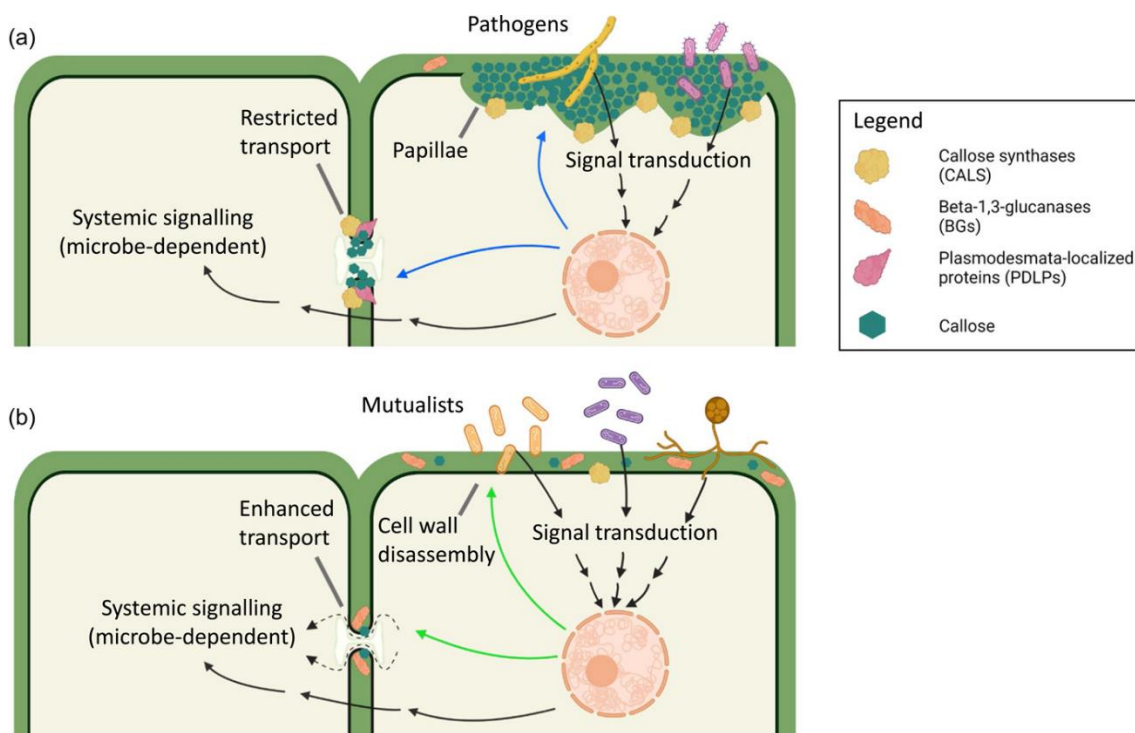


Fig. 5.2.2. Callose responses to plant-microbe interactions. (a) In response to pathogens, callose is deposited at the site of infection and results either in papillae forming around penetration pegs to strengthen the cell wall barrier or at plasmodesmata to restrict microbe signalling or pathogen spread to adjacent cells. (b) In response to some mutualistic microbes, callose is

disassembled at plasmodesmata to promote cell-to-cell signalling. From German, Yeshvekar and Benitez-Alfonso (2022).

In addition to the deposition of callose at PD as discussed throughout this thesis, callose is also deposited in epidermal cells around extra-haustorial membranes of papillae produced by fungal pathogens, such as the powdery mildew fungus *Blumeria graminis* f. sp. *hordei* (*Bgt*). Overexpression of *POWDERY MILDEW RESISTANCE 4* (*PMR4*), which encodes a stress induced callose synthase, leads to reduced penetration by *Bgt* in Arabidopsis (Elligner et al., 2013). Callose deposition in phloem sieve tubes may also act as a plug against vascular pathogens. A recent study showed that during infection of citrus species by the proteobacterium *Candidatus*, transmitted by the Asian citrus psyllid (*Diaphorina citri*), callose deposition is upregulated in phloem sieve tubes and postulated to be a part of the hypersensitive response to reduce bacterial colonisation; a number of callose synthases were shown to be upregulated in inoculated vs healthy plants (Granato et al., 2019). However, complete occlusion of sieve tubes could be detrimental to the host plant if photosynthates are unable to pass.

Fungal cell walls are mostly composed of β -glucans, notably the β -1,3 and β -1,6-varieties which are covalently bound through branches (Fig. 5.2.3; Fesel and Zuccaro, 2016). β -1,3-glucans are the most abundant at 65-90% of the total β -glucan content (Bowman and Free, 2006) and are synthesised by a β -1,3-glucan synthase embedded within the plasma membrane and transfers a glucose molecule to the glucan fibre via uridine diphosphate-N-glucose. Interestingly β -1,6-glucans are not present in plants and so present themselves as candidates for PAMP/ MAMP recognition.

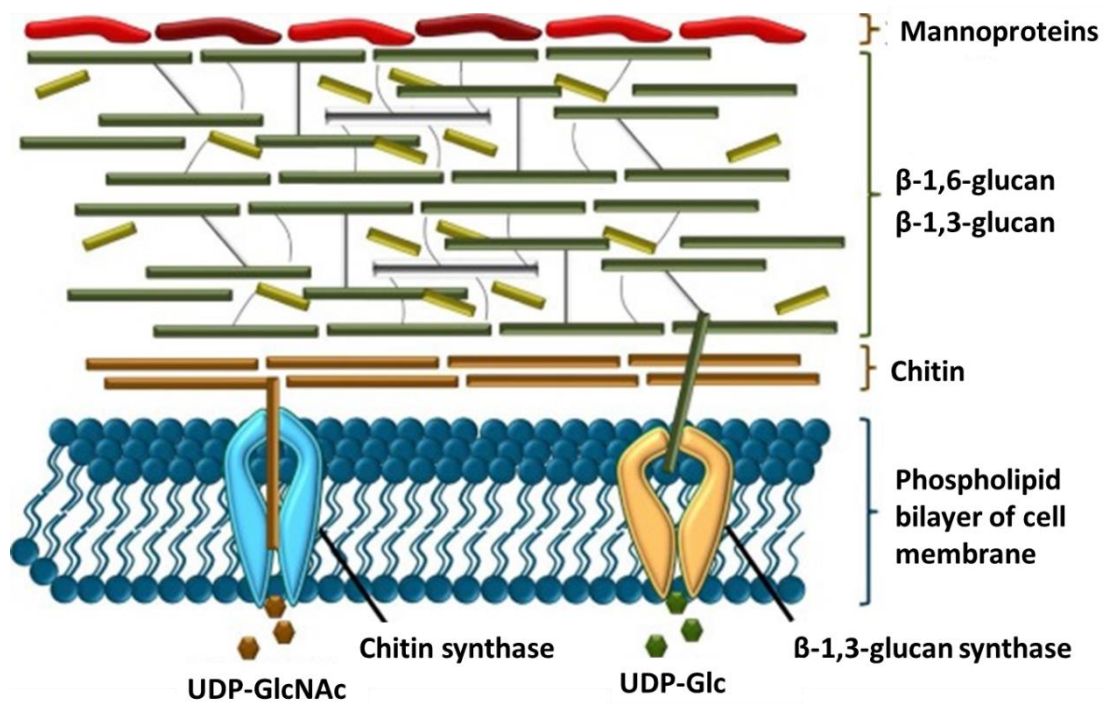


Fig. 5.2.3. Schematic diagram of fungal cell wall composition. β -1,3-glucans are synthesised at the plasma membrane by β -1,3-glucan synthases. The glucan layer, composed of both β -1,3 and β -1,6-glucans, is sandwiched between an outer mannoprotein layer and an inner chitin layer, which is immediately adjacent to the plasma membrane. From Fesel and Zuccaro (2016).

Plants and fungi contain GH enzymes that are secreted, with the aim of targeting the other's nascent and/or mature cell walls. During infection, release of sugar oligos from the polysaccharides can activate the PTI arm of plant immunity as a PAMP. The GH81 family of carbohydrate active enzymes cleaves the glycosidic linkages between carbon 1 and 3 in the glucose polymer callose, and have the interpro description of endo-1,3- β -glucanase. In Barley (*Hordeum vulgare*), a GH81-type glucan-binding protein was identified through a protein pull down with the biotinylated β -glucan laminarin (another β -1-3-glucan polymer), and named GBP1. Mutation of this and its paralog GBP2 led to decreased colonisation by both beneficial root mycorrhizal fungi and pathogens and was accompanied by an increased callose response at cell wall appositions (Wanke et al., 2023). This indicates that by disrupting proteins that bind to β -glucans, and perhaps preventing their hydrolysis by GH81 enzymes, either from plant or fungal origin, leads to increased callose presence at the fungal-plant interface. However, research into the action of GH81 enzymes from both plant and fungal origin in plant-pathogen interactions is currently, entirely, lacking.

In yeasts, GH81 proteins have been shown to be involved in the cell separation process. For example, disruption of the GH81 gene *ENG1* in the pathogenic yeast *Candida albicans* was shown not to attenuate growth or hyphal morphogenesis but was essential for septum degradation (Esteban et al., 2005). Similarly in the yeast *Saccharomyces cerevisiae* the enzyme was shown to localise to the daughter side of the septum during cell separation (Baladrón et al., 2002). However, these enzymes are not secreted and thus likely target β -1-3-glucans in the fungal cell wall.

Although the genomes of several fungi have been shown to contain gene(s) coding for GH81 enzymes, the active degradation of callose by a secreted GH81 enzyme by a fungal species, or any other phytopathogen, has not yet been explored, despite its relevance across plant pathology. This chapter explores the effect of single gene deletion of a highly conserved GH81 enzyme in *F. graminearum*, with a predicted signal peptide sequence, on virulence in wheat.

5.3 Methods

The methods outlined here are in addition to those detailed in the [general materials and methods chapter](#).

5.3.1 Identification of putative GH81 targets in *F. graminearum*

The *F. graminearum* reference genome (PH-1, version 5 (King et al., 2015) was used for the identification of putative GH81 target genes. A search was done using the FungiDB (Basenko et al., 2018; fungidb.org/) for genes with the annotated GO term 'glucan endo-1,3-beta-glucanase activity', as predicted by the CaZy database for the hydrolysis of β -1,3-glycosidic bonds in callose (Drula et al., 2022; www.cazy.org/). Candidate genes were also screened for the presence of a signal peptide using SignalP (SignalP v. 6.0; Teufel et al., 2022; <https://services.healthtech.dtu.dk/services/SignalP-6.0/>) and subcellular localisations checked with WolfPSort (<https://wolfpsort.hgc.jp/>). To ensure that the gene is expressed during *in planta* infection, RNASeq analysis from Dilks et al. (2019) and processed for Kroll et al. (2024) will be analysed.

5.3.2 Structural prediction of putative GH81 target

Structures of target GH81 enzymes were predicted using Alpha Fold 3 (DeepMind; Abramson et al., 2024) to confirm classified structures of the GH81 family.

5.3.3 Phylogenetic analysis of GH81 orthologues

The open-source software Egnogmapper-v5 (Huerta-Cepas et al., 2019) was used to map FgGH81 (FGRAMPH1_01G10749) to the Orthologue Group (OG) ENOG503NTYF, encompassing the whole fungal kingdom, and to generate the phylogenetic tree. The tree was visualised and annotated using the interactive Tree of Life (iTOL) software (Letunic and Bork, 2024).

For analysis within the FSAMSC, orthologues were pulled from EnsemblFungi (<https://fungi.ensembl.org/>; release 59), and sequences retrieved from Uniprot (<https://www.uniprot.org/>; release 2024_03). Phylogenetic analysis was conducted in Geneious (version 10.2) using standard neighbour joining tree parameters bootstrapping. Sequence alignment was also conducted in Geneious (version 10.2).

5.3.2 Fragment amplification

For the single gene deletion of FGRAMPH1_01G10749, Gibson split-marker assembly was employed (Gibson et al., 2009; King et al., 2017). For designing of constructs, NEBuilder assembly tool (<https://nebulderv1.neb.com/>) was used to generate primers for ligation of fragments (Table 5.3.2). Briefly, two constructs were inserted into the pGEM-T Easy plasmid vector (Promega, UK), one of either the 1kb upstream region of the 5' flank of the target gene (FGRAMPH1_01G10749) or 1kb downstream of the 3' flank and half of the split selection marker hygromycin B phosphotransferase gene (hph) that confers resistance to the antibiotic hygromycin (Figure 5.3.2 (a)). For Gibson Assembly, four fragments were prepared: 1kb 5'upstream of FgGH81, the first half of the hygromycin split marker, second half of the split marker, and 1kb 3' downstream of FgGH81. Primers were sourced from Eurofins genomics (Eurofins, EU) as salt-free lyophilised oligos, reconstituted in dH₂O and diluted to 10µM for use. Each of the fragments was amplified by PCR using Phusion high-fidelity Taq polymerase with HF buffer (NEB, USA). Each 50µl reaction included 25µl 2x

Phusion master mix, 1µl DMSO, 21µl dH₂O, 1µl of template DNA (reactions 1 and 4 = WT (PH-1) gDNA; reactions 2 and 3 = pHYG1.4 plasmid containing the hygromycin resistance gene) and 1µl of each of the forward and reverse primers, as detailed in Table 5.3.2. The PCR cycle specifications used were as follows {98°C (30s) [(98°C (10s), Ta°C (30s), 72°C (45s)) x 34], 72°C 10 min final extension} and conducted using a thermocycler (T100 Thermal Cycler, BioRad, USA). For Ta°C values see Table 5.3.1. A 25µl aliquot from each reaction was loaded into a 1% (w/v) agarose gel amended with ethidium bromide for confirmation of expected band size (Table 5.3.2). PCR products were cut from the gel, and then the DNA extraction and purification was conducted using a QIAquick Gel Extraction Kit (Qiagen, UK) according to kit instructions. DNA yields >10ng/ µl were used for Gibson Assembly.

5.3.3 Gibson Assembly

To join the 5'+HY or YG+3' fragments, Gibson Assembly master mix (NEB, USA) was used. Each 10µl reaction contained 5µl mastermix, 1µl pGEMt easy vector at 50ng/µl, and 100ng (variable volume) of each of the HY or YG fragment and 100ng (variable volume) 5' or 3' flank, resulting in 2-fold excess ratio of fragment inserts to vector. The reactions are incubated for 1 hour at 50°C in a PCR thermocycler (T100 Thermal Cycler, BioRad, USA) for cloning into *E. coli* competent cells.

Table 5.3.1. Primers used for Gibson Assembly. Preparations of fragments for Gibson assembly in *F. graminearum* joined 5' + HY (PCR 1 and 2) and YG + 3' (PCR 3 and 4) fragments that were prepared through PCR amplification.

Primer name	PCR	Product size	Overlaps	Oligo (UPPERCASE = gene-specific primer)	Anneals	3' Tm	3' Ta*
1_LB_FgGH81_5'_F	1	1010	pGEMt-easy	ccgcggaattcgatCCGGGAGCGCAAGCCAAG	5'_FgGH81	73.2°C	68.5°C
2_HY_FgGH81_5'_R			HY-	gttatcgaatGGCTTCATGGCTCTTCTAATATAGTCGG	5'_FgGH81	68.5°C	68.5°C
3_FgGH81_5'_HY_F	2	1156	5'_FgGH81	atgaagccATTCGATAACTGATATTGAAGGAGCATTTTTT	HY-	67.8°C	67.8°C
4_RB_HY_R			pGEMt-easy	gcgaattcactagtgatGGATGCCTCCGCTCGAAG	HY-	68.0°C	67.8°C
5_LB_YG_3'_F	3	1264	pGEMt-easy	ccgcggaattcgatCGTTGCAAGACCTGCCTG	-YG	65.4°C	60.4°C
6_FgGH81_YG_3'_R			3'_FgGH81	gaatgaaataCTCGAGGTTCGACGGTATC	-YG	60.4°C	60.4°C
7_YG_FgGH81_3'_F	4	1025	-YG	acctcgagTATTTTCATTCGTTACTTTCAATATTTTG	3'_FgGH81	60.8°C	60.8°C
8_RB_FgGH81_3'_R			pGEMt-easy	gcgaattcactagtgatCGAGGTCCAGGTCCAATTG	3'_FgGH81	65.1°C	60.8°C

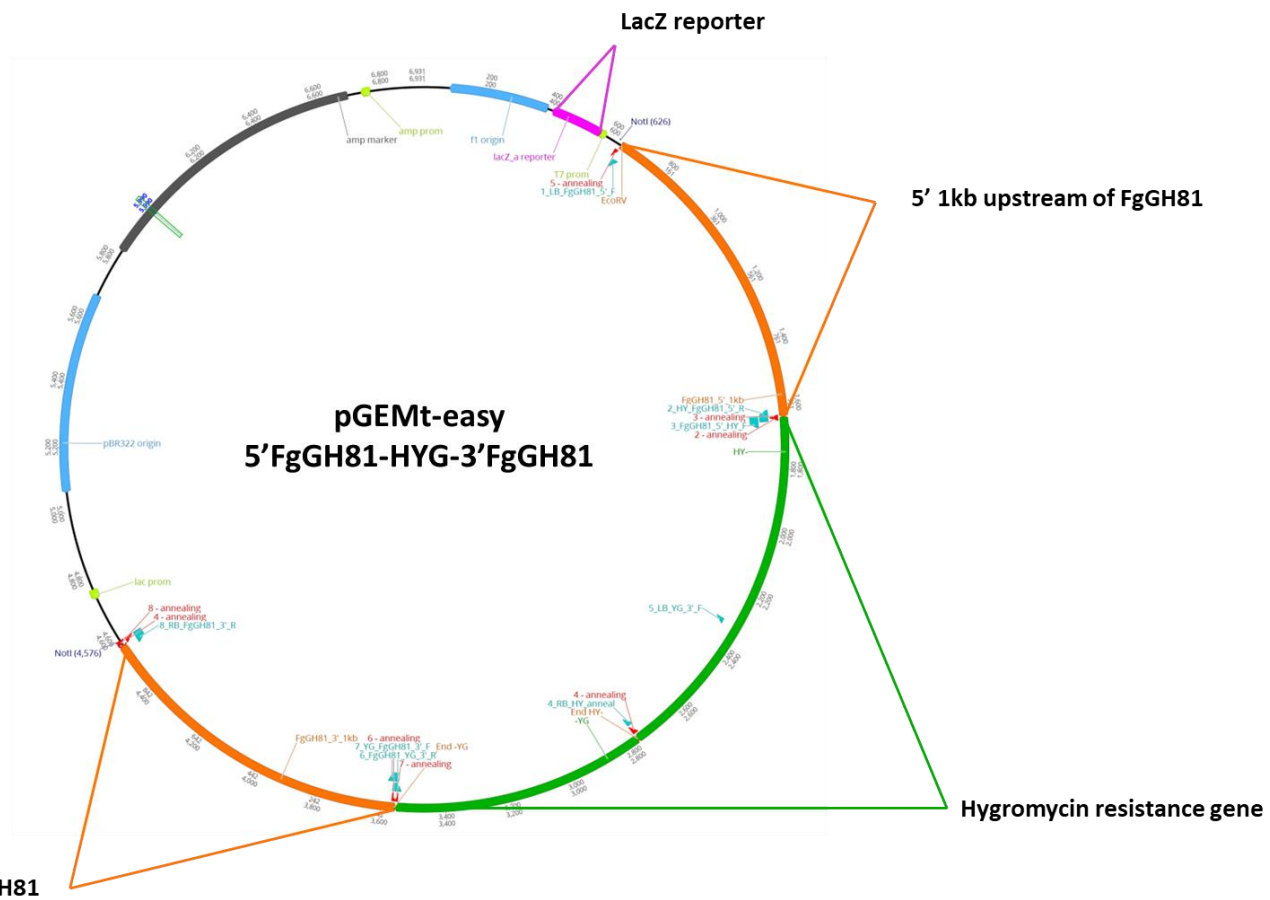


Fig. 5.3.1 Schematic diagram of pGEM-T Easy vector used for split-marker fragment ligation. At the EcoRV restriction cut sites, the 5' 1kb upstream of the target gene FgGH81, Hygromycin split marker and 3' 1kb downstream of FgGH81 fragments are inserted into the vector. Note this figure shows only the completely ligated vector, which is not generated in the split marker transformation process in *E. coli*, but anneals during fungal transformation as described in Figure 5.3.2 (a).

5.3.4 *E. coli* cloning

For the amplification of desired constructs for *E. coli* transformation, commercially purchased NEB DH5 α *E. coli* competent cells (NEB, USA) were used. Briefly, chemically competent cells were thawed on ice and 2 μ l of the desired assembly added to 25 μ l cell aliquots, mixed by pipetting and incubated on ice for 30 mins. Reactions were then heat shocked at 42°C for 30s, incubated on ice for 2 mins and made up to 1ml with 975 μ l of SOC media (Thermo Fisher Scientific). *E. coli* cells were then incubated at 37°C for 60 mins with agitation at 250rpm for recovery. For selection of positive transformants, YT agar plates with 75 μ l/ml Hygromycin were prepared. Ampicillin plates were used as the positive control and no selection as the negative control. The pGEMt-easy vector contains the LacZ colorimetric reporter and so 100 μ l XGAL (5-bromo-4-chloro-3-indolyl- β -D-galactopyranoside; Thermo Fisher Scientific, UK) was added to the surface of all plates and allowed to dry prior to plating of *E. coli*. Plates were incubated overnight at 37°C.

Positive colonies for 5'-HY and YG-3' were screened visually and 5 positive (white) colonies were selected for colony PCR (cPCR) to confirm presence of desired constructs. cPCR was conducted using HotStart Master Mix in 25 μ l reaction volumes using primers 1 and 4, and 5 and 8 for respective fragments (Table 5.3.2). PCR cycle specification as follows {98°C (30s) [(98°C (30s), Ta°C (30s), 72°C (2.5 mins)) x 34], 72°C 10 min final extension}.

From the pool of confirmed positive transformants, three were selected and individually incubated overnight in 50ml falcon tubes in 25 ml of YT medium with hygromycin selection (75 μ g/ml) and shaking (180 RPM). The next day, the cultures were mini-prepped using a GeneJET plasmid miniprep (Thermo Fisher Scientific) kit according to instructions. Plasmids were sequenced using pUC19_F and pUC19_R primers (Table 5.3.3) to ensure correct assembly and check for mutations in the hygromycin cassette. Sequencing was done by Eurofins Genomics (UK).

5.3.5 Preparation of bulk PCR fragments for fungal transformation

To generate the large quantity of DNA required (~1ug/μl) for each transformation, a bulk PCR amplification was conducted. The primers from each reaction that overlap the vector were used (primers 1 and 8 in Table 5.3.2). Eight 50μl PCR assays were established using Hot Star Master Mix Kit (Qiagen) and the PCR cycle used was {95°C (15 mins) [(94°C (60s), 58°C (30s), 72°C (150s)) x 34], 72°C 10 min final extension}. DNA was extracted using the phenol-chloroform protocol outlined in section [2.3.1](#).

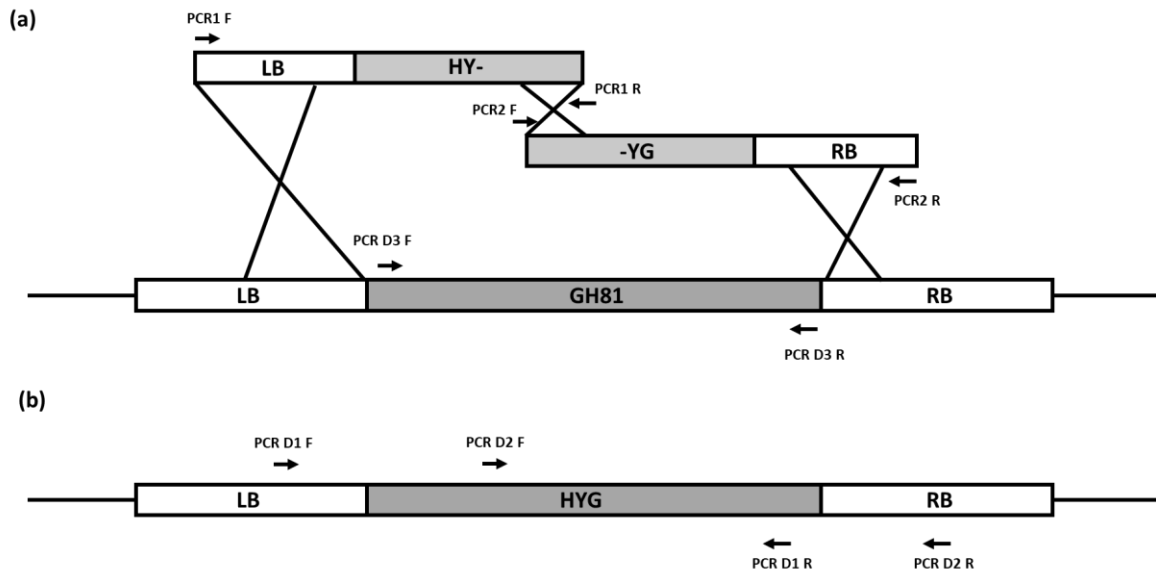


Fig. 5.3.2 Schematic diagram of Gibson Assembly. (a) The split marker technique using the resistance gene for the antibiotic selection hygromycin. Two fragments are assembled *in vitro*, one containing the first half of the hygromycin (HYG) gene (denoted HY-), annealed to the 1kb 5' of left border of the target gene. The second fragment contains the second half of the HYG gene (denoted -YG) annealed to 1kb 3' of the right border of the target gene. Primers used to generate the fragments for assembly are annotated and detailed in Table 5.3.1. (b) Split marker deletion of the gene of interest *in situ* in the genome. The GH81 and 1kb 5' and 3' have been replaced by the gene conferring resistance to hygromycin (HYG). Primers for diagnostic PCRs are annotated and detailed in Table 5.3.2.

5.3.6 Fungal transformation

Transformations for single gene deletion of FgGH81 was conducted using the split-marker method as previously described (Urban, Cuzick and Hammond-Kosack, 2008; King et al., 2017). Briefly, *F. graminearum* was cultured for 2 days on PDA plates and conidia harvested into 200 ml flasks of TB3 (Table 5.3.3) medium. Conidia were germinated overnight and harvested through miracloth under a mild vacuum, washed twice with dH₂O and once with 1.2M KCl. Germinated conidia were resuspended in 25ml KCl containing 750mg driselase (Sigma, D9515) and 400mg Lysing enzyme (Sigma, L1412) and the cell wall

digested for 2 hrs with agitation at 80rpm at 30°C. Protoplasts were then harvested by centrifugation (13.2krpm, 10 mins, RT), the supernatant discarded, and pellet resuspended in STC media (Table 5.3.3). For each transformation 100µl of protoplast suspension was mixed with 5µl of each of the 5' and 3' vector flanks at 2µg/µl before adding 1ml of 40% PEG in STC media and mixed carefully with a pipette tip. The protoplast-PEG solution was incubated for 20 mins at RT before adding 5ml TB3 and then left overnight on a vertical rotating mixer.

If the protoplasts were viable, cell wall regeneration is evident with a cloudy solution. The regeneration (REG) agar (Table 5.3.3) was prepared and mixed with an equal volume of 1.6M sucrose. When the agar cools to 45°C the selective antibiotic was added (hygromycin, 75µg/µl) and the protoplast solution was split into 25ml aliquots of the REG agar with sucrose media (Table 5.3.3) for each plate (four plates per transformation including positive and negative controls). Positive control was protoplasts alone (no DNA or selection) to ensure protoplasts were viable throughout transformation process and negative control was protoplasts alone with selection (hygromycin, 75µg/µl) to ensure that the selection inhibited non-transformant *F. graminearum* growth. Plates were placed in a 28°C incubator with the lids untapped and colonies of transformed *F. graminearum* became visible from 5 days onwards.

5.3.7 Transformant diagnostics

After 5 days, positive *F. graminearum* colonies were observed on the transformation plates. The positive control plates have extensive colony development across the surface while the negative control plate lacked colonies. For verification, putative transformants were lifted onto fresh 6cm petri dishes of SNA amended with the selective antibiotic hygromycin (75µg/ml). From these plates, eight well growing transformants were brought forwarded for PCR diagnostics to test for hygromycin insertion into the FgGH81 gene site.

Transformants with positive growth on the second selection plate were cultured in YPD media with 75µg/µl hygromycin for 2 days at 22°C with 120rpm agitation. DNA was extracted using the CTAB extraction method as outlined in section [2.3.1](#).

Three PCR diagnostics were conducted on each sample, spanning from the left border (LB) into the second half of the split marker (-YG) and from the first half of the split marker (HY-) into the right border (RB). The final PCR checks for the presence of the FgGH81 gene. Fig 5.3.3. shows a schematic of primer diagnostics and Table 5.3.2 outlines the primers used. Gel electrophoreses were run as outlined in section [2.3.5](#).

Table 5.3.2. Primers used for sequencing and diagnostics of *ΔFgGH81*.

PCR	Primer name	Product size	Overlaps		Anneals	3' Tm
	pUC19_F	For sequencing plasmids (-ve 180bp)		TATTTAGGTGACACTATAG		58°C
	pUC19_R			TAATACGACTCACTATAGGG		58°C
D1	F_LB_YG_GH81	2632	LB	GTCGCTATCGTGGGACCAAT	-YG	60.5°C
	R_LB_YG_GH81		-YG	CTCCAGTCAATGACCGCTGT	LB	59.8°C
D2	F_HY-RB_GH81	2306	HY-	CTGATCCCATGTGTATCACTGG	RB	60.5°C
	R_HY-RB_GH81		RB	CTTTCGAGTTGGTTGTACAGCC	HY-	59.8°C
D3	F_GH81_internal	1812	5' GH81	ACTCACCCAGTCTCCAAGGA	3' GH81	59.8°C
	R_GH81_internal		3' GH81	TCGTGACATGACTGCAAGCT	5' GH81	60°C

Table 5.3.3 Media preparations for fungal transformation.

Media	Components
TB3	0.3% Yeast extract, 0.3% Bacto Peptone, 20% Sucrose
Enzyme mix	<i>For 300ml:</i> 400mg Sigma Lysing Enzyme, 0.5g Driselase, 25ml 1.2M KCl, up to 300ml with dH ₂ O
STC sucrose	20% sucrose, 50mM Tris-HCl, pH 8.0, 50mM CaCl ₂
40% PEG8000 in STC sucrose	40% (v/v) PEG8000 in STC sucrose
2x Regeneration medium (REG)	0.4% Yeast extract, 0.4% Casein-Hydrolysate (N-Z_amine A)
1.6M sucrose	<i>For 500ml:</i> 500g sucrose in 912ml dH ₂ O
Regeneration (REG) agar	<i>For 100ml:</i> 0.7g low melting point agarose in 50ml 2x REG and 50ml 1.6M sucrose
REG agar + sucrose	<i>1:1 ratio of REG agar and 1.6M sucrose i.e., 50ml REG agar + 50ml 1.6M sucrose per transformation plate.</i>

5.3.8 Generation of conidia for wheat inoculations

After three days, a small sample from the edge of the hyphal growth front was lifted and transferred to a fresh 9cm petri dish of SNA supplemented with a lower concentration of hygromycin at 20ug/ml. The lids of the plates were tapped close to prevent water loss but left with a small breathing gap (< 5 mm) to allow oxygen in. The plates were left for nine days until transformant hyphal growth covers the plate surface. Once the hyphal front has reached the edge of the plate, 300µl of TB3 (Table 5.3.4) was added to the plate and spread with an L-shaped sterile plastic spreader, removing hyphae from the surface. This was done to stimulate spore production. After 2 days, spores were harvested, diluted to 5×10^5 spores/ml and stored at -80°C in aliquots until use.

5.3.10 Phenotyping $\Delta GH81$ transformants *in vitro*

The growth rate of the $\Delta GH81$ transformants were analysed against the WT strain PH-1 on complete (PDA) and minimal (SNA) media.

To mimic stresses encounter by *F. graminearum* during colonisation of wheat spikes, transformants were subjected to a series of chemical stressors aimed to test the cell wall integrity. These were osmotic stress (NaCl), membrane stress (Tergitol), Congo Red, a cell wall integrity stressor, and calcofluor white (CFW), a cell wall perturbing agent that binds chitin the fungal cell wall. PDA plates supplemented with either 0.02% Tergitol, 1.5M NaCl, 250µg/ml Congo Red or 150µg/ml CFW were prepared and 20µl of 5×10^5 spores/ml spore suspension of WT and each transformant dropped onto the plates, followed by a 3-fold dilution series. Control plates of nutrient poor media (SNA) and nutrient rich media (PDA) were also included in this assay. Plates were grown in the dark at RT and imaged after 3 days using an Olympus E-M10-Mark IV mirrorless digital camera (Olympus, Tokyo, Japan).

To determine if conidiospore (asexual spore) morphology was affected by transformation and/or deletion of the GH81 gene, spores of WT and three $\Delta GH81$ transformants were imaged under BF illumination on a Zeiss Axioimager (Zeiss, UK). Equally, to determine if KO of GH81 led to an inability to sexually reproduce, perithecia were induced *in vitro* as previously described ([3.3.9](#)).

5.3.11 Plant inoculations

Point inoculation of the susceptible dwarf spring wheat cultivar 'Apogee', grown as in section [2.4.2](#), were conducted at mid-anthesis, as outlined in section [2.4.4](#).

5.3.12 Disease assessment

For initial determination of a reduced virulence phenotype, three positive transformants confirmed by diagnostic PCR were included in a disease progression assay and analysed as outlined in section [2.4.5](#). To assess if $\Delta GH81$ had an attenuated pathogenicity *in planta*, disease progression was tracked across a 14-day period.

5.3.12 DON quantification

DON was quantified in whole wheat spike rachis internodes at the end of disease progression (14dpi) for WT and $\Delta GH81$ T1 using the methods outlined in [2.4.7](#).

5.4 Results

5.4.1 Identification of target GH81 gene

On bioinformatic search for a β -1,3-glucanase, one gene from the GH81 family was returned, FGRAMPH1_01G10749 (Chromosome 2: 2,536,310-2,539,412, forward strand). Analysis in Uniprot (uniprot.org/uniprotkb/I1RWS7/entry) confirmed the prediction of glucan endo-1,3-beta-glucanase activity and predicted a signal peptide sequence, indicating that the enzyme is secreted and may be targeted towards callose at plasmodesmata in host cell walls. SignalP v. 6.0 (Teufel et al., 2022; <https://services.healthtech.dtu.dk/services/SignalP-6.0/>) predict a cleavage site of the signal peptide between amino acid positions 21 and 22, with probability of 0.9769. WolfPSort analysis predicted extracellular localisation of the putative FgGH81 protein at 22, mitochondrial localisation at 2 and vacuolar at 2. Together, this evidence supports extracellular secretion of FGRAMPH1_01G10749 by *F. graminearum* and thus probable involvement in pathogenicity.

Next, RNASeq data during plant infection by *F. graminearum* WT strain PH-1 on the susceptible spring wheat cultivar 'Bobwhite', analysed by Kroll et al. (2024) was used to investigate expression patterns during infection. Figure 5.4.2 demonstrates locations of sampling for RNASeq analysis, adapted from Kroll et al. (2024). The putative FgGH81 target gene of FGRAMPH1_01G10749 has negligible expression in YPD culture at 0.912 (Table 5.4.1). In rachis internodes 1 and 2 (R1-2), which represent high fungal biomass *in planta* and advanced stages of infection, FgGH81 expression was highest at 31.07 FKPM. Subsequently, expression during the increasingly earlier stages of infection towards the advancing hyphal front in R3-4, R5-6 and R7-8 are 8.62, 2.10 and 4.20 FKPM, respectively. In whole spikelet tissues at 3 days post inoculation, expression was assessed to be 8.76 FKPM, dropping to 3.56 FKPM in spikelets at 7 days post inoculation. This analysis confirmed the expression of the gene *in planta*, and low expression *in vitro*. RNASeq expression data indicates a role for FgGH81 during later stages of infection. However, spikelet expression patterns of FGRAMPH1_01G10749 opposes the expression pattern observed in rachis internodes, which identified higher expression during early and late stages of infection, respectively.

Table 5.4.1. Expression of FgGH81 (FGRAMPH1_01G10749). In YPD culture at 72 hours, rachis internodes (R) at 15 dpi (grouped into pairs: R11-2, R13-4, R15-6, R17-8) and whole spikelets (Sp) infected with PH-1 at 3dpi and 7dpi. Values are in FPKM and analysed from Dilks et al. (2019) by Erika Kroll, Rothamsted Research for Kroll et al. (2024).

ID	YPD 72hr	R11-2	R13-4	R15-6	R17-8	Sp 3dpi	Sp 7dpi
FgGH81 (FPKM)	0.912	31.07	8.62	2.10	4.20	8.76	3.56

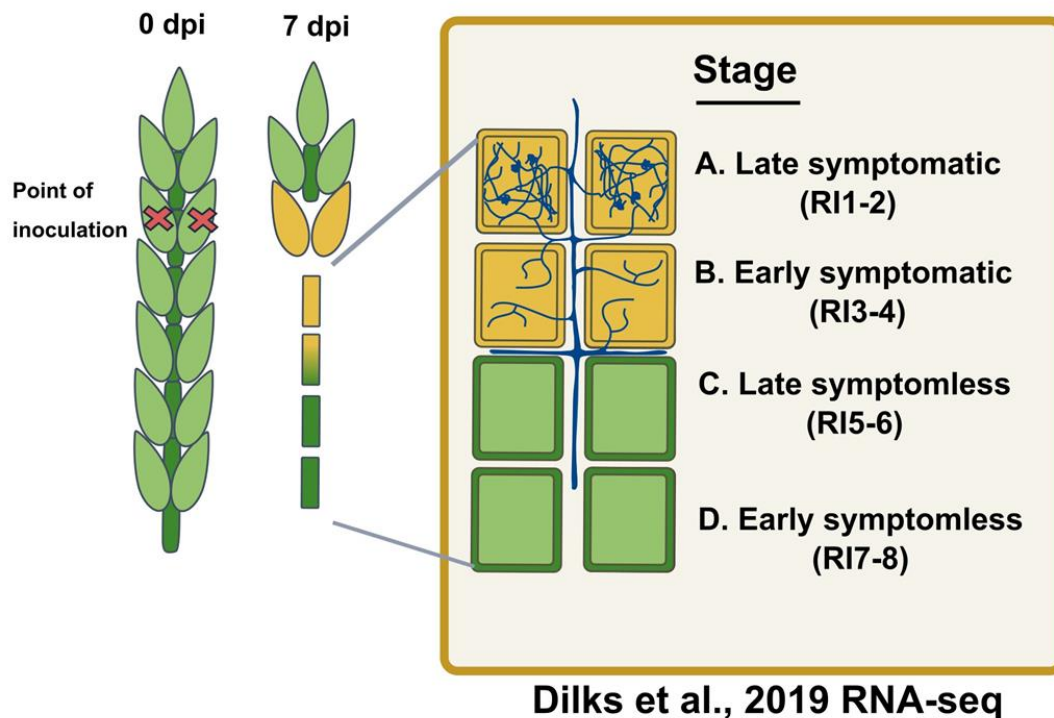


Fig. 5.4.2. Schematic diagram of rachis internode samples from point of infection used for RNASeq analysis. Stages A (RI1-2) and B (RI3-4) indicate late and early symptomatic stages of *F. graminearum* infection respectively and are in yellow, and C (RI5-6) and D (RI7-8) represent late and early symptomless stages respectively, shown in green. Fungal hyphae are shown in blue, with high levels of colonisation in the late symptomatic, low intracellular colonisation in the early symptomatic, apoplastic growth in the late symptomless and very low apoplastic growth in the early symptomless. Rachis internodes (RI) correspond to RNASeq expression data in Table 5.3.1. Data is from Dilks et al. (2019) and figure is from Kroll et al. (2024).

5.4.2 Structural prediction of FgGH81

FGRAMPH1_01G10749 is a protein with 850 amino acid residues, a transcript length of 2,891 base pairs and molecular weight of 93,721.97 g/mol. Composed of five coding exons, the gene is located on the forward strand of chromosome 2 (fungi.ensembl.org/). Structural predictions of FgGH81 in AlphaFold 3 (DeepMind; Abramson et al., 2024) confirmed a $(\alpha/\alpha)_6$ barrel structure, which is predicted by the CaZy database (<http://www.cazy.org/GH81.html>) with high quality prediction value pTM = 0.91. The predicted catalytic domain is situated between Glu533 (E; base) and Glu557 (E; proton donor) (Fig. 5.4.3; Zhou et al., 2013), but due to sequence and slight structural differences, the catalytic site of FgGH81 is yet to be determined.

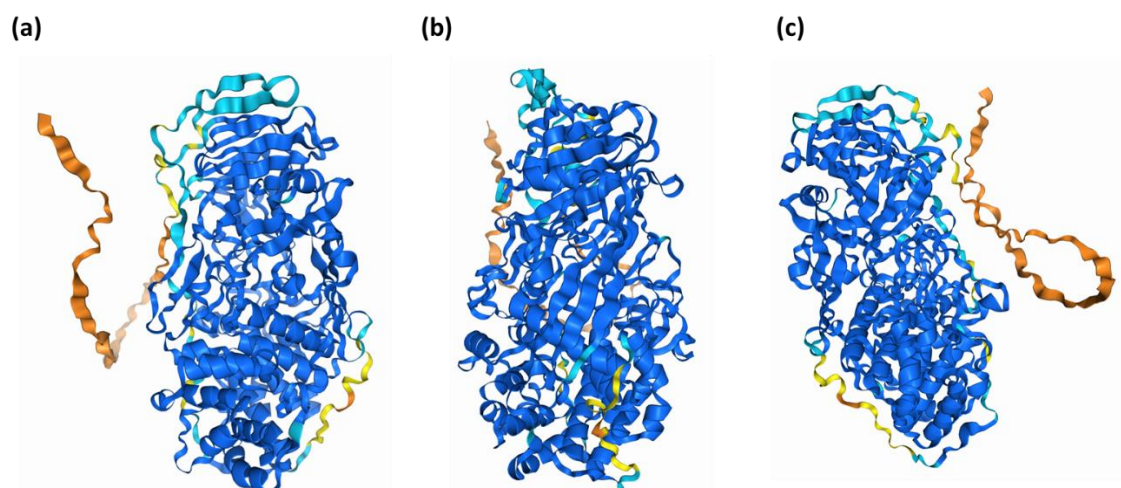


Fig. 5.4.3. AlphaFold 3 (DeepMind) structural predictions of FGRAMPH1_01G10749 (FgGH81). Structure contains $(\alpha/\alpha)_6$ barrel structure as diagnostic of GH81 family proteins. Structural prediction confidence intervals are as follows: very high; dark blue >90%, high; light blue 90-70%, low; yellow 70 to 50% and very low; orange (<50%). Low-confidence structural prediction (orange) in FGRAMPH1_01G10749 correlates with predicted signal peptide sequence. (a) Left hand side view, (b) front view and (c) right hand side view with a 90° turn between each view.

5.4.2 GH81 target orthologues in *Fusarium* species complex

A search of available genomes in Ensembl Fungi (<https://fungi.ensembl.org/index.html>, release 59 – May 2024) using the comparison tool for orthologues resulted in 6 closely related orthologues within the wider *Fusarium* Species Complex with high sequence homology (Table 5.4.2).

Table 5.4.2 Sequence identity of orthologues in top 6 *Fusarium* species. Taken from ensembl fungi BLAST results of FGRAMPH1_01G10749.

Species	Orthologue	Target % ID
<i>F. pseudograminearum</i>	FPSE_07741 K3UJH2	98.82%
<i>F. culmorum</i>	FCUL_04608.1 No Uniprot	89.31%
<i>F. fujikuroi</i>	FFUJ_06299 S0E794	85.48%
<i>F. oxysporum</i> (<i>f. sp. lycopersici</i>)	FOXG_03014 A0A0J9UHW4	85.13%
<i>F. verticilloides</i>	FVEG_01870 W7LJP9	83.92%
<i>F. solani</i> (<i>subsp. Pisi</i>)	NechaG99620 C7YM19	74.30%

Phylogenetically, sequences cluster with host-specificity, with the cereal infecting *F. graminearum*, *F. pseudograminearum*, and *F. culmorum* and *F. fujikuroi* clustering together (Fig. 5.4.4). The non-cereal infecting species, *F. fujikuroi*, *F. verticilloides* and *F. oxysporum* group together also, with *F. solani* present as an outgroup. All the top 6 *Fusarium* orthologues have higher than 83% sequence identity to *F. graminearum* (Table 5.4.2).

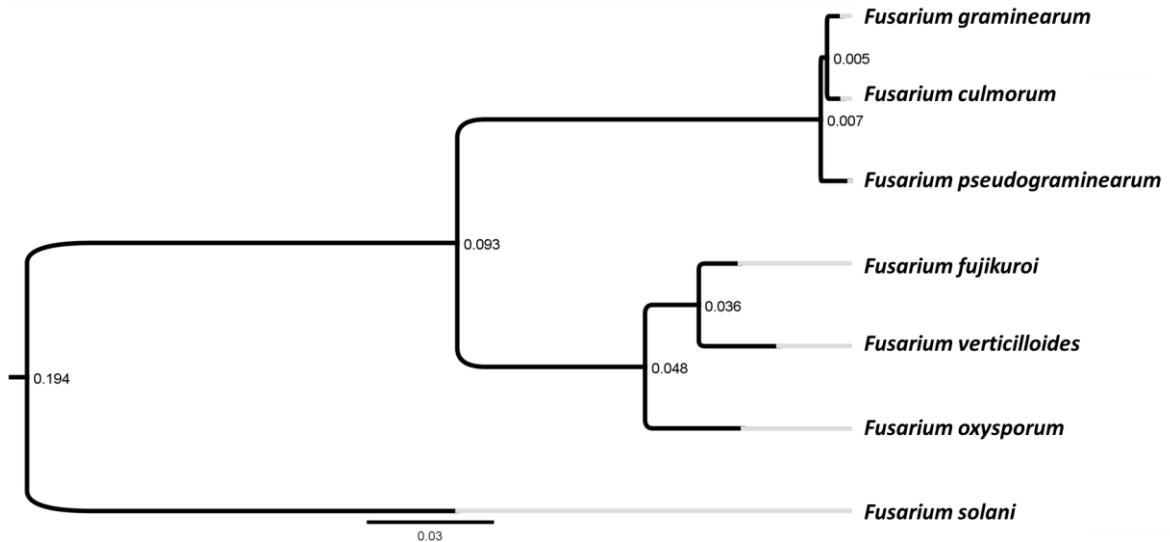


Fig. 5.4.4 Phylogenetic tree of FgGH81 orthologues in *Fusarium* species. Made in Geneious v 10.2.3 with protein sequences from Uniprot.

Sequence alignment of high identity orthologues across the *Fusarium* species complex confirms high homology. Each *Fusarium* species has only one copy of the GH81 orthologue, indicating a conserved use for the enzyme in cereal-infecting *Fusarium* species (Fig. 5.4.5). Sequence homology diverges as host range diverges.

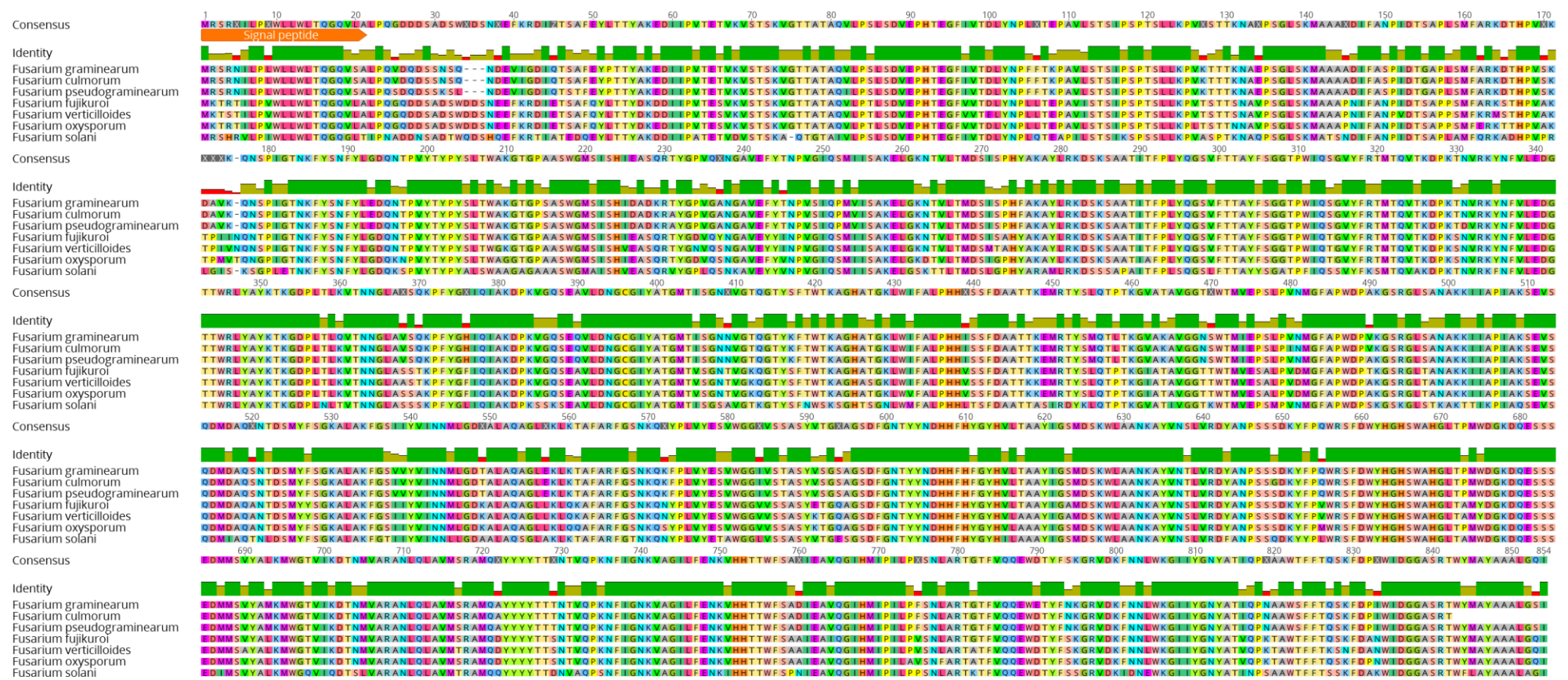


Fig. 5.4.5. Alignment of top 6 *Fusarium* species orthologues. Signal peptide cleavage site is precited between amino acid residues 21 and 22 with probability of 0.977 (signal v.6.0) in *F. graminearum* and is conserved in *F. culmorum* and *F. pseudograminearum*. Made in Geneious v 10.2.3 sequence alignment tool.

5.4.3. Fungal orthologues of FgGH81

Identification of fungal orthologues of FgGH81 yielded 214 proteins from 153 species (Fig. 5.4.6). Conservation is mostly restricted to the ascomycetes, with most species having a single copy of the orthologue. Several basidiomycete species, including the wheat rust pathogen *Puccinia graminis*, have a highly conserved sequence homology to the FgGH81 gene. High confidence bootstrap values are present across the fungal kingdom, supporting the notion that the gene is highly conserved and has a similar function.

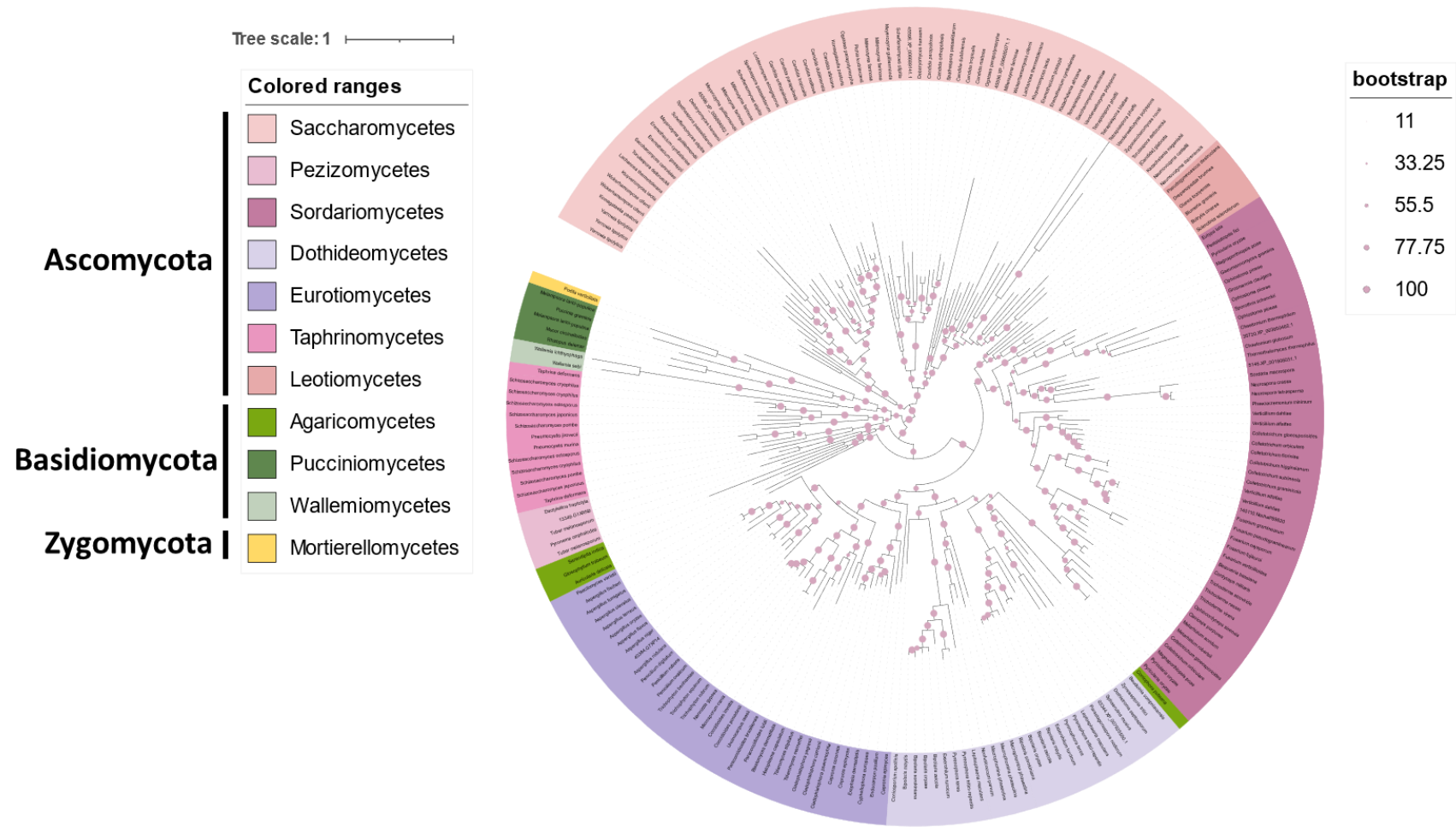


Fig. 5.4.6. Phylogenetic tree across the fungal kingdom of FgGH81 orthologues. Orthologues are grouped by class. Ascomycota are shown in the pink palette, Basidiomycota in green and Zygomycota in yellow. Tree scale is shown above the colour key and bootstrap key to the right of the phylogenetic tree. Fungal orthologues were curated from Egnognmapper-v5 and tree generated in interactive Tree of Life (iTOL) software.

5.4.5 PCR confirmation of GH81 transformants

To confirm single gene deletion knock out of the putative GH81 gene by split marker, PCR diagnostics were conducted, as outlined in Fig. 5.3.2. Diagnostic PCR 1 confirms the presence of the second half of the hygromycin split marker cassette from the left border, with PCR D2 from the first half of the split marker to the right border. Together these check for the correct assembly of the hygromycin cassette in the native locus of the putative GH81 gene. PCR D3 has two internal primers for the GH81 gene, and so positive bands in this PCR indicate presence of the gene. Due to the multiple nuclei (< 8) in each *F. graminearum* cell, some PCRs indicate that not all nuclei have been transformed, and contain both the GH81 gene and the hygromycin resistance cassette. Transformants T1, T7, T13 and T20 are indicated to be correct, with correct band sizes for D1 and D2, and absent in D3. These are renamed T1=T1, T7=T2, T13=T3 for future experiments.

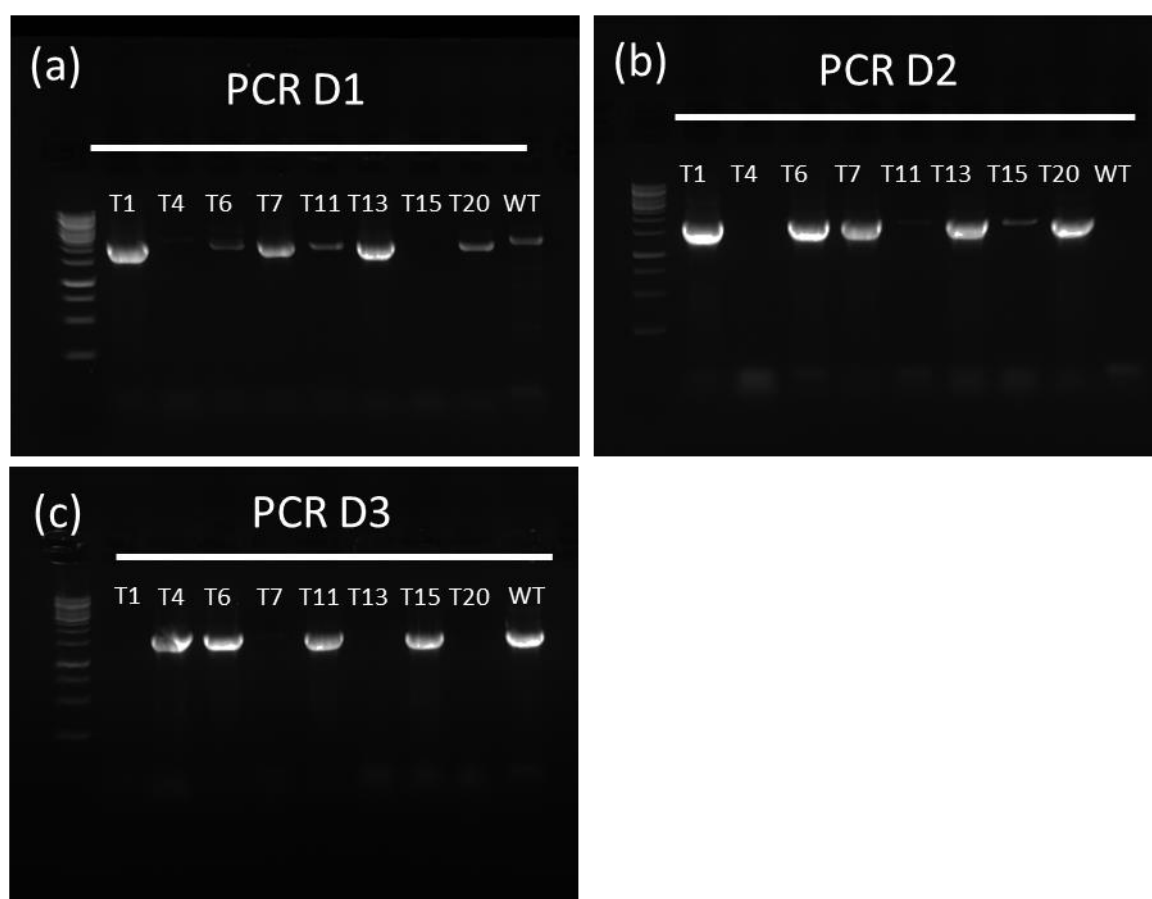


Fig. 5.4.7. Transformant diagnostics by PCR. Transformants selected from sub-cultured HYG selection plates were diagnosed through PCR. PCR D1 confirms presence of 5' LB to -YG fragment of split marker, with PCR D2 confirming presence of HY- fragment of split marker to 3' RB of target gene. PCR D3 checks for the presence of the GH81 gene. Expected band sizes are

PCR D1 = 2632, PCR D2 = 2306 and PCR D3 = 1812 (Table 5.3). Gel electrophoresis with 1% agarose in 1x TBE buffer amended with ethidium bromide, run at 100V, 400mA in 1 x TBE.

5.4.6 *In vitro* phenotyping of $\Delta GH81$ growth

To ensure the transformation procedure and KO of the putative FgGH81 gene had any effect on the spore morphology, spores of WT strain PH-1 and transformants 1-3 were checked by light microscopy. No discernible effects were noted on visualisation (Fig. 5.4.8), with all spores showing typical septa and 'banana' shape of similar sizes to the WT.

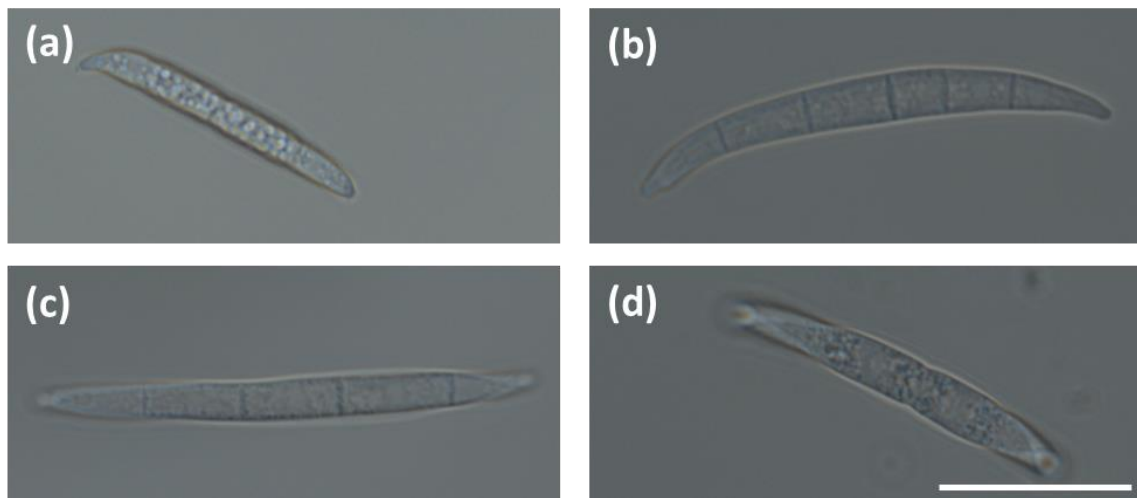


Fig. 5.4.8. Spore morphology. (a) WT, (b) T1, (c) T2 and (d) T3, imaged by light microscopy under BF illumination. Scale bar = 20 μ m.

To determine whether the KO of FgGH81 has any effect on *in vitro* growth in stress conditions designed to mimic *in planta* stress experienced during infection, a series of stress tests were conducted (Fig. 5.4.9). Across all treatments, no discernible effects of membrane or nutrient stress were evident on transformant growth vs WT. This indicates that FgGH81 is likely secreted and/or is not expressed highly *in vitro*, as indicated by RNASeq data, and is likely not rearranging β -1,3-glucans in the fungal cell wall. Overall, this supports the bioinformatic dataset used to identify the putative FgGH81 gene.

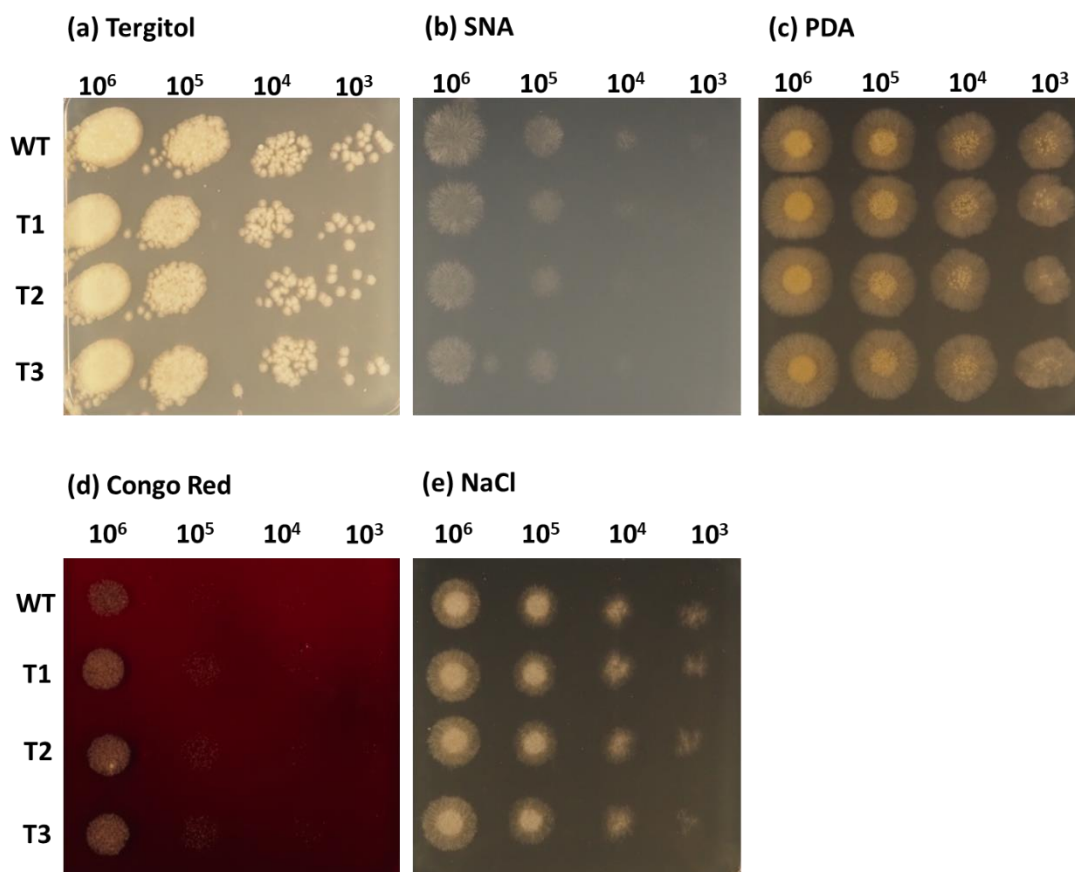


Fig. 5.4.9. Stress test plates of WT and $\Delta GH81$ transformants. (a) PDA (rich media), (b) SNA (poor media), (c) PDA with Tergitol (0.02%), (d) PDA with Congo Red (250 μ g/ml), and (e) PDA with NaCl 150 μ g/ml. All *F. graminearum* strains underwent a serial dilution from 1×10^6 to 1×10^3 . 20 μ l of each fungal spore dilution was added to plates for phenotyping and grown at RT in the dark for 2 days before imaging.

To determine if KO of FgGH81 has any (unexpected) effect on the ability of *F. graminearum* to form perithecia *in vitro*, a carrot agar assay to induce sexual reproduction was set up. All three transformants were able to produce perithecia (Fig. 5.4.10).

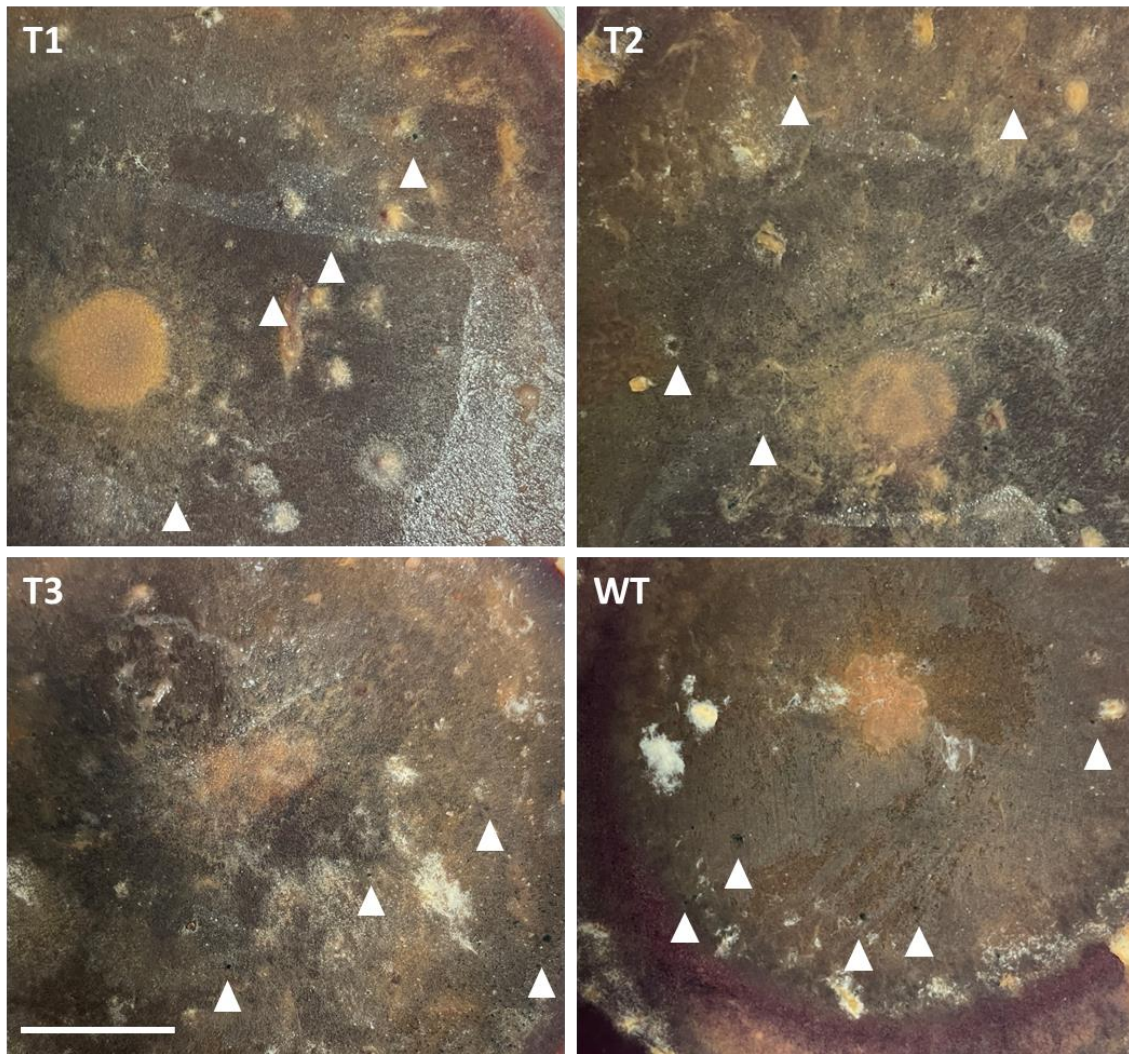


Fig. 5.4.10. Production of perithecia *in vitro*. Carrot agar plates inoculated with (a) T1, (b) T2, (c) T3 and (d) WT were all able to produce perithecia, which are visible as black structures above indicated white arrows. Scale bar = 20mm.

5.4.7 Wheat spike disease assessment of $\Delta GH81$

In planta phenotyping of GH81 single gene deletion mutants were conducted with three independent transformants. Disease progression of GH81 down the wheat spike from the 7th spikelet tracked behind WT, with reduced virulence (Fig. 5.4.11. (a)). Further analysis of disease progression through Area Under Disease Progression Curve (AUDPC) and subsequent ANOVA statistical analysis determined statistically reduced virulence between the WT PH-1 strain and all three independent transformants, which behaved similarly (Fig. 5.4.11. (b)). The disease progression was conducted three times with five independent biological replicates for each treatment per experimental replicate. Example images of inoculated wheat spikelets at 10dpi are shown in Fig. 5.4.11. (c), with inoculated

spikelet indicated by the yellow arrow. Wheat spikes inoculated with WT are, on average, fully symptomatic on 7 spikelets by 10dpi, whereas wheat spikes inoculated with transformants T1, T2 and T3 have symptoms evident on 5.5 spikelets on average. This is visible in Fig. 5.4.11 (c) with green spikelets at the bottom of the wheat spike.

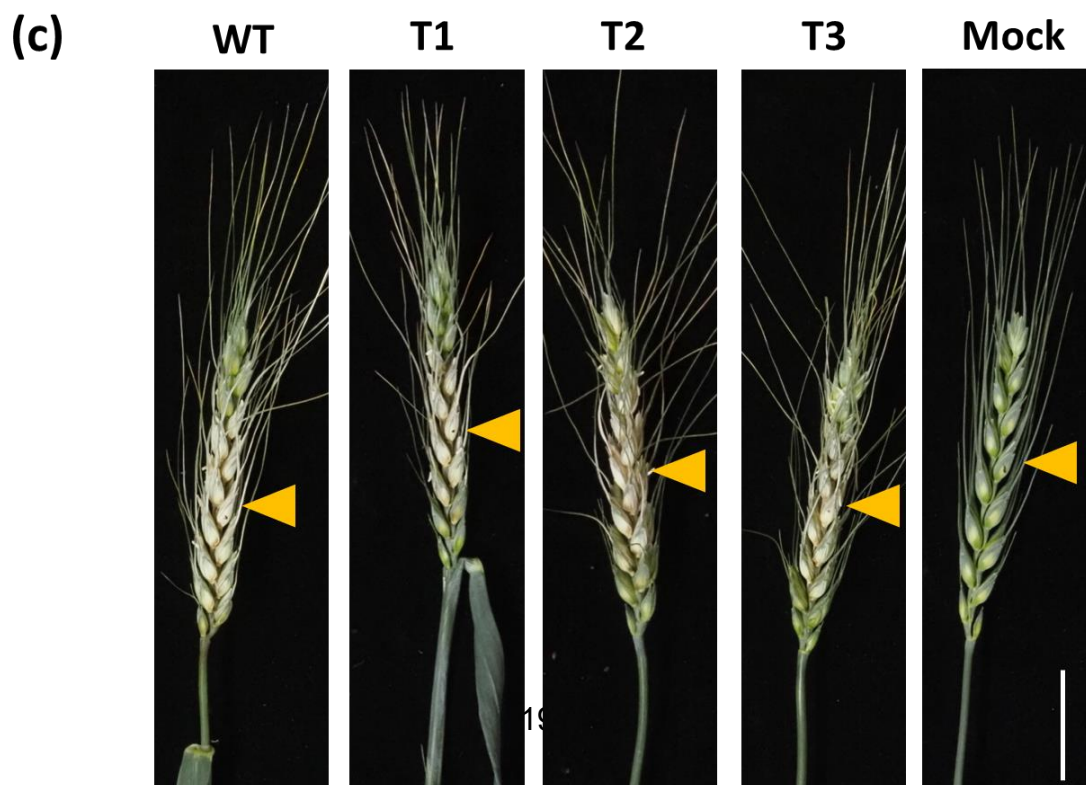
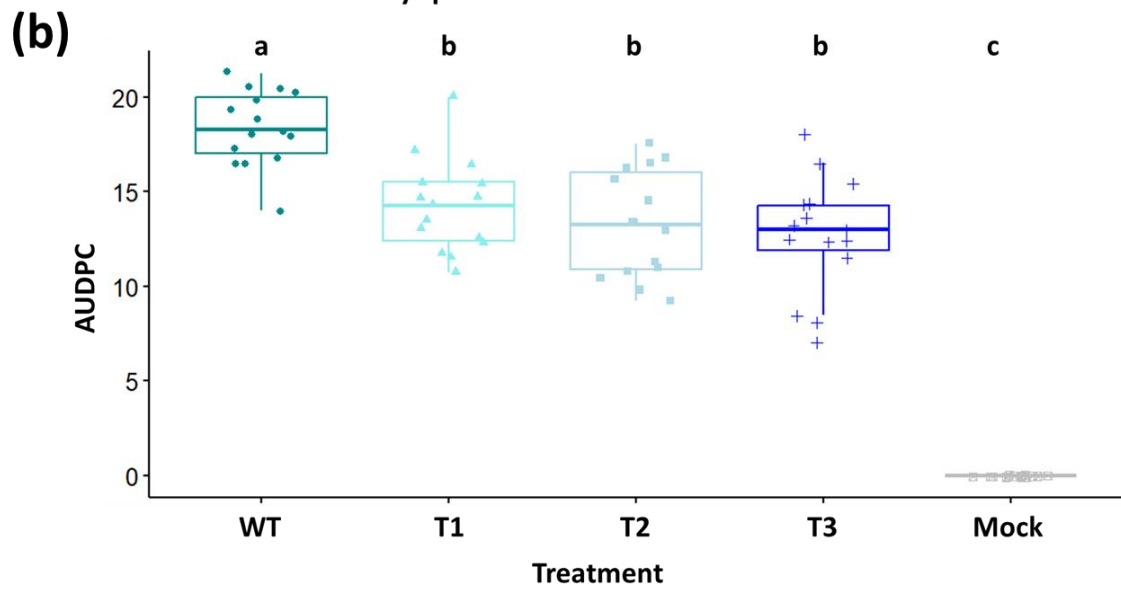
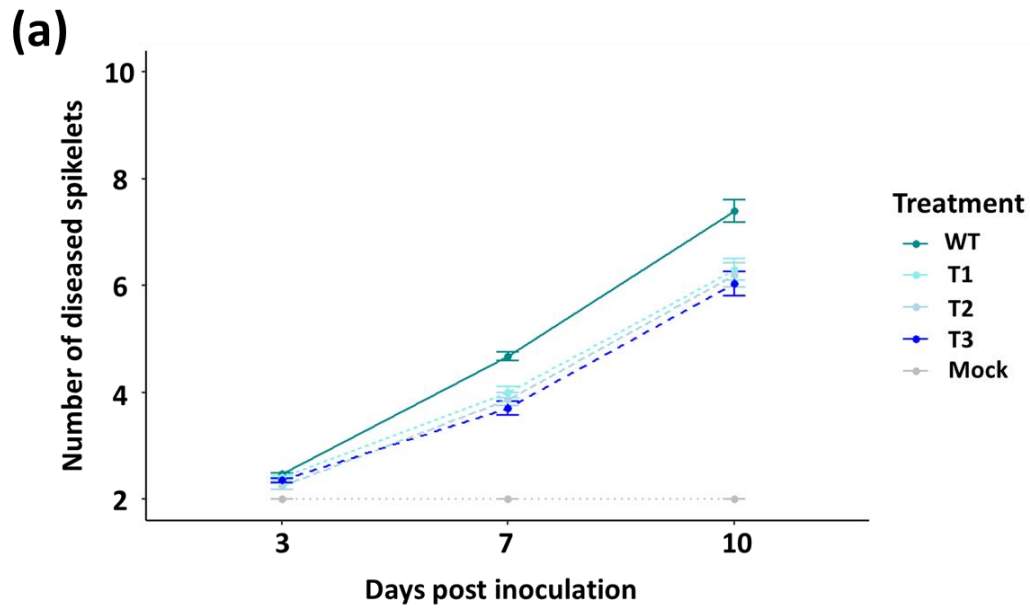


Fig. 5.4.11. Wheat spike disease assessment for $\Delta GH81$ in planta phenotype. (a) Disease progression of WT, 3 independent transformants T1, T2, and T3 and Mock inoculated spikelets. The 7th true spikelet from the base was inoculated with 5 μ l 5x10⁵ spores/ml on both sides. (b) Area Under Disease Progression Curve (AUDPC) for disease progression at 10dpi. ANOVA = F(4, 70)= 132.6, p < 0.005, n=15. Letters denoted group significance as determined by Tukey post-hoc test. (c) Example wheat spikes at 10dpi (from left to right) WT, T1, T2, T3 and Mock. Yellow arrow indicates inoculated spikelet. Scale bar = 20mm.

5.4.8 DON quantification

To determine if the production of the trichothecene mycotoxin DON was affected by the deletion of FgGH81, a DON ELISA test was conducted on wheat rachis internodes collected at the end of disease progression at 14dpi. Tests confirmed presence of DON in all WT and $\Delta GH81$ T1 samples above the detectable limit of 2.5ppm in whole spike rachis internodes.

5.5 Discussion

Identification of an endo- β -1,3-glucanases of the GH81 enzyme family in *F. graminearum* yielded a single gene with very low expression *in vitro* and moderate expression *in planta*, as indicated by RNASeq transcripts by Dilks et al. (2019). This indicates that expression is upregulated in response to infection and has a role in host tissue colonisation. The single gene copy made this gene an ideal candidate for single gene deletion knock out (KO) and subsequent phenotyping. The expression pattern in rachis internodes indicated a high expression in the later stages of infection (RI 1-2), but in whole spikelets expression is higher at 3dpi than 7dpi. Given callose deposition at plasmodesmata is a generic response to biotic and abiotic stress in plants, it would be biologically sensible to remove the deposition to facilitate host tissue colonisation, particularly in the thicker, lignified rachis tissue. In WT *F. graminearum* growth, macroscopic symptoms in the first rachis internode occurs between 3 and 7 days, so expression may peak between these two timepoints.

Structural prediction of the FgGH81 enzyme confirmed the predicted structure and had high homology to a GH81 enzyme crystallised from the mucoromycete fungus *Rhizomucor miehei* (RmLam81A; Zhou et al., 2013). While they predict a catalytic site between Glu553 and Glu557 (proton donor and recipient,

respectively) in their crystallised structure, this has not yet been confirmed experimentally, and a lack of sequence homology between FgGH81 and the crystallised structure mean that the active site is yet to be determined.

Further afield in the fungal kingdom, a phylogenetic analysis was conducted to investigate the relative expansion and/or contraction of the GH81 gene family. Using the orthologue finder tool EggNog (Huerta-Cepas et al., 2019), 214 proteins from 153 species were returned. Many of the species that returned more than one copy were in the yeasts (Saccharomycetes), such as *Yarrowia lipolytica*. Whether this is an expansion of the GH81 family due to evolutionary advantage or has contracted in the ascomycetes and basidiomycetes has not yet been determined. Other ascomycete fungal pathogens of wheat that contain a GH81 orthologue include *Zymoseptoria tritici*, the causal agent of Septoria tritici blotch, and *Magnaporthe oryzae*, the causal agent of blast disease. Other foliar pathogens include the rust species *Puccinia graminis*, which although is a basidiomycete, also infects wheat. The high conservation of the GH81 enzyme across the wheat infecting fungal pathogens may indicate a conserved use for the enzyme. However, expression patterns and/or determination of secretion signal peptides were not analysed across the fungal kingdom.

Single gene deletion of FgGH81 was successfully achieved through Gibson split marker. Diagnostic PCRs of eight selected transformants confirmed KO of the gene in all nuclei in *F. graminearum* protoplasts in four of the transformants, three of which were carried forward to further phenotyping and renamed T1-3. *In vitro* phenotyping of the transformants were conducted to ensure that no other genes were accidentally targeted during transformation and that the gene in question had no effect on reproductive fitness or hyphal growth in stressful conditions prior to moving into *in planta* phenotyping. These experiments were particularly pertinent with the gene in question, as there was a chance that the signal peptide prediction was incorrect and the FgGH81 enzyme in fact degraded and/or rearranged β -1,3-glucans in the fungal cell wall. However, no *in vitro* phenotypes differing from WT growth were observed in stress test plates and formation of perithecia *in vitro*.

During disease progression, the Δ GH81 transformants tracked behind the WT disease symptoms. This became evident from 3 days, after macroscopic symptoms became apparent in the inoculated spikelets. However, unlike the

$\Delta Tri5$ mutant, which was the subject of investigations in [chapter 3](#), the $\Delta GH81$ mutants were able to pass beyond the inoculated spikelet, with similar symptoms to WT infection of bleached spikelets and attenuation of the awns, albeit slower. By 14dpi, all spikelets of WT and the three $\Delta GH81$ mutants had reached full infection of 7 spikelets. All three single gene deletion mutants also behaved similarly throughout infections, with similar mean AUDPC values that were significantly different to WT infection.

While it is likely that callose is being deposited in response to the fungal infection, the $\Delta GH81$ mutants all have the ability to produce the trichothecene mycotoxin DON. It is hypothesised that one of the roles of DON during infection is to dampen the host wheat immune response, specifically the deposition of callose at plasmodesmata which is a component of the PTI arm of plant immunity. As previously reported, lack of DON leads to restriction of infection to the inoculated spikelet and, by as yet undetermined means, prevents cell-to-cell movement through plasmodesmatal pit fields (Proctor et al., 1995; Armer et al. (2024a); [chapter 3](#)). It was also postulated previously that *F. graminearum* invasive hyphae utilise pit fields to facilitate colonisation of the rachis tissue due to its inherent high lignification and thick cell walls which are difficult for CWDEs to digest. Thus plant immune responses defend these portals by callose deposition to symplastically isolate the infected cell from healthy tissue, and slow the spread of secreted components of infection ahead of the invasive hyphae, such as mycotoxins, CWDEs and effectors.

The reduced virulence phenotype observed may be due to an inability to break down callose at critical junctions in the rachis internode. It may also be the case that the lack of restriction to the inoculated spikelet is due to the overproduction of mycotoxins, which may compensate for lack of GH81 enzyme and so inhibits callose deposition before it needs to be degraded. When the rachis internodes of the inoculated wheat spikes were tested for DON production at the end of disease progression, both WT and $\Delta GH81$ transformants had detectable levels of DON. Limitations of ELISA tests designed for more natural (i.e. lower) levels of infection and lead to large errors in the data due to the large dilutions required. Hence, it can only be concluded that the $\Delta GH81$ transformants all produce DON during infection. It would be interesting to investigate whether mycotoxin production is

increased during infection to compensate for a critical component of infection, such as deletion of CWDEs.

Several studies have so far looked at the relative importance of CWDEs in *F. graminearum*, finding that it often takes the deletion of more than one cell wall component-digesting enzyme to have a phenotype *in planta*. In the *Fusarium oxysporum* f. sp., which cause vascular wilt diseases across a wide range of crops, KO of either individual proteases or CWDEs does not typically lead to detectable reduced virulence (Michielse and Rep, 2009). Analyses of *F. graminearum* gene expression in coleoptiles identified a large number of CWDEs that are upregulated during infection (Zhang et al., 2012), of which expression increased as infection progressed to 64 hours post inoculation, indicating an important role for cell wall degradation during infection. Previously, Walter et al. (2010) had identified 70 CWDEs that are expressed either during infection or when exposed to plant host extracts, indicating that the fungus actively senses host cell walls and expresses degrading enzymes in response. In *F. graminearum* infection cushion structures and runner hyphae on plant tissues during early infection, 140 carbohydrate degrading enzymes (CAZymes) have been identified as being upregulated (Mentges et al., 2020). Despite these identifications, no study has thus far investigated the role of GH81 enzymes that are predicted to degrade callose directly during plant-pathogen interactions. However, a recent study in the mutualistic arbuscular mycorrhizal fungus *Rhizophagus irregularis* in Barley (*Hordeum vulgare*), a GH81-type glucan-binding protein was found to promote colonisation of root tissues, with mutations in the gene and its paralogue reduced colonisation (Wanke et al., 2023). Although not specifically a degrading enzyme, it does demonstrate that interactions with β -1,3-glucans during host-tissue colonisation, whether beneficial or detrimental to the host, are important.

It is hypothesised that *F. graminearum* degrades callose during host tissue colonisation due to the relative cost of excreting and degrading host cell walls to advance infection. The relative importance of cell wall components, and inferred their respective CWDEs, during phytopathogenic interactions are further explored in [chapter 6](#) through application of the *Arabidopsis thaliana* SALK lines and exploration of wheat rachis tissue during the *F. graminearum* infection window surrounding anthesis.

It is worth noting that the release of β -1,3-glucans from callose through the action of FgGH81 may induce plant immunity through by acting as DAMPs. In tobacco, application of the linear β -1,3-glucan laminarin, extracted from brown algae, was shown to induce members of the lignin pathway PAL, CAOMT and SA accumulation (Klarzynski et al., 2000). Lignification of cell walls is a defence component and the role of lignin in wheat-*F. graminearum* infections is further explored in [chapter 6](#). As discussed previously in [chapter 1](#), fragments of cell walls can act as DAMPs and activate PTI, but as β -1,3-glucans are also present in the fungal cell wall they could equally be perceived as PAMPs during infection. However, with the remaining CWDE arsenal of *F. graminearum* functionally intact in Δ GH81, although compensatory expression of other CWDEs were not analysed in this study, this is unlikely to affect DAMP/PAMP responses during infection.

The work presented in this chapter may indicate an integral role for the FgGH81 during infection of wheat spikes. Data presented here indicates that the putative FgGH81 enzyme is expressed and has a role in virulence during infection of the susceptible wheat cultivar 'Apogee'. While this enzyme is predicted to degrade callose, its secretion and degradation of callose are yet to be confirmed. The following section outlines future experiments that will be conducted to confirm these and elucidate the role of FgGH81 during infection of wheat spikes.

5.5.1 Future experiments

To ensure that the *in planta* phenotype presented here in this chapter is due only to the KO of the FgGH81 gene, sequencing of the three transformants will be conducted. From these, one transformant will be selected for genetic complementation which will occur in the neutral locus of *F. graminearum* by Golden Gate assembly (Darino et al., 2024). Generation of the Δ GH81::GH81 complement strain will confirm a role for FgGH81 *in planta*.

To confirm that the putative FgGH81 enzyme degrades callose at plasmodesmata *in planta*, it is proposed to generate an overexpression (OE) strain of *Agrobacterium tumefaciens* to apply the transient protein expression system in *Nicotiana benthamiana*. By first eliciting the PTI pathway of plant immunity through application of the PAMP chitin, to induce callose deposition at

plasmodesmata, infusion of the FgGH81 OE *Agrobacterium* will be conducted. This assay will contain stains with and without the signal peptide, as well as a fluorophore-tagged FgGH81 protein to demonstrate localisation to PD. It is proposed that resulting callose deposits in controls and the OE line will be quantified through aniline blue staining for callose and subsequent image analysis (Sankoh et al., 2024). Further experiments could explore alterations to molecular flux, perhaps through transient expression of the fluorescent protein GFP, with and without the presence of the OE *Agrobacterium* strain to elude whether the movement of proteins, such as effectors, to adjacent cells is affected by the action of FgGH81.

5.6 References

Abramson J, Adler J, Dunger J. *et al.* (2024). Accurate structure prediction of biomolecular interactions with AlphaFold 3. *Nature*. doi: /10.1038/s41586-024-07487-w

Baladrón V, Ufano S, Dueñas E, Martín-Cuadrado AB, del Rey F, Vázquez de Aldana CR. (2002). *Eng1p*, an endo-1,3-beta-glucanase localized at the daughter side of the septum, is involved in cell separation in *Saccharomyces cerevisiae*. *Eukaryotic cell*. **1**(5): 774–786. doi: 10.1128/EC.1.5.774-786.2002

Basenko EY, Pulman JA, Shanmugasundram A, Harb OS, Crouch K, Starns D, Warrenfeltz S, Aurrecochea C, Stoeckert CJ Jr, Kissinger JC, Roos DS, Hertz-Fowler C (2018). FungiDB: An Integrated Bioinformatic Resource for Fungi and Oomycetes. *Journal of Fungi (Basel)*. **4**(1):39. doi: 10.3390/jof4010039.

Bowman SM, Free SJ. (2006). The structure and synthesis of the fungal cell wall. *Bioessays*. **28**(8): 799-808. doi: 10.1002/bies.20441.

Dilks T, Halsey K, De Vos RP, Hammond-Kosack KE, Brown NA (2019). Non-canonical fungal G-protein coupled receptors promote *Fusarium* head blight on wheat. *PLoS Pathogens*. **15**(4): e1007666. doi: 10.1371/journal.ppat.1007666.

Drula E, Garron ML, Dogan S, Lombard V, Henrissat B, Terrapon N (2022). The carbohydrate-active enzyme database: functions and literature. *Nucleic Acids Research*. **50**: D571–D577. doi: 10.1093/nar/gkab1045.

Esteban PF, Ríos I, García R, Dueñas E, Plá J, Sánchez M, Vázquez de Aldana CR, del Rey F. (2005). Characterization of the *CaENG1* Gene Encoding an Endo-1,3- β -Glucanase Involved in Cell Separation in *Candida albicans*. *Current Microbiology*. **51**: 385–392. doi: 10.1007/s00284-005-0066-2.

- Fesel PH, Zuccaro A. (2016). β -glucan: Crucial component of the fungal cell wall and elusive MAMP in plants. *Fungal Genetics and Biology*. **90**: 53-60. doi: 10.1016/j.fgb.2015.12.004.
- Gibson DG, Young L, Chuang RY, Venter JC, Hutchinson III CA, Smith HO (2009). Enzymatic assembly of DNA molecules up to several hundred kilobases. *Nature Methods*. **6**: 343-345. doi: 10.1038/nmeth.1318.
- Granato LM, Galdeano DM, D'Alessandre NDR, Breton MC, Machao MA. (2019). Callose synthase family genes plays an important role in the *Citrus* defense response to *Candidatus Liberibacter asiaticus*. *European Journal of Plant Pathology*. **155**: 25–38. doi: 10.1007/s10658-019-01747-6
- Han X, Hyun TK, Zhang M, Kumar R, Koh E, Kang B, Lucas WJ, Kim J. (2014). Auxin-Callose-Mediated Plasmodesmal Gating Is Essential for Tropic Auxin Gradient Formation and Signaling. *Developmental Cell*. **28**(2): 132-146. doi: 10.1016/j.devcel.2013.12.008
- Holdaway-Clarke TL, Walker NA, Hepler PK, Overall RL. (2000). Physiological elevations in cytoplasmic free calcium by cold or ion injection result in transient closure of higher plant plasmodesmata. *Planta*. **210**: 329-335. doi: 10.1007/PL00008141.
- Huerta-Cepas J, Szklarczyk D, Heller D, Hernández-Plaza A, Forslund SK, Cook H, Mende DR, Letunic I, Rattei T, Jensen LJ, von Mering C, Bork P. (2019). eggNOG 5.0: a hierarchical, functionally and phylogenetically annotated orthology resource based on 5090 organisms and 2502 viruses. *Nucleic Acids Research*, **47**(D1): D309–D314. doi: 10.1093/nar/gky1085
- King R, Urban M, Hammond-Kosack MC, Hassani-Pak K, Hammond-Kosack KE. (2015). The completed genome sequence of the pathogenic ascomycete fungus *Fusarium graminearum*. *BMC genomics*. **16**(1): 544. doi: 10.1186/s12864-015-1756-1.
- Klarzynski O, Plesse B, Joubert J, Yvin J, Kopp M, Kloareg B, Fritig B. (2000). Linear β -1,3 Glucans Are Elicitors of Defense Responses in Tobacco. *Plant Physiology*, **124**(3): 1027–1038, doi: 10.1104/pp.124.3.1027
- Kroll EK, Bayon C, Rudd J, Armer V, Magaji- Umashankar A, Ames R, Urban M, Brown NA, Hammond-Kosack KE. (2024). A conserved fungal Knr4/Smi1 protein is vital for maintaining cell wall integrity and host plant pathogenesis. *bioRxiv*, 2024.05.31.596832; doi: 10.1101/2024.05.31.596832.
- Letunic I, Bork P. (2024). Interactive Tree of Life (iTOL) v6: recent updates to the phylogenetic tree display and annotation tool. *Nucleic Acids Research*. **52**(W1): W78–W82, doi: 10.1093/nar/gkae268.
- Michielse CB, Rep M. (2009). Pathogen profile update: *Fusarium oxysporum*. *Molecular Plant Pathology*. **10**: 311–324. doi: 10.1111/j.1364-3703.2009.00538.x.
- Rafiei V, Véléz H, Tzelepis G. (2021). The Role of Glycoside Hydrolases in Phytopathogenic Fungi and Oomycetes Virulence. *International Journal of Molecular Sciences*. **22**(17): 9359. doi: 10.3390/ijms22179359.

- Sankoh AF, Adjei J, Roberts DM, Burch-Smith TM. (2024). Comparing Methods for Detection and Quantification of Plasmodesmal Callose in *Nicotiana benthamiana* Leaves During Defense Responses. *Molecular Plant Microbe Interactions*. **37**(5): 427-431. doi: 10.1094/MPMI-09-23-0152-SC.
- Scheider R, Hanak T, Persson S, Voigt CA. (2016). Cellulose and callose synthesis and organization in focus, what's new? *Current Opinion in Plant Biology*. **34**: 9-16. doi: 10.1016/j.pbi.2016.07.007.
- Teufel F, Almagro Armenteros JJ, Johansen AR, Halldór Gíslason M, Pihl SI, Tsirigos KD, Winther O, Brunak S, von Heijne G, Nielsen H (2022). SignalP 6.0 predicts all five types of signal peptides using protein language models. *Nature Biotechnology* 40, 1023–1025. doi: 10.1038/s41587-021-01156-3.
- Underwood W. (2012). The plant cell wall: a dynamic barrier against pathogen invasion. *Frontiers in Plant Science*. **3**:85. doi: 10.3389/fpls.2012.00085.
- Wang B, Andargie M, Fang R. (2022). The function and biosynthesis of callose in high plants. *Heliyon*. **8**(4):e09248. doi: 10.1016/j.heliyon.2022.e09248.
- Wanke A, van Boerdonk S, Mahdi LK, Wawra S, Neidert M, Chandrasekar B, Saake P, Saur IML, Derbyshire P, Holton N, Menke FLH, Brands M, Pauly M, Acosta IF, Zipfel C, Zuccaro A. (2023). A GH81-type β -glucan-binding protein enhances colonization by mutualistic fungi in barley. *Current Biology*. **33**(23): 5071-5084.e7. doi: 10.1016/j.cub.2023.10.048.
- Zhou P, Chen Z, Yan Q, Yang S, Hilgenfeld R, Jiang Z. (2013). The structure of a glycoside hydrolase family 81 endo- β -1,3-glucanase. *Acta Crystallographica*. D69: 2027-2038. doi: 10.1107/S090744491301799X.

Chapter 6: The role of plant cell wall composition and fungal resistance

6.1 Acknowledgement of contributions

Part of the *Arabidopsis thaliana* detached leaf assay experiments were funded by the British Society of Plant Pathology (BSPP) summer vacation bursary and conducted by University of Bath undergraduate student Max Fontaine. I would like to thank him personally for his hard work, patience and diligent lab work in the summer of 2022. In addition, I would like to thank Dr Paul Ebersbach, University of Exeter, for conducting the BCARS-Raman analysis shown in this chapter.

I would also like to thank the efforts of Prof Jurriaan Ton (University of Sheffield), Dr Dominique Arnaud and Prof Nicholas Smirnov (Central European Institute of Technology and University of Exeter), and Prof. Ohkmae K. Park (Korea University) for providing the seed of various *At* mutants for use in this chapter.

I also thank the Salk Institute Genomic Analysis Laboratory for providing the sequence-indexed *Arabidopsis* T-DNA insertion mutants and the Nottingham *Arabidopsis* Stock Centre (NASC) for distributing the material. In the interest of FAIR science, a protocol for the *Arabidopsis thaliana* detached leaf assay was published on protocols.io (Armer, Deeks and Hammond-Kosack, 2024) due to alterations to previously published protocols and is included in thesis Appendix 3.

6.2 Introduction

The plant cell wall provides a relatively durable, physical barrier to invading plant pathogens (Underwood, 2012). Split into the primary and secondary cell wall, it is largely composed of polysaccharides cellulose, hemicellulose, pectin and callose (Fig. 6.2.1). The secondary cell wall, closer to the plasma membrane of the plant cell, also contains lignin, a phenolic biopolymer made up of the monolignol subunits paracoumaryl alcohol (H), coniferyl alcohol (G), and sinapyl alcohol (S). Lignin adds strength and, due to its hydrophobic properties, waterproofs tissues, as such lining of the xylem vessels for water transport.

Between cell walls of adjacent cells, a structure known as the middle lamella resides. The middle lamella glues the cells together and is primarily composed of calcium-rich pectates, which is further broken down into ‘hairy’ and ‘smooth’ with biases for rhamnogalacturonan (with side branches) and homogalacturonan (linear polymers), respectively (Reignault, Valette-Collet and Boccara, 2007).

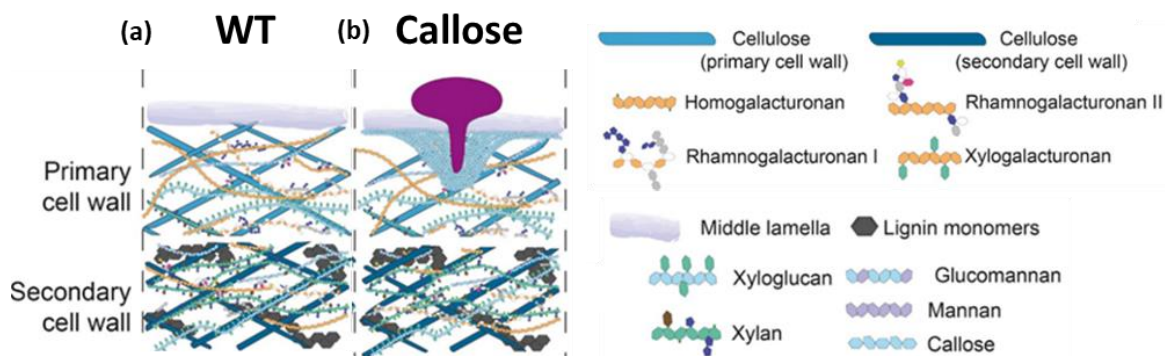


Fig. 6.2.1. Example diagram of the plant cell wall matrix. (a) Wild type cell wall structure and (b) Callose localisation around penetration peg from phytopathogen. Although this varies between tissue types, the plant cell wall is composed of the primary and secondary cell walls, with a structure known as the middle lamella, composed largely of pectates, between adjacent cells in plant tissues. The primary cell wall is largely composed of polysaccharides of cellulose, various hemicelluloses, and pectin, with the strengthening addition of lignin in the secondary cell wall closest to the plant plasma membrane. Adapted from Bacete et al. (2017).

During the early stages of plant-pathogen interactions, the invading pathogen must break into the tissue through a cell wall in most instances. Thus, the cell wall provides the first barrier of defence. Pathogens secrete hydrolysing enzymes to disassemble carbohydrate polymers in the cell wall matrix (see also [chapter 5](#)) and it is emerging that plants sense the reduction in cell wall integrity (CWI) during this stage (Narváez-Barragán et al., 2022). *F. graminearum* has many genes encoding these hydrolytic enzymes in its genome (Table 6.2.1; Kubicek, Starr and Glass (2014)) which disassemble the cell wall matrix. Pathogens often need to break through efficiently, thus reducing damage and producing DAMPs, to minimise recognition by the PTI branch of the plant immune system ([section 1.3](#)).

Table 6.2.1 Plant cell wall (CW) components, relative enzyme classes for degradation and number of CWDEs present in *F. graminearum* (*Fg*) genome. Data from Kubicek, Starr and Glass (2014).

CW component	Enzyme classes	Number in <i>Fg</i> (PH-1)
--------------	----------------	----------------------------

Cellulose	Cellulases, β -Glycosidases and accessory enzymes GH61 and carbohydrate binding module (CBM)	83
Hemicelluloses	Xylanases, xyloglucanases, α -Galactosidases, β -Mannanase, α -Arabinosidases, β -Galactosidases and β -Glucuronidases	46
Pectin	Polygalacturonases and Polygalacturonate lyases	33

The CWI maintenance system in plant cell walls monitors the matrix and responds to perturbations as a result of abiotic wounding or biotic attack. Sensing this occurs through a set of plasma membrane receptors that work with PRRs to detect cell wall components that have been damaged which act as DAMPs (Narváez-Barragán et al., 2022; [section 1.3](#)). Rapid alkalisation Factors (RALFs), which largely reside extracellularly, are also implicated in these responses by binding to pectin in the cell wall and environmental stimuli trigger the decoupling of RALF from pectin. Further, they recruit the known receptor-like kinase Feronia (FER) and its co-receptor LLG1 to initiate cell surface responses (Liu et al., 2023). The Feronia signaling network also contain MLO proteins, the widely characterised gene family that have recently been identified as Ca^{2+} channels and act downstream of the RALF signaling pathway (Gao et al., 2023). Pectin is heavily methylated when secreted to the cell wall and has been shown to be demethylated during infection with *F. oxysporum* and is sensed by a plasma-membrane localised receptor known as RESISTANT TO FUSARIUM OXYSPORUM 1 (RFO1), leads to upregulation of WAK signaling and downstream defence responses (Huerta et al., 2023).

In response to damage, the plant reinforces the cell wall by altering cell wall composition or increasing cell wall thickness (Narváez-Barragán et al., 2022). However, this reinforcement fitness cost must be balanced with efforts towards growth and reproduction. To prevent cell wall damage, plants also inhibit the action of CWDEs through the secretion of proteins into the extracellular matrix that bind to microbial enzymes (Juge, 2006). Cell wall alterations during plant-pathogen interactions have been widely reported in the literature. In *Arabidopsis* leaves in response to the PTI inducing avirulent strains of the bacterial pathogen *Pseudomonas syringae*, a lignin barrier forms as demonstrated by phloroglucinol

staining, but this effect was actually increased in virulent strains activating the ETI branch of plant immunity (Lee et al., 2019), demonstrating the increased response of ETI as proposed in the zig-zag model by Jones and Dangl (2006). This has recently been proposed by Yuan et al. (2021) whereby 'potentiation' of PTI is essential for ETI responses. The accumulation of lignin in leaves in *the At-Pseudomonas syringae* interaction is driven by a group of proteins called casparian strip membrane domain protein (CASP)-like proteins (CASPLs), to prevent wider spread of the invading bacterial pathogen. Disruption of two CASPLs, by T-DNA insertion and microRNA silencing respectively in the *CASPL4D1/amiCASPL1D1* double mutant, attenuated the ability for the plant to deposit a lignin barrier in *Arabidopsis* leaves (Lee et al., 2019). Disruptions to parts of the lignin biosynthesis pathway (Fig. 6.2.2) have been shown to increase resistance to some fungal pathogens. In rapeseed (*Brassica napus*), knock out of the ferulate-5-hydroxylase (F5H) gene, which converts G monolignols to S, decreases the ratio of S to G lignin, and increases resistance to the stem rot causing fungus *Sclerotinia sclerotiorum* (Cao et al., 2022). Impairment of other enzymes in the lignin biosynthesis pathway including caffeic acid O-methyltransferase (CAOMT) and cinnamyl alcohol dehydrogenase (CAD) in the crop Sorghum (*Sorghum bicolor*) leads to reduces *Fusarium* spp. colonisation (Funnell-Harris, Pedersen and Sattler, 2010). While disruptions to CAD genes generally interrupt the formation of lignin from respective monolignol subunits, CAOMT specifically interrupts the methylation of the 5-hydroxyl group of 5-hydroxyconiferylaldehyde substrates that form S subunits of lignin (Humphreys and Chapple, 2002).

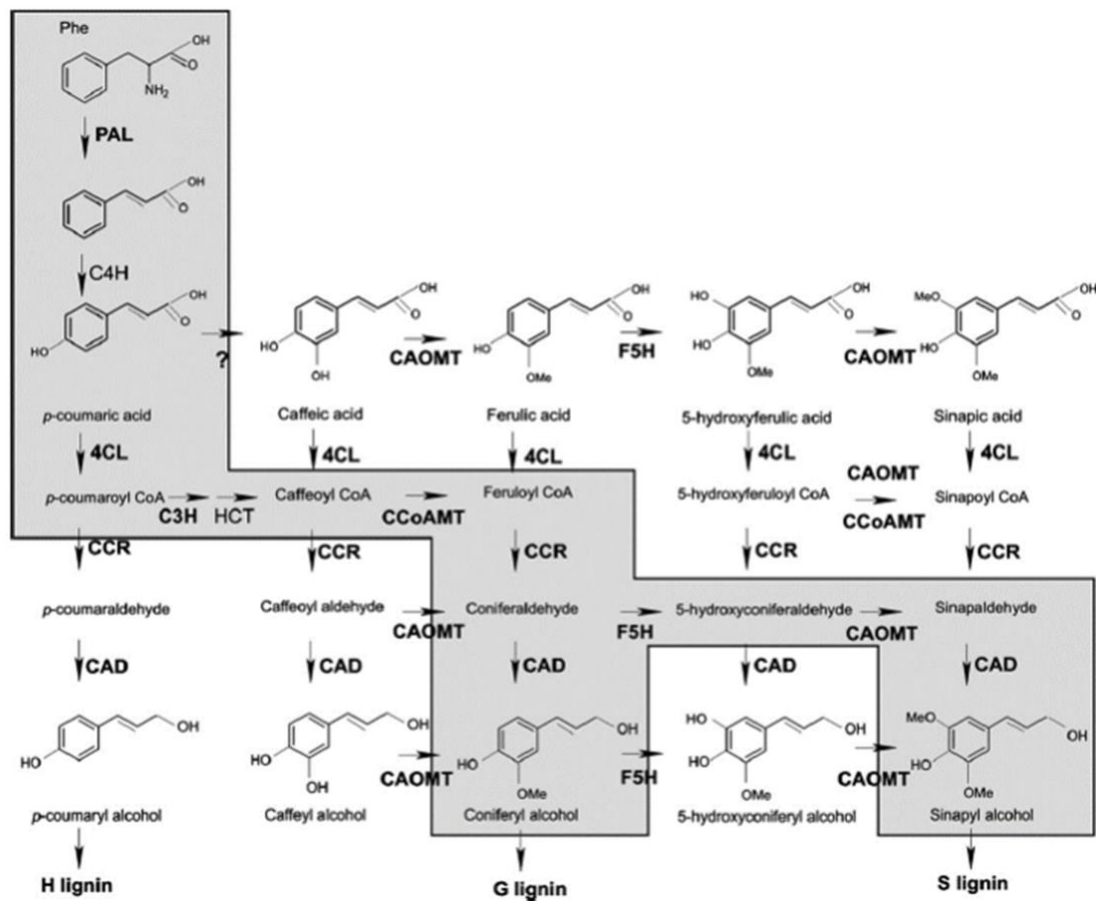


Fig. 6.2.2. Lignin biosynthesis pathway. Key pathway involved in lignin-based defence is highlighted in grey, and the noted enzymes are caffeoyl-CoA 3-O-methyltransferase (CCoAMT), cinnamyl alcohol dehydrogenase (CAD) and caffeic acid O-methyltransferase (CAOMT). Other enzymes are as follows: Phenylalanine ammonia lyase (PAL), cinnamate 4-hydroxylase (C4H), 4-coumarate (4CL), cinnamoyl-CoA-reductase (CCR), coumarate 3-hydroxylase (C3H) ferulate 5-hydroxylase (F5H). From Bhuiyan et al. (2009).

In diploid wheat (*Triticum monococcum*), appositions by the obligate biotrophic pathogen powdery mildew (*Blumeria graminis* f. sp. *tritici*; *Bgt*) are countered by cell wall lignification, and expression transcripts of key enzymes (PAL, CAOMT, FAH, CCoAMT and CAD) accumulate in the epidermis. When these are transiently silenced through RNAi, incidences of *Bgt* penetration into the leaf surface increase (Bhuiyan et al., 2009). A pattern emerges where resistance to fungal pathogens is increased when G subunits of lignin are more abundant than S subunits (Fig. 6.2.2). Stronger and stiffer cell walls have a greater ratio of S monolignols to G in the cell wall (Yoon, Choi and An, 2015). These innate differences may lead to misleading results in translational research between *At* and wheat but can still indicate a role for lignin in infection. It was also decided to include two apoplastic peroxidases, *prx33-3* and *prx34-2*, in the *Arabidopsis*

screen due to previous reports that these remove H₂O₂ which are used to oxidise G and S monolignols for the generation of lignin (Demont-Caulet et al., 2010).

Disruption of other cell wall components can lead to increased resistance, such as cellulose synthases (CESA), three subunits of which are required for cellulose synthesis in *At* in the secondary cell wall, CESA4/IRX5, CESA7/IRX3 and CESA8/IRX1, named for IRREGULAR XYLEM phenotype, lead to increased resistance to the necrotrophic fungus *Plectosphaerella cucumerina* (Hernández-Blanco et al., 2007). However, mutations in the CESA subunits in the primary cell wall had no altered disease phenotype (Hernández-Blanco et al., 2007). Disrupting cellulose microfibrils in the cell wall may impact the overall integrity and disrupting the secondary cell wall, where lignin is present, could disrupt structural integrity of the entire cell.

For pectin, loss of function mutants in glucuronate 4-epimerase (GAE) genes, which produce the subunits of pectin, UDP-d-galacturonic acid, are brittle and had increased susceptibility to some *Botrytis cinerea* isolates when both *gae1* and *gae6* are knocked out (Bethke et al., 2016). The authors of this study also report how the bacterial pathogen *Pseudomonas syringae* pv. *maculicola* represses the expression of GAE1 and GAE6 in WT Col-0 plants.

Arabidopsis thaliana has previously been shown to be susceptible to *F. graminearum* infection in the floral (Urban et al., 2002) and leaf tissues (Chen et al., 2006). As a plant model organism with a small genome, *Arabidopsis* is ideal for dissecting gene/protein function(s) and thus cell wall components that may be implicated in disease resistance and/or susceptibility in the native pathosystem. This can be particularly useful when generating reverse genetic mutants in the native host, such as wheat, because of the high demand on time and resources. The *A. thaliana* genomic resource of the SALK lines have been widely used to investigate cell wall components that are implicated in plant pathogen interactions (O'Malley, Barragan and Ecker, 2015), some of which have been discussed and used in this chapter. A table summarising the *Arabidopsis* mutants used for the initial detached leaf assay screen is provided in Table 6.4.1.

The first aim of this chapter is to harness the genetic resources available from the SALK collection of T-DNA insertion mutants in cell wall synthesis genes to explore responses to leaf infection by *F. graminearum*. By utilising T-DNA insertion

mutants, we may be able to ascertain which cell wall components are more important for defence against *F. graminearum*. Results of the initial screen guided a more detailed analysis of specific cell wall mutants in the lignin biosynthesis pathway and initiated an exploration of lignification through rachis development in the native host. The second aim of this chapter is to answer the research question ‘Why does *F. graminearum* have such a limited infection window around anthesis?’ This is done by exploring the extent of lignification in the wheat rachis from anthesis through grain filling stages of wheat development.

6.3 Materials and methods

The methods outlined here are in addition to those detailed in the [general materials and methods chapter](#).

6.3.1 Curation of cell wall mutants

In order to identify potential cell wall composition mutants that may be implicated in resistance and/or susceptibility to *F. graminearum* infection in the native wheat pathosystem, a search of the literature was conducted. Often in the plant model organism *Arabidopsis thaliana*, wheat gene orthologues were identified using the Ensembl Compara tool (ensembl.org) and expression levels during PAMP-triggered immunity and/or *Fusarium graminearum* infection checked on the wheat expression browser (wheatexpression.org). A table of wheat gene orthologues of lignin cell wall components as a secondary focussed literature search is available in [Appendix 6.7.1](#).

6.3.2 SALK line T-DNA insertion model and genotyping

DNA extraction of *A. thaliana* T-DNA insertion lines for homozygous verification of gene disruption followed the CTAB method, as outlined in chapter 2, section [2.3.1](#). Genotyping of *At* lines was conducted by PCR. Each PCR included 3 primers: LB = left border of the T-DNA insertion, LP = Left border of gene of interest, RP = right border of gene of interest (Fig. 6.3.1 (a)). A WT band is 900bps, with the insertion band at 410+ N (0-300bps). For genotyping purposes, a sample that yields two bands on the gel electrophoresis is deemed heterozygous for the T-DNA insertion and is discarded from further analysis, as

are plants that yield a WT band (Fig. 6.3.1 (b)). NASC-acquired SALK lines are segregating T3 lines.

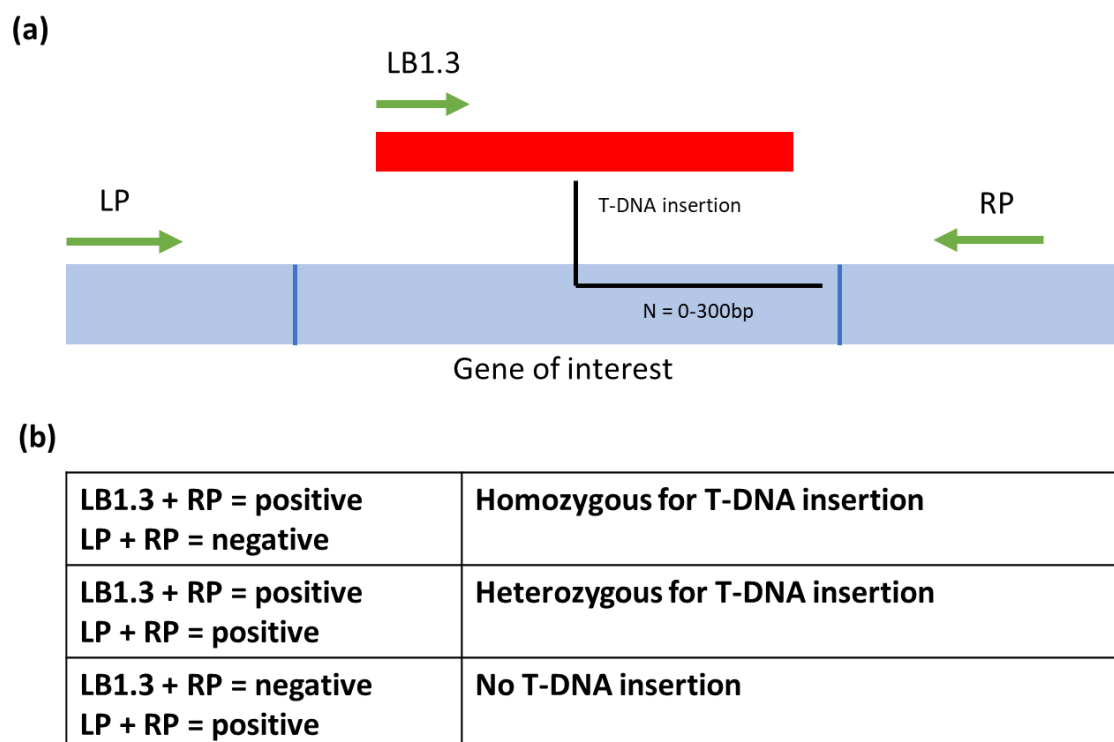


Fig. 6.3.1 Schematic representation of SALK line verification for T-DNA insertion. (a) LP and RP are specific to the gene of interest being studied, with LB1.3 specific to the 5' end of the T-DNA insertion. (b) Three primers, as outlined in Table 6.3.1, are used to genotype the T-DNA *A. thaliana* lines, determining if they are homozygous, heterozygous or lack the presence of the T-DNA insertion in the gene of interest.

Primers were designed in the freely available T-DNA Primer Design Tool software (<http://signal.salk.edu/tdnaprimers.2.html>) and ordered as lyophilised salt-free oligos from Eurofins Genomics (Germany). Primers used for genotyping SALK lines are present in Table 6.3.1. Non-SALK line mutants *prx33* and *prx34* were also included in the analysis and verified by donor.

Table 6.3.1. Primers used for genotyping *A. thaliana* SALK lines.

Mutant	Left Primer	Right Primer
<i>min7</i>	TTCTTCTCTGCTGTCAGGCTC	TTGACCAACGAATTTTTCACC
<i>omt1</i>	TTGAAACTAGCTTGGTCGGTG	AATTCTTGATGGTGGGATTCC
<i>cad4</i>	GGAAAACCTACTCAAGGTGGC	CAGTTTCAATTGGTGTGAGCC
<i>cad5</i>	GGAAAACCTACTCAAGGTGGC	ACTTAGCCCAAAGTTGGTTGG
<i>cad4cad5</i>	GGAATAATGGAGGCAGAGAGG	CCTCTTAGGCCTGGTTGTTTC
<i>caspl4a3</i>	GACGATACGAAGCAAAAGCAC	CACCTTCGACCTCTGTTTGAG

<i>caspl4d1</i>	ATCGTGAAGGACTCAAAAGCC	ATGAAGATACATGCTGTCCGC
<i>gae1</i>	ATCACGTGAGTGAAAGCAACC	AATTAGTTGCAAGTTGGTCCG
<i>gae6</i>	CATAGGCCTAATTTGGGGATC	TTGGTCTGTTCCGGTGTTC
<i>irx9</i>	GCTGGTAAGGCCTCATTTTTTC	AACTTACCAACCCACCCATTC
<i>irx10-1</i>	ACCATGTCTGTTTGGACGAAG	AAAATCCACTCGGAGGACTTG
<i>irx14-1</i>	AACGACACGTGTACCTCCTTG	AACATCACAATCCCATCAAGC
<i>irx14-2</i>	TTCCATCGACAAAACCATCTC	AATCGCCGGAGTAATAGCTTC
<i>irx14-3</i>	TCCCCGAAAAACCCTGTATAC	TTGGGATATTGGCTCATTAG
LB1.3	ATTTTGCCGATTTGGAAC	-

6.3.3 *Arabidopsis thaliana* detached leaf assay

The protocol utilised for the *Arabidopsis thaliana* (*At*) SALK line detached leaf assay has been published on protocols.io (Armer et al., 2024a). Briefly, *At* seed were germinated on ½ MS agar, incubated at 4°C for 2 days and grown in conditions outlined in section [2.4.3](#). At fluorescence emergence, at approximately 4 weeks, one mature rosette leaf from each plant was excised and the petiole placed at 90° into 1% water agar square plates amended with Tergitol (Sigma Aldrich) to prevent *F. graminearum* hyphae extending into the agar. Two wounds were scored into the upper epidermis of the detached *At* leaf using a sterile 20µl pipette tips and 5µl of each treatment (water control, WT *F. graminearum*, WT amended with 20µM DON, and 20µM DON alone). Spore suspensions of WT *F. graminearum* were prepared to 5x10⁵ spores/ml.

6.3.4 *Arabidopsis thaliana* leaf disease assessment

To ascertain the relative susceptibility or resistance of the *Arabidopsis thaliana* SALK lines were put through a large screen for relative resistance and/or susceptibility to *F. graminearum* infection in detached leaves. This work was conducted by BSPP-funded student Max Fontaine. After a large screen of 15 cell wall *At* mutants, the cell wall component lignin was identified as contributing to susceptibility when genes of the lignin biosynthesis pathway were perturbed. Namely, these are *cad4*, *cad5*, the *cad4cad5* double mutant and *omt1*. The apoplastic peroxidases *prx33* and *prx34* were also carried through to a second, detailed screen for disease assessment.

6.3.5 Morphological assessment of wheat tissues throughout growth

To assess why *F. graminearum* infection is restricted to the period around anthesis, a study of morphological changes in the wheat rachis was conducted, as well as an analysis of lignification in wheat tissues throughout growth. The dwarf wheat cultivar Apogee was grown as outlined in section [2.4.2](#) and, for the assessment of disease progression 2 weeks after anthesis, were inoculated as outlined in section [2.4.5](#) with the WT *F. graminearum* strain PH-1. Tissues were fixed in LR white resin, following the methods outlined in [2.5.2](#) and sectioned as in [2.5.3](#). Micron-thick (1µm) resin sections were then stained either with the polychromatic dye Toluidine blue (0.1% w/v in PBS) or the lignin stain potassium permanganate (1% w/v in PBS).

For sequential rachis sections throughout the structure, sections were taken every 20µm.

6.3.6 Lignin staining and quantification in wheat tissue sections

LR White resins prepared as detailed in chapter 2 (sections [2.5.2](#) and [2.5.3](#)). 1µm sections were taken every 10 microns throughout the rachis from the outer edge to the centre (approximately 50 sections per sample). Sections were stained for 10 mins with 1% (w/v) potassium permanganate (Sigma Aldrich, UK) as described in Chancellor et al. (2024).

Relative lignification in wheat tissues throughout growth was determined through image analysis of potassium permanganate-stained sections. Entire sections imaged were parsed using the threshold colour function in Fiji (ImageJ) in the HSB colour space to remove the background. Using the selected area, the area of cell wall was recorded using the measure function. Subsequently, a second measurement of the image was taken to determine the proportion of darker stained cell walls, indicating a greater lignin presence, using the thresholding parameters of: Hue 0-255, Saturation 0-255, Brightness 0-120 (Fig. 6.3.2). The percentage of the total area stained dark was calculated. For each evaluated tissue, the average of three technical replicates (sections) from each of 3 biological samples was calculated to account for minor variations in potassium permanganate staining.

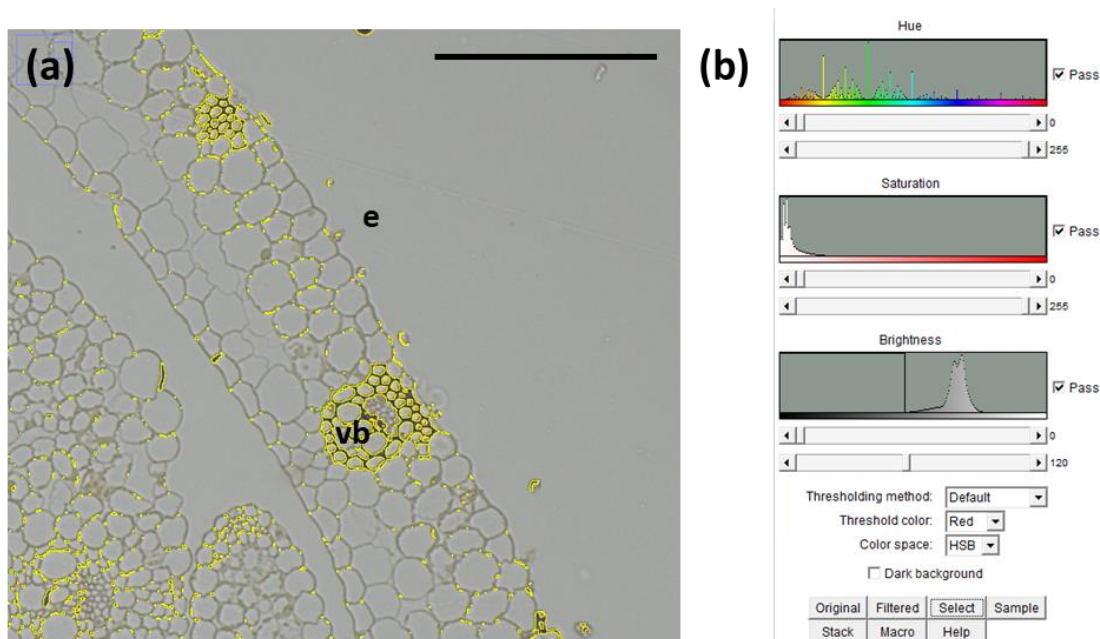


Fig. 6.3.2. Demonstration of image analysis for relative lignification in wheat tissues stained with potassium permanganate. (a) Example of Apogee wheat stem section at 2 weeks, with highly lignified areas highlighted in yellow around vascular bundles. Scale bar = 200µm. (b) Colour thresholding tool adjustments in ImageJ for dark-staining selection in image. vb = vascular bundle; e = epidermis.

6.3.7 RAMAN spectroscopy of rachis cell wall matrix

In order to view the cell wall matrix of the wheat rachis tissue, Raman microscopy was employed. Raman microscopy has the advantage of detecting biomolecules based on spectral data without destroying the sample. Broadband coherent anti-Stokes Raman scattering (BCARS) is able to enhance signals from weaker Raman spectral bands. In conjunction with linear unmixing, different cell wall components are able to be deciphered *in situ*.

For sample preparation, fresh wheat rachis tissues at anthesis from the 7th true spikelet from the base of the spike, were excised using a sterile razor blade. To preserve the sample and prevent degradation, the rachis samples were fixed in paraformaldehyde- glutaraldehyde fixative as outlined in section 5.5.2. Once in 0.05M Sorensen's phosphate buffer, samples are stored at 4°C prior to sectioning.

The rachis samples were then fixed in frozen TissueTek (Sakura, Alphen aan den Rijn) at -20°C to hold samples in place and sectioned at 60µm on a cryo-microtome (CM1850 Cryostat, Leica Microsystems). Samples were placed on

standard microscopy slides and stored at 4°C for up to several weeks before imaging.

Broadband Coherent anti-Stokes Scattering (BCARS) microscopy was conducted on the rachis samples using an inverted microscope (Olympus, IX7) with two seeded co-fibre lasers generating the pump (770 nm; ~16 mW, 3.4 ps) and broadband stokes beams (~900 – 1350 nm; ~9.5 mW, ~16 fs) that are focussed onto the sample under water-immersion objective with temporary laser superimposition through application of a delay line (ThorLabs, MCM 3000). By shifting the delay between laser pulses, various Raman shifts can be optimised for the sample to achieve the brightest image for further analysis. BCARS is a nonlinear optical imaging method that enables full Raman spectral fingerprint hyperspectral imaging similar to spontaneous Raman imaging (linear optical method) but much faster. A schematic diagram of the BCARS set up is shown in Fig. 6.3.3.

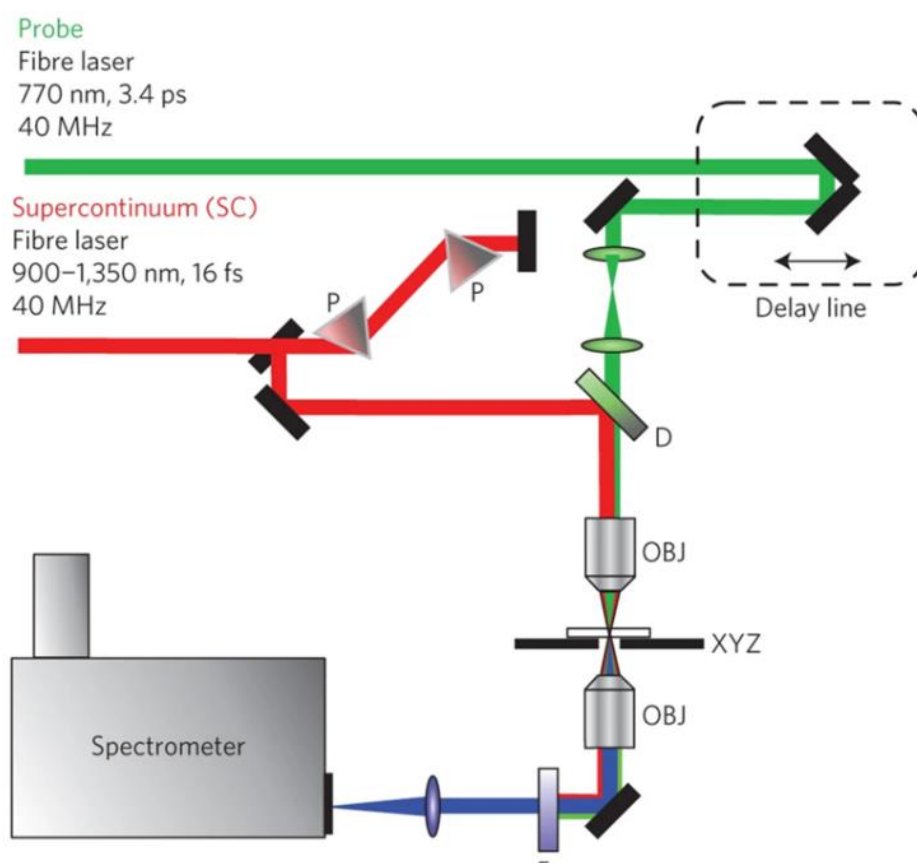


Fig. 6.3.3. Schematic diagram of BCARS imaging system. Set up produces high resolution spectra across entire biologically relevant Raman window ($\sim 500\text{--}3,500\text{ cm}^{-1}$). P = prism; D = dichroic mirror; OBJ = objective lens; XYZ = sample stage; F = filters. Image from Camp Jr. et al. (2014).

6.4 Results

6.4.1 Identification of wheat cell wall components postulated for susceptibility and/or resistance to *F. graminearum* infection

As a result of a literature search for cell wall components that have been implicated in the susceptibility and/or resistance to various fungal pathogens, wheat homologues were identified using the Ensembl Compara function and expression patterns during *F. graminearum* infection verified through the wheat expression browser. Wheat homologues of lignin genes were analysed in further depth in the literature with respect to pathogen resistance (Appendix 6.7.1). This check verified some involvement of the genes of interest pulled from the literature search in the native wheat-*F. graminearum* pathosystem, but also the involvement of some other pathogens.

6.4.2 Identification of *Arabidopsis* orthologues and SALK lines

After identification of genes putatively implicated in cell wall rearrangements during infection in wheat were identified, *At* orthologues were identified and/or curated from original literature search, with many of the plant-pathogen studies being conducted in the *At* model plant system. A list of the *At* genotypes used, their relative cell wall component, reason for inclusion and source are detailed in Table 6.4.1.

Table 6.4.1. *Arabidopsis thaliana* genotypes used in the initial detached leaf assay study. Relevant cell wall component and reason for inclusion detailed and seed source.

<i>A. thaliana</i> genotype	Cell wall component	Reason for inclusion – literature	Seed source
Col-0 (WT)	-	Parental background control	-
<i>min7-1</i> HopM1 interactor 7	-	Vesicular trafficking component. Knock out (KO) shows severe susceptibility to <i>F. graminearum</i> infection (Machado Wood et al., 2021).	NASC
<i>prx33-3</i>	-	Apoplastic peroxidases that take up H ₂ O ₂ to then oxidase G and S monolignols to catalyse lignin polymerisation (Demont-Caulet et al., 2010).	Exeter
<i>prx34-2</i>			

<i>pmr5</i> POWDERY MILDEW RESISTANT 5	Pectin	Mutations in the gene, which encodes a pectin acetyltransferase, leads to increased resistance to powdery mildew (Chiniquy et al., 2019).	NASC
<i>gae1-1</i> UDP-D-glucuronate 4-epimerase	Pectin	Increases susceptibility to <i>B. cinerea</i> and expression is repressed by <i>Pseudomonas</i> spp. Bethke et al. (2016).	NASC
<i>gae1-1gae6-1</i> as above	Pectin		NASC
<i>cad5</i> CINNAMYL ALCOHOL DEHYDROGENASE	Lignin	KO leads to increased susceptibility in <i>At</i> to virulent and avirulent strains of <i>Pseudomonas syringae</i> (Tronchet et al., 2010).	NASC
<i>cad4cad5</i> as above	Lignin		NASC
<i>omt1</i>	Lignin	Silencing in wheat leads to increased susceptibility to powdery mildew in wheat. (Bhuiyan et al., 2009).	NASC
<i>caspl4a3</i> CASPARIAN STRIP MEMBRANE DOMAIN (CASP)-LIKE	Lignin	Loss of function mutants lead to increased susceptibility to <i>Pseudomonas syringae</i> (Lee et al., 2019).	NASC
<i>caspl4d1</i> as above	Lignin		Korea
<i>amiCASPL1D1</i> as above	Lignin		Korea
<i>amiCASPL1D1 caspl4d1</i> as above	Lignin		Korea
<i>irx9</i> IRREGULAR XYLEM	Hemicellulose	Silencing of xylanases in <i>Botrytis cinerea</i> (Noda, Brito and González, 2010) and <i>Magnaporthe oryzae</i> (Nguyen et al., 2011) both lead to reduced virulence, indicating role in resistance.	NASC
<i>irx10</i> as above	Hemicellulose		NASC
<i>irx14-1,14-2,14-3</i> as above	Hemicellulose		NASC

6.4.3 *Arabidopsis thaliana* detached leaf assay

To determine if *At* cell wall mutants had differing disease phenotypes in response to *F. graminearum* infection, a detached leaf assay was conducted. This was a high-throughput and repeatable experiment to screen through a large number of cell wall mutants. The SALK line background ecotype Col-0 was used as the control and *min7*, which encodes an ADP-ribosylation factor guanine nucleotide exchange factor (ARF-GEF) family protein targeted by HopM1 involved in vesicular trafficking control, was used as the susceptible control (Machado Wood et al., 2021).

After a pilot detached leaf assay, it was determined that mutants in lignin signaling and/or synthesis pathways had increased susceptibility to *F. graminearum* infection in detached leaf assays. The cell wall mutants of *omt1*, *cad4*, *cad5*, *cad4cad5* and the apoplastic peroxidases *prx33* and *prx34* were taken forward for more detailed detached leaf assay analysis and are all involved in the lignin biosynthesis pathway or lignin polymerisation. Interestingly, the lignin responsive genes of the CASPL family did not have attenuated susceptibility to *F. graminearum* infection, nor did the pectin or hemicellulose *At* mutants. Some of the *At* cell wall mutants had altered phenotypes during growth, particularly the *pmr4* and *pmr5* pectin mutants which had small rosettes with rounded leaves (Fig. 6.4.1).



Fig 6.4.1. Exemplary rosettes for *Arabidopsis thaliana* mutants at 4 weeks old. Left to right, top to bottom: Col-0 = Columbia (WT); *cad4* = Cinnamyl Alcohol Dehydrogenase 4; *cad4cad5* = Cinnamyl Alcohol Dehydrogenase 4 and Cinnamyl Alcohol Dehydrogenase 5 double mutant; *prx33* = peroxidase 33; *min7* = HopM1 Interactor 7 (susceptible control); *cad5* = Cinnamyl Alcohol Dehydrogenase 5; *omt1* = caffeic acid O-methyltransferase 1; *prx34* = peroxidase 34; *caspl4a3* = Casparian strip membrane domain protein (CASP)-like protein (CASPLs) 4 a3; *caspl4d1* = CASPL 4d1; *amiCaspl1d1* = microRNA disrupted CASPL1d1; *amiCaspl1d1caspl4d1* = CASPL double mutant; *pmr4* = powdery mildew resistant 4; *pmr5* = powdery mildew resistant 5; *gae1* = UDP-D-glucuronate 4-epimerase 1; *gae1gae6* = *gae1* and *gae6* double mutant. Scale bar = 2cm.

In the detached leaf assay, no cell wall mutant was a susceptible to *F. graminearum* infection as the *min7* positive control (Fig. 6.4.2). Example images of detached leaves at 5dpi are shown in Fig. 6.4.2, but it is worth noting that large variations in diseased area were observed across replicates. For infection to take hold, inoculum was supplemented with DON and reduced variability in the detached leaf infection severity (Fig. 6.4.3). Typically, *At* leaves responded to *F.*

graminearum infection with localised necrosis to the wound site, and in *cad4*, *cad5* and the susceptible control *min7*, widespread necrosis was evident (Fig. 6.4.2). Interestingly, the *cad4cad5* double mutant did not match the increased susceptibility observed in the single mutants.

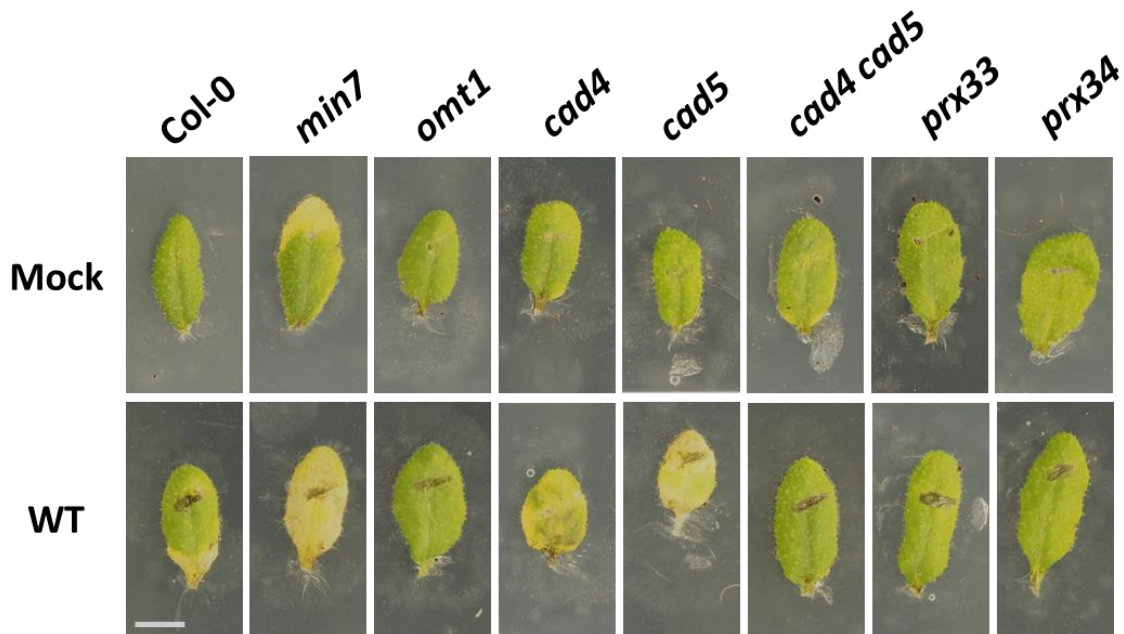


Fig. 6.4.2. Example images of *Arabidopsis thaliana* detached leaf assay mutants. Mock inoculated with dH₂O (top) and inoculated with WT *F. graminearum* (PH-1) at 5x10⁵ spores/ml, supplemented with 20µm DON. Scale bar = 20mm.

6.4.5 Exploration of wheat stem and floral tissue morphology

As *F. graminearum* is a pathogen, almost exclusively, of the wheat floral tissues around the period of anthesis, an exploration of the morphological changes that may pertain this was executed. No literature has so far been published on the internal morphology of the wheat rachis tissue throughout growth, despite this having implications in FHB development. This exploration focussed on lignification, as this cell wall component has been both implicated in disease resistance within the literature and also within the *Arabidopsis* detached leaf assay. Tissues were selected from wheat plants throughout growth for analysis of lignin content and floral tissue morphology. Example images of plants at each week in growth are shown in Fig. 6.4.3, with relevant Feekes growth stages in Fig. 6.4.3(a). Anthesis occurs at 6 weeks, where *F. graminearum* typically infects.

(a)

Week	Apogee	Feekes growth stages
1		1
2		2
3		3-4
4		5
5		8-9
6		10.1
7		10.5
8		11
9		11
10		11
11		11 (Harvest)

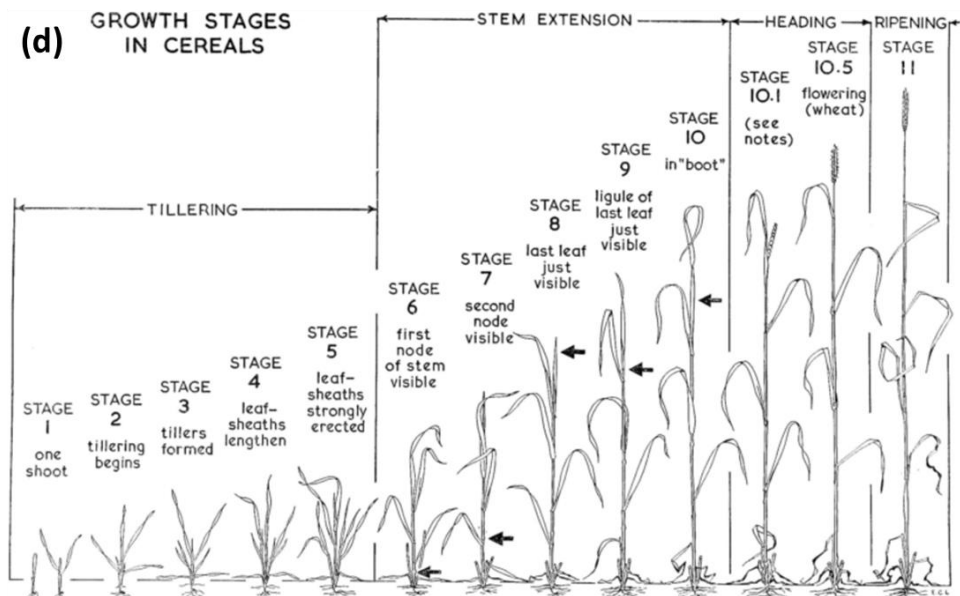


Fig. 6.4.3. Apogee wheat growth. (a) Weeks of growth of the dwarf wheat cultivar Apogee in controlled conditions relative to Feekes growth scale, as outlined in (d). (b) Example images of

Apogee growth from week 1 to week 6 and (c) week 7 to week 11. (d) Feeks growth scale of wheat from Large (1954). Scale bar = 50mm.

During this exploration, the infection window around anthesis in Apogee was tested. While it is generally accepted in the field that infection is restricted to ~5 days around anthesis, it has not yet been reported explicitly in this cultivar. Prior to further morphological explorations, it was deemed necessary to check this. WT *F. graminearum* was inoculated two weeks (14 days) after mid-anthesis (week 8; Fig. 6.4.3 (c)). By 7 days, when WT symptoms have typically advanced beyond the inoculated spikelet, very limited macroscopic symptoms were visible. However, by 10 days, symptoms on the glume were apparent as was attenuation of the awns. Surprisingly, by 14 days post inoculation (week 10 in growth, typical disease symptoms of premature bleaching of the wheat spike had spread widely above the point of inoculation and, although to a limited extent, also below. Although bleaching associated with senescence can start to occur around 10 weeks, attenuation of the awns and bending of the whole spike are indicative of *F. graminearum* infection. What caused this sudden spread is currently known.



Fig. 6.4.4. WT *F. graminearum* infection two weeks after anthesis infection window. Infection progression shown from side (left) and front (right) angles for each imaged timepoint of 7, 10 and 14 days post inoculation. inoculated spikelet is indicated by the yellow arrow. Scale bar = 20mm.

Next, an analysis the wheat rachis morphological changes throughout the period from anthesis to the appearance of macroscopic FHB symptoms as demonstrated in Fig. 6.4.4 was conducted through microscopy,

First, transverse sections of the wheat rachis internode were explored through 1 μ m thick resin sections stained with Toluidine blue (TB). Between weeks 7 and 11, the period after anthesis and during grain filling before wheat senescence, it is observed that the distance between vascular bundles (vb) increase as the cells in the tissue between them becomes devoid of contents and may convert from parenchyma cells to aerenchyma (aer). From weeks 6 through 11, the epidermal layer (e) becomes consistently stained a lighter blue, indicating a higher degree of lignification, with cell wall becoming evidently thicker. Evidence of stomatal pores are also absent by 11 weeks, which coincides with the thickening of the epidermal cell layer and senescence (Fig. 6.4.3 (c)).

To better explore morphological changes in the rachis node in the period around anthesis, through which *F. graminearum* hyphae must pass to colonise other wheat spikelet, a small exploration through the staining of longitudinal sections with TB staining was conducted. In rachis nodes between weeks 6 and 7, a high degree of cell growth with lignification is observed between the lemma (L) and palea (P) axes (Fig. 6.4.6). It is also observed that aerenchyma appear between 7 and 11 weeks in both transverse sections of rachis internodes (Fig.6.4.5) and longitudinal sections of rachis nodes (Fig. 6.4.6). Whether this is an artefact of the exactly where tissue sampling occurred, or a true component of rachis development requires further exploration.

To build on this, a serial exploration of the wheat rachis and rachis node to dissect the structural changes throughout the rachis around anthesis (week 7) was conducted. By sectioning every 20 μ m from the outer edge to the centre of the rachis, a picture of the constituent tissue layers of this structure was explored for the first time (Fig. 6.4.7).

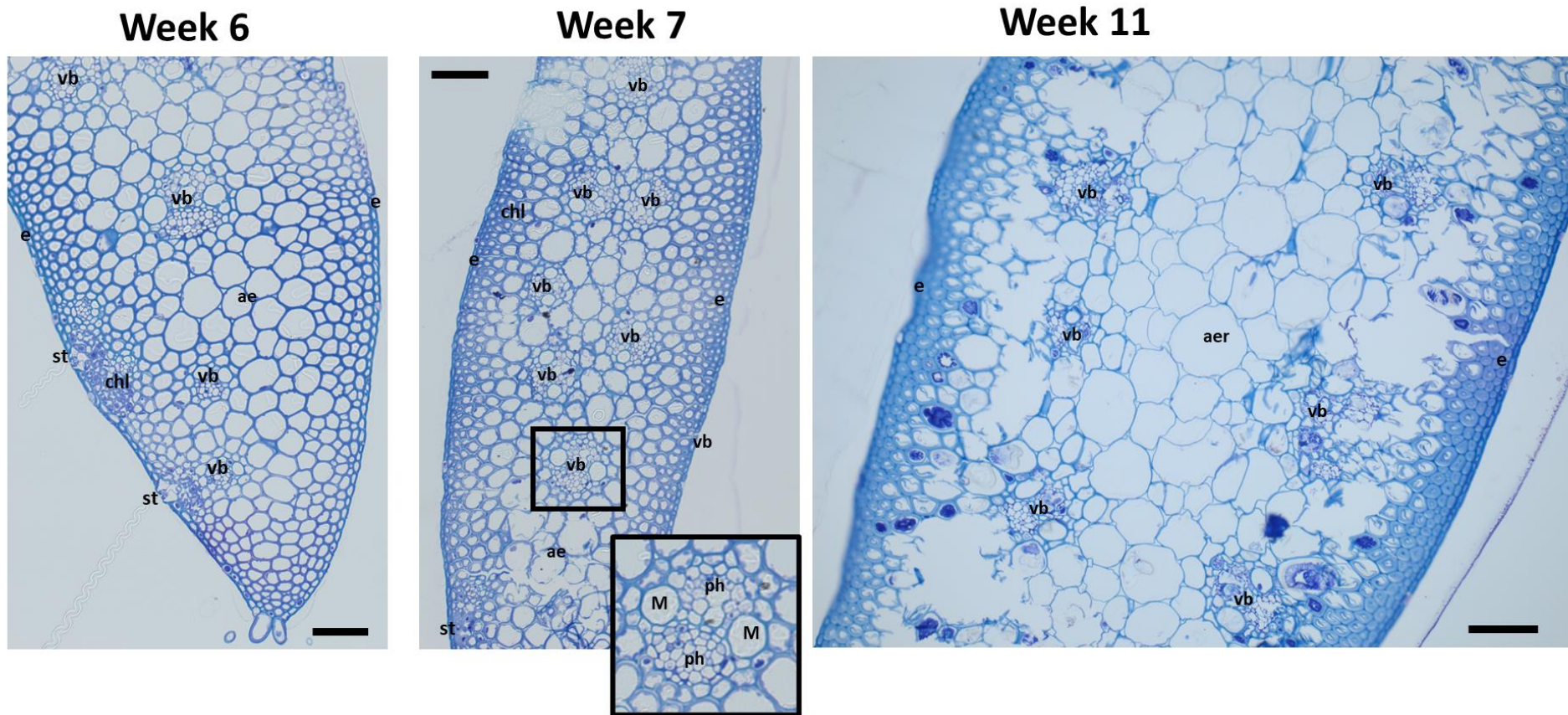


Fig. 6.4.5. Transverse sections of rachis internodes of wheat cv. 'Apogee' stained with TB showing morphology through growth at 6, 7 and 12 weeks. vb = vascular bundle; s = stomata; e = epidermal parenchyma; aer = aerenchyma; chl = chlorenchyma; m = metaxylem; x = xylem; ph = phloem; s = sieve tubes. Scale bar = 100µm.

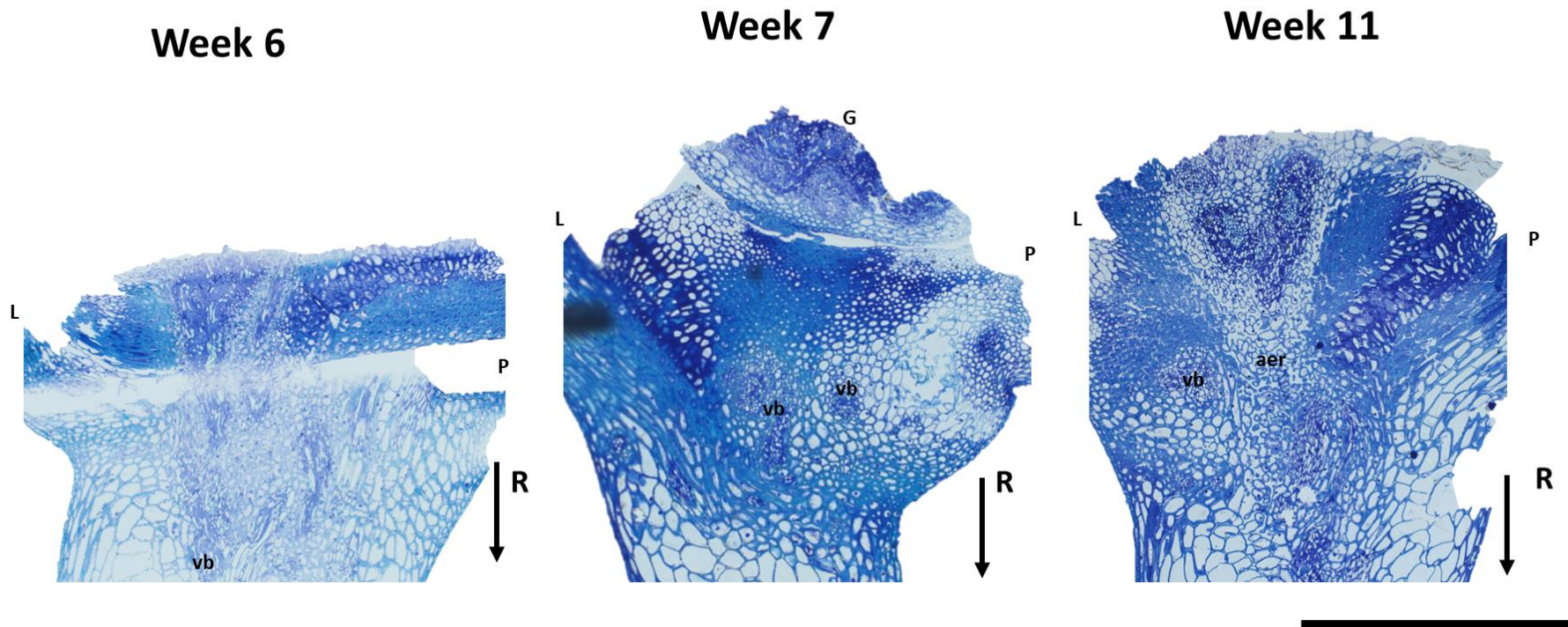
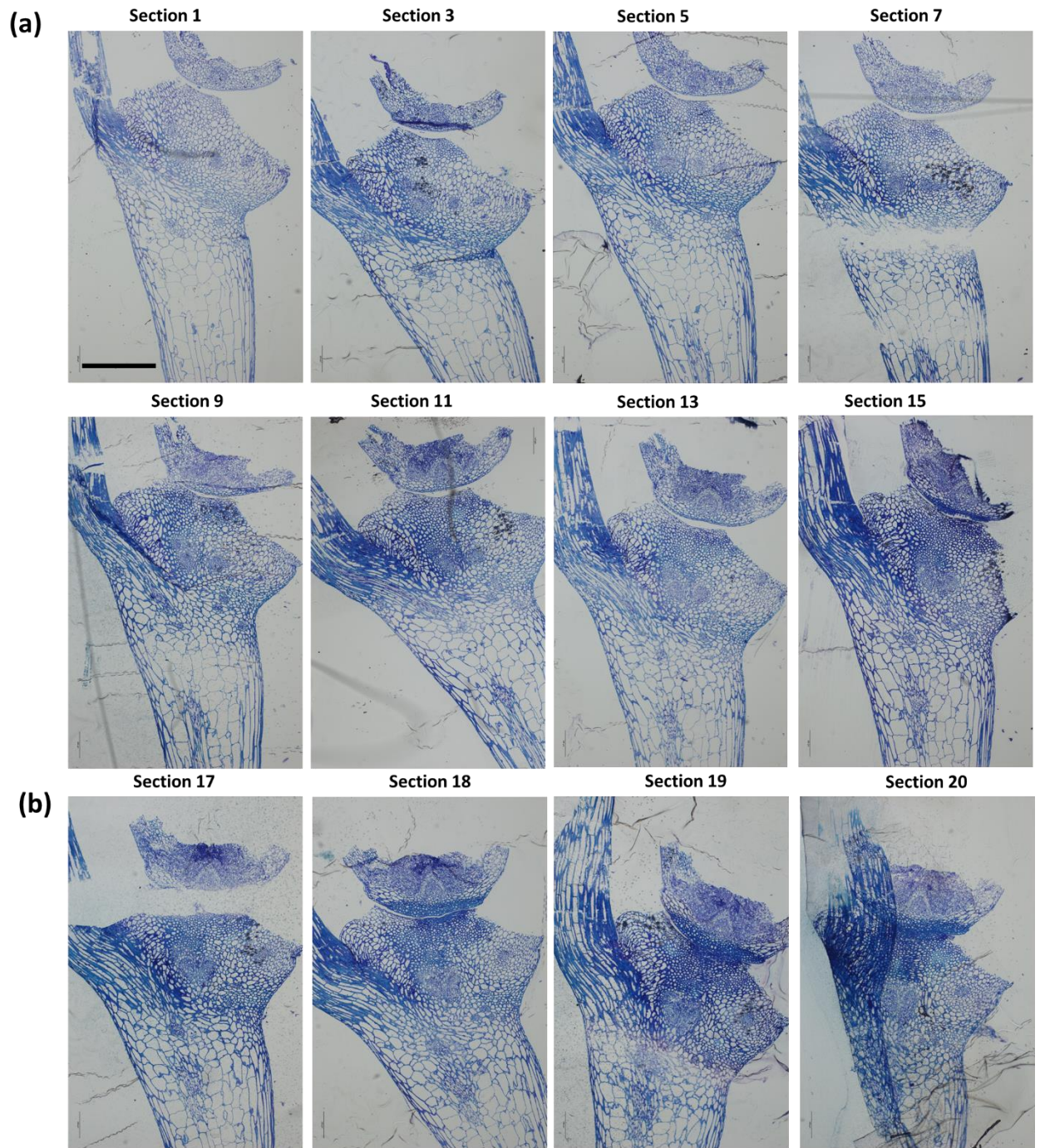


Fig. 6.4.6. Longitudinal sections of rachis nodes stained with TB showing morphology through growth at 6, 7 and 12 weeks (left to right). TB staining shows high degree of lignification (stained in blue) with many areas of thick, dense cells. L = lemma; P = palea; G = grain; vb = vascular bundle; aer = aerenchyma; R = rachis. Arrow shows where rest of rachis would begin and continue. Scale bar = 500 μ m.



(c)

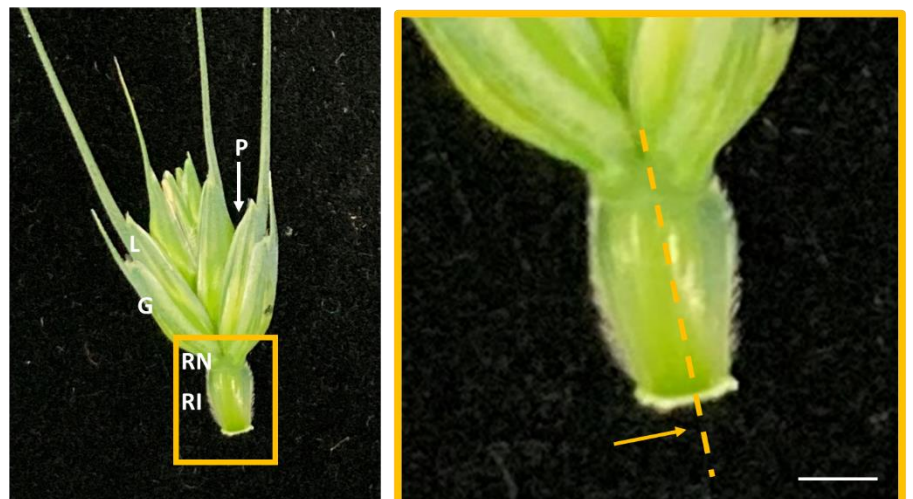


Fig. 6.4.7. Serial longitudinal sections of rachis nodes and internodes stained with Toluidine Blue at week 7 of growth (anthesis). (a) Approximately 40 μ m between shown sections (left to right, top to bottom). (b) Approximately 20 μ m between shown sections in the centre of the rachis (left to right). Scale bar = 500 μ m. (c) Schematic image of wheat spikelet, with enlarged panel on left showing direction of sectioning from outer edge to centre. L = lemma; P = palea; G = glume; RN = rachis node; RI = rachis internode. Scale bar = 500 μ m.

By sectioning from the outside to the inner edge of the combined rachis node and internode, it is possible to see where *F. graminearum* hyphae might colonise (Fig. 6.4.7). Further into the rachis (sections 15-19), cells directly beneath the developing grain are denser and more lignified than those on the outer edges (sections 3 and 11). Vascular bundles are evident throughout the rachis node and within the rachis internode from section 11 onwards (approximately 200 μ m into the rachis), which correlates with the location of vascular bundles from the edge as seen in Fig. 6.4.6. The majority of cells in the rachis internode itself are parenchyma cells. Colonization of the lemma tissue itself may pose a faster route to bypass the lignification seen in the rachis node at 7 weeks in Fig. 6.4.6, and to some extent in Fig. 6.4.8 and Fig. 6.4.9.

To better explore the alterations in lignification, longitudinal rachis nodes and internodes, with directly adjacent sections to those in Fig. 6.4.6., were stained with the lignin stain potassium permanganate (PP) (Fig. 6.4.9). Results from the PP stain confirm the TB staining, where light blue staining indicates lignin, with high levels in the lemma axis between the rachis node and rachis internode, and the high-density cells sitting beneath the developing grain also containing high lignin quantities. Interestingly, sections at week 9 in both Fig. 6.4.6 and Fig. 6.4.9 showed the highest degree of lignification particularly along the epidermal edges and spanning the junction between the rachis node (RN) and the rachis internode (RI).

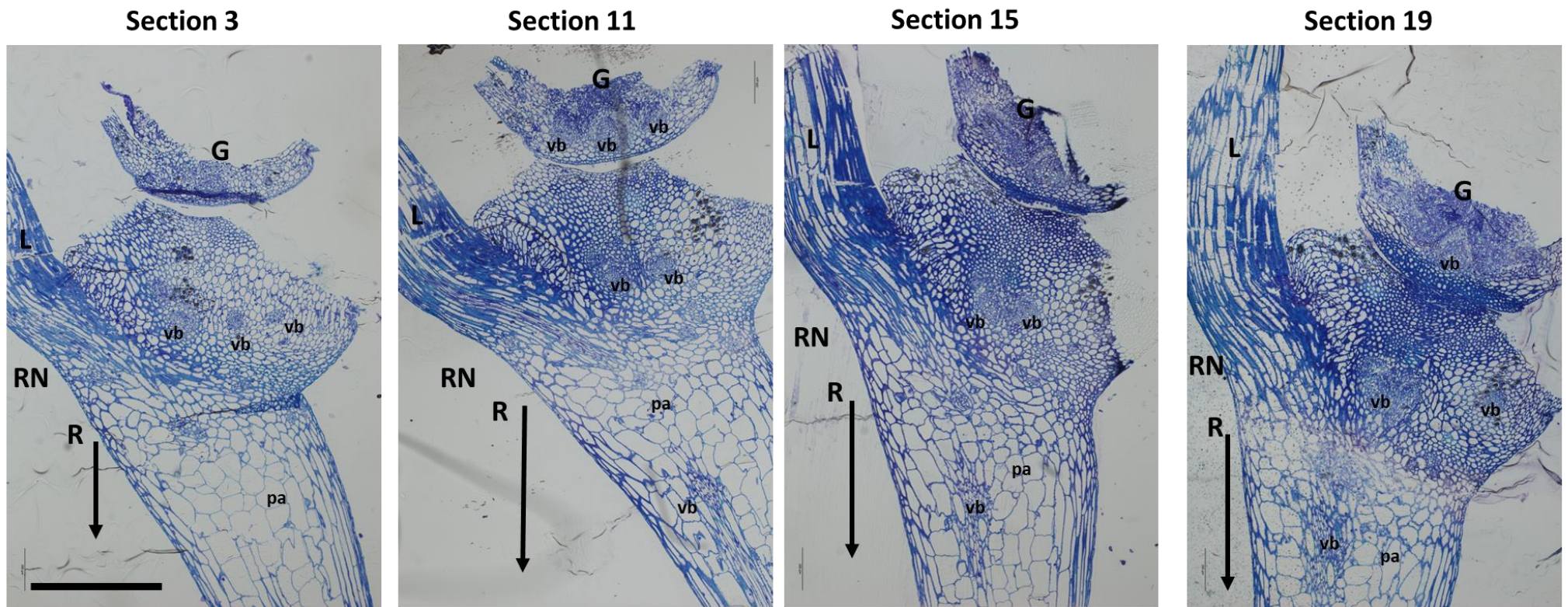


Fig. 6.4.8. Selected sections from Fig. 6.4.8 from outer edge to centre of rachis, stained with Toluidine Blue. RN = rachis node; R = rachis (arrow indicates orientation and direction of rest of rachis); G = developing grain; L = lemma; vb = vascular bundle; pa = parenchyma cells. Scale bar = 500µm.

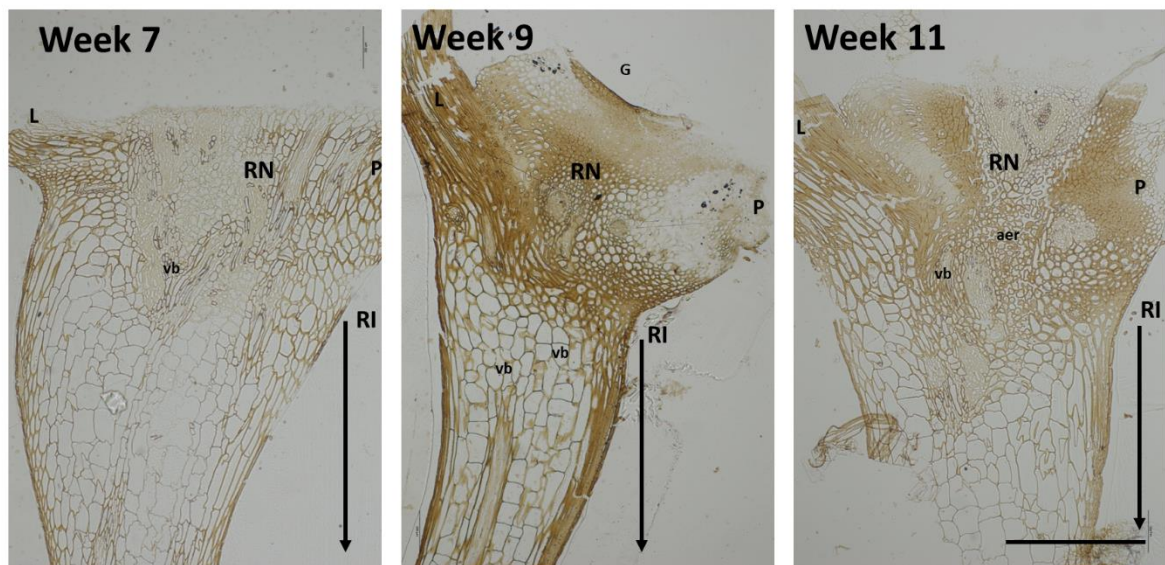


Fig. 6.4.9. Longitudinal rachis sections stained with potassium permanganate for lignin visualisation. Sampled timepoints are week 7, 9 and 11. L = lemma; P = palea; G = grain; vb = vascular bundle; aer = aerenchyma; RI = rachis internode; RN = rachis node. Arrow shows where rest of rachis would begin and continue. Scale bar = 500 μ m.

To further explore how lignin is distributed throughout wheat spikelet tissues throughout development, and quantify the changes in lignification, image analysis on PP-stained sections was conducted (Fig. 6.4.10). In early stages of wheat growth from weeks 2 to 6, whole stems were sampled and had no significant difference in lignin as growth progressed ($F(2,3)=3.666$, $p = 0.156$). In the spikelet tissues of lemma ($F(3,8) = 1.519$, $p=0.282$) and palea ($F(2,6)=4.053$, $p = 0.077$), while an upward trend was observed as growth progressed this was not significant. This trend was also true for the rachis ($F(3,6) = 1.339$, $p = 0.347$), but interestingly not for the rachis node which remained relatively stable in lignin quantity ($F(2,5) = 0.455$, $p = 0.658$). Each biological sample is a mean value of lignification from three technical replicates to account for the subtle variation in staining, with three biological replicates per tissue type and week. The experiment was conducted once.

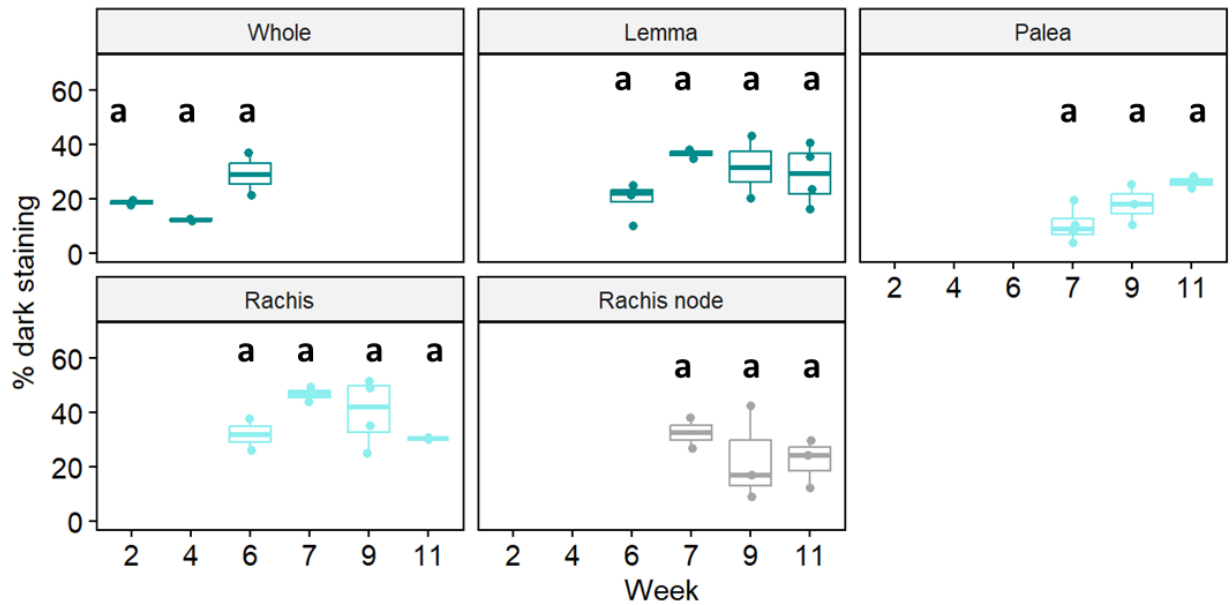


Fig. 6.4.10. Percentage of high lignification in wheat tissues at different growth stages. Whole, lemma, palea and rachis tissues of the wheat spikelet and rachis node also included. ANOVA followed by Tukey-post hoc test conducted on each tissue type individually. Letters denote significance groupings. Values are mean of three technical replicates, with three biological replicates per sample type (i.e., week and tissue type).

Example images at 5x objective, imaged under BF illumination are shown in Fig. 6.4.11, for each of the tissue types and timepoints sampled. In the stem, lignification is mainly present around the numerous vascular bundles, but in the lemma, palea and rachis, lignification staining is darker on the adaxial layer, and in the case of the rachis, also the abaxial layer (entire epidermis). These tissue layers provide structural support to the tissue. While shown here, it is worth noting that transverse sections of the rachis node are hard to acquire, often falling apart on sectioning due to insufficient support by the resin.

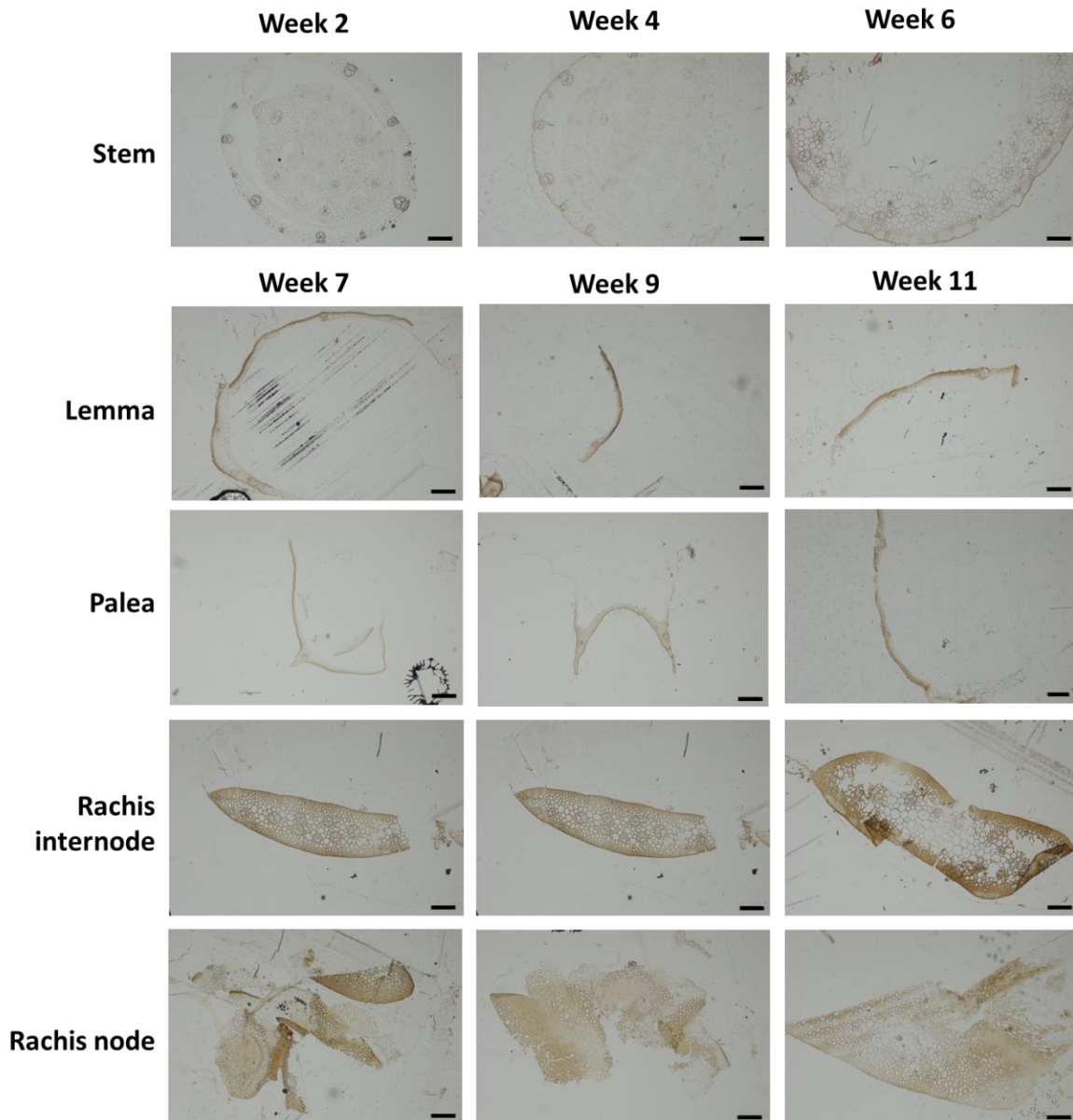


Fig. 6.4.11. Example images of potassium permanganate-stained 1 μ m thick sections. Weeks 2, 4 and 6 for the stem and weeks 7, 9 and 11 for all other tissues are shown. Images captured with BF illumination with 5x objective lens. Where more lignin is present, staining is darker. All scale bars = 200 μ m.

6.4.7 BCARS-Raman spectroscopy for exploration of rachis cell wall matrix

While much of the rachis exploration throughout growth, and a focus on the period around anthesis, has thus far looked at lignification, an alternative imaging method was sought to decipher further the cell wall matrix at week 7/ period of anthesis. BCARS-Raman spectroscopy of the rachis localised lignin, cellulose and pectin with the tissue (Fig. 6.4.12), with specific component spectra shown

in Fig. 6.4.12 (a). Pectin ($800\text{-}900\text{ cm}^{-1}$), putative syringyl units of lignin (1093 , 1335 and 1451 cm^{-1}) and an aromatic ring of lignin alcohols at 1602 cm^{-1} are highlighted in the spectra. Lignin syringyl units disperse between cellulose fibres in the secondary cell wall, shown in red. Cellulose fibrils have differing spectra depending on their orientation, with peaks at 1093 cm^{-1} and 2900 cm^{-1} for 90° and 0° orientation respectively (Fig. 6.4.13).

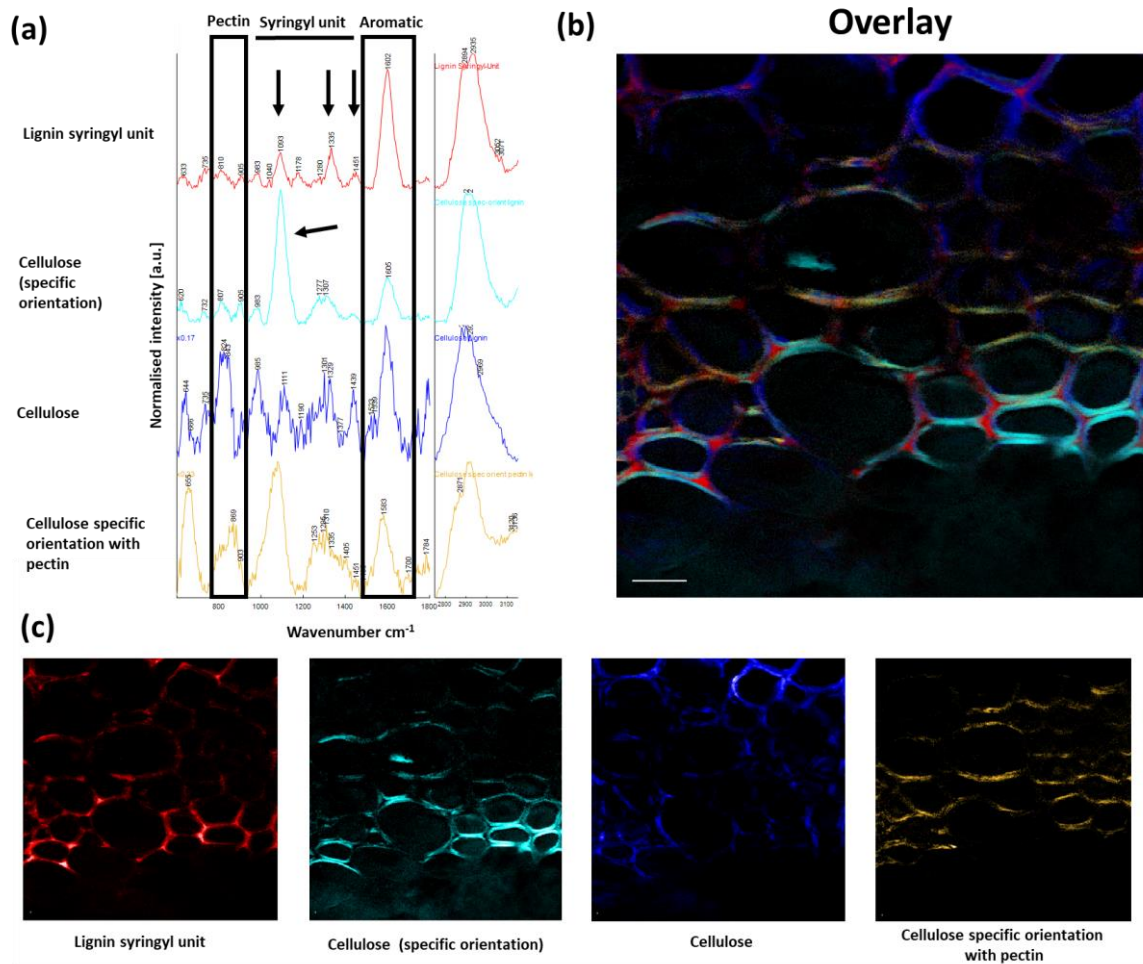


Fig. 6.4.12. BCARS-Raman spectroscopy. (a) Normalised intensity spectra of estimated cell wall components. Highlighted areas of interest include pectin ($800\text{-}900\text{ cm}^{-1}$), putative syringyl units at 1093 , 1335 and 1451 cm^{-1} and an aromatic ring of lignin monomers at 1602 cm^{-1} . (b) Overlay of four cell wall specific channels showing localisations. Scale bar = $50\mu\text{m}$ (c) individual channels showing localisations of cell wall components from left to right: Lignin syringyl unit (red), cellulose (specific orientation; light blue), cellulose (dark blue), and cellulose specific orientation with pectin (yellow).

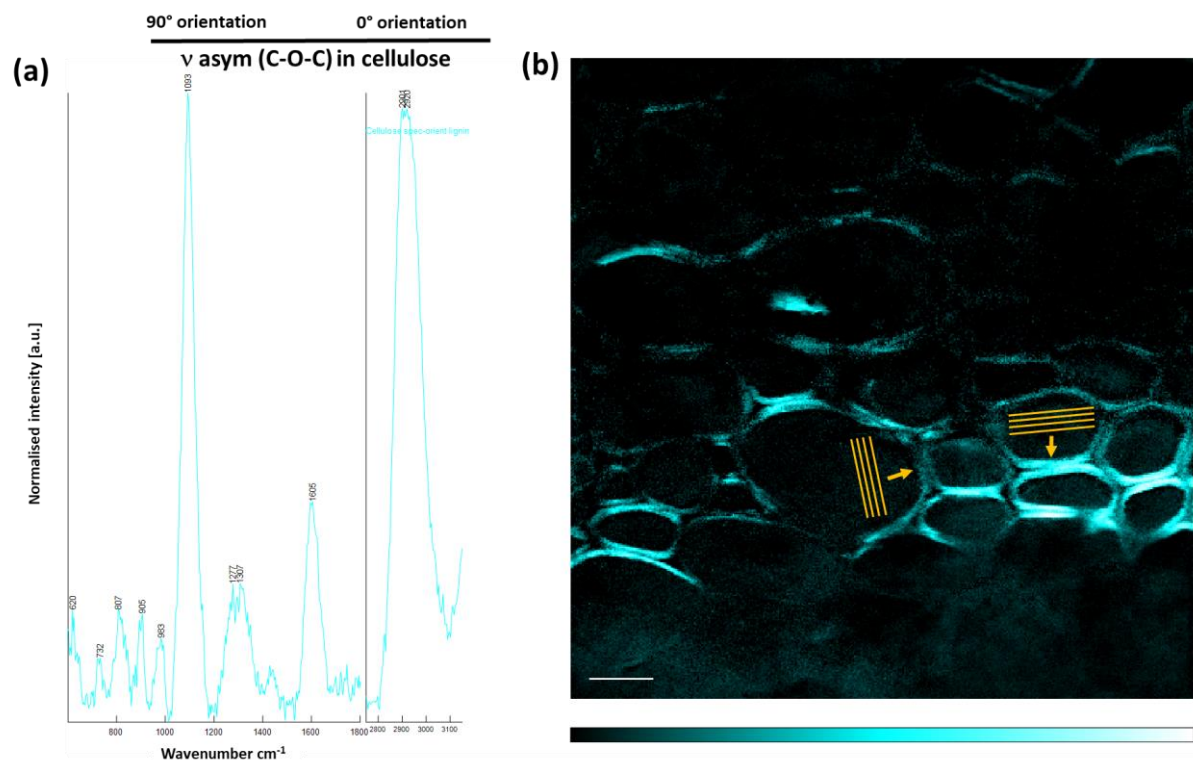


Fig. 6.4.13. Cellulose microfibrils in wheat rachis tissue. (a) Orientation of cellulose microfibrils in wheat rachis tissue, with peaks at 1093 cm^{-1} for 90° and 2900 cm^{-1} for 0° . (b) Direction of cellulose microfibrils shown and relative intensity in blue, dark = less intensity, bright = higher intensity. Scale bar = $50\mu\text{m}$.

6.5 Discussion

Searching the prevailing literature on cell wall mutants that pertain altered disease phenotypes to a number of diseases yielded mutants in pectin, lignin, callose and hemicelluloses. Confirmation of expression of wheat orthologues during *F. graminearum* infection and/or PAMP elicitation refined the shortlist of *Arabidopsis* mutants to test in a high throughput detached leaf assay screen. Unfortunately, the detached leaf assay required a high degree of fine-tuning, and it was finally determined that the addition of the mycotoxin DON was required to reduce the disease phenotype variability and the addition of the detergent Tergitol to the water agar medium, that prevents senescence of the detached leaves, was required to prevent *F. graminearum* hyphae preferentially colonising the agar. This supports previously reported literature whereby addition of DON at $75\mu\text{M}$ to *F. graminearum* inoculum in *Arabidopsis* detached leaf assays increased disease severity (Chen et al., 2006). In addition, surface sterilisation of *At* seed and removal of sucrose typically added to $\frac{1}{2}$ MS agar used to germinate the seed was

required to eliminate contamination. To reflect these changes to previously published detached leaf assays (Chen et al., 2006; Machado Wood et al., 2021), a protocol was published to accompany this chapter (Armer et al., 2024).

Despite these alterations, diseased area of detached leaves remained variable. This is consistent with a previous detached leaf assay screen of *Arabidopsis* mutants (Machado Wood et al., 2021). While not reported here, fungal burden was attempted to better quantify disease in detached leaves but remained equally variable. Unavoidable changes to containment growth rooms during building refurbishment during this period meant moving to rooms with no humidity control, and soil was contaminated with a non-pathogenic soil saprotrophic fungus, which cross-reacted to actin primers used to quantify *F. graminearum* in *Arabidopsis* leaves. This demonstrates difficulties in translational science between some model species, such as the dicot *Brassica Arabidopsis thaliana* and the monocot cereal wheat (*Triticum aestivum*). *Fusarium graminearum* and its closely related species *F. culmorum*, although have been shown to infect *Arabidopsis* previously (Urban et al., 2002), do not typically infect species beyond the small grain cereals and has a limited host range (Armer et al., 2024b). This may explain why addition of the mycotoxin DON is required to reduce disease variability. Interestingly, although it has long been known that the TRI gene biosynthetic cluster that is responsible for trichothecene mycotoxin production is not induced *in vitro* in typical culturing mediums (Chen et al., 2000), expression and/or detection of DON in *F. graminearum*-infected *Arabidopsis* leaves has not yet been studied. In infected floral tissues however, DON levels of 1ppm, much lower than that found in wheat, have been reported (Urban et al., 2002).

From the *Arabidopsis* detached leaf assay, some of the selected mutants of the lignin biosynthesis pathway had visibly increased disease severity compared to other cell wall mutants. Hence, the lignin biosynthesis mutants, along with the apoplastic peroxidase mutants, were selected for further analysis. Lignification of plant cell walls is a known defence response to a wide range of pathogens. However, this increase in severity was very smaller, with *F. graminearum* infection still being localised with the hypersensitive response. With the difficulties in infection establishment in *Arabidopsis*, this supports the idea that plant-pathogen interactions should be largely studied in the native pathosystem. *F. graminearum* has a very small host range and is thus very adapted to floral tissues of small

grain cereals, and specifically wheat. However, it makes sense that lignin is a key defence component in the cell wall as the wheat rachis is a highly lignified tissue, as demonstrated with potassium permanganate staining in the rachis node and internode. Of the lignin gene targets, a further search of the literature revealed widespread increase in disease susceptibility to *Fusarium graminearum*, as well as some other fungal pathogens, in wheat species *Triticum monococcum* and *Triticum aestivum* as well as Sorghum (*Sorghum bicolor*) and Barley (*Hordeum vulgare*). As a hexaploid, wheat often has three, if not more, alleles of lignin biosynthesis genes. Some alleles may only be active in certain tissues, which has implications for selecting those with relevant expression for the pathosystem. However, these studies further supported the notion of lignin involvement in resistance to *F. graminearum* infection and guided a focus towards spatial localisation in the wheat rachis and further postulation of involvement in restriction of *Fusarium graminearum* infection to the period around anthesis.

Unfortunately, some of the identified key targets weren't able to be acquired or tested. Some were due to lack of homozygosity in the T-DNA insertion SALK lines, but also lack of germination. One of these was PMR4, the callose synthase so named for its resistance to powdery mildew, has shown to have complete lack of callose in Arabidopsis leaves (Vogel and Somerville, 2000). Also known as GLUCAN SYNTHASE-LIKE 5, this gene has been shown to be implicated in papillary callose formation, although this gene is not required for the callose-lacking structure formation (Jacobs et al., 2003). Although lacking in callose, the *pmr4* mutants have increased resistance to penetration by fungal pathogens and this is likely due to upregulation of salicylic acid (SA) in the *pmr4* mutant compared to the WT control which leads to localised cell death, similar to that of the hypersensitive response (HR), around penetration sites (Nishimura et al., 2003). Overexpression lines of PMR4 have increased resistance due to increased callose deposition at penetration sites, but here SA is not upregulated (Ellinger et al., 2013). Knock down of SA-induced defence responses in the *pmr4* mutants restores susceptibility (Nishimura et al., 2003) and indicates a potentially link and/or shared regulatory pattern. Translating this to wheat, silencing the orthologue to GLS5 with VIGS led to increased susceptibility to the wheat powdery mildew pathogen *Blumeria graminis* f. sp. *tritici* (Cheng et al., 2021) and was also found to be similar in Barley (Chowdhury et al., 2016). While in both

studies decreased callose accumulation was observed in papillae around penetration sites, no difference in SA regulation was observed between WT and VIGS lines indicating that this may be decoupled in the monocots.

The wheat rachis is an inherently lignified tissue. It has a structural role in supporting the developing grain and facilitating the passage of water and sugars through the vascular elements to facilitate grain development. Throughout this study it became clear that no anatomical study has been conducted in depth to explore the development and infection related morphological changes that occur in the wheat rachis, particularly with respect to lignin. While recent studies have explored rachis ultrastructure with a focus on vasculature in barley (Rutten et al., 2024) and in wheat (Houshmandfar and Asli, 2011), a detailed microscopic analysis of wheat rachis ultrastructure at anthesis was required to fully understand host-tissue colonisation mechanisms undertaken by *F. graminearum*. Most importantly, WT *F. graminearum* does not have the same disease phenotype in Barley as in wheat, which has restriction of infection to the inoculated spikelet, similar to that described in [chapter 3](#) with the $\Delta Tri5$ KO mutant. This makes comparable studies between barley and wheat difficult, with respect to differing disease phenotypes.

While the microscopic analysis of the wheat rachis in this chapter may give an indication to the importance of lignin, and perhaps a wheat developmental stage through which arises an opportunity for *F. graminearum* infection advancement, further studies must be undertaken. Emerging technologies are improving in their resolution. One such example is micro-CT scanning of wheat rachis tissues to spatially map *F. graminearum* infection *in planta*, which has been applied to study wheat grain morphology throughout development (Quoc Le et al., 2019), however resolutions are not yet high enough to model *F. graminearum* hyphae. Alternatively, serial block scanning face electron microscopy allows for a better resolution, with 3D reconstruction of cells by serial sectioning, but is more costly and requires significant sample preparation time. This scale, requiring significant computational power, allows for multiple cell resolution but not yet at the tissue level required for the wheat rachis. However, this is likely to change in the coming years and offers the best opportunity for modelling aspects of cellular morphology, such as plasmodesmatal pit fields, that cannot be viewed by light microscopy by nature of being smaller than the wavelength of visible light. Other

technologies such as focused ion beam SEM and serial sectioning TEM are not yet widely used in plant sciences but are gaining popularity (Zechman, Möstl and Zellnig, 2022).

Many experimental techniques that assess the composition and/or quantity of particular cell wall components do so in relative isolation, and without the spatial information that is so important in plant-pathogen interactions. Raman spectroscopy is a technique that provides the chemical signature of samples *in situ* without destroying the sample, as is the case in GCMS. The Raman effect, where different molecules respond to a monochromatic laser with a spectra of vibrations in what is known as inelastic scattering, in combination with linear unmixing, as used in this study, this allows for the simultaneous deciphering of cell wall components, with spatial resolution to 300nm (Mateu, Bock and Gierlinger, 2020). Despite only recently being applied to plant tissues, Raman has recently been shown to differentiate healthy from infected tomato plants with two viral pathogens, Tomato yellow leaf curl Sardinia virus (TYLCSV) and Tomato spotted wilt virus (TSWV), within 2 weeks of inoculation (Mandrile et al., 2019). In wheat, Raman has also been used to differentiate between biotic and abiotic stresses, namely drought, nitrogen deficiency, aphid infestation and viral infection (Higgins et al., 2022). Spectra shown to shift are related to chlorophylls, carotenoids and specifically lutein, which is an antioxidant implicated in protection of plant tissues against ROS, released as part of the plant immune system.

Overall, the work presented in this chapter indicates an integral role for lignin in the wheat rachis and *F. graminearum* resistance. Putative analyses of lignification throughout spikelet development shows increasing lignification as the tissue senesces and is required to support an increasingly heavy wheat grain. This chapter also highlights the difficulties of using distantly related model organisms to decipher disparate tissues, such as *At* leaves and wheat spikelet tissues which hold very different roles in the plant. Further, it highlights the possibility of emerging technologies for examining the cell wall matrix *in situ* but require further experimentation to elucidate the specific cell wall changes that occur during plant pathogen interactions.

6.6 References

- Armer VJ, Deeks MJ, Hammond-Kosack KE. (2024c). *Arabidopsis thaliana* detached leaf assay for the disease assessment of *Fusarium graminearum*. *Protocols.io*. doi: 10.17504/protocols.io.261gedmwov47/v1.
- Armer VJ, Deeks MJ, Hammond-Kosack KE. (2024a). *Arabidopsis thaliana* detached leaf assay for the disease assessment of *Fusarium graminearum* infection. *Protocols.io*. doi: 10.17504/protocols.io.261gedmwov47/v1.
- Armer VJ, Kroll E, Darino M, Smith DP, Urban M, Hammond-Kosack KE. (2024b). Navigating the *Fusarium* species complex: Host-range plasticity and genome variations. *Fungal Biology*. **In press**. doi: 10.1016/j.funbio.2024.07.004.
- Barros J, Serrani-Yarce JC, Chen F, Baxter D, Venables BJ, Dixon RA. (2016). Role of bifunctional ammonia-lyase in grass cell wall biosynthesis. *Nature Plants*. **2**: 16050. doi: 10.1038/nplants.2016.50.
- Bethke G, Thao A, Xiong G, Li B, Soltis NE, Hatsugai N, Hillmer RA, Katagiri F, Kliebenstein DJ, Pauly M, Glazebrook J. (2016). Pectin Biosynthesis Is Critical for Cell Wall Integrity and Immunity in *Arabidopsis thaliana*. *The Plant Cell*. **28**(2): 537–556. doi: 10.1105/tpc.15.00404.
- Bhuiyan NH, Selvaraj G, Wei Y, King J. (2009). Gene expression profiling and silencing reveal that monolignol biosynthesis plays a critical role in penetration defence in wheat against powdery mildew invasion. *Journal of Experimental Botany*. **60**(2): 509-521. doi: 10.1093/jxb/ern290.
- Camp Jr CH, Lee YJ, Heddleston JM, Hartshorn CM, Hight Walker AR, Rich JN, Lathia JD, Cicerone MT. (2014). High-speed coherent Raman fingerprint imaging of biological tissues. *Nature Photonics*. **8**: 627–634. doi: 10.1038/nphoton.2014.145.
- Cao Y, Yan X, Ran S, Ralph J, Smith RA, Chen X, Qu C, Li J, Liu L. (2022). *Plant, Cell & The Environment*. **45**(1): 248-261. doi: 10.1111/pce.14208.
- Chancellor T, Smith DP, Chen W, Clack SJ, Venter E, Halsey K, Carrera E, McMillan V, Canning G, Armer VJ, Hammond-Kosack KE, Palma-Guerrero J. (2024). A fungal endophyte induces local cell-wall mediated resistance in wheat roots against take-all disease. *Frontiers in Plant Science*. **In press**. doi: 10.3389/fpls.2024.1444271.
- Chen X, Steed A, Harden C, Nicholson P. (2006). Characterization of *Arabidopsis thaliana*–*Fusarium graminearum* interactions and identification of variation in resistance among ecotypes. *Molecular Plant Pathology*. **7**(5): 391-403. doi: 10.1111/j.1364-3703.2006.00349.x.
- Cheng P, Wang Z, Ren Y, Jin P, Ma K, Wang B. (2021). Silencing of a Wheat Ortholog of Glucan Synthase-Like Gene Reduced Resistance to *Blumeria graminis* f. sp. *tritici*. *Frontiers in Plant Science*. **12**: 800077. doi: 10.3389/fpls.2021.800077
- Chiniquy D, Underwood W, Corwin J, Ryan A, Szemenyei H, Lim CC, Stonebloom SH, Birdseye DS, Vogel J, Kliebenstein D, Scheller HV, Somerville S. (2019). PMR5, an acetylation protein at the intersection of pectin biosynthesis and defense against fungal pathogens. *The Plant Journal*. **100**(5): 1022-1035. doi: 10.1111/tpj.14497.

- Chowdhury J, Schober MS, Shirley NJ, Singh RR, Jacobs AK, Douchkov D, Schweizer P, Fincher GB, Burton RA, Little A. (2016). Down-regulation of the *glucan synthase-like 6* gene (HvGsl6) in barley leads to decreased callose accumulation and increased cell wall penetration by *Blumeria graminis* f. sp. *hordei*. *New Phytologist*. **212**: 434–43.
- Demont-Caulet N, Lapierre C, Jouanin L, Baumberger S, Méchin V. (2010). *Arabidopsis* peroxidase-catalyzed copolymerization of coniferyl and sinapyl alcohols: kinetics of an endwise process. *Phytochemistry*. **71**(14–15): 1673–1683. doi: 10.1016/j.phytochem.2010.06.011.
- Dhokane D, Karre S, Kushalappa AC, McCartney C. (2016). Integrated Metabolo-Transcriptomics Reveals *Fusarium* Head Blight Candidate Resistance Genes in Wheat QTL-Fhb2. *PLoS ONE*. **11**(5): e0155851. doi: 10.1371/journal.pone.0155851.
- Ellinger D, Naumann M, Falter C, Zwikowics C, Jamrow T, Manisseri C, Somerville SC, Voigt CA. (2013). Elevated early callose deposition results in complete penetration resistance to powdery mildew in *Arabidopsis*. *Plant Physiology*. **161**:1433–44. doi: 10.1104/pp.112.211011.
- Funnell-Harris DL, Pedersen JF, Sattler SE. (2010). Alteration in Lignin Biosynthesis Restricts Growth of *Fusarium* spp. in Brown Midrib Sorghum. *Phytopathology*. **100**(7): 632-728. doi: 10.1094/PHYTO-100-7-0671.
- Funnell-Harris DL, Pedersen JF, Sattler SE. (2010). Alteration in Lignin Biosynthesis Restricts Growth of *Fusarium* spp. in Brown Midrib Sorghum. **100**(7): 632-728. doi: 10.1094/PHYTO-100-7-0671.
- Gao Q, Wang C, Xi Y, Shao Q, Hou C, Li L, Luan S. (2023). RALF signaling pathway activates MLO calcium channels to maintain pollen tube integrity. *Cell Research*. **33**: 71-79. doi: 10.1038/s41422-022-00754-3.
- Hernández-Blanco C, Feng DX, Hu J, Sánchez-Vallet A, Deslandes L, Llorente F, Berrocal-Lobo M, Keller H, Barlet X, Sánchez-Rodríguez C, Anderson LK, Somerville S, Marco Y, Molina A. (2007). Impairment of Cellulose Synthases Required for *Arabidopsis* Secondary Cell Wall Formation Enhances Disease Resistance. *The Plant Cell*, **19**(3): 890–903. doi: 10.1105/tpc.106.048058.
- Higgins S, Serada V, Herron B, Gadhave KR, Kurouski D. (2022). Confirmatory detection and identification of biotic and abiotic stresses in wheat using Raman spectroscopy. *Frontiers in Plant Science*. **13**: 1035522. doi: 10.3389/fpls.2022.1035522
- Houshmandfar A, Asli DE. (2011). An Anatomical Study of Vascular System of Spike: Dynamics of Central Vascular Bundles at Successive Internodes along the Rachis of Wheat. *Advances in Environmental Biology*. **5**(7): 1531-1535. No doi available.
- Huerta AI, Sancho-Andrés G, Montesinos JC, Silva-Navas J, Bassard S, Pau-Roblot C, Kesten C, Schlechter R, Dora S, Ayupov T, Pelloux J, Santiago J, Sánchez-Rodríguez C. (2023). The WAK-like protein RFO1 acts as a sensor of the pectin methylation status in *Arabidopsis* cell walls

to modulate root growth and defense. *Molecular Plant*. **16**(5): P865-881. doi: 10.1016/j.molp.2023.03.015.

Humphreys JM, and Chapple C. (2002). Rewriting the lignin roadmap. *Current Opinion in Plant Biology*. **5**(3):224-229. doi: 10.1016/s1369-5266(02)00257-1.

Jacobs AK, Lipka V, Burton RA, Panstruga R, Strizhov N, Schulze-Lefert P, Fincher GB. (2003). An *Arabidopsis* callose synthase, GSL5, is required for wound and papillary callose formation. *Plant Cell*. **15**:2503–13. doi: 10.1105/tpc.016097

Jang CS, Johnson JW, Seo YW. (2005). Differential expression of TaLTP3 and TaCOMT1 induced by Hessian fly larval infestation in a wheat line possessing H21 resistance gene. *Plant Science*. **168**(5): 1319-1326. doi: 10.1016/j.plantsci.2005.01.014.

Kubicek CP, Starr TL, Glass NL. (2014). Plant Cell Wall–Degrading Enzymes and Their Secretion in Plant-Pathogenic Fungi. *Annual Review of Phytopathology*. **52**: 427-451. doi: 10.1146/annurev-phyto-102313-045831.

Large EC. (1954). Growth stages in cereals illustration of the Feekes growth scale. **3**(4): 128-129. doi: 10.1111/j.1365-3059.1954.tb00716.x.

Le TDQ, Alvarado C, Girousse C, Legland D, Chateigner-Boutin A. (2019). Use of X-ray micro computed tomography imaging to analyze the morphology of wheat grain through its development. *Plant Methods*. **15**: 84. doi: 10.1186/s13007-019-0468-y

Lee M, Jeon HS, Kim SH, Chung, JH, Roppolo D, Lee H, Cho HJ, Tobimatsu Y, Ralph J, Park OK. (2019). Lignin-based barrier restricts pathogens to the infection site and confers resistance in plants. *The EMBO Journal*. **38**: e101948. doi: doi.org/10.15252/embj.2019101948.

Liu MJ, Yeh FJ, Yvon R, Simpson K, Jordan S, Chambers J, Wu H, Cheung AY. (2023). Extracellular pectin-RALF phase separation mediates FERONIA global signaling function. *Cell*. **187**(2): P312-330.E22. doi: 10.1016/j.cell.2023.11.038.

Ma Q. (2007). Characterization of a cinnamoyl-CoA reductase that is associated with stem development in wheat. *Journal of Experimental Botany*. **58**(8): 2011-2021. doi: 10.1093/jxb/erm064.

Ma Q. (2010). Functional analysis of a cinnamyl alcohol dehydrogenase involved in lignin biosynthesis in wheat. *Journal of Experimental Botany*. **61**(10): 2735–2744, doi: 10.1093/jxb/erq107.

Machado Wood AK, Panwar V, Grimwade-Mann M, Ashfield T, Hammond-Kosack KE, Kanyuka K. (2021). The vesicular trafficking system component MIN7 is required for minimizing *Fusarium graminearum* infection. *Journal of Experimental Botany*. **72**(13): 5010–5023. doi: 10.1093/jxb/erab170.

Mandrile L, Rotunno S, Miozzi L, Vaira AM, Giovannozzi AM, Rossi AM, Noris E. (2019). Nondestructive Raman Spectroscopy as a Tool for Early Detection and Discrimination of the

- Infection of Tomato Plants by Two Economically Important Viruses. *Analytical Chemistry*. **91**(14): 9025-9031. doi: 10.1021/acs.analchem.9b01323.
- Mateu BP, Bock P, Gierlinger N. (2020). Raman Imaging of Plant Cell Walls. *Methods in molecular biology (Clifton, N.J.)*, 2149: 251–295. doi: 10.1007/978-1-0716-0621-6_15.
- Narváez-Barragán DA, Tovar-Herrera OE, Guevara-García A, Serrano M, Martínez-Anaya C. (2022). Mechanisms of plant cell wall surveillance in response to pathogens, cell wall-derived ligands and the effect of expansins to infection resistance or susceptibility. *Frontiers in Plant Science*. **13**: 969343. doi: 10.3389/fpls.2022.969343.
- Nguyen QB, Itoh K, Van Vu B, Tosa Y, Nakayashiki H. (2011). Simultaneous silencing of endo- β -1,4 xylanase genes reveals their roles in the virulence of *Magnaporthe oryzae*. *Molecular Microbiology*. **81**: 1008–1019. doi: 10.1111/j.1365-2958.2011.07746.x.
- Nishimura MT, Stein M, Hou BH, Vogel JP, Edwards H, Somerville SC. (2003). Loss of a callose synthase results in salicylic acid – dependent disease resistance. *Science*. **301**:969–72. doi: 10.1126/science.1086716.
- Noda J, Brito N, González C. (2010). The *Botrytis cinerea* xylanase Xyn11A contributes to virulence with its necrotizing activity, not with its catalytic activity. *BMC Plant Biology*. **10**:38. doi: 10.1186/1471-2229-10-38.
- O'Malley RC, Barragan CC, Ecker JR. (2015). A User's Guide to the Arabidopsis T-DNA Insertional Mutant Collections. *Methods in Molecular Biology*. **1284**: 323-342. doi: 10.1007/978-1-4939-2444-8_16.
- Reignault P, Valette-Collet O, Boccara M. (2008). The importance of fungal pectinolytic enzymes in plant invasion, host adaptability and symptom type. *European Journal of Plant Pathology*. **120**: 1–11. doi: 10.1007/s10658-007-9184-y.
- Rong W, Luo M, Shan T, Wei X, Du L, Xu H, Zhang Z. (2016). A Wheat Cinnamyl Alcohol Dehydrogenase TaCAD12 Contributes to Host Resistance to the Sharp Eyespot Disease. *Frontiers in Plant Science*. **7**: 1723. doi: 10.3389/fpls.2016.01723.
- Rutten T, Thirulogachandar V, Huang Y, Shanmugaraj N, Koppolu R, Ortleb S, Hensel G, Kumlehn J, Melzer M, Schnurbusch T. (2024). Anatomical insights into the vascular layout of the barley rachis: implications for transport and spikelet connection. *Annals of Botany*. **133**(7):983-996. doi: 10.1093/aob/mcae025.
- Soni N, Altartouri B, Hegde N, Duggavathi R, Nazarian-Firouzabadi F, Kushalappa AC. (2021). TaNAC032 transcription factor regulates lignin-biosynthetic genes to combat *Fusarium* head blight in wheat. *Plant Science*. **204**: 110820. doi: 10.1016/j.plantsci.2021.110820
- Soni N, Hedge N, Dhariwal A, Kushalappa AC. (2020). Role of laccase gene in wheat NILs differing at QTL-Fhb1 for resistance against *Fusarium* head blight. *Plant Science*. **298**:110574. doi: 10.1016/j.plantsci.2020.110574.

- Tronchet M, Balagué C, Kroj T, Jouanin L, Roby D. (2010). Cinnamyl alcohol dehydrogenases-C and D, key enzymes in lignin biosynthesis, play an essential role in disease resistance in *Arabidopsis*. *Molecular Plant Pathology*. **11**(1): 83-92. doi: 10.1111/j.1364-3703.2009.00578.x.
- Underwood W. (2012). The plant cell wall: a dynamic barrier against pathogen invasion. *Frontiers in Plant Science*. **3**:85. doi: 10.3389/fpls.2012.00085.
- Urban M, Daniels S, Mott E, Hammond-Kosack K. (2002). *Arabidopsis* is susceptible to the cereal ear blight fungal pathogens *Fusarium graminearum* and *Fusarium culmorum*. *The Plant Journal*. **32**(6): 961-973. doi: 10.1046/j.1365-313X.2002.01480.x.
- Vogel J, Somerville S. (2000). Isolation and characterization of powdery mildew-resistant *Arabidopsis* mutants. *PNAS*. **97**(4): 1897-1902. doi: 10.1073/pnas.030531997
- Wang M, Zhu X, Wang K, Lu C, Luo M, Shan T, Zhang Z. (2018). A wheat caffeic acid 3-O-methyltransferase TaCOMT-3D positively contributes to both resistance to sharp eyespot disease and stem mechanical strength. *Scientific Reports*. **8**: 6543. doi: 10.1038/s41598-018-24884-0
- Yoon J, Choi H, An G. (2015). Roles of lignin biosynthesis and regulatory genes in plant development. *Journal of Integrated Plant Biology*. **57**(11): 902-912. doi: 10.1111/jipb.12422.
- Yuan M, Jiang Z, Bi G, Nomura K, Liu M, Wang Y, Cai B, Zhou JM, He SY, Xin XF. (2021). Pattern-recognition receptors are required for NLR-mediated plant immunity. *Nature*. **592**(7852):105-109. doi: 10.1038/s41586-021-03316-6.
- Zechmann B, Möstl S, Zellnig G (2022). Volumetric 3D reconstruction of plant leaf cells using SEM, ion milling, TEM, and serial sectioning. *Planta*. **255**: 118. doi: 10.1007/s00425-022-03905-3.

6.7 Appendix

6.7.1 Wheat cell wall orthologues for lignin targets

List of wheat orthologues identified from literature search and expression patterns confirmed through the wheat expression browser. Due to the hexaploid nature of wheat, the top three orthologues are identified for each gene. Plant species are *Triticum aestivum* (*Ta*), *Triticum monococcum* (*Tm*), *Sorghum bicolor* (*Sb*), *Hordeum vulgare* (*Hv*).

Name	ID info	Gene	Rationale	Species	Reference	Orthologues
TaCOMT-3D	AK332908	COMT	Eyespot resistance, identified via transcriptomics. Confirmed function by silencing and overexpression. S-lignin.	<i>Ta</i>	Wang et al. (2018)	TraesCS3A02G534900
						TraesCS3B02G612000
						TraesCS3D02G540200
TaCAD	Traes_6BS_6477 278C5	CAD	Potential QTL-Fhb2 to FHB	<i>Ta</i>	Dhokane et al. (2016)	-
Ta4CL	Traes_6BS_CC8 E63D7F	4CL	Potential QTL-Fhb2 to FHB	<i>Ta</i>	Dhokane et al. (2016)	-
TmPAL	EU099348	PAL	Role in powdery mildew penetration defence	<i>Tm</i>	Bhuiyan et al. (2009)	TraesCS6A02G222800
						TraesCS6B02G258500
						TraesCS6D02G212400
TmC3H	EU099347	C3H	Role in powdery mildew penetration defence	<i>Tm</i>	Bhuiyan et al. (2009)	TraesCS5A02G214800
						TraesCS5B02G209100
						TraesCS5D02G217200
TmF5H	EU099349	F5H	Role in powdery mildew penetration defence (expression analysis followed by TIGS RNAi).	<i>Tm</i>	Bhuiyan et al. (2009)	TraesCS2A02G490100
						TraesCS2B02G518400
						TraesCS2D02G490500

Tm4CL	EU099350	4CL	Role in powdery mildew penetration defence (expression analysis followed by TIGS RNAi).	<i>Tm</i>	Bhuiyan et al. (2009)	TraesCS2A02G145800
						TraesCS2D02G150400
						TraesCS2B02G171200
TmCCoAMT	EU099351	CCoAMT	Role in powdery mildew penetration defence (expression analysis followed by TIGS RNAi).	<i>Tm</i>	Bhuiyan et al. (2009)	TraesCS7A02G240300
						TraesCS7B02G135900
						TraesCS7D02G239200
TmCCR	EU099352	CCR	Role in powdery mildew penetration defence (expression analysis followed by TIGS RNAi).	<i>Tm</i>	Bhuiyan et al. (2009)	TraesCS7A02G149000
						TraesCS7B02G052600
						TraesCS7D02G150500
TmCAD	EU099353	CAD	Role in powdery mildew penetration defence (expression analysis followed by TIGS RNAi).	<i>Tm</i>	Bhuiyan et al. (2009)	TraesCS6A02G173700
						TraesCS6B02G201600
						TraesCS6D02G162800
TmCAOMT	DQ862834	CAOMT	Role in powdery mildew penetration defence (expression analysis followed by TIGS RNAi).	<i>Tm</i>	Bhuiyan et al. (2009)	TraesCS7A02G333900
						-
						-
TaCOMT1	AY226581	COMT	Induction by Hessian fly larvae.	<i>Tm</i>	Jang, Johnson and Seo (2005)	TraesCS7B02G245500
						TraesCS7D02G341500
						-
		COMT		<i>Sb</i>		TraesCS3B02G612000

SbCOMT (bmr12)	SORBI_3007G04 7300		<i>Fusarium</i> susceptibility gene from Sorghum. Impairment leads to reduced <i>Fusarium</i> colonisation.		Funnell-Harris, Pedersen and Sattler (2010)	TraesCS3D02G540200
						TraesCS3A02G534900
SbCAD (bmr6)	SORBI_3004G07 1000	CAD	<i>Fusarium</i> susceptibility gene from Sorghum. Impairment leads to reduced <i>Fusarium</i> colonisation.	<i>Sb</i>	Funnell-Harris, Pedersen and Sattler (2010)	TraesCS6A02G173700
						-
						-
TaCAD1	GU563724	CAD	No pathology data.	<i>Ta</i>	Ma (2010)	TraesCS6B02G201600
						TraesCS6D02G162800
						-
TaCAD12	BT008979	CAD	Eyespot resistance	<i>Ta</i>	Rong et al. (2016)	TraesCS7A02G350500
						TraesCS7B02G232400
						TraesCS7D02G328300
BdPTAL	BdPTAL1 XP_003575396	PTAL	Tyrosine lignin synthesis shortcut identified in <i>Bd</i> , preference for S monolignols. Role in defence not yet studied.	<i>Bd</i>	Barros et al. (2016)	TraesCS6B02G258400
						TraesCS6D02G212200
						TraesCS6A02G222900
TaCCR	DQ449508	CCR	No pathology data.	<i>Ta</i>	Ma (2007)	TraesCS5A02G225100
						TraesCS5B02G223700
						TraesCS5D02G232400
HvPAL	CUST_2684_PI39 0587928	PAL		<i>Hv</i>	-	TraesCS2A02G196700.1
						TraesCS2B02G224300.1

			Expressed with <i>Blumeria graminis</i> , <i>Magnaporthe oryzae</i> , <i>Puccinia graminis</i>			TraesCS2D02G204700.1
HvCOMT	CUST_17725_PI3 90587928	COMT	Expressed with <i>Blumeria graminis</i> , <i>Magnaporthe oryzae</i> , <i>Puccinia graminis</i>	Hv	-	TraesCS1A02G032400.1
						TraesCS1B02G040900.1
						TraesCS1D02G033900.1
TaLAC4	TraesCS3B02G3 92700	LAC	Closest to stem laccase LAC17	Ta	Soni et al. (2020)	TraesCS3B02G392700
						TraesCS3D02G354200
						TraesCS3A02G360400
TaNAC032	CDM82556.1	NAC	Role in <i>Fusarium graminearum</i> resistance- in Fhb1. Regulates lignin biosynthesis - including TaLAC4	Ta	Soni et al. (2021)	TraesCS3B02G194000
						TraesCS3D02G170000
						TraesCS3A02G162900

Chapter 7: General discussion

This thesis has explored the colonisation mechanisms deployed by *F. graminearum* by taking a number of different experimental approaches. This chapter summarises the key findings, implications and future perspectives for further understanding the wheat-*F. graminearum* pathosystem. This chapter also discusses new, unanswered questions that have arisen and the technological advances that have occurred over the duration of this PhD project. Finally, in this chapter I discuss future control strategies for Fusarium Head Blight in light of these findings.

7.1 Summary of Key findings

Findings from this PhD project have contributed to our understanding of the wheat-*F. graminearum* interaction and are briefly summarised below:

- DON is secreted during early infection stages to dampen host defence responses, one of which is the deposition of callose at plasmodesmatal pit fields.
- *F. graminearum* hyphae use plasmodesmatal pit fields to traverse between adjacent cells in highly lignified tissues, such as the wheat rachis. DON may facilitate this by preventing callose deposition.
- Callose deposition may be locally induced in the absence of DON using the $\Delta Tri5$ strain and provides durable disease resistance to subsequent WT infection.
- *F. graminearum* secretes a glycoside hydrolase 81 family enzyme (GH81) that is predicted to catalyse the breakdown of callose at plasmodesmata during infection.
- Cell wall composition in the wheat rachis, specifically lignification at specific developmental stages, may cause the restricted infection period around anthesis as well as force *F. graminearum* hyphae through plasmodesmatal pit fields.

Together, these novel findings have altered the current working model for *F. graminearum*-wheat host tissue colonisation by cell wall traversing and are summarised in Fig. 7.1.

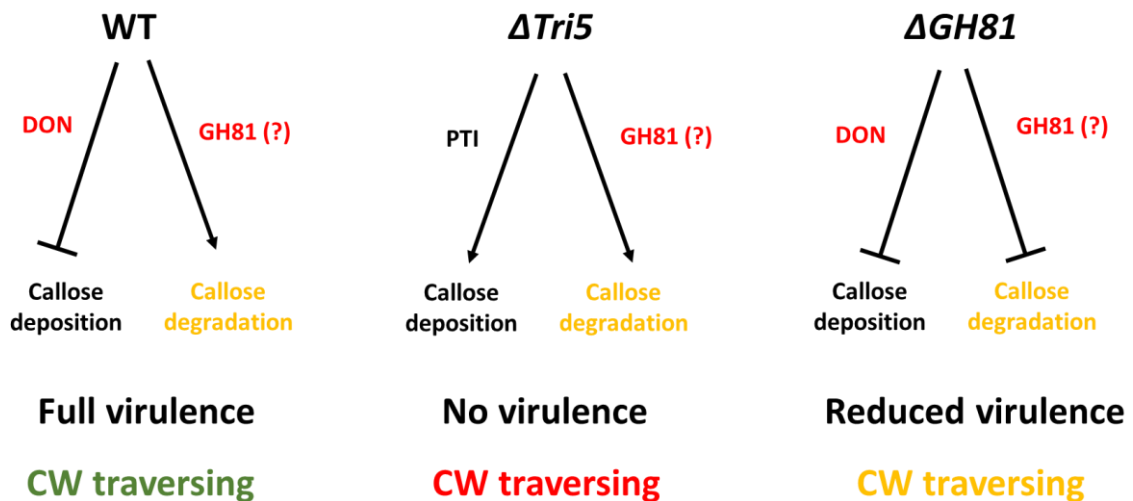


Fig. 7.1 Working model for cell wall (CW) traversing through plasmodesmatal pit fields in wheat rachis tissue by *Fusarium graminearum*. In the WT interaction, *F. graminearum* secretes the trichothecene mycotoxin DON, which putatively prevents callose deposition and the GH81 enzyme which is hypothesised to catalyse the degradation of β -1,3-glycosidic bonds in the glucose polymer callose. In the WT interaction, with both DON and FgGH81, full virulence is observed with cell wall traversing by invasive hyphae. In the single gene deletion mutant $\Delta Tri5$, the DON mycotoxin is not synthesised, and the PTI branch of plant immunity is not dampened so callose deposition is increased. While it is hypothesised that GH81 is still secreted during early infection, the presence of GH81 does not overcome the wheat immune responses and virulence in the wheat rachis is completely attenuated with no cell wall crossings observed. In the $\Delta GH81$ single gene deletion mutant, DON is still synthesised whereas the ability to degrade callose is hypothesised to be attenuated, pending further confirmation. This led to reduced virulence into the neighbouring wheat spikelets, however it has not yet been explored whether cell wall crossings are reduced in this interaction.

7.2 Original hypotheses and research questions

As set out at the beginning of this thesis, four hypotheses were proposed to guide exploration into the wheat rachis colonisation mechanisms by *F. graminearum*. These will now be explored and discussed based on the findings obtained.

1. The mycotoxin Deoxynivalenol (DON) facilitates host-tissue colonisation in wheat rachis tissue.

This hypothesis was first set out at the onset of this PhD project following prior reports in the literature regarding a single gene deletion mutant in the trichothecene mycotoxin biosynthesis pathway, $\Delta Tri5$, which encodes the essential enzyme trichodiene synthase (TRI5) and marks the first committed step

of DON biosynthesis (Jansen et al., 2005; Procter et al., 1995). While it has long been known that TRI5, and thus DON, is an essential virulence factor in the wheat- *F. graminearum* compatible interaction, the specific underlying mechanisms had not yet been elucidated. DON is a toxin known to target the ribosomes (Brown et al., 2004) and thus has a role in the broad-spectrum dampening of protein translation. Subsequently, ribotoxicity also causes apoptosis (programmed cell death) (Pestka, 2008). What specific proteins and/or signaling pathways that DON targets to facilitate infection remained unanswered at the beginning of this project.

To decipher the differences in host-tissue colonisation between $\Delta Tri5$ and WT *F. graminearum*, a microscopic analysis of wheat spikelet tissues during early stages of infection was initiated. In the lemma and palea tissues, widespread colonisation and cellular degradation was observed, but this was restricted to the thinner-walled abaxial cell layers during $\Delta Tri5$ colonisation. Most surprisingly, cell-to-cell traversing through plasmodesmatal pit fields, as previously reported in the WT interaction in wheat rachis tissue by Brown et al. (2012), into adaxial cell layers was never observed. Adaxial cell layers of the lemma and palea contain more lignin, as shown by Toluidine blue staining and later in chapter 6 with potassium permanganate staining, and are visibly thicker. It was then hypothesised that DON dampens callose deposition at plasmodesmata during biotic stress, which is an effective host defence response to *F. graminearum* infection when CWDEs are less effective and/or require more energy to break down cell walls. If DON was a potential key to this interaction, it was then hypothesised that the lack of biosynthesis of DON by $\Delta Tri5$ could be chemically complemented by addition of DON with spore inoculum. This was not the case and led us further to hypothesise that DON is secreted with spatial and temporal precision during host-tissue colonisation. In addition, DON has been shown to be rapidly conjugated to the less toxic DON-3-glucoside in barley (Li et al., 2015) and becomes both undetectable by standard ELISA competitive assay kits and trafficable throughout the plant.

2. Callose deposition is a defence response to *F. graminearum* infection in wheat spikes.

With regards to the potential interaction between callose and DON, obtaining many samples for statistically robust experiments through bioimaging was

challenging. Resin embedding and sectioning of wheat spikelet tissues was incredibly time consuming, even prior to immunolabelling and confocal imaging. Microtomy was a major bottleneck in this PhD project and although this could in part be solved by automatic sample preparation, resin integrity was not good on all sections and required vetted by eye before transferring to slides. For simpler modelling of hyphal colonisation of wheat rachis tissues, μ CT scanning is emerging as a non-invasive alternative (Le et al., 2019), but still requires improvements to resolution before this technique can be utilised to great effect.

Despite sample preparation bottlenecks, results from immunolabelling callose deposits in chapter 3 indicated that callose is upregulated in both the WT and $\Delta Tri5$ interactions, and also when DON is applied. Due to the toxicity of DON, it is likely that DON acts as a DAMP and activates the PTI branch of the plant immune system, which involves callose deposition at plasmodesmatal pit fields. Due to generic application here, it is not surprising that callose deposition is upregulated compared to the control, but it was interesting that the DON-deficient mutant $\Delta Tri5$ had comparable callose deposits per cell at both sampled time points to WT *F. graminearum*. If DON was the only hindrance on callose deposition, we would expect comparable levels to the DON treatment. This led to further experiments in chapter 4, exploring the PTI responses to $\Delta Tri5$ and whether specific secretion of DON by subsequent inoculation of spikelet with WT *F. graminearum* could overcome the wheat defence responses. Very surprisingly, pre-inoculation of wheat spikelets with $\Delta Tri5$ and the PAMP-elicitor chitin prevented subsequent WT infection across 24 and 48hr timescales. This indicates that wheat defences are actually robust against *F. graminearum* and that toxins, specifically of the trichothecene class, have evolved to overcome these. This is supported by a recent analysis by Qu et al. (2024), who reviewed the presence of various toxin families across the *Fusarium* spp. In the *Fusarium sambucinum* species complex, to which *Fusarium graminearum* belongs, toxin classes are most numerous across the entire *Fusarium* spp. phylogeny and this also correlates with a reduction in genome size (Armer et al., 2024b). It is postulated that the reduction in lineage specific (LS) chromosomes and genome size is due to functional redundancy induced by toxin presence. Hence, when the ability to produce these toxins is removed, *F. graminearum* cannot compensate (Fig. 7.2). This may also explain why very few effectors have so far been identified

single copy is present in the *F. graminearum* genome. The FgGH81 predicted protein sequence is also highly conserved across the Ascomycota indicating an important role for this enzyme. Single gene deletion analysis of FgGH81 led to a reduced, but not completely attenuated, disease phenotype. However, further experiments are required to confirm callose degradation *in planta*, as outlined in chapter 5.

3. Developmental changes in wheat rachis morphology control the short infection window surrounding anthesis for successful *F. graminearum* disease formation in wheat spikes.

The infection window of *F. graminearum* is typically restricted to the period of anthesis, which lasts ~5 days for the entire wheat spike. Infections either much before or after this time period leads to reduced, or completely attenuated, virulence. However, as presented in section [6.4.5](#) infections 2 weeks after anthesis lead to a sudden breakthrough of infection between 10 and 14 days later (i.e. between 3 and 4 weeks from the typical infection timepoint). Therefore, it is hypothesised that the opening and/or route(s) through which *F. graminearum* hyphae use to grow through the wheat rachis closes and subsequently re-opens. Sectioning indicated that this could revolve around a lignin barrier through which even WT *F. graminearum* producing trichothecene mycotoxins cannot overcome. The timing of this opening during development may be one of the differences between resistant and susceptible wheat cultivars, but this requires further investigation.

4. *F. graminearum* hyphae need to pass through plasmodesmatal pit fields due to the lignin-rich cell wall composition in the wheat rachis.

As an inherently highly lignified tissue, the cell walls of the wheat rachis are difficult to degrade through the secretion and action of CWDEs. Equally, fragments of the cell wall which result from hydrolysis act as DAMPs (Hou et al., 2019) and activate the PTI branch of plant immunity, one aspect of which is callose deposition at plasmodesmata, as discussed. There is also reason to postulate that maintaining host cell wall structural integrity is essential for *F. graminearum* infection, with fitness penalties incurred when navigating through highly degraded host tissues. This balance to ensure retention of cell wall structural integrity is likely to be particularly pertinent to keep active host sink

tissues such as the wheat spikelet, thereby ensuring a continuous nutrient supply for the fungal hyphae.

As a result of devising and carrying out experiments to test the four hypotheses originally set, the following research questions set out at the beginning of this thesis could be answered:

1. What is the role of DON during infection of wheat floral tissues?

To dampen wheat host defence response, which include the deposition of callose at plasmodesmata pit fields.

2. Does DON overcome PAMP-tiggered immunity?

Excretion of DON by hyphae after PTI induction does not overcome PTI.

3. Does *Fg* directly degrade specific cell wall component(s) at plasmodesmata through the excretion of glycoside hydrolase enzymes?

Putatively yes through the secretion of a glycoside hydrolase 81 enzyme.

4. What cell wall components pose an effective barrier to *Fg*, forcing cell wall traversing through plasmodesmatal pores?

Lignin appears to be integral to cell wall resistance and encouragement of cell wall traversing.

7.3 Technological advancements

This PhD was initiated at an exciting time in the field of plant-pathogen interactions. While the first *Fusarium graminearum* reference genome was published back in 2003 by the BROAD institute and subsequently improved by Cuomo et al. (2007), advances in annotations and more comprehensive sequencing reads have expanded our ability to use the genome with more accuracy (King et al., 2017). The full first wheat genome was published in 2018 (IWGSC, 2018) and tools such as the wheat expression browser (wheatexpression.org) that collates RNASeq data with a useable user interface are making bioinformatic tools more widespread and accessible. Also more recently, RNASeq analysis of the wheat – *F. graminearum* interaction across different disease stages has allowed for stage specific analysis of infection (Dilks et al., 2019; Kroll et al., 2024).

Since beginning this project, a number of technologies have emerged that would further help to elucidate the spatial and temporal stages of *F. graminearum* infection in the wheat rachis, alongside new and remaining research questions that have arisen as a result of the outcomes of this PhD project:

1. What is the size exclusion limit for *Fusarium graminearum* hyphal constriction?

One remaining question from the observations obtained from the resin microscopic analysis in chapter 3 was the size exclusion limit of hyphal constriction that occurred when passing from one adjacent cell to another through plasmodesmatal pit fields. While typical constriction appeared to be around 1µm, the size exclusion limit of hyphae has not yet been determined and the size of pit fields in wheat crops may be a source of resistance to *F. graminearum* infection if below this physical limit. Microfluidics, often referred to as ‘organ-on-a-chip’ technology, could provide an *in vitro* opportunity to study this interaction, particularly as it is nearly impossible to conduct live-cell imaging of this interaction in the wheat rachis tissue. Fukuda et al. (2021) have explored these systems, determining that hyphal polarity post-constriction correlates with speed of growth, but more importantly that the related *Fusarium oxysporum* appeared unphased when challenged with constriction. This may indicate that *F. graminearum* is also well adapted to constriction. Current limitations of these technologies have yet to determine the hyphal constriction / size exclusion limit for fungal hyphae to pass through, but nitrocellulose-based systems have found that hyphae of another *Fusarium* species are able to pass through filters with diameters of 0.38µm (Cho et al., 2023). Whether microfluidic systems are able to go beyond this, with some advancements, is yet to be determined but this technologies are well posed to explore what triggers and/or how hyphae begin constriction *in planta*, forming the basis of chemotropism and/or thigmotropism experiments.

2. How durable is PAMP-triggered immunity to *F. graminearum* infection in wheat spikes?

Co-inoculation experiments, as set out in chapter 4, demonstrated how pre-inoculation with the avirulent, DON-deficient $\Delta Tri5$ strain of *F. graminearum* prevented subsequent infection by the WT strain PH-1. Similar phenotypes were observed when the pre-inoculation of the wheat spike was replaced with the

PAMP elicitor, and fungal cell wall component, chitin. Exactly what wheat defences are upregulated were not dissected in this project, but have been explored with respect to *F. graminearum* previously (Hao et al., 2022). In the future, it would be possible to explore if these responses are chitin specific, or if resistance is equally upheld with other elicitors of the PTI branch of plant immunity such as flg22. However, this resistance was not observed through spray inoculation experiments, and the duration of resistance in point-inoculated spikelets was not thoroughly tested in this project due to time and financial constraints. For example, this could be further tested beyond 48hrs. The differential responses to chitin and/or $\Delta Tri5$ and the WT strain could be explored through single-cell spatial transcriptomics (otherwise known as single-cell RNA-sequencing; Giacomello, 2021). This could elucidate the differential defence responses across tissues, in this instance the outer glume in spray inoculations, and the rachis, lemma and palea tissues in the point inoculation experiments. Sensitivity to PAMPs could relate to the relative fitness importance of each tissue, but also their role in reproduction (lemma and palea), support (rachis) and protection (glume).

From an alternate angle on the fungal side, single-cell spatial transcriptomics could help to pinpoint at exactly which spatial point TRI5 and other genes of the TRI gene biosynthetic cluster, are upregulated during infection and confirm our hypothesis that DON is excreted with spatial and temporal precision *in planta*. To this end, the development of Förster resonance energy transfer (FRET) biosensors for tracking DON and its interactors *in planta*, similarly to plant hormones such as auxin (Isoda et al., 2021), could help to truly understand the spatial and temporal role of this essential component of infection. Proximity labelling can similar be used for tracking interactors of proteins (Qin et al., 2021) and has been explored in wheat in response to abiotic stress (Zhang et al., 2022), but both of these technologies have difficulties in the rachis tissue.

3. Are plasmodesmatal pit field crossings essential for virulence in wheat spikes?

While it is hypothesised in this thesis, and alluded to in the results presented, that plasmodesmatal pit field crossings are essential for traversing through lignified wheat rachis tissue, this could be further supported by full tissue modelling of infection. Several technologies are developing in the field of plant-pathogen

interactions, and include (micro) μ CT scanning and serial block SEM/ TEM imaging for modelling infection. Micro CT scanning, or equally nanoCT of the wheat rachis alone, could be used as a non-invasive technique to model hyphal infections over time, pinpointing where and how often cell wall crossings take place. This has so far been conducted at the whole wheat grain scale (Le et al., 2019), but not yet to the resolution required for visualising hyphae. Other technical advances, albeit time and cost intensive, include serial block SEM/ TEM (Paterlini and Belevich, 2022), which would be able to capture the resolution required for imaging plasmodesmata themselves, and High-Resolution Volume Electron Microscopy (Using Plasma-Focused Ion Beam Scanning Electron Microscopy) which similarly may aid the mapping of plasmodesmatal pit fields across whole plant cells (Rotkina et al., 2024).

7.4 Challenges and future perspectives

Further new technologies could be applied to the wheat-*F. graminearum* interaction. Underpinning much of the bottleneck in elucidating aspects of the wheat- *F. graminearum* infection is the fact that it is inherently difficult to do any live cell bioimaging in wheat spikelet and rachis tissues. Utilising other organisms, as attempted within this thesis with *Arabidopsis thaliana*, was not successful. There remains a need for a PH-1 vs $\Delta Tri5$ wheat infection time course RNASeq dataset to fully explore the compensatory mechanisms of a lack of DON from the fungal side, and determine which wheat specific defence responses are dampened by the presence of DON in the WT interaction. In addition, a *F. graminearum* pangenome would allow researchers to account for the genetic variety of field isolates and best pinpoint mutual targets for chemical and genetic control of this destructive pathogen.

In light of the findings presented in this thesis, novel control strategies surrounding the revealed essentialism of hyphal constriction through plasmodesmatal pit fields have emerged. While it appears that DON dampens host immune responses, including the deposition of callose at plasmodesmata, the mechanisms by which *F. graminearum* actually constrict could be exploited as a source of novel chemical and/or genetic control. For a hyphae to retain normal growth after constrained growth, repolarisation of its membrane must occur for orientation (Gow, Latge and Munro, 2017). While many other, faster

growing phytopathogens seem unable to repolarise (Fukuda et al. 2021), *Fusarium* spp. have so far not been tested to its limit and thus may indicate an evolutionary pressure for this. The Spitzenkörper (apical body) is a structure that sits behind the growing hyphal front (apex) and organises hyphal growth through the arrangement of macro- and microvesicles (which contain different cell wall synthesis functions), actin and ribosomes (Riquelme and Sánchez-León, 2014). Interrupting this structure could pose as a filamentous fungal-specific target for chemical control of *F. graminearum*.

Other preliminary findings of this thesis suggest that a window for infection around anthesis closes and reopens as senescence begins in the wheat head. The speed of this change could be explored to prevent *F. graminearum* infection, with further studies for genetic control looking at the pace of closing this window and may be the underlying factor between resistant and susceptible wheat varieties.

7.5 Final conclusion and summary

The experiments and results presented within this thesis have advanced our knowledge of the wheat- *F. graminearum* pathosystem, particularly with respect to the hyphal navigation through the wheat spikelet tissue. The trichothecene mycotoxin DON is essential for this process and likely dampens callose deposition at plasmodesmatal pit fields, but through as yet unknown mechanisms. RNASeq of the wheat- $\Delta Tri5$ interaction will help to solve this puzzle. In the absence of DON, wheat defences activated through the PTI branch of plant immunity are sufficient to prevent subsequent infection with WT *F. graminearum*, highlighting the importance of rapid and sustained upregulation of general wheat responses to biotic stress, which likely includes callose deposition at plasmodesmata. On the other side of this interaction, single gene deletion of a secreted enzyme predicted to degrade callose led to a reduction in virulence, but further experiments are required to validate this interaction. Finally, it appears that restriction of the infection window to anthesis may be due to a developmental change, and new technologies such as μ CT scanning could elucidate through non-invasive modelling of development of this largely understudied tissue. Lignin in wheat cell walls appears to be a durable barrier to hyphae *in planta* and upregulation of this cell wall component could be further studied through transcriptomics.

Trichothecene mycotoxins were first discovered as virulence factors in the wheat-*F. graminearum* prior to my own existence on this planet. However, how they facilitated infection was not revealed until this project, which has also been published in *Molecular Plant Pathology* (Armer et al., 2024a). This goes to show that often picking up interesting leads from years past with new angles and technologies can yield new and interesting results. However, while this PhD has provided some answers, it has stimulated many more research questions. I have high hopes for the future of this field and look forward to tracking advancements in years to come. As I leave my PhD, the prospect of utilising gene editing technologies errs ever closer in the UK, and hope for controlling not just *F. graminearum*, but also many other plant pathogens, by genetic means becomes a realistic prospect. However, to underpin this and provide durable resistance, we must better understand the infection mechanisms of phytopathogens in their plant hosts.

7.6 References

Armer VJ, Kroll E, Darino M, Smith DP, Urban M, Hammond-Kosack KE, (2024b). Navigating the *Fusarium* Species Complex: Host-Range Plasticity, Niche Diversification and Genome Variations. *Fungal Biology*. **In Press**. doi: 10.1016/j.funbio.2024.07.004.

Armer VJ, Urban M, Ashfield T, Deeks MJ, Hammond-Kosack KE. (2024a). The trichothecene mycotoxin deoxynivalenol facilitates cell-to-cell invasion during wheat-tissue colonisation by *Fusarium graminearum*. *Molecular Plant Pathology*. **25**(6): e13485. doi: 10.1111/mpp.13485.

Brown DW, Dyer RB, McCormick SP, Kendra DF, Plattner RD. (2004). Functional demarcation of the *Fusarium* core trichothecene gene cluster. *Fungal Genetics and Biology*. **41**(4), 454-462. doi: 10.1016/j.fgb.2003.12.002.

Cho E, SH Lee, Jeong M, De Mandal S, Park S, Nam SW, Byeun DG, Choi JK, Lee Y, Shin J, Jeon J. (2023). Genetic and transcriptomic analysis of hyphal constriction based on a novel assay method in the rice blast fungus. *bioRxiv*. doi: 10.1101/2023.06.14.545034.

Cuomo CA, et al. (2007) The *Fusarium graminearum* Genome Reveals a Link Between Localized Polymorphism and Pathogen Specialization. *Science*. **317**:1400-1402. doi: 10.1126/science.1143708.

Dilks T, Halsey K, De Vos RP, Hammond-Kosack KE, Brown NA (2019). Non-canonical fungal G-protein coupled receptors promote *Fusarium* head blight on wheat. *PLoS Pathogens*. **15**(4): e1007666. doi: 10.1371/journal.ppat.1007666.

- Fukuda S, Yamamoto R, Yanagisawa, N, Takaya N, Sato Y, Riquelme M, Takeshita N. (2021). Trade-off between Plasticity and Velocity in Mycelial Growth. *mBio*, **12**(2): e03196-20. doi: 10.1128/mbio.03196-20.
- Giacomello S. (2021). A new era for plant science: spatial single-cell transcriptomics. *Current Opinion in Plant Biology*. **60**: 102041. doi: 10.1016/j.pbi.2021.102041.
- Gow NAR, Latge J, Munro CA. (2017). The Fungal Cell Wall: Structure, Biosynthesis, and Function. *Microbiology Spectrum*. **5**(3). doi: 10.1128/microbiolspec.funk-0035-2016.
- Hao G, Tiley H, McCormick S. (2022). Chitin Triggers Tissue-Specific Immunity in Wheat Associated with Fusarium Head Blight. *Frontiers in Plant Science*. **13**: 832502. doi: 10.3389/fpls.2022.832502.
- Hou S, Liu Z, Shen H, Wu D. (2019). Damage-Associated Molecular Pattern-Triggered Immunity in Plants. *Frontiers in Plant Science*. **10**: 646. doi: 10.3389/fpls.2019.00646.
- Isoda R, Yoshinari A, Ishikawa Y, Sadoine M, Simon R, Frommer WB. (2021). Sensors for the quantification, localization and analysis of the dynamics of plant hormones. *The Plant Journal*. **105**(2): 542-557. doi: 10.1111/tpj.15096.
- Jansen C, von Wettstein D, Schäfer W, Kogel K-H, Felk A, Maier FJ. (2005). Infection patterns in barley and wheat spikes inoculated with wild-type and trichodiene synthase gene disrupted *Fusarium graminearum*. *PNAS*. 102(46), 16892- 16897. doi: 10.1073/pnas.0508467102.
- Kanja C, Hammond-Kosack KE. (2020). Proteinaceous effector discovery and characterization in filamentous plant pathogens. *Molecular Plant Pathology*. **21**(10): 1353-1376. doi: 10.1111/mpp.12980.
- King R, Urban M, Hammond-Kosack KE. (2017). Annotation of *Fusarium graminearum* (PH-1) version 5.0. *Genome Announcements*. **5**. doi: 10.1128/genomea.01479-16.
- Kroll EK, Bayon C, Rudd J, Armer V, Magaji- Umashankar A, Ames R, Urban M, Brown NA, Hammond-Kosack KE. (2024). A conserved fungal Knr4/Smi1 protein is vital for maintaining cell wall integrity and host plant pathogenesis. *bioRxiv*, 2024.05.31.596832; doi: 10.1101/2024.05.31.596832.
- Le TDQ, Alvarado C, Girousse C, Legland D, Chateigner-Boutin A. (2019). Use of X-ray micro computed tomography imaging to analyze the morphology of wheat grain through its development. *Plant Methods*. **15**:84. doi: 10.1186/s13007-019-0468-y.
- Li X, Shin S, Heinen S, Dill-Macky R, Berthiller F, Nersesian N, Clemente T, McCormick S, Muehlbauer GJ. (2015). Transgenic Wheat Expressing a Barley UDP-Glucosyltransferase Detoxifies Deoxynivalenol and Provides High Levels of Resistance to *Fusarium graminearum*. *Molecular Plant Microbe Interactions*. **28**(11): 1237–1246. doi: 10.1094/MPMI-03-15-0062-R.
- Riquelme M, Sánchez-León E. (2014). The Spitzenkörper: a choreographer of fungal growth and morphogenesis. *Current Opinion in Microbiology*. **20**: 27-33. doi: 10.1016/j.mib.2014.04.003.

- Paterlini A, Belevich I. (2022). Serial Block Electron Microscopy to Study Plasmodesmata in the Vasculature of *Arabidopsis thaliana* Roots. In: Benitez-Alfonso Y, Heinlein M. (eds) Plasmodesmata. *Methods in Molecular Biology*, **2457**. Humana, New York, NY. doi: 10.1007/978-1-0716-2132-5_5
- Pestka JJ. (2008). Mechanisms of Deoxynivalenol-Induced Gene Expression and Apoptosis. *Food Additives and Contamination Part A: Chemistry, Analysis, Control, Exposure and Risk Assessment*. **25**(9): 1128–1140. doi: 10.1080/02652030802056626.
- Proctor RH, Hohn TM, McCormick SP. (1995). Reduced virulence of *Gibberella zeae* caused by disruption of a trichothecene toxin biosynthetic gene. *Molecular Plant Microbe Interactions*. **8**(4), 593-601. doi: 10.1094/mpmi-8-0593.
- Qin W, Cho KF, Cavanagh PE, Ting AY. (2021). Deciphering molecular interactions by proximity labelling. *Nature Methods*. **18**: 133-143. doi: 10.1038/s41592-020-01010-5.
- Qu Z, Ren X, Du Z, Hou J, Li Y, Yao Y, An Y. (2024). *Fusarium* mycotoxins: The major food contaminants. *mLife*. **3**(2): 176-206. doi: 10.1002/mlf2.12112.
- The International Wheat Genome Sequencing Consortium (IWGSC) *et al.* (2018). Shifting the limits in wheat research and breeding using a fully annotated reference genome. *Science*. **361**(6403): 7191. doi: 10.1126/science.aar7191.
- Zhang K, Li Y, Huang T, Li Z. (2022). Potential application of TurboID-based proximity labeling in studying the protein interaction network in plant response to abiotic stress. *Frontiers in Plant Science*. **13**: 974598. doi: 10.3389/fpls.2022.974598.

Appendix 1

Armer VJ, Kroll E, Darino M, Smith DP, Urban M, Hammond-Kosack KE, (2024). Navigating the *Fusarium* Species Complex: Host-Range Plasticity, Niche Diversification and Genome Variations. *Fungal Biology*. **In Press**. doi: 10.1016/j.funbio.2024.07.004.



British Mycological
Society promoting fungal science

Contents lists available at ScienceDirect

Fungal Biology

journal homepage: www.elsevier.com/locate/funbio



Navigating the *Fusarium* species complex: Host-range plasticity and genome variations

Victoria J. Armer^a, Erika Kroll^{a,1}, Martin Darino^{a,1}, Daniel P. Smith^{b,1}, Martin Urban^{a,1}, Kim E. Hammond-Kosack^{a,*}

^a *Protecting Crops and the Environment, Rothamsted Research, Harpenden, Herts, AL5 2JQ, UK*

^b *Intelligent Data Ecosystems, Rothamsted Research, Harpenden, Herts, AL5 2JQ, UK*

ARTICLE INFO

Handling Editor: Prof. G.M. Gadd

Keywords:

Genus *Fusarium*, diverse biologies
Non-pathogenic and pathogenic
Fusariosis
Mycotoxicosis
Niches and environments
Industrial uses
Genomes and pangenomes

ABSTRACT

The Ascomycete genus *Fusarium*, first introduced by Link in 1809, currently consists of 431 species and 3558 unclassified isolates and hybrids (according to NCBI Taxonomy lists). Collectively, these fungi have diverse lifestyles and infection cycles exploiting a wide range of environments, hosts, ecological niches, and nutrient sources. Here, we carried out a pan-*Fusarium* species review to describe and explore the glamorous, and the less attractive niches, exploited by pathogenic and endophytic species. We survey species that infect plant, human, animal and/or invertebrate hosts, free-living non-pathogenic species dwelling in land, air or water-based natural ecosystems, through to those species that exploit human-modified environments or are cultivated in industrial production systems. Fully sequenced, assembled and annotated reference genomes are already available for 189 *Fusarium* species, many at chromosome scale. In addition, for some of the world's most important species extensive single species pangenomes or closely related *formae speciales* genome clusters are readily available. Previous comparative genomics studies have focussed on taxonomically restricted clusters of *Fusarium* species. We now investigate potential new relationships between these vastly contrasting *Fusarium* biologies, niches and environmental occupancies and the evolution of their respective genomes.

1. Introduction

Fusarium species represent a vast and diverse group of filamentous ascomycete fungi (order *Hypocreales*, family *Nectriaceae*) that have gained considerable attention, primarily as plant pathogens and soil-dwelling saprotrophs (Dean et al., 2012; Leslie and Summerell, 2013; Coleman, 2016; Gordon, 2017; Figueroa et al., 2018; Abdel-Azeem et al., 2019a; Kanja et al., 2021; Moonjely et al., 2023; Nikitin et al., 2023), but more recently as human and animal pathogens (O'Donnell et al., 2016; Sáenz et al., 2020; Batista et al., 2020) as well as industrially useful species (Abdel-Azeem et al., 2019b). These fungi occupy an extensive range of niches and environments, demonstrating their ability to adapt and thrive in both ubiquitous and rarer ecological settings. Infectious *Fusaria* are typically present within moist soils, as hyphae associated with decaying plant debris or present as longer-lived resting spores for survival. Many species produce air and/or water-dispersed spores that either facilitate host infection cycles and/or transfer to additional

non-pathogenic niches. This pan-*Fusarium* species review will encompass several of the well-known pathogenic and sometimes mycogenic (toxin-producing) species, as well as the less well-known occurrences of *Fusarium* species thriving in the wide range of habitats this planet has to offer: snow to arid grasslands, marine life to oil.

For many *Fusarium* species, fully sequenced, assembled and annotated genomes and pangenomes are already available, many at chromosome scale (Appendix A.1). Typically, their genomes comprise between four and 12 core chromosomes with or without the presence of a smaller number of additional lineage specific (LS) chromosomes (technical terms are explained in Table 1; Li et al., 2020a), also known as accessory or supernumerary chromosomes. As in other fungal species, the presence or absence of a sexual cycle for a given species greatly influences the extent and range of repetitive sequences and transposons, and whether paralogous genes and gene family expansions are maintained or lost in each *Fusarium* genome/pangenome.

Many of the species in the genus *Fusarium* are now grouped within

* Corresponding author.

E-mail address: kim.hammond-kosack@rothamsted.ac.uk (K.E. Hammond-Kosack).

¹ EK, MD, DS and MU have contributed equally to this article.

<https://doi.org/10.1016/j.funbio.2024.07.004>

Received 1 October 2023; Received in revised form 8 May 2024; Accepted 4 July 2024

Available online 14 July 2024

1878-6146/© 2024 Published by Elsevier Ltd on behalf of British Mycological Society.

Table 1

Glossary of terms and abbreviations used in this review.

Term	Definition
Effectors	Small molecules or proteins secreted by pathogens including fungi to alter host-cell structure and function, and thus promote infection (Kamoun, 2006; Wilson and McDowell, 2022).
<i>Forma specialis</i> (pl. <i>Formae speciales</i> ; abbreviated as f. sp.)	An individual, or group of individuals (plural), within a fungal species adapted to a specific host.
Lineage-specific chromosome/s	Also known as accessory or supernumerary chromosomes that can be distinguished from core chromosomes of a species. Lineage-specific chromosomes are dispensable but can play important roles under specific conditions such as conferring pathogenicity towards a particular host (Li et al., 2020a).
Secondary metabolites	Organic compounds produced by organisms and not directly involved in growth, development, and reproduction. Primary metabolites are fundamentally required for normal cellular processes, whilst secondary metabolites are molecules used to communicate or interfere with other organisms (Khachatourians and Arora, 1999; Cray et al., 2013). Secondary metabolites are frequently synthesised from a single to a few small tightly clustered groups of genes which are co-ordinately expressed under specific conditions.
Species complex (SC)	A group of closely related fungal species. In <i>Fusarium</i> more than 430 species have been identified and are grouped in 23 species complexes (Bansal et al., 2019; Geiser et al., 2021). Some of the larger species complexes, which are also intensively investigated, include the <i>F. solani</i> complex, <i>F. oxysporum</i> complex, <i>F. sambucinum</i> complex, <i>F. incarnatum-equiseti</i> complex and <i>F. fujikuroi</i> complex.

specific species complexes based on phylogenomic and phylogenetic analyses. The most recent *Fusarium* phylogeny arising from a 19 orthologous protein-coding gene study (Geiser et al., 2021) is shown in Fig. 1. Within this phylogeny the largest species complexes identified include *F. sambucinum* (FSAMSC) (typically four or five core chromosomes and zero or two accessory chromosomes), *F. incarnatum-equiseti* (FIESC) (typically eight or nine core chromosomes and one accessory chromosome), *F. fujikuroi* (FFC) (typically 10–13 core chromosomes and zero to two accessory chromosomes), *F. oxysporum* (FOSC) (typically 11 core chromosomes and two to four accessory chromosomes) and one of the more basal lineages *F. solani* (FSSC) (typically nine to 12 core chromosomes and zero to three accessory chromosomes). A total of 23 species complexes are recognised within the genus *Fusarium* (Geiser et al., 2021).

This review will investigate interrelationships recently discovered between the vast and diverse range of *Fusarium* biologies (Fig. 2), nutrient acquisition strategies, host and non-host niche occupancies (Fig. 2) and the evolution of their genomes/pangenomes. This aims to be an extensive and comprehensive analysis of the *Fusarium* genus, summarising the knowns and unknowns, and inspiring future research into these fascinating filamentous fungi.

2. Impacts of *Fusarium* species on global food security

Wherever crops are grown, *Fusarium* spp. typically follow. The range of infection strategies employed by *Fusarium* allows for a wide range of host threats and the development of disease symptoms ranging from wilts, stem base, root and/or fruit rots to floral blights and seed/grain discolorations and/or shrivelling. Cultivation of the top primary and commodity crops (Fig. 2; Table 2; FAO, 2020a) are all, to some extent, infected by *Fusarium* spp. *Fusarium* species that are pathogenic to crops are ubiquitous in the environment. Reproduction is often fast, for example the *Fusarium* Head Blight-causing species *F. graminearum* can form ascospores (sexual spores) from an infected wheat plant within weeks to a few months from initial infection, and can be observed in as little as two weeks in culture in laboratory settings (Trail et al., 2002). The *Fusarium oxysporum* and *Fusarium solani* species complexes (described later) are responsible for vascular wilts across a vast range of crop hosts and can enter the vicinity of plants through groundwater, paradoxically blocking vascular elements, leading to a reduction in water uptake and the typically wilting disease phenotypes (Coleman, 2016; Edel-Hermann and Lecomte, 2019). Groundwater mediated spore dispersal of these species makes control incredibly hard in non-glasshouse food production systems.

2.1. *Fusarium* spp. infect a wide range of crops

F. sacchari causes the wilt Pokkah Boeng disease on sugarcane from the seedling stage onwards (Yao et al., 2020). *F. graminearum* and *F. culmorum* cause cereal seedling root rots and death, but later on head blight/head scab formation within the floral tissues of most small grain cereals, including wheat, barley, maize and rice from crop anthesis onwards (McMullen et al., 2012; Moonjely et al., 2023). *F. solani* and *F. oxysporum* are most often attributed to wilts and root rots found in dicotyledonous crops, but the same disease symptoms can also be caused by a wide range of other *Fusarium* species within other disease complexes (Table 2). Amongst the commodity crops, notable occurrences of *Fusarium* spp. in recent years have included the emergence of *F. oxysporum* f. sp. *cubense* Tropical Race 4, which causes Panama disease (vascular wilt) of bananas (Ploetz, 2015), and *F. xylarioides* which causes coffee wilt disease (Rutherford, 2007; Peck and Boa, 2023). Disease issues occur when new banana or coffee plantations are established in locations where the soil already contains the fungal propagules or where biosecurity procedures have not been strictly followed. Both of these interactions are explored further in our section on arborescent habitats. Whilst not exhaustive, these examples highlight the breadth of infection strategies deployed by *Fusarium* species to successfully cause such a range of diseases in so many different plant host species, host niches and cropping systems (Fig. 2). Collectively, *Fusarium* species are an ever-growing global threat to food security.

2.2. *Fusarium* Head Blight/Head Scab in cereals

In the small grain cereals, including oats, barley and wheat, many members of the *Fusarium sambucinum* species complex, including *F. graminearum* and *F. culmorum*, are the primary causal agents of *Fusarium* Head Blight disease, aka *Fusarium* Head Scab (reviewed McMullen et al., 2012; Kanja et al., 2021; Moonjely et al., 2023) (Fig. 3). The ongoing global importance of the *Fusarium*-cereal pathosystem cannot be underestimated due to the presence of large epidemic/pandemic-scale outbreaks occurring on an almost annual basis in one or more continents (Vaughan et al., 2016). Besides reduced grain yield and grain quality, these species contaminate the developing grain with harmful mycotoxins which are damaging to human, livestock and natural ecosystem health (Kanja et al., 2021; Johns et al., 2022; Moonjely et al., 2023). Those of the trichothecene class, such as the water soluble deoxynivalenol (DON) and its acetyl derivatives (3-A-DON and 15-A-DON) pose such high risks that harvested grains and shipped grains are routinely tested for their presence. Many individual

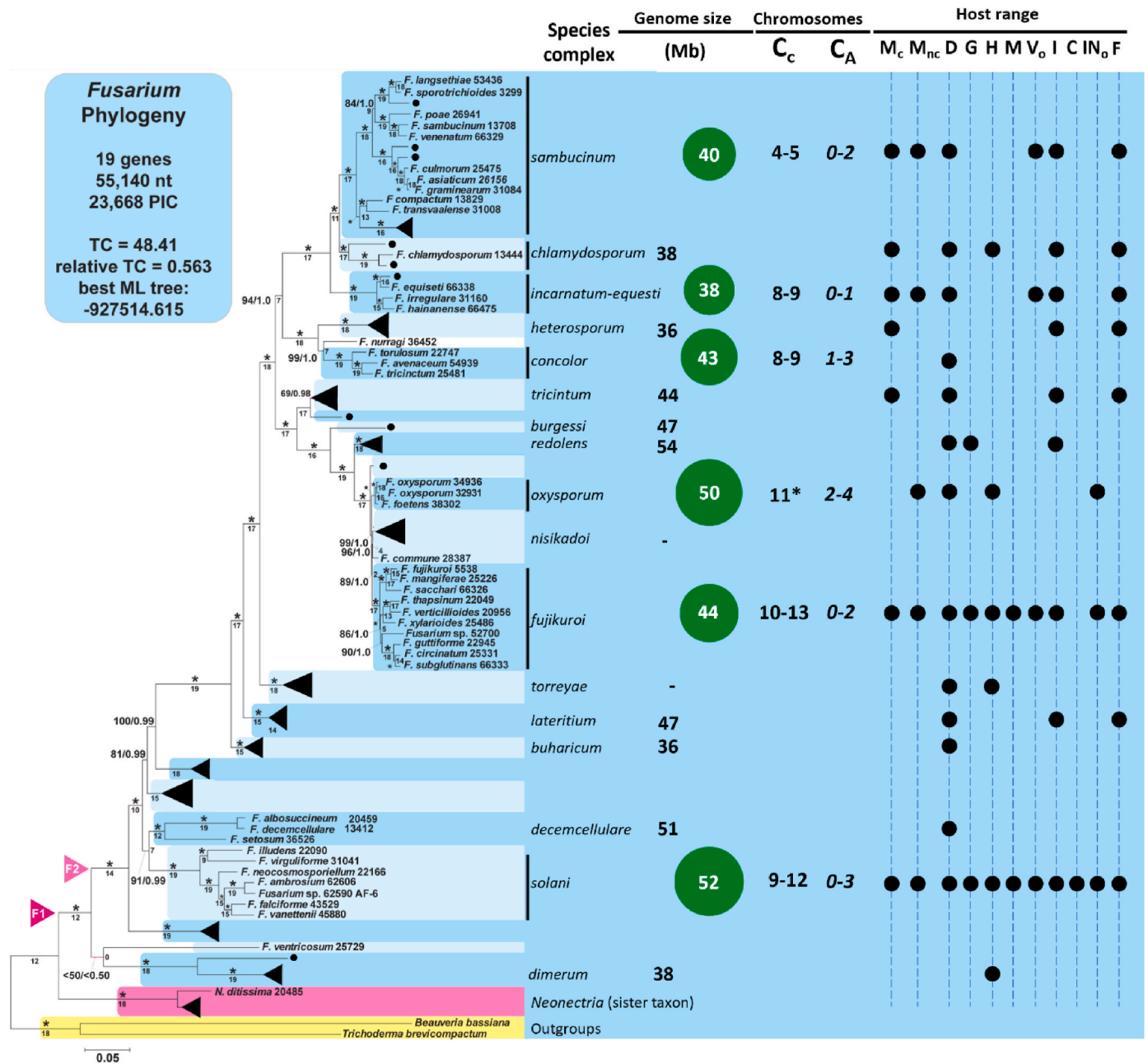


Fig. 1. The genus *Fusarium*: Phylogeny tree, adapted from Geiser et al. (2021), also indicating the breadth of genomic variation and host ranges of pathogenic species within each clade. Genome size is expressed as an average (to zero d.p.) of all available ungapped genomes (Appendix A.1). Many complexes are yet to have genomes sequenced. Species complexes with chromosome scale genome assemblies are highlighted with green circles and also given the relative genome core (C_c) and accessory chromosome/non-core (C_A) numbers determined by the germ tube burst method Waalwijk et al. (2018). *For the *F. oxysporum* species complex the typical genome size and structure is given; accessory chromosomes in this complex often confer host specificity. The host ranges indicate known *Fusarium*-host interactions reported in the available literature but are speculated to increase as surveillance studies and genomic identification based methodologies improve. Host range abbreviations in order of appearance. *Plant Hosts*: M_c – Monocot cereal, M_{nc} – Monocot – non-cereal, D – Dicots, G – Gymnosperm, *Vertebrate Hosts*: H – Human, M – Mammal, V_o – Vertebrate (other), I – Insect, C – Crustacea, IN_o – Invertebrate (other), F – Fungi.

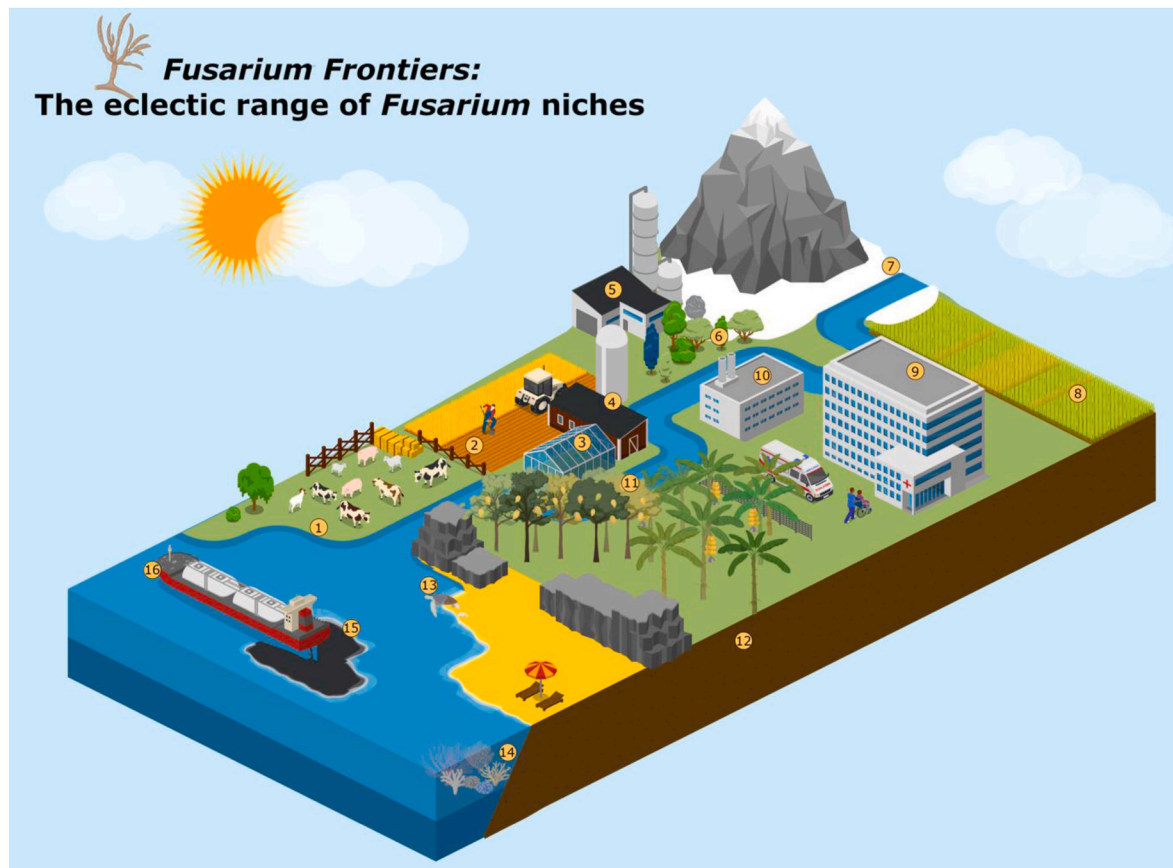


Fig. 2. *Fusarium* Frontiers: Examples of the range of niches occupied by different *Fusarium* species. (1) **Animal husbandry:** *Fusarium*-infected cereal grain feed contains mycotoxins that are hazardous to livestock health, (2) **Cereal production:** *Fusarium* infection of small grain cereals (wheat, barley, triticale, oats and maize) reduces yields, grain quality, and renders grain unfit for human or animal consumption due to mycotoxin content, (3) **Horticulture crop production in glasshouses:** root infecting *Fusarium* species, primarily *F. oxysporum* f. sp. and *F. solani*, arise through soil contamination leading to wilt diseases and/or stem base diseases, (4) **Cereal grain storage:** *Fusarium*-infected grain can proliferate during incorrect storage, further spoiling grain post-harvest, (5) **Bioethanol production/distillation processes:** *Fusarium* species, primarily *F. oxysporum*, may be utilised for the production of bioethanol from lignocellulosic materials, such as garden and food waste, due to its ability to breakdown the material into D-xylose, which is subsequently fermented into ethanol and organic acids. Whereas, if *Fusarium*-infected cereal grain is used for distillation processes, the valuable by-product of dried distillers grain solids may be contaminated with mycotoxins and is therefore unsuitable for use as an animal feed, (6) **Commercial, native, arboretum and ornamental tree infections:** *Fusarium* infects trees via contaminated soil, wounds, wind/rain dispersed spores and/or when vectored by specific insect species causing tree decline, reduced productivity and/or eventual tree deaths at any plant age, (7) **Snow moulds:** *Fusarium* was once described as a snow mould when cereals crops were grown in colder regions, although recent phylogenetic analysis has now reassigned these to a different species (*Microdochium nivale*), (8) **Natural grasslands:** known to act as a *Fusarium* reservoir, proposed to facilitate host jumps from closely related grass species to those in modern crop cultivation thereby inducing *Fusarium* epidemics, (9) **Hospitals:** Human fusariosis in immunocompromised patients can be caused by various *Fusarium* species. Limited effective fungal treatments may cause fusariosis to be a greater problem in the future, (10) **Industrial uses:** since the 1980s, *Fusarium venenatum*, a soil-dwelling species, has been cultivated in air-lift fermenters and sold for human consumption as a non-meat alternative mycoprotein suitable for vegetarian or vegan consumption, (11) **Mango and banana production:** *Fusarium* has caused great economic losses to both global crops, the latter largely affected by the emergence and spread of *Fusarium oxysporum* f. sp. *cubense* Tropical Race 4, (12) **Soil:** *Fusarium* species are typically found in the soil, which can act as a reservoir for plant infections between compatible crop cycles, (13) **Vertebrate infections:** *Fusarium* species can act as pathogens within the animal kingdom in natural environments and in captivity, (14) **Marine environments:** Isolation of *Fusarium* species from across the globe's oceans and seas indicate roles for *Fusarium* in the marine environment, (15) **Mycoremediation:** *Fusarium*'s ability to grow in adverse conditions makes this genus a prime candidate for cleaning anthropogenic environmental damage, such as oil spill or heavy metal contamination, (16) **Accidental movement:** *Fusarium* transport through shipping routes within infected raw commodities can be a leading cause of inter-continental and/or within continent *Fusarium* outbreaks, for example shipping low-level infected non-processed grain in bulk carriers followed by lack of detection at the receiving port.

Table 2

Fusarium species infecting globally important crop plants.

Crops		
<i>Coffea arabica</i> and <i>C. canephora</i> (Cultivated Coffee)	<i>F. xylarioides</i> causes coffee wilt disease	Rutherford (2007)
Cucurbitaceae family (Cucumber, melons, squashes, etc.)	<i>F. oxysporum</i> causes root rots and vascular wilts. Mobile pathogenic accessory chromosomes determine f. sp. and host ranges.	Li et al. (2020b)
Fabaceae or Leguminosae family (Legume, pea or bean family, including chickpeas and lentils)	Large range of <i>Fusarium</i> species cause root rots either alone or in complexes with non- <i>Fusarium</i> species, predominantly caused by <i>F. avenaceum</i> , <i>F. acuminatum</i> , <i>F. poae</i> and <i>F. oxysporum</i> .	Moparthi et al. (2021)
<i>Glycine max</i> (Soybean)	A wide range of <i>Fusarium</i> species cause wilt and root rot diseases. <i>F. solani</i> and <i>F. oxysporum</i> are most frequently associated with root rots, as well as <i>F. graminearum</i> , <i>F. proliferatum</i> , and <i>F. virguliforme</i> .	Diaz Arias et al. (2013)
<i>Hordeum vulgare</i> (Barley)	<i>F. graminearum</i> causes <i>Fusarium</i> Head Blight on barley, including mycotoxin contamination of grain and causes gushing issues for the brewing and distilling industries.	Wegulo et al. (2015)
<i>Musa</i> spp. (Cultivated Banana)	<i>F. oxysporum</i> f. sp. <i>cubense</i> (<i>Foc</i>) causes Panama disease, a vascular wilt on bananas. Tropical Race 4 is currently of greatest global concern for its impact on Cavendish banana production.	Ploetz (2015)
<i>Oryza sativa</i> (Rice)	<i>F. proliferatum</i> causes rice spikelet and sheath rot disease; <i>F. fujikuroi</i> causes Bakanae disease; <i>F. graminearum</i> causes <i>Fusarium</i> Head Blight	Abbas et al. (1999) Chen et al. (2020) Gomes et al. (2014)
<i>Saccharum officinarum</i> (Sugarcane)	<i>F. verticillioides</i> (formally <i>F. moniliforme</i>) causes wilts and Pokkah Boeng disease, as does <i>F. sacchari</i> .	Vishwakarma et al. (2013) Yao et al. (2020) Tiwari et al. (2020)
<i>Solanum tuberosum</i> (Potato)	Thirteen reported species of <i>Fusarium</i> cause tuber dry rot of potatoes, including <i>F. graminearum</i> , <i>F. oxysporum</i> , <i>F. solani</i> var. <i>coeruleum</i> , <i>F. avenaceum</i> and <i>F. culmorum</i> .	Takken and Rep (2010)
Solanaceae family (tomato, pepper, aubergine, potatoes, etc.)	<i>F. oxysporum</i> causes root rots and vascular wilts. Mobile pathogenic chromosomes determine f. sp. and host ranges.	Brown et al. (2010) McMullen et al. (2012)
<i>Triticum aestivum</i> (Wheat)	<i>F. graminearum</i> and <i>F. culmorum</i> cause <i>Fusarium</i> Head Blight globally. <i>F. avenaceum</i> and <i>F. poae</i> cause <i>Fusarium</i> Head Blight in more geographically restricted regions.	Duncan and Howard (2010) Bacon and Williamson (1992)
<i>Zea mays</i> (Maize)	<i>F. graminearum</i> and <i>F. verticillioides</i> cause post-flowering stalk rot, also infects floral tissues, roots and kernels.	

countries/trading regions globally have strict maximum threshold limits for unprocessed cereal grains intended for both human and animal uses (AHDB, 2023). In most years, the harvested grain levels are below officially set limits, but these limits are sometimes exceeded in years when the periods around crop flowering have been particularly wet, facilitating *Fusarium* infection (Johns et al., 2022). Feed contaminated with mycotoxins is not suitable for livestock consumption (Tian et al., 2022), or for further processes such as brewing (Pascari et al., 2022) or bioethanol distilling (Lopes et al., 2023). In addition, *Fusarium*-derived non-toxic, secreted hydrophobin proteins cause the highly undesirable phenomenon of spontaneous ‘gushing’ or foaming during beer fermentation (Sarlin et al., 2012). Post-harvest, during grain transportation and/or storage, *Fusarium* Head Blight can further reduce grain quality and eventual usability, due to additional fungal hyphal proliferation and/or resumption of mycotoxin biosynthesis if the water content within the grain is not carefully controlled (Magan et al., 2010).

2.3. Mycotoxin contamination of grain

As previously described, pathogenic *Fusarium* strains produce various mycotoxins harmful to plants and animals. Of these, the most prevalent and well-studied *Fusarium* toxins include: trichothecenes, zearalenone and fumonisins. One of the most toxic trichothecene toxins is T-2 toxin (Janik et al., 2021), which induces alimentary toxic aleukia in humans and was previously used as an aerosol bioweapon (Adhikari et al., 2017). While not the most toxic, Type-B sesquiterpenoid trichothecene mycotoxins deoxynivalenol (DON) and nivalenol (NIV) are of high economic importance because these secondary metabolites frequently contaminate grain at levels high enough to cause adverse effects for humans and livestock (Mishra et al., 2022). The DON mycotoxin inhibits the function of the peptidyl transferase enzyme in eukaryotic ribosomes, thereby inhibiting protein translation, which leads to vomiting, feed refusal and lack of body weight gain in farmed animals (Kamle et al., 2022). *F. graminearum* DON is synthesised by the

functionally diverse *TRI* gene family which resides at one major locus and two minor loci in the genome. The major cluster, comprising of 12 genes, is retained across *F. graminearum*, *F. culmorum*, *F. sporotrichioides*, *F. langsethiae* and *F. venenatum*. *TRI* gene expression is tightly transcriptionally regulated by two transcription factors residing within the major *TRI* gene clusters (Merhej et al., 2011). The *TRI* cluster of the largely non-pathogenic (see later) *F. venenatum* only produces the Type-A trichothecene, diacetoxyscirpenol (DAS), under certain conditions (O'Donnell et al., 1998; King et al., 2018). Similarly, zearalenone (ZEA) is a phytoestrogenic toxin and results in mycotoxicoses of farm animals, especially pigs as it appears as a field contaminant (Fink-Gremmels and Malekinejad, 2007). Studies have shown that ZEA can stimulate the production of breast cancer cells (Belhassen et al., 2015). Finally, fumonisins are highly toxic to animals and humans and are also classed as cancer-promoting metabolites (Chen et al., 2021; Norred et al., 1996).

2.4. Soil dormancy of *Fusarium* causes infection cycles

The ability of *Fusarium* species to ‘overwinter’ or remain dormant in the soil for decades, through sexual spore production, hyphal fragments and/or the presence of hyphae within slowly decaying buried infected crop residues (Parry et al., 1995; McMullen et al., 2012), makes elimination through crop rotation near-impossible. Fungal spores, like many other types of microbes, can remain dormant for vast timescales, sometimes even for decades, centuries, or longer (Bosch et al., 2021; Pedrós-Alió, 2021; Hallsworth, 2022). Many *Fusarium* species can remain asymptomatic on non-host plants until a suitable host becomes available for reproduction. *Fusarium* spp. are also proficient pathogens of ornamental plants, including *Pelargonium hortorum* (*Geranium*) Yang et al., 2022) and *Lilium* spp. (Yang et al., 2023). Horticulture systems can often provide alternative hosts to pathogenic *Fusarium* spp., creating an opportunistic reservoir to jump back to arable crop species when hosts become available.

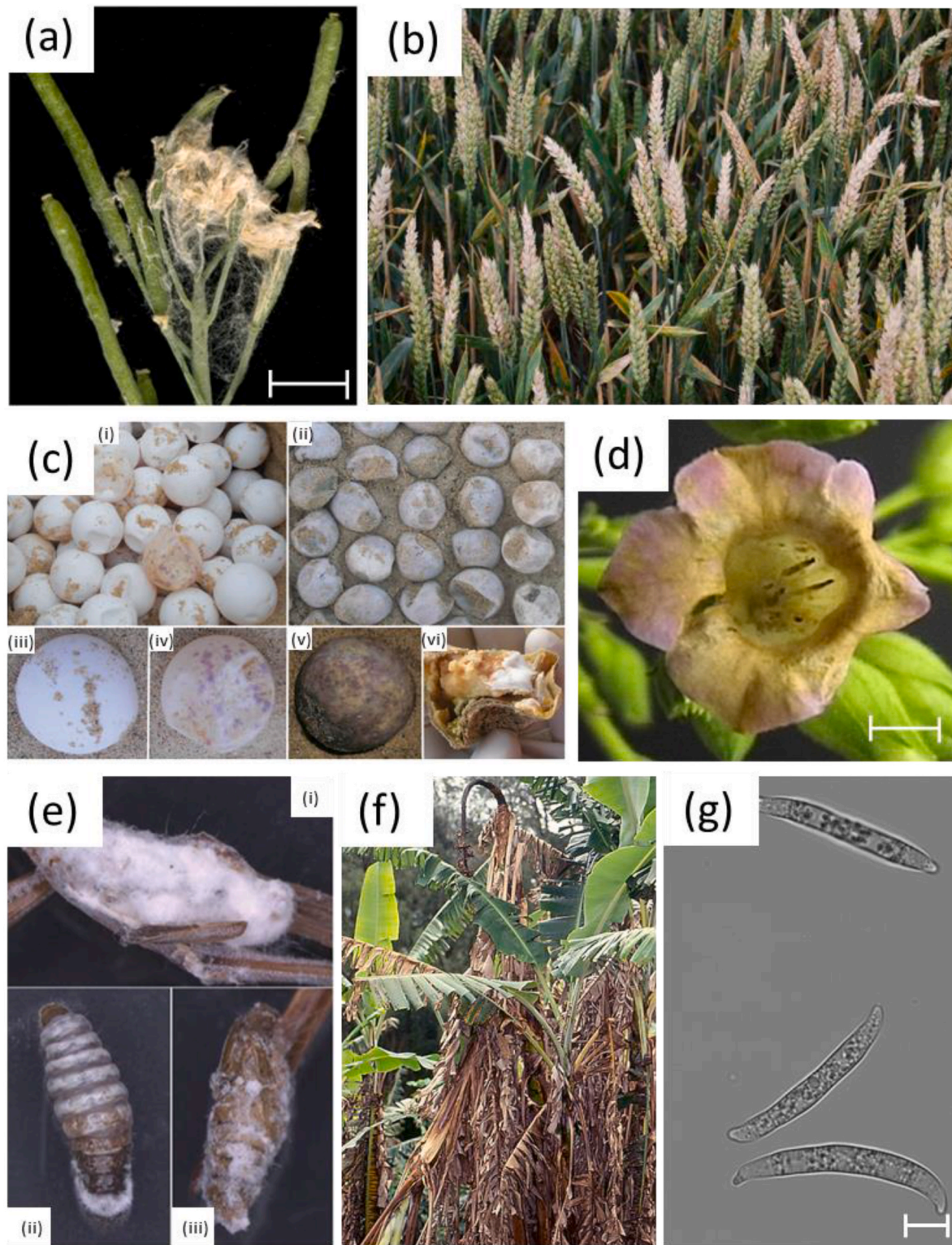


Fig. 3. *Fusarium* infections on native plant and animal hosts and model organisms. (a) *F. graminearum* (wild-type global reference strain PH-1) infection of *Arabidopsis thaliana* ecotype Landsberg Erecta at 11 dpi (spray inoculated). Scale bar = 4 mm, Image courtesy of Martin Urban, Rothamsted Research, (b) *F. graminearum* causing Fusarium Head Blight on wheat spikes, image courtesy of Martin Urban, Rothamsted Research, (c) Sea turtle (*Caretta caretta*) nests (top, (i) healthy and (ii) *Fusarium*-infected) and individual eggs (bottom) infected with *Fusarium* species. The four lower insets labelled (iii) to (vi) within panel c show increasing severity of turtle egg infection left (least) to right (most). Image reproduced from [Sarmiento-Ramirez et al. \(2014\)](#), (d) *Nicotiana tabacum* (tobacco) flowers infected with *F. graminearum* at 4 dpi. Scale bar = 4 mm. Image courtesy of Martin Urban, Rothamsted Research, (e) *F. concentricum* infection of dead larvae and pupae from the moth *Polychrosis cunninhamicola*, figure adapted from [Qiu et al. \(2023\)](#). The insets labelled indicate (i) dead larva severely covered with white hyphae, (ii) dead larva and (iii) pupa sprouting white hyphae. (f) *F. oxysporum* f. sp. *cubense* Tropical Race 4, otherwise known as Panama Disease, infection of banana trees. Image by Scott Nelson and utilised under the Creative Commons Zero Licence, (g) *F. graminearum* (strain PH-1) spores under light microscope, showing typical curved morphology of *Fusarium* spores. Scale bar = 10 μ m. Image by Erika Kroll, Rothamsted Research.

3. *Fusarium* in the natural environment

Fusarium spp. occur naturally in a myriad of niches. Whilst these can sometimes spill into monoculture cropping systems causing disease epidemics as discussed throughout this review, many other interesting components of the environment harbour *Fusarium* species, to either detrimental or beneficial ends.

3.1. *Fusarium* species infecting vertebrates

Members of at least seven *Fusarium* species complexes have been reported to infect human and/or animal hosts (Table 3) and cause fusariosis, including *F. solani*, *F. oxysporum*, *F. fujikuroi*, *F. incarnatum-equiseti*, *F. chlamydosporum* and *F. dimerum* (van Diepeningen et al., 2014). Members of the *F. solani* and *F. oxysporum* complexes are the most common among those infecting humans (Batista et al., 2020). In humans, *Fusarium*-caused diseases include keratomycosis (infection of the cornea), onychomycosis (infection of the nail) and dermatitis (infection of the skin). Most *Fusarium* spp. infecting humans are considered opportunistic pathogens. Infections in healthy patients usually remain local, are typically located in externally facing tissues and can be controlled by normal immune responses. However, in immunocompromised patients *Fusarium* infections can spread to the blood and other tissues/organs increasing the chances of morbidity and mortality of the patients (Low and Rotstein, 2011). *Fusarium* species infecting humans are distributed worldwide and are usually detected by PCR amplification of different marker genes (Al-Hatmi et al., 2016). So far, few efforts have been made to fully sequence the genomes of clinical strains to identify specific genes and/or accessory chromosomes connected with pathogenicity in humans or animals (Appendix A.1).

Many members of the *F. oxysporum* species complex have lineage-specific (LS) chromosomes which in the tomato infecting f. sp. were elegantly demonstrated more than a decade ago to define host specificity (Ma et al., 2010). In an approach to identify specific genes and/or LS chromosomes connected with human infections, inter-isolate comparisons were undertaken. The genomes of two clinical *F. oxysporum* isolates NRRL 32931 and NRRL 47514 were fully sequenced and compared to the genome of the tomato infecting strain *F. oxysporum* f. sp. *lycopersici* (Fol 4287) (Zhang et al., 2020). The two clinical isolates shared 11 chromosomes with Fol 4287, but each possessed an additional four unique LS chromosomes. These LS chromosomes were found to be enriched in genes involved in metal ion transport and cation transport that may allow the pathogen to overcome the micronutrient starvation induced by human host defences. Whereas plant-specific effector genes such as Secreted In Xylem (SIX) and plant cell wall degrading enzymes were absent from both genomes of the clinical isolates (Zhang et al., 2020). This study suggests that isolates able to proliferate in human tissues have become adapted due to the repertoire of specific genes present in LS chromosomes.

Fusarium species can infect many different classes of animals (Table 3). Disease reports are usually obtained from animals kept in captivity, with poor living conditions and stress possibly increasing the chance of infection by different *Fusarium* species (Smith et al., 1989; Crow et al., 1995; Perpiñán et al., 2010; Cafarchia et al., 2020). Often when *Fusarium* species are isolated from infected tissues they are in association with other fungal or bacterial species (Hatai et al., 1986; Perpiñán et al., 2010; Cafarchia et al., 2020). As a result, the true causal species of observed symptoms is often difficult to ascertain. Nevertheless, some infections do occur in natural conditions, as is the case with eggs from different species of marine turtles (Fig. 3, panel C) (Sarmiento-Ramirez et al., 2014; Greeff-Laubscher and Jacobs, 2022). Sea turtle eggs are incubated in sand in coastal beaches and can come in contact with different *Fusarium* spp. such as *F. falciforme*, *F. keratoplasticum* and *F. crassum* (Sarmiento-Ramirez et al., 2010; Sarmiento-Ramirez et al., 2014; Greeff-Laubscher and Jacobs, 2022). Infected eggs do not produce viable embryos, and this leads to a reduction in the hatch

rate. Finally, some *Fusarium* isolates can infect both plants and animals. For example, *F. oxysporum* f. sp. *lycopersici* isolate FGSC 9935 can infect tomato as well as immunocompromised mice (Navarro-Velasco et al., 2011). Future genomic analysis of this isolate will help to determine whether the presence of specific genes in either LS chromosomes or those present in the core chromosomes are responsible for the infection of hosts from different kingdoms.

Over the last decade there has been a steady rise in the number of reports of opportunistic *Fusarium* species infecting humans and animals. A potential explanation could be the development of better detection tools that allows for the discrimination between fungi species. However, poor captivity conditions of animals, as well as changes in habitat conditions worldwide can favour fungal proliferation, which can also increase the number of immunocompromised human individuals that are exposed to and are susceptible to *Fusarium* infection. In addition, many different *Fusarium* species have been reported to have developed resistance to various fungicides, thereby making solely anti-fungal based control strategies more difficult (Batista et al., 2020). Going forward, future comparative genomic projects involving *Fusarium* species and isolates infecting animals and/or humans, where the host species are often taxonomically distantly related, will be essential to understand how this genus is able to harbour multiple trans-kingdom pathogens.

3.2. *Fusarium* in marine environments

The marine environment, although globally relatively stable, can be hostile to the proliferation and even existence of many fungal species. Localised and regional changes to pH, salinity, temperature, wave action, water pressure, nutrient availability and/or human activity associated polluting chemistries has led to the evolution of many unique metabolic processes. To this end, the ubiquitous *Fusarium* genus is no exception, having developed unique secondary metabolites to carve out many niches in the marine world.

Some *Fusarium* species discovered in marine environments have notable anthropogenic benefits, such as the halogenated sesterterpene Neomangicol B compound, which was isolated from a marine *Fusarium* spp. and has antimicrobial properties similar to the antibiotic gentamicin (Renner et al., 1998). Many approved pharmaceutical compounds were originally isolated from endophytic marine fungi, often hosted within marine sponges (Gao et al., 2018) and corals (Couttolenc et al., 2016). In fact, *F. oxysporum* strains derived from coral have demonstrated potential as anti-cancer therapeutics when tested against cancer cell lines *in vitro* (Couttolenc et al., 2016).

Thermal adaptations to both warm and cool oceans have occurred. *F. equiseti* strains isolated from tropical marine environments in Malaysia grow optimally at 25 °C, and also have significant cellulase activity (Tajuddin et al., 2017). However, whether this has evolved in response to nutrient acquisition from seaweed/kelps with predominantly cellulose based cell walls or is a legacy from a prior land-based evolutionary niche occupied, is yet to be explored. Another abiotic factor of marine environments is low water activity (the effective concentration of water molecules) or the increased osmotic potential, or salt stress, endured by organisms (Lee et al., 2018; Hallsworth, 2019). In marine fungal organisms, including *Fusarium* spp., salt tolerance is largely unexplored, yet the breadth of marine environments in which they are found would indicate mechanisms for such tolerance. Studies investigating salt tolerance of the halotolerant black yeast *Hortaea werneckii* and *Aspergillus penicillioides*, a species that can tolerate concentrations up to 30 % NaCl, have indicated that salt is not required for growth (Plemenitaš et al., 2008; Stevenson et al., 2017a, 2017b). However, solute stress has been shown to induce the fumonisin mycotoxin biosynthesis *FUM* genes in *F. verticillioides* (Jurado et al., 2008).

Discussions around *Fusarium* spp. and aspects of the marine environment were first initiated through a description of different pathogenic interactions. As far back as the 1980s, *F. solani* had been highlighted as a pathogen of both marine and freshwater crustaceans,

Table 3
Animal species infected with *Fusarium* spp.

Vertebrates: Class	Ecosystem	Species	Symptoms	<i>Fusarium</i> species complex (SC)*	Reference
Amphibia	Fresh water	<i>Bufo baxteri</i> (Wyoming toad)	Dermatitis, kidney infection.	<i>Fusarium fujikuroi</i> SC (<i>F. proliferatum</i> , <i>F. verticilliooides</i>), <i>Fusarium oxysporum</i> SC (<i>F. oxysporum</i>), <i>Fusarium solani</i> SC (<i>F. solani</i>)	Perpiñán et al. (2010)
Fish	Marine	<i>Pagrus</i> sp. (Red sea bream) <i>Sphyrna lewini</i> (Hammerhead sharks), <i>Sphyrna tiburo</i> (Bonnethead shark)	Kidney infection. Dermatitis in the lateral line canal system. Infection of hyaline cartilage.	<i>Fusarium oxysporum</i> SC (<i>F. oxysporum</i>) <i>Fusarium solani</i> SC (<i>F. solani</i>)	Hatai et al. (1986) Crow et al. (1995) Smith et al. (1989)
Mammalia	Marine	<i>Pseudorca crassidens</i> (False killer whale) <i>Tursiops truncatus</i> (Bottlenose dolphin)	Skin lesion. Infection of the central nervous system.	<i>Fusarium solani</i> SC (<i>F. solani</i>) <i>Fusarium oxysporum</i> SC (<i>F. oxysporum</i>)	Tanaka et al. (2012) Staggs et al. (2010)
	Terrestrial	<i>Canis lupus familiaris</i> (Dogs) <i>Mus musculus</i> (Mice)	Infection of the central nervous system. Invasive hyphae in different organs.	<i>Fusarium solani</i> SC (<i>F. solani</i>) <i>Fusarium oxysporum</i> SC (<i>F. oxysporum</i>)	Evans et al. (2004) Schäfer et al. (2014)
Reptilia	Marine	<i>Caretta caretta</i> (Loggerhead sea turtle) <i>Chelonia mydas</i> (Green sea turtle) <i>Dermochelys coriacea</i> (Leatherback sea turtle) <i>Eretmochelys imbricata</i> (Hawksbill sea turtle) <i>Lepidochelys kempii</i> (Kemp's ridley sea turtle) <i>Lepidochelys olivacea</i> (Olive ridley sea turtle) <i>Natator depressus</i> (Flatback sea turtle)	Superficial lesions in shell and skin. Invasive infections (lung infection). Egg infections (lower hatching success).	<i>Fusarium sambucinum</i> SC (<i>F. brachygibbosum</i>) <i>Fusarium oxysporum</i> SC (<i>F. oxysporum</i>) <i>Fusarium solani</i> SC (<i>F. solani</i> , <i>F. falciforme</i> , <i>F. crassum</i>)	Cafarchia et al. (2020) (1) Orós et al. (2004) Greeff-Laubacher and Jacobs (2022); Sarmiento-Ramirez et al. (2014) (1); Sarmiento-Ramirez et al., 2010 (1)
	Terrestrial	<i>Acanthodactylus nilsoni</i> <i>Rastegar-Pooyani</i> (Fringe-Toed Lizard) <i>Gopherus berlandieri</i> (Texas tortoise)	Dermatitis in the neck and fingers. Necrosis of the scute that form the shell.	<i>Fusarium fujikuroi</i> SC (<i>F. proliferatum</i>) <i>Fusarium incarnatum-equiseti</i> SC (<i>F. incarnatum-equiseti</i>)	Chehri et al. (2015) (1) Rose et al. (2001) (1)
Invertebrate: Class					
Arthropoda	Marine	<i>Limulus polyphemus</i> (Atlantic horseshoe crab)	Shell and gill lesions.	<i>Fusarium solani</i> SC (<i>F. solani</i>)	Tuxbury et al. (2014) (1)
	Terrestrial	<i>Galleria mellonella</i> and <i>Polychrosis cunninhamiacola</i> (Moth and caterpillars) <i>Acythopeus curvirostris</i> , <i>Brahmina coriacea</i> , <i>Tenebrio molitor</i> , and <i>Tribolium confusum</i> (Beetles) <i>Tetanops myopaeformis</i> (Fly) <i>Ronderosia bergii</i> (Grasshopper) <i>Heterotermes indicola</i> (Termites) <i>Frankliniella occidentalis</i> and <i>Ceratothripoides claratris</i> (Thrips) <i>Planococcus ficus</i> (Vine mealybug) <i>Dryocosmus kuriphilus</i> (Wasp) <i>Cephus cinctus</i> (Wheat stem sawfly)	Hyphae colonisation of inner tissues leads to death.	<i>Fusarium fujikuroi</i> SC (<i>F. fujikuroi</i>), <i>Fusarium oxysporum</i> SC (<i>F. oxysporum</i>), <i>Fusarium fujikuroi</i> SC (<i>F. fujikuroi</i>), <i>Fusarium oxysporum</i> SC (<i>F. oxysporum</i>), <i>Fusarium solani</i> SC (<i>F. solani</i>), <i>Fusarium incarnatum-equiseti</i> SC (<i>F. incarnatum-equiseti</i>), <i>Fusarium sambucinum</i> SC (<i>F. sambucinum</i>), alongside members of <i>Fusarium chlamydosporum</i> , <i>Fusarium tricinctum</i> , <i>Fusarium heterosporum</i> , <i>Fusarium redolens</i> , and <i>Fusarium lateritium</i> SCs.	Qiu et al. (2023) (1) Navarro-Velasco et al. (2011) (1) Reviewed in: Santos et al. (2020).
Cnidaria	Marine	<i>Hydra vulgaris</i> (Fresh-water polyp)	Removal of the bacterial community from epithelial cells results in lethal infection by different <i>Fusarium</i> spp.	<i>Fusarium</i> spp.	Fraune et al. (2015) (1)
Nematoda	Terrestrial	<i>Caenorhabditis elegans</i> (Nematode)	Lethal infection after consumption of conidia.	<i>Fusarium solani</i> SC, <i>F. oxysporum</i> SC, <i>F. fujikuroi</i> SC	Muhammed et al. (2012) (1,2)

(1) Reference contains images of host species with *Fusarium* symptoms.

(2) Infections were done artificially to establish the soil nematode *Caenorhabditis elegans* as a model to study human *Fusarium* infections.

causing localised lesions in the exoskeleton of shrimp, succeeded by mycelium growth into deeper tissues (Hose et al., 1984). Alderman (1982) demonstrated that artificial wounds prior to inoculation were required to induce similar infections as reported in the wild, indicating that, whilst well adapted, *Fusarium* is likely to be an opportunistic pathogen. *F. solani* is known for its ability to infect crustaceans (Alderman and Polglase, 1986), turtle eggs (Greeff-Laubscher and Jacobs, 2022) and stingrays (Hsu et al., 2021) (Table 3).

Fusarium's presence in the marine environment has indicated a possible use as removers of environmental pollutants. In hostile, nutrient poor environments, fungi evolve unique modes of nutrient acquisition and subsequently produce secondary metabolites of interest. In the South China Sea, a *Fusarium* species (denoted #ZZF51) was isolated from coastal mangrove forests and noted for its potential as a bio-accumulator of the radioactive element uranium (VI) from uranyl ions (UO_2^{2+}) present in the marine environment (Yang et al., 2012). Possibly, future development in metal extractions from fungi could provide a source of fuel for nuclear energy or extraction of heavy metal pollution from environments. Conversely, mycoremediation of heavy metal and hydrocarbon (oil) pollution is considered a relatively easy and low-cost solution to anthropogenic damage to the environment. Under artificial saline stress, a *Fusarium* species (denoted F092) performed relatively well, being able to break down some aliphatic fractions of crude oil in just two months (Hidayat and Tachibana, 2012).

The marine environment has been relatively little-explored, and this is true too for marine microorganisms, including fungi. From the wide range of *Fusarium* species discovered, it is likely that a wealth of species remains undiscovered and some of these could have potentially beneficial uses in mycoremediation of hostile environments and pharmaceutical applications. However, as anthropogenic activity continues to encroach on the marine world, host-jumps of *Fusarium* species to marine living organisms is likely to become ever more frequent.

3.3. *Fusarium* and snow

The snow mould *Microdochium nivale* (previously named *Fusarium nivale* ex Berlese and Voglino; Wollenweber, 1931; Gerlach and Nirenberg, 1982), is the causative agent of *Fusarium* Patch Disease of forage and turf grasses and seedling blight disease of winter cereals (Ponomareva et al., 2021; Tronsmo et al., 2001). Snow mould develops under the protection of snow cover and is particularly severe when the snow cover fully melts during mild winter periods and then reforms. Plant infections from seed or soil-borne inoculum (mycelia, conidia and ascospores) occur at low near freezing temperatures, under the dark and humid conditions of snow cover. Freeze-thaw cycles are likely to be more unpredictable and more frequent, due to increased climatic fluctuations as a result of climate change. Therefore, snow mould disease is also likely to increase in incidence, severity and distribution in the near future. The specialisation of this fungus to such conditions suggests a robust stress biology, as surviving freeze-thaw cycles can be challenging and the changes in the density of water that occur close to 0 °C may also cause unusual forms of cellular stress to microbes that undergo fluctuations in the range 0 to 4 °C (Pavankumar et al., 2021).

3.4. Fungicolous *Fusarium* species

Associations between *Fusarium* species and other species across the fungal kingdom have been reported, with 80 *Fusarium* isolates confirmed to have fungicolous interactions across the Basidiomycota, Ascomycota and Mucoromycota, as well as the Oomycota that is composed of fungi-like protist organisms (Torbaty et al., 2021) (Fig. 1). Some *Fusarium* species may have the potential to be mycological control agents of fungal plant pathogens. For example, *F. proliferatum* in the *fujikuroi* species complex and *F. persianum* in the *incarnatum-equiseti* complex have noted hyperparasitic associations with smuts (Torbaty et al., 2019), whilst members of the *F. lateritium*, *F. oxysporum*, and *F.*

avenaceum species complexes are necrotrophic towards *Botrytis cinerea*, the causal agent of grey moulds on multiple plant species (Domsch et al., 2007). In addition, *F. heterosporum* is a reported hyperparasite of the cereal infecting fungus *Claviceps purpurea*, more commonly known as ergot (Preece et al., 1994). Within the Basidiomycota, the widely cultivated common mushroom *Agaricus bisporus* has been reported to have necrotrophic associations with several members of the *tricinatum* and *oxysporum* species complexes (Torbaty et al., 2019). In addition, in natural ecosystems, *Fusarium* species associations have been noted with several macrofungi including tree bracket fungi (*Polyporus radiatus*, *Fomes fomentarius*), *Tuber* spp. (e.g. truffles), *Coprinus* spp. (e.g. shaggy ink cap) and *Boletus* spp. (e.g. porcini mushrooms) (Torbaty et al., 2019).

3.5. Bacterial - *Fusarium* interactions

During the typical infection process of plants, as well as during soil colonisation, *F. graminearum* has to compete with the residing microbial population. A study by Chen et al. (2018) reported that the bacterial community present in wheat spikes changes upon *F. graminearum* infection, indicating that the pathogen can favour some bacterial species over others. *F. oxysporum* also alters the microbiome during infection of tubers from the medicinal plant species, *Pseudostellaria heterophylla*, commonly known as false starwort (Yuan et al., 2022). The microbiome modification could be a plant protection mechanism known as “cry-for-help” where the plant secretes different metabolites to attract beneficial microorganisms that help the plant to minimise the effect of infection (Rizaludin et al., 2021). However, some studies have reported that specific *Fusarium* species can establish beneficial interactions with the microbiome. For example, *F. graminearum* can establish a beneficial interaction with *Burkholderia glumae*, a seed-borne pathogenic bacteria infecting rice panicles (Jung et al., 2018). The interaction promotes fungal and bacterial dispersion as well as disease progression of both pathogens. In addition, a preliminary report revealed the soil bacteria species, *Stenotrophomonas maltophilia*, was able to live inside *F. graminearum* (Ali et al., 2022). This symbiotic relationship would benefit the nitrogen fixation capacity of the fungus. Finally, *Fusarium* spp. can produce different secondary metabolites that play different roles during microbial encounters (reviewed in Venkatesh and Keller, 2019). Overall, a limited number of cooperative interactions with bacteria have been described so far for the *Fusarium* genus. Future research is required to identify new beneficial and disadvantageous interactions between *Fusarium* spp. and the microbiome, as well as the molecular mechanisms controlling these interactions in natural and human-made environments.

3.6. *Fusarium* in arborescent habitats and tree plantations

Fusarium species pose significant threats to a wide range of arborescent vegetation such as trees, shrubs (treelets), and other tree-like plants. Forests cover 31 percent of the global land area (FAO, 2020b). They provide species-rich habitats for various types of flora, fauna and microorganisms. Both natural and cultivated tree habitats face increasing threats from *Fusarium* due to travel and climate change (Fisher et al., 2012) and reports of *Fusarium*-incited disease outbreaks have increased in intensive monoculture plantations since the 1950s (Gaba et al., 2015).

Trees are perennial woody plants that play a vital ecological role in terrestrial ecosystems. They possess well-developed stems or trunks, undergo secondary growth to increase stem thickness, and have distinct crowns of branches and leaves. Trees promote human well-being by supporting agriculture, aiding carbon sequestration, regulating water resources, lowering local air temperatures through providing shade and ensuring soil conservation. Additionally, trees provide valuable resources such as timber and fibres. The arborescent monocotyledonous tree-like plants, such as *Musa* spp. (banana), *Elaeis guineensis* (oil palm), date palm (*Phoenix canariensis*) and *Cocos nucifera* (coconut), provide

sources of fruits, nuts, and oils. In this context, we describe some major *Fusarium* tree pathogens of high global concern.

As opportunistic fungi with a wide range of metabolic adaptability and ability to produce toxins, an increasing number of *Fusarium* species have been recognised for their capacity to exploit the niches provided by trees (Perincherry et al., 2019; Stack et al., 2022). *Fusarium* species can infect and become devastating pathogens when newly introduced into naive environments where the hosts are not adapted (Dobbs et al., 2021). Various major routes of tree infection are described.

First, soil-borne wilting diseases can spread due to human activities, trade and via contaminated soil and seedlings. *Fusarium* wilt of bananas, commonly called Panama disease, threatens banana plantations worldwide and is mainly caused by *F. odoratissimum*, previously known as *F. oxysporum* f. sp. *cubense*, including the Tropical Race 4 (TR4) strain (Maryani et al., 2019). Since the early 1990s, TR4 has spread to various countries in Southeast Asia, South Asia, the Middle East, and Africa and has increasingly affected the Cavendish cultivar, which accounts for 99 % of banana exports (Dita et al., 2018).

Various specialised *F. oxysporum formae speciales* can infect different tree species, including *Acer* spp. (maples), *Carya* spp. (hickories), *E. guineensis* (oil palm) leading to vascular browning, wilting, and eventual decline (Zhao et al., 2020a; Lazarotto et al., 2014; Rusli, 2017). Other tree and seedling pathogens include *F. circinatum*, and *F. solani*. *F. circinatum* causes pine pitch canker disease in various pine species, including *Pinus radiata* (Monterey pine), *Pinus pinaster* (maritime pine), and *Pinus taeda* (loblolly pine) (Drenkhan et al., 2020). The primary infection routes of these species are through wounds or natural openings such as resin ducts. Rapid colonisation of xylem causes blockage and impairs water and nutrient transport, leading to resinous cankers on branches, trunks, or stems, eventually resulting in wilting, dieback, and tree mortality. The ubiquitous species *F. solani* (formerly named *Nectria haematococca*) causes root rot and damping-off under high humidity from contaminated soil in a broad range of hosts and seedlings including cultivated tree species such as *Olea europaea* (olive) (Kacprzak et al., 2001; Babbitt et al., 2002).

F. decemcellulare causes a condition known as oversprouting disease in the Brazilian Guaraná shrub (*Paullinia cupana* var. *sorbilis*) leading to the excessive growth of shoots or sprouts on the plant. When the fungus infects the shrub, it disrupts the plant's normal growth processes triggering a high number of shoots and galls, likely due to plant hormone imbalances (Queiroz et al., 2023). Guaraná shrubs produce fruit the size of a coffee berry and their seeds produce stimulants including caffeine, which are widely used as supplements in energy drinks. *F. decemcellulare* infects 85 woody hosts in tropical and subtropical regions. Additionally, mangoes (*Mangifera indica*) can be affected by malformation in shoots and inflorescences. A survey of diseased mango tissues in Australia identified additional *Fusarium* species, including *F. mangiferae* and *F. proliferatum* (Liew et al., 2016) that affect shoot formation in a similar way to *F. decemcellulare*.

Several *Fusarium* species have been described as being transmitted by insects. *Fusarium* Dieback disease affects avocados and many other tree species. This disease is caused by *F. euwallacea*, a symbiont of the Asian ambrosia beetle (*Euwallacea* sp.) (Bonilla-Landa et al., 2018). Ambrosia beetles store symbiotic fungal inocula in specialised structures adapted for the transport of symbiotic fungi, called mycangia. The fungal insect symbiont is speculated to weaken tree resistance thereby benefitting the insect and provide additional nutrients during growth through wood fibres. Another significant threat is *F. circinatum*, the cause of Pine Pitch Canker, which is one of the most devastating forest diseases worldwide (Zamora-Ballesteros et al., 2019). The transportation of asymptomatic or infected seeds and seedlings due to human activities is responsible for long-range dissemination. The fungus is locally transmitted by insect vectors, wind and rain. The physical damage caused by insects provides the primary fungal infection sites for *F. circinatum* (Selikhovkin et al., 2018; Fernández-Fernández et al., 2019). In summary, tree diseases can be caused by various *Fusarium* species that infect roots, wounds, cause

hypertrophic growth or are transmitted in association with insects.

3.7. Natural grassland ecosystems: an ever-growing reservoir of *Fusarium* diversity

Biogeographical surveys in Australia, USA and Brazil of *Fusarium* in highly diverse naturally dry prairie grassland or wet tropical savannah ecosystems have led to the identification of many novel species. These studies historically focussed on *Fusarium* species associated with soil or plant debris, but more recently have also included the isolation of endophytic species. Some of these *Fusarium* species are now recognised to be restricted to a specific geographical area or climatic condition. Some species typically identified in natural grasslands have so far been rarely or never reported in the *Poaceae* (grasses) dominated cultivated arable lands including dry prairie grassland. For example, *F. sporotrichioides* var. *chlamydosporum*, *F. equiseti* and *F. konzum* (Zeller et al., 2003; Walsh et al., 2010; Summerell et al., 2011). Species solely recovered from tropical savannah include *F. gaditjirrii* (Phan et al., 2004), *F. lyarnte* and *F. werrikimbe* (Walsh et al., 2010), *F. coicis* (Laurence et al., 2016) and very recently *F. caapi* and *F. brachiariae* recovered from symptomless native seeds taken from several locations in Brazil (Costa et al., 2021). The interest in the identification, phylogenetic classification and long-term storage of *Fusarium* species from natural ecosystems associated with minimal anthropogenic activities arose from an original idea published by Leslie and colleagues in 2004, suggesting that native or introduced grasses could act as inoculum reservoirs of known or unknown and potentially plant pathogenic and mycotoxigenic *Fusarium* species (Leslie et al., 2004).

4. *Fusarium* in anthropogenic environments

The human-made environment is no exception to the proliferation of *Fusarium*. Members of the genus thrive in fuel and have even made it to space. However, the positive potential of *Fusarium* species is arguably in its infancy. *F. venenatum* is cultivated as a climate-friendly protein source, and the metabolic powerhouse that is *Fusarium* is used to produce various industrial enzymes, for undertaking complex bioconversion processes involving raw commodities and/or waste products, for the production of a vast array of different types of commercially important secondary metabolites and for nanoparticle biosynthesis.

4.1. Fuel contamination and space

Various studies employing re-isolation and different diagnostic techniques have provided insights into the adaptability and survival capabilities of *Fusarium* species in human-made environments and their role as fungal contaminants. For instance, investigations conducted on samples from aircraft tanks and kerosene have confirmed the presence of uncharacterised *Fusarium* species as active contaminants (Darby et al., 2001; Krohn et al., 2021). Among the species highly adapted to grow on jet fuel is a *F. fujikuroi* isolate, FUS01, for which a draft genome sequence is available (Radwan et al., 2018). The authors reported the presence of two AlkB-related alkane hydroxylases and an n-alkane inducible cytochrome P-450 gene that may enable *F. fujikuroi* strain FUS01 to grow on jet fuel. Further research focusing on the specific genetic and physiological traits that enable *Fusarium* species to persist and thrive in these human-made niches can offer a better understanding of their ecological dynamics, as well as identify potential implications and issues for industries involved in fuel storage and transportation that may need to be addressed.

In another case, involving plant cultivation on the International Space Station, two fungal strains (VEG-01C1, VEG-01C2) isolated from ornamental plants (*Zinnia hybrida*) had their genomes sequenced and were identified as *F. oxysporum* species (Urbaniak et al., 2018). Both strains bear a striking resemblance to the clinical strain FOSC 3-a, which was isolated from the blood of a US patient suffering from fusariosis

(Appendix A.1). This finding emphasises the importance of implementing stringent hygiene measures during space travel to mitigate potential issues associated with *Fusarium* contamination.

4.2. Mycoprotein producer and bioconversion agent

The saprotrophic soil dwelling fungus *F. venenatum* was initially taxonomically misclassified as *F. graminearum* prior to molecular phylogenetic analyses (O'Donnell et al., 1998). In England in the 1980's under the guidance of Prof. Toni Trinci and sponsored jointly by the companies Rank Hovis McDougall and ICI, *F. venenatum* was developed as an alternative to meat, high in protein and dietary fibre, but low in fat. The *F. venenatum* A3/5 strain was selected for commercialisation because this strain routinely produced masses of unusually long, unbranched filamentous hyphae when grown in specially developed air lift fermenters. These unusual hyphae could then be used to produce the required long mycofibres. *F. venenatum* was commercialised in 1985 under the name Quorn® (Trinci, 1992, 1994) and is now sold as a human food in more than 25 countries (quorn.com). Quorn® production involves fungal biomass accumulation in fermentation towers under specific growth conditions. The harvested long hyphae are then heated, mixed with egg albumin (for vegetarian options) or potato starch (for vegan options) and rolled into meat-like fibres. Globally, Quorn® is the only commercially available, human consumption-approved mycoprotein. In an industrial context, *F. venenatum* is also used for the production of various recombinant proteins, including, lipases, phytases, trypsin and xylanases (Royer et al., 1995; Berka et al., 1998, 2003). Whereas the *F. venenatum* strain ATCC20334 is used for the bioconversion of pre-treated wheat straw to ethanol using a simultaneous saccharification and fermentation process (Yudianto et al., 2019). *Fusarium* toxins have not been detected in any of these industrial applications. However, *F. venenatum* was found to produce the Type A trichothecene, diacetoxyscirpenol (DAS) when grown in rice grain cultures (O'Donnell et al., 1998).

In recent years, *F. venenatum* research has focussed on establishing stable transformation/high throughput gene deletions and CRISPR/Cas9 gene editing systems with the overall aim of improving and further extending the metabolic engineering potential of this species (Wilson and Harrison, 2021; Tong et al., 2022, 2023). The search is also on to identify natural strains with the opposite mating type to increase the overall diversity, through sexual recombination, available for future industrial exploitation. Interestingly, *F. venenatum* was recently reported to cause a foot, root, lower stem reddish-brown rot disease in a wheat crop under sown with peas in Germany. This hitherto unsuspected pathogenic potential was confirmed using controlled single isolate glasshouse inoculations (Rigorth et al., 2021).

4.3. Secondary metabolites - dangers and industrial applications

Fusarium species have impressive biosynthetic capabilities, producing substances that are toxic and stressors, including chaotropic and hydrophobic stressors that function as antimicrobials (Cray et al., 2013; Noel et al., 2023).

While *Fusarium* species can produce an arsenal of dangerous and health debilitating metabolites, they can also act as biosynthetic powerhouses. In fungal genomes, genes involved in the synthesis of secondary metabolites have been observed to form tightly linked clusters often located in discrete non-randomly distributed regions on chromosomes (Cuomo et al., 2007). These clusters, known as biosynthetic gene clusters, consist of secondary metabolite biosynthetic enzymes which are often accompanied by regulatory or transport genes within the cluster. Analysis of these biosynthetic gene clusters in *Fusarium* identified numerous classes containing polyketide synthases, nonribosomal peptide synthetases, and terpene synthases as signature enzymes (Hoogendoorn et al., 2018; Kanja et al., 2021). As of December 2022, the Dictionary of Natural Products database listed 783 *Fusarium*-derived

secondary metabolites, encompassing various pharmacologically significant compounds like alkaloids, peptides, amides, terpenoids, quinones, and pyranones. Among these *Fusarium*-derived secondary metabolites, 50 have demonstrated bactericidal effects against Gram-positive strains, 12 against Gram-negative strains, and 17 compounds were effective against both Gram-negative and Gram-positive bacteria. Furthermore, *Fusarium* species were found to be rich in antifungal secondary metabolites, with 27 exhibiting antifungal activity and 41 having dual antifungal and antibacterial properties. Additionally, 23 *Fusarium*-derived secondary metabolites showed antiviral effects, and 39 demonstrated antiparasitic effects (Xu et al., 2023).

Fusaric acid was originally isolated from *F. heterosporum* and is a compound that is used for the industrial synthesis of the pharmaceutical vasodilator bupicomide (Velasco et al., 1975). Fusaric acid has also been clinically studied as a potential treatment of cancers (Fernandez-Pol et al., 1993; Stack et al., 2004), salmonella infection (Li et al., 2014) and tardive dyskinesia (Viukari and Linnoila, 1977). Gibberellic acid, a hormone found both in plants and fungi, was originally isolated from *F. fujikuroi* (Kurosawa, 1926). Gibberellic acid affects plant developmental processes including germination and is used in glasshouses to induce the germination of dormant seeds. Gibberellic acid is also widely used in the barley malting industry (Palmer, 1974). *Fusarium* species are also primary contenders for improving the production of bioethanol from organic waste due to their large array of cell wall degrading enzymes that can break down lignocellulosic materials (Prasoulas et al., 2020). The breakdown products of lignocellulosic materials include D-xylose, which can be fermented into ethanol and other organic acids (Singh and Kumar, 1991).

Fusarium species have been utilised for synthesising metal nanoparticles, such as silver, gold, platinum, silica, and palladium (Rai et al., 2021). The fungus secretes metabolites as a response to environmental stress, which act as reducing and stabilising agents of metal ions in solution. Consequently, metal nanoparticles can be generated from aqueous metal ions using cultured fungal extract (Rai et al., 2021).

Furthermore, the extension of native biosynthetic gene clusters by incorporating genes from non-native homologous clusters has been demonstrated in *F. graminearum*. The polyketide synthase cluster, *PKS15*, was extended using a gene from the homologous gene cluster of *Arthrinium sacchari*, resulting in the production of a novel compound with insecticidal properties (Tsukada et al., 2020).

In the future, *Fusarium* species along with other fungi will increasingly be utilised to power circular solutions in industry and build sustainable net-zero value chains.

5. *Fusarium* species complexes, genomes and research

Over the past 25 years, fully sequenced, assembled and annotated reference genomes have become available for over 189 *Fusarium* species through the vision, technical advances and efforts of large international research collaborations, specific research clusters and/or individual research teams (Fig. 1 and Appendix A.1). In addition, for many of the economically important and most problematic *Fusarium* species, chromosome-scale pangenomes are beginning to emerge. With this wealth of genomic resources and the associated species and strain specific metadata, collectively the community has successfully captured the incredible biological diversity represented by the *Fusarium* genus. Therefore, we have taken this opportunity to further describe and explore how the physical organisation of the different *Fusarium* genomes and the overall genome sizes present amongst the 23 species complexes may or may not have influenced the evolution of *Fusarium* lifestyles and niche occupancies.

5.1. Physical *Fusarium* genome structures and potential relationships to pathogenic and niche occupancy

The current understanding of *Fusarium* genome structures has arisen

from a combination of whole genome sequencing using various longer read sequencing technologies (Hamim et al., 2022) and direct chromosome karyotyping using the germ tube burst method (Waalwijk et al., 2018). When genome structure is considered within a phylogenetic context (Fig. 1), a striking evolutionary pattern of decreasing chromosome numbers is evident across the 23 *Fusarium* species complexes. This compaction of the *Fusarium* genome was originally noted in the first reported comparative whole genome sequencing study, i.e. the *F. graminearum* versus *F. oxysporum* f. sp. *lycopersici* comparison (Cuomo et al., 2007; Ma et al., 2010) and has subsequently been reinforced as additional genomes became available for species in the same and other complexes. The *F. sambucinum* species complex, within which *F. graminearum* resides, is dominated by species with either four or five core chromosomes and either no or two accessory chromosomes (Fig. 1). This genome structure is recognised in all the *F. sambucinum* species complex-assigned species and represents the greatest reduction in core chromosome number. The *F. sambucinum* species complex is considered to be evolutionarily the youngest. Within the global reference *F. graminearum* PH-1 isolate genome, the positions of the presumed ancient chromosome fusion events have been defined (Cuomo et al., 2007; King et al., 2015, 2017; Lu et al., 2022) (the latest PH-1 genome annotation).

The *F. sambucinum* complex contains species that are soil saprotrophs, and most are plant pathogens of cropped cereal species and various temperate field vegetable species. However, increasingly non-cereal species included in cereal rotations are known to be *Fusarium* hosts, for example, soybean, sugar beet, potato, as well as wild grass growing within the cropped cereal landscape, although not all of these additional hosts go on to develop disease symptoms. A few species are non-pathogenic, for example *F. longipes*. The host range for many pathogenic *sambucinum* species is > 100 plant species. Many species in the *sambucinum* complex are mycogenic, with the majority producing either Type A or Type B sesquiterpenoid trichothecene mycotoxins such as HT2 and T2, DON, NIV, NX2 or NX3 (Johns et al., 2022; Perochon and Doohan, 2024). Some species also produce the nonsteroidal estrogenic mycotoxin zearalenone (Gajęcki and Gajęcka, 2023). For the majority of mycogenic species, mycotoxin production only occurs *in planta* but can be induced in cultures by the addition of reactive oxygen species, specific polyamines and/or altering solute concentrations (reviewed by Kanja et al., 2021). Globally and regionally some of the most important plant pathogens affecting food security reside in this species complex, including *F. graminearum* (discussed above), *F. culmorum*, *F. pseudograminearum*, *F. asiaticum* and *F. poae*. Single isolates recovered for five species in this complex can infect the Lepidoptera and Hymenoptera insect orders (Santos et al., 2020). The industrial fungus *F. venenatum* also resides in this species complex (King et al., 2018).

Four other *Fusarium* species complexes have a relatively low number and consistent number of core chromosomes, namely *chlamydosporum* $n =$ eight, *incarnatum-equiseti* $n =$ eight or nine, *heterosporum* $n =$ seven and *tricinctum* $n =$ eight (Fig. 1). Within each of these complexes there are species and isolates with or without the presence of a limited number of lineage specific chromosomes. Unfortunately, none of these species complexes have a chromosome scale genome assembly available. The *chlamydosporum* species complex contains various plant pathogens of cereal species as well as the human pathogen *F. chlamydosporum*. Some isolates of the latter species can infect specific insect orders. The *incarnatum-equiseti* species complex contains various plant pathogens mostly of non-cereal species and a couple that infect cereal species. Some mycogenic species are present. Each of these plant pathogenic species has only a limited host range reported, typically one to ten species. *F. scripi*, originally isolated from plant debris washed from soil, has not been demonstrated to have a pathogenic lifestyle. This species is now used in the industrial production of silver nanoparticles (as described above). Also present in the *incarnatum-equiseti* species complex is the human pathogen *F. incarnatum-equiseti*, the plant endophytic species *Fusarium hainanense* and five other species that are pathogenic towards one or more insect orders. The *heterosporum* species complex contains

isolates either pathogenic towards *Claviceps purpurea*, a cereal infecting fungus or a specific insect order. The *tricinctum* species complex contains various plant pathogens of cereal and/or non-cereal species which may or may not produce harmful mycotoxins, including enniatins (ENs) and moniliformin (MON) (Laraba et al., 2022). In summary, the majority of the species in these four complexes, with a relatively low and consistent number of core chromosomes, are not human pathogens. A high proportion are pathogens of cereals and/or non-cereal species and a few are known to produce mycotoxins or other secondary metabolites during plant infections. Other life strategies such as free-living and endophytic are present but uncommon and only present in the *incarnatum-equiseti* complex. Fungal and insect-infecting species are present in all four complexes.

Species in the *F. oxysporum* complex consistently have 11 core chromosomes, some with smaller 1–1.5 Mb lineage specific regions at the ends of specific chromosomes, accompanied by a variable number of lineage specific (LS) chromosomes, typically two to four (Fig. 1; Appendix A.1). Unlike in the *F. sambucinum* species complex, most of the *F. oxysporum* species complex memberships are soil saprotrophs and plant pathogenic fungi with a narrow host range of predominantly annual vegetable, perennial shrub, tree or tree-like species. To date, the majority of the genes identified in determining plant species host range are located on the accessory chromosomes (see below). *F. oxysporum* and *F. solani* are capable of infecting immunocompromised mice, although up to 12 species of *Fusarium* have been reported to cause fusariosis of immunocompromised human patients (Nucci and Anaissie, 2007). *F. oxysporum* strains have so far been reported to infect insect hosts of the orders *Coleoptera* (beetles), *Hemiptera* (true bugs) and *Lepidoptera* (butterflies and moths) (Santos et al., 2020). Various fungal infecting species are also present in this complex.

Two *Fusarium* species complexes have a relatively high number of core chromosomes, and these numbers are not as consistent as in the aforementioned species complexes. Species in the *fujikuroi* complex have 10–13 core chromosomes, whilst species in the *solani* complex have 9–12 core chromosomes. The lineage specific chromosomes of both species complexes are also inconsistent in number, ranging from zero to two in *fujikuroi* and zero to three in *solani* species. The *fujikuroi* species complex includes more than 60 species and contains almost exclusively pathogenic species important in agricultural or medical settings (Yilmaz et al., 2021). A few species, including *F. fujikuroi*, *F. proliferatum* and *F. verticillioides*, are mycogenic and produce various mycotoxins including the potentially carcinogenic fumonisin B1, and *F. torulosum* which produces a toxin during infection of the pasture grass species kikuyu (*Cenchrus clandestinus*) which then poisons grazing cattle. To date 26 species have sequenced genomes present in public databases. Chromosome scale genomes are only present for three species: *F. circinatum* which causes bark cankers on specific conifer tree species, *F. fujikuroi* causes major disease problems in maize and wheat production in warmer regions and *F. verticillioides* is a major maize pathogen. The core chromosome numbers range from 12 or 13 in *F. circinatum* with or without two LS chromosomes, to 10 or 11 core chromosomes in *F. fujikuroi* each with two LS chromosomes or a consistent 10 core chromosomes in *F. verticillioides* with a single LS chromosome (Chiara et al., 2015; Yao et al., 2023; Wingfield et al., 2012; Waalwijk et al., 2018). Notable amongst the plant pathogenic species are several that cause malformation disease in mango trees and flowers due to induced hormone imbalances, namely *F. mangiferae*, *F. mexicanum* and *F. sterilihyphosum*. *F. fujikuroi* causes bakanae/foolish disease of rice seedlings due to gibberellin production. In addition to causing serious cereal diseases, other monocotyledonous hosts include banana, pineapple, palms, onions, asparagus and an orchid species (Appendix A.1). Some species have very wide host ranges, for example *F. proliferatum* can also be a plant endophyte, whereas others have so far only been reported to cause disease on one or a few species. One species in the *fujikuroi* complex infects the fungal host *Cronartium conigenum* which causes blister canker of pine trees in some USA states, whilst other isolates are

pathogenic towards commercial *Laelia* orchids in Malaysia. In addition, specific isolates of seven *F. fujikuroi* species can infect different insect hosts present in five orders, including the sole report of a pathogenic *F. verticilloides* isolate on the order *Orthoptera* (grasshoppers, locusts and crickets) (Santos et al., 2020). In summary, the species in the *fujikuroi* complex have probably the most diverse terrestrial hosts and lifestyles and, similar to fungi in the genus *Metarhizium*, likely act as generalists and keystone species (Brancini et al., 2022). Most species in the *fujikori* and *solani* species complexes discussed here are underexplored, with the exception of the mycogenic producing species.

Amongst the other *Fusarium* species, genome sizes vary considerably even when the phylogenetic analyses have indicated a relatively close evolutionary relatedness. For example, the genomes of *F. lateritium* and *F. buharicum* differ in size by 9 Mb at 47 Mb and 36 Mb, respectively, and the *F. burgessi* and *F. redolens* genomes by 13 Mb, at 47 Mb and 54 Mb, respectively (Fig. 1). Whereas the basal species *F. dimerum* has a genome size of 36 Mb which is very similar in size to many species residing within the youngest species complex, *F. sambucinum*. Other *Fusarium* species predicted to reside close to the base of the phylogenetic tree, namely *F. decemcellulare* and *F. redolens* have far larger genomes at 51 Mb and 54 Mb, respectively. These dramatic differences in genome size indicate that various known, as well as currently unreported evolutionary processes and mechanisms potentially controlling the expansion and contraction of *Fusarium* genome sizes are likely to be operating either globally, regionally, or locally in these different *Fusarium* species. Some of the genome structure and size changes are potential responses to physical and chemical stresses encountered during environmental and/or during host niche occupancy. Others genome structure changes may have arisen through non-*Fusarium* interspecies biological interactions with either antagonistic or symbiotic pathogenic fungal species, free-living fungal species and/or other types of microorganisms. Alternatively, the strains used to generate the sequenced and assembled genome may in the future turn out to be a species outlier which possess either atypical evolutionary histories and/or adaptive mechanisms to protect unique niche occupancy/lifestyle patterns.

6. The known and potential roles of lineage-specific chromosomes in two *Fusarium* species complexes

LS-chromosomes are typically 1-3 Mbp in size, vary in number between strain within a fungal species and can be artificially transferred between strains to confer novel traits (Ma et al., 2010). LS-chromosomes are dispensable but can play important roles under specific conditions such as conferring pathogenicity towards a particular host (Li et al., 2020a).

6.1. The *F. oxysporum* species complex and gene-for-gene relationships

F. oxysporum isolates are soil saprotrophs, plant pathogens and plant endophytes grouped into more than 150 *formae speciales* based on which of the ~120 known hosts each species does or does not infect (Edel-Hermann and Lecomte, 2019). Most species infect via wounded roots and then enter the host. Pathogenic isolates go on to colonise and block xylem vessels in the roots and lower stem tissues and this results in entire plant wilting symptoms. Each *Fusarium* species' host range varies from a single species to multiple genera. In addition, particular host specificities have arisen multiple times in different lineages by horizontal gene transfer (van Dam et al., 2017; Carmona et al., 2020; Brenes Guallar et al., 2022). Often host species specialisation has been altered by specific genomic selection events (Afordoanyi et al., 2022). For example, the transfer of complete (Ma et al., 2010) or parts (Li et al., 2020a) of LS chromosomes between strains can confer alterations to pathogenicity. *F. oxysporum* is the most intensively sequenced *Fusarium*, with 724 genome assemblies available: (<https://www.ncbi.nlm.nih.gov/assembly/?term=Fusarium%20oxysporum>; [27/6/2023]), and many strains continually being published (Sabahi et al., 2022).

Unlike other *Fusarium*-cereal interactions (Kanja et al., 2021), many *F. oxysporum* f. sp. - plant interactions conform to Flor's classic gene-for-gene concept in plant pathology (Flor, 1942). Put simply into a biological context, the production of a single pathogen gene product, usually at the onset of the infection cycle, leads the host to directly or indirectly detect the pathogen's presence and then successfully activate an effective defence response to stop further colonisation by the now detected pathogen. In the case of *F. oxysporum* f. sp. and many other filamentous pathogen-plant interactions, the detected pathogen gene products are small, secreted proteins called effectors which are hypothesised or known to contribute to the disease-causing ability of the pathogen (Kamoun, 2006; Wilson and McDowell, 2022). For *F. oxysporum* f. sp. different lineage-specific Secreted In Xylem (SIX) effectors, encoded on discrete regions of LS chromosomes, were shown to be responsible for host-specific pathogenicity (Van Dam et al., 2017). In a recent study, a hierarchical clustering of the repertoire of predicted secreted protein effectors for all *F. oxysporum* f. sp. was also shown to correlate well with the host specificity of many isolates (Brenes Guallar et al., 2022). However, this correlation was less obvious for some isolates which have introgressed transposon-rich accessory regions within core chromosomes. Accessory genome elements are present in LS chromosomes in many fungal taxa (Bertazzoni et al., 2018). It is increasingly evident that the significant abilities of *F. oxysporum* f. sp. to exploit different scenarios have arisen through the acquisition or loss of accessory genome elements. For example, changes to the many host niches *F. oxysporum* spp. can occupy (Bertazzoni et al., 2018; Yang et al., 2020), adapt to host resistance (Biju et al., 2017) and exploit increased temperatures (Epstein et al., 2017; Kaur et al., 2022) by carrying LS polyketide genes (Yang et al., 2020), LS effectors (Ma et al., 2010) and/or LS transcription factors that promote their expression (van der Does et al., 2016).

Interestingly, isolates of *F. oxysporum* that exhibit host-specific pathogenicity, can also colonise the outer layers of the roots of many other plant species asymptotically as apoplastically-localised endophytes. A recent study has revealed that an additional set of effectors, called Early Root Colonisation (ERC) effectors are secreted during the initial biotrophic growth phase on both the main and alternative host plant species (Redkar et al., 2022b). Unlike the SIX effectors, the ERC genes have homologous sequences across the entire *oxysporum* species complex, are located on the core chromosomes and are present in other phytopathogenic fungi. *ERC* gene deletion in a pathogenic *F. oxysporum* f. sp. *lycopersici* isolate led to reduced virulence and rapid activation of plant immune responses, whilst in a nonpathogenic isolate *ERC* gene deletion resulted in impaired root colonisation (Redkar et al., 2022b).

Genomic signatures of sexual reproduction have been reported for *F. oxysporum* f. sp. *ciceris* (Fayyaz et al., 2023) but although Mating Type (MAT) genes remain and are expressed in *F. oxysporum* field isolates (Yun et al., 2000), no sexual morphs have been successfully characterised and sexual reproduction is likely rare at best in the *F. oxysporum* lineage. The *F. oxysporum formae speciales* form a complex of closely related, asexual taxa in which parasexual crossing can promote diversity. Conidial anastomoses between incompatible isolates can produce viable heterokaryons (Shahi et al., 2016; Kurian et al., 2018; Epstein et al., 2022) in which parasexual recombination could generate new pathotypes (Teunissen et al., 2002; Epstein et al., 2022). Active transpositions in genomes have also resulted in loss of gene function which has enabled adaptation to host resistance (Inami et al., 2012; Kashiwa et al., 2016).

6.2. The *F. solani* species complex

Most of the 100+ species in the *F. solani* species complex (FSSC) are ubiquitous in natural environments and are often soil saprotrophs (Zhang et al., 2006). Many species are responsible for mortality in farmed or wild animals, immunocompromised humans or plant hosts (Coleman 2016; Hoh et al., 2022). Whereas, in immunocompetent

humans the diseases are more localised and less invasive, including abscesses, onychomycosis and/or keratitis. In veterinary and clinical settings, the general disease name given is fusariosis. In agricultural settings the typical disease symptoms are necrotic stem base and/or root rots and these subsequently result in the wilting, stunting and chlorosis of stems and/or leaves and in the case of soybean crops sudden-death syndrome caused by *F. virguliforme* is particularly problematic. Many species in the *solani* complex infect more than one plant species but typically <10 hosts. For most interactions the underlying pathogenicity processes have not been fully investigated. But in a few cases the mechanism is known. For example, *F. vanettenii* (formerly *F. solani* f. sp. *pisi*) inactivates by demethylation the inducible plant specific defence compound pisatin to cause a root disease on pea plants (Milani et al., 2012). The required *PDA1* and *PEP* genes are located in a discrete region of an LS chromosome. Recently, the *solani* species complex has been re-organised based on a three-loci phylogenetic analysis into three major clades, with the majority of species, many with highly contrasting lifestyles, placed in clade 3 (Geiser et al., 2021) (as described above).

In summary, LS chromosomes in some *Fusarium* species are increasing being recognised to play important and diverse roles in niche occupancy and ‘in host’ lifestyles. The recognition that some LS fragments are also found to reside at the ends of core chromosomes also now hints to the relocation of key genetic information by a mechanism(s) currently underexplored in *Fusarium* species.

6.3. Model organisms for *Fusarium* research

Studying *Fusarium* infection and colonisation strategies using model species (Table 4, Fig. 3) allows for the exploration of various mechanisms underlying successful or unsuccessful host infections. One of the first reported use of a model species – *Fusarium* interaction was the study by Urban et al. (2002). To date, the use of nine plants, one vertebrate and one invertebrate host species as models to explore *Fusarium*-host interaction research have been documented (Table 4). Probably the most widely used model plant species is *Arabidopsis thaliana* (thale cress) for root, stem-base, leaf and/or floral infection analyses. Recently, basal land plants, such as *Physcomitrella patens* have been utilised. For example, *P. patens* is now known to induce immune responses following *F. solani* infection even though disease symptoms are mild (Mamaeva et al., 2023). As with most biological research, use of model organisms is a convenient and reproducible strategy for studying interactions, phenotypes and genomic factors. However, as many *Fusarium* species have restricted host ranges, there is a growing consensus that specific host-pathogen interactions need to be studied in their native hosts. In addition, the growing availability of host genomes/pan-genomes, especially for cropped plant species, combined with the use of dwarf

cultivars and/or faster generation cycling methods/lines, may decrease the necessity to use model organisms in future *Fusarium* research.

7. Future research directions

Numerous *Fusarium* species remain problematic and impose challenges for many agricultural, clinical and veterinary sectors: the range of disease control options is generally poor with only low efficacy and/or multi-site fungicides now available (for example, Fusarium Head blight in wheat (Barro et al., 2023), Panama disease of banana caused by Tropical Race 4 (Cannon et al., 2022), and human fusariosis (Batista et al., 2020)). Most agricultural practice alterations such as crop rotations or crop residue removal are at best only partially effective. Breeding in new sources of host resistance without compromising yields or quality remains quite problematic. Whilst strict sanitation/quarantine restrictions are increasingly difficult to implement due to the daily high volumes of fresh/dried goods traded and transported locally and globally. There is an urgent need to discover new accessible targets for chemical intervention and to find new ways to enhance host resistance mechanisms. In this regard, fungal pathogenomics inspired approaches are gaining momentum because pangenome analyses are revealing the core gene repertoires potentially deployed by each problematic species for invasive purposes (Rampersad, 2020; Kanja et al., 2021). Inhibiting the biosynthesis of specific fungal inner and outer cell wall components is also emerging as an attractive option to target with novel antifungal drugs (Gow and Lenardon, 2023). In addition, the repurposing of already registered non-antifungal drugs through computer modelling, docking simulations and then experimental validation for potential antifungal purposes is another option under serious consideration (Kim et al., 2020; Reddy et al., 2022). To fully achieve these pathogens focussed approaches for *Fusarium* species, additional fundamental knowledge needs to be gained on the *Fusarium* genes, pathways and processes required for initial infection and the subsequent disease formation processes. In the Pathogen-Host Interactions database (www.PHI-base.org, Urban et al., 2022; Cuzick et al., 2023), 601 *Fusarium* genes from 11 species have been formally demonstrated to be required for one or more aspects of the pathogenic process in one to a few host species. However, the vast majority of these gene function studies have involved just two *Fusarium* species namely, *F. graminearum* and *F. oxysporum* f. sp. *lycopersici*. Therefore, our understanding of the mechanisms underlying the wealth of different *Fusarium* lifestyles occurring on and within different host tissue niches still remains highly fragmentary and incomplete. To enhance host disease resistance and deliver sustainable disease control there is a need to discover and understand which plant and animal defence mechanisms are effective against different *Fusarium* species as well as other problematic fungal

Table 4
Fusarium species known to have the ability to infect model organisms.

Model organisms		
<i>Arabidopsis thaliana</i> (Thale cress)	Main plant model organism. Dicot angiosperm with small genome. <i>F. oxysporum</i> naturally causes wilt disease via the roots. Young seedlings, rosette leaves and floral tissues susceptible to cereal head blight causing species <i>F. graminearum</i> and <i>F. culmorum</i> .	Wang et al. (2024) Wood et al. (2020) Wang et al. (2022) Urban et al. (2002) Peraldi et al. (2011)
<i>Brachypodium distachyon</i> (Purple false brome)	Monocot model grass species, smaller genome than cultivated relatives and faster generation time. <i>F. graminearum</i> causes Fusarium Head Blight.	
<i>C. elegans</i> (Free living nematode, roundworm)	Model species for a variety of biological and genomic applications. Lethal infection after consumption of conidia of <i>F. solani</i> , <i>F. oxysporum</i> or <i>F. proliferatum</i> .	Muhammed et al. (2012)
<i>Marchantia polymorpha</i> (Common liverwort)	Nonvascular model land plant species. <i>F. oxysporum</i> was shown to cause endophytic root colonisation.	Redkar et al. (2022a)
<i>Mus</i> spp. (Mouse)	Mouse model for human and mammal fusariosis studies. <i>F. oxysporum</i> infection in various organs.	Schäfer et al. (2014)
<i>Nicotiana benthamiana</i> and <i>N. tabacum</i> (Tobacco)	Dicot model organisms used for plant-pathogen interactions, particularly for protein interactions. <i>F. graminearum</i> causes floral infections.	Urban et al. (2002)
<i>Physcomitrium patens</i> (Spreading earthmoss)	Bryophyte that represents more ancient lineages of vascular plants. <i>F. solani</i> can infect with mild symptoms.	Mamaeva et al. (2023)
<i>Populus trichocarpa</i> (Black cottonwood)	Model tree/woody plant genus with small genome (<i>Populus trichocarpa</i> sequence is available) and fast growth. <i>F. solani</i> causes root and vascular wilt.	Su et al. (2021)

species (Case et al., 2022). New approaches to *Fusarium* disease control include genetically engineered and/or modified crops by gene editing, alongside traditional plant breeding to enhance disease resistance whilst maintaining high yields and good product quality. For some *Fusarium* species and agricultural crop production systems, cross kingdom small RNA interference (ckRNAi) focussing on specific *Fusarium*-specific targets may become a viable option (reviewed Machado et al., 2018; Moonjely et al., 2023). For other *Fusarium* problems, biological control methods with suitable bacterial and/or other fungal species (Mulik et al., 2022; Attia et al., 2022) or by designing a synthetic microbial community (Prigigallo et al., 2022) or via manipulation of below- and/or above-ground microbiomes (Karlsson et al., 2021; Hong et al., 2023) are already considered to be viable options to limit outbreaks and/or reduce the overall disease pressures.

In the last 20 years, an increasing number of reports connecting *Fusarium* species with vertebrate infection has been observed (Bansal et al., 2019; Batista et al., 2020). The sequenced genomes available for different *Fusarium* species should permit the future development of multiplex detection techniques that can accurately establish the presence or absence of different *Fusarium* species in lesions/infected tissues from a diverse number of vertebrates. This approach is already increasingly in use for *Fusarium* incited plant disease diagnostics (Vázquez-Rosas-Landa et al., 2021; Achari et al., 2023) and for phylogenetic analyses (O'Donnell et al., 2022). Global warming and modifications to the natural environments may render animals more susceptible to infection by one or more opportunistic pathogens, including *Fusarium* species. Studies that evaluate the impact of climate change and habitat modification where increased fusariosis cases are suspected must be established. Vertebrates and/or plants could serve as reservoirs for fungi including different *Fusarium* species with the potential to jump to humans (Casadevall, 2019). Therefore, the identification of these reservoirs is required to avoid new epidemics.

Many of the *Fusarium* species described in this review can thrive in a wide range of stressful environments including water environments (marine, brackish and/or freshwater), soils that are continually waterlogged, arid, or anywhere in between and in anthropomorphic environments, including terrestrial and aquatic sites contaminated with pollutants such as oil and heavy metals, jet fuel, and have even made it into space, as illustrated in Fig. 2. Collectively, *Fusarium* species must have further evolved various known gene, protein and metabolite networks and other physiological mechanisms already well investigated in other fungal species needed for carbon and nitrogen metabolism (Huberman et al., 2021; Wu et al., 2020), osmoregulation (Pérez-Llano et al., 2020), coping with various oxidative stresses (Shay et al., 2022; Yaakoub et al., 2022), using different signalling molecules, for example nitrous oxide (Zhao et al., 2020b) as well as evolving or acquiring specific mechanisms to ward off potential competitor species that could also be occupying these highly specialised niches (Magan, 2007). *Fusarium* species are also highly likely to possess many yet to be discovered constitutive or inducible *Fusarium* specific mechanisms, both possibly regulated in new and highly flexible ways to maintain successful living within these stressful and potentially ever changing micro- and macro-niches. Several fundamental questions that remain to be answered include: Is this colonisation and reproductive success in these stressful environments due to specialist fungal characteristics *per se* or the 'genius of the genome evolution still ongoing in the *Fusarium* genus' that the required mechanisms only become triggered at specific interfaces for example fuel/air, water/air/physical surfaces, etc? Or is the overall success of the *Fusarium* genus due to the additional flexibility of their baseline saprotrophic lifestyles and predominantly soil/plant debris based mycelial networks which also includes inducible systems conferring the ability to produce a wider range of secondary metabolites as and when required? Or do *Fusarium* species occupy a wider and more complex range of stressful conditions because hyphal growth/viability

can be maintained for longer, and/or different types of hyphal dormancy are triggered and/or because a different repertoire of dormant resting spore types are made?

Increasingly *Fusarium* species are recognised as being part of disease complexes either with other *Fusarium* species, other pathogenic fungal species and/or other types of microbes and insects. The role(s) of *Fusarium* species in each of these disease complexes is for the most part under-explored. Whether the *Fusarium* dominated disease complexes will remain with the same species membership in crop monocultures, specific crop rotations, in farmed animals or natural vertebrate and invertebrate populations will change as agricultural systems alter in the face of climate change pressures or as agricultural production further encroaches into additional natural habitats is currently unknown (Chaloner et al., 2021). A changing species membership would likely have implications for the durability of anticipated new approaches to disease control. Also, how many more of these *Fusarium* dominated disease complexes have yet to be discovered and will any of these have beneficial rather than detrimental consequences?

There currently exists in the public databases numerous *Fusarium* genomes without annotations or with only minimal annotations (Appendix A.1). Going forward, as a minimum, it is essential that existing high coverage genome sequences are assembled and annotated into the core and accessory portions as well as where data are already available that global pangenomes are established for at least a few species from within each of the 23 recognised *Fusarium* species complexes. This will then provide the necessary framework to undertake detailed inter-species comparative analyses and to develop new diagnostic and surveillance technologies that could be deployed in a wide range of agricultural, medical, and other anthropomorphic settings to aid disease modelling and disease prediction studies locally and/or globally.

Extensive research has been directed towards comprehending the diversity of *Fusarium* biosynthetic pathways and characterising resultant products. Prospective research avenues lie in the exploration of industrial utilities for these compounds (Abdel-Azeem et al., 2019b). Thus, we envision a proliferation of industrially significant *Fusarium*-derived products in the near future. Furthermore, to aid in our unceasing endeavour to abate environmental pollution, such as that arising from heavy metal accumulation, we are optimistic about leveraging the potential of *Fusarium* spp. to effectively mitigate these challenges.

Functional genomics approaches to investigate gene function in *Fusarium* species began ~30 years ago with the deletion of the *TRI5* gene in *F. graminearum* (Proctor et al., 1995). Since the early days of gene deletions in *Fusarium*, an additional 12 pathogenic *Fusarium* species have been successfully transformed. These species are listed in the Pathogen-Host Interactions database (Urban et al., 2022). In addition, the Quorn fungus *F. venenatum* is transformable (Wilson and Harrison, 2021). The transformation techniques used include both *Agrobacterium*-mediated transformation and polyethylene glycol-mediated protoplast transformation to modify gene function (Weld et al., 2006). Recently, the first target site integration locus for *F. graminearum* transformation has been identified and successfully used for gene complementation, promoter reporter and protein localisation construct evaluation (Darino et al., 2024). Overall, the genus *Fusarium* seems quite amenable to functional genomics analysis, and we expect this to hold true for the majority of the 431 *Fusarium* species in the NCBI Taxonomy list. This opens up the possibility of analysing and understanding the variety and diversity of *Fusarium* protein functions to increase our understanding of many new aspects of fundamental fungal biology. In addition, the new knowledge gained from these functional genomics analyses will help to formulate new ways to prevent *Fusarium* epidemics and enable the development of new bioremediation and protection processes.

8. Take home messages

- 431 *Fusarium* species have been formally described and classified. These are organised into 23 *Fusarium* species complexes. Many 1000s more await formal taxonomic classification.
- The genome sizes and chromosome organisation present in each of the *Fusarium* species complexes is distinct. The more recently evolved species have fewer core chromosomes and also no or two lineage specific chromosomes.
- No *Fusarium* species have so far been described as an obligate biotrophic pathogen. The majority are either free-living saprotrophs or have hemibiotrophic or necrotrophic pathogenic lifestyles. In natural ecosystems, a few species are plant endophytes or insect symbionts.
- Genome-based analyses can provide important insights into *in-situ* ecology (see also [Hallsworth et al., 2023a](#)).
- A very diverse range of disease symptoms have been reported to be associated with pathogenic *Fusarium* species, including for plants soft or dry rots of roots, stem bases and/or fruits, vascular wilts, floral blights and grain shrivelling, floral/stem hypertrophy or sudden defoliation/death. For immunocompetent humans and other vertebrates and invertebrate hosts, disease symptoms include superficial skin or shell lesions or progressive egg infections. For immunocompromised humans, diseases include deeper eye, lung, kidney, vascular infections and in some cases death.
- Only some *Fusarium* species produce problematic mycotoxins. The chemical entities secreted are diverse in structure and function. For mycogenic species, mycotoxin production is only essential for disease formation on some but not all host species and/or the specific tissues or organs colonised.
- The host ranges of *Fusarium* species are highly plastic and where the underlying mechanisms have been investigated are often linked to the acquisition of new genetic materials via predominantly asexual mechanisms, including hyphal tip fusion, gain and loss of lineage specific chromosomes. For many species the identified host range determinants so far reported are small proteinaceous effectors or chemical detoxification enzymes.
- Many *Fusarium* species have important industrial, medical and nutritional uses, but most *Fusarium* species remain underutilised.

9. Final remarks

The information in this review has been obtained from >100 specialist research journals spanning the life sciences, organic and inorganic chemistry, food science, food security and climate change. By reviewing this wealth of highly fragmented knowledge we have been able to explore many of the positive and negative ways *Fusarium* species impact on the daily lives of humans, animals, plants, invertebrates, bacteria, and other fungi, whilst living in different natural or artificial habitats and communities present on land, in the soil, in fresh or marine water, in the air or in outer space. There is much still to be discovered in the fascinating and ever-growing world of *Fusarium* species.

CRedit authorship contribution statement

Victoria J. Armer: Conceptualization, Data curation, Formal analysis, Investigation, Methodology, Visualization, Writing – original draft, Writing – review & editing. **Erika Kroll:** Conceptualization, Visualization, Writing – original draft, Writing – review & editing. **Martin Darino:** Conceptualization, Writing – original draft, Writing – review & editing. **Daniel P. Smith:** Conceptualization, Data curation, Formal analysis, Resources, Writing – original draft, Writing – review & editing. **Martin Urban:** Conceptualization, Visualization, Writing – original draft, Writing – review & editing. **Kim E. Hammond-Kosack:** Conceptualization, Data curation, Formal analysis, Funding acquisition, Investigation, Project administration, Supervision, Validation, Visualization, Writing – original draft, Writing – review & editing.

Acknowledgements

We apologise to authors and researchers who have renamed species recently which we have failed to include here. Martin Darino, Martin Urban and Kim Hammond-Kosack are supported by the Biotechnology and Biological Sciences Research Council (BBSRC) Institute Strategic Programme (ISP) Grant, Delivering Sustainable Wheat (BB/X011003/1) within the Work package Delivering Resilience to Biotic Stress (BBS/E/RH/230001B) and the BBSRC grants (BB/X012131/1 and BB/W007134/1). Dan Smith was supported by the BBSRC ISP Grant (BB/CCG2280/1). Victoria Armer and Erika Kroll are supported by the BBSRC-funded South West Biosciences Doctoral Training Partnership

(BB/T008741/1). Fig. 2 was produced in Icograms and combined with modified images obtained from a licenced version of Biorender. This review article is dedicated to the memory of Professor Naresh Magan (1953–2023) who was an exceptional scientist and both a great mentor and friend within and beyond the global fungal community; [Hallsworth et al. \(2023b\)](#).

Appendix A. Supplementary data

Supplementary data to this article can be found online at <https://doi.org/10.1016/j.funbio.2024.07.004> and also as a dataset at DOI: [10.5281/zenodo.12762856](https://doi.org/10.5281/zenodo.12762856). The information within this Appendix was correct as of March 2024 and includes information on Species, NCBI identifier, Assigned Phylogenetic Clade, the number of genomes available on NCBI, Ungapped Genome Size, Number of Chromosomes, Number of Core and Lineage Specific (LS) Chromosomes (by karyotyping), the Sequencing Methodology and Source. It also includes an extensive, but not universal, curation of known host ranges for each species with accompanying literature citations for many species.

References

- Abbas, H.K., Cartwright, R.D., Xie, W., Mirocha, C.J., Richard, J.L., Dvorak, T.J., Sciumbato, G.L., Shier, W.T., 1999. Mycotoxin production by *Fusarium proliferatum* isolates from rice with *Fusarium* sheath rot disease. *Mycopathologia* 147 (2), 97–104.
- Abdel-Azeem, A.M., Abdel-Azeem, M.A., Abdul-Hadi, S.Y., Darwish, A.G., 2019a. *Aspergillus*: Biodiversity, ecological Significances, and industrial applications. In: Yadav, A., Mishra, S., Singh, S., Gupta, A. (Eds.), *Recent Advancement in White Biotechnology through Fungi*. Springer, Cham.
- Abdel-Azeem, A.M., Abdel-Azeem, M.A., Darwish, A.G., Nafady, N.A., Ibrahim, N.A., 2019b. *Fusarium*: biodiversity, ecological significances, and industrial applications. In: Yadav, A., Mishra, S., Singh, S., Gupta, A. (Eds.), *Recent Advancement in White Biotechnology through Fungi*. Springer, Cham.
- Achari, S.R., Mann, R.C., Sharma, M., Edwards, J., 2023. Diagnosis of *Fusarium oxysporum* f. sp. *Ciceris* causing *Fusarium* wilt of chickpea using loop-mediated isothermal amplification (LAMP) and conventional end-point PCR. *Sci. Rep.* 13, 2640.
- Adhikari, M., Negi, B., Kaushik, N., Adhikari, A., Al-Khedhairi, A.A., Kaushik, N.K., Choi, E.H., 2017. T-2 mycotoxin: toxicological effects and decontamination strategies. *Oncotarget* 8 (20), 33933–33952.
- Afordoanyi, D.M., Diabankana, R.G.C., Akosah, Y.A., Validov, S.Z., 2022. *Are formae speciales* pathogens really host specific? A broadened host specificity in *Fusarium oxysporum* f.sp. *umonis-cucumerinum*. *Braz. J. Microbiol.* 53 (4), 1745–1759.
- AHDB, 2023. Risk assessment for fusarium mycotoxins in wheat. Available at. <https://ahdb.org.uk/mycotoxins>. Accessed 1st September 2023.
- Alderman, D.J., 1982. Fungal diseases of aquatic animals. In: Roberts RJ (Eds) *Microbial Diseases of Fish*, Society for General Microbiology, Special Publication. Academic Press, London, pp. 189–242, 9.

- Alderman, D.J., Polglase, J.L., 1986. Are fungal diseases significant in the marine environment? In: Moss, S.T. (Ed.), *The Biology of Marine Fungi*. Cambridge University Press, London, pp. 189–198.
- Al-Hatmi, A.M., Hagen, F., Menken, S.B., Meis, J.F., De Hoog, G.S., 2016. Global molecular epidemiology and genetic diversity of *Fusarium*, a significant emerging group of human opportunists from 1958 to 2015. *Emerg. Microb. Infect.* 5 (1), 1–11.
- Ali, H., Pei, M., Li, H., Fang, W., Mao, H., Khan, H.A., Nadeem, T., Lu, G., Olsson, S., 2022. The wheat head blight pathogen *Fusarium graminearum* can recruit collaborating bacteria from soil. *Cells* 11 (19), 3004.
- Attia, M.S., Abdelaziz, A.M., Al-Askar, A.A., Arishi, A.A., Abdelhakim, A.M., Hashem, A.H., 2022. Plant growth-promoting fungi as biocontrol tool against *Fusarium* wilt disease of tomato plant. *J. Fungi* 8 (8), 775.
- Babbitt, S., Gally, M., Pérez, B.A., Barreto, D., 2002. First report of *Nectria haematococca* causing wilt of olive plants in Argentina. *Plant Dis.* 86, 326.
- Bacon, C.W., Williamson, J.W., 1992. Interactions of *Fusarium moniliforme*, its metabolites and bacteria with corn. *Mycopathologia* 117, 65–71.
- Bansal, Y., Singla, N., Kaistha, N., Sood, S., Chander, J., 2019. Molecular identification of *Fusarium* species complex isolated from clinical samples and its antifungal susceptibility patterns. *Curr. Med. Mycol.* 5 (4), 43–49.
- Barro, J.P., Santana, F.M., Tibola, C.S., Machado, F.J., Schipanski, C.A., Chagas, D.F., Guterres, C.W., Casarotto, G., Capitano, C.G., Dallagnol, L.J., Kuhnem, P., Feksa, H.R., Venancio, W.S., Del Ponte, E.M., 2023. Comparison of single- or multi-active ingredient fungicides for controlling *Fusarium* head blight and deoxynivalenol in Brazilian wheat. *Crop Protect.* 174, 106402.
- Batista, B.G., Chaves, M.A., Reginatto, P., Saraiva, O.J., Fuentesfria, A.M., 2020. Human fusariosis: an emerging infection that is difficult to treat. *Rev. Soc. Bras. Med. Trop.* 53, e20200013.
- Belhassen, H., Jiménez-Díaz, I., Arrebola, J.P., Ghali, R., Ghorbel, H., Olea, N., Hedili, A., 2015. Zearalenone and its metabolites in urine and breast cancer risk: a case-control study in Tunisia. *Chemosphere* 128, 1–6.
- Berka, R.M., Rey, M.W., Brown, K.M., Byun, T., Klotz, A.V., 1998. Molecular characterization and expression of a phytase gene from the thermophilic fungus *Thermomyces lanuginosus*. *Appl. Environ. Microbiol.* 64 (11), 4423–4427.
- Berka, R.M., Nelson, B.A., Zaretsky, E.J., Yoder, W.T., Rey, M.W., 2003. Genomics of *Fusarium venenatum*: an alternative fungal host for making enzymes. In: Arora, D.K., Khachatourians, G.G. (Eds.), *Applied Mycology & Biotechnology, Fungal Genomics*. Elsevier Science, Amsterdam.
- Bertazzoni, S., Williams, A.H., Jones, D.A., Syme, R.A., Tan, K.C., Hane, J.K., 2018. Accessories make the outfit: accessory chromosomes and other dispensable DNA regions in plant-pathogenic fungi. *Molecular Plant Microbe Interactions* 31 (8), 779–788.
- Biju, V.C., Fokkens, L., Houterman, P.M., Rep, M., Cornelissen, B.J.C., 2017. Multiple evolutionary trajectories have led to the emergence of races in *Fusarium oxysporum* f. sp. *Lycopersici*. *Appl. Environ. Microbiol.* 83 (4).
- Bonilla-Landa, I., de la Cruz, O.L., Sanchez-Rangel, D., Ortiz-Castro, R., Rodríguez-Haas, B., Barrera-Mendez, F., Gomez, R., Enriquez-Medrano, F.J., Olivares-Romero, J.L., 2018. Design, synthesis and biological evaluation of novel fungicides for the management of *Fusarium* DieBack disease. *Journal of the Mexican Chemical Society* 62, 86–98.
- Bosch, J., Varliero, G., Hallsworth, J.E., Dallas, T.D., Hopkins, D., Frey, B., Kong, W., Lebr, P., Makhallanyane, T.P., Cowan, D.A., 2021. Microbial anhydrobiosis. *Environ. Microbiol.* 23, 6377–6390.
- Brancini, G.T.P., Hallsworth, J.E., Corrochano, L.M., GÜL, Braga, 2022. Photobiology of the keystone genus *Metarhizium*. *J. Photochem. Photobiol. B Biol.* 226, 112374.
- Brenes Guallar, M.A., Fokkens, L., Rep, M., Berke, L., van Dam, P., 2022. *Fusarium oxysporum* effector clustering version 2: an updated pipeline to infer host range. *Front. Plant Sci.* 13, 1012688.
- Brown, N.A., Urban, M., Van De Meene, A.M.L., Hammond-Kosack, K.E., 2010. The infection biology of *Fusarium graminearum*: defining the pathways of spikelet to spikelet colonisation in wheat ears. *Fungal Biol.* 114, 555–571.
- Cafarchia, C., Paradies, R., Figueredo, L.A., Iatta, R., Desantis, S., Di Bello, A.V.F., Zizzo, N., van Diepeningen, A.D., 2020. *Fusarium* spp. in loggerhead sea turtles (*Caretta caretta*): from colonization to infection. *Veterinary Pathology* 57 (1), 139–146.
- Cannon, S., Kay, W., Kilaru, S., Schuster, M., Gurr, S.J., Steinberg, G., 2022. Multi-site fungicides suppress banana Panama disease, caused by *Fusarium oxysporum* f. sp. *Cubense* Tropical Race 4. *PLoS Pathog.* 18 (10), e1010860.
- Carmona, S.L., Burbano-David, D., Gómez, M.R., Lopez, W., Ceballos, N., Castaño-Zapata, J., Simbaqueba, J., Soto-Suárez, M., 2020. Characterization of pathogenic and nonpathogenic *Fusarium oxysporum* isolates associated with commercial tomato crops in the Andean region of Colombia. *Pathogens* 9 (1), 70.
- Casadevall, A., 2019. Global catastrophic threats from the fungal kingdom. In: Inglesby, T., Adalja, A. (Eds.), *Global Catastrophic Biological Risks. Current Topics in Microbiology and Immunology*, 424. Springer, Cham.
- Case, N.T., Berman, J., Blehert, D.S., Cramer, R.A., Cuomo, C., Currie, C.R., Ene, I.V., Fisher, M.C., et al., 2022. The future of fungi: threats and opportunities. *G3 Genes|Genomes|Genetics* 12 (11) jkac224.
- Chaloner, T.M., Gurr, S.J., Bebbler, D.P., 2021. Plant pathogen infection risk tracks global crop yields under climate change. *Nat. Clim. Change* 11, 710–715.
- Chehri, K., Rastegar-Pouyani, N., Sayyadi, F., 2015. Dermatitis in the fringe-toed lizard, *Acanthodactylus nilsoni rastegar-pouyani*, 1998 (Sauria: Lacertidae) Associated with *Fusarium proliferatum*. *Curr. Microbiol.* 71, 607–612.
- Chen, C., Chen, S., Liu, C., Wu, D., Kuo, C., Lin, C., Chou, H., Wang, Y., Tsai, Y., Lai, M., Chung, C., 2020. Invasion and colonization pattern of *Fusarium fujikuroi* in rice. *Phytopathology* 110 (12), 1934–1945.
- Chen, Y., Wang, J., Yang, N., Wen, Z., Sun, X., Chai, Y., Ma, Z., 2018. Wheat microbiome bacteria can reduce virulence of a plant pathogenic fungus by altering histone acetylation. *Nat. Commun.* 9 (1), 3429.
- Chen, J., Wen, J., Tang, Y., Shi, J., Mu, G., Yan, R., Cai, J., Long, M., 2021. Research progress on fumonisins B1 contamination and toxicity: a review. *Molecules* 26 (17), 5238.
- Chiara, M., Fanelli, F., Mulè, G., Logrieco, A.F., Pesole, G., Leslie, J.F., Horner, D.S., Toomajian, C., 2015. Genome sequencing of multiple isolates highlights subtelomeric genomic diversity within *Fusarium fujikuroi*. *Genome Biol. Evolution* 7 (11), 3062–3069.
- Coleman, J.J., 2016. The *Fusarium solani* species complex: ubiquitous pathogens of agricultural importance. *Mol. Plant Pathol.* 17 (2), 146–158.
- Costa, M.M., Melo, M.P., Carmo, F.S., Moreira, G.M., 2021. *Fusarium* species from tropical grasses in Brazil and description of two new taxa. *Mycol. Prog.* 20 (1), 61–72.
- Couttolenc, A., Espinoza, C., Fernández, J.J., Norte, M., Plata, G.B., Padrón, J.M., Shnyreva, A., Trigoso, A., 2016. Antiproliferative effect of extract from endophytic fungus *Curvularia trifolii* isolated from the Veracruz Reef System in Mexico. *Pharmaceut. Biol.* 54 (8), 1392–1397.
- Cray, J.A., Bell, A.N.W., Bhaganna, P., Mswaka, A.Y., Timson, D.J., Hallsworth, J.E., 2013. The biology of habitat dominance; can microbes behave as weeds? *Microb. Biotechnol.* 6, 453–492.
- Crow, G.L., Brock, J.A., Kaiser, S., 1995. *Fusarium solani* fungal infection of the lateral line canal system in captive scalloped hammerhead sharks (*Sphyrna lewini*) in Hawaii. *J. Wildl. Dis.* 31 (4), 562–565.
- Cuomo, C.A., Güldener, U., Xu, J., Trail, F., Turgeon, B.G., Di Pietro, A., Walton, J.D., Ma, L., et al., 2007. The genome sequence of *F. graminearum* reveals localized diversity and pathogen specialization. *Science* 317, 1400–1402.
- Cuzick, A., Seager, J., Wood, V., Urban, M., Rutherford, K., Hammond-Kosack, K.E., 2023. A framework for community curation of interspecies interactions literature. *Elife* 12, e84658.
- Darby, R.T., Simmons, E.G., Wiley, B.J., 2001. A survey of fungi in a military aircraft fuel supply system. *Int. Biodeterior. Biodegrad.* 48, 159–161.
- Darino, M., Urban, M., Kaur, N., Machado Wood, A., Grimwade-Mann, M., Smith, D., Andrew Beacham, A., Hammond-Kosack, K.E., 2024. Identification and functional characterisation of a locus for target site integration in *Fusarium graminearum*. *Fungal Biol. Biotechnol.* 11, 1–21.
- Dean, R., Van Kan, J.A.L., Pretorius, Z.A., Hammond-Kosack, K.E., Di Pietro, A., Spanu, P.D., Rudd, J.J., Dickman, M., Kahmann, R., Ellis, J., Foster, G.D., 2012. The top 10 fungal pathogens in molecular plant pathology. *Mol. Plant Pathol.* 13 (4), 414–430.
- Diaz Arias, M.M., Leandro, L.F., Munkvold, G.P., 2013. Aggressiveness of *Fusarium* species and impact of root infection on growth and yield of soybeans. *Phytopathology* 103 (8), 768–776.
- Dita, M., Barquero, M., Heck, D., Mizubuti, E.S.G., Staver, C.P., 2018. *Fusarium* wilt of banana: current knowledge on epidemiology and research needs toward sustainable disease management. *Front. Plant Sci.* 9, 1468.
- Dobbs, J.T., Kim, M.S., Dudley, N.S., Jones, T.C., Yeh, A., Dumroese, R.K., Canon, P.G., Hauff, R.D., Klopfenstein, N.B., Wright, S., Stewart, J.E., 2021. *Fusarium* spp. diversity associated with symptomatic *Acacia koa* in Hawai'i. *For. Pathol.* 51 (6), e12713.
- Domsch, K.H., Gams, W., Anderson, T., 2007. *Compendium of Soil Fungi*, second ed. (IHW-Verlag: Germany).
- Drenkhan, R., Ganley, B., Martin-Garcia, J., Vahalik, P., Adamson, K., Adamčíková, K., Ahumada, R., Blank, L., et al., 2020. Global geographic distribution and host range of *Fusarium circinatum*, the causal agent of pine pitch canker. *Forests* 11 (7), 724.
- Duncan, K.E., Howard, R.J., 2010. Biology of maize kernel infection by *Fusarium verticillioides*. *Mol. Plant Microbe Interactions* 23 (1), 6–16.
- Edel-Hermann, V., Lecomte, C., 2019. Current status of *Fusarium oxysporum* formae speciales and races. *Phytopathology* 109 (4), 512–530.
- Epstein, L., Kaur, S., Chang, P.L., Carrasquilla-Garcia, N., Lyu, G., Cook, D.R., Subbarao, K.V., O'Donnell, K., 2017. Races of the celery pathogen *Fusarium oxysporum* f. sp. *Apii* are polyphyletic. *Phytopathology* 107 (4), 463–473.
- Epstein, L., Kaur, S., Henry, P.M., 2022. The emergence of *Fusarium oxysporum* f. sp. *Apii* Race 4 and *Fusarium oxysporum* f. sp. *Coriandrii* highlights major obstacles facing agricultural production in coastal California in a warming climate: a case study. *Front. Plant Sci.* 13, 921516.
- Evans, J., Levesque, D., de Lahunta, A., Jensen, H.E., 2004. Intracranial Fusariosis: a novel cause of fungal meningoencephalitis in a dog. *Veterinary Pathology* 41 (5), 510–514.
- FAO, 2020a. *World Food and Agriculture – Statistical Yearbook 2020*. FAO, Rome.
- FAO, 2020b. *Nations environment Programme. The State of the World's Forests 2020. Forests, biodiversity and people* FAO, Rome.
- Fayyaz, A., Robinson, G., Chang, P.L., Bekele, D., Yimer, S., Carrasquilla-Garcia, N., Negash, K., Surendrarao, A., et al., 2023. Hiding in plain sight: genome-wide recombination and a dynamic accessory genome drive diversity in *Fusarium oxysporum* f. sp. *ciceris*. *PNAS* 120 (27), e2220570120.
- Fernández-Fernández, M., Naves, P., Witzell, J., Musolin, D.L., Selikhovkin, A.V., Paraschiv, M., Chira, D., Martínez-Álvarez, P., et al., 2019. Pine pitch canker and insects: relationships and implications for disease spread in Europe. *Forests* 10 (8), 627.
- Fernandez-Pol, J.A., Klos, D.J., Hamilton, P.D., 1993. Cytotoxic activity of fusaric acid on human adenocarcinoma cells in tissue culture. *Anticancer Res.* 13 (1), 57–64.
- Figuerola, M., Hammond-Kosack, K.E., Solomon, P.S., 2018. A review of wheat diseases—a field perspective. *Mol. Plant Pathol.* 19 (6), 1523–1536.

- Fink-Gremmels, J., Malekinejad, H.J.A.F., 2007. Clinical effects and biochemical mechanisms associated with exposure to the mycoestrogen zearalenone. *Anim. Feed Sci. Technol.* 137, 326–341.
- Fisher, M.C., Henk, D.A., Briggs, C.J., Brownstein, J.S., Madoff, L.C., McCraw, S.L., Gurr, S.J., 2012. Emerging fungal threats to animal, plant and ecosystem health. *Nature* 484, 186–194.
- Flor, H.H., 1942. Inheritance of pathogenicity in a cross between physiological races 22 and 24 of *Melampsora lini*. *Phytopathology* 32 (1), 5.
- Fraune, S., Anton-Erxleben, F., Augustin, R., Franzburg, S., Knop, M., Schröder, K., Willoweit-Ohl, D., Bosch, T.C., 2015. Bacteria–bacteria interactions within the microbiota of the ancestral metazoan Hydra contribute to fungal resistance. *ISME J.* 9 (7), 1543–1556.
- Gaba, S., Lescourret, F., Boudsocq, S., Enjalbert, J., Hinsinger, P., Journet, E., Navas, M., et al., 2015. Multiple cropping systems as drivers for providing multiple ecosystem services: from concepts to design. *Agron. Sustain. Dev.* 35, 607–623.
- Gajecki, M.T., Gajecka, M., 2023. The multidirectional influence of feed-borne deoxynivalenol and zearalenone on animal health. *Toxins* 15 (7), 419.
- Gao, H., Li, G., Lou, H., 2018. Structural diversity and biological activities of novel secondary metabolites from endophytes. *Molecules* 23 (3), 646.
- Geiser, D.M., Al-Hatmi, A.M.S., Aoki, T., Arie, T., Balmas, V., Barnes, I., Bergstrom, G.C., Bhattacharyya, M.K., et al., 2021. Phylogenomic Analysis of a 55.1-kb 19-gene dataset resolves a monophyletic *Fusarium* that includes the *Fusarium solani* species complex. *Phytopathology* 111, 1064–1079.
- Gerlach, W., Nirenberg, H., 1982. The genus *Fusarium*. a pictorial atlas 209, 1–406 (Berlin, Germany: Kommissionsverlag P. Parey).
- Gomes, L.B., Ward, T.J., Badiale-Furlong, E., Del Ponte, E.M., 2014. Species composition, toxigenic potential and pathogenicity of *Fusarium graminearum* species complex isolates from southern Brazilian rice. *Plant Pathol.* 64 (4), 980–987.
- Gordon, T.R., 2017. *Fusarium oxysporum* and the *Fusarium* wilt syndrome. *Annu. Rev. Phytopathol.* 55, 23–39.
- Gow, N.A.R., Lenardon, M.D., 2023. Architecture of the dynamic fungal cell wall. *Nat. Rev. Microbiol.* 21, 248–259.
- Greeff-Laubscher, M.R., Jacobs, K., 2022. *Fusarium* species isolated from post-hatchling loggerhead sea turtles (*Caretta caretta*) in South Africa. *Sci. Rep.* 12 (1), 5874.
- Hallsworth, J.E., 2019. Microbial unknowns at the saline limits for life. *Nature Ecology and Evolution.* 3, 1503–1504.
- Hallsworth, J.E., 2022. Water is a preservative of microbes. *Microb. Biotechnol.* 15 (1), 191–214.
- Hallsworth, J.E., Udaondo, Z., Pedrós-Alió, C., Höfer, J., Benison, K.C., Lloyd, K.G., Cordero, R.J.B., de Campos, C.B.L., et al., 2023a. Scientific novelty beyond the experiment. *Microb. Biotechnol.* 16 (6), 1131–1173.
- Hallsworth, J.E., Mswaka, A.Y., Patriarca, A., Verheecke-Vaessen, C., Medina, A., 2023b. The life and works of professor Naresh magan. *World Mycotoxin J.* 16, 195–197.
- Hamim, I., Sekine, K.-T., Komatsu, K., 2022. How do emerging long-read sequencing technologies function in transforming the plant pathology research landscape? *Plant Mol. Biol.* 110 (6), 469–484.
- Hatai, K., Kubota, S.S., Kida, N., Udagawa, S.I., 1986. *Fusarium oxysporum* in red sea bream (*Pagrus sp.*). *J. Wildl. Dis.* 22 (4), 570–571.
- Hidayat, A., Tachibana, S., 2012. Biodegradation of aliphatic hydrocarbon in three types of crude oil by *Fusarium sp.* F092 under stress with artificial sea water. *J. Environ. Sci. Technol.* 5 (1), 64–73.
- Hoh, D.Z., Lee, H.H., Wada, N., Liu, W.A., Lu, M.R., Lai, C.K., Ke, H.M., Sun, P.F., et al., 2022. Comparative genomic and transcriptomic analyses of trans-kingdom pathogen *Fusarium solani* species complex reveal degrees of compartmentalization. *BMC Biol.* 20 (1), 236.
- Hong, S., Yuan, X., Yang, J., Yang, Y., Jv, H., Li, R., Jia, Z., Ruan, Y., 2023. Selection of rhizosphere communities of diverse rotation crops reveals unique core microbiome associated with reduced banana *Fusarium* wilt disease. *New Phytol.* 238 (5), 2194–2209.
- Hoogendoorn, K., Barra, L., Waalwijk, C., Dickschat, J.S., van der Lee, T.A.J., Medema, M.H., 2018. Evolution and diversity of biosynthetic gene clusters in *Fusarium*. *Front. Microbiol.* 9, 1158.
- Hose, J.E., Lightner, D.V., Redman, R.M., Danald, D.A., 1984. Observations on the pathogenesis of the imperfect fungus, *Fusarium solani*, in the California brown shrimp, *Penaeus californiensis*. *J. Invertebr. Pathol.* 44 (3), 292–303.
- Hsu, L., Su, C., Sun, P., Chen, Y., 2021. *Fusarium solani* species complex infection in elasmobranchs: a case report for rough-tail stingray with valid antifungal therapy. *Med. Mycol. Case Reports* 32, 34–38.
- Huberman, L.B., Wu, V.W., Kowbel, D.J., Glass, N.L., 2021. DNA affinity purification sequencing and transcriptional profiling reveal new aspects of nitrogen regulation in a filamentous fungus. *Proc. Natl. Acad. Sci. U.S.A.* 118 (13), e2009501118.
- Inami, K., Yoshioka-Akiyama, C., Morita, Y., Yamasaki, M., Teraoka, T., Arie, T., 2012. A genetic mechanism for emergence of races in *Fusarium oxysporum* f. sp. *Lycopersici*: inactivation of virulence gene AVR1 by transposon insertion. *PLoS One* 7 (8), e44101.
- Janik, E., Niemcewicz, M., Podogrocki, M., Ceremuga, M., Stela, M., Bijak, M., 2021. T-2 toxin—the most toxic trichothecene mycotoxin: metabolism, toxicity, and decontamination strategies. *Molecules* 26 (22), 6868.
- Johns, L.E., Bebbler, D.P., Gurr, S.J., Brown, N.A., 2022. Emerging health threat and cost of *Fusarium* mycotoxins in European wheat. *Nat. Food.* 3, 1014–1019.
- Jung, B., Park, J., Kim, N., Li, T., Kim, S., Bartley, L.E., Kim, J., Kim, I., Kang, Y., Yun, K., Choi, Y., 2018. Cooperative interactions between seed-borne bacterial and air-borne fungal pathogens on rice. *Nat. Commun.* 9 (1), 31.
- Jurado, M., Marín, P., Magan, N., González-Jaén, M.T., 2008. Relationship between solute and matrix potential stress, temperature, growth, and *FUM1* gene expression in two *Fusarium verticillioides* strains from Spain. *Appl. Environ. Microbiol.* 74 (4), 2032–2036.
- Kacprzak, M., Asiegbu, F.O., Daniel, G., Stenlid, J., Mańka, M., Johansson, M., 2001. Resistance reaction of Conifer species (European Larch, Norway Spruce, Scots Pine) to infection by selected necrotrophic damping-off pathogens. *Eur. J. Plant Pathol.* 107, 191–207.
- Kamle, M., Mahato, D.K., Gupta, A., Pandhi, S., Sharme, B., Dhawan, K., Vasundhara, Mishra S., Kumar, M., Tripathi, A.D., Rasane, P., Selvakumar, R., Kumar, A., Gamlath, S., Kumar, P., 2022. Deoxynivalenol: an overview on occurrence, chemistry, biosynthesis, health effects and its detection, management, and control strategies in food and feed. *Microbiol. Res.* 13 (2), 292–314.
- Kamoun, S., 2006. A catalogue of the effector secretome of plant pathogenic oomycetes. *Annu. Rev. Phytopathol.* 44, 41–60.
- Kanja, C., Machado Wood, A.K., Baggaley, L., Walker, C., Hammond-Kosack, K.E., 2021. Cereal-*Fusarium* interactions: improved fundamental insights into *Fusarium* pathogenomics and cereal host resistance reveals new ways to achieve durable disease control. In: *Achieving Durable Disease Resistance in Cereals*, Ed R. Oliver. Burleigh Dodds Science Publishing, UK.
- Karlsson, I., Persson, P., Friberg, H., 2021. *Fusarium* head blight from a microbiome perspective. *Front. Microbiol.* 12, 628373.
- Kashiwa, T., Suzuki, T., Sato, A., Akai, K., Teraoka, T., Komatsu, K., Arie, T., 2016. A new biotype of *Fusarium oxysporum* f. sp. *Lycopersici* race 2 emerged by a transposon-driven mutation of virulence gene AVR1. *FEMS Microbiol. Lett.* 363 (14) ffw132.
- Kaur, S., Barakat, R., Kaur, J., Epstein, L., 2022. The effect of temperature on disease severity and growth of *Fusarium oxysporum* f. sp. *Apii* Races 2 and 4 in celery. *Phytopathology* 112 (2), 364–372.
- Khachatourians, G.G., Arora, D.K., 1999. Biochemical and modern identification techniques: microfloras of fermented foods. In: *Encyclopaedia of Food Microbiology*. Robinson RK. Elsevier.
- Kim, J.H., Cheng, L.W., Chan, K.L., Tam, C.C., Mahoney, N., Friedman, M., Shilman, M.M., Land, K.M., 2020. Antifungal drug repurposing. *Antibiotics* (Basel), 9 (11), 812.
- King, R., Urban, M., Hammond-Kosack, M.C.U., Hassani-Pak, K., Hammond-Kosack, K.E., 2015. The completed genome sequence of the pathogenic ascomycete fungus *Fusarium graminearum*. *BMC Genomics* 16, 544.
- King, R., Urban, M., Hammond-Kosack, K.E., 2017. Annotation of *Fusarium graminearum* (PH-1) version 5.0. *Genome Announce.* 5 <https://doi.org/10.1128/genomea.01479-16>.
- King, R., Brown, N.A., Urban, M., Hammond-Kosack, K.E., 2018. Inter-genome comparison of the Quorn fungus *Fusarium venenatum* and the closely related plant infecting pathogen *Fusarium graminearum*. *BMC Genom.* 19, 269.
- Krohn, I., Bergmann, L., Qi, M., Indenbirken, D., Han, Y., Perez-Garcia, P., Katzwitsch, E., Hägele, B., et al., 2021. Deep (Meta)genomics and (Meta) transcriptome analyses of fungal and bacteria consortia from aircraft tanks and kerosene identify key genes in fuel and tank corrosion. *Front. Microbiol.* 12, 722259.
- Kurian, S.M., Di Pietro, A., Read, N.D., 2018. Live-cell imaging of conidial anastomosis tube fusion during colony initiation in *Fusarium oxysporum*. *PLoS One.* 13 (5), e0195634.
- Kurosawa, E., 1926. Experimental studies on the nature of the substance secreted by the 'bakanae' fungus. *Trans. Nat. History Soc. Formosa* 16, 213–227.
- Laraba, I., Busman, M., Geiser, D.M., O'Donnell, K., 2022. Phylogenetic diversity and mycotoxin potential of emergent *Fusarium* species within the *Fusarium tricinctum* species complex. *Phytopathology* 112 (6), 1284–1298.
- Laurence, M.H., Walsh, J.L., Shuttleworth, L.A., Robinson, D.M., Johansen, R.M., Petrovic, T., Vu, T.T.H., Burgess, L.W., Summerell, B.A., Liew, E.C.Y., 2016. Six novel species of *Fusarium* from natural ecosystems in Australia. *Fungal Divers.* 77, 349–366.
- Lazarotto, M., Milanese, P.M., Muniz, M.F.B., Reiniger, L.R.S., Beltrame, R., Harakava, R., Blume, E., 2014. Morphological and molecular characterization of *Fusarium spp* pathogenic to pecan tree in Brazil. *Genet. Mol. Res.* 13, 9390–9402.
- Lee, C.J.D., McMullan, P.E., O'Kane, C.J., Stevenson, A., Santos, I.C., Roy, C., Ghosh, W., Mancinelli, R.L., Mormile, M.R., McMullan, G., Banciu, H.L., Fares, M.A., Benison, K.C., Oren, A., Dyall-Smith, M.L., Hallsworth, J.E., 2018. NaCl-saturated brines are thermodynamically moderate, rather than extreme, microbial habitats. *FEMS (Fed. Eur. Microbiol. Soc.) Microbiol. Rev.* 42, 672–693.
- Leslie, J.F., Summerell, B.A., 2013. An overview of *Fusarium*. In: *Fusarium: Genomics, Molecular and Cellular Biology*. Eds Proctor RH and Brown D. Caister Academic Press, Norfolk (UK).
- Leslie, J.F., Zeller, K.A., Logrieco, A., Mulè, G., Moretti, A., Ritieni, A., 2004. Species diversity of and toxin production by *Gibberella fujikuroi* species complex strains isolated from native prairie grasses in Kansas. *Appl. Environ. Microbiol.* 70 (4), 2254–2262.
- Li, J., Fokkens, L., Conneely, L.J., Rep, M., 2020a. Partial pathogenicity chromosomes in *Fusarium oxysporum* are sufficient to cause disease and can be horizontally transferred. *Environ. Microbiol.* 22 (12), 4985–5004.
- Li, J., Fokkens, L., van Dam, P., Rep, M., 2020b. Related mobile pathogenicity chromosomes in *Fusarium oxysporum* determine host range on cucurbits. *Mol. Plant Pathol.* 21 (6), 761–776.
- Li, J., Sun, W., Guo, Z., Lu, C., Shen, Y., 2014. Fusaric acid modulates type three secretion system of *Salmonella enterica* serovar *Typhimurium*. *Biochem. Biophys. Res. Commun.* 449 (4), 455–459.
- Liew, E.C.Y., Laurence, M.H., Pearce, C.A., Shivas, R.G., Johnson, G.I., Tan, Y.P., Edwards, J., Perry, S., Cooke, A.W., Summerell, B.A., 2016. Review of *Fusarium* species isolated in association with mango malformation in Australia. *Australas. Plant Pathol.* 45 (6), 547–559.

- Lopes, P., Sobari, M.M.C., Lopes, G.R., Martins, Z.E., Passos, C.P., Petronilho, S., Ferreira, L.M., 2023. Mycotoxins' prevalence in food industry by-products: a systematic review. *Toxins* 15 (4), 249.
- Low, C.Y., Rotstein, C., 2011. Emerging fungal infections in immunocompromised patients. *F1000 Med. Reports* 3, 14.
- Lu, P., Chen, D., Qi, Z., Wang, H., Chen, Y., Wang, Q., Jiang, C., Xu, J.R., Liu, H., 2022. Landscape and regulation of alternative splicing and alternative polyadenylation in a plant pathogenic fungus. *New Phytol.* 235 (2), 674–689.
- Ma, L., van der Does, H.C., Borkovich, K.A., Coleman, J.J., Daboussi, M., Di Pietro, A., Dufresne, M., Freitag, M., et al., 2010. Comparative genomics reveals mobile pathogenicity chromosomes in *Fusarium*. *Nature*. 464, 367–373.
- Machado, A.K., Brown, N.A., Urban, M., Kanyuka, K., Hammond-Kosack, K.E., 2018. RNAi as an emerging approach to control *Fusarium* head blight disease and mycotoxin contamination in cereals. *Pest Manag. Sci.* 74 (4), 790–799.
- Magan, N., 2007. Fungi in extreme environments. In: Kubicek, C., Druzhinina, I. (Eds.), *Environmental and Microbial Relationships. The Mycota*, 4. Springer, Berlin, Heidelberg.
- Magan, N., Aldred, D., Mylona, K., Lambert, R.J.W., 2010. Limiting mycotoxins in stored wheat. *Food Addit. Contam.* 27 (5), 64–650.
- Mamaeva, A., Lyapina, I., Knyazev, A., Golub, N., Mollaev, T., Chudinova, E., Elansky, S., Babenko, V.V., et al., 2023. RALF peptides modulate immune response in the moss *Physcomitrium patens*. *Front. Plant Sci.* 14, 1077301.
- Maryani, N., Lombard, L., Poerba, Y.S., Subandiyah, S., Crous, P.W., Kema, G.H.J., 2019. Phylogeny and genetic diversity of the banana *Fusarium* wilt pathogen *Fusarium oxysporum* f. sp. *cubense* in the Indonesian centre of origin. *Stud. Mycol.* 92, 155–194.
- McMullen, M., Bergstrom, G., De Wolf, E., Dill-Mackay, R., Hershman, D., Shaner, G., Van Sanford, D., 2012. A united effort to fight an enemy of wheat and barley: *Fusarium* Head Blight. *Plant Dis.* 96 (12), 1712–1855.
- Merhej, J., Richard-Forget, F., Barreau, C., 2011. Regulation of trichothecene biosynthesis in *Fusarium*: recent advances and new insights. *Appl. Microbiol. Biotechnol.* 91, 519–528.
- Milani, N.A., Lawrence, D.P., Arnold, A.E., VanEtten, H.D., 2012. Origin of pisatin demethylase (PDA) in the genus *Fusarium*. *Fungal Genet. Biol.* 49 (11), 933–942.
- Mishra, S., Srivastava, S., Dewangan, J., Divakar, A., Rath, S.K., 2022. Global occurrence of deoxynivalenol in food commodities and exposure risk assessment in humans in the last decade: a survey. *Crit. Rev. Food Sci. Nutr.* 60 (8), 1346–1374.
- Moonjely, S., Ebert, M., Patan-Glassbrook, D., Noel, Z.A., Roze, L., Shay, R., Watkins, T., Trail, F., 2023. Update on the state of research to manage *Fusarium* head blight. *Fungal Genet. Biol.* 169, 103829.
- Moparthi, S., Burrows, M., Mgbeci-Ezeri, J., Agindotan, B., 2021. *Fusarium* spp. associated with root rot of pulse crops and their cross-pathogenicity to cereal crops in Montana. *Plant Dis.* 105 (3), 525–719.
- Muhammed, M., Fuchs, B.B., Wu, M.P., Breger, J., Coleman, J.J., Mylonakis, E., 2012. The role of mycelium production and a MAPK-mediated immune response in the *C. elegans*-*Fusarium* model system. *Med. Mycol.* 50 (5), 488–496.
- Mulk, S., Wahab, A., Yasmin, H., Mumtaz, S., El-Serehy, H.A., Khan, N., Hassan, M.N., 2022. Prevalence of wheat associated *Bacillus* spp. and their bio-control efficacy against *Fusarium* root rot. *Front. Microbiol.* 12, 798619.
- Navarro-Velasco, G.Y., Prados-Rosales, R.C., Ortiz-Urquiza, A., Quesada-Moraga, E., Di Pietro, A., 2011. *Galleria mellonella* as model host for the trans-kingdom pathogen *Fusarium oxysporum*. *Fungal Genet. Biol.* 48 (12), 1124–1129.
- Nikitin, D.A., Ivanova, E.A., Semenov, M.V., Zhelezova, A.D., Ksenofontova, N.A., Tkhakakhova, A.K., Kholodov, V.A., 2023. Diversity, ecological characteristics and identification of some problematic phytopathogenic *Fusarium* in soil: a review. *Diversity* 15 (1), 49.
- Noel, D., Hallsworth, J.E., Gelhaye, E., Darnet, S., Sormani, R., Morel-Rouhier, M., 2023. Modes-of-action of antifungal compounds: stressors and (target-site-specific) toxins, toxicants, or toxin-stressors. *Microb. Biotechnol.* 16 (7), 1438–1455.
- Norred, W.P., Voss, K.A., Riley, R.T., Plattner, R.D., 1996. Fumonisin toxicity and metabolism studies at the USDA: fumonisin toxicity and metabolism. *Adv. Exp. Med. Biol.* 392, 225–236.
- Nucci, M., Anaissie, W., 2007. *Fusarium* infections in immunocompromised patients. *Clin. Microbiol. Rev.* 20 (4), 695–704.
- O'Donnell, K., Sutton, D.A., Wiederhold, N., Robert, V.A.R.G., Crous, P.W., Geiser, D.M., 2016. Veterinary fusarioses within the United States. *J. Clin. Microbiol.* 54 (11), 2813–2819.
- O'Donnell, K., Whitaker, B.K., Laraba, I., Proctor, R.H., Brown, D.W., Broders, K., Kim, H., McCormick, S.P., et al., 2022. DNA Sequence-based identification of *Fusarium*: a work in progress. *Plant Dis.* 106 (6), 1597–1609.
- O'Donnell, K., Cigelnik, E., Casper, H.H., 1998. Molecular phylogenetic, morphological, and mycotoxin data support reidentification of the Quorn mycoprotein fungus as *Fusarium venenatum*. *Fungal Genet. Biol.* 23 (1), 57–67.
- Orós, J., Delgado, C., Fernández, L., Jensen, H.E., 2004. Pulmonary hyalohyphomycosis caused by *Fusarium* spp. in a Kemp's ridley sea turtle (*Lepidochelys kempi*): an immunohistochemical study. *N. Z. Vet. J.* 52 (3), 150–152.
- Palmer, G.H., 1974. The industrial use of gibberellic acid and its scientific basis—a review. *J. Inst. Brew.* 80 (1), 13–30.
- Parry, D.W., Jenkinson, P., McLeod, L., 1995. *Fusarium* ear blight (scab) in small grain cereals – a review. *Plant Pathol.* 44 (2), 207–238.
- Pascari, X., Marin, S., Ramos, A.J., Sanchis, V., 2022. Relevant *Fusarium* mycotoxins in malt and beer. *Foods* 11 (2), 246.
- Pavankumar, T.L., Mittal, P., Hallsworth, J.E., 2021. Molecular insights into the ecology of a psychrotolerant *Pseudomonas syringae*. *Environ. Microbiol.* 23 (7), 3665–3681.
- Peck, L.D., Boa, E., 2023. Coffee wilt disease: the forgotten threat to coffee. *Plant Pathol.* 00, 1–16.
- Pedrés-Alió, C., 2021. Time travel in microorganisms. *Syst. Appl. Microbiol.* 44 (4), 126227.
- Peraldi, A., Beccari, G., Steed, A., Nicholson, P., 2011. *Brachypodium distachyon*: a new pathosystem to study *Fusarium* Head Blight and other *Fusarium* diseases of wheat. *BMC Plant Biol.* 11, 100.
- Pérez-Llano, Y., Rodríguez-Pupo, E.C., Druzhinina, I.S., Chenthamara, K., Cai, F., Gunde-Cimerman, N., Zalar, P., Gostinčar, C., Kostanjšek, R., Folch-Mallol, J.L., et al., 2020. Stress reshapes the physiological response of halophile fungi to salinity. *Cells* 9 (3), 525.
- Perincheri, L., Lalak-Kańczugowska, J., Stepień Ł., 2019. *Fusarium*-produced mycotoxins in plant-pathogen interactions. *Toxins* 11 (11), 664.
- Perochon, A., Doohan, F.M., 2024. Trichothecenes and Fumonisin: key players in *Fusarium*-cereal ecosystem interactions. *Toxins* 16 (2), 90.
- Perpiñán, D., Trupkiewicz, J.G., Armbrust, A.L., Geiser, D.M., Armstrong, S., Garner, M. M., Armstrong, D.L., 2010. Dermatitis in captive Wyoming toads (*Bufo baxteri*) associated with *Fusarium* spp. *J. Wildl. Dis.* 46 (4), 1185–1195.
- Phan, H.T., Burgess, L.W., Summerell, B.A., Bullock, S., Liew, E.C., SmithWhite, J.L., Clarkson, J.R., 2004. *Gibberella gadijirrii* (*Fusarium gadijirrii*) sp. Nov., a new species from tropical grasses in Australia. *Plant Dis.* 88, 261–272.
- Plemenitaš, A., Vauptič, T., Lenassi, M., Kogej, T., Gunde-Cimerman, N., 2008. Adaptation of extremely halotolerant black yeast *Hortaea werneckii* to increased osmolarity: a molecular perspective at a glance. *Stud. Mycol.* 61 (1), 67–75.
- Ploetz, R., 2015. Management of *Fusarium* wilt of banana: a review with special reference to tropical race 4. *Crop Protect.* 73, 7–15.
- Ponomareva, M.L., Gorshkov, V.U., Ponomarev, S.N., Korzun, V., Miedaner, T., 2021. Snow mold of winter cereals: a complex disease and a challenge for resistance breeding. *Theor. Appl. Genet.* 139, 419–433.
- Prasoula, G., Gentikis, A., Konti, A., Kalantzi, S., Kekos, D., Mamma, D., 2020. Bioethanol production from food waste applying the multienzyme system produced on-site by *Fusarium oxysporum* F3 and mixed microbial cultures. *Fermentation* 6 (2), 39.
- Preece, T.F., Pettitt, T.R., Biggs, D.T., 1994. *Fusarium heterosporum* growing on ergots (*Claviceps purpurea*) in spikelets of common cord-grass (*Spartina anglica*) in the Isle of Wight. *Mycologist* 8 (1), 9–11.
- Prigigallo, M.I., Cabanás, Mercado-Blanco J., Bubic, G., 2022. Designing a synthetic microbial community devoted to biological control: the case study of *Fusarium* wilt of banana. *Front. Microbiol.* 13, 967885.
- Proctor, R.H., Hohn, T.M., McCormick, S.P., 1995. Reduced virulence of *Gibberella zeae* caused by disruption of a trichothecene toxin biosynthetic gene. *Mol. Plant Microbe Interact.* 8 (4), 593–601.
- Qiu, H.L., Fox, E.G., Qin, C.S., Yang, H., Tian, L.Y., Wang, D.S., Xu, J.Z., 2023. First record of *Fusarium concentricum* (Hypocreales: hypocreaceae) isolated from the moth *Polychrosis cuninhamiacola* (Lepidoptera: tortricidae) as an entomopathogenic fungus. *J. Insect Sci.* 23 (2), 2.
- Queiroz, C.A., Caniato, F.F., Siqueira, V.K.S., de Moraes Catarino, A., Hanada, R.E., O'Donnell, K., Laraba, I., 2023. Population genetic analysis of *Fusarium decemcellulare*, a Guaraná pathogen, reveals high genetic diversity in the Amazonas state, Brazil. *Plant Dis.* 107, 1343–1354.
- Radwan, O., Gunasekera, T.S., Ruiz, O.N., 2018. Draft genome sequence of *Fusarium fujikuroi*, a fungus adapted to the fuel environment. *Genome Announc.* 6 (3).
- Rai, M., Bonde, S., Golinska, P., Trzcińska-Wencel, J., Gade, A., Abd-Elisalam, K.A., Shende, S., Gaikwad, S., Ingle, A.P., 2021. *Fusarium* as a novel fungus for the synthesis of nanoparticles: mechanism and applications. *J. Fungi* 7 (2), 139.
- Rampersad, S.N., 2020. Pathogenomics and management of *Fusarium* diseases in plants. *Pathogens* 9 (5), 340.
- Reddy, G.K.K., Padmavathi, A.R., Nancharaiya, Y.V., 2022. Fungal infections: pathogenesis, antifungals and alternate treatment approaches. *Curr. Res. Microbiol. Sci.* 3, 100137.
- Redkar, A., Ibanez, S.G., Sabale, M., Zechmann, B., Solano, R., Di Pietro, A., 2022a. Marchantia polymorpha model reveals conserved infection mechanisms in the vascular wilt fungal pathogen *Fusarium oxysporum*. *New Phytol.* 234 (1), 227–24.
- Redkar, A., Sabale, M., Schudoma, C., Zechmann, B., Gupta, Y.K., López-Berges, M.S., Venturini, G., Gimenez-Ibanez, S., Turrà, D., Solano, R., Di Pietro, A., 2022b. Conserved secreted effectors contribute to endophytic growth and multihost plant compatibility in a vascular wilt fungus. *Plant Cell* 34 (9), 3214–3232.
- Renner, M.K., Jensen, P.R., Fenical, W., 1998. Neomanglicols: structures and absolute stereochemistries of unprecedented halogenated sesterpenes from a marine fungus of the genus *Fusarium*. *J. Org. Chem.* 63 (23), 8346–8354.
- Rigorth, K.S., Finckh, M., Šišić, A., 2021. First report of *Fusarium venenatum* causing foot and root rot of wheat (*Triticum aestivum*) in Germany. *Plant Dis.* 105 (6), 1855.
- Rizaludin, M.S., Stopnisek, N., Raaijmakers, J.M., Garbeva, P., 2021. The chemistry of stress: understanding the 'cry for help' of plant roots. *Metabolites* 11 (6), 357.
- Rose, F.L., Koke, J., Koehn, R., Smith, D., 2001. Identification of the etiological agent for necrotizing scute disease in the Texas tortoise. *J. Wildl. Dis.* 37 (2), 223–228.
- Royer, J.C., Moyer, D.L., Reiwitich, S.G., Madden, M.S., Jensen, E.B., Brown, S.H., Yonker, C.C., Johnstone, J.A., Golightly, E.J., Yoder, W.T., et al., 1995. *Fusarium graminearum* A 3/5 as a novel host for heterologous protein production. *Biotechnology* 13 (13), 1479–1483.
- Rusli, M.H., 2017. Disease epidemiology and genetic diversity of *Fusarium oxysporum* f. sp. *elaedis*, cause of *Fusarium* wilt of oil palm (*Elaeis guineensis* Jacq.). *J. Oil Palm Res.* 29 (4), 548–561.
- Rutherford, M.A., 2007. Current knowledge of coffee wilt disease, a major constraint to coffee production in Africa. *Phytopathology* 96, 663–666.
- Sabahi, F., Banihashemi, Z., de Sain, M., Rep, M., 2022. Genome sequences of 38 *Fusarium oxysporum* strains. *BMC Res. Notes* 15, 229.

- Sáenz, V., Alvarez-Moreno, C., Pape, P.L., Restrepo, S., Guarro, J., Ramírez, A.M.C., 2020. A one health perspective to recognize *Fusarium* as important in clinical practice. *J. Fungi* 6 (4), 235.
- Santos, A.C.S., Diniz, A.G., Tiago, P.V., Oliveira, N.T., 2020. Entomopathogenic *Fusarium* species: a review of their potential for the biological control of insects, implications and prospects. *Fungal Biol. Rev.* 34 (1), 41–57.
- Sarlin, T., Kivioja, T., Kalkkinen, N., Linder, M.B., Nakari-Setälä, T., 2012. Identification and characterization of gushing-active hydrophobins from *Fusarium graminearum* and related species. *J. Basic Microbiol.* 52 (2), 184–194.
- Sarmiento-Ramírez, J.M., Abella, E., Martín, M.P., Tellería, M.T., Lopez-Jurado, L.F., Marco, A., Dieguez-Urbeondo, J., 2010. *Fusarium solani* is responsible for mass mortalities in nests of loggerhead sea turtle, *Caretta caretta*, in Boavista, Cape Verde. *FEMS (Fed. Eur. Microbiol. Soc.) Microbiol. Lett.* 312 (2), 192–200.
- Sarmiento-Ramírez, J.M., Abella-Perez, E., Phillott, A.D., Sim, J., Van West, P., Martín, M.P., Marco, A., Dieguez-Urbeondo, J., 2014. Global distribution of two fungal pathogens threatening endangered sea turtles. *PLoS One* 9 (1), e85853.
- Schäfer, K., Di Pietro, A., Gow, N.A., MacCallum, D., 2014. Murine model for *Fusarium oxysporum* invasive fusariosis reveals organ-specific structures for dissemination and long-term persistence. *PLoS One* 9 (2), e89920.
- Selikhovkin, A.V., Markovskaja, S., Vasaitis, R., Martynov, A.N., Musolin, D.L., 2018. Phytopathogenic fungus *Fusarium circinatum* and potential for its transmission in Russia by insects. *Russian J. Biol. Invasions* 9, 245–252.
- Shahi, S., Beerens, B., Bosch, M., Linnmans, J., Rep, M., 2016. Nuclear dynamics and genetic rearrangement in heterokaryotic colonies of *Fusarium oxysporum*. *Fungal Genet. Biol.* 91, 20–31.
- Shay, R., Wiegand, A.A., Trail, F., 2022. Biofilm formation and structure in the filamentous fungus *Fusarium graminearum*, a plant pathogen. *Microbiol. Spectr.* 10 (4).
- Singh, A., Kumar, P.K., 1991. *Fusarium oxysporum*: status in bioethanol production. *Crit. Rev. Biotechnol.* 11 (2), 129–147.
- Smith, A.G., Muhvich, A.G., Muhvich, K.H., Wood, C., 1989. Fatal *Fusarium solani* infections in baby sharks. *J. Med. Vet. Mycol.* 27 (2), 83–91.
- Stack, A.J., Marek, S.M., Gordon, T.R., Bostock, R.M., 2022. Genetic diversity and potential inoculum sources of *Fusarium* species causing cankers in bareroot-propagated almond trees in California nurseries. *Plant Dis.* 106, 1401–1407.
- Stack Jr., B.C., Hansen, J.P., Ruda, J.M., Jaglowski, J., Shvidler, J., Hollenbeak, C.S., 2004. Fusaric acid: a novel agent and mechanism to treat HNSCC. *Otolaryngol. Head Neck Surg.* 131 (1), 54–60.
- Staggs, L., Leger, J.S., Bossart, G., Townsend, F.I., Hicks, C., Rinaldi, M., 2010. A novel case of *Fusarium oxysporum* infection in an Atlantic bottlenose dolphin (*Tursiops truncatus*). *J. Zoo Wildl. Med.* 41 (2), 287–290.
- Stevenson, A., Hamill, P.G., Dijksterhuis, J., Hallsworth, J.E., 2017a. Water-, pH- and temperature relations of germination for the extreme xerophiles *Xeromyces bisporus* (FRR 0025), *Aspergillus penicillioides* (JH06THJ) and *Eurotium halophilicum* (FRR 2471). *Microb. Biotechnol.* 10, 330–340.
- Stevenson, A., Hamill, P.G., O’Kane, C.J., Kminek, G., Rummel, J.D., Voytek, M.A., Dijksterhuis, J., Hallsworth, J.E., 2017b. *Aspergillus penicillioides* differentiation and cell division at 0.585 water activity. *Environ. Microbiol.* 19 (2), 687–697.
- Su, T., Zhou, B., Cao, D., Pan, Y., Hu, M., Zhang, M., Wei, H., Han, M., 2021. Transcriptomic profiling of *Populus* roots challenged with *Fusarium* reveals differential responsive patterns of invertase and invertase-inhibitor-like families within carbohydrate metabolism. *J. Fungi.* 7 (2), 89.
- Summerell, B.A., Leslie, J.F., Liew, E.C.Y., Laurence, M.H., Bullock, S., Petrovic, T., Bentley, A.R., Howard, M.H., Peterson, S.A., Walsh, J.L., Burgess, L.W., 2011. *Fusarium* species associated with plants in Australia. *Fungal Divers.* 46, 1–27.
- Tajuddin, N., Rizman-Idid, M., Convey, P., Alias, S.A., 2017. Thermal adaptation in a marine-derived tropical strain of *Fusarium equiseti* and polar strains of *Pseudogymnoascus spp.* under different nutrient sources. *Bot. Mar.* 61 (1), 9–20.
- Takken, F., Rep, M., 2010. The arms race between tomato and *Fusarium oxysporum*. *Mol. Plant Pathol.* 11 (2), 309–314.
- Tanaka, M., Izawa, T., Kuwamura, M., Nakao, T., Maezono, Y., Ito, S., Murata, M., Murakami, M., Sano, A., Yamate, J., 2012. Deep granulomatous dermatitis of the fin caused by *Fusarium solani* in a false killer whale (*Pseudorca crassidens*). *J. Vet. Med. Sci.* 74 (6), 779–782.
- Teunissen, H.A., Verkooijen, J., Cornelissen, B.J., Haring, M.A., 2002. Genetic exchange of avirulence determinants and extensive karyotype rearrangements in parasexual recombinants of *Fusarium oxysporum*. *Mol. Genet. Genomics* 268 (3), 298–310.
- Tian, M., Feng, Y., He, X., Zhang, D., Wang, W., Liu, D., 2022. Mycotoxins in livestock feed in China - current status and future challenges. *Toxicol* 214, 112–120.
- Tiwari, R.K., Kumar, R., Sharma, S., Sagar, V., Aggarwal, R., Naga, K.C., Lal, M.K., Chourasia, K.N., Kumar, D., Kumar, M., 2020. Potato dry rot disease: current status, pathogenomics and management. *3 Biotech* 10 (11), 503.
- Tong, S., An, K., Chen, W., Chai, M., Sun, Y., Wang, Q., Li, D., 2023. Identification of neutral genome integration sites with high expression and high integration efficiency in *Fusarium venenatum* TB01. *Synthetic and Systems Biotechnology* 8 (1), 141–14.
- Tong, S., An, K., Zhou, W., Chen, W., Sun, Y., Wang, Q., Li, D., 2022. Establishment of high-efficiency screening system for gene deletion in *Fusarium venenatum* TB01. *J. Fungi* 8 (2), 169.
- Torbati, M., Arzanlou, M., Santos, A.C.S., 2021. Fungicolous *Fusarium* species: ecology, diversity, isolation, and identification. *Curr. Microbiol.* 78, 2850–2859.
- Torbati, M., Arzanlou, M., Sandoval-Denis, M., Crous, P.W., 2019. Multigene phylogeny reveals new fungicolous species in the *Fusarium tricinctum* species complex and novel hosts in the genus *Fusarium* from Iran. *Mycol. Prog.* 18, 119–133.
- Trail, F., Xu, H., Loranger, R., Gadoury, D., 2002. Physiological and environmental aspects of ascospore discharge in *Gibberella zeae* (anamorph *Fusarium graminearum*). *Mycologia* 94 (2), 181–189.
- Trinci, A.P.J., 1992. Myco-protein: a twenty-year overnight success story. *Mycological Research* 96 (1), 1–13.
- Trinci, A.P.J., 1994. Evolution of the Quorn® myco-protein fungus, *Fusarium graminearum* A3/5. *Microbiology* 140, 2181–2188.
- Tronsmo, A.M., Hsiang, T., Okuyama, H., Nakajima, T., 2001. Low temperature diseases caused by *Microdochium nivale*. In: *Low Temperature Plant Microbe Interactions under Snow*. Ed: Iriki N, Gaudet DA, Tronsmo AM, Matsumoto N, Yoshida M, Nishimune A (Eds). Published by the Hokkaido National Agricultural Experiment Station.
- Tsukada, K., Shinki, S., Kaneko, A., Murakami, K., Irie, K., Murai, M., Miyoshi, H., Dan, S., et al., 2020. Synthetic biology based construction of biological activity-related library of fungal decalin-containing diterpenoid pyrones. *Nat. Commun.* 11, 1830.
- Tuxbury, K.A., Shaw, G.C., Montali, R.J., Clayton, L.A., Kwiatkowski, N.P., Dykstra, M.J., Mankowski, J.L., 2014. *Fusarium solani* species complex associated with carapace lesions and branchitis in captive American horseshoe crabs *Limulus polyphemus*. *Dis. Aquat. Org.* 109 (3), 223–230.
- Urban, M., Czick, A., Seager, J., Wood, V., Rutherford, K., Venkatesh, S.Y., Sahu, J., Iyer, S.V., et al., 2022. PHI-base in 2022: a multi-species phenotype database for Pathogen-Host Interactions. *Nucleic Acids Res.* 50 (D1), D837–847.
- Urban, M., Daniels, S., Mott, E., Hammond-Kosack, K.E., 2002. *Arabidopsis* is susceptible to the cereal ear blight pathogens *Fusarium graminearum* and *Fusarium culmorum*. *Plant J.* 32 (6), 961–973.
- Urbaniak, C., Massa, G., Hummerick, M., Khodadad, C., Schuerger, A., Venkateswaran, K., 2018. Draft genome sequences of two *Fusarium oxysporum* isolates cultured from infected *Zinnia hybrida* plants grown on the international space station. *Genome Announc.* 6 (20).
- van Dam, P., de Sain, M., Ter Horst, A., van der Gragt, M., Rep, M., 2017. Use of comparative genomics-based markers for discrimination of host specificity in *Fusarium oxysporum*. *Appl. Environ. Microbiol.* 84 (1).
- van der Does, H.C., Fokkens, L., Yang, A., Schmidt, S.M., Langereis, L., Lukaszewicz, J.M., Hughes, T.R., Rep, M., 2016. Transcription factors encoded on core and accessory chromosomes of *Fusarium oxysporum* induce expression of effector genes. *PLoS Genet.* 12 (11), e1006401.
- van Diepeningen, A.D., Al-Hatmi, A.M., Brankovics, B., de Hoog, G.S., 2014. Taxonomy and clinical spectra of *Fusarium* species: where do we stand in 2014? *Curr. Clin. Microbiol. Rep.* 1, 10–18.
- Vaughan, M., Backhouse, D., Del Ponte, E.M., 2016. Climate change impacts on the ecology of *Fusarium graminearum* species complex and susceptibility of wheat to *Fusarium* head blight: a review. *World Mycotoxin J.* 9 (5), 685–700.
- Vázquez-Rosas-Landa, M., Sánchez-Rangel, D., Hernández-Domínguez, E.E., Pérez-Torres, C.A., López-Buenfil, A., et al., 2021. Design of a diagnostic system based on molecular markers derived from the ascomycetes pan-genome analysis: the case of *Fusarium* dieback disease. *PLoS One* 16 (1), e0246079.
- Velasco, M., Gilbert, C.A., Rutledge, C.O., McNay, J.L., 1975. Antihypertensive effect of a dopamine beta hydroxylase inhibitor, bucipamide: a comparison with hydralazine. *Clin. Pharmacol. Therapeut.* 18 (2), 145–153.
- Venkatesh, N., Keller, N.P., 2019. Mycotoxins in conversation with bacteria and fungi. *Front. Microbiol.* 10, 403.
- Vishwakarma, S.K., Kumar, P., Nigam, A., Singh, A., Kumar, A., 2013. Pokkah Boeng: an emerging disease of sugarcane. *J. Plant Pathol. Microbiol.* 4, 170.
- Viukari, M., Linnoila, M., 1977. Effect of fusaric acid on tardive dyskinesia and mental state in psychogeriatric patients: a pilot study. *Acta Psychiatr. Scand.* 56 (1), 57–61.
- Waalwijk, C., Taga, M., Zheng, S., Proctor, R.H., Vaughan, M.M., O’Donnell, K., 2018. Karyotype evolution in *Fusarium*. *IMA Fungus.* 9 (1), 13–26.
- Walsh, J.L., Laurence, M.H., Liew, E.C.Y., Sagalang, A.E., Burgess, L.W., Summerell, B.A., Petrovic, T., 2010. *Fusarium*: two endophytic novel species from tropical grasses of northern Australia. *Fungal Divers.* 44, 149–159.
- Wang, L., Calabria, J., Chen, H., Somssich, M., 2022. The *Arabidopsis thaliana* - *Fusarium oxysporum* strain 5176 pathosystem: an overview. *J. Exp. Bot.* 73 (18), 6052–6067.
- Wang, Y., Liu, X., Yuan, B., Chen, X., Zhao, H., Ali, Q., Zheng, M., Tan, Z., Yao, H., Zheng, S., Wu, J., Xu, J., Shi, J., Wu, H., Gao, X., Gu, Q., 2024. *Fusarium graminearum* rapid alkalization factor peptide negatively regulates plant immunity and cell growth via the FERONIA receptor kinase. *Plant Biotechnol. J.* 22 (7), 1800–1811.
- Wegulo, S.N., Baenziger, P.S., Nopsa, J.H., Bockus, W.W., Hallen-Adams, H., 2015. Management of *Fusarium* head blight of wheat and barley. *Crop Protect.* 73, 100–107.
- Weld, R.J., Plummer, K.M., Carpenter, M.A., Ridgway, H.J., 2006. Approaches to functional genomics in filamentous fungi. *Cell Res.* 16, 31–44.
- Wilson, F.M., Harrison, R.J., 2021. CRISPR/Cas9 mediated editing of the Quorn fungus *Fusarium venenatum* A3/5 by transient expression of Cas9 and sgRNAs targeting endogenous marker gene PKS12. *Fungal Biol. Biotechnol.* 8, 15.
- Wilson, R.A., McDowell, J.M., 2022. Recent advances in understanding of fungal and oomycete effectors. *Curr. Opin. Plant Biol.* 68, 102228.
- Wingfield, B.D., Steenkamp, E.T., Santana, Q.C., Coetzee, M.P., Bam, S., Barnes, I., Beukes, C.W., Chan, W.Y., et al., 2012. First fungal genome sequence from Africa: a preliminary analysis. *South Afr. J. Sci.* 108, 93–98.
- Wollenweber, H.W., 1931. *Fusarium monoglyphi*. Parasitic and saprophytic fungi. *Zeitschrift Fur Parasitenkunde* 3, 269–516.
- Wood, A.K.M., Walker, C., Lee, W., Urban, M., Hammond-Kosack, K.E., 2020. Functional evaluation of a homologue of plant rapid alkalisation factor (RALF) peptides in *Fusarium graminearum*. *Fungal Biol.* 124 (9), 753–765.
- Wu, V.W., Thieme, N., Huberman, L.B., Glass, N.L., 2020. The regulatory and transcriptional landscape associated with carbon utilization in a filamentous fungus. *Proc. Natl. Acad. Sci. U.S.A.* 17 (11), 6003–6013.

- Xu, M., Huang, Z., Zhu, W., Liu, Y., Bai, X., Zhang, H., 2023. *Fusarium*-derived secondary metabolites with antimicrobial effects. *Molecules* 28 (8), 3424.
- Yaakoub, H., Mina, S., Calenda, A., Bouchara, J.P., Papon, N., 2022. Oxidative stress response pathways in fungi. *Cell. Mol. Life Sci.* 79 (6), 333.
- Yang, H., Tan, N., Wu, F., Liu, H., Sun, Z., 2012. Biosorption of uranium (VI) by a mangrove endophytic fungus *Fusarium sp.* #ZZF51 from the South China Sea. *J. Radioanal. Nucl. Chem.* 292 (3), 1011–1016.
- Yang, H., Yu, H., Ma, L.J., 2020. Accessory chromosomes in *Fusarium oxysporum*. *Phytopathology*. 110 (9), 1488–1496.
- Yang, L., Gao, W., Huo, J., Zhang, C., Xu, L., Wang, Y., 2022. First report of stem and root rot caused by *Fusarium oxysporum* on *Geranium* in China. *Plant Dis.* 107 (5), 1623.
- Yang, P., Hao, Z., Qu, Y., Liang, R., Xu, L., Zhang, K., Ming, J., 2023. First report of *Fusarium equiseti* causing bulb rot on lily (*Lilium* 'White planet') in China. *Plant Dis.* 107 (9), 2847.
- Yao, G., Chen, W., Sun, J., Wang, X., Wang, H., Meng, T., Zhang, L., Guo, L., 2023. Gapless genome assembly of *Fusarium verticillioides*, a filamentous fungus threatening plant and human health. *Sci. Data* 10, 229.
- Yao, Z., Zou, C., Peng, N., Zhu, Y., Bao, Y., Zhou, Q., Wu, Q., Chen, B., Zhang, M., 2020. Virome identification and characterization of *Fusarium sacchari* and *F. andiyazi*: causative agents of Pokkah Boeng disease in sugarcane. *Front. Microbiol.* 11, 240.
- Yilmaz, N., Sandoval-Denis, M., Lombard, L., Visagie, C.M., Wingfield, B.D., Crous, P.W., 2021. Redefining species limits in the *Fusarium fujikuroi* species complex. *Persoonia* 46, 129–162.
- Yuan, Q.S., Wang, L., Wang, H., Wang, X., Jiang, W., Ou, X., Xiao, C., Gao, Y., Xu, J., Yang, Y., Cui, X., 2022. Pathogen-mediated assembly of plant-beneficial bacteria to alleviate *Fusarium* wilt in *Pseudostellaria heterophylla*. *Front. Microbiol.* 13, 842372.
- Yudianto, D., Nainggolan, E.A., Millati, R., Hidayat, C., Lennartsson, P., Taherzadeh, M. J., Niklasson, C., 2019. Bioconversion of pretreated wheat straw to ethanol by *Monascus purpureus* CBS 109.07 and *Fusarium venenatum* ATCC 20334 using simultaneous saccharification and fermentation. *Biodiversitas: J. Biodiversity* 20, 2229–2235.
- Yun, S.H., Arie, T., Kaneko, I., Yoder, O.C., Turgeon, B.G., 2000. Molecular organization of mating type loci in heterothallic, homothallic, and asexual *Gibberella/Fusarium* species. *Fungal Genet. Biol.* 31 (1), 7–20.
- Zamora-Ballesteros, C., Diez, J.J., Martín-García, J., Witzell, J., Solla, A., Ahumada, R., Capretti, P., Cleary, M., Drenkhan, R., Dvořák, M., et al., 2019. Pine Pitch Canker (PPC): pathways of pathogen spread and preventive measures. *Forests* 10 (12), 1158.
- Zeller, K.A., Summerell, B.A., Bullock, S., Leslie, J.F., 2003. *Gibberella konza* (*Fusarium konzum*) sp. nov., a new biological species within the *Gibberella fujikuroi* species complex from prairie grasses. *Mycologia* 95, 943–954.
- Zhang, N., O'Donnell, K., Sutton, D.A., Nalim, F.A., Summerbell, R.C., Padhye, A.A., Geiser, D.M., 2006. Members of the *Fusarium solani* species complex that cause infections in both humans and plants are common in the environment. *J. Clin. Microbiol.* 44 (6), 2186–2190.
- Zhang, Y., Yang, H., Turra, D., Zhou, S., Ayhan, D.H., DeJulio, G.A., Guo, L., Broz, K., Wiederhold, N., Coleman, J.J., Donnell, K.O., 2020. The genome of opportunistic fungal pathogen *Fusarium oxysporum* carries a unique set of lineage-specific chromosomes. *Commun. Biol.* 3 (1), 50.
- Zhao, X., Li, H., Zhou, L., Chen, F., Chen, F., 2020a. Wilt of *Acer negundo* L. caused by *Fusarium nirenbergiae* in China. *J. For. Res.* 31, 2013–2022.
- Zhao, Y., Lim, J., Xu, J., Yu, J.H., Zheng, W., 2020b. Nitric oxide as a developmental and metabolic signal in filamentous fungi. *Mol. Microbiol.* 113 (5), 872–882.

Appendix 2

Armer VJ, Urban M, Ashfield T, Deeks MJ, Hammond-Kosack KE. (2024). The trichothecene mycotoxin deoxynivalenol facilitates cell-to-cell invasion during wheat-tissue colonisation by *Fusarium graminearum*. *Molecular Plant Pathology*. **25**(6): e13485. doi: 10.1111/mpp.13485.

The trichothecene mycotoxin deoxynivalenol facilitates cell-to-cell invasion during wheat-tissue colonization by *Fusarium graminearum*

Victoria J. Armer^{1,2}  | Martin Urban¹  | Tom Ashfield^{1,3}  | Michael J. Deeks²  | Kim E. Hammond-Kosack¹ 

¹Protecting Crops and the Environment, Rothamsted Research, Harpenden, UK

²Biosciences, University of Exeter, Exeter, UK

³Crop Health and Protection (CHAP), Rothamsted Research, Harpenden, UK

Correspondence

Kim E. Hammond-Kosack, Protecting Crops and the Environment, Rothamsted Research, Harpenden, AL5 2JQ, UK.
Email: kim.hammond-kosack@rothamsted.ac.uk

Funding information

Biotechnology and Biological Sciences Research Council, Grant/Award Number: BB/T008741/1, BB/W007134/1, BB/X011003/1, BB/X012131/1, BBS/E/C/00010250 and BBS/E/RH/230001B

Abstract

Fusarium head blight disease on small-grain cereals is primarily caused by the ascomycete fungal pathogen *Fusarium graminearum*. Infection of floral spike tissues is characterized by the biosynthesis and secretion of potent trichothecene mycotoxins, of which deoxynivalenol (DON) is widely reported due to its negative impacts on grain quality and consumer safety. The *TRI5* gene encodes an essential enzyme in the DON biosynthesis pathway and the single gene deletion mutant, $\Delta Tri5$, is widely reported to restrict disease progression to the inoculated spikelet. In this study, we present novel bioimaging evidence revealing that DON facilitates the traversal of the cell wall through plasmodesmata, a process essential for successful colonization of host tissue. Chemical complementation of $\Delta Tri5$ did not restore macro- or microscopic phenotypes, indicating that DON secretion is tightly regulated both spatially and temporally. A comparative qualitative and quantitative morphological cellular analysis revealed infections had no impact on plant cell wall thickness. Immunolabelling of callose at plasmodesmata during infection indicates that DON can increase deposits when applied exogenously but is reduced when *F. graminearum* hyphae are present. This study highlights the complexity of the interconnected roles of mycotoxin production, cell wall architecture and plasmodesmata in this highly specialized interaction.

KEYWORDS

deoxynivalenol, *Fusarium graminearum*, head scab disease, plasmodesmata, wheat (*Triticum aestivum*)

1 | INTRODUCTION

Fusarium graminearum (teleomorph *Gibberella zeae*) is an ascomycete fungal pathogen and the main causative agent of *Fusarium* head blight (FHB), or scab disease, on wheat. *F. graminearum* infects wheat floral tissues at flowering (anthesis), secreting many cell

wall-degrading enzymes (CWDEs), other proteins and metabolites as well as mycotoxins that contaminate the developing grain, rendering it unsuitable for both human and livestock consumption (McMullen et al., 2012). Among these mycotoxins, the sesquiterpenoid type B toxins of the trichothecene class are particularly potent and include deoxynivalenol (DON), nivalenol (NIV), zearalenone (ZEA)

This is an open access article under the terms of the [Creative Commons Attribution](https://creativecommons.org/licenses/by/4.0/) License, which permits use, distribution and reproduction in any medium, provided the original work is properly cited.

© 2024 The Author(s). *Molecular Plant Pathology* published by British Society for Plant Pathology and John Wiley & Sons Ltd.

and T-2 toxin (reviewed McCormick et al., 2011), all of which target the ribosome and inhibit protein synthesis (Brown et al., 2004). Trichothecene contamination of grain causes significant economic losses annually (McMullen et al., 1997), destroying wheat crops weeks before harvest and subsequently proliferating during ineffective grain storage/shipment. Epidemics of FHB occur when warm, wet weather coincides with anthesis and are particularly prominent in the mid-west United States, Asia, Brazil and northern Europe (McMullen et al., 1997; Vaughan et al., 2016). Novel genetic targets are required to help control outbreaks of FHB disease due to the prevalence of resistance to the major class of azole fungicides in global *F. graminearum* strains (Fan et al., 2013). Incidences of FHB outbreaks are expected to increase as climate change increases precipitation around wheat harvests (Vaughan et al., 2016). Hence, it is imperative that the infection biology of *F. graminearum* is explored further to aid in the development of resistant wheat varieties and precise chemical control, with the overall aim of minimizing FHB-associated reductions in cereal yields, grain quality and to improve human/animal health.

The infection cycle of FHB commences with the dispersal of conidia (asexual) or ascospores (sexual) by rain droplet-induced splashes or wind onto wheat plants. During a typical infection of wheat at crop anthesis, germinating spores enter the host floral tissues through natural openings, such as stomata (Pritsch et al., 2007) and cracked open anther sacs, or have been reported to form penetration pegs on the abaxial surface of the palea and lemma tissues of the wheat spikelet (Wanjiru et al., 2002). Host-tissue colonization continues with the invasive hyphae growing both intercellularly and intracellularly. *F. graminearum* has been noted to have a biphasic lifestyle, whereby the advancing infection front is split between macroscopically symptomatic and symptomless phases (Brown et al., 2011). The symptomless phase is hallmarked by apoplastic growth, and the symptomatic by extensive intracellular growth. What initiates this switch is not yet known and is a subject of great interest. During later stages of infection, *F. graminearum* secretes CWDEs in abundance (Brown et al., 2012) to facilitate infection by deconstructing wheat cell walls. At the rachis internode, invasive hyphae have been reported to enter vascular elements (Wanjiru et al., 2002) and grow through the remaining wheat spike within the vasculature as well as in the cortical tissue surrounding the vascular bundles (Brown et al., 2010). Furthermore, within the chlorenchyma band of the rachis, *F. graminearum* produces perithecia, sexual reproductive structures, completing its lifecycle (Guenther & Trail, 2005). Post-harvest, *F. graminearum* overwinters saprophytically on crop debris or within the soil, thereby infecting subsequent crop cycles. The presence of *F. graminearum* in the soil can be the primary cause of seedling blight and root rot in subsequent wheat crops (Parry et al., 1995).

Intracellular growth by *F. graminearum* has been previously reported to traverse wheat cell walls through pits or pit fields, where plasmodesmata (PD) are present (Brown et al., 2010; Guenther &

Trail, 2005; Jansen et al., 2005). PD are cytoplasmic communication channels that symplastically bridge the cell walls by an appressed endoplasmic reticulum (ER), known as a desmotubule, within a plasma membrane (PM) continuum stabilized by proteins connected to both the ER and PM (Sager & Lee, 2018). PD are instrumental to cellular signalling, allowing for the transport of sugars, ions and small proteins, to name a few. However, plants can adjust the permeability of PD by the deposition of callose, mediated by the action of callose synthases and β -1,3-glucanases (Lee & Lu, 2011) at PD junctions. This callose plugging leads to the symplastic isolation of cells that are damaged or under pathogen attack, thereby restricting the movement of secreted pathogen effector proteins, toxins and other metabolites. PD have a major role in host plant defence against viruses, bacteria and fungi (Lee & Lu, 2011). *F. graminearum* exploits the plasmodesmatal transit highways by excreting β -1,3-glucanases: enzymes that catalyse the breakdown of the 1,3-O-glycosidic bond between glucose molecules in callose. RNA-seq analysis of *F. graminearum* infection of wheat spikes found that several *Fusarium* β -1,3-glucanases are upregulated in the host plant from as early as 6 h post-infection and peaking at 36–48 h after inoculation (Pritsch et al., 2007).

The trichothecene mycotoxin DON is a well-reported virulence factor in wheat floral tissues (Cuzick et al., 2008; Jansen et al., 2005; Proctor et al., 1995) and biosynthesis of the toxin requires the *TRI5* gene, encoding the enzyme trichodiene synthase (Hohn et al., 1993). DON is synthesized and then secreted by *F. graminearum* hyphae during infection and is a potent ribosomal-binding translational inhibitor. This broad-spectrum dampening of induced protein-dependent defence responses has thus far prevented the elucidation of specific components of host immunity that restrict *F. graminearum* in the DON-deficient interaction. The low molecular weight of trichothecenes and their water-solubility allow them to rapidly enter cells and target eukaryotic ribosomes. This causes what is known as the 'ribotoxic stress response' that can activate, among other processes, mitogen-activated protein kinases (MAPKs) and apoptosis (reviewed Pestka, 2008). Deletion of *TRI5* eliminates the ability of *F. graminearum* to synthesize DON (Proctor et al., 1995), and infection of wheat floral tissues by the single gene deletion mutant ($\Delta Tri5$) is restricted to the inoculated spikelet, and results in the production of eye-shaped lesions on the outer glume (Cuzick et al., 2008; Jansen et al., 2005). Conversely, expression of *TRI5* in wild-type *F. graminearum* is correlated with DON accumulation in planta (Hallen-Adams et al., 2011). In non-host pathosystems, such as the model plant species *Arabidopsis thaliana*, infection of floral tissues with the single gene deletion mutant $\Delta Tri5$ causes a wild-type disease phenotype, indicating that DON is not a virulence factor in this interaction (Cuzick et al., 2008). Current evidence indicates that the *TRI4* gene, which encodes a multifunctional cytochrome P450 monooxygenase and resides within the main trichothecene mycotoxin biosynthetic cluster (Tokai et al., 2007), is expressed during the *F. graminearum*-wheat coleoptile interaction (Qui et al., 2019), but the role

of *TRI4* or *TRI5* as a virulence factors in coleoptiles has not yet been reported. The *TRI4* protein is required for four consecutive oxygenation steps in trichothecene mycotoxin biosynthesis (Tokai et al., 2007), thus indicating a role for trichothecene mycotoxins during coleoptile infection. Through the use of fluorescent marker reporter strains, the *TRI5* gene has been shown to be induced during infection structure formation on wheat palea (Boenisch & Schafer, 2011). However, the absence of *TRI5* in a *F. graminearum* $\Delta Tri5$ -GFP strain did not impact the ability of *F. graminearum* to form infection cushions during initial time points of infection (Boenisch & Schafer, 2011). The DON mycotoxin naturally occurs as two chemotypes, 15-ADON and 3-ADON, and individual *F. graminearum* strains secrete either toxin type. The wild-type (WT) strain used in this study, PH-1, synthesizes 15-ADON. Host-plant resistance to DON is a characteristic of type II FHB resistance, whereby fungal advancement does not proceed beyond the rachis node (reviewed Mesterházy, 1995).

Whilst the macrobiology and some aspects of the cellular biology of the single-gene deletion mutant $\Delta Tri5$ have been previously studied, the mode of restriction of $\Delta Tri5$ remains to be elucidated. Postulations have been made around the role of DON during host-tissue colonization, specifically relating to the targeting of ribosomes and the subsequent, broad-spectrum, protein translation inhibition (Pestka, 2010). However, what host defence mechanisms are targeted/specifically affected by DON have not been explored in planta. This study aims to re-evaluate the infection biology of the $\Delta Tri5$ strain, and hence the role(s) of DON, during host-tissue colonization through a combination of molecular and microscopy techniques. Through qualitative and quantitative image analysis of wheat floral tissues during WT and $\Delta Tri5$ infection, we report that the $\Delta Tri5$ single gene deletion mutant has an impaired ability to traverse PD. We also find no evidence to support the hypothesis that a general increase in plant cell wall thickening occurs in the absence of DON production, whereby the upregulation of cell wall defences occurs during pathogen attack. From the data gathered, we infer that the secretion of DON during host-tissue colonization is highly specific both spatially and temporally. This is indicated by the lack of increase in virulence in the $\Delta Tri5$ mutant when supplied with DON at the point of inoculation in our study. In light of these discoveries, we pose new questions surrounding *F. graminearum* infection biology, cell wall colonization and wheat host defence mechanisms.

2 | RESULTS

The role(s) of DON during *F. graminearum* infection of different wheat tissues was addressed through a multifaceted approach. We applied a combination of detailed cell and molecular biology and morphological analyses of floral and coleoptile infections to analyse the effect of DON on hyphae traversing cell walls at PD and the occurrence of the defence response, callose deposition, at PD during

infections caused by either the WT strain or the single gene deletion mutant $\Delta Tri5$ *F. graminearum* strain.

2.1 | DON is not required for virulence on wheat coleoptiles and chemical complementation does not restore the WT disease phenotype on wheat spikes

To determine whether DON is or is not required for virulence on wheat coleoptiles under our conditions the fully susceptible cv. Apogee was tested. Inoculation of wheat coleoptiles revealed no differences in lesion length between the WT PH-1 strain and single gene deletion mutant $\Delta Tri5$ (Figure 1a,b). However, reverse transcription-quantitative PCR (RT-qPCR) analysis showed that the WT strain expressed *TRI5* during coleoptile infection at 3, 5 and 7 days post-inoculation (dpi), but remains at very low levels ($\times 0.8$ *FgActin*) and stationary throughout the infection progression (Figure 1c), indicating that *TRI5* mRNA levels are not temporally altered for this interaction during the early to mid-time points explored. This finding supports a previous study by Qui et al. (2019), who reported accumulation of transcripts of the *TRI4* gene, also required for trichothecene mycotoxin biosynthesis.

Next, we asked whether the same host and pathogen genotypes showed different DON dependencies during floral tissue interactions. Disease progression of WT, $\Delta Tri5$ and DON-complemented strains were analysed by tracking visible disease symptom development on the outer glume and rachis of inoculated wheat spikes. The single $\Delta Tri5$ mutant was restricted to the inoculated spikelet in all instances. Chemical complementation of the $\Delta Tri5$ mutant with DON (35 ppm) applied along with the conidia failed to restore the macroscopic WT spikelet phenotype occurring on the inoculated spikelet or spikelet-to-spikelet symptom development. This DON concentration was not detrimental to either spore germination or early spore germling growth (Data S1). Interestingly, co-inoculation of WT *F. graminearum* with DON at the same concentration did not result in any observable advancement of disease symptoms (Figure 2a). Application of DON (35 ppm) alone did not induce any macroscopic disease symptoms and visually equated to the water only (distilled water) mock-inoculated samples (Figures 2d and 3a). The area under the disease progression curve (AUDPC) analysis revealed that the PH-1 and PH-1 + DON supplementation floral infections had significantly greater disease progression than the $\Delta Tri5$, $\Delta Tri5$ + DON, DON only and mock-inoculated treatments (Kruskal-Wallis, $p = 2.8e^{-10}$; Figure 2b). To quantify the levels of DON present in all treatments at the end of disease progression (Day 14), a DON-ELISA test was carried out to determine the final 15-ADON concentrations. PH-1 and PH-1 + DON samples had an average DON concentration of over 30 ppm, whilst all other treatments had no detectable (< 0.5 ppm) DON (Figure 2c). This indicates that the addition of DON to WT inoculum did not stimulate further DON production and confirms that the PH-1 $\Delta Tri5$ mutant is impaired in DON biosynthesis. Of

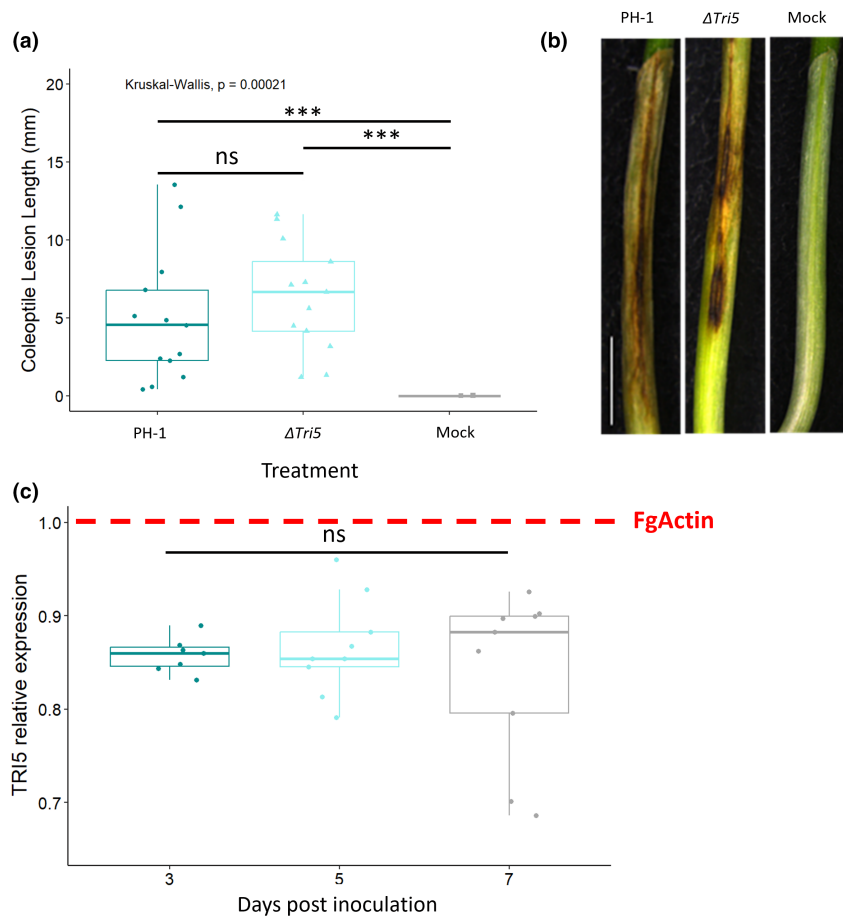


FIGURE 1 *Fusarium graminearum* disease formation on wheat coleoptiles. (a) Length lesion at 7 days post-inoculation (dpi) for PH-1, the $\Delta Tri5$ mutant and mock inoculations, Kruskal-Wallis *** $p < 0.005$. (b) Examples of disease lesion phenotypes at 7 dpi for PH-1, $\Delta Tri5$ and mock inoculations from rep 2, scale bar = 20 mm and (c) relative expression of *TR15* measured using reverse transcription-quantitative PCR at 3, 5 and 7 dpi in wheat coleoptiles, normalized against *FgActin* expression. Analysis of variance $F(2,22) = 0.421$, $p = 0.662$ (ns).

note, the lack of detection of DON in the $\Delta Tri5$ + DON and DON alone samples is probably due to the detoxification of DON by wheat plants to DON-3-glucoside, the latter is undetectable by the competitive ELISA kit used in this study. The conjugation of DON to DON-3-glucoside, catalysed by a UDP-glucosyltransferase, in planta is difficult to detect through its increased molecule polarity and is thus known as a 'masked mycotoxin' (Berthiller et al., 2005). A visual representation of disease progression occurring in each treatment is shown in Figure 2d.

Cuzick et al. (2008) had previously shown a qualitative difference in the appearance of macroscopic disease symptoms on the glumes between the WT and the $\Delta Tri5$ mutant. In this study, we have extended this observation and explored the macroscopic and microscopic disease symptoms. Macroscopically, we were able to confirm the $\Delta Tri5$ -inoculated spikelets exhibited 'eye-shaped' lesions on the outer surface of the glume by 7 dpi (Figure 3a). These differed from the characteristic fawn brown 'bleaching' of the spikelet tissues observed in the WT interaction at 7 dpi (Figure 3a). Chemical complementation of $\Delta Tri5$ did not restore the WT phenotype nor visibly increase the severity of the WT disease phenotype. To quantify the diseased area, inoculated spikelets were imaged at 5 and 7 dpi and analysed using the Lemnagrid software. The PH-1 and PH-1 + DON spikelets had a greater area exhibiting disease symptoms than both the $\Delta Tri5$ and $\Delta Tri5$ + DON treatments

(Figure 3b). Note that computational restrictions in spikelet parsing from background led to minor, insignificant disease symptoms for DON and mock samples.

2.2 | The $\Delta Tri5$ mutant is inhibited in its ability to traverse PD during host-tissue colonization

Resin-embedded samples of the lemma, palea and rachis spikelet components revealed changes in cellular morphology at different points of infection (Figure 4). In the palea and lemma parenchyma tissue layer, the $\Delta Tri5$ and $\Delta Tri5$ + DON infected samples exhibited extensive cell wall degradation and colonization by invasive hyphae (Figure 5), similarly to the WT infection. However, in the adaxial layer of the palea and lemma tissues, the hyphae in the $\Delta Tri5$ and $\Delta Tri5$ + DON samples rarely penetrated into the thicker-walled cells (Figure 5a-d). Mirroring the macroscopic lack of symptoms in the rachis, the $\Delta Tri5$ rachis samples never contained invasive hyphae at either 5 or 7 dpi (Figure 5e). In the PH-1 and PH-1 + DON-infected samples, invasive hyphae proliferated throughout the entirety of the lemma, palea and rachis tissues, causing extensive cell wall degradation (Figure 4). To penetrate the adaxial layer, the PH-1 hyphae utilized cell wall pits resembling PD pit fields (Figure 4c). In these instances, the hyphae constricted considerably to traverse the

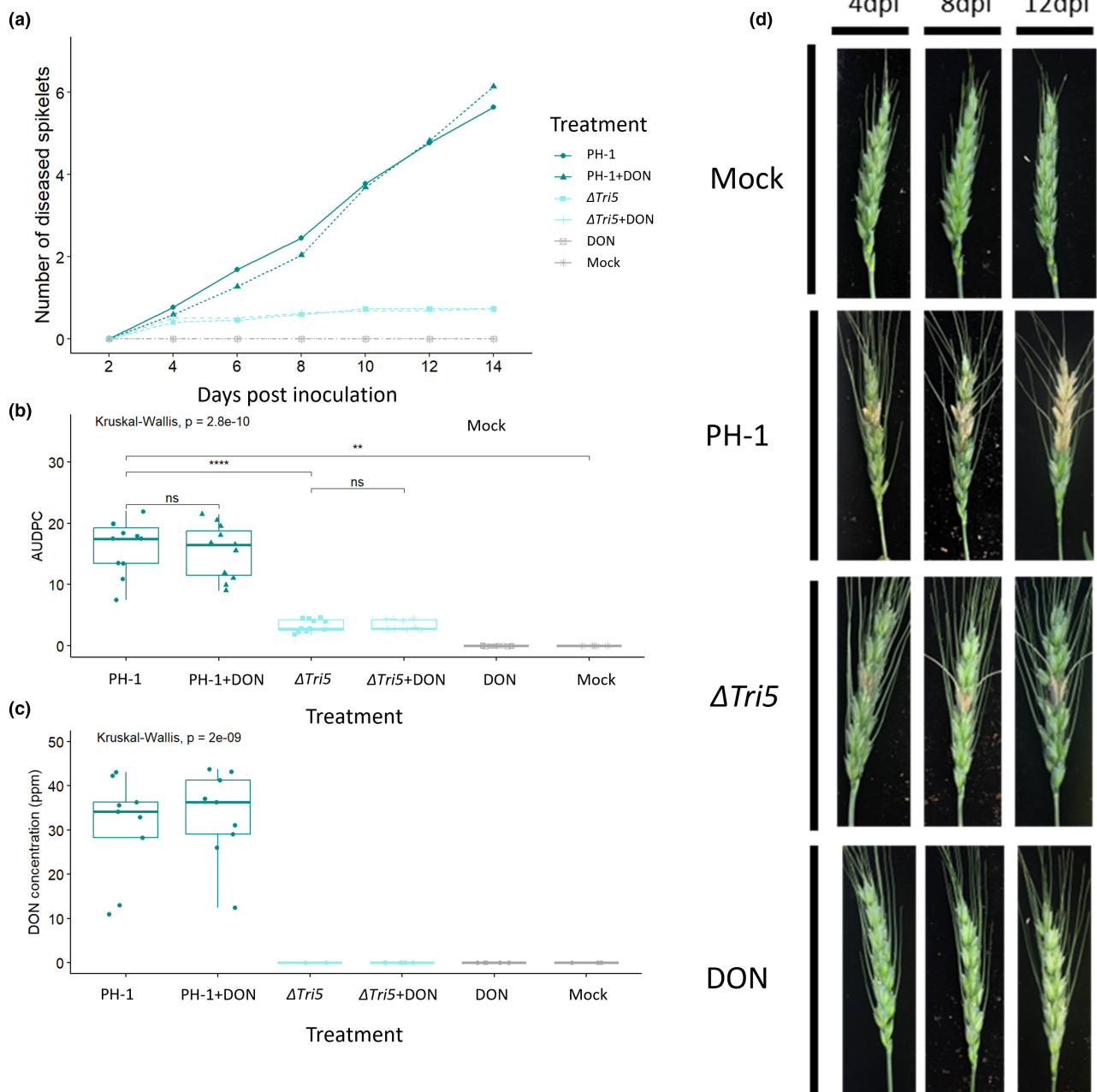


FIGURE 2 Analysis of whole wheat floral tissues following point inoculations. (a) Tracked visible disease progression at 2 day intervals to 14 days post-inoculation (dpi) from below the inoculated spikelet. (b) Area under disease progression curve (AUDPC) for disease progression in panel (a) Kruskal-Wallis $***p < 0.005$. (c) Deoxynivalenol (DON) concentrations of wheat spikes at 14 dpi, Kruskal-Wallis $***p < 0.005$. (d) Representative disease progression images at selected time points of 4, 8 and 12 days.

cell wall. Traversing of the cell wall through PD pit fields was not observed in $\Delta Tri5$ and $\Delta Tri5$ +DON samples at either time point (Figure 5). In general, where hyphae had invaded cells, the cell contents, notably nuclei, chloroplasts and evidence of cytoplasm, were not observed, indicating cell death. In the palea and lemma tissues of the PH-1 infected samples at 7 dpi, putative evidence of 'ghost' hyphae was identified, which are characterized by a lack of cellular contents (Brown et al., 2011) in older infection structures as the infection front advances into the host plant.

To aid elucidation of the role of DON during infection of wheat floral tissues, cell wall thickness from resin-embedded wheat samples was measured along the adaxial layer of lemma and palea tissues, and in the visibly reinforced regions of rachis tissue, for all treatments. In the adaxial layer of the lemma, palea and rachis tissues, cell wall thickness of resin-embedded samples imaged by light microscopy was found not to differ between treatments, particularly between those with and without the presence of DON (Data S5). This unanticipated result indicates that cell wall reinforcements are

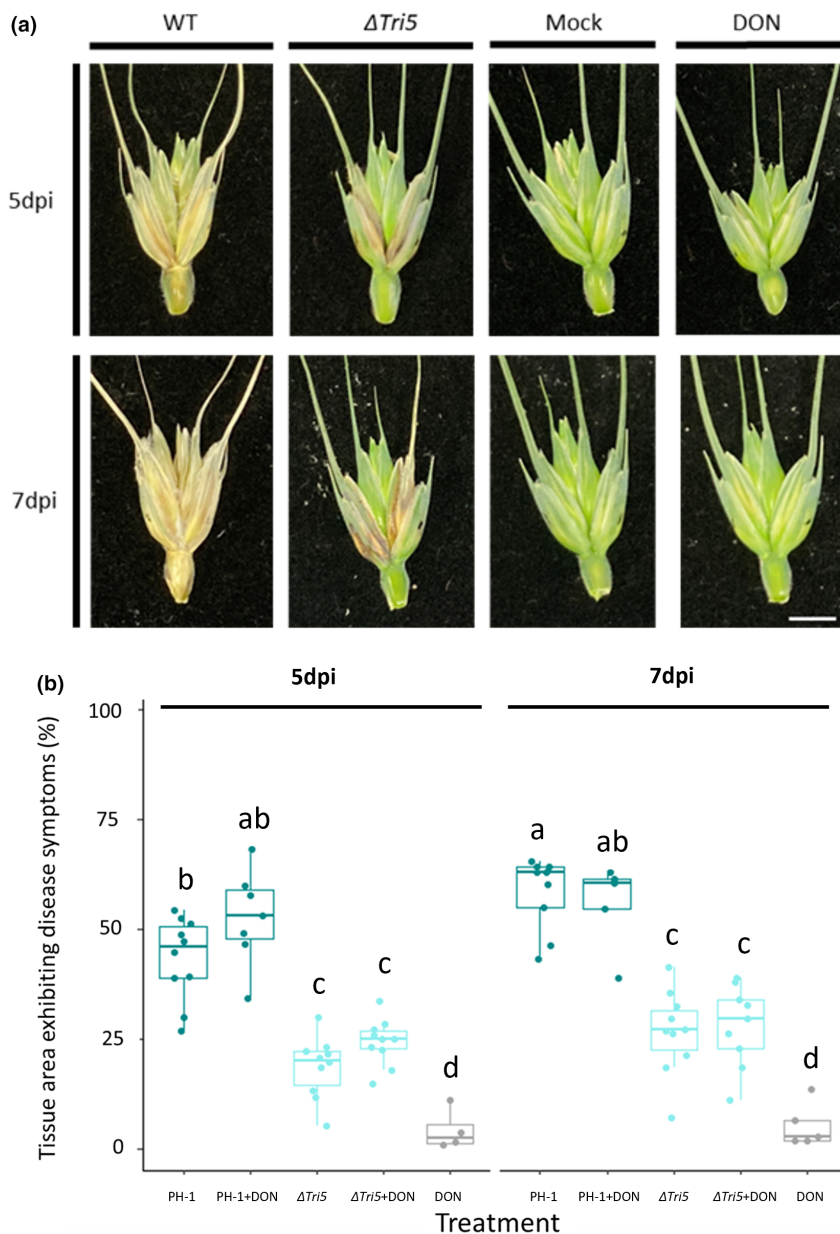


FIGURE 3 Quantitative spikelet analysis for disease symptom development. (a) Examples of dissected spikelets at 5 and 7 days post-inoculation (dpi), scale bar = 10 mm. (b) External tissue areas exhibiting disease symptoms at 5 and 7 dpi as determined by Lemnagrid computational software. Analysis of variance, *** $p < 0.005$, Tukey post hoc denotes group significance.

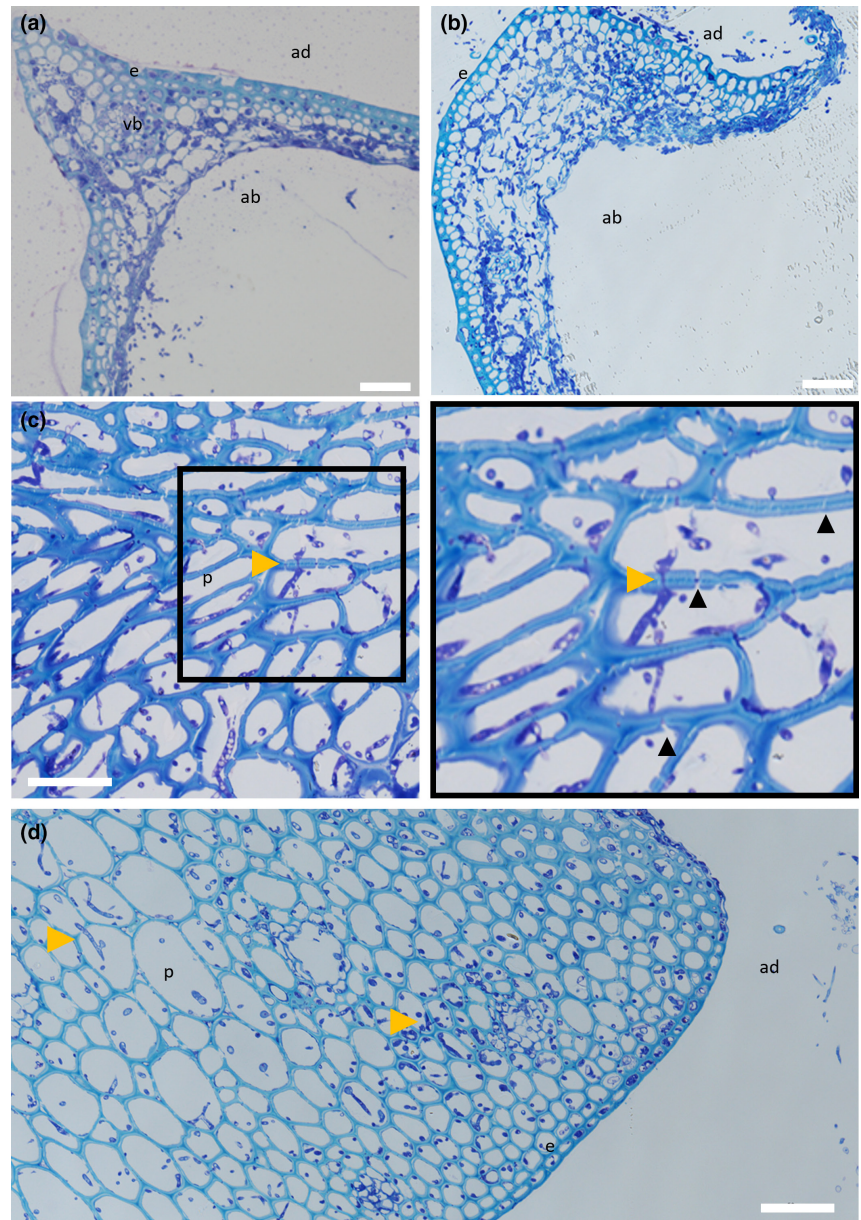
not evident at this level of resolution and are not impacted by the presence of DON. However, it is worth noting that extensive cell wall degradation was present in the abaxial layer of palea and lemma tissues. This microscopic phenotype was not quantified but is most likely caused by the release of CWDEs from *F. graminearum* hyphae (Data S5).

In order to gain a thorough understanding of infection, a scanning electron microscopy (SEM) analysis was used. SEM micrographs of rachis post-spikelet inoculation with WT PH-1 at 5 dpi revealed several notable interactions, including intracellular growth through cells still containing cytoplasm, apoplastic growth between cells, hyphal constriction and cell wall traversing and gaps in rachis cell walls (Figure 6a,b,d). Micrographs of $\Delta Tri5$ -infected lemma tissue at 5 dpi confirmed the resin analysis, whereby extensive cell wall degradation was observed in the parenchyma tissue layer (Figure 6c).

2.3 | Immunolabelling of callose during infection reveals reduced deposits in the WT infection and phloroglucinol staining indicates lignin-based defence response(s)

Resin sections of PH-1, $\Delta Tri5$ and mock-inoculated wheat floral tissues were analysed for the presence of callose at junctions in the cell wall (Figure 7). Immunolabelling for the presence of callose confirmed the material of pit structures was consistent with PD. Imaging revealed that in both WT (PH-1) and DON-deficient ($\Delta Tri5$) *F. graminearum*-inoculated spikes there was an increased frequency of instances where callose was deposited at PD junctions compared to mock-inoculated controls (Figure 7). However, the DON-only inoculated samples exhibited a marked increase in callose in both lemma and rachis tissues, indicating that callose deposition had been induced in a manner consistent with a basal

FIGURE 4 Wild-type (WT)-infected wheat floral tissues at 5 and 7 days post-inoculation (dpi) demonstrating aspects of typical infection. (a) Lemma at 5 dpi infected with WT *Fusarium graminearum* showing widespread hyphal colonization throughout the tissue accompanied by hyphal proliferation protruding from the abaxial layer. (b) A 7 dpi WT-infected lemma showing further tissue degradation by cell wall-degrading enzymes and considerable hyphal proliferation. (c) Rachis at 5 dpi infected with WT *F. graminearum* showing a number of plasmodesmata (PD) crossings by invasive hyphae, indicated by yellow arrowheads, and extensive cell wall degradation of the mesophyll layer by *F. graminearum*-secreted cell wall-degrading enzymes. PD can be identified as gaps in the parenchyma layer cell walls, a number of which are indicated by black arrowheads. (d) A 7 dpi WT-infected rachis demonstrating durability of parenchyma tissue against cell wall-degrading enzymes at later infection time points. ab=abaxial layer, ad=adaxial layer, e=epidermal layer, p=parenchyma tissue, vb=vascular bundle. Yellow arrowheads indicate PD crossings by invasive *F. graminearum* hyphae. Scale bar = 50 μ m.



immune response to symplastically isolate cells after the detection of the DON toxin.

Spikelets of wheat inoculated with WT, PH-1 and $\Delta Tri5$ were sampled at 5 dpi for analysis of the lignin response. This investigation was prompted by the presence of localized eye-shaped lesions in the $\Delta Tri5$ -infected samples. Darker staining by the phloroglucinol indicates a higher lignin content, which was found to be most notable in the $\Delta Tri5$ -infected lemma tissue (Data S8). This was surprising, as the lesions were present on the glume. Whilst this was not quantified, the WT PH-1 and mock-inoculated controls were visually comparable, indicating that WT *F. graminearum* may have a role in dampening pathogen-induced lignin upregulations, possibly through the action of DON. This proposes the hypotheses that in the absence of trichothecene mycotoxins, wheat is able to upregulate lignin defence pathways.

3 | DISCUSSION

This study has re-examined and extended knowledge on the restricted host tissue colonization phenotype previously reported in wheat spikes for the non-DON-producing $\Delta Tri5$ single gene deletion mutant of *F. graminearum*. The study was catalysed by the lack of published cellular information available on how DON, produced and secreted by the advancing *F. graminearum* hyphae, actually facilitates the extraordinary effective and speedy disease progression consistently observed in the spikes of susceptible wheat cultivars. DON has long been classified as a key virulence factor in the *F. graminearum*-wheat interaction (Hohn et al., 1993; Jansen et al., 2005) and facilitates the host-tissue colonization of the rachis and thus is essential for successful internal spikelet-to-spikelet growth of hyphae through the entire floral spike. However, prior to this study, the

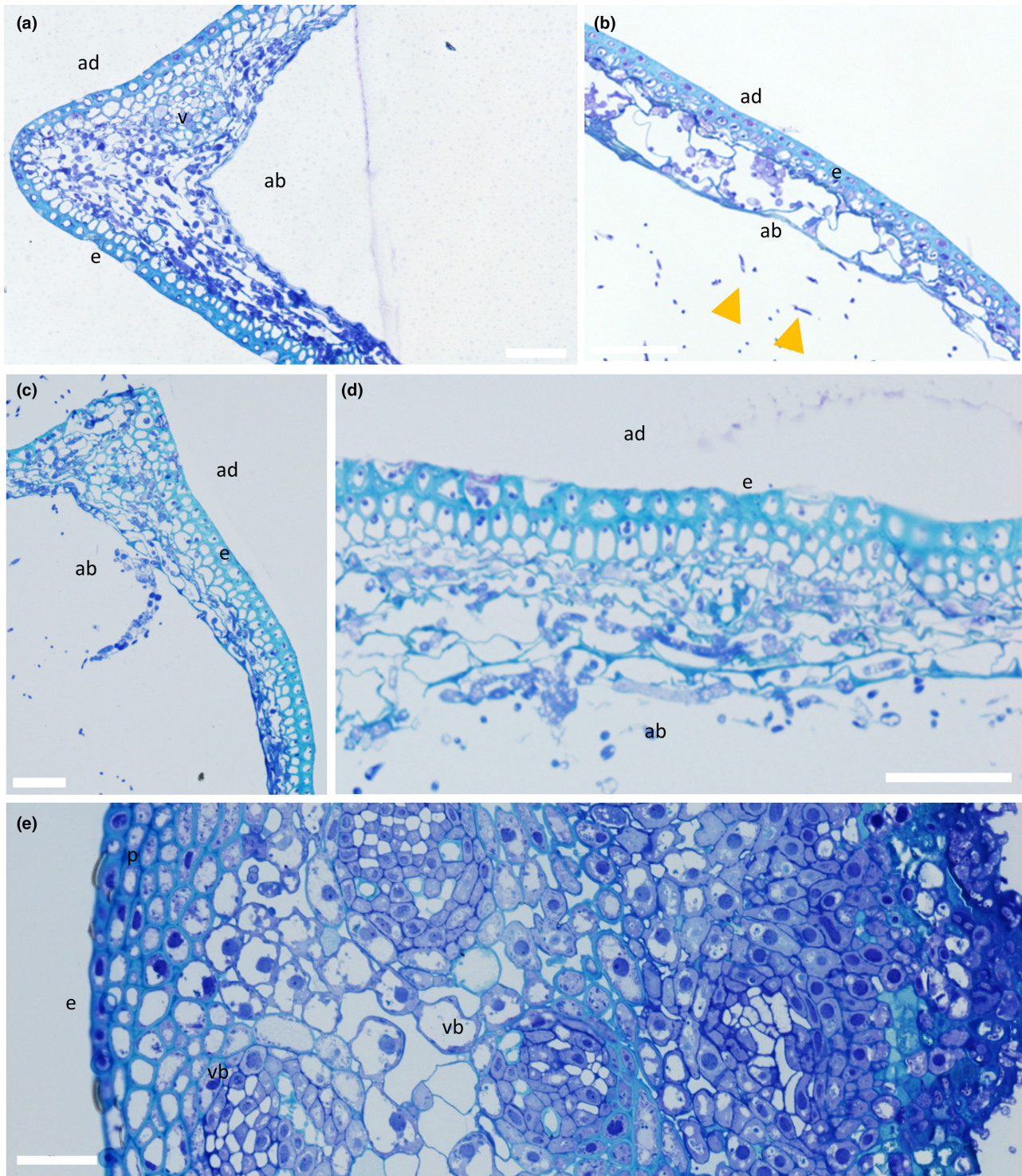


FIGURE 5 Comparison of $\Delta Tri5$ -infected and $\Delta Tri5$ + deoxynivalenol (DON) infected wheat floral tissues at 5 and 7 days post-inoculation (dpi) showing the similarities and differences between tissue types in various aspects of a typical infection. (a) Lemma at 7 dpi infected with $\Delta Tri5$ *Fusarium graminearum* with extensive proliferation of invasive hyphae throughout the abaxial layer, but rarely any penetration into the adaxial layer. (b) Palea at 5 dpi infected with $\Delta Tri5$ and supplemented with 35 ppm DON showing cell wall degradation in the abaxial layer and evidence of external fungal hyphae. Yellow arrows indicate hyphae external to the plant tissue. (c) Palea at 7 dpi infected with $\Delta Tri5$, with similar symptoms to the lemma at the earlier 5 dpi time point. (d) Lemma infected with $\Delta Tri5$ and supplemented with 35 ppm DON at 7 dpi showing cell wall degradation of the abaxial layer. (e) A rachis section at 5 dpi infected with $\Delta Tri5$ and supplemented with 35 ppm DON. No evidence of hyphae or cell wall degradation throughout the sample. ab=abaxial layer, ad=adaxial layer, e=epidermal layer, p=parenchyma tissue, vb=vascular bundle. No plasmodesmata crossings by invasive *F. graminearum* hyphae are evident. Scale bar=50 μ m.

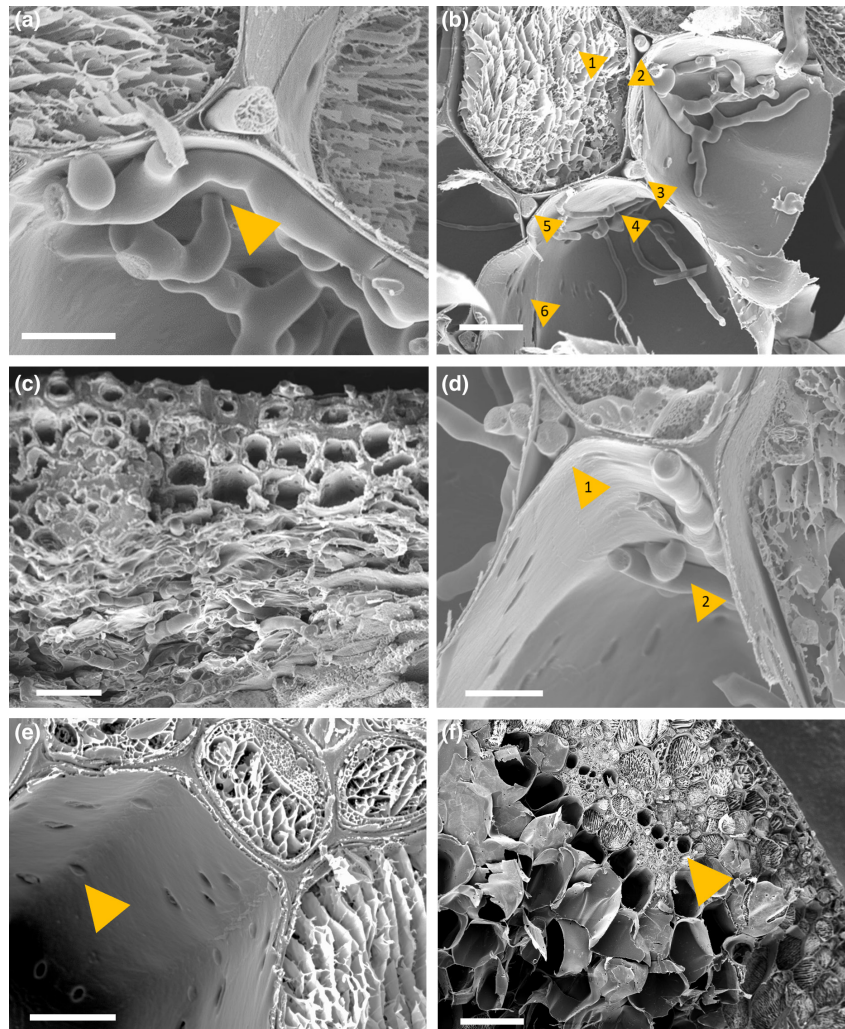


FIGURE 6 Scanning electron micrographs of *Fusarium graminearum* PH-1 and $\Delta Tri5$ - wheat floral interactions. (a) A hypha of the wild-type PH-1 strain appears to cross through the cell wall at 5 days post-inoculation (dpi) in rachis tissue. Scale bar = 10 μ m. (b) Wild-type PH-1 infecting rachis tissue at 5 dpi, the numbered yellow arrowhead indicates point of interest. 1. Intracellular growth in a cell where cytoplasm is still present; 2., 3., and 5. Apoplastic growth between cells, 4. Potential crossing of the cell wall by a hypha through a plasmodesma and 6. 'Holes' in the cell wall that are potential sites of plasmodesmata. Scale bar = 20 μ m. (c) $\Delta Tri5$ -infected lemma tissue at 5 dpi demonstrating extensive hyphal colonization and cell wall degradation of the parenchyma tissue layer (bottom), but minimal infection in the thicker-walled adaxial layer (top), scale bar = 20 μ m. (d) Wild-type PH-1 infection of the rachis at 5 dpi, 1. Growth of two hyphae through the same apoplastic space in parallel to hyphae growing intracellularly in neighbouring cells to the left and right. 2. Hypha appear to constrict to traverse the cell wall. (e) Mock-inoculated rachis tissue, yellow arrow indicates pores in cell wall. (f) Mock-inoculated rachis tissue showing lack of cellular contents in the central regions of the tissue. Yellow arrow indicates vascular bundle. (a)–(e) Scale bar = 10 μ m, (f) scale bar = 100 μ m.

morphological and cellular responses underlying this macroscopically well-documented phenomenon had not been explored. In this study our two primary aims were (a) to identify the morphological differences in the hyphal infection routes between the WT and $\Delta Tri5$ strains during wheat floral infections compared to coleoptile infections, and (b) to focus on the multifaceted role(s) of the cell wall and its constituent components as well as the pit fields during hyphal colonization due to their potential to delay, minimize or cease fungal progression through the numerous internal complexities that the wheat spike architecture presents to the *Fusarium* hyphae.

As described above, our experimentation confirmed that the $\Delta Tri5$ mutant could sufficiently colonize the lemma and palea tissues

but not the rachis (Cuzick et al., 2008; Jansen et al., 2005). Similarly, our results concurred with those of Jansen et al. (2005) that the DON-deficient *F. graminearum* strain could not grow beyond the rachis node due to the presence of inherently thicker cell walls in this tissue. However, our quantitative comparative analysis of the WT and DON-deficient interactions revealed no differences between cell wall thickness at two time points, or with the control mock-inoculated tissues, indicating that cell walls do not increase in thickness per se as part of a locally occurring defence response. Upon further microscopic analysis in the current study, we observed that the DON-deficient $\Delta Tri5$ mutant could not enter wheat cells with inherently thicker cell walls because the hyphae could not pass

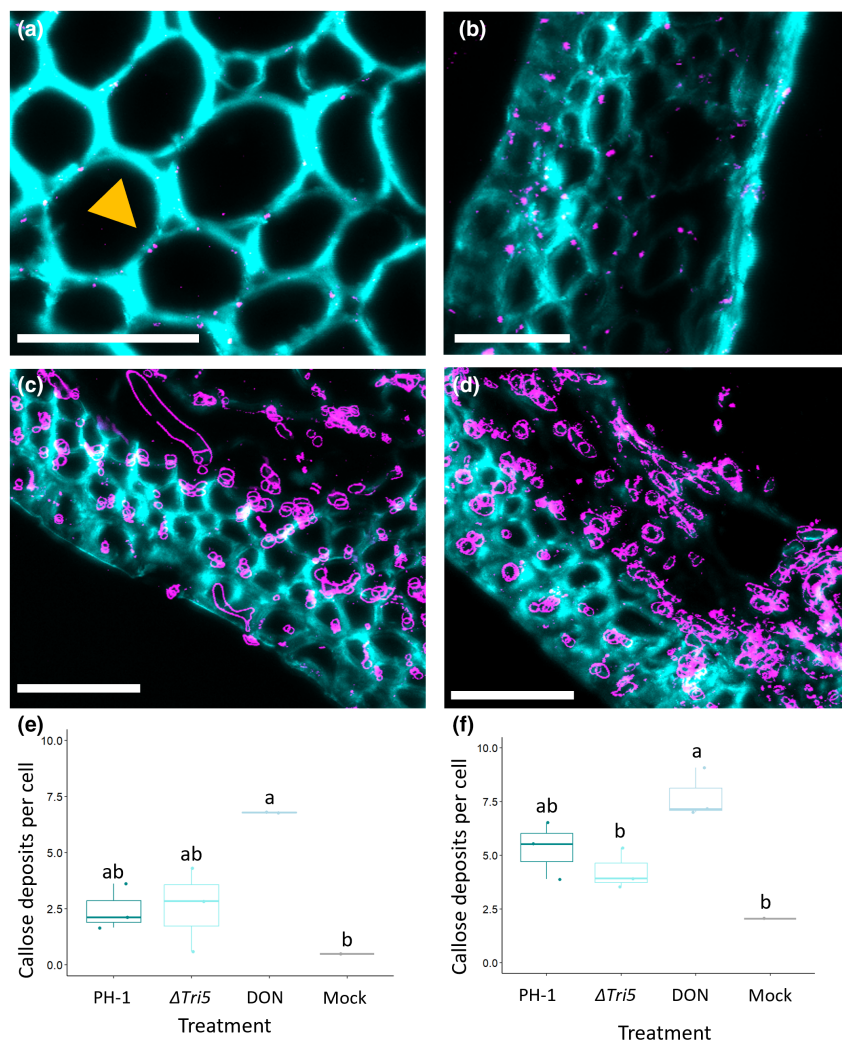


FIGURE 7 Immunofluorescence detection of callose in rachis and lemma tissues. Magnified region of interest of the *Fusarium graminearum*-wheat interaction demonstrating callose deposits at plasmodesmata. (a) Control rachis, yellow arrow indicates callose deposit at break in cell wall staining, (b) dexylnivalenol (DON)-inoculated lemma tissue, (c) *F. graminearum* PH-1 infected lemma at 5 days post-inoculation (dpi), (d) $\Delta Tri5$ -infected lemma at 5 dpi. Sections were imaged by confocal microscopy with excitation-emission spectra for Alexa Fluor-488 at 488 nm, 510–530 nm and 405 nm, 450–475 nm for Calcofluor white. Callose deposits are labelled in magenta with wheat cell walls in cyan. Scale bars = 50 μ m. In panels (c) and (d) the *Fusarium* hyphae also react positively to the antibody due to β -1,3-glucans in the fungal cell wall and are labelled in magenta. (e) Quantification of the number of immunolabelled callose deposits, averaged across number of cells in the sample area, in lemma tissues at 5 dpi infected with wild-type (PH-1), $\Delta Tri5$, DON and mock control, analysis of variance (ANOVA), * $p < 0.05$, and (f) rachis tissues at 5 dpi infected with PH-1, $\Delta Tri5$, DON and mock controls, ANOVA, * $p < 0.05$. Letters indicate significance differences between groups from Tukey post hoc analysis following one-way ANOVA.

through pit fields containing PD. This phenomenon was frequently observed in both the cortical and sclerenchyma cell layers. As a result, the $\Delta Tri5$ hyphae accumulated within and between the neighbouring thinner-walled parenchyma cells. In the absence of DON, potentially other so far uncharacterized secreted proteinaceous effectors fail to correctly manipulate these potential gateways into the neighbouring wheat cells. The analysis of resin sections revealed that cell walls within the adaxial layer of lemma and palea tissues were not thicker in infected samples. Although this rules out additional cell wall reinforcements, these findings do not eliminate cell wall compositional changes. Our results indicate that lignin content increases in the lemma tissue, which strengthens the tissue and

hence emphasizes the role of PD as cell wall portals in host-tissue colonization. We hypothesize that DON, through its intracellular target of the ribosomes, inhibits local protein-translation-based defence responses, whereas symplastic isolation of neighbouring cells by the deposition of callose at PD is a largely post-translationally regulated process induced within the generic plant defence response (Wu et al., 2018). Our SEM inquiry of the infected tissues indicates that PD, when used by the advancing hyphal front, are potentially 'dead portals' that lack the desmotubule symplastic bridge between neighbouring cells, but this needs to be confirmed through further analysis by transmission electron microscopy. This would also confirm whether callose deposits are eliminated prior to or coincident

with hyphal constriction and traversing of the cell wall. Although again a static analysis method, transmission electron microscopy can be used to explore whether desmotubule connections, and callose deposits, are consistently present or absent at the point of hyphal traverse. Collectively, these data suggest that the broad-spectrum consequences of DON targeting could prevent the synthesis and action of key defence enzymes at PD. This could be explored by a combined comparative proteomics, phosphoproteomics and RNA-seq analysis of the WT and $\Delta Tri5$ -infections to elucidate the wheat defence responses occurring at the advancing *Fusarium* hyphal front that are reduced and/or eliminated by the presence of DON.

The deposition of callose at the PD junction by callose synthases has been demonstrated to be induced by various biotic stress-inducing pathogens (Wu et al., 2018). The role of callose differs with cellular location: callose polymers are a structural component of papillae in various cereal species that form below appressoria produced by fungal pathogens such as the powdery mildew *Blumeria graminis* f. sp. *hordei*, whereby elevated callose deposition in highly localized papillae in epidermal cells results in resistance to fungal infection (Ellinger et al., 2013). In vascular tissue, callose can be deposited to restrict vascular advancements by wilt pathogens, including by *Fusarium* and *Verticillium* species (reviewed in Kashyap et al., 2021). To investigate the potential of DON impacting upon PD occlusion following our discovery of the impeded traversal of PD by the $\Delta Tri5$ strain, we immunolabelled callose in resin-embedded sections of wheat floral tissues. We found that DON strongly induced callose depositions, and callose deposition was also moderately increased in WT- and $\Delta Tri5$ -infected lemma and palea tissues. This indicates that callose deposition is increased as a defence response when DON or *Fusarium* hyphae are present. However, in the WT infection, we observed a frequency of callose depositions similar to the non-DON producing $\Delta Tri5$ strain indicating an interruption or targeted degradation of callose occlusions by *F. graminearum* invasive hyphae. We note, however, that the chemical fixation process employed for this analysis could affect the integrity of callose deposits. The secretion of glycoside hydrolase (GH) proteins that break down β -1,3-glucans such as callose has not been explored with respect to the *F. graminearum*-wheat interaction, although GH12 family proteins that break down xyloglucan in plant cell walls appear to be implicated in virulence (Wang et al., 2022). In the $\Delta Tri5$ infections, in the absence of DON other hyphal components and/or secreted molecules may be responsible for the modest callose deposition at the PD junction.

Intracellular colonization through the rachis node and beyond in the rachis internode possibly requires DON and is therefore required for the second intracellular phase of the biphasic life-style described for *F. graminearum*, where extracellular apoplastic growth characterizes the initial 'stealth' phase of infection (Brown et al., 2010). If this is the case, then lacking the ability to traverse PD would restrict direct acquisition of nutrients from host cells by the fungal hyphae. The *TRI* biosynthetic gene cluster required for DON biosynthesis is transcriptionally activated early during wheat spike infection, peaking between 72 and 120h post-inoculation (Chen et al., 2019; Evans et al., 2000), when infection is largely

restricted to the palea, lemma and glume tissues. Trichothecene biosynthesis is regulated by two transcription factors, *TRI6* and *TRI10*, within the biosynthetic pathway. Of note, DON is not required for full virulence of the developing wheat kernel seed coat (Jansen et al., 2005). In addition to our finding in coleoptiles, Ilgen et al. (2009) identified that trichothecene biosynthesis pathway induction was potentially tissue specific and somewhat restricted to the developing grain kernel and rachis node, and suggested that 'kernel tissue perception' by the *Fusarium* hyphae induces the biosynthesis of trichothecene mycotoxins. This suggestion concurs with Zhang et al. (2012) who reported that the trichothecene biosynthesis genes were not induced during *F. graminearum* infection of wheat coleoptiles, whereas Qui et al. (2019) reported the expression of *TRI4* in wheat coleoptiles. We found *TRI5* expression to be detectable at low levels in the wheat coleoptiles, remaining around 0.8 \times the expression levels of *FgActin*. This is lower than the *TRI5* expression level reported by Brown et al. (2011), who reported a level over 3 \times that of *FgActin* in wheat spikes.

Gardiner, Osbourne, et al. (2009) presented evidence that, in addition to their previous reports that exogenous application of amines, such as agmatine, in vitro induces *TRI5* expression (Gardiner, Kazan, & Manners, 2009), low pH further accelerates expression of the *TRI* gene cluster. Other inducers of the DON biosynthetic pathway genes include carbon, nitrogen and light (Gardiner, Osbourne, et al., 2009). These factors could explain the low and stationary levels of *TRI5* gene expression throughout infection of wheat coleoptiles, which have been noted to be particularly acidic plant tissue due to the optimum activity of expansion proteins around pH4 (Gao et al., 2008). Other fungal pathogens that are reported to use PD during infection of cereals include *Magnaporthe oryzae* and *M. oryzae* pathotype *tritricum*, which respectively cause rice blast and wheat blast diseases on the floral panicles and floral spikes (Fernandez & Orth, 2018; Sakulkoo et al., 2018). Although *M. oryzae* does not synthesize trichothecene mycotoxins, the invading hyphae secrete another potent general protein translation inhibitor, namely tenuazonic acid (Wilson & Talbot, 2009). The effect of this mycotoxin on PD traversing and virulence in *Magnaporthe* spp. has not yet been reported.

F. graminearum progression into the rachis and through sequential rachis nodes and internodes allows for the successful completion of the disease infection cycle in wheat crops. Typically, perithecia form from the chlorenchyma band of the rachis following prolific hyphal colonization of this highly specialized photosynthetic tissue layer within the wheat spike (Guenther & Trail, 2005). Hence, interruption of WT disease progression prior to this crucial point in the primarily monocyclic infection cycle is of great interest for reducing full virulence of FHB and in particular in reducing the abundance of air-dispersed ascospores. Interestingly, infection of barley spikelets with WT *F. graminearum* is solely restricted to the inoculated spikelet, similarly to $\Delta Tri5$ infection of wheat (Jansen et al., 2005). How this occurs has not yet been explored, but we hypothesize that a lack of traversing of PD by hyphae may have a role to play in barley rachis node tissue.

Overall, our study indicates that PD are the key to successful host-tissue colonization by *F. graminearum* and that DON, directly or

(a) WT interaction

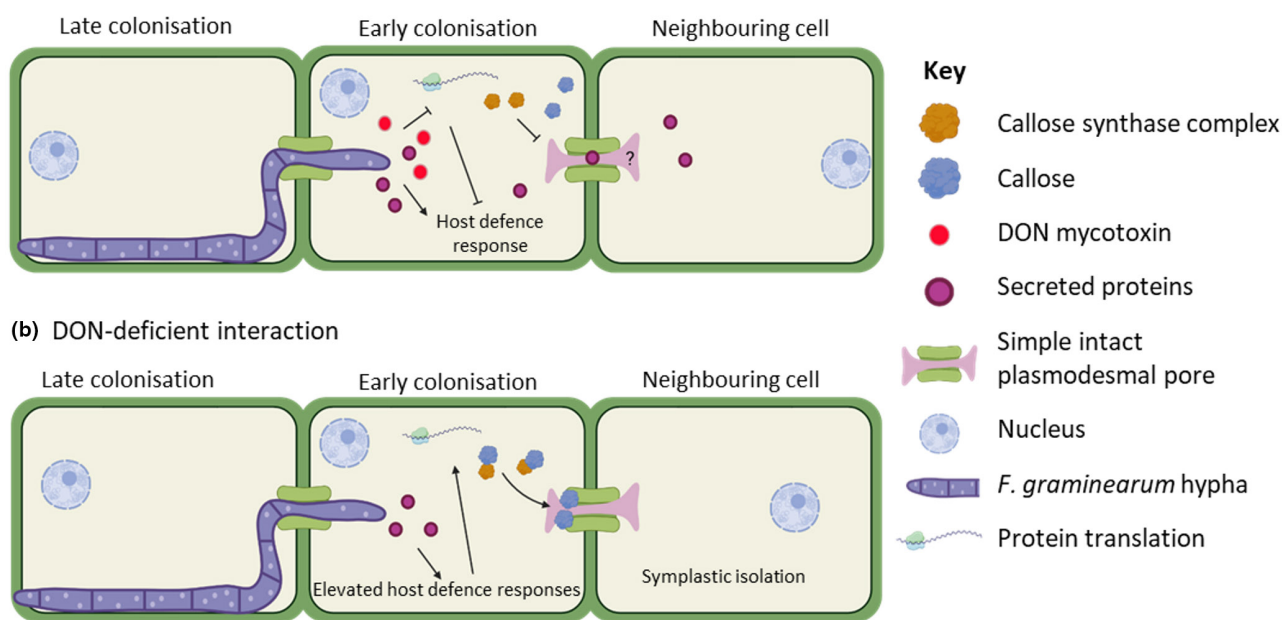


FIGURE 8 Proposed working model for the role of deoxynivalenol (DON) in the *Fusarium graminearum*–wheat interaction. (a) In the wild-type (WT) interaction, DON interferes with the wheat host defence response by inhibiting protein translation and reducing the ability of the host to deposit callose at plasmodesmata (PD) to restrict further hyphal infection. It is currently unknown how long the desmotubule remains functional or in place. (b) In the absence of DON, *F. graminearum*-secreted proteins are detected by the host and trigger host defence responses, including the symplastic isolation of neighbouring cells by the deposition of callose at PD.

indirectly, facilitates this interaction. We anticipate that the results of this study are considered in future working disease models of the *F. graminearum*–wheat interaction and suggest these incorporate a greater emphasis on tissue and cell wall architecture and composition when considering host susceptibility to fungal pathogens. To this end, we have proposed a new working model (Figure 8) that summarizes our findings around the presence of DON during wheat infection and the impact on callose deposition at PD.

4 | EXPERIMENTAL PROCEDURES

4.1 | Fungal growth

The *F. graminearum* reference strain PH-1 (NCBI: txid229533) and the DON-deficient single gene deletion mutant $\Delta Tri5$, within the PH-1 parental background (Cuzick et al., 2008), were used in this study. Conidia for glycerol stocks were prepared by culturing on synthetic nutrient-poor agar (SNA) plates containing 0.1% KH_2PO_4 , 0.1% KNO_3 , 0.1% $\text{MgSO}_4 \cdot 7\text{H}_2\text{O}$, 0.05% KCl, 0.02% glucose, 0.02% sucrose and 2% agar. Plates were left to grow for 8 days at room temperature (RT) with constant illumination under near-UV light (Philips TLD 36W/08). TB3 liquid medium (0.3% yeast extract, 0.3% Bacto peptone and 20% sucrose) was added to plates to stimulate spore production and left for a further 2 days. Conidia were harvested and stored in 15% glycerol at -80°C in 2 mL cryotubes (Thermo Fisher

Scientific). Conidial suspensions in water to be used for inoculations were prepared by spreading conidia from glycerol stocks onto potato dextrose agar (PDA; Sigma Aldrich) plates. The plates were then incubated at RT for 2 days. After incubation, conidia were harvested with distilled water. Spore concentrations were measured with the aid of a haemocytometer (Hausser Bright-line). Experiments were conducted under APHA plant licence number 101948/198285/6.

4.2 | Plant growth

The susceptible dwarf spring wheat (*Triticum aestivum*) cultivar Apogee was used for all wheat experiments, sourced from the National Small Grains Collection, USDA-ARS, Aberdeen, Idaho, United States. Seeds were sown in Rothamsted Prescription Mix (RPM) soil (Petersfield Growing Mediums) in P15 pots (approx. volume 7 cm^3) and grown in controlled environment facilities at HSE category 2 (Fitotron; Weiss Gallenkamp), 16h light:8h dark cycle at 22°C and 18°C , respectively, 70% relative humidity and illumination at $2200\mu\text{mol m}^{-2}\text{s}^{-1}$.

4.3 | Coleoptile inoculations

For coleoptile inoculations, Apogee grains were left for 2 days at 5°C in water for imbibition before being placed individually onto cotton wool plugs in a 24-well tissue culture plate (VWR) and left

to germinate for 3 days under high humidity conditions (<90% relative humidity) under normal wheat growth conditions. At 3 days after sowing, approximately 5 mm from the tip of each coleoptile was cut to encourage infection. Inoculations occurred through the placement of a cut pipette tip with a filter paper insert soaked with 5×10^5 spores/mL solution, with distilled water used as a negative control. The coleoptiles were left in the dark for 3 days to aid infection, after which inoculation tips were subsequently removed, and coleoptiles were left to grow under normal growth conditions for a further 4 days (Darino et al., 2024). Disease phenotypes on the coleoptiles were assessed at 7 days post-inoculation by imaging lesions on an M205 FA stereomicroscope (Leica Microsystems). Each experimental replicate contained five biological samples for each treatment (three mock-inoculated) and the experiment was repeated three times.

4.4 | Floral inoculations

At mid-anthesis, wheat plants were inoculated with 5×10^5 spores/mL water conidial suspension of PH-1 or $\Delta Tri5$, conidial suspension supplemented with DON, DON alone or water (distilled water) control. DON supplementation of inoculum was 35 ppm (Sigma-Aldrich). As described in Lemmens et al. (2005), a 5- μ L droplet was placed between the palea and the lemma on each side of the seventh true spikelet from the base. Inoculated plants were placed in a high (<90%) humidity for the first 72 h of infection, with the first 24 h in darkness. After 72 h plants were returned to normal growth conditions.

4.5 | Determination of DON concentration for exogenous application

To determine the concentration of DON to use for the chemical complementation experiments, a number of experiments were undertaken. These scoped for a concentration that was not detrimental to both *F. graminearum* spore germination and growth (Data S1), as well as sufficient to cause physiological stress to plant-tissue in the plant model *Arabidopsis thaliana* (Data S2). *A. thaliana* was grown as detailed in Armer et al. (2024). Concentrations up to 350 ppm were not detrimental to fungal proliferation in media and as low as 10 ppm demonstrated considerable reduction in growth in *A. thaliana* seedlings. The concentration of 35 ppm (118 μ M) was determined as a result of these experiments.

4.6 | Disease progression

As above, Apogee at mid-anthesis was inoculated and disease progression was assessed by counting spikelets showing visible symptoms every 2 days after inoculation until 14 dpi. Area under disease progression curve (AUDPC) (Van der Plank, 1963) values were calculated using the 'agricolae' package (v. 1.4.0; de Mendiburu &

Yaseen, 2020) in R (v. 4.0.2). Statistical significance was determined by Kruskal–Wallis one-way analysis of variance through the R package 'ggplot2' (v. 3.4.0; Wickham, 2016).

4.7 | Red green blue colour classification for disease assessment of dissected spikelets

To quantify disease progression on wheat spikelets at 5 and 7 dpi, colour (RGB) spikelets were imaged (iPhone 6s; Apple) on both sides with consistent illumination. Diseased area was quantified using a curated program on the LemnaTec Lemnagrid software (CHAP). Diseased area was classified by pixel colour segmentation after application of filters to threshold from the background, identify misclassified pixels and fill in gaps. Area attributed to anthers were omitted from further analysis. The relative area attributed to each classification was then calculated in a custom R script and all samples were normalized to the mean value of 'diseased' of the mock treatment due to background parsing error.

4.8 | Bioimaging

Inoculated spikelets were dissected from the wheat spikes for internal observations of infected floral tissues. Spikelets were fixed for 24 h in a solution of 4% paraformaldehyde, 2.5% glutaraldehyde and 0.05 M Sorensen's phosphate buffer ($\text{NaH}_2\text{PO}_4 \cdot \text{Na}_2\text{HPO}_4 \cdot 7\text{H}_2\text{O}$, pH 7.2), in the presence of Tween 20 (Sigma-Aldrich) and subject to a light vacuum for 20 s to ensure tissue infiltration. Fixed spikelets were washed three times with 0.05 M Sorensen's phosphate buffer and subsequently underwent an ethanol dehydration protocol at 10% ethanol increments, up to 100% ethanol. Spikelets were dissected into component tissues and embedded with LR White resin (TAAB) at increasing resin ratios (1:4, 2:3, 3:2, 4:1), followed by polymerization in the presence of nitrogen at 60°C for 16 h. Ultrathin 1 μ m resin sections were cut from resin blocks using a microtome (Reichert-Jung; Ultracut), placed onto polysine microscope slides (Agar Scientific) and stained with 0.1% (wt/vol) Toluidine Blue O in 0.1 M Sorensen's phosphate buffer. Every 10th section was collected for a total of 10 sections per embedded block to fully explore floral tissues and mounted with Permunt (Fisher Scientific) prior to imaging on an Axioimager 512 (Zeiss) at 20 \times magnification under brightfield illumination. The experiment was repeated three times, with a total of five biological replicates for each treatment, with two mock samples per batch. In total, 111 resin blocks were explored across a 100 μ m in the centre of the sample, with sections cut every 10 μ m. Image analysis was conducted in Fiji for ImageJ (v. 2.3.0) and statistical analysis was conducted in R (v. 4.0.2).

For SEM exploration of floral tissues, spikelets at 5 dpi were excised and coated in 50:50 OCT compound (Sakura FineTek) with colloidal graphite (TAAB). SEM analysis was conducted on rachis tissue infected with the WT reference strain PH-1 at 5 dpi. Sample

preparation occurred in a Quorum cryo low-pressure system before imaging on a JEOL LV6360 SEM at 5 kV with software v. 6.04.

For the analysis of cell wall thickness in WT, WT+DON, $\Delta Tri5$, $\Delta Tri5$ +DON, DON and mock treatments at 5 and 7 dpi, fixed resin sections were used. For each treatment, five biological replicates were used and 10 non-adjacent cell wall measurements across the sample made using Fiji for ImageJ (v. 2.3.0), with the average used for statistical analysis.

Callose immunolabelling of resin-embedded sectioned material was conducted according to Amsbury and Benitez-Alfonso (2022). Briefly, callose was localized by anti- β -1,3-glucan antibodies (Biosupplies) and secondarily conjugated with rabbit anti-mouse Alexa Fluor-488. Wheat cell walls were counterstained with Calcofluor white. Sections were imaged by confocal microscopy on a Leica SP8 confocal microscope, with excitation-emission spectra for Alexa Fluor-488 at 488 nm, 510–530 nm and 405 nm, 450–475 nm for Calcofluor white. Image analysis for the quantification of callose deposits per cell was conducted in Fiji (ImageJ) using maximum projections of Z stacks and channels converted to binary masks. The number of cells in the sample area was calculated using the cell counter tool and callose deposits were counted by the number of discrete Alexa Fluor-488 fluorescent objects between the size of 2 to 12 pixel units to eliminate cross-reactivity with β -1,3-glucans in the fungal cell walls. The number of callose deposits were averaged across the number of complete cells (all cell walls visible) in the sample area. The same image analysis parameters were set to all images, including mock treatments. Callose deposits were quantified in the lemma and rachis tissues only, with three biological replicates for each treatment (PH-1, $\Delta Tri5$, DON, Mock). Further examples are present in Data S6 and image analysis methodology is demonstrated in Data S7.

4.9 | DON quantification

To determine if the presence of DON in the WT strain inoculum stimulated further DON production, if administered DON could be detected in wheat spike tissues at the end of disease progression (14 dpi), and the absence of DON in the $\Delta Tri5$ mutant interaction a competitive ELISA for 15-ADON was employed. Whole wheat spikes were used for this quantification in the case the DON was trafficked or secreted beyond the inoculated spikelet due to its high water solubility. Whole wheat spikes after 14 days of disease progression were ground to a fine powder in the presence of liquid nitrogen and 1 g of each sample was resuspended in 5 mL distilled water, vortexed until dissolved, incubated in a 30°C water bath for 30 min and centrifuged for 15 min at full speed (13,100g). The supernatant was removed and analysed using the Beacon Analytical Systems Inc. Deoxynivalenol (DON) Plate Kit according to kit instructions. The A_{450} values were measured on a Varioskan microplate reader (Thermo Scientific). Three technical replicates of each biological replicate (a single wheat spike) were conducted, and the experiment was repeated three times.

4.10 | Expression of the mycotoxin biosynthesis gene *TRI5* during coleoptile infection

The trichodiene synthase gene *TRI5* was used as a proxy for the relative expression of the trichothecene biosynthesis pathway during coleoptile infection. Total RNA was extracted from whole coleoptiles at 3, 5 and 7 dpi using a total RNA extraction kit (NEB) and following the kit instructions. First-strand cDNA was synthesized using RevertAid First Strand cDNA synthesis kit (ThermoFisher Scientific) as per kit instructions and using random hexamer primers provided. *TRI5* expression was then assessed by qPCR with melt curve using the primers in Data S3, with SYBR Green as the reporter, ROX as passive reference and NFQ-MGB as the quencher. The qPCR with melt curve was conducted in technical and biological triplicate on a QuantStudio 6 Pro and results analysed on the complementary Design & Analysis Software v. 2.6.0 (ThermoFisher Scientific). The experiment was conducted three times. Quantification of *TRI5* expression was normalized against the housekeeping gene *FgActin* (primers in Data S3) for each sample, also included within the qPCR run in triplicate. At least one primer in a primer pair for qPCR targets was designed to span an exon-exon junction to avoid annealing to residual DNA.

4.11 | Phloroglucinol staining for presence of lignin

A 3% phloroglucinol (Sigma Aldrich)-HCl solution (Weisner stain) was prepared fresh in accordance with methods by Mitra and Loque (2014). Inoculated wheat spikelets were sampled at 5 dpi and cleared in 100% ethanol for 4 days before going through a rehydration series (75%, 50%, 25% and 0% ethanol) at 1 h per stage. Cleared spikelets were bathed in Weisner stain for 1 h, or until staining of the tissues became evidently saturated. Spikelets were then imaged (OM-D E-M10; Olympus) under constant illumination and, subsequently, dissected tissues were imaged individually.

4.12 | Formation of perithecia in vitro

Carrot agar was prepared using the method outlined by Cavinder et al. (2012) and supplemented with DON at 35 ppm (wt/vol) to test for the ability of the WT strain, and the DON trichothecene-deficient deletion mutant, $\Delta Tri5$, to develop perithecia in vitro, for lifecycle completion viability (Data S4). Ability of perithecia to discharge ascospores in the presence of DON was assessed using the same method as described in Cavinder et al. (2012).

4.13 | Statistical analysis

Scripts were written in R (v. 4.0.2) for each experimental analysis. Unless otherwise stated, analysis of variance followed by Tukey post hoc test was conducted for parametric datasets and Kruskal–Wallis

for nonparametric datasets. The significance threshold was set to $\alpha=0.05$ in all cases.

ACKNOWLEDGEMENTS

The authors would like to thank the CHAP organization at Rothamsted Research for access to their Lemnagrid image analysis software. Special thanks are given to Hannah Walpole and Kirstie Halsey from Rothamsted Research Bioimaging department for continued training, advice and expertise. We also thank Harold Bockelman, the curator of the National Small Grains Collection, USDA-ARS, for providing the wheat variety used in this study. Kim Hammond-Kosack and Martin Urban are supported by the Biotechnology and Biological Sciences Research Council (BBSRC) Institute Strategic Programme (ISP) Grants Designing Future Wheat (BBS/E/C/000I0250) and Delivering Sustainable Wheat (BB/X011003/1 and BBS/E/RH/230001B) and the BBSRC grants (BB/X012131/1 and BB/W007134/1). Victoria J. Armer is supported by the BBSRC-funded South West Biosciences Doctoral Training Partnership (BB/T008741/1).

CONFLICT OF INTEREST STATEMENT

The authors declare no financial or non-financial competing interests.

DATA AVAILABILITY STATEMENT

The research data supporting this publication are provided within this paper. Requests for materials relating to this paper should be made to Kim Hammond-Kosack (kim.hammond-kosack@rothamsted.ac.uk) at Rothamsted Research.

ORCID

Victoria J. Armer  <https://orcid.org/0000-0002-1008-520X>

Martin Urban  <https://orcid.org/0000-0003-2440-4352>

Tom Ashfield  <https://orcid.org/0000-0003-3356-2248>

Michael J. Deeks  <https://orcid.org/0000-0001-5487-5732>

Kim E. Hammond-Kosack  <https://orcid.org/0000-0002-9699-485X>

REFERENCES

- Amsbury, S. & Benitez-Alfonso, Y. (2022) Immunofluorescence detection of callose in plant tissue sections. *Methods in Molecular Biology*, 2457, 167–176.
- Armer, V.J., Deeks, M.J. & Hammond-Kosack, K.E. (2024) *Arabidopsis thaliana* detached leaf assay for the disease assessment of *Fusarium graminearum*. *Protocols.io*. Available from: <https://doi.org/10.17504/protocols.io.261gedmwov47/v1>
- Berthiller, F., Dall'Asta, C., Schuhmacher, R., Lemmens, M., Adam, G. & Krska, R. (2005) Masked mycotoxins: determination of a deoxynivalenol glucoside in artificially and naturally contaminated wheat by liquid chromatography–tandem mass spectrometry. *Journal of Agricultural and Food Chemistry*, 53, 3421–3425.
- Boenisch, M.J. & Schafer, W. (2011) *Fusarium graminearum* forms mycotoxin producing infection structures on wheat. *BMC Plant Biology*, 11, 110.
- Brown, D.W., Dyer, R.B., McCormick, S.P., Kendra, D.F. & Plattner, R.D. (2004) Functional demarcation of the *Fusarium* core trichothecene gene cluster. *Fungal Genetics and Biology*, 41, 454–462.
- Brown, N.A., Antoniw, J. & Hammond-Kosack, K.E. (2012) The predicted secretome of the plant pathogenic fungus *Fusarium graminearum*: a refined comparative analysis. *PLoS One*, 7, e33731.
- Brown, N.A., Bass, C., Baldwin, T.K., Chen, H., Massot, F., Carion, P.W.C. et al. (2011) Characterisation of the *Fusarium graminearum*–wheat floral interaction. *Journal of Pathogens*, 2011, 626345.
- Brown, N.A., Urban, M., van de Meene, A.M.L. & Hammond-Kosack, K.E. (2010) The infection biology of *Fusarium graminearum*: defining the pathways of spikelet to spikelet colonisation in wheat ears. *Fungal Biology*, 114, 555–571.
- Cavinder, B., Sikhakolli, U., Fellows, K.M. & Trail, F. (2012) Sexual development and ascospore discharge in *Fusarium graminearum*. *Journal of Visualized Experiments*, 61, 3895.
- Chen, Y., Kistler, H.C. & Ma, Z. (2019) *Fusarium graminearum* trichothecene mycotoxins: biosynthesis, regulation, and management. *Annual Review of Phytopathology*, 57, 15–39.
- Cuzick, A., Urban, M. & Hammond-Kosack, K. (2008) *Fusarium graminearum* gene deletion mutants *map1* and *tri5* reveal similarities and differences in the pathogenicity requirements to cause disease on *Arabidopsis* and wheat floral tissue. *New Phytologist*, 177, 990–1000.
- Darino, M., Urban, M., Kaur, N., Machado-Wood, A., Grimwade-Mann, M., Smith, D. et al. (2024) Identification and functional characterisation of a locus for target site integration in *Fusarium graminearum*. *Fungal Biology and Biotechnology*, 11, 2.
- Ellinger, D., Naumann, M., Falter, C., Zwickowics, C., Jamrow, T., Manisseri, C. et al. (2013) Elevated early callose deposition results in complete penetration resistance to powdery mildew in *Arabidopsis*. *Plant Physiology*, 161, 1433–1444.
- Evans, C.K., Xie, W., Dill-Macky, R. & Mirocha, C.J. (2000) Biosynthesis of deoxynivalenol in spikelets of barley inoculated with macrocladia of *Fusarium graminearum*. *Plant Disease*, 84, 654–660.
- Fan, J., Urban, M., Parker, J.E., Brewer, H.C., Kelly, S.L., Hammond-Kosack, K.E. et al. (2013) Characterization of the sterol 14 α -demethylases of *Fusarium graminearum* identifies a novel genus-specific CYP51 function. *New Phytologist*, 198, 821–835.
- Fernandez, J. & Orth, K. (2018) Rise of a cereal killer: the biology of *Magnaporthe oryzae* biotrophic growth. *Trends in Microbiology*, 26, 582–597.
- Gao, Q., Zhao, M., Li, F., Gau, Q., Xing, S. & Wang, W. (2008) Expansins and coleoptile elongation in wheat. *Protoplasma*, 233, 73–81.
- Gardiner, D.M., Kazan, K. & Manners, J.M. (2009) Nutrient profiling reveals potent inducers of trichothecene biosynthesis in *Fusarium graminearum*. *Fungal Genetics and Biology*, 46, 604–613.
- Gardiner, D.M., Osbourne, S., Kazan, K. & Manners, J.M. (2009) Low pH regulates the productions of deoxynivalenol by *Fusarium graminearum*. *Microbiology*, 155, 3149–3156.
- Guenther, J.C. & Trail, F. (2005) The development and differentiation of *Gibberella zeae* (anamorph: *Fusarium graminearum*) during colonization of wheat. *Mycologia*, 97, 229–237.
- Hallen-Adams, H.E., Wenner, N., Kuldau, G.A. & Trail, F. (2011) Deoxynivalenol biosynthesis-related gene expression during wheat kernel colonization by *Fusarium graminearum*. *Phytopathology*, 101, 1091–1096.
- Hohn, T.M., McCormick, S.P. & Desjardins, A.E. (1993) Evidence for a gene cluster involving trichothecene-pathway biosynthetic genes in *Fusarium sporotrichioides*. *Current Genetics*, 24, 291–295.
- Ilgen, P., Hader, B., Maier, F.J. & Schäfer, W. (2009) Developing kernel and rachis node induce the trichothecene pathway of *Fusarium graminearum* during wheat head infection. *Molecular Plant-Microbe Interactions*, 22, 899–908.
- Jansen, C., von Wettstein, D., Schäfer, W., Kogel, K.-H., Felk, A. & Maier, F.J. (2005) Infection patterns in barley and wheat spikes inoculated with wild-type and trichodiene synthase gene disrupted *Fusarium graminearum*. *Proceedings of the National Academy of Sciences of the United States of America*, 102, 16892–16897.

- Kashyap, A., Planas-Marquès, M., Capellades, M., Valls, M. & Coll, N.S. (2021) Blocking intruders: inducible physico-chemical barriers against plant vascular wilt pathogens. *Journal of Experimental Botany*, 72, 184–198.
- Lee, J. & Lu, H. (2011) Plasmodesmata: the battleground against intruders. *Trends in Plant Science*, 16, 201–210.
- Lemmens, M., Scholz, U., Berthiller, F., Dall'Asta, C., Koutnik, A., Schuhmacher, R. et al. (2005) The ability to detoxify the mycotoxin deoxynivalenol colocalizes with a major quantitative trait locus for Fusarium head blight resistance in wheat. *Molecular Plant-Microbe Interactions*, 18, 1318–1324.
- McCormick, S.P., Stanley, A.M., Stover, N.A. & Alexander, N.J. (2011) Trichothecenes: from simple to complex mycotoxins. *Toxins*, 3, 802–814.
- McMullen, M., Bergstrom, G., De Wolf, E., Dill-Macky, R., Hershman, D., Shaner, G. et al. (2012) A unified effort to fight an enemy of wheat and barley: Fusarium head blight. *Plant Disease*, 96, 1712–1728.
- McMullen, M., Jones, R. & Gallenberg, D. (1997) Scab of wheat and barley: a re-emerging disease of devastating impact. *Plant Disease*, 81, 1340–1348.
- Mendiburu, F. & Yaseen, M. (2020) *Agricolae*: statistical procedures for agricultural research. R package version 1.4.0. Available from: <https://CRAN.R-project.org/package=agricolae>. [Accessed 23rd May 2024]
- Mesterházy, A. (1995) Types and components of resistance to Fusarium head blight of wheat. *Plant Breeding*, 114, 377–386.
- Mitra, P.P. & Loque, D. (2014) Histochemical staining of *Arabidopsis thaliana* secondary cell wall elements. *Journal of Visualized Experiments*, 87, 51381.
- Parry, D.W., Jenkinson, P. & McLeod, L. (1995) Fusarium ear blight (scab) in small grain cereals—a review. *Plant Pathology*, 44, 207–238.
- Pestka, J.J. (2008) Mechanisms of deoxynivalenol-induced gene expression and apoptosis. *Food Additives and Contamination Part A: Chemistry, Analysis, Control, Exposure and Risk Assessment*, 25, 1128–1140.
- Pestka, J.J. (2010) Deoxynivalenol: mechanisms of action, human exposure, and toxicological relevance. *Archives of Toxicology*, 84, 663–679.
- Pritsch, C., Muehlbauer, G.J., Bushnell, W.R., Somers, D.A. & Vance, C.P. (2007) Fungal development and induction of defense response genes during early infection of wheat spikes by *Fusarium graminearum*. *Molecular Plant-Microbe Interactions*, 13, 159–169.
- Proctor, R.H., Hohn, T.M. & McCormick, S.P. (1995) Reduced virulence of *Gibberella zeae* caused by disruption of a trichothecene toxin biosynthetic gene. *Molecular Plant-Microbe Interactions*, 8, 593–601.
- Qui, H., Zhao, X., Fang, W., Wu, H., Abubakar, Y.S., Lu, G. et al. (2019) Spatiotemporal nature of *Fusarium graminearum*-wheat coleoptile interactions. *Phytopathology Research*, 1, 26.
- Sager, R.E. & Lee, J. (2018) Plasmodesmata at a glance. *Journal of Cell Science*, 131, jcs209346.
- Sakulkoo, W., Osés-Ruiz, M., Garcia, E.O., Soanes, D.M., Littlejohn, G.R., Hacker, C. et al. (2018) A single fungal MAP kinase controls plant cell-to-cell invasion by the rice blast fungus. *Science*, 359, 1399–1403.
- Tokai, T., Koshino, H., Takahashi-Ando, N., Sato, M., Fujimura, M. & Kimura, M. (2007) *Fusarium Tri4* encodes a key multifunctional cytochrome P450 monooxygenase for four consecutive oxygenation steps in trichothecene biosynthesis. *Biochemical and Biophysical Research Communications*, 353, 412–417.
- Van der Plank, J.E. (1963) *Plant diseases: epidemics and control*. New York: Academic Press.
- Vaughan, M., Backhouse, D. & Ponte, E.M.D. (2016) Climate change impacts on the ecology of *Fusarium graminearum* species complex and susceptibility of wheat to Fusarium head blight: a review. *World Mycotoxin Journal*, 9, 685–700.
- Wang, Z., Yang, B., Zheng, W., Wang, L., Cai, X., Yang, J. et al. (2022) Recognition of glycoside hydrolase 12 proteins by the immune receptor RXEG1 confers *Fusarium* head blight resistance in wheat. *Plant Biotechnology Journal*, 21, 769–781.
- Wanjiru, W.M., Zhensheng, K. & Buchenauer, H. (2002) Importance of cell wall degrading enzymes produced by *Fusarium graminearum* during infection of wheat heads. *European Journal of Plant Pathology*, 108, 803–810.
- Wickham, H. (2016) *ggplot2: elegant graphics for data analysis*. New York: Springer-Verlag.
- Wilson, R.A. & Talbot, N.J. (2009) Under pressure: investigating the biology of plant infection by *Magnaporthe oryzae*. *Nature Reviews Microbiology*, 7, 185–195.
- Wu, S., Kumar, R., Iswanto, A.B.B. & Kim, J. (2018) Callose balancing at plasmodesmata. *Journal of Experimental Botany*, 69, 5325–5339.
- Zhang, X.-W., Jia, L.-J., Zhang, Y., Li, X., Zhang, D. & Tang, W.-H. (2012) In planta stage-specific fungal gene profiling elucidates the molecular strategies of *Fusarium graminearum* growing inside wheat coleoptiles. *The Plant Cell*, 24, 5159–5176.

SUPPORTING INFORMATION

Additional supporting information can be found online in the Supporting Information section at the end of this article.

How to cite this article: Armer, V.J., Urban, M., Ashfield, T., Deeks, M.J. & Hammond-Kosack, K.E. (2024) The trichothecene mycotoxin deoxynivalenol facilitates cell-to-cell invasion during wheat-tissue colonization by *Fusarium graminearum*. *Molecular Plant Pathology*, 25, e13485. Available from: <https://doi.org/10.1111/mpp.13485>

Appendix 3

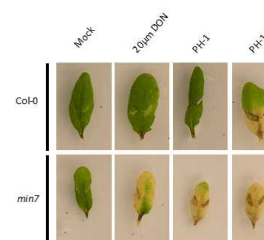
Armer VJ, Deeks MJ, Hammond-Kosack KE. (2024). *Arabidopsis thaliana* detached leaf assay for the disease assessment of *Fusarium graminearum*. *Protocols.io*. doi: 10.17504/protocols.io.261gedmwov47/v1.

Mar 07, 2024

🌐 *Arabidopsis thaliana* detached leaf assay for the disease assessment of *Fusarium graminearum* infection

DOI

dx.doi.org/10.17504/protocols.io.261gedmwov47/v1



Victoria J Armer^{1,2}, Michael J. Deeks², Kim E. Hammond-Kosack¹

¹Rothamsted Research; ²University of Exeter



Victoria J Armer

Rothamsted Research, University of Exeter

OPEN  ACCESS



DOI: dx.doi.org/10.17504/protocols.io.261gedmwov47/v1

Protocol Citation: Victoria J Armer, Michael J. Deeks, Kim E. Hammond-Kosack 2024. *Arabidopsis thaliana* detached leaf assay for the disease assessment of *Fusarium graminearum* infection. [protocols.io https://dx.doi.org/10.17504/protocols.io.261gedmwov47/v1](https://dx.doi.org/10.17504/protocols.io.261gedmwov47/v1)

License: This is an open access protocol distributed under the terms of the [Creative Commons Attribution License](https://creativecommons.org/licenses/by/4.0/), which permits unrestricted use, distribution, and reproduction in any medium, provided the original author and source are credited

Protocol status: Working

We use this protocol and it's working

Created: February 05, 2024

Last Modified: March 07, 2024

Protocol Integer ID: 94706

Keywords: *Fusarium graminearum*, *Arabidopsis thaliana*, detached leaf, Deoxynivalenol (DON)

Funders Acknowledgement:

**UK BBSRC South West
Biosciences Doctoral Training
Partnership**

Grant ID: BB/T008741/1

**UK BBSRC Delivering
Sustainable Wheat Grant
(DSW)**

Grant ID: BB/X011003/1

**UK BBSRC Delivering
Resilience to Biotic Stress**

Grant ID: BBS/E/RH/230001B

**UK BBSRC Designing Future
Wheat**

Grant ID: BB/P016855/1

Abstract

Arabidopsis thaliana (*At*), as the plant model organism, has the advantage of a bank of genotypes in stock centres worldwide. This allows for the assessment of genotypes and their contributes to disease resistance and/or susceptibility to a wide range of pathogens. We found that, through utilising the SALK lines (Alonso *et al.*, 2003) provided by NASC (Nottingham, UK), to ensure reproducible disease phenotypes for disease analysis required additional specific steps not detailed in the current literature. This is likely due to the specificity of *Fusarium graminearum* (*Fg*) infection to the floral tissues of small grain cereals and the fact that *At* is a non-host of *Fg*. Whilst this protocol has been written and tested for the assessment of detached *At* leaves infected with *Fg*, it may be adapted for use for exploring other plant-pathogen interactions.

This protocol is designed for the assessment of disease on *Arabidopsis thaliana* leaves by the fungal pathogen *Fusarium graminearum*. The nuances of this protocol that have been troubleshot have encouraged us to publish this as its own entity. The protocol described has been adapted from previous protocols published by Machado-Wood *et al.* (2021) and Chen *et al.* (2003), as well as by taking several components from Cuzick *et al.* (2008). Loosely, this protocol details seed sterilisation and plant growth, inoculations and diseases assessment.

Image Attribution

All images included in this protocol were taken by Victoria Armer, Rothamsted Research.

Materials

Protocol specific materials

1. *Arabidopsis thaliana* seed of desired genotype (NASC, UK)
2. Murashige and Skoog (MS) Basal Salt media (Sigma Aldrich, UK)
3. Deoxynivalenol (DON) (Sigma Aldrich, UK) *
**please read and follow the COSHH data sheet because DON is toxic to life.*
(<https://www.sigmaaldrich.com/GB/en/sds/sigma/d0156>).
4. Thin bleach (4.5% (v/v) Sodium hypochlorite)
5. Tergitol (Sigma Aldrich, UK)
6. 1M KOH

General lab consumables

1. 2ml microcentrifuge tubes
2. Toothpicks
3. dH₂O
4. Agar
5. Square petri dishes (120mm x 120mm)

General plant growth consumables

1. Levington's F2+S soil (Everris Ltd, UK)
2. Pots P7 (approx. volume 350cm³)
3. Plant trays
4. Capillary matting
5. Humidity lids

Equipment

1. Scales, weigh boats and spatulas
2. Stir bar
3. Duran flasks
4. Autoclave
5. pH meter
6. Fridge or cold room (5°C)
7. Flow hood
8. Controlled growth environment
8. Light meter

Safety warnings

⚠ Deoxynivalenol (DON) is a trichothecene mycotoxin that targets eukaryotic ribosomes, inhibiting protein translation. At chronic, low concentrations it can cause Leukaemia, and at higher, acute doses it induces nausea and vomiting, and can be fatal if swallowed. DON cannot be effectively destroyed by autoclaving. Please carefully read and follow the below COSHH data sheet and use appropriate PPE when handling DON.

(<https://www.sigmaaldrich.com/GB/en/sds/sigma/d0156>).



1.1. Preparation of ½ MS plates for *At* germination

1 *This step was found necessary to eliminate plate contamination from other fungal and bacterial species during seed germination on ½ MS agar plates. Unlike usual ½ MS preparations, this one does not contain sucrose to limit contamination. This can be done ahead of time and stored at room temperature for a matter of weeks after autoclaving.*

1.1 Prepare ½ MS media using the following recipe (makes 1000ml – scale as required):


1.2 a.  1.1 g MS

1.3 b. Up to  1000 mL with dH₂O

1.4 c. Add stir bar and stir until suspended

1.5 d. Adjust to  5.7 with  1 Molarity (M) KOH

2 Aliquot into Duran flasks for autoclaving, removing stir bar





3 Add agar to  1 % (v/v) in each flask (e.g. 2.5g for 250ml) and autoclave before use

4 Pour ½ MS media into square plates to a depth of 25mm for seed germination.

1.2. Sterilisation and plating of *At* seed

5 *This was found to be the most 'fool proof' method of thorough seed surface sterilisation whilst ensuring high germination rates. N.B. don't rush the serial dilution or miss steps – 5 washes ensures that the sterilisation solution is sufficiently diluted to not inhibit seed germination. Seed stratification in a cold room or fridge ensures even germination of *At* seed.*





- 5.1 Create the sterilisation solution by mixing 50:50 dH₂O and thin bleach (4.5% (v/v) sodium hypochlorite). This must be made fresh on day of use.
- 5.2 Aliquot required seed into 2ml microcentrifuge tubes and add  500 µL of the sterilisation solution. Invert to mix, ensuring all seed are suspended before settling and leave for 10 mins, inverting several times to ensure sufficient coating of seeds.
- 5.3 Conduct a dilution series of the bleach solution, pipetting out  450 µL of the sterilisation solution and replacing with  1000 µL of dH₂O. Invert to suspend all seed and remove solution once seed settles. Repeat 4 times with subsequent additions of  1000 µL of dH₂O to ensure sufficient dilution of the sterilising solution.
- 5.4 Pour seed onto an absorbent surface (e.g. blue roll) for pricking out onto ½ MS plates, at least 20mm apart, using (autoclaved) toothpicks.
- 5.5 Place ½ MS plates into a plastic bag and place in the dark in a cold room or fridge for 48hrs.

1.3. Plant Growth

6 **Plant growth**

Plant growth can occur at neutral (12 hour) or long (16 hour) day length. We found that long day length worked well and sped up the experiment progression, allowing detached leaf inoculations to take place 4 weeks from germination.

- 6.1 Place square plates into a controlled growth room or cabinet with the following settings:
 - 6.2 a. 16hr day length
 - 6.3 b.  22 °C day temperature,  18 °C night temperature
 - 6.4 c. 70% Humidity
 - 6.5 d. 140µmol m⁻² s⁻¹ light intensity.
 - 6.6 Leave to germinate for 7 days.

7 Seedling transplantation

- 7.1 Prepare trays and pots for seed transplantation by lining trays with capillary matting and filling P7 pots with Levington's F2+S soil. Press until soil is firm and hydrate with dH₂O until moist to touch on the surface. Leave space (i.e. cut out one pot from the tray) for easy watering from beneath to avoid disturbing delicate seedlings.
- 7.2 At 7 days, transplant *At* seedlings from ½ MS plates into F2+S using sterilised tweezers. Ensure roots are carefully tucked into the soil, pressing around the base of the developing rosette.
- 7.3 Spray the surface of the soil with dH₂O and place a vent closed humidity lid over the tray, leaving under normal growth conditions for a further 14 days (Fig. 1).

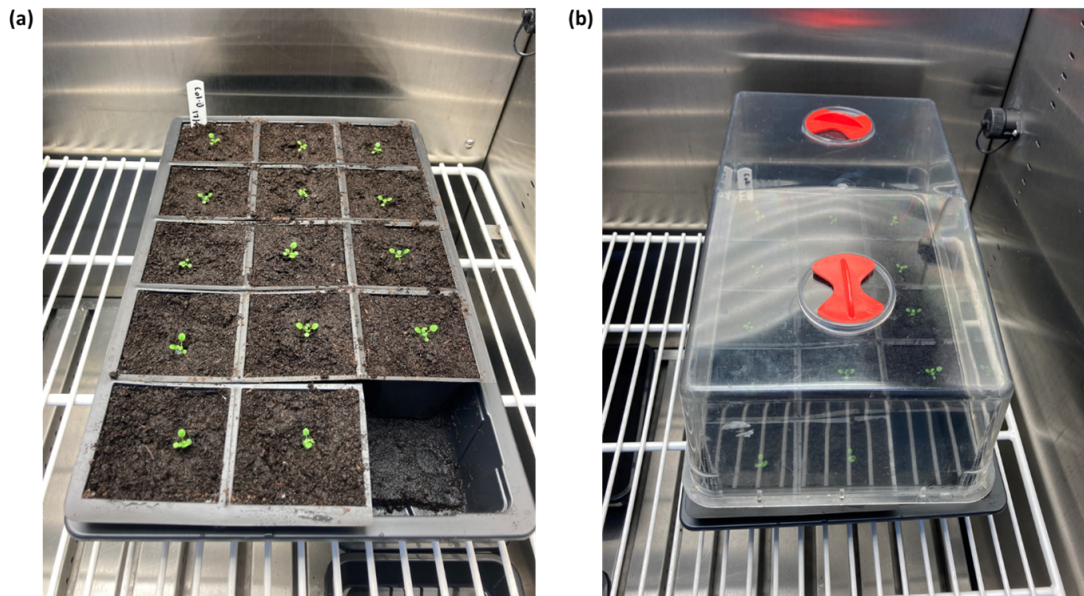


Fig. 1. Growth conditions of *Arabidopsis thaliana* in trays of P7 pots. Image of 21-day old seedlings. (a) Example growth tray lined with capillary matting and (b) with humidity lid (vent closed) for plant growth.

- 7.4 At 21 days old (14 days after transplantation) remove the humidity lid and leave for another 7 days. Ensure soil is well hydrated throughout plant growth, watering from the bottom of the tray. Capillary matting should be moist to the touch and ensures even watering across the tray.

1.4. Detached leaf inoculations

- 8 *Detached leaf assay plates can be prepared a couple of days before inoculation if stored in a sealed bag in a cold room or fridge. The addition of Tergitol (a detergent and therefore fungal*



membrane stressor) encourages fungal growth on the At leaves rather than on the 1% water agar plates.

8.1 Preparation of 1% (w/v) water agar plates for detached leaf assay:

8.2 a. Add  4 g Agar to a 400ml Duran bottle

8.3 b. Top up to  400 mL with dH₂O

8.4 c. Autoclave

8.5 d. Store at RT until use (can be prepared months in advance).

8.6 Melt 1% (w/v) water agar in the microwave (800W, 5.5 minutes)

8.7 Leave to cool until lukewarm

8.8 Add  200 μ L Tergitol to each  400 mL 1% (w/v) bottle of water agar solution

8.9 Gently swirl flasks to disperse Tergitol without creating bubbles (about 20s of gentle motion)

8.10 Pour 1% (w/v) water agar plates to 25mm depth in flow hood and ensure plates are dry before use.

1.5. Rosette examples and leaf selection

9 At 4 weeks old, *At* plants should have well-developed vegetative growth but have minimal evidence of apical bud development (Fig. 2).



Fig. 2. Example rosettes of *At* wild-type Col-0 and susceptible control *min7* at 4 weeks under growth conditions described; scale bar = 20mm.

- 10 For the detached leaf assay, select leaves that are relatively small and flat for ease of inoculating, imaging and scoring. Leaves must be in active vegetative growth and not close to senescence – for easy identification, do not choose leaves that are particularly rounded indicating they originated in the early growth stages of the plant.
- 11 Cut leaves with sterile scissors and stick the petiole into the 1% (w/v) agar plate at a 45° angle. Ideally, leaves should not sit flush on the agar. Square plates can fit 6 leaves, spaced 30mm apart (Fig. 3).
- 12 Leaves should be selected and inoculated in quick succession i.e., leaves should be selected, cut and inoculated for each plate before moving onto the next plate.
- 13 Each plant is a biological replicate. Unless including technical replicates, only one leaf per plant is taken. The addition of Tergitol to the water agar prevents hyphal growth between replicates. The experiment should be repeated 3 times before conducting statistical analysis.

1.6. Inoculations

- 14 *The addition of DON is a requirement to make infection of At with Fg occur routinely. Efforts to achieve a reliable and reproducible assay without the application of DON have been unsuccessful.*
- 14.1 Selected leaves are gently scored on the agar plates using the end of a sterile 20µl (small) tip, either side of the midrib vein. This needs to be done very carefully to break through the adaxial epidermis layer, but not the palisade mesophyll layer. Several gentle strokes of the pipette tip may be required. This artificial wounding is necessary to allow *F. graminearum* to cause disease (Fig. 3.)



Fig. 3. Example square plate, filled with 1% water agar amended with Tergitol, laid with *Arabidopsis* WT Col-0 detached leaves. Wounding must damage the adaxial epidermis so that fungal infection can access the palisade mesophyll, but not penetrate the leaf entirely.

- 14.2 With gloved hands, drop 2 μ l of a 5×10^5 spores/ml water conidial suspension amended with [M] 20 micromolar (μ M) DON onto each wound. Appropriate controls should be used for each treatment to assess for the impact of scoring (dH₂O) and DON only application (20 μ M DON).
- 14.3 Plates should be placed in the dark for 2 days in otherwise normal growth conditions and subsequently left for a further 5 days under low light (70 μ mol m⁻² s⁻¹ light). N.B. this can be achieved by moving plates further from light sources and under cover. Use a light meter to ensure that light levels are appropriate. Low light levels prevent senescence of

leaves, which interferes with disease assessment.

- 14.4 Detached leaves should be assessed at 7 days post infection (dpi), although particularly strong phenotypes may be visible at 4dpi in susceptible genotypes.

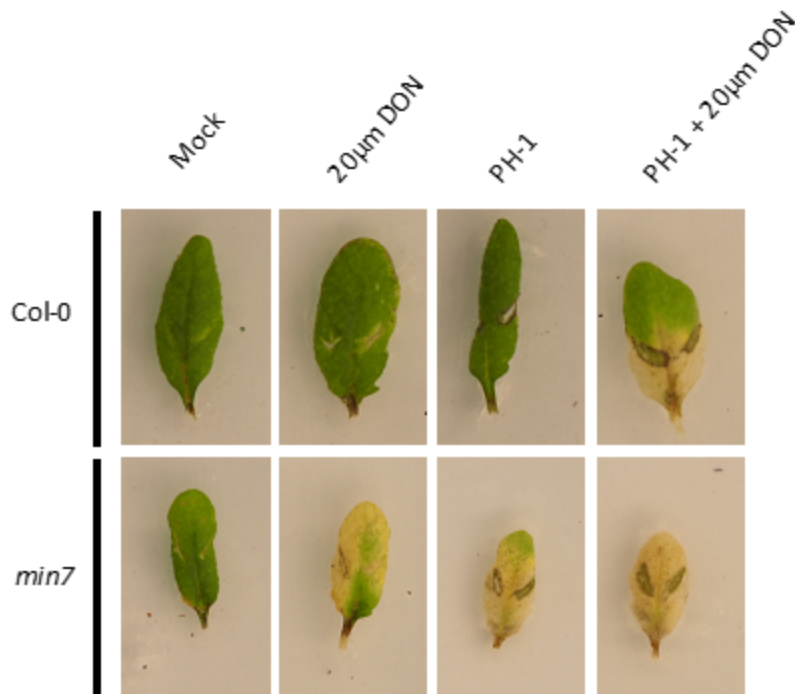


Fig.4. Example images of detached leaf assay at 7dpi for WT Col-0 and susceptible control *min7*.

14.5

Safety information

Deoxynivalenol (DON) is a trichothecene mycotoxin that targets eukaryotic ribosomes, inhibiting protein translation. At chronic, low concentrations it can cause Leukaemia, and at higher, acute doses it induces nausea and vomiting, and can be fatal if swallowed. DON cannot be effectively destroyed by autoclaving. Please carefully read and follow the below COSHH data sheet and use appropriate PPE when handling DON.

(<https://www.sigmaaldrich.com/GB/en/sds/sigma/d0156>).

Follow COSHH data sheet for the safe disposal of unused DON.

1.7. Disease assessment

15 **Image analysis**

Photographs of diseased images should be taken with a high-quality camera for recording purposes using a camera mount on a dark or light background.

16 **Visual scoring**



A DS index for visually scoring leaf disease severity is detailed by Chen *et al.* (2006) and offers a simple, reproducible way of assessing a large number of samples without downstream analysis.

17 **Fungal burden**

Fungal burden, the ratio of fungal to host gDNA, can be used to analyse the internal disease burden. A protocol for this is detailed in Machado-Wood *et al.* (2021), but briefly entails gDNA extraction followed by qPCR, with species-specific primers for quantification of entire gDNA.

18 **DON mycotoxin analysis**

The production of the DON mycotoxin by *Fusarium graminearum* can be measured as described in Cuzick, Urban and Hammond-Kosack (2008) using a commercially available enzyme-linked immunosorbent assay (ELISA). Ensure that the kit purchased matches the designated *Fg* chemotype of the strain to be used in the experiment; the WT reference strain PH-1 is a 15-ADON producer, an ester of deoxynivalenol (Miller, Taylor and Greenhalgh, 1983).

Protocol references

1. Alonso, J.M. *et al.* (2003). Genome-wide insertional mutagenesis of *Arabidopsis thaliana*. *Science*. **301**(5633):653-7. doi: 10.1126/science.1086391
2. Chen, X., Steed, A., Harden, C. and Nicholson, P. (2006). Characterization of *Arabidopsis thaliana-Fusarium graminearum* interactions and identification of variation in resistance among ecotypes. *Mol. Plant Pathol.* **7**(5):391-403. doi: 10.1111/j.1364-3703.2006.00349.x
3. Cuzick, A., Urban, M., and Hammond-Kosack, K. (2008). *Fusarium graminearum* gene deletion mutants map1 and tri5 reveal similarities and differences in the pathogenicity requirements to cause disease on Arabidopsis and wheat floral tissue. *New Phytol.* **177**(4): 990-1000. doi: 10.1111/j.1469-8137.2007.02333.x
4. Machado-Wood, A. K., Panwar, V., Grimwade-Mann, M., Ashfield, T., Hammond-Kosack, K. E. and Kanyuka, K. (2021). The vesicular trafficking system component MIN7 is required for minimizing *Fusarium graminearum* infection. *J. Exp. Bot.* **72**(13):5010-5023. doi: 10.1093/jxb/erab170
5. Miller, J. D., Taylor, A., Greenhalgh, R. (1983). Production of deoxynivalenol and related compounds in liquid culture by *Fusarium graminearum*. *Can. J. Microbiol.* **29**(9): 1171-1178. doi: 10.1139/m83-179